

Editor's preface

There are certain problems that must be solved in developing an attractive definition for modern Physical Organic Chemistry. The definition should be as broad as possible and should not restrict the scope of our field in a manner that excludes high quality work from it. At the same time, definitions that place Physical Organic Chemistry at the center around which modern scientific activity revolves are pretentious and may not be entirely accurate or widely accepted. I have not solved these problems, but hope with time to have developed an ability to recognize work in Physical Organic Chemistry deserving of publication in this monograph.

The vast improvement over the past thirty years in our understanding of the mechanism of enzyme catalysis is due, most importantly, to the development of site-directed mutagenesis of enzyme structure as a routine laboratory tool, and to the explosion in the number of enzyme structures that have been solved by X-ray crystallography. X-ray crystallographic determination of an enzyme structure might have been expected to reveal everything needed to explain enzyme catalysis. In fact, the use of an X-ray structure in developing the mechanism of the corresponding protein-catalyzed reaction most often raises questions about whether one is gifted enough to *see*. For example, the contribution of hydrogen tunneling to the rate acceleration for enzyme-catalyzed hydrogen transfer cannot be determined by inspection of a static crystal structure, but this structure provides a starting point for modern high-level calculations to determine whether hydrogen passes over, or tunnels through, the reaction coordinate for hydrogen transfer. Presently, the only experimental method for determining the importance of hydrogen tunneling in enzyme catalysis is through the determination of kinetic isotope effects. The chapter by Floyd Romesberg and Richard Schowen presents a lucid description of tunneling in solution and enzyme-catalyzed reactions; and, reviews the evidence for tunneling that has been obtained through the determination of kinetic isotope effects on these reactions.

Selenium and tellurium are not found commonly in organic compounds, and the rich chemistry of organoselenium and organotellurium compounds is therefore under appreciated by many organic chemists, including this editor. Michael Detty and Margaret Logan have prepared a detailed and cogent review of work to characterize the mechanism of one electron and two electron oxidation/reduction reactions of organochalcogens. Readers of this chapter might note that extensions of relatively simple concepts developed in the study of more familiar organic compounds are fully sufficient to rationalize the chemistry that is unique to organochalcogens.

Interest within the physical organic community on the mechanism for the formation and reaction of ion-pair and ion-dipole intermediates of solvolysis peaked sometime in the 1970s and has declined in recent years. The concepts developed during the heyday of this work have stood the test of time, but these reactions have not been fully characterized, even for relatively simple systems. Richard and coworkers have prepared a short chapter that summarizes their recent determinations of absolute rate constants for the reactions of these weak association complexes in water. This work provides a quantitative basis for the formerly largely qualitative discussions of competing carbocation-nucleophile addition and rearrangement reactions of ion and dipole pairs.

This volume seeks in a small way to bridge the wide gap between organic chemistry in the gas and condensed phases. The same types of chiral ion-dipole complexes that form as intermediates of solvolysis may be generated in the gas phase by allowing neutral molecules to cluster with chiral cations. The reactions of these "chiral" clusters have been characterized in exquisite detail by mass spectrometry. The results of this work are summarized by Maurizio Speranza in a chapter that is notable for its breadth and thoroughness of coverage. This presentation leaves the distinct impression that further breakthroughs on the problems discussed await us in the near future.

J. P. Richard

Contents

Editor's preface vii

Contributors to Volume 39 ix

Dynamics for the reactions of ion pair intermediates of solvolysis 1

JOHN P. RICHARD, TINA L. AMYES, MARIA M. TOTEVA and YUTAKA TSUJI

- 1 Introduction 1
- 2 A "Global" scheme for solvolysis 2
- 3 Clocks for reactions of ion pairs 3
- 4 Addition of solvent to carbocation–anion pairs 6
- 5 Protonation of a carbocation–anion pair 11
- 6 Isomerization of ion pair reaction intermediates 12
- 7 Racemization of ion pairs 22
- 8 Concluding remarks 24
 - Acknowledgements 24
 - References 24

Isotope effects and quantum tunneling in enzyme-catalyzed hydrogen transfer. Part I. The experimental basis 27

FLOYD E. ROMESBERG and RICHARD L. SCHOWEN

- 1 Introduction 28
- 2 Experimental phenomenology of quantum tunneling in enzyme-catalyzed reactions 48
- 3 Experimental signatures of tunneling 70
- 4 Models for tunneling in enzyme reactions 72
- 5 Tunneling as a contribution to catalysis: prospects and problems 73
 - References 74

One- and two-electron oxidations and reductions of organoselenium and organotellurium compounds 79

MICHAEL R. DETTY and MARGARET E. LOGAN

- 1 Introduction 79

2 Two-electron oxidations and reductions of selenium and tellurium compounds	80
3 One-electron oxidation of selenium and tellurium compounds	117
References	140

Chiral clusters in the gas phase **147**

MAURIZIO SPERANZA

1 Introduction	147
2 Ionic and molecular clusters in the gas phase	149
3 Experimental methodologies	155
4 Chiral recognition in molecular clusters	178
5 Chiral recognition in ionic clusters	196
6 Concluding remarks	266
Acknowledgements	267
References	267

Author Index **283**

Cumulative Index of Authors **297**

Cumulative Index of Titles **299**

Subject Index **307**

Isotope effects and quantum tunneling in enzyme-catalyzed hydrogen transfer.

Part I. The experimental basis

FLOYD E. ROMESBERG[†] and RICHARD L. SCHOWEN[‡]

[†]*Department of Chemistry, CVN-22, 10550 N. Torrey Pines Road, The Scripps Research Institute, La Jolla, CA 92037 USA*

[‡]*University of Kansas, Department of Pharmaceutical Chemistry, 2095 Constant Avenue, Lawrence, KS 66047 USA*

- 1 Introduction 28
 - Quantum tunneling in chemical reactions 28
 - Quantum tunneling in solution reactions 29
 - Quantum tunneling in enzyme-catalyzed reactions: early indications 35
 - The rule of the geometric mean (“no isotope effects on isotope effects”) 36
 - The Swain–Schaad relationship 36
 - The normal temperature dependence of isotope effects (see Chart 1) 37
 - Secondary isotope effects measure transition-state structure 37
 - Quantum tunneling in enzyme-catalyzed reactions: breakthroughs 42
- 2 Experimental phenomenology of quantum tunneling in enzyme-catalyzed reactions 48
 - Hydride-transfer reactions involving nicotinamide cofactors 48
 - Commitments 55
 - Hydride-transfer reactions involving other cofactors 64
 - Hydrogen-atom transfer reactions 67
 - Proton-transfer reactions 69
- 3 Experimental signatures of tunneling 70
 - Observations that do not definitively indicate tunneling 70
 - Observations that likely indicate tunneling 71
- 4 Models for tunneling in enzyme reactions 72
 - Bell tunneling 72
 - Tunneling assisted by protein dynamics 72
- 5 Tunneling as a contribution to catalysis: prospects and problems 73
 - References 74

Preamble

The last decade has seen the growth of a substantial literature on the role of quantum tunneling as a mechanism of the transfer of hydrogenic entities

E-mail address: floyd@scripps.edu (F.E. Romesberg), rschowen@ku.edu (R.L. Schowen).

(protons, hydrogen atoms, and hydride ions) during enzyme-catalyzed reactions. Much of the evidence for these ideas derives from kinetic isotope effects. This article is intended as a review of the background of the subject, the conceptual apparatus that underlies the isotopic studies, the phenomenology of the experimental observations, and a qualitative sketch of the interpretative, mechanistic models that have emerged.

This is a subject in which the role of sophisticated theoretical work has been especially crucial already, and its importance continues to grow. The most controversial aspect of the subject is the question of whether and how protein vibrations are directly linked to the catalysis of hydrogen tunneling by enzymes. The full nature and value of the theoretical work is not covered in the present article, nor are the evidence and concepts that underlie proposals for the involvement of protein dynamics. It is our intention to follow the present article with a later treatment of the theoretical contributions and the dynamical questions.

1 Introduction

QUANTUM TUNNELING IN CHEMICAL REACTIONS

The Heisenberg Uncertainty Principle,^{1,2} describing a dispersion in location and momentum of material particles that depends inversely on their mass, gives rise to vibrational zero-point energy differences between molecules that differ only isotopically. These zero-point energy differences are the main origin of *equilibrium* chemical isotope effects, i.e., non-unit isotopic ratios of equilibrium constants such as K_H/K_D for a reaction of molecules bearing a protium (H) atom or a deuterium (D) atom.

Non-unit *kinetic* isotope effects such as the rate-constant ratio k_H/k_D also derive from isotopic zero-point energy differences in the reactant state and in the transition state. A second manifestation of the Uncertainty Principle may also contribute to kinetic isotope effects, namely isotopic differences in the probability of quantum tunneling through the energy barrier between the reactant state and the product state.

For years, solution chemists (including enzymologists) took little note of the tunneling in chemical processes of particles other than electrons, chiefly because, for reactions that were of interest to them, no experimental data demanding the consideration of nuclear tunneling were in hand. Gas-phase reactions, such as the hydrogen-transfer reaction from methane to a trifluoromethyl radical, were well known to involve hydrogen tunneling, as is discussed in H.S. Johnston's book, "*Gas Phase Reaction Rate Theory*", which appeared in 1966.³

The simplest physical picture for the tunneling of a hydrogen nucleus during a hydrogen-transfer reaction takes note of the nuclear probability-density function for

the hydrogen nucleus, which describes the dispersion of the nucleus in three-dimensional space. If the distance over which the nucleus must move from a point on the reactant-state side of the potential-energy barrier to a point on the product-state side of the barrier is smaller than the dispersion of the hydrogen nucleus, then the hydrogen nucleus will possess probability density on both sides of the barrier. The fractional probability density on the product side measures the likelihood that the hydrogen-transfer process will have occurred for this molecule, in spite of the fact that the molecule had never reached the energy required classically to cross over the top of the barrier through the transition state. The distance through the energy barrier might be sufficiently small for one of two reasons. The barrier itself might be inherently thin, implying that the energy rises steeply on the reactant side and then falls steeply on the product side. Alternatively, the reacting molecules might be approaching the energy maximum at the transition state, where the distance between reactant side and product side approaches zero.

QUANTUM TUNNELING IN SOLUTION REACTIONS

In the 1950s and 1960s, experimental observations began to suggest that in solution reactions of complex molecules, tunneling of hydrogen nuclei might sometimes be an aspect of hydrogen-transfer mechanisms. Much of this work was reviewed in detail by Caldin in 1969.⁴ Kinetic isotope effects and their temperature dependences were the primary measurements that supported tunneling, just as is true today. The pioneering studies of R.P. Bell and his coworkers were focused on typical acid-based catalyzed organic reactions such as ketone enolization. By 1956 their observations encompassed: (a) isotope effects so large that tunneling seemed required, and (b) temperature dependences of the isotope effects that were difficult to explain without the inclusion of tunneling. Such indications were missing in other, quite similar reactions and a certain amount of confusion began to develop over why tunneling occurred in some hydrogen-transfer reactions and not in others.

It may have been the dramatic 1964 publication of E.S. Lewis and L. Funderburk⁵ that forced the question of hydrogen tunneling in complex solution reactions near room temperature into the consciousness of a larger scientific public, particularly in physical-organic chemistry. This article presented isotope effects for proton abstraction from 2-nitropropane by a series of substituted pyridines, and the values rose sharply as the degree of steric hindrance to the reaction increased (Fig. 1). All the observed H/D isotope effects, from 9.6 to 24, were larger than expected from the simplest version of the so-called semiclassical theory of isotope effects (Fig. 2).

On this theory, it is assumed (a) that the motion of the reactant-state C–H/D bonds can be thought of as one stretching and two bending motions, and (b) that the bending motions are little different in the transition state than in the reactant state. Then, the maximum possible isotope effect will be determined by the isotopic zero-point energy difference in the reactant-state C–H/D motion. For a stretching motion with a C–H frequency of 2900 and CD frequency 2130 cm^{-1} , the isotopic

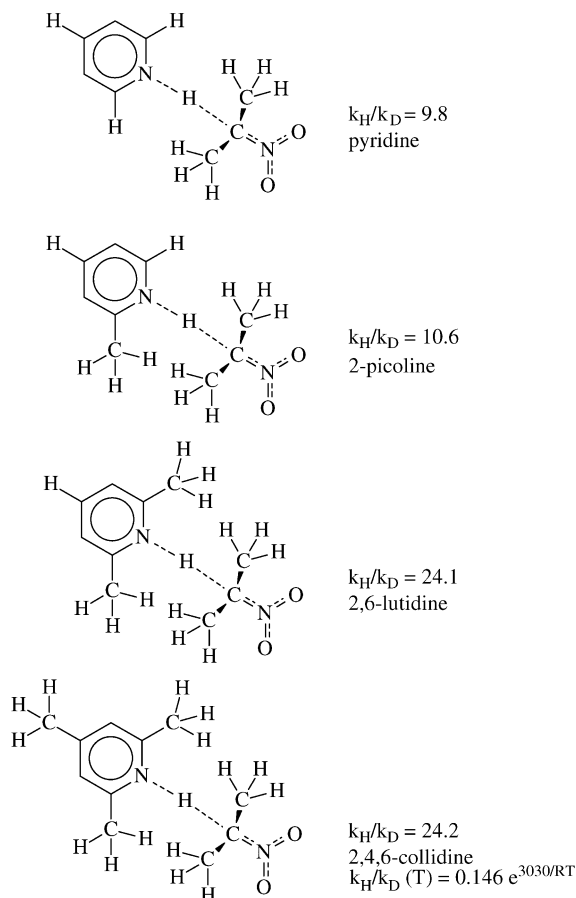


Fig. 1 Lewis and Funderburk⁵ found that the H/D primary kinetic isotope effects (25 °C in aqueous *t*-butyl alcohol) for proton abstraction from 2-nitropropane by pyridine derivatives all exceed the maximum isotope effect that could have been derived from the isotopic difference in reactant-state zero-point energies alone (a value around 7). The magnitude of the isotope effect increases with the degree of steric hindrance to reaction presented by the pyridine derivative, the identical results for 2,6-lutidine and 2,4,6-collidine ruling out any role for electronic effects of the substituents. The temperature dependence shown for 2,4,6-collidine is exceedingly anomalous: the pre-exponential factor A_H/A_D is expected to be near unity but is instead about 1/7, while the value of $\Delta H_D^\ddagger - \Delta H_H^\ddagger = 3030$ cal/mol would have generated an isotope effect at 25 °C of 165 if the pre-exponential factor had indeed been unity.

zero-point energy difference is 385 cm^{-1} and with RT of 207 cm^{-1} , the maximum isotope effect is predicted to be 6.4. This value is exceeded even by the pyridine reaction. Even if the bending motions produced no zero-point energy in the transition state (a circumstance hard to imagine), the predicted maximum isotope effect is around 23, which is slightly smaller than the values of 24 seen here for

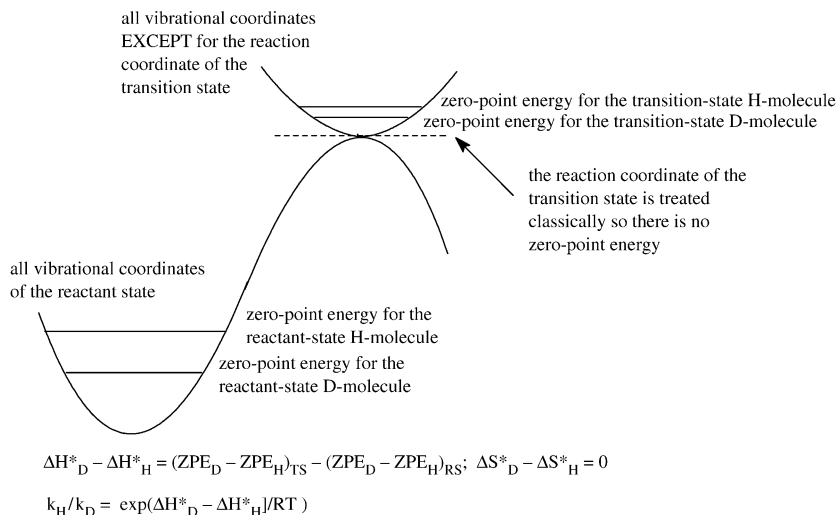


Fig. 2 Schematic representation of the so-called semiclassical treatment of kinetic isotope effects for hydrogen transfer. All vibrational motions of the reactant state are quantized and all vibrational motions of the transition state except for the reaction coordinate are quantized; the reaction coordinate is taken as classical. In the simplest version, only the zero-point levels are considered as occupied and the isotope effect and temperature dependence shown at the bottom are expected. Because the quantization of all stable degrees of freedom is taken into account (thus the zero-point energies and the isotope effects) but the reaction-coordinate degree of freedom for the transition state is considered as classical (thus omitting tunneling), the model is called semiclassical.

the most sterically hindered bases. At the time, this isotope effect was the largest ever observed in a solution reaction at room temperature.

The temperature dependence of the large isotope effect for the 2,4,6-collidine is just as striking (see Chart 1 and Fig. 2). In place of the expected unit value of A_H/A_D , a value around 0.15 was found accompanied by an enormous isotopic difference in enthalpies of activation, equivalent to an isotope effect of 165. Both of these results had earlier been shown by Bell (as summarized by Caldin⁴) to be predicted by a one-dimensional model for tunneling through a parabolic barrier. The outlines of Bell's treatment of tunneling are given in Chart 2, while Fig. 3 shows that the departure of the isotopic ratios of pre-exponential factors from unity and isotopic activation energy differences from the expected values are both predicted by the Bell approach.

The most significant point about the Lewis and Funderburk results, however, was not the observation of tunneling. Bell and his coworkers had already succeeded in observing tunneling, large isotope effects, and their apparently characteristic temperature dependence in similar reactions. What was notable here was the clear trend in the isotope effects with increasing steric hindrance. Steric repulsion of the pyridine methyl groups (at C2 and C6) by the two methyl groups of 2-nitropropane is a short-range interaction with a steep dependence on the distance between the

Chart 1. Data reduction for isotope-effect temperature dependences

Isotope-effect temperature dependences have been treated by means of the Eyring equation:

$$k = (k_b T/h) \exp([\Delta S^\ddagger/R] - [\Delta H^\ddagger/RT])$$

where k is the rate constant; k_b the Boltzmann constant; T the temperature in K ; h the Planck constant, ΔS^\ddagger the standard entropy of activation; ΔH^\ddagger the standard enthalpy of activation; and the Arrhenius equation:

$$k = A \exp(-[E_a/RT])$$

where k is the rate constant; A the pre-exponential factor and E_a the activation energy.

The parameters of the two equations are related by:

$$\Delta H^\ddagger = E_a - RT$$

$$\Delta S^\ddagger = R(\ln[hA/kT]) - 1$$

For an isotope effect K_H/K_D , one has for the two treatments:

$$\ln(k_H/k_D) = (\Delta S_H^\ddagger - \Delta S_D^\ddagger)/R - (\Delta H_H^\ddagger - \Delta H_D^\ddagger)/RT$$

$$\ln(k_H/k_D) = \ln(A_H/A_D) - (E_{aH} - E_{aD})/RT$$

so that:

$$(\Delta S_H^\ddagger - \Delta S_D^\ddagger) = R \ln[A_H/A_D]$$

$$(\Delta H_H^\ddagger - \Delta H_D^\ddagger) = [E_{aH} - E_{aD}]$$

interacting methyl groups.⁶ As a result, the repulsion will become a factor only as the two reacting molecules enter the transition state, and as they approach still more closely the energy will rise sharply. As the hydrogen-transfer event is completed and the product molecules move apart, the energy will then drop steeply. The effect of introducing increasing steric hindrance is therefore to produce a barrier to reaction which is high and thin. Crossing over the barrier is made more difficult but crossing through the barrier is made easier. Lewis and Funderburk made this argument and thus offered a proposal for how the degree of tunneling, in this case assumed to correlate with the magnitude of the isotope effect, could be controlled by the molecular structure of the reactants. As the structure generated greater steric repulsion, it resulted in a sharper barrier, more easily penetrated in the tunneling event. So this study provided a mechanistic basis for the occurrence of tunneling, satisfying at the time.

Chart 2. A simplified account of the Bell tunneling model⁸

The transition state theory holds that the reaction rate ν will be given by the product of transition-state concentration $[T]$ and the imaginary frequency[†] $i\nu$ ($i = \sqrt{-1}$) with which the transition-state molecule decomposes to product:

$$\nu = i\nu[T]$$

Let K^* be the true thermodynamic equilibrium constant for formation of the transition-state species T from the reactant-state species R and let k be the experimental rate constant for the reaction of R . Neglecting activity coefficients:

$$\nu = i\nu K^*[R] = k[R]$$

$$k = i\nu K^* = i\nu Q_T/Q_R$$

where the Q s are partition functions. Factor from Q_T the vibrational partition function for the reaction coordinate q^\ddagger and (a) let Q^\ddagger be the “defective” partition function that lacks this reaction-coordinate degree of freedom (thus $Q_T = q^\ddagger Q^\ddagger$); (b) let K^\ddagger be the corresponding “defective” equilibrium constant (thus $K^\ddagger = Q^\ddagger/Q_R$):

$$k = i\nu Q_T/Q_R = i\nu q^\ddagger Q^\ddagger/Q_R = i\nu q^\ddagger K^\ddagger = i\nu q^\ddagger \exp(-\Delta G^\ddagger/RT)$$

Ascribe to q^\ddagger the form of a harmonic-oscillator partition function so that the pre-exponential factor becomes:

$$i\nu q^\ddagger = i\nu[(1/(e^{iu/2} - e^{-iu/2}))] = (k_b T/h)[(iu/(e^{iu/2} - e^{-iu/2}))]$$

where $u = h\nu/k_b T$. If u is small (gently curved barrier), then $(e^{iu/2} - e^{-iu/2}) = (1 + iu/2 - 1 + iu/2) = iu$ and the pre-exponential factor becomes $k_b T/h$. This is the “ultrasimple” transition-state theory, with no provision for tunneling. If the barrier is more sharply curved, then the full expression is used. The relationship $(e^{iu/2} - e^{-iu/2}) = 2i \sin(u/2)$ can be introduced to emphasize that the quantity i cancels, and the Bell tunneling correction at this simple level is given by:

$$(u/2)/\sin(u/2)$$

with u restricted to values of less than 2π .

[†] The frequency is an imaginary number because it is given by $(1/2\pi)[F/\mu]^{1/2}$, where F is the force constant and μ the reduced mass for the reaction coordinate along which the reactant molecules pass through the transition state. The force constant $F = [\partial^2 V/\partial q^2]_{q=0}$ (V is the potential energy and q the distance along the reaction coordinate, equal to zero at the transition state). F is a negative number because V experiences a maximum at $q = 0$ and the frequency is, therefore, imaginary.

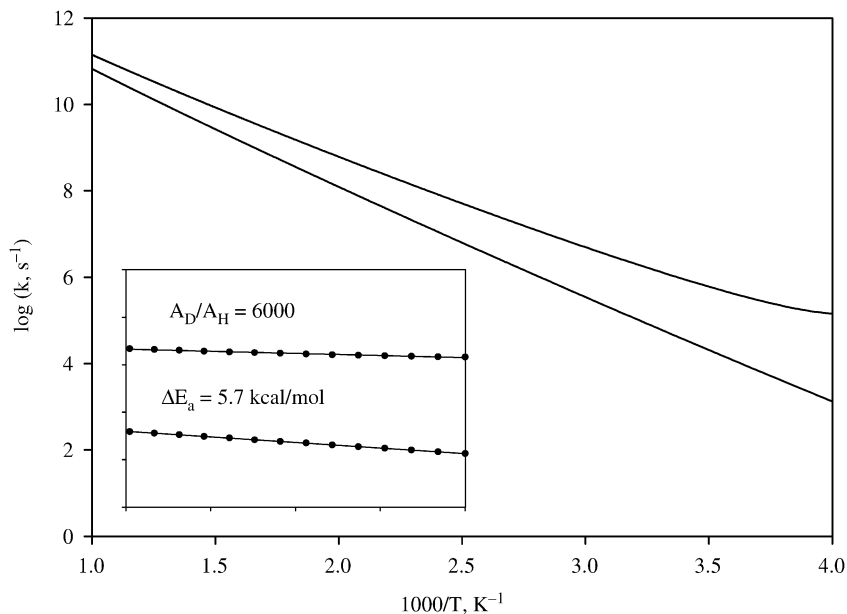


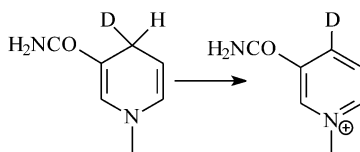
Fig. 3 Hydrogen tunneling according to the Bell model can generate anomalous isotopic Arrhenius parameters. A semiclassical model with $\Delta S_{\text{H}}^{\ddagger} = \Delta S_{\text{D}}^{\ddagger} = 0$ (thus $A_{\text{H}} = A_{\text{D}}$) and $\Delta H_{\text{H}}^{\ddagger} = 10.0$ kcal/mol, $\Delta H_{\text{D}}^{\ddagger} = 11.4$ kcal/mol (an isotope effect of about 10 at room temperature) was corrected for tunneling by Bell's simplified correction $Q_t = (u/2)/\sin(u/2)$ where $u = h\nu/kT$ and $i\nu$ is the imaginary frequency for barrier crossing; ν_{H} was taken as 1000 cm^{-1} , ν_{D} as 735 cm^{-1} . The solid lines (H above, D below) are plotted for temperatures from 250 to 1000 K. At high temperatures, the observed rate constants approach the semiclassical values, while at low temperatures the rate-increasing effect of tunneling produces upward curvature. Curvature appears at higher temperatures with H than D, leading to a lower apparent A_{H} and lower apparent E_{a} than for the semiclassical reaction. The inset shows that linear least-squares fits to the data between 250 and 263 K yield $A_{\text{D}}/A_{\text{H}} = 6000$ (instead of 1.0) and $\Delta E_{\text{a}} = 5.7$ kcal/mol rather than 1.4 kcal/mol. The isotope effect $k_{\text{H}}/k_{\text{D}}$ is about 75 at 256 K and appears to be the product of a pre-exponential ratio of (1/6000) and an isotope effect from activation energy differences of 460,000.

E.S. Lewis reviewed the situation in the 1975 *Festschrift* for R.P. Bell⁷ and R.P. Bell brought the subject to 1980 in his book.⁸ In the same year, the subject was included in the monograph on isotope effects by L. Melander and W. H. Saunders.⁹ Work in this period on organic reactions in solution clarified not only some mechanistic aspects of tunneling but also clarified many of the experimental criteria for tunneling. A major contributor is W. H. Saunders, whose studies of tunneling in elimination and related reactions involving proton transfer have been widely influential. For example,¹⁰ the 1,2-elimination of *p*-toluenesulfonic (“tosylic”) acid (TsOH) from $(\text{C}_6\text{H}_5)_2\text{CLCH}_2\text{OTs}$ (where L (“label”) can be H or T), in *t*-butanol

with *t*-butoxide ion as base, generated isotope effects (H/T) from 30.6 at 40 °C to 18.3 at 80 °C. The isotope effects are larger than the expected maximum values (the H/T effect of 30.6 is the equivalent of an H/D effect of 10.8), and their temperature dependence is anomalous: $A_H/A_T = 0.31$ and the isotopic difference in enthalpies of activation is 2.85 kcal/mol, corresponding to an isotope effect of 125 at 25 °C. The authors calculated the magnitude of the Bell tunnel correction (Chart 2, Fig. 3) to the semiclassical rate constant to be 2.0 for the data just described, implying that the occurrence of tunneling increases the rate by this factor. A systematic picture of the mechanistic basis for the presence or absence of tunneling, however, was still lacking¹⁰: “Although (the present results) confirm our earlier observations of virtually ubiquitous tunneling in E2 reactions, there are almost no clear-cut trends in either isotope effects or tunnel corrections”.

QUANTUM TUNNELING IN ENZYME-CATALYZED REACTIONS: EARLY INDICATIONS

Just as in the preceding examples, early indications of tunneling in enzyme-catalyzed reactions depended on the failure of experiments to conform to the traditional expectations for kinetic isotope effects (Chart 3). Table 1 describes experimental determinations of α -secondary isotope effects for redox reactions of the cofactors NADH and NAD⁺. The two hydrogenic positions at C4 of NADH are stereochemically distinct and can be labeled individually by synthetic use of enzyme-catalyzed reactions. In reactions where the deuterium label is not transferred (see below), an



α -secondary isotope effect can be determined. As recounted in the last item of Chart 3, such effects are expected to be measures of transition-state structure. If the transition state closely resembled reactants, then no change in the force field at the isotopic center would occur as the reactant state is converted to the transition state and the α -secondary kinetic isotope effect should be 1.00. If the transition state closely resembled products, then the transition-state force field at the isotopic center would be very similar to that in the product state, and the α -secondary kinetic isotope effect should be equal to the equilibrium isotope effect, shown by Cook, Blanchard, and Cleland¹⁴ to be 1.13. Between these limits, the kinetic isotope effect should change monotonically from 1.00 to 1.13.

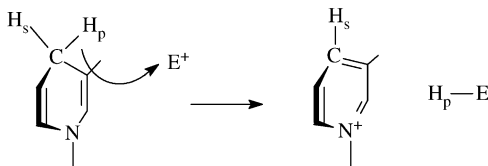
Kurz and Frieden^{11,13} in 1977 and 1980 determined α -secondary kinetic isotope effects for the unusual desulfonation reaction shown in Table 1, both in free solution and with enzyme catalysis by glutamate dehydrogenase. The isotope effects (H/D) were in the range of 1.14–1.20. At the time, the correct equilibrium isotope effect had not been reported and their measurements yielded an erroneous value

Chart 3. Traditionally expected features of hydrogen isotope effects⁹

THE RULE OF THE GEOMETRIC MEAN ("NO ISOTOPE EFFECTS ON ISOTOPE EFFECTS")

Isotope effects at different positions in a molecule are independent and multiplicative (the isotope effects on the free energy of reaction or activation are additive).

For example, primary and secondary isotope effects in reduction by NADH:



The primary isotope effect $(k_H/k_D)_P$ can be measured with $H_s = H$ or with $H_s = D$; the Rule states the two measurements should be equal to each other. The secondary isotope effect $(k_H/k_D)_S$ can be measured with $H_p = H$ and with $H_p = D$; the Rule states the two measurements should be equal to each other.

The Rule is a rough expectation based on the local character of vibrational motions and becomes more reliable as the locations of the two isotopic sites become more distant.

THE SWAIN-SCHAAD RELATIONSHIP

The simplest version of the origin of kinetic isotope effects holds that, say k_H/k_D will given by:

$$k_H/k_D = \exp(1/2)(\sum[\nu_h - \nu_d]_{TS} - \sum[\nu_h - \nu_d]_{RS}/kT)$$

where the sums give the isotopic frequency differences in the transition state (TS) and the reactant state (RS), so that the argument of the exponential is the change in isotopic zero-point energy differential upon activation. Assuming that the reduced masses of all the isotopically sensitive vibrations can be approximated by $1/\sqrt{1}$ for H vibrations and $1/\sqrt{2}$ for D vibrations, then:

$$k_H/k_D = (\text{constant})^{(1-1/\sqrt{2})}$$

where the constant is a property of only the H vibration frequencies. A similar procedure gives:

$$k_H/k_T = (\text{constant})^{(1-1/\sqrt{3})}$$

so that:

$$k_{\text{H}}/k_{\text{T}} = (k_{\text{H}}/k_{\text{D}})^{(1-1/\sqrt{3})/(1-1/\sqrt{2})} = (k_{\text{H}}/k_{\text{D}})^{1.44}$$

This apparently naive expectation has been confirmed theoretically and experimentally. The exponent 1.44 is known as the Swain–Schaad exponent or coefficient, and is used in various forms of which the most common are:

$$\ln(k_{\text{H}}/k_{\text{T}})/\ln(k_{\text{H}}/k_{\text{D}}) = 1.44$$

$$\ln(k_{\text{H}}/k_{\text{T}})/\ln(k_{\text{D}}/k_{\text{T}}) = 3.26$$

THE NORMAL TEMPERATURE DEPENDENCE OF ISOTOPE EFFECTS (SEE CHART 1)

If isotope effects arise solely from the difference between isotopic zero-point energy differentials in the reactant state and transition state, with no role of excited vibrational states, then $(\Delta S_{\text{H}}^{\ddagger} - \Delta S_{\text{D}}^{\ddagger}) = 0$ on the Eyring model and $A_{\text{H}} = A_{\text{D}}$ on the Arrhenius model. Thus:

$$k_{\text{H}}/k_{\text{D}} = \exp[-(\Delta H_{\text{H}}^{\ddagger} - \Delta H_{\text{D}}^{\ddagger})/RT] = \exp[-(E_{\text{aH}} - E_{\text{aD}})/RT]$$

If the isotope effect at T_1 is $(k_{\text{H}}/k_{\text{D}})_1$, then the temperature dependence is predicted as:

$$\ln(k_{\text{H}}/k_{\text{D}}) = (T_1/T)\ln[(k_{\text{H}}/k_{\text{D}})_1]$$

SECONDARY ISOTOPE EFFECTS MEASURE TRANSITION-STATE STRUCTURE

If secondary isotope effects arise strictly from changes in force constants at the position of substitution, with none of the vibrations of the isotopic atom being coupled into the reaction coordinate, then a secondary isotope effect will vary from 1.00 when the transition state exactly resembles the reactant state (thus no change in force constants when reactant state is converted to transition state) to the value of the equilibrium isotope effect when the transition state exactly resembles the product state (so that conversion of reactant state to transition state produces the same change in force constants as conversion of reactant state to product state). For example in the hydride-transfer reaction shown under point 1 above, the equilibrium secondary isotope effect on conversion of NADH to NAD^+ is 1.13. The kinetic secondary isotope effect is expected to vary from 1.00 (reactant-like transition state), through $(1.13)^{0.5}$ when the structural changes from reactant state to transition state are 50% advanced toward the product state, to 1.13 (product-like transition state). That this naïve expectation is unlikely to be exact has been shown by Glad and Jensen⁷⁶.

Table 1 Experimental studies that led to the coupled motion and tunneling model

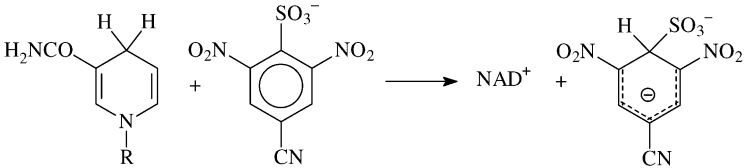
Reference	System	Observations
11		Without enzyme catalysis, the secondary KIE (H/D) is 1.21. With catalysis by glutamate dehydrogenase, the secondary KIE is 1.14 ± 0.07 .
12	Yeast alcohol dehydrogenase, catalysis of oxidation by NAD^+ of benzyl alcohol; equilibrium interconversion of benzyl alcohol and benzaldehyde	With label in the benzyl alcohol, the secondary KIE (H/T) is 1.34–1.38 while the equilibrium isotope effect is 1.33–1.34. Substituent effects, by contrast, indicate a transition state that resembles the reactant state, not the product state.
13	Same as for Ref. 11	Without enzyme catalysis, the secondary KIE is 1.15–1.16. The equilibrium secondary isotope effect was estimated as 1.01–1.03 (but see entry below). The exalted secondary isotope effect was suggested to originate in reaction-coordinate motion of the secondary center.
14	Equilibrium interconversion of NAD^+ to NADH.	The equilibrium secondary isotope effect (H/D) for conversion of NAD^+ to NADH is 0.89 (1.13 for conversion of NADH to NAD^+).

Table 1 (*continued*)

Reference	System	Observations
15	Yeast alcohol dehydrogenase (YADH), catalysis of reduction by NADH of acetone; formate dehydrogenase (FDH), oxidation by NAD ⁺ of formate; horse-liver alcohol dehydrogenase (HLAD), catalysis of reduction by NADH of cyclohexanone	With label in NADH, the secondary KIE is 1.38 for reduction of acetone (YADH); with label in NAD ⁺ , the secondary KIE is 1.22 for oxidation of formate (FDH); with label in NADH, the secondary KIE is 1.50 for reduction of cyclohexanone (HLAD). The exalted secondary isotope effects were suggested to originate in reaction-coordinate motion of the secondary center.

of 1.01–1.03. The kinetic effects thus appeared to be *exalted*, much larger than the equilibrium effect and in violation of the expectation of Chart 3. Even when the correct equilibrium isotope effect of 1.13 became known,¹⁴ the exaltation was still apparent, although less dramatic. The explanation suggested by Kurz and Frieden^{11,13} was that the reaction-coordinate motion could involve both the transferring motion of one of the C4-hydrogens of NADH and the motion into the ring plane of the other, non-transferring hydrogen. This “coupled motion” would make the isotope effect at the non-transferring center a partially primary isotope effect and not a typical secondary isotope effect. The important subject of coupled motion will be discussed in rigorous detail in a treatment to be published later.

At about the same time, Welsh, Creighton, and Klinman¹² identified a confusing contradiction between secondary isotope effects and substituent effects in the action of yeast alcohol dehydrogenase on benzyl alcohol. The substituent effect studies¹⁶ had shown that k_{cat} for oxidation of benzyl alcohol was independent of electronic and steric substitution in the benzyl ring, while reduction of benzaldehyde exhibited large substituent effects. Both findings suggested that the transition state resembled the unchanged alcohol much more than the benzaldehyde. However, α -secondary kinetic isotope effects (H/T) for the oxidation of benzyl alcohol were identical to the equilibrium effects, suggesting exactly the opposite conclusion. These observations would later be understood as an example of exaltation of the secondary isotope effect from a small value consistent with the substituent effects to a large value, coincidentally equal to the equilibrium effect.

In the following year, Cleland and his coworkers¹⁵ reported further and more emphatic examples of the phenomenon of exaltation of the α -secondary isotope effects in enzymic hydride-transfer reactions. The cases shown in Table 1 for their studies of yeast alcohol dehydrogenase and horse-liver alcohol dehydrogenase would have been expected on traditional grounds to show kinetic isotope effects between 1.00 and 1.13 but in fact values of 1.38 and 1.50 were found. Even more impressively, the oxidation of formate by NAD^+ was expected to exhibit an isotope effect between 1.00 and $1/1.13 = 0.89$ – an inverse isotope effect because NAD^+ was being converted to NADH. The observed value was 1.22, normal rather than inverse. Again the model of coupled motion, with a citation to Kurz and Frieden, was invoked to interpret the findings.

In 1983, Huskey and Schowen¹⁷ tested the coupled-motion hypothesis and showed it to be inadequate in its purest form to account for the results. If, however, tunneling along the reaction coordinate were included along with coupled motion, then not only was the exaltation of the secondary isotope effects explained but also several other unusual features of the data as well. Fig. 4 shows the model used and the results. The calculated equilibrium isotope effect for the NCMH model (the models employed are defined in Fig. 4) was 1.069 (this value fails to agree with the measured value of 1.13 because of the general simplicity of the model and particularly defects in the force field). If the coupled-motion hypothesis were correct, then sufficient coupling, as measured by the secondary/primary reaction-coordinate amplitude ratio $r_{\text{H2}}/r_{\text{H1}}$ should generate secondary isotope effects that

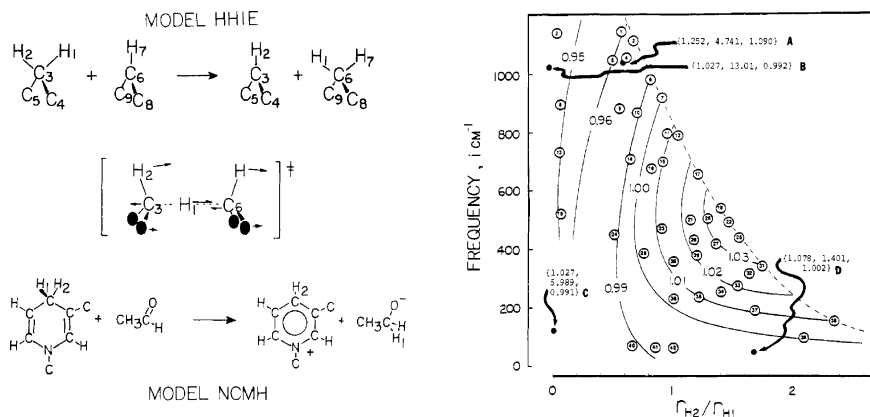


Fig. 4 Models and results from the Huskey and Schowen¹⁷ test of the coupled-motion hypothesis in 1983. Two models are defined in the left-hand part of the figure: HHIE, a simplified model for general exploration, and NCMH, a more extensive model for detailed examinations. Standard force constants, bond lengths, angles, and atomic masses were used for reactant states. For transition states, the force fields and geometries were varied according to a bond-energy bond-order (BEBO) paradigm as described in detail by Rodgers, Femec and Schowen⁷³. For the reaction-coordinate motion (left center), the bending coordinates shown and the two C–H stretching coordinates were coupled to varying degrees by adjustment of off-diagonal elements in the force-constant matrix. Two features of the resulting reaction coordinates were then considered: the imaginary frequency and the amplitude ratio $r_{\text{H}2}/r_{\text{H}1}$, where H2 refers to the non-transferring (“secondary”) hydrogen and H1 to the transferring (“primary”) hydrogen. On the right, the results are shown with values for some NCMH models of the primary isotope effect, the secondary isotope effects, and ratio of the secondary isotope effect for H-transfer to the secondary isotope effect for D-transfer. The many small circles represent HHIE calculations, and their main significance is that only models to the left of the dashed line can represent true transition states with one and only one reaction coordinate; models in the remainder of the two-dimensional space have multiple unstable coordinates. Other features of the results are discussed in the text. Reproduced from Ref. 17 with the permission of the American Chemical Society.

exceed the equilibrium effect. In addition, it was required that the calculated primary isotope effect should fall in or near the experimental range of 4.9–5.5.

On the right side of Fig. 4, the two points C and D represent models with a small imaginary frequency (see Chart 2 for an explanation of this term and its role in tunneling) and thus gentle curvature at the top of the activation barrier. Point C has an amplitude ratio of zero, and thus no coupling of the bending motions of the secondary hydrogen into the reaction coordinate. The secondary isotope effect is 1.027 and roughly corresponds to the transition-state structure (half-transferred hydrogen), being very roughly midway between 1.00 and 1.069. The primary effect is 6.0, adequately close to the experimental range. Point D introduces a very large amount of coupled motion, producing an amplitude ratio of 1.7: the secondary hydrogen moves over a distance almost twice that for the primary hydrogen. In fact, the secondary isotope effect somewhat exceeds the equilibrium effect

(1.078 vs. 1.069). But the primary isotope effect is reduced by an unacceptable amount to only 1.4, far from the experimental values. This reduction is a result of increasing the reaction-coordinate amplitude for the secondary hydrogen at the expense of the motion of all other atoms, including the primary hydrogen. Tunneling corrections on the truncated Bell model (Chart 2) are included for points C and D but are very small (1.000–1.006). It was concluded that coupled motion with a gently curved barrier could not produce the observations.

Points A and B on the plot represent models with a sharply curved barrier, the reaction-coordinate frequency being around $i1000\text{ cm}^{-1}$ (where $i = \sqrt{-1}$). Point B (no coupled motion) shows a modest secondary effect (1.027) but a very large primary effect of 13, distant from the experimental values, and so fails on all counts. Point A, with an amplitude ratio of 0.5 (primary hydrogen moves twice as far as the secondary hydrogen), however, exhibits a secondary isotope effect of 1.252, well in excess of the equilibrium effect of 1.069. Furthermore, the primary isotope effect is 4.7, quite close to the experimental range. The tunneling correction for the secondary isotope effect at point A is 1.19 so the semiclassical secondary isotope effect would be 1.052. This value is not in excess of the equilibrium effect of 1.069, further emphasizing that the introduction of coupled motion alone cannot explain the exaltation of the secondary isotope effect. The tunneling correction for the primary isotope effect is 1.57 so the semiclassical primary effect is 3.0; thus the coupled motion without tunneling would also produce an unacceptably low primary isotope effect.

The overall conclusion drawn by Huskey and Schowen¹⁷ was that a combination of coupled motion and tunneling through a relatively sharp barrier was required to explain the exaltation of secondary isotope effects. They also noted that this combination predicts that a reduction of exaltation in the secondary effect will occur if the transferring hydrogen is changed from protium to deuterium: for point A in Fig. 4, the secondary effect is reduced by a factor of 1.09. Experimentally, reduction factors of 1.03 to 1.14 had been reported. For points B, C, and D on the diagram, all of which lack a combination of coupled motion and tunneling, no such reductions in the secondary isotope effect were calculated.

These studies had therefore found the tunneling phenomenon, with coupled motion, as the explanation for failures of these systems to conform to the expectations that the kinetic secondary isotope effects would be bounded by unity and the equilibrium effect and that the primary and secondary effects would obey the Rule of the Geometric Mean (Chart 3), as well as being consistent with the unusual temperature dependences for isotope effects that were predicted by Bell for cases involving tunneling.

QUANTUM TUNNELING IN ENZYME-CATALYZED REACTIONS: BREAKTHROUGHS

A few years later, Cha, Murray and Klinman¹⁸ published a report on isotope effects in the redox interconversion of benzyl alcohol–benzaldehyde/NAD⁺–NADH, with catalysis by yeast alcohol dehydrogenase. This article effected among biochemists

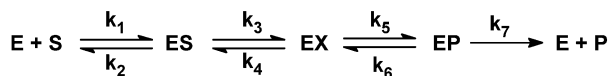
much the same shift in attitude that Lewis and Funderburk's article had produced with organic chemists. The centerpiece of this article was a new approach to violations of the Swain–Schaad relationship (Chart 3) that provided a diagnostic criterion for tunneling.

There are two ways in which an enzymic reaction can fail to satisfy the Swain–Schaad relationship, one of which is if tunneling occurs. In order to use violations of this rule to diagnose the presence of tunneling, it is necessary to eliminate the other possible reason for a violation, namely, limitation of the rate by more than one step. The derivation of the Swain–Schaad equation in Chart 3 assumes that the step that produces the isotope effect is fully rate-limiting, and if this should be untrue, then the relationship should fail without any significance for tunneling.

Chart 4 shows how isotope effects are influenced if more than a single step limits the rate and illustrates the situation for an irreversible one-substrate enzyme-catalyzed reaction. In any multistep steady-state reaction, the isotope effects on the observable kinetic parameters (the *observed isotope effects*) are weighted averages of the individual isotope effects on each of the microscopic rate constants (the *intrinsic isotope effects*). The weighting factor for each intrinsic isotope effect is the fractional degree to which the corresponding step limits the rate for the H reactant. The value of the weighting factor is 1.0 if the individual step fully limits the rate (and the corresponding rate constant is thus equal to the observable rate constant) and falls to zero as the individual step becomes faster (larger rate constant) and no longer influences the observable rate. The last two equations of Chart 4 give the algebraic expressions for enzyme kinetics when one and only one individual step has an isotope effect.

Enzymologists often refer to the situation in which more than a single step limits the rate as “kinetic complexity”. Cha, Murray, and Klinman¹⁸ advocated a particularly effective manner of treating isotope-effect data to check for kinetic complexity. Chart 5 shows an illustrative example in which it is assumed that the isotope sensitive step is only 50% rate limiting for the H case, with an H/D primary isotope effect of 5 and H/T primary isotope effect of 10.2 (calculated from the Swain–Schaad relationship) on the isotope-sensitive step. In this case, the observed H/D isotope effect is 3 and the observed H/T effect is 5.6. If the Swain–Schaad exponent is calculated from the observed effects, a value of 1.56 rather than 1.44 is obtained. A prediction of the H/T effect from the H/D effect, using the standard exponent of 1.44, gives 4.9 instead of the observed 5.6 while the reverse prediction of the H/D effect from the H/T effect gives 3.3 instead of the observed 3.0. The disagreements between expectations for a single rate-limiting step and the observed quantities are modest, on the order of 15% or less. If the observed isotope effects cannot be determined with considerably greater precision than 15%, then these isotope effects will be poor indicators of kinetic complexity.

Cha, Murray, and Klinman¹⁸ proposed using the same data differently, by comparing expectations for the isotope effects k_H/k_T and k_D/k_T . The difference is purely algebraic but it has an advantage based on the fact that the isotope-sensitive step is least rate-limiting for the H case, more nearly rate-limiting for the D

Chart 4. The expression of intrinsic isotope effects in multistep reactions


For the deuterated substrate, the observable rate constants are given by:

$$1/k_{\text{cat}}/K_{\text{M}})_{\text{D}} = (1/k_1)_{\text{D}} + (k_2/k_1k_3)_{\text{D}} + (k_2k_4/k_1k_3k_5)_{\text{D}} + (k_2k_4k_6/k_1k_3k_5k_7)_{\text{D}}$$

$$1/(k_{\text{cat}})_{\text{D}} = (1/k_3)_{\text{D}} + (k_4/k_3k_5)_{\text{D}} + (k_4k_6/k_3k_5k_7)_{\text{D}} + (1/k_5)_{\text{D}} + (k_6/k_5k_7)_{\text{D}} \\ + (1/k_7)_{\text{D}}$$

Let m_{xy} be the microscopic or net rate constant that links reactant state x with transition state y ($x = 0$ for $E + S$; $x = 1$ for ES , etc; $y = 1$ for the transition state associated with k_1 and k_2 ; $y = 3$ for the transition state associated with k_3 and k_4 , etc):

$$1/(k/c(k/(k_{\text{cat}}/K_{\text{M}}))_{\text{D}} = (1/m_{01})_{\text{D}} + (1/m_{03})_{\text{D}} + (1/m_{05})_{\text{D}} + (1/m_{07})_{\text{D}}$$

$$1/(k_{\text{cat}})_{\text{D}} = (1/m_{13})_{\text{D}} + (1/m_{15})_{\text{D}} + (1/m_{17})_{\text{D}} + (1/m_{25})_{\text{D}} + (1/m_{27})_{\text{D}} + (1/m_{37})_{\text{D}}$$

Multiply by the observable rate constants for the protiated substrate:

$$(k_{\text{cat}}/K_{\text{M}})_{\text{H}}/(k_{\text{cat}}/K_{\text{M}})_{\text{D}} \\ = (k_{\text{cat}}/K_{\text{M}})_{\text{H}}(1/m_{01})_{\text{D}} + (k_{\text{cat}}/K_{\text{M}})_{\text{H}}(1/m_{03})_{\text{D}} + (k_{\text{cat}}/K_{\text{M}})_{\text{H}}(1/m_{05})_{\text{D}} \\ + ((k_{\text{cat}}/K_{\text{M}})_{\text{H}}1/m_{07})_{\text{D}}$$

$$(k_{\text{cat}})_{\text{H}}/(k_{\text{cat}})_{\text{D}} = (k_{\text{cat}})_{\text{H}}(1/m_{13})_{\text{D}} + (k_{\text{cat}})_{\text{H}}(1/m_{15})_{\text{D}} + (k_{\text{cat}})_{\text{H}}(1/m_{17})_{\text{D}} \\ + (k_{\text{cat}})_{\text{H}}(1/m_{25})_{\text{D}} + (k_{\text{cat}})_{\text{H}}(1/m_{27})_{\text{D}} + (k_{\text{cat}})_{\text{H}}(1/m_{37})_{\text{D}}$$

Multiply and divide by the microscopic rate constants for the protiated substrate:

$$(k_{\text{cat}}/K_{\text{M}})_{\text{H}}/(k_{\text{cat}}/K_{\text{M}})_{\text{D}} \\ = [(k_{\text{cat}}/K_{\text{M}})_{\text{H}}/m_{01\text{H}}](m_{01\text{H}}/m_{01\text{D}}) + [(k_{\text{cat}}/K_{\text{M}})_{\text{H}}/m_{03\text{H}}](m_{03\text{H}}/m_{03\text{D}}) \\ + [(k_{\text{cat}}/K_{\text{M}})_{\text{H}}/m_{05\text{H}}](m_{05\text{H}}/m_{05\text{D}}) + [(k_{\text{cat}}/K_{\text{M}})_{\text{H}}/m_{07\text{H}}](m_{07\text{H}}/m_{07\text{D}})$$

$$(k_{\text{cat}})_{\text{H}}/(k_{\text{cat}})_{\text{D}} = [(k_{\text{cat}})_{\text{H}}/m_{13\text{H}}](m_{13\text{H}}/m_{13\text{D}}) + [(k_{\text{cat}})_{\text{H}}/m_{15\text{H}}](m_{15\text{H}}/m_{15\text{D}}) \\ + [(k_{\text{cat}})_{\text{H}}/m_{17\text{H}}](m_{17\text{H}}/m_{17\text{D}}) + [(k_{\text{cat}})_{\text{H}}/m_{25\text{H}}](m_{25\text{H}}/m_{25\text{D}}) \\ + [(k_{\text{cat}})_{\text{H}}/m_{27\text{H}}](m_{27\text{H}}/m_{27\text{D}}) + [(k_{\text{cat}})_{\text{H}}/m_{37\text{H}}](m_{37\text{H}}/m_{37\text{D}})$$

Change to Northrop notation for the isotope effects:

$${}^D(k_{\text{cat}}/K_M) = [(k_{\text{cat}}/K_M)_H/m_{01H}]({}^Dm_{01}) + [(k_{\text{cat}}/K_M)_H/m_{03H}]({}^Dm_{03}) \\ + [(k_{\text{cat}}/K_M)_H/m_{05H}]({}^Dm_{05}) + [(k_{\text{cat}}/K_M)_H/m_{07H}]({}^Dm_{07})$$

$${}^D(k_{\text{cat}}) = [(k_{\text{cat}})_H/m_{13H}]({}^Dm_{13}) + [(k_{\text{cat}})_H/m_{15H}]({}^Dm_{15}) + [(k_{\text{cat}})_H/m_{17H}]({}^Dm_{17}) \\ + [(k_{\text{cat}})_H/m_{25H}]({}^Dm_{25}) + [(k_{\text{cat}})_H/m_{27H}]({}^Dm_{27}) + [(k_{\text{cat}})_H/m_{37H}]({}^Dm_{37})$$

Note that the ratios of observable to microscopic rate constants (in square brackets) determine the fractional degree to which the microscopic rate constant determines the rate with protiated substrate (i.e., $[(k_{\text{cat}}/K_M)_H/m_{01H}] = 1$ when $m_{01H} = (k_{\text{cat}}/K_M)_H$ and m_{01H} is fully rate-limiting; $[(k_{\text{cat}}/K_M)_H/m_{01H}] = 0$ when $m_{01H} \gg (k_{\text{cat}}/K_M)_H$ and m_{01H} has no effect on the rate). These quantities are weighting factors for the individual isotope effects:

$${}^D(k_{\text{cat}}/K_M) = [v_{01H}]({}^Dm_{01}) + [v_{03H}]({}^Dm_{03}) + [v_{05H}]({}^Dm_{05}) + [v_{07H}]({}^Dm_{07})$$

$${}^D(k_{\text{cat}}) = [w_{13H}]({}^Dm_{13}) + [w_{15H}]({}^Dm_{15}) + [w_{17H}]({}^Dm_{17}) + [w_{25H}]({}^Dm_{25}) \\ + [w_{27H}]({}^Dm_{27}) + [w_{37H}]({}^Dm_{37})$$

so that:

$$1 = [v_{01H}] + [v_{03H}] + [v_{05H}] + [v_{07H}]$$

$$1 = [w_{13H}] + [w_{15H}] + [w_{17H}] + [w_{25H}] + [w_{27H}] + [w_{37H}]$$

Note that if only one step, say the k_3 step, has a kinetic isotope effect and there are no equilibrium isotope effects, then:

$${}^D(k_{\text{cat}}/K_M) = [v_{03H}]({}^Dm_3) + (1 - [v_{03H}])$$

$${}^D(k_{\text{cat}}) = [w_{13H}]({}^Dm_3) + (1 - [w_{15H}])$$

(which slows the isotope-sensitive step but not the non-isotope-sensitive step), and rate-limiting most of all for the T case. In the example of Chart 5, the isotope-sensitive step is 50% rate-limiting in the H case ($k_H/k_{SH} = 0.50$; see Chart 5 for the definitions of these rate constants), 83% rate-limiting in the D case ($k_D/k_{SD} = 0.83$), and 91% rate-limiting in the T case ($k_T/k_{ST} = 0.91$). By aggregation of the D and T rate constants in one ratio, one selects the isotope effect that is as close as possible to the isotope effect on the isotope-sensitive step and thus most likely to obey the Swain–Schaad relation. By aggregation of H and T rate constants in the comparison

Chart 5. Klinman's approach to kinetic complexity¹⁸

Consider a multistep reaction with a single isotope-sensitive step. Let the observable isotopic rate constants be denoted k_H , k_D , and k_T and the microscopic rate constants be denoted k_N (*Not* isotope sensitive) and k_{SH} , k_{SD} , and k_{ST} (isotope *Sensitive*). Let $k_{SH}/k_{SD} = 5$ and $k_{SH}/k_{ST} = 10.2$, so that $k_{SD}/k_{ST} = 1.9$ according to the Swain–Schaad rule (Chart 3). Assume that the isotope-sensitive step is 50% rate-limiting for the H case (i.e., $k_H/k_{SH} = 0.5$), so that (from the expressions in Chart 4).

$$k_H/k_D = 0.5 + 0.5(5) = 3$$

$$k_H/k_T = 0.5 + 0.5(10.2) = 5.6$$

and thus

$$k_D/k_T = 1.9$$

The following calculations can be made on the basis of the traditional comparison of k_H/k_D with k_H/k_T or the more effective comparison of k_D/k_T with k_H/k_T .

Calculated quantity	Result and remarks
<i>Comparison of k_H/k_D with k_H/k_T</i>	
$[\ln(k_H/k_T)]/[\ln(k_H/k_D)]$	1.56 instead of the expected 1.44
$(k_H/k_D)^{1.44} = (k_H/k_T)_{\text{predicted}}$	4.9 instead of the observed 5.6
$(k_H/k_T)^{[1/1.44]} = (k_H/k_D)_{\text{predicted}}$	3.3 instead of the observed 3.0
<i>Comparison of k_D/k_T with k_H/k_T</i>	
$[\ln(k_H/k_T)]/[\ln(k_D/k_T)]$	2.68 instead of the expected 3.26
$(k_D/k_T)^{3.26} = (k_H/k_T)_{\text{predicted}}$	8.1 instead of the observed 5.6
$(k_H/k_T)^{[1/3.26]} = (k_D/k_T)_{\text{predicted}}$	1.7 instead of the observed 1.9

ratio, one achieves the greatest distortion possible by combining the case where the isotope-sensitive step is most nearly rate-limiting with the case where it is least rate-limiting. Now the failures of the expectations for lack of kinetic complexity are considerably more dramatic, the calculations differing from the observations by as much as 45%. The most powerful of the tests is the prediction of the H/T effect from the D/T effect, and the signature of kinetic complexity is that *the H/T effect calculated from the D/T effect must be larger than the observed H/T effect if kinetic complexity is present.*

This stratagem is still more impressive when the possibility of quantum tunneling is introduced. Cha, Murray, and Klinman followed calculations performed by

W. H. Saunders,¹⁹ in which he noted that the tunneling probabilities for the isotopic species should be in the order H highest, D less, and T least. Again the aggregation of D and T measurements produces an isotope effect with the least possible contribution of tunneling and thus most likely to follow the semiclassical Swain–Schaad formula. By comparing predictions with the H/T isotope effect, one dramatizes any contribution of tunneling by combining the isotopic species with the greatest tunneling propensity to that with the smallest tunneling propensity. Most pleasing of all is the fact that *the H/T effect calculated from the D/T effect must be smaller than the observed H/T effect if tunneling is present.*

A neat trichotomy is thus established. Prediction of the H/T effect from the D/T effect must result in a value that is either larger than the observed effect, indicating kinetic complexity, or smaller than the observed effect, indicating quantum tunneling, or equal to the observed effect, indicating a single rate-limiting step with no tunneling.

Experiments with the oxidation of benzyl alcohol by NAD^+ , catalyzed by yeast alcohol dehydrogenase, yielded $(k_{\text{cat}}/K_{\text{M}})_{\text{D}}/(k_{\text{cat}}/K_{\text{M}})_{\text{T}} = 1.72 - 1.76$ (standard deviations about 0.03–0.06). These experiments involved multiple labeling so an exact interpretation must take into account Huskey's rules for this situation (Chart 7 below). Application of the Swain–Schaad relationship predicts an H/T effect of 5.9–6.3 (propagated errors 0.2–0.6). The observed H/T effects are 7.0–7.2 (standard deviations about 0.1), providing a very strong indication of the importance of tunneling in this reaction.

Similar determinations of the α -secondary isotope effects were also made. The D/T effects were 1.03–1.04, leading to predicted H/T effects of 1.10–1.14. The observed H/T effects were 1.33–1.37, confirming (a) that the motion of the non-transferring hydrogen is coupled into the reaction coordinate, and (b) that tunneling is occurring with the non-transferring hydrogen as well as with the transferring hydrogen, as would be expected if the motions of both are components of the reaction coordinate.

The effective Swain–Schaad exponent required to account for the primary isotope effects is given by $[\ln(k_{\text{H}}/k_{\text{T}})]/[\ln(k_{\text{D}}/k_{\text{T}})] = [\ln(7.1)]/[\ln(1.73)] = 3.58$, which is larger than the canonical 3.26 but not impressively so. The secondary isotope effects tell a different story, where the required value is $[\ln(1.35)]/[\ln(1.03)] = 10.2$. This enormous departure from the standard 3.26 is a tremendously effective indicator of both coupled motion and tunneling. The phenomenon appears to be general that when secondary isotope effects result from tunneling with motion at the secondary center coupled into the reaction coordinate, the Swain–Schaad failures are far stronger than in the primary isotope effects for the same reaction. One factor has to do with the experimental design and will be discussed below. The other factor is inherent in the data. To the extent that the D/T isotope effect involves little tunneling by either nucleus, then the canonical Swain–Schaad prediction should give the semiclassical part of the H/T isotope effect. This H/T effect is about 6.0 at the primary center; the observed value of 7.1 then suggests that an approximate tunnel correction of $(7.1)/6 = 1.2$ is required for

the primary isotope effect. For the secondary center, the corresponding ratio is $1.35/1.12 = 1.2$, showing that a tunneling correction of about 20% is required at both positions. However, for the secondary effect, the effect of tunneling is to increase a 12% isotope effect to a 35% isotope effect, or a factor of 3. Clearly tunneling contributes to the magnitude of the secondary isotope effect much more than it does to the magnitude of the primary isotope effect.

Finally the temperature dependence of the primary isotope effects was determined. Here the traditional expectations of Chart 3 were fully met: the results translate into $A_{\text{H}}/A_{\text{D}} = 1.1 \pm 0.1$, $E_{\text{aD}} - E_{\text{aH}} = 0.8$ kcal/mol. Thus the amount of tunneling present, adequate to produce the observed exaltation of secondary isotope effects, violations of the Swain–Schaad relationship, and violations of the Rule of the Geometric Mean in the neighborhood of room temperature, does not lead to anomalies in either the ratio of isotopic pre-exponential factors nor the isotopic activation energy difference over the temperature range studied (approximately 0–40 °C). As will be seen later, the temperature dependence of isotope effects for reactions that include tunneling is in general a complex, unresolved issue.

2 Experimental phenomenology of quantum tunneling in enzyme-catalyzed reactions

Table 2 contains, in reverse chronological order, detailed information about the results of 15 experimental studies of tunneling in enzymic reactions, conducted in the last five years. These examples will be used to explore the range of evidence, reaction types, enzymes, and concepts currently under study. Other progress made during the preceding decade will be referred to in the discussion of these examples and has been treated in a number of reviews.^{35–50}

HYDRIDE-TRANSFER REACTIONS INVOLVING NICOTINAMIDE COFACTORS

Dihydrofolate reductases

Kohen, Benkovic and their coworkers²⁰ have suggested on the basis of the data summarized under entry 1 of Table 2 that hydride transfer from NADPH to the imine center of 7,8-dihydrofolate (see Fig. 5 for a schematic picture of the reaction), catalyzed by dihydrofolate reductase (DHFR) of *Escherichia coli*, occurs with quantum tunneling of the hydrogen nucleus. The magnitudes of the isotope effects are smaller than the semiclassical limits and not especially large on any scale (the H/T value around 4.8 while the semiclassical limit is around 16–17). The observation that led the authors to favor a tunneling mechanism is the temperature independence of the isotope effects: when the intrinsic isotope effects (i.e., those for the hydride-transfer step itself) are calculated by Northrop's method (Chart 6), they remain constant over the accessible temperature range, from 5 to 45 °C. Fitting the isotope effects to an Arrhenius dependence (Chart 1) yields

Table 2 Recent experimental studies of quantum tunneling in enzyme action

Entry number; reference	Enzyme; reaction catalyzed	Results
(1) 20	Dihydrofolate reductase from <i>E. coli</i> ; hydride transfer from NADPH to 7,8-DHF	Competitive isotope effects H/T (ca. 4.8) and D/T (ca. 1.7) on k_{cat}/K_M , 5–45 °C. Conversion to intrinsic H/T, D/T, H/D. Intrinsic primary isotope effects are temperature-independent (A-ratio = 7.4 ± 4 [H/T], 4.0 ± 1.5 [H/D], 1.8 ± 0.3 [D/T]; E-difference = 0.1 ± 0.3 [H/T], 0.1 ± 0.2 [H/D], 0.03 ± 0.09 [D/T] kcal/mol). Intrinsic secondary isotope effects are 1.194 ± 0.007 [H/T] and 1.052 ± 0.007 [D/T] with Swain–Schaad exponent 3.5 ± 0.5 (H/D 1.13). The activation energy for k_{cat}/K_M is ca. 3 kcal/mol.
(2) 21	Thymidylate synthase from <i>E. coli</i> ; hydride transfer from H ₄ folate to form the methyl group of dTMP	Competitive isotope effects H/T and D/T on k_{cat}/K_M , 5–45 °C. Conversion to intrinsic H/T, D/T isotope effects, which are temperature independent (A-ratio 6.8 ± 2.8 [H/T], 1.9 [D/T], E-difference = 0.02 ± 0.25 [H/T], -0.04 ± 0.08 [D/T] kcal/mol). The activation energy for k_{cat} (same rate-determining step as k_{cat}/K_M) is 4.0 ± 0.1 kcal/mol.
(3) 22	Peptidylglycine α -hydroxylating monooxygenase, WT and Y318F mutant; H-atom transfer to Cu–O from benzoyl-glycine	Primary H/D isotope effects on k_{cat} : WT (Y318F) 1.6(2.0); k_{cat}/K_S NA (8.3); k_{cat}/K_O 3.2 (8.1); K_{10} 0.64 (3.2). Isotope effects on k_{cat}/K_S WT (Y318F) Primary H/D 3.9 (4.5), H/T 9.7 (11.2), secondary H/T 1.09 (1.11). Intrinsic H/D WT (Y318F) primary 10.7 (9.4); secondary 1.21 (1.17). Primary 18-O isotope effects: WT (Y318F) 1.0173 (1.0169) [H-substrate]; 1.0212 (not measured) [D-substrate]; intrinsic 1.023.
(4) 23	Dihydrofolate reductase from <i>Thermotoga maritima</i> ; hydride transfer from NADPH to 7,8-DHF	Primary H/D isotope effects for the single-turnover rate constant, 6–65 °C (range 6.7–3.7). The temperature dependence of the isotope effect shows a break at 25 °C; below, $A_H/A_D = 0.002 \pm 0.001$; above $A_H/A_D = 1.56 \pm 0.47$. Below, $E_{\text{aH}} = 49.9 \pm 1.7$ kJ/mol; $E_{\text{aD}} = 69.2 \pm 3.7$ kJ/mol; above, $E_{\text{aH}} = 53.5 \pm 0.4$ kJ/mol; $E_{\text{aD}} = 56.0 \pm 0.8$ kJ/mol.

(continued on next page)

Table 2 (continued)

Entry number; reference	Enzyme; reaction catalyzed	Results
(5a) 24	Morphinone reductase from <i>Pseudomonas putida</i> : (1) hydride transfer from NADH to enzyme-bound FMN; (2) hydride transfer to 2-cyclohexenone from FMNH ₂ .	(1) Primary H/D for k_{cat} at 5–36 °C (IE 3.9 ± 0.1 at 25 °C). Linear T-dependences with $A_{\text{H}}/A_{\text{D}} = 0.126 \pm 0.005$, $\Delta H_{\text{H}}^{\ddagger} = 35.3 \pm 0.5$; $\Delta H_{\text{H}}^{\ddagger} = 43.5 \pm 0.8$ kJ/mol. Solvent isotope effect HOH/DOD = 1.05 ± 0.02 . (2) Linear T-dependences for k_{cat} with primary H/D labeling. $A_{\text{H}}/A_{\text{D}} = 3.7 \pm 2.1$, $\Delta H_{\text{H}}^{\ddagger} = 17.6 \pm 2.9$; $\Delta H_{\text{D}}^{\ddagger} = 17.1 \pm 0.9$ kJ/mol. HOH/DOD $A_{\text{H}}/A_{\text{D}} = 3.1 \pm 2.0$, $\Delta H_{\text{HOH}}^{\ddagger} = 17.6 \pm 2.9$; $\Delta H_{\text{DOD}}^{\ddagger} = 16.7 \pm 0.7$ kJ/mol. Strict adherence to the Rule of the Geometric Mean for H and D cofactors in HOH and DOD.
(5b) 24	Pentaerythritol tetranitrate (PETN) reductase, hydride transfer from NADH to FMN.	For B, with NADPH, primary H/D is linear with $A_{\text{H}}/A_{\text{D}} = 4.1 \pm 0.3$, $\Delta H_{\text{H}}^{\ddagger} = 36.4 \pm 0.9$; $\Delta H_{\text{D}}^{\ddagger} = 36.6 \pm 0.9$ kJ/mol. For T-independent IE, “gating”, i.e., tunneling from ground states. For T-dependent IE, “Franck-Condon” i.e., tunneling between various vibrational states, all on the Kuznetsov–Ulstrup model. See their alternative in footnote 3, p. 43981.
(6) 25	Glucose oxidase modified with differing levels of glycolation or pegolation; hydride transfer from C1 of 2-deoxyglucose to FAD	Competitive isotope effects on $k_{\text{cat}}/K_{\text{M}}$ H/D = 2.22–2.26 (33 °C) for MW = 155–320. $A_{\text{D}}/A_{\text{T}} = 0.55$ –1.04 (intrinsic) for various modifications. Values of $A_{\text{D}}/A_{\text{T}}$ show positive slope vs. ΔH^{\ddagger} ; increased as the deviation from the mean melting temperature became negative.
(7) 26	Peptidylglycine α -hydroxylating monooxygenase, H-atom transfer to Cu–O from benzoyl-glycine	Competitive H/T primary IE, 5–45 °C. Convert primary to intrinsic effects which yield $A_{\text{H}}/A_{\text{D}} = 5.9 \pm 3.2$, $\Delta E_{\text{a}} = 0.37 \pm 0.33$. Estimate $k(\text{chem})$ at 870 s^{-1} (37 °C) and 180 s^{-1} (15 °C) to obtain E_{a} ca. 13 kcal/mol for the chemical step.

Table 2 (continued)

Entry number; reference	Enzyme; reaction catalyzed	Results
(8) 27	Horse liver alcohol dehydrogenase and the F93W mutant, hydride transfer from benzyl alcohol to NAD in MeOH/water.	From ± 3 to -50 °C, 50% MeOH, H/DIE on k_{cat} . Values are 1.53 ± 0.09 and 1.52 ± 0.08 at extremes but as low as 1.03 ± 0.09 at -42 °C. For k_{cat}/K_M 3.2 ± 0.5 and 4.3 ± 0.5 at extremes but 2.4 ± 0.2 at -20 °C. Primary H/T IE decrease monotonically 9.0–2.2; D/T 2.2–0.99. Secondary H/T 1.32–1.12 then 1.25; D/T roughly constant at 1.0–1.1. Primary Swain–Schaad exponents 2.2–2.9; secondary 1.3–2.9. F93W mutant $+3$ to -35 °C; H/D on k_{cat} 1.12–1.5 irregularly; for k_{cat}/K_M H/D IE increases at lower temperature from 3.5–7.5. Primary H/T irregular 8.6–13.0; D/T about 2. Secondary H/T constant at 1.4; D/T roughly constant at 1.0–1.1.
(9) 28	Horse liver alcohol dehydrogenase, F93W mutant with I224 also mutated to G,A,V,L.; hydride transfer from benzyl alcohol to NAD	Competitive H/D/T IE for 1 single, 4 double mutants. Primary H/T: 7.4–7.8 for all; secondary H/T: 1.29–1.31 for all; Primary D/T 1.81–1.86 for all; secondary D/T 1.03–1.05 for all.
(10) 29	Heterotetrameric sarcosine oxidase of <i>Arthrobacter sp.</i> 1-IN, proton transfer from adduct of FAD with sarcosine-(CH ₃) and sarcosine-(CD ₃)	Swain–Schaad exponents: primary 3.3–3.4 for all, secondary 6.2, 8.6, 9.1; 6.9, 5.9. For 10 mutants this exponent is linear in $\ln(k_{\text{cat}}/K_M)$. k_{cat} for the partial reaction, primary H/D IE 7.3 constant over 5–37 °C. $A_H/A_D = 4.5 \pm 0.5$, $\Delta H_D^\ddagger = 39.4 \pm 0.9$; $\Delta H_H^\ddagger = 39.4 \pm 0.9$; $\Delta H_D^\ddagger = 40.0 \pm 1.2$ kJ/mol.

(continued on next page)

Table 2 (*continued*)

Entry number; reference	Enzyme; reaction catalyzed	Results
(11) 30	Human 15-lipoxygenase and soybean LO-1; H/D-atom transfer from per-H vs. per-D linoleic acid C11 to Fe–O	Competitive IE temperature-independent >30 °C, 47 ± 7 (15-HLO), 48 ± 5 (SLO-1). Below 30 °C, IE decreases at 5 μM S, but remains constant or increases at 100 μM S to ca. 10–20.
(12) 31	Soybean lipoxygenase-1, WT and L546A mutant, H-atom transfer from H, D labeled linoleic acid C11 to Fe–O	Solvent IE 2 at high temperature, disappears at low temperature. Recemic 11-(R,S)- ² H-linoleic acid and 11-S- ² H-linoleic acid (the 11-S hydrogen is transferred) were used to obtain primary and secondary isotope effects: the intrinsic primary H/D effect is 76 ± 8 for the WT, 78 ± 8 for the L546A mutant; the intrinsic secondary H/D effect is 1.1 ± 0.1 for the WT, 1.2 ± 0.1 for the L546A mutant. Small values of ΔH^\ddagger (kcal/mol) were observed for k_{cat} for all isotopic forms and both mutants: 1.3 ± 0.2 (WT, H), 0.7 ± 0.2 (WT, 11-S-D), 2.4 ± 0.2 (WT, 11, 11-D ₂), 2.4 ± 0.4 (L546A, H) with $A_{\text{H}}/A_{\text{D}} = 110 \pm 70$ (WT, H vs. 11-S-D) 10 ± 7 (WT, H vs. 11, 11-D ₂).
(13) 32	NAD-malic enzyme, hydride transfer from C2 of malate to NAD or APAD, concomitant with decarboxylation.	Competitive IE: Mn, NAD, Primary H/T 3.56 ± 0.08 , D/T 1.72 ± 0.03 . Application of Swain–Schaad predicts H/T 5.8 ± 0.3 . Mn APAD H/T 4.84 ± 0.04 , D/T 1.63 ± 0.04 . Secondary T/H 1.025(16) Mg/NAD, 1.028(18) Mn/NAD, 0.874(18) Mn/APAD, 1.006(1) Cd/NAD. D/T 1.018(17) Mg/NAD, 1.019(18) Mn/NAD, 0.920(18) Mn/APAD, 1.004(2), Cd/NAD.

Table 2 (continued)

Entry number; reference	Enzyme; reaction catalyzed	Results
(14) 33	Alcohol dehydrogenase of <i>Bacillus stearothermophilus</i> ; hydride transfer from PhCH ₂ OH and stereospecifically labeled PhCDHOH to NAD ⁺	Competitive primary and secondary IE, H/D/T 5–65 °C. Primary H/T IE 5.5 at high temperature, rising to 7 at low temperature; D/T 1.62–1.75; Swain–Schaad exponent ca. 3.5 throughout. Secondary H/T IE 1.23 to 1.33; D/T 1.01–1.06; Swain–Schaad exponent 11 (high temperature) to 5 (low temperature). H/T, D/T A-ratio 0.26 ± 0.23, 0.26 ± 0.14 (5–30 °C), 4.3 ± 0.6, 1.73 ± 0.26 (30–65 °C). IE on <i>k</i> _{cat} primary H/D, 5–30 °C; ΔH^\ddagger 23.6 ± 0.6 (H), 31.4 ± 1.7(D); $\Delta\Delta H^\ddagger$ 7.8 ± 1.8; A-ratio 10 ⁻⁵ . 30–65 °C: ΔH^\ddagger 14.6 ± 0.3 (H), 15.1 ± 0.5(D); $\Delta\Delta H^\ddagger$ 0.5 ± 0.6; A-ratio 2.2 ± 1.1; H/D 2.5 at high temperature, up to 8 at low temperature.
(15) 34	Methylamine dehydrogenase of <i>Methylophilus methylotrophus</i> , proton transfer from the methylamine adduct of tryptophan tryptophylquinone (TTQ)	CH ₃ -amine vs. CD ₃ -amine, transient kinetics studies of H-transfer step, H/D IE 5–40 °C, <i>A</i> _H / <i>A</i> _D = 16.8 ± 0.5, ΔH^\ddagger 42.2 ± 1.1 (H), 43.2 ± 1.8 (D) kJ/mol, rate constant unchanged.

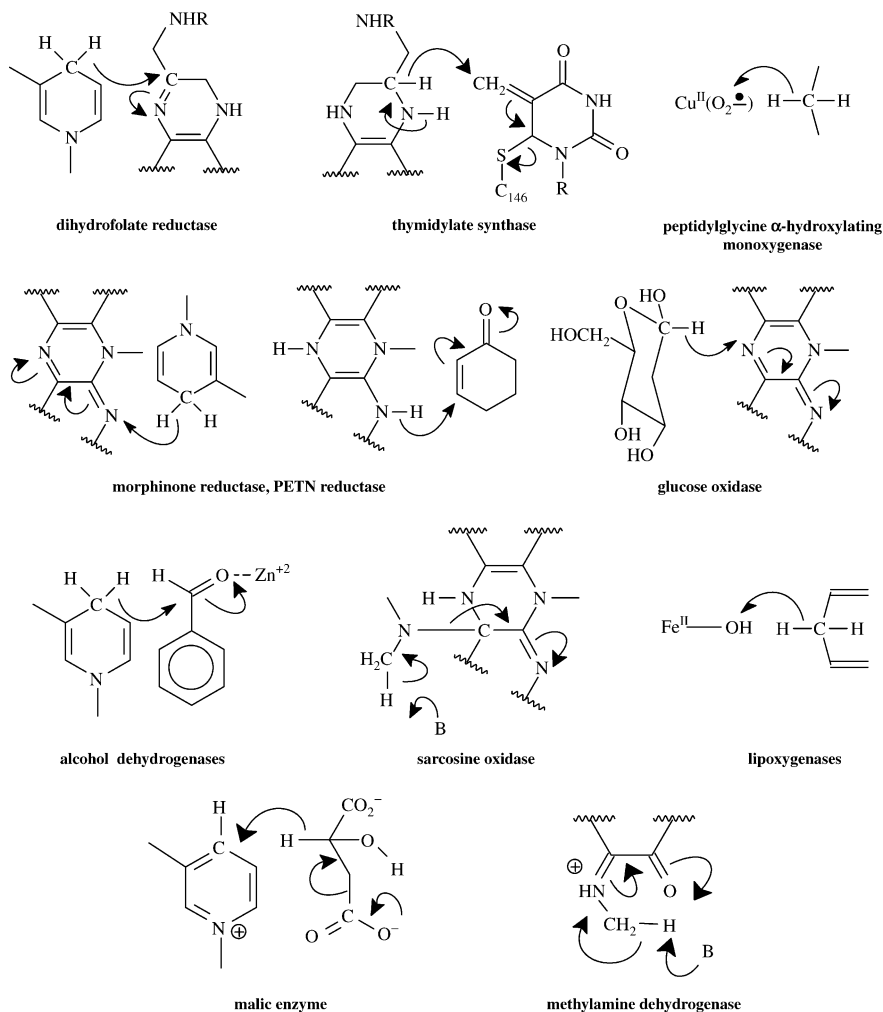


Fig. 5 Schematic reaction diagrams for the enzymic systems of Table 2.

$A_H/A_T = 7.4$ and $A_D/A_T = 1.8$ and isotopic activation energy differences that are within the experimental error of zero. The values of the two A-ratios correspond to a Swain-Schaad exponent of 3.4, not much different from the semiclassical expectation of 3.3. The α -secondary isotope effects are 1.19 (H/T), 1.13 (H/D), and 1.05 (D/T), which are exactly at the limiting semiclassical value of the equilibrium isotope effect. The secondary isotope effects generate a Swain-Schaad exponent of 3.5, again close to the semiclassical expectation. At the same time that the isotope effects are temperature-independent, the kinetic parameter k_{cat}/K_M shows (for any of the isotopic species) an activation energy of around 3 kcal/mol.

Chart 6. Northrop's method for intrinsic isotope effects

From Chart 4, the observed isotope effect (H/D) for a multistep reaction with a single isotope-sensitive step will be given by:

$${}^Dk = [w_H]({}^Dm) + (1 - [w_H])$$

where Dm is the intrinsic isotope effect (defined as the isotope effect on the single isotope-sensitive step), and w_H (a weighting factor) is the fractional degree to which the isotope-sensitive step limits the rate of reaction of the H-labeled reactant ($w_H = k_H/m_H$). A similar equation applies to the H/T isotope effect:

$${}^Tk = [w_H]({}^Tm) + (1 - [w_H])$$

The weighting factor can be eliminated to yield:

$$({}^Tk - 1)/({}^Tm - 1) = ({}^Dk - 1)/({}^Dm - 1)$$

and if the Swain–Schaad relationship holds, $({}^Tm) = ({}^Dm)^{1.44}$ so that

$$({}^Tk - 1)/([{}^Dm]^{1.44} - 1) = ({}^Dk - 1)/({}^Dm - 1)$$

where Dm is the only unknown quantity. The equation cannot be solved analytically; it is subject to iterative solution and will give reliable values if the determination of Tk and Dk is very precise and Dk falls within a limited range of values around 2⁷⁷. For such cases, the intrinsic isotope effect can be obtained by iterative solution of the equation, for which Kohen and his coworkers have provided a program at <http://cricket.chem.uiowa.edu/~kohen>.

COMMITMENTS

The first equation above is frequently written by enzymologists as:

$${}^Dk = [{}^Dm + C]/[1 + C]$$

where $C = (1 - w_H)/w_H$. C is called the “commitment to catalysis” (Northrop, D.B. (1991). In *Enzyme Mechanism from Isotope Effects*, Cook, P.F. (ed.), pp. 181–202. CRC Press, Boca Raton, FL). Since w_H varies from zero when the isotope-sensitive step is very fast and has no effect on the observed rate constant to unity when the isotope-sensitive rate constant is equal to the observed rate constant and completely limits the rate, C will vary from infinity in the former case to zero in the latter case. If binding of substrate to the enzyme precedes the single isotope-sensitive step, and if every molecule that binds continues rapidly to product then binding is the rate-limiting step, C is infinite, and ${}^Dk = 1$ since the isotope-sensitive step is much faster than binding. The enzyme is said to exhibit “a large commitment”. If binding is rapid and reversible, and no other step is as slow as the isotope-sensitive step, then C is zero and ${}^Dk = {}^Dm$. The enzyme is said to exhibit “no commitment”.

Thus the primary and secondary isotope effects are all within the semiclassical limits and their relationship is in full accord with the semiclassical Swain–Schaad relationship. There is no indication from the magnitudes of the secondary isotope effects in particular of any coupling between motion at the secondary center and the reaction-coordinate for hydride transfer. Thus the sole evidence taken to indicate tunneling is the rigorous temperature-independence of the primary isotope effects.

One very primitive model that might explain such behavior is one in which the enzyme–substrate-cofactor complex fluctuates rapidly and reversibly until it encounters a (probably rare) state such that tunneling from a reactant-like energy well into a product-like energy well can occur between the lowest vibrational states for the two energy wells. Then the rate constant k should be given by $k = KP$ where K is the equilibrium constant for conversion of the reactant state to the sub-state prepared for efficient tunneling, and P is the probability that tunneling will occur between the reactant-like and product-like sub-states. The equilibrium constant K will depend on temperature, reflecting the free-energy cost of conversion to the tunneling sub-state but K will be the same for all isotopic species if, as expected, the force constants at the isotopic centers are the same in the reactant state and the tunneling sub-state. The probability P will be temperature independent because it is essentially a property of the nuclear wave-functions in the two sub-states, but it will be different for the three isotopic species, largest for that labeled with H, which has the most dispersed nuclear wave function, and smallest for that labeled with T, which has the least dispersed wave function. Thus for any isotopic species with label L (= H, D, or T), $k_L = KP_L$. Each of the isotopic rate constants will have the temperature dependence of K , but the isotope effects will be temperature-independent: $k_H/k_T = P_H/P_T$; $k_H/k_D = P_H/P_D$; $k_D/k_T = P_D/P_T$. This kind of model, customarily treated within a much more sophisticated formalism, is the essence of the concept of *vibrationally assisted*, *vibrationally enhanced*, or *environmentally modulated tunneling*. The quantitative evaluation of such models will be undertaken in a subsequent part of our treatment.

A related experimental study by Maglia and Allemann²³ (entry 4 of Table 2) of the DHFR from *Thermotoga maritima* gave a different picture. The single-turnover rate constants were measured with isotopically labeled (H, D) NADPH from 6 to 65 °C. The observed isotope effect (H/D) is 6.7 at the lowest temperature, around 4 at room temperature and 3.7 at the highest temperature. No attempt seems to have been made to deal with possible kinetic complexity and indeed the temperature dependences have an unusual form. At around 25 °C, the Arrhenius plot for k_H departs from linearity such that the observed rate constants at lower temperatures are larger than those extrapolated from higher temperatures; the plot for k_D departs from linearity such that the observed rate constants at lower temperatures are smaller than those extrapolated from higher temperatures. The resulting temperature dependence of the ratio k_H/k_D then shows a break at 25 °C, with the isotope effects below this temperature being highly dependent on temperature and those above this

temperature being much less dependent on temperature, generating the Arrhenius parameters shown in Table 2. A full interpretation of these results requires correction for or at least a test for possible kinetic complexity.

Thymidylate synthase

Agrawal et al.²¹ (entry 2 of Table 2) examined the thymidylate-synthase (*E. coli*) catalyzed hydride-transfer reaction shown schematically in Fig. 5, with correction of the observed data to intrinsic isotope effects. As with *E. coli* DHFR, the isotope effects themselves are of modest size, k_H/k_T being around 7, and thus well below the semiclassical limit of about 17. The intrinsic isotope effects, also similar to the DHFR case, are rigorously temperature independent, while the rate constants themselves (k_{cat}/K_M) are temperature dependent. A model similar to that above was employed in explanation: search for an effective tunneling configuration, that is isotope-independent but temperature-dependent over the temperature range studied, precedes a tunneling event that carries the system from a reactant-like state to a product-like state without vibrational excitation. The tunneling event is isotope-dependent but temperature independent. Also, as before, far more sophisticated theoretical descriptions can be used. The description and evaluation of these descriptions will be undertaken in later parts of our treatment.

Morphinone reductase and pentaerythritoltetranitrate reductase

The report of Basran et al.²⁴ (entry 5 of Table 2) contains two studies involving hydride transfer with nicotinamide cofactors. In morphinone-reductase catalyzed reduction by NADH of the flavin cofactor FMN (schematic mechanism in Fig. 5), the primary isotope effects are modest (around 4 for H/D), but exhibit a small value of A_H/A_D (0.13) and an exalted isotopic difference in energies of activation (8.2 kJ/mol) that alone would have generated an isotope effect around 30. The enthalpies of activation are in the range of 35–45 kJ/mol. This is behavior typical of “Bell tunneling” as discussed above. It can also be reproduced by more complex models, as will be discussed in later parts of this review.

The similar reaction of NADH with FMN in the active site of pentaerythritol-tetranitrate reductase, also with overall isotope effects around 4, shows A_H/A_D of 4 and no isotopic difference in the enthalpies of activation, which are about 36 kJ/mol in magnitude. These findings were taken to be consistent with enzyme fluctuations, occasioning the isotope-independent energy cost, to a tunneling configuration such that react-to-product tunneling occurs from the vibrational ground state.

Alcohol dehydrogenases

Two studies in Table 2 (entries 8 and 9) proceed from previous reports^{51,52} on the question of tunneling in the action of horse-liver alcohol dehydrogenase.

Initial studies of the wild-type dehydrogenase had indicated the product-release step for oxidation of benzyl alcohol to benzaldehyde to be partially rate-limiting, so the situation was expected to be complicated. Bahnson et al.⁵¹ found modest primary isotope effects of 7.1 (H/T) and 1.9 (D/T), corresponding to a Swain–Schaad exponent of 3.1, in agreement with the semiclassical value of 3.26. The α -secondary isotope effects (label in the alcohol) were 1.335 ± 0.003 (H/T) and 1.073 ± 0.008 (D/T); here the Swain–Schaad exponent is 4.1 ± 0.4 , probably exceeding the semiclassical value and raising the question of a possible role for tunneling (but see Kohen et al.⁶¹). If the tunneling phenomenon were being hidden by the partially rate-limiting product release, the authors reasoned, an appropriate mutation in the active site might make the product-release step more rapid and the hydride-transfer step more nearly rate-limiting. The result would be to “unmask” the contribution of tunneling. The most effective mutation in this regard was the L57F mutant, designed to decrease the size of the alcohol binding-site and increase the rate of product release. This mutant showed very little change from the wild-type enzyme in the kinetic parameters, in the primary isotope effects, or in the Swain–Schaad exponent for the primary effects. But the secondary isotope effects became 1.318 ± 0.007 (H/T) and 1.033 ± 0.004 (D/T) with a Swain–Schaad exponent of 8.5 ± 0.4 , a clear indication of tunneling with coupled motion. As has already been seen, indications of tunneling are much more readily detected in the smaller secondary effects than in the larger primary effects. Even so, these data dramatize the vital importance of (a) obtaining extremely precise data and (b) correctly propagating the error estimates for the isotope effects into an error estimate for the Swain–Schaad exponent.

Bahnson et al.⁵² extended the series of mutations to include ones in which reductions occurred in the second-order rate constant $k_{\text{cat}}/K_{\text{M}}$ by as much as a factor of 100. No substantial changes were observed in the primary isotope effects or their Swain–Schaad exponent. However, the precisely measured secondary isotope effects changed systematically as the rate constant decreased, such that the Swain–Schaad exponent decreased monotonically with decreasing $k_{\text{cat}}/K_{\text{M}}$ from an exponent of 8.5 for the L57F mutant (reactivity equivalent to the wild-type enzyme) to an exponent of 3.3 for the V203G mutant, slower by 100-fold.

Chin and Klinman²⁸ (entry 9, Table 2) extended this work in a highly informative direction. Bahnson et al.⁵² had focused on mutation of active-site residues, and determined crystal structures for a mutant exhibiting an emphatic sign of tunneling (F93W with a Swain–Schaad exponent for the secondary isotope effects of 6.1) and for a mutant showing a more modest indication of tunneling (V203A with an exponent of 4.9). In the F93W structure, the distance over which hydride transfer must occur (i.e., the distance from C4 of the cofactor nicotinamide ring to C1 of the trifluoroethanol surrogate for substrate) is 3.2 Å; the side chain of V203 buttresses the nicotinamide ring at this position. Mutation of V203 to Ala results in an increase of the hydride-transfer distance to 4 Å, providing a straightforward structural rationale for decreased tunneling in the mutants that place residues at position 203 with smaller side-chains than that of Val. Chin and Klinman now produced double mutants of the F93W mutant, a “high-tunneling” enzyme, in which side-chain

structures were altered at a residue (I224) that is 20 Å from the active site and makes contact with the adenine ring of the cofactor. Mutation of I224 to Ala, Leu, Gly, and Val resulted in no change in kinetic parameters, primary isotope effects, or the Swain–Schaad exponent for the primary effects. Mutation to Ala and Gly (smaller side chains than Ile) also left unchanged the secondary isotope effects and their Swain–Schaad exponents (6.9 for Ala and 5.9 for Gly vs. 6.2 for the Ile enzyme). Mutation to Leu and Val, with side chains as large as or larger than that of Ile, produced Swain–Schaad exponents more emphatically signalling a role for tunneling (8.6 for Leu and 9.1 for Val). All of the newly studied mutants gave results that fell on the monotonic curve of Bahnson et al.,⁵² relating larger $k_{\text{cat}}/K_{\text{M}}$ to a larger Swain–Schaad exponent for the secondary isotope effects: the plot is shown in Fig. 6. Among the significant contributions of this publication are:

(a) It confirms that structural features of the enzyme are required for the occurrence of tunneling in the hydride-transfer reaction the enzyme catalyzes.

(b) It demonstrates that structural features both within the active site and remote from the active site can affect the degree of tunneling.

(c) It demonstrates that catalytic activity correlates positively with the degree of tunneling, suggesting that induction of tunneling by the enzyme is a mechanism of catalytic acceleration. A plot similar to that for Fig. 6, leading to the same conclusion, can also be constructed for formate dehydrogenase with the catalytic activity being varied by the use of structurally altered cofactors.⁵³

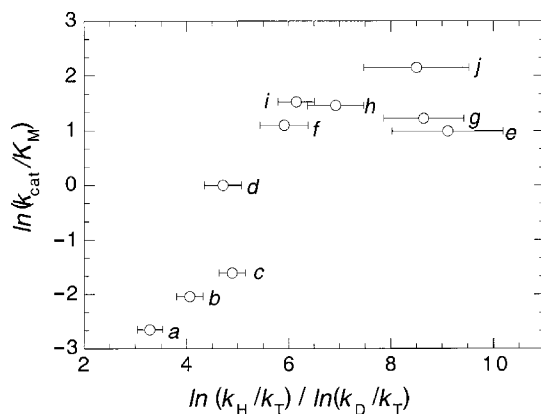


Fig. 6 Illustration from Chin and Klinman²⁸. Increased catalytic activity of horse-liver alcohol dehydrogenase in the oxidation of benzyl alcohol to benzaldehyde by NAD^+ , measured by $k_{\text{cat}}/K_{\text{M}}$ (ordinate), correlates with the Swain–Schaad exponent for the α -secondary isotope effect (abscissa), for which values above about four are indicators of tunneling. This is a direct test of the hypothesis that tunneling in the action of this enzyme contributes to catalysis. As the rate increases by over two orders of magnitude and then levels off, the anomalous Swain–Schaad exponents also increase and then level off. Reproduced from Ref. 28 with the permission of the American Chemical Society.

Tsai and Klinman²⁷ (entry 8 of Table 2) have obtained temperature dependences of the kinetic isotope effects for horse-liver alcohol dehydrogenase, most significantly for the F93W mutant, where the hydride-transfer step is fully rate-limiting for k_{cat}/K_M , and the observed isotope effects on this rate constant are the intrinsic isotope effects for hydride transfer. The measurements were carried out from -35 to $+3$ °C by using 40% methanol in water as the solvent. For non-competitive determination of the H-rate constants and the D-rate constants, the primary (H/D) isotope effects fell from 7.5 at -35 °C to 3.5 at $+3$ °C. An Arrhenius treatment showed a linear dependence and gave $A_H/A_D = 0.015 \pm 0.013$, with E_a values of 11.2 (H) and 12.7 (D) kcal/mol. This is a strong enough indication of the presence of tunneling but the detailed situation is less than completely clear. Competitive measurements of H, D, and T-labeled substrates were therefore undertaken. The Swain–Schaad exponent for the primary H/T vs. D/T isotope effects remained indistinguishable from the semiclassical value, while the exponent for the secondary isotope effects was generally above the semiclassical value (from 16 ± 8 to 4.4 ± 0.5 but with an irregular relationship to the temperature. The primary H/T effects extrapolate to $A_H/A_T = 0.33 \pm 0.16$, again indicative of tunneling. Some evidence was obtained that the mechanism may shift in the low-temperature methanol-containing solutions away from the room temperature, aqueous-solution mechanism in which the cofactor binds first and the alcohol binds second, toward a mechanism with some random component of binding by the cofactor and substrate. This complication may be preventing a clearer definition of the situation, although it is apparent that tunneling is occurring.

An alcohol dehydrogenase from the thermophilic organism *Bacillus stearothermophilus*, closely similar in sequence and structure to the enzymes from yeast and from horse liver, was examined by Kohen et al.³³ (entry 14 in Table 2), with isotopically labeled benzyl alcohols as substrates over the temperature range 5 – 65 °C. The primary isotope effects were small, between 5.5 and 7 (H/T), 1.62 and 1.75 (D/T), the relationship yielding a Swain–Schaad exponent of 3.5, essentially the semiclassical value. The secondary isotope effects, in a now-familiar picture, required exponents of 11 in the higher range of temperatures and 5 in the lower range. In fact, plots of $\log k_{\text{cat}}$ against $1/T$ show a distinct break for both H-labeled and D-labeled substrates (labeled at the primary site) at 30 °C; above and below this temperature the data are quite linear. In the high-temperature regime, ΔH^\ddagger is the nearly the same for H-labeled (14.6 kcal/mol) and D-labeled (15.1 kcal/mol) substrates and A_H/A_D is 2.2. In the low temperature regime, ΔH^\ddagger is far smaller for H-labeled (23.6 kcal/mol) than for D-labeled (31.4 kcal/mol) substrates. This difference would have produced an isotope effect of around 380,000, had the value of A_H/A_D not been 10^{-5} . In both regimes, therefore, tunneling is strongly indicated but on differing models. Above 30 °C, the data were taken as consistent with a fluctuational search by the enzyme for a sub-state about 15 kcal/mol in energy above the reactant-state ternary complex, with tunneling then occurring in the sub-state from low-lying vibrational states with a probability ratio (H/D) of about 2. Below 30 °C, a simple viewpoint would hold that, over the temperature range studied,

tunneling plays no part in reaction of the D-labeled substrate but a considerable part in reaction of the H-labeled substrate, making the observed values of $\Delta H_{\text{H}}^{\ddagger}$ and A_{H} far smaller than would have been expected from the semiclassical route followed by the D-labeled substrate.

Why the break at 30 °C? Kohen and Klinman⁵⁴ suggest that the fluctuational excursions to locate a tunneling sub-state depend on low-frequency vibrational modes of the enzyme, which are freely operational in the high-temperature regime. At lower temperatures, the enzyme structure may become rigid and incapable of such motions and a slower reaction, perhaps involving some tunneling near the transition state of the semiclassical reaction, sets in.

To test the hypothesis that the conformational flexibility of the thermophilic enzyme is lower at room temperature than at higher temperatures, Kohen and Klinman measured, by FTIR, the time course of H/D exchange of protein N–H sites in deuterium oxide for the thermophilic alcohol dehydrogenase. Their measurements were made at the optimal host–organism temperature of 65 °C and at 25 °C, below the transition temperature. They also included yeast alcohol dehydrogenase at 25 °C, which is the optimal temperature for its own host organism.

In such experiments,^{55,56} the fraction of remaining unexchanged N–H sites is expected to decay as a multi-exponential function of time with one exponential contributor for each N–H site or class of N–H sites. The assumed mechanism is that fluctuations of the enzyme that lead to solvent exposure are rapid and reversible compared to the exchange event. The rate constant k_0 for exchange of the fully exposed site is determined to a fair extent merely by acid–base catalysis of N–H exchange and by the temperature; both effects can be estimated from studies with model compounds and are roughly independent of other structural considerations. The effective overall rate constant for exchange at the i th N–H site or class of sites then becomes $\rho_i k_0$, where ρ_i is the probability that the i th N–H site will be fully solvent exposed. Typically k_0 is around 10 s^{-1} at neutral pH and room temperature and values of ρ vary from 1 for rapidly exchanging surface residues to 10^{-8} or less for deeply buried residues that are rarely exposed. The half-life times for exchange in a typical experiment, therefore, can vary from 100 ms to 80 days or longer. The customary presentation of the data is a plot of the fraction of unexchanged sites vs. $\log(k_0 t)$, thus compressing the enormous scales of time logarithmically and measuring the time t in units of k_0^{-1} , which allows experiments at different pH and temperature to be compared with each other.

Kohen and Klinman⁵⁴ found that yeast alcohol dehydrogenase at 25 °C, the optimal temperature of its host, and the thermophilic alcohol dehydrogenase at 65 °C, the optimal temperature of its host, gave a time dependence for exchange that lay on a common curve, with 50% of their sites having exchanged at $t = (3000)/k_0$, and 80% of their sites having exchanged at $t = (3 \times 10^6)/k_0$. The thermophilic alcohol dehydrogenase at 25 °C, below the break-point in its temperature dependence, gave a different time dependence indicative of a smaller tendency to expose exchangeable sites: at $t = (3000)/k_0$ only 20% exchange had occurred instead of 50% and at $t = (3 \times 10_6)/k_0$, only 50% exchange had occurred

instead of 80%. These results confirm two suspicions. First, it is confirmed for these two cases that enzymes near the thermal optima of their host organisms tend to exhibit similar structural flexibility. Second, the thermophilic enzyme is shown to be more flexible in the high-temperature regime where a conformational search for a tunneling sub-state (followed by tunneling within the sub-state) is proposed as the dominant mechanism, while it is more rigid in the low-temperature-regime where the isotope effects are consistent with tunneling near a transition-state configuration.

The books, however, cannot yet be closed. Although the flexibilities of the yeast enzyme at 25 °C and thermophilic enzyme at 65 °C are similar, and although both show unmistakable evidence of tunneling, the nature of the tunneling process appears to be different. This is another instance in which the temperature dependences of the isotope effects generate a complex and ill-understood picture.

NAD-Malic enzyme

The study of Karsten et al.³² (entry 13 in Table 2) is of special interest because the reaction under catalysis (see Figure 5 for the schematic mechanism) may involve hydride transfer simultaneous with the fission of a C–C bond in the decarboxylation component of the reaction. If the two events are concerted (evidence in related enzymes does not provide a clear guideline on this point) then tunneling might become more difficult because of the increased effective mass.

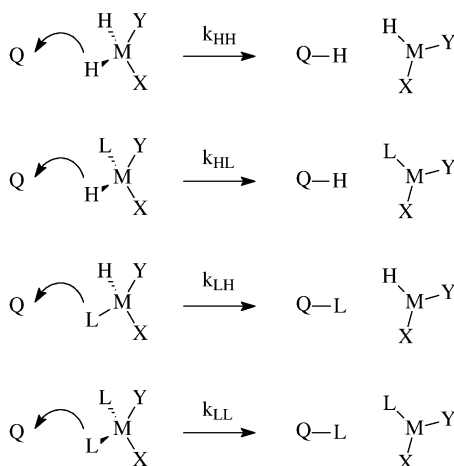
For the enzyme from *Ascaris suum*, α -secondary isotope effects (T-label in NAD^+) were determined on the rate constant under four sets of circumstances: use of the cofactor NAD^+ with the divalent metal ions Mn^{2+} ; Mg^{2+} ; and Cd^{2+} ; and use of the cofactor 3-acetylpyridine adenine dinucleotide (APAD) with the divalent metal ion Mn^{2+} . Previous work⁵⁷ had shown that the intrinsic primary isotope effect depends on the metal ion employed (the metal is thought to interact with the hydroxyl substituent of malate). As the ionic radius of the metal ion increases from the smallest value (for Mn^{2+}) to the largest value (for Cd^{2+}), the primary isotope effect (H/D) rises from 3 to 30. It was suggested that the larger metal ions compressed the malate against the cofactor, decreasing the hydride-transfer distance and thus increasing the level of tunneling.

The equilibrium secondary isotope effect (H/D) for reduction of NAD^+ is $1/1.13 = 0.89$ (Table 1), which translates to an effect of 0.84 (H/T). The traditional expectation would, therefore, be that the kinetic secondary effect would be inverse, between the limits of 1.00 and 0.84 (H/T). In fact, the effects are 1.028 ± 0.018 (Mn^{2+} , NAD^+), 1.025 ± 0.016 (Mg^{2+} , NAD^+), 1.006 ± 0.001 (Cd^{2+} , NAD^+), 0.874 ± 0.018 (Mn^{2+} , APAD) when H^- is transferring. When D^- is transferring, the effects are 1.0015 ± 0.0005 (Mn^{2+} , NAD^+), 1.002 ± 0.01 (Mg^{2+} , NAD^+), 0.976 (one determination: Cd^{2+} , NAD^+) and was not determined for the Mn^{2+} , APAD combination. As the authors explain, the errors are too large to allow detailed trends to be discerned, but it is clear (a) that the secondary effects are exalted, clearly

normal effects where inverse effects are expected; (b) that the secondary effects observed when D is transferred are less exalted than when H is transferred. These expectations for reactions in which motion of the secondary center is incorporated into the reaction coordinate and where tunneling is contributing to the hydrogen transfer reaction were laid out with particular clarity by Huskey⁵⁸ and the paper of Karsten et al.³² is a particularly clean demonstration of his points. A summary of those points is given in Chart 7.

Chart 7. Huskey's rules for violations of the rule of the geometric mean and the Swain–Schaad relationships

Consider a substrate with two hydrogenic sites from which a single hydrogen is transferred stereospecifically (e.g., in an enzymic reaction):



A label (L = D or T) can be introduced in the transferable position (left subscript of the rate constant) or in the non-transferable position (right subscript of the rate-constant): Then k_{HH}/k_{DH} and k_{HD}/k_{DD} are *primary deuterium isotope effects*, while k_{HH}/k_{HD} and k_{DH}/k_{DD} are *secondary deuterium isotope effects*. In the general case, we can relate each of the two effects by:

$$k_{HH}/k_{DH} = (k_{HD}/k_{DD})^{R_p}$$

$$k_{HH}/k_{HD} = (k_{DH}/k_{DD})^{R_s}$$

R_p is an exponent that describes the relationship of a primary isotope effect with H in the secondary position to a primary isotope effect with D in the secondary position. R_s is an exponent that describes the relationship of a secondary isotope effect with H in the primary position to a secondary isotope effect with D in the primary position. According to the Rule of the

Geometric Mean (Chart 3), $R_p = R_s = 1$. *If the Rule of the Geometric Mean is invalid, e.g., as a result of strong vibrational coupling between the primary and secondary centers, R_p and R_s may not be unity.*

If a protium/tritium (H/T) primary isotope effect is measured with protium at the secondary position (k_{HH}/k_{TH}) and a D/T primary isotope effect with deuterium at the secondary position (k_{DD}/k_{TD}), then a complicated situation ensues. If both primary isotope effects had been measured with protium at the secondary position, then

$$k_{HH}/k_{TH} = (k_{DH}/k_{TH})^{S_p}$$

where S_p is the Swain–Schaad exponent (Chart 3) with a semiclassical value of 3.26. For secondary isotope effects measured with a common isotope at the primary position, the Swain–Schaad exponent S_s has the same semiclassical value of 3.26. For the circumstance envisioned above, which may be dictated by synthetic necessity or some other consideration of experimental design, the relationship between k_{HH}/k_{TH} and k_{DD}/k_{TD} derives from a combination of the Swain–Schaad relationship (just above) and the Rule of the Geometric Mean:

$$k_{DH}/k_{TH} = (k_{DD}/k_{TD})^{R_s}$$

Combining the last two equations gives

$$k_{HH}/k_{TH} = (k_{DD}/k_{TD})^{S_p R_s}$$

showing that *the deviation of the values from the semiclassical expectation is potentially produced by violations of either the Swain–Schaad relationship or the Rule of the Geometric Mean or both.*

For further important work on this and related concepts, see Rucker, J. and Kliman, J.P. (1999). Computational study of tunneling and coupled motion in alcohol dehydrogenase-catalyzed reactions: Implication for measured hydrogen and carbon isotope effects. *J. Am. Chem. Soc.* **121**, 1997–2006, and Kohen, A. and Jensen, J.H. (2002). Boundary conditions for the Swain–Schaad relationship as a criterion for hydrogen tunneling. *J. Am. Chem. Soc.* April 17, **124**(15), 3858–3864.

HYDRIDE-TRANSFER REACTIONS INVOLVING OTHER COFACTORS

Morphinone reductase

Basran et al.²⁴ (entry 5, Table 2) obtained primary (H/D) isotope effects and solvent isotope effects for the hydride transfer from FMN_H to cyclohexenone (see Figure 5 for the schematic mechanism) from 5 to 36 °C. It was established that the N5 hydrogen of FMN_H, which is transferred in the rate-limiting step of the reaction, did not exchange rapidly with solvent hydrogen following *in-situ* steady-state generation of the cofactor deuterated at this site. At 25 °C, primary isotope

effects (H/D) were about 3.5 in both protium oxide (HOH) and deuterium oxide (DOD), and solvent isotope effects (HOH/DOD) were 2.3 regardless of whether the cofactor was transferring H or D. The combined isotope effect (H, HOH)/(D, DOD) was 8.2, approximately equal to 3.5×2.3 . Thus the Rule of the Geometric Mean (Chart 3) is strictly obeyed. These findings are strong evidence that a single step determines the rate, and that both isotope effects arise in that step. The findings suggest that the motions of the isotopic center(s) that generate the two effects are not coupled to each other.

The temperature dependence of the primary isotope effect (H/D) on k_{cat} yields an Arrhenius A-ratio of 3.7 with the isotopic values of ΔH^\ddagger equal within experimental error, each being around 17–18 kJ/mol. This was again assigned, in effect, to a fluctuational search by the enzyme for an efficient tunneling sub-state (which would seem to be energetically elevated by around 17–18 kJ/mol) with tunneling then proceeding from the vibrational ground state of the tunneling sub-state.

The solvent isotope effect produces an A-ratio (HOH/DOD) of three with isotope-independent ΔH^\ddagger of 17–18 kJ/mol. This result is more difficult to interpret, because it is unknown how many isotopic sites in the enzyme or water structure contribute to the isotope effect of 2–3. If a single site should be the origin of the effect, then the site could reasonably be a solvent-derived protonic site of the enzyme involved in general-acid catalysis of the hydride transfer, most simply by protonic interaction with the carbonyl oxygen of cyclohexenone or possibly by proton transfer to an olefinic carbon of cyclohexenone.

The apparent temperature-independence of the solvent isotope effect is particularly interesting. The calculated value of ΔH^\ddagger for the reaction in DOD is *smaller* than that in HOH by 0.9 ± 0.2 kJ/mol. This is hard to account for on any model and may be a signal of some hidden kinetic complexity or other anomaly. If the isotope-effect generating site is a proton being transferred to carbon, then many studies indicate tunneling to be a possible mechanism (see, e.g., Saunders¹⁹ for references to many of his important contributions establishing this point). If the site involves a general-acid catalytic interaction with a carbonyl oxygen of cyclohexenone, then there are also precedents for temperature-independent isotope effects.

Krishtalik⁵⁹ (Table 11, p 273) tabulates seven examples of solvent isotope effects in the action of serine proteases on N-blocked amino-acid derivatives. These effects arise from protonic interactions in general catalysis and are known to arise from a single site.⁶⁰ The isotope effects are between 2 and 3 and the isotopic activation energy differences are all within 0.3 kcal/mol (1–2 kJ/mol) of zero. The situation is thus quite similar to that reported by Basran et al. Its explanation is not completely clear. Krishtalik and his coworkers believe that the general-catalysis interaction involves tunneling on exactly the model described several times above: fluctuation of the enzyme to a tunneling sub-state (isotope-independent, temperature-dependent), followed by tunneling from a ground vibrational state (isotope-dependent, temperature-independent). However, a different view⁶⁰ has been that these interactions are basically hydrogen-bonding interactions involving

shorter and somewhat stronger hydrogen bonds than the ordinary ones. The temperature dependence of the isotope effect for such interactions is not known, but the fact that the potential-energy well for such interactions is commonly thought to be broad, and relatively flat could mean that excited vibrational states and, therefore, entropy contributions could play an unusual role, and possibly lead to a smaller temperature dependence of the isotope effect.

Glucose oxidase

Seymour and Klinman²⁵ (entry 6 in Table 2; see Fig. 5 for a schematic mechanism) measured relative rate constants for the hydride-transfer reaction (H, D, T) from C1 of 2-deoxyglucose to the cofactor FAD. To explore the model for enzymically enhanced tunneling, according to which the enzyme conducts a fluctuational search for an efficient tunneling sub-state, five variants of glucose oxidase, anticipated to have differing capacities for the fluctuational search, were generated.

Previous work⁶¹ had shown that with three differently glycosylated forms of glucose oxidase, as the degree of glycosylation increased the enthalpy of activation for k_{cat} increased and indications of tunneling disappeared. For example, with the least glycosylated variant (136 kDa) $A_{\text{D}}/A_{\text{T}}$ was 1.47, well above the semiclassical value of approximately unity, and ΔH^{\ddagger} was 8.1 kcal/mol, while for the most heavily glycosylated variant (205 kDa), $A_{\text{D}}/A_{\text{T}}$ was 0.89, near the semiclassical value of unity, and ΔH^{\ddagger} was 13.7 kcal/mol. The reasonable conclusion was drawn that the glycosyl appendages could render the conformational exploration for a tunneling sub-state more difficult and thus force the reaction to proceed semiclassically.

Seymour and Klinman made use of: (a) the deglycosylated form of the enzyme isolated from *Aspergillus niger* (136 kDa); (b) the deglycosylated enzyme modified with polyethylene glycol (PEG) units of relatively short length (146 kDa); (c) the wild-type enzyme as isolated in a glycosylated state from *A. niger* (155 kDa); (d) the deglycosylated enzyme modified with PEG units of greater length (211 kDa); (e) a glycosylated form of the enzyme obtained by expression of the *A. niger* gene in yeast (320 kDa). The values of k_{cat} for enzymes (a) through (e) lay within the range 5.2–6.1 s⁻¹ and the isotope effects $k_{\text{D}}/k_{\text{T}}$ covered only the range 2.22–2.26, the range being smaller than the standard deviation of a single measurement (data at 33 °C). A heroic exercise in analysis of the data, particularly the temperature dependence of the isotope effects (D/T and H/T), revealed a diabolical level of kinetic complexity (more than a single rate-limiting step). Also revealed were artifacts arising from changes in oxygen-concentration upon mixing that rendered incorrect the magnitudes and trends in isotopic A-ratios that were reported by Kohen et al.⁶¹ and recounted above.

After an exceedingly cautious extraction had been made of the intrinsic isotope effects from the data, the wild-type enzyme (c, 155 kDa) gave an A-ratio (D/T) of 0.98, essentially consistent with a semiclassical mechanism, and the deglycosylated enzyme (a, 136 kDa) 0.81, a borderline indication of tunneling, while the fully glycosylated enzyme (e, 320 kDa) and the two PEG-derivatives

(b and d, 146 and 211) gave the values most indicative of tunneling, 0.61 and 0.55, respectively. The straightforward idea of a correlation between tunneling and light, mobile structures is clearly wrong. Upon further exhaustive analysis, there is some indication that as the enthalpies of activation rise, the sign of tunneling disappears, but at the least it is unclear whether this correlation represents cause or effect.

This extraordinary study shows with great clarity how far we now are from a reliable understanding of either the linkage between protein flexibility and tunneling in the most general sense, or the physical models that underlie anomalous temperature dependences of isotope effects.

HYDROGEN-ATOM TRANSFER REACTIONS

Peptidyl- α -hydroxylating monooxygenase

Two entries in [Table 2](#) (entries 3 and 7) describe isotope-effect studies for this enzyme (PHM). A schematic mechanism for the isotope-sensitive step is shown in [Fig. 5](#). Francisco et al.²⁶ (entry 7) commenced this work by obtaining primary and secondary isotope effects (H, D, T) for the kinetic parameter $k_{\text{cat}}/K_{\text{M}}$ at temperatures from 5 to 45 °C. The substrate was a simple model substance, N-benzoylglycine (hippuric acid). The observed primary isotope effects rose as the temperature increased from values near 2 at 5 °C to values around 12 (H/T) and 5 (H/D) at 45 °C. Such behavior is contrary to the traditional expectations ([Chart 3](#)) and also contrary to expectations on any model of quantum tunneling. It is, however, the anticipated behavior if kinetic complexity is present, i.e., if more than a single step limits the rate and if the importance of the isotope-sensitive step in limiting the rate decreases as the temperature decreases. The latter effect is simply a matter of the relative enthalpies of activation for the isotope-sensitive step vs. the non-sensitive steps for the particular reaction: if the isotope-sensitive step has the smaller enthalpy of activation, it will not decrease in rate as the temperature falls as much as the other steps, and will, therefore, be less important in limiting the rate at lower temperatures. Northrop's method ([Chart 6](#)) was used to obtain the intrinsic values of the isotope effects, which emerged as wholly independent of temperature. The primary (H/D) effect is around 11–12 over the entire range of temperatures. The same is true of the secondary (H/D) effect, which averaged 1.27. Using their knowledge of the intrinsic isotope effects, they could obtain the values of the hydrogen-atom transfer step at different temperatures ([Chart 4⁶²](#)), thus estimating an enthalpy of activation around 13 kcal/mol for this step.

These data led to the model already described several times above. The enzyme executes a search for a tunneling sub-state, apparently 13 kcal/mol in energy above the principal state; from this state the hydrogen atom tunnels with no further vibrational excitation. Probably motion of the secondary center is coupled into the tunneling coordinate. The result is large, temperature-independent primary and secondary isotope effects in the context of an isotope-independent activation energy.

Francisco et al.²² (Table 2, entry 3) found that for PHM, ¹⁸O primary isotope effects (16/18) were different for the H-labeled substrate (1.0173 ± 0.0009) and the D-labeled substrate (1.0212 ± 0.0018). Such a result had previously been obtained with dopamine- β -hydroxylase,⁶³ an enzyme that shares many mechanistic properties with PHM. The isotope effects with dopamine- β -hydroxylase were 1.0197 (H-substrate) and 1.0256 (D-substrate), very close in both cases to those for PHM. Francisco et al. point out that the H/D sensitivity of the primary oxygen isotope effect requires that the oxygen cleavage and activation event (which generates the primary oxygen isotope effect) and the hydrogen-atom transfer event (which generates the primary hydrogen isotope effect) must be linked by a set of reversible steps. The occurrence of an irreversible step between the two events would insulate them kinetically from each other and make the observed effect of substrate isotopic composition on the oxygen isotope effect impossible. Some difficult questions remain about what the activation event is and the identity of the hydrogen-abstracting species shown in Figure 5 (but see Evans, Ahn and Klinman⁷⁴ and Chen and Solomon⁷⁵).

Lipoxygenases

These enzymes remove a hydrogen atom from C11 of linoleic acid to generate a pentadienyl radical that reacts with dioxygen at C13, giving rise eventually to a 13-hydroperoxyl species. Rickert and Klinman³¹ (entry 12 of Table 2) succeeded in measuring the primary and α -secondary isotope effects for the soybean enzyme; previous workers had measured only the combined effects. They prepared by chemical synthesis a racemic mixture (equimolar in R and S enantiomers) of the monodeuterated 11-²H-linoleic acid. The enzyme is known to remove stereospecifically the 11-S hydrogen with a large isotope effect (H/D, more than 40), so when the racemic mixture was oxidized with lipoxygenase catalysis, the 11-S-¹H, 11-R-²H species was rapidly consumed, leaving behind 11-R-¹H, 11-S-²H-linoleic acid in greater than 95% enantiomeric excess. This compound allowed the eventual determination of the intrinsic primary and secondary isotope effects but only after realization that, while the wild-type enzyme is about 99% stereoselective for the 11-S hydrogen in the 11-H,H substrate, the very large isotope effect causes the stereoselectivity to drop to 55% with the 11-R-H, S-D substrate. This circumstance led to wildly misleading results with the secondary isotope effect appearing to be as large as five. With the L54A mutant, in which the binding site is opened to allow increased mobility of the substrate, the stereoselectivities for the 11-S hydrogen dropped to 95% (HH) and 23% (HD). Careful extraction of the intrinsic isotope effects yielded a primary effect (H/D) of 75–85 and a secondary effect (H/D) of 1.1–1.2 for both the wild-type and mutant enzyme. The very large primary isotope effect can only be reconciled with an important role for tunneling, but the secondary isotope effect is not indicative of whether motion at this center is coupled to the tunneling event. The apparent primary isotope effects are nearly or completely independent of temperature and the kinetic parameter k_{cat} exhibits a ΔH^\ddagger of only

1–3 kcal/mol. A simple hypothesis might be that tunneling occurs directly from the ground vibrational state of the main enzyme–substrate complex. A further important contribution from this group on tunneling in soybean lipoxygenase⁶⁴ will be discussed in a later publication in connection with the role of protein dynamics.

Lewis et al.³⁰ (entry 11 of Table 2) examined the temperature-dependence of isotope effects in the action of both the human enzyme and the soybean enzyme, by measuring the relative amounts of per-protio and per-deuterio-13-hydroperoxy-products by HPLC. The observed effects are, therefore, composed of primary, secondary, and perhaps remote isotope-effect contributions. Isotope effects on k_{cat}/K_M for both enzymes (determined by competition between labeled substrates) are increased by high total substrate concentration, an effect previously observed but still ill-understood. At 100 μM substrate, the effects are roughly independent of temperature below about 15 °C, and are about 60 (H/D) for the human enzyme and 100 (H/D) for the soybean enzyme. Above 15 °C, the effects decline to about 50 for the human enzyme and about 60 for the soybean enzyme, perhaps because non-isotope-sensitive steps become more nearly rate-limiting (see Chart 4).

These findings are consistent with the reactant ground-state tunneling hypothesis indicated by the findings of Rickert and Klinman discussed above. If the decline in isotope effect at higher temperatures results from other steps than the tunneling event becoming more nearly rate-limiting at higher temperatures, these other steps would be required to have even lower activation enthalpies than the very low value estimated by Rickert and Klinman for the tunneling event. An alternative hypothesis would be that the higher temperature disrupts the delicate structural and/or dynamical balance required for the ground-state tunneling mechanism.

PROTON-TRANSFER REACTIONS

Sarcosine oxidase

Harris et al.²⁹ (entry 10 of Table 2; see Fig. 5 for a schematic mechanism) have obtained isotope effects arising from proton abstraction from the CH_3 or CD_3 groups of the correspondingly labeled sarcosine adducts of FAD. The isotope effects, therefore, contain contributions from both primary and α -secondary effects. The overall effects (H/D) are 7.3 and independent of temperature between 5 and 37 °C (the isotopic difference in activation energies is 0.6 ± 2.1 kJ/mol). The rate constants for the overall process have ΔH^\ddagger about 39–40 kJ/mol. The interpretation proposed by the authors is a vibrationally driven search for the tunneling sub-state (presumably about 40 kJ/mol elevated in energy over the reactant adduct complex), followed by temperature-independent tunneling with a modest advantage the proton over the deuterium.

Methylamine dehydrogenase

This enzyme makes use of the novel cofactor TTQ (tryptophan tryptophyl quinone) which contains an ortho-quinone functional array. The substrate forms an imine

adduct with one of the carbonyl groups and an enzymic base abstracts a proton from the methyl group with activation by the second carbonyl group (see Fig. 5 for a schematic mechanism). The chemistry is, therefore, somewhat similar to that of sarcosine oxidase, described above. Basran et al.³⁴ (entry 15 of Table 2) measured kinetic isotope effects from 5 to 40 °C by using CH₃NH₂ and CD₃NH₂ so, as with sarcosine oxidase, the effects will contain contributions from both primary and secondary effects. The rate constant here too was temperature-dependent with ΔH^\ddagger about 45 kJ/mol, with a negligible difference between the isotopic reactions. The overall isotope effect (H/D) is, therefore, temperature-independent and equal to about 13. The isotope effect and the enthalpies of activation are unaffected by the presence of 30% glycerol in the solvent. The authors take this as excluding any large-scale enzyme reorganization as contributing to the rate the process that generates the isotope effects and requires the activation energy. The model proposed is a rapid reversible search for a tunneling sub-state from which temperature-independent tunneling generates the observed isotope effect.

3 Experimental signatures of tunneling

OBSERVATIONS THAT DO NOT DEFINITELY INDICATE TUNNELING

Large isotope effects per se do not indicate tunneling

As the examples in the preceding section have shown, tunneling perhaps most commonly in the cases so far examined occurs with modest and even with small isotope effects, well within the limits of semiclassical ideas (Fig. 2). Even if isotope effects beyond the semiclassical limits are observed, other sources of large apparent isotope effects must be ruled out. Among these are isotope effects arising from reaction-path branching.⁶⁵ If, for example, hydrogen transfer occurs in an irreversible step generating an intermediate that branches between a major product formed with no isotope effect and a minor product formed in a second hydrogen-transfer process, the initial rates of formation of the minor product will exhibit isotope effects that are the product of the two individual hydrogen-transfer isotope effects. If each individual isotope effect were within the semiclassical limit and equal to, say, 6 (H/D), then the observed apparent isotope effect would be 36.

Non-linear Eyring or Arrhenius dependences per se do not indicate tunneling

It is a natural expectation, if a semiclassical mechanism that governs the rate at high temperatures gives way at lower temperatures to a tunneling process with no activation energy or a very low activation energy, to observe curvature in Eyring or Arrhenius plots. The expected form of the curvature is that the enthalpy of activation is reduced at lower temperatures, so that the plot is “bowl-shaped” or concave upwards. There are, however, other origins for such observations that must be

excluded before such an observation can be attributed to tunneling. Two commonplace origins for curvature of this kind are:

- (1) A substantial, positive heat capacity of activation, ΔC_p^\ddagger . In this case, the enthalpy of activation will be given by $\Delta H^\ddagger = \Delta H_0^\ddagger + T\Delta C_p^\ddagger$. Then ΔH^\ddagger will rise with temperature and the plots will be curved in the sense expected for tunneling.
- (2) A change in mechanism between two semiclassical pathways, one with a larger enthalpy of activation and more positive entropy of activation that dominates at higher temperatures and the other with a smaller enthalpy of activation and more negative entropy of activation that dominates at low temperatures.

Temperature-independent isotope effects per se do not indicate tunneling

There are ways in which temperature-independent isotope effects can arise in the absence of tunneling.

- (1) Kinetic complexity can produce apparently temperature-independent isotope effects. For example, a rise in temperature produces a smaller intrinsic isotope effect, in agreement with the conventional expectations of Chart 3, for an isotope-sensitive step that is partially rate limiting. If at the same time the rise in temperature makes other steps relatively more rapid so that the isotope-sensitive step then becomes more nearly rate-limiting, then the intrinsic isotope effect will be more fully expressed (Chart 4). If these effects roughly balance, then the isotope effect may appear to be independent of temperature while in fact fully in accord with semiclassical expectations. Seymour and Klinman²⁵ have discussed in detail the problem of kinetic complexity in isotope-effect temperature dependences.
- (2) In a more trivial sense, small isotope effects may appear temperature-independent simply because the expected isotopic difference in enthalpies or energies of activation is small. It is thus, of course, important to compare the apparent isotopic temperature dependences and their error estimates with the semiclassical expectations.

OBSERVATIONS THAT LIKELY INDICATE TUNNELING

The valid criteria for establishing tunneling in hydrogen-transfer processes that have been encountered in the consideration of various examples above are:

- (1) The observation of ratios of isotopic Arrhenius pre-exponential factors that are substantially distant from the semiclassical expectation of unity (Charts 1 and 3). The deviant values may be either substantially smaller than unity or substantially greater than unity.
- (2) The related observation of isotopic differences in energies or enthalpies of activation that are substantially larger or smaller than the semiclassical

- expectation of $RT \ln$ (isotope effect) (Charts 1 and 3). The larger differences are coupled with A-ratios that are small, the smaller differences should be greater than or equal to zero and coupled to an A-factor ratio that is equal to or larger than the isotope effect.
- (3) The observation of a primary tritium isotope effect (H/T) that is substantially larger than the value predicted on the basis of the semiclassical Swain–Schaad relation (Chart 3) from a heavy-hydrogen (D/T) isotope effect. The same information can be expressed in terms of a Swain–Schaad exponent required to relate the two isotope effects that is substantially larger than the semiclassical value of 3.26.
 - (4) The observation of exalted secondary isotope effects, i.e., those that are substantially beyond the semiclassical limits of unity and the equilibrium isotope effect. These observations require coupling between the motion at the primary center and motion at the secondary center in the transition-state reaction coordinate, and in addition that tunneling is occurring along the reaction coordinate.
 - (5) The observation of systematic deviations from the Rule of the Geometric Mean between primary and α -secondary isotope effects. The magnitude of both effects should be greater (more normal) when the other position is occupied by a lighter isotope than when it is occupied by a heavier isotope.

4 Models for tunneling in enzyme reactions

The detailed description of the models currently being used to describe tunneling in enzyme-catalyzed reactions will be undertaken in a later part of our treatment in which theoretical studies will be reviewed and ideas about the role of protein motions will be a focus. At this point, we will briefly sketch the most commonly used ideas.

BELL TUNNELING

This approach was originally used to account for cases in which low values of the isotopic A-factor ratio and inflated values of the isotopic difference in activation energies were the main indicators of tunneling. The underlying formalism is one in which modest amounts of tunneling are considered to occur in the neighborhood of the transition state. Modern transition-state theory^{66–68} can account for greater degrees of tunneling. Approaches outside the transition-state theoretical framework are also being used to account for enzymic data that fit the Bell model (see below).

TUNNELING ASSISTED BY PROTEIN MOTION

Currently suggested models for tunneling increasingly invoke “protein dynamics”. These models envision either a series of conformational fluctuations that lead to a suitable tunneling configuration (“passive dynamics”) or a more active role for the enzyme motions (“active dynamics” or “gating”).⁶⁴ On the model of

“active dynamics”, enzyme vibrational modes are recruited to vary the tunneling distance and the relative energies of the vibrational levels between which tunneling will occur. Such a modulation of the tunneling probabilities can occur either in a higher-energy sub-state or in the ground state of the reactive enzyme complex. Models of this type are related to long-standing contributions from the school of Dogonadze and recent interpretations have commonly relied on the formulation of this approach by Ulstrup and Kuznetsov⁶⁹.

Because both the passive fluctuations and the modulating vibrations can require thermal excitation, this model is capable of accounting for temperature-dependent isotope effects, including those traditionally described by the Bell model. Theoretical studies, which will be the topic of the second and third parts of this three-part series of articles, have not yet produced a consensus on the contribution of specific protein motions to enzyme catalysis.

A version of the model is also becoming an increasingly common explanation for the observation of temperature-independent isotope effects when the rate constants themselves are temperature-dependent. While the theoretical formulations employed^{64,69} are capable of reproducing the data, the underlying physical picture seems problematic. That the vibrational modulation of barrier height and width by quite low-frequency protein motions can effectively maintain a relative tunneling probability for the two isotopic species that is identical over a considerable temperature range seems an enormously stringent requirement. As both experimental and theoretical studies move forward, it remains true at this point that isotope-effect temperature-dependences that fall outside the semiclassical expectations are the least well-understood part of the picture.

5 Tunneling as a contribution to catalysis: prospects and problems

A central question for those interested in enzyme catalysis of hydrogen transfer is, to what degree is tunneling an evolutionarily developed component of the catalytic power of enzymes? It has long been known that non-enzymic hydrogen-transfer reactions frequently occur with tunneling. The work of Saunders and others on proton-transfer reactions has been discussed in this article. Non-enzymic hydride transfer from nicotinamide species was shown by Powell and Bruce in 1983 to proceed with tunneling.⁷⁰ Finke et al. have confirmed for enzyme models that hydrogen-atom transfers also show the signatures of tunneling.⁷² None of these demonstrations and few of the experimental enzymic studies to date actually address the question of what factor the phenomenon of tunneling contributes to the rate of either a non-enzymic or an enzymic reaction (Notable exceptions are represented by Chin and Klinman²⁸ and Bahnsen et al.⁵²; see Fig. 6 above and the accompanying discussion.) Thus the question of the evolutionary development of tunneling as a catalytic strategy in enzymes remains, from an experimental viewpoint, completely open. The current best hope for resolving this question is with the sophisticated and powerful new forms of theory.

References

1. Christofferson, R.E. (1989). *Basic Principles and Techniques of Molecular Quantum Mechanics*, pp. 195–198. Springer, New York
2. Kauzmann, W. (1957). *Quantum Chemistry*, pp. 241–246. Academic Press, New York
3. Johnston, H.S. (1966). *Gas Phase Reaction Rate Theory*. Ronald Press, New York
4. Caldin, E.F. (1969). Tunneling in proton-transfer reactions in solution. *Chem. Rev.* **69**, 135–156
5. Lewis, E.S. and Funderburk, L. (1964). Tunneling in a proton transfer. A large isotope effect. *J. Am. Chem. Soc.* **86**, 2531–2532
6. Burkert, U. and Allinger, N.L. (1982). *Molecular Mechanics*, pp. 29–31. American Chemical Society, Washington
7. Lewis, E.S. (1975). In *Tunneling in Hydrogen Transfer Reactions in Proton-Transfer Reactions*, Caldin, E. and Gold, V. (eds), p. 317–338. Chapman and Hall, London
8. Bell, R.P. (1980). *The Tunnel Effect in Chemistry*. Chapman and Hall, London
9. Melander, L. and Saunders, W.H. (1980). *Reaction Rates of Isotopic Molecules*. Wiley Interscience, New York
10. Kaldor, S.B., Fredenburg, M.E. and Saunders, W.H. (1980). Mechanisms of elimination reactions 32. Tritium isotope effects and tunnel effects in the reaction of 2,2-diphenylethyl-2-t derivatives with various bases. *J. Am. Chem. Soc.* **102**, 6296–6299
11. Kurz, L.C. and Frieden, C. (1977). Comparison of the structures of enzymatic and nonenzymatic transition states. Reductive desulfonation of 4-X-2,6-dinitrobenzene-sulfonates by reduced nicotinamide adenine dinucleotide. *Biochemistry* **16**, 5207–5216
12. Welsh, K.M., Creighton, D.J. and Klinman, J.P. (1980). Transition-state structure in the yeast alcohol dehydrogenase reaction: the magnitude of solvent and alpha-secondary hydrogen isotope effects. *Biochemistry* **19**, 2005–2016
13. Kurz, L.C. and Frieden, C. (1980). Anomalous equilibrium and kinetic alpha-deuterium secondary isotope effects accompanying hydride transfer from reduced nicotinamide adenine dinucleotide. *J. Am. Chem. Soc.* **102**, 4198–4203
14. Cook, P.F., Blanchard, J.S. and Cleland, W.W. (1980). Primary and secondary deuterium isotope effects on equilibrium constants for enzyme-catalyzed reactions. *Biochemistry* **19**, 4853–4858
15. Cook, P.F., Oppenheimer, N.J. and Cleland, W.W. (1981). Secondary deuterium and nitrogen-15 isotope effects in enzyme-catalyzed reactions. Chemical mechanism of liver alcohol dehydrogenase. *Biochemistry* **20**, 1817–1825
16. Klinman, J.P. (1976). Isotope effects and structure-reactivity correlations in the yeast alcohol dehydrogenase reaction. A study of the enzyme-catalyzed oxidation of aromatic alcohols. *Biochemistry* **15**, 2018–2026
17. Huskey, W.P. and Schowen, R.L. (1983). Reaction-coordinate tunneling in hydride-transfer reactions. *J. Am. Chem. Soc.* **105**, 5704–5706
18. Cha, Y., Murray, C.J. and Klinman, J.P. (1989). Hydrogen tunneling in enzyme reactions. *Science* **243**, 1325–1330
19. Saunders, W.H. (1985). Calculations of isotope effects in elimination reactions. New experimental criteria for tunneling in slow proton transfers. *J. Am. Chem. Soc.* **107**, 164–169
20. Sikorski, R.S., Wang, L., Markham, K.A., Ravi Rajagopalan, P.T., Benkovic, S.J. and Kohen, A. (2004). Tunneling and coupled motion in the *E. coli* dihydrofolate reductase catalysis. *J. Am. Chem. Soc.* **126**, 4778–4779
21. Agrawal, N., Hong, B., Mihai, C. and Kohen, A. (2004). Vibrationally enhanced hydrogen tunneling in the *Escherichia coli* thymidylate synthase catalyzed reaction. *Biochemistry* **43**, 1998–2006

22. Francisco, W.A., Blackburn, N.J. and Klinman, J.P. (2003). Oxygen and hydrogen isotope effects in an active site tyrosine to phenylalanine mutant of peptidylglycine alpha-hydroxylating monooxygenase: mechanistic implications. *Biochemistry* **42**, 1813–1819
23. Maglia, G. and Allemann, R.K. (2003). Evidence for environmentally coupled hydrogen tunneling during dihydrofolate reductase catalysis. *J. Am. Chem. Soc.* **125**, 13372–13373
24. Basran, J., Harris, R.J., Sutcliffe, M.J. and Scrutton, N.S. (2003). H-tunneling in the multiple H-transfers of the catalytic cycle of morphinone reductase and in the reductive half-reaction of the homologous pentaerythritol tetranitrate reductase. *J. Biol. Chem.* **278**, 43973–43982
25. Seymour, S.L. and Klinman, J.P. (2002). Comparison of rates and kinetic isotope effects using PEG-modified variants and glycoforms of glucose oxidase: the relationship of modification of the protein envelope to C–H activation and tunneling. *Biochemistry* **41**, 8747–8758
26. Francisco, W.A., Knapp, M.J., Blackburn, N.J. and Klinman, J.P. (2002). Hydrogen tunneling in peptidylglycine alpha-hydroxylating monooxygenase. *J. Am. Chem. Soc.* **124**, 8194–8195
27. Tsai, S. and Klinman, J.P. (2001). Probes of hydrogen tunneling with horse liver alcohol dehydrogenase at subzero temperatures. *Biochemistry* **40**, 2303–2311
28. Chin, J.K. and Klinman, J.P. (2000). Probes of a role for remote binding interactions on hydrogen tunneling in the horse liver alcohol dehydrogenase reaction. *Biochemistry* **39**, 1278–1284
29. Harris, R.J., Meskys, R., Sutcliffe, M.J. and Scrutton, N.S. (2000). Kinetic studies of the mechanism of carbon-hydrogen bond breakage by the tetrameric sarcosine oxidase of *Arthrobacter* sp. 1-IN. *Biochemistry* **39**, 1189–1198
30. Lewis, E.R., Johansen, E. and Holman, T.R. (1999). Large competitive kinetic isotope effects in human 15-lipoxygenase catalysis measured by a novel HPLC method. *J. Am. Chem. Soc.* **121**, 1395–1396
31. Rickert, K.W. and Klinman, J.P. (1999). Nature of hydrogen transfer in soybean lipoxygenase 1: separation of primary and secondary isotope effects. *Biochemistry* **38**, 12218–12228
32. Karsten, W.E., Hwang, C.C. and Cook, P.F. (1999). Alpha-secondary tritium kinetic isotope effects indicate hydrogen tunneling and coupled motion occur in the oxidation of L-malate by NAD-malic enzyme. *Biochemistry* **38**, 4398–4402
33. Kohen, A., Cannio, R., Bartolucci, S. and Klinman, J.P. (1999). Enzyme dynamics and hydrogen tunnelling in a thermophilic alcohol dehydrogenase. *Nature* **399**, 496–499
34. Basran, J., Sutcliffe, M.J. and Scrutton, N.S. (1999). Enzymatic H-transfer requires vibration-driven extreme tunneling. *Biochemistry* **38**, 3218–3222
35. Antoniou, D., Caratzoulas, S., Kalyanaraman, C., Mincer, J.S. and Schwartz, S.D. (2002). Barrier passage and protein dynamics in enzymatically catalyzed reactions. *Eur. J. Biochem.* **269**, 3103–3112
36. Bahnson, B.J. and Klinman, J.P. (1995). Hydrogen tunneling in enzyme catalysis. *Methods Enzymol.* **249**, 373–397
37. Benkovic, S.J. and Hammes-Schiffer, S. (2003). A perspective on enzyme catalysis. *Science* **301**, 1196–1202
38. Cha, Y., Murray, C.J. and Klinman, J.P. (1989). Hydrogen tunneling in enzyme reactions. *Science* **243**, 1325–1330
39. Klinman, J.P. (1991). Hydrogen tunneling and coupled motion in enzyme reactions. In *Enzyme Mechanism from Isotope Effects*, Cook, P.F. (ed.), pp. 127–148. CRC Press, Boca Raton
40. Klinman, J.P. (1989). Quantum mechanical effects in enzyme-catalysed hydrogen transfer reactions. *Trends Biochem. Sci.* **14**, 368–373

41. Klinman, J.P. (1981). Probes of mechanism and transition-state structure in the alcohol dehydrogenase reaction. *CRC Crit. Rev. Biochem.* **10**, 39–78
42. Klinman, J.P. (1978). Kinetic isotope effects in enzymology. *Adv. Enzymol. Relat. Areas Mol. Biol.* **46**, 415–494
43. Klinman, J.P. (1978). Primary hydrogen isotope effects. In *Transition States of Biochemical Processes*. Gandour, R.D. and Schowen, R.L. (eds), pp. 165–200. Plenum, New York
44. Knapp, M.J. and Klinman, J.P. (2002). Environmentally coupled hydrogen tunneling. Linking catalysis to dynamics. *Eur. J. Biochem.* **269**, 3113–3121
45. Kohen, A. and Klinman, J.P. (1999). Hydrogen tunneling in biology. *Chem. Biol.* **6**, R191–R198
46. Miller, S.M. and Klinman, J.P. (1982). Deduction of kinetic mechanisms from primary hydrogen isotope effects: dopamine beta-monoxygenase – a case history. *Methods Enzymol.* **87**, 711–732
47. Northrop, D.B. (2002). Effects of high pressure on enzymatic activity. *Biochim. Biophys. Acta.* **1595**, 71–79
48. Scrutton, N.S., Basran, J. and Sutcliffe, M.J. (1999). New insights into enzyme catalysis. Ground state tunnelling driven by protein dynamics. *Eur. J. Biochem.* **264**, 666–671
49. Sutcliffe, M.J. and Scrutton, N.S. (2002). A new conceptual framework for enzyme catalysis. Hydrogen tunnelling coupled to enzyme dynamics in flavoprotein and quinoprotein enzymes. *Eur. J. Biochem.* **269**, 3096–3102
50. Sutcliffe, M.J. and Scrutton, N.S. (2000). Enzyme catalysis: over-the-barrier or through-the-barrier? *Trends Biochem. Sci.* **25**, 405–408
51. Bahnson, B.J., Park, D.H., Kim, K., Plapp, B.V. and Klinman, J.P. (1993). Unmasking of hydrogen tunneling in the horse liver alcohol dehydrogenase reaction by site-directed mutagenesis. *Biochemistry* **32**, 5503–5507
52. Bahnson, B.J., Colby, T.D., Chin, J.K., Goldstein, B.M. and Klinman, J.P. (1997). A link between protein structure and enzyme catalyzed hydrogen tunneling. *Proc Natl Acad. Sci. USA* **94**, 12797–12802
53. Bibbs, J.A., Demuth, H.U., Huskey, W.P., Mordy, C.W. and Schowen, R.L. (1988). On the role of quantum tunneling phenomena in the catalytic power of enzymes. *J. Mol. Catal.* **47**, 187–197
54. Kohen, A. and Klinman, J.P. (2000). Protein flexibility correlates with degree of hydrogen tunneling in thermophilic and mesophilic alcohol dehydrogenases. *J. Am. Chem. Soc.* **122**, 10738–10739
55. Zavodszky, P., Kardos, J., Svingor, A. and Petsko, G.A. (1998). Adjustment of conformational flexibility is a key event in the thermal adaptation of proteins. *Proc. Natl Acad. Sci. USA* **95**, 7406–7411
56. Hvidt, A. and Wallevik, K. (1972). Conformational changes in human serum albumin as revealed by hydrogen–deuterium exchange studies. *J. Biol. Chem.* **247**, 1530–1535
57. Karsten, W.E., Gavva, S.R., Park, S.H. and Cook, P.F. (1995). Metal ion activator effects on intrinsic isotope effects for hydride transfer from decarboxylation in the reaction catalyzed by the NAD-malic enzyme from *Ascaris suum*. *Biochemistry* **34**, 3253–3260
58. Huskey, W.P. (1991). Origin of apparent Swain–Schaad deviations in criteria for tunneling. *J. Phys. Org. Chem.* **4**, 361–366
59. Krishtalik, L.I. (1986). *Charge Transfer Reactions in Electrochemical and Chemical Processes*. Consultants Bureau, New York
60. Schowen, R.L. (1988). Structural and energetic aspects of protolytic catalysis by enzymes: charge-relay catalysis in the function of serine proteases. In *Mechanistic Principles of Enzyme Activity*, Liebman, J.F. and Greenberg, A. (eds), pp. 119–168. VCH Publishers, New York

61. Kohen, A., Jonsson, T. and Klinman, J.P. (1997). Effects of protein glycosylation on catalysis: changes in hydrogen tunneling and enthalpy of activation in the glucose oxidase reaction. *Biochemistry* **36**, 2603–2611
62. Miller, S.M. and Klinman, J.P. (1985). Secondary isotope effects and structure–reactivity correlations in the dopamine beta-monooxygenase reaction: evidence for a chemical mechanism. *Biochemistry* **24**, 2114–2127
63. Tian, G., Berry, J.A. and Klinman, J.P. (1994). Oxygen-18 kinetic isotope effects in the dopamine beta-monooxygenase reaction: evidence for a new chemical mechanism in non-heme metallomonooxygenases. *Biochemistry* **33**, 226–234
64. Knapp, M.J., Rickert, K. and Klinman, J.P. (2002). Temperature-dependent isotope effects in soybean lipoxygenase-1: correlating hydrogen tunneling with protein dynamics. *J. Am. Chem. Soc.* **124**, 3865–3874
65. Thibblin, A. and Ahlberg, P. (1989). Reaction branching and extreme kinetic isotope effects in the study of reaction mechanisms. *Chem. Soc. Rev.* **18**, 209–224
66. Garcia-Viloca, M., Gao, J., Karplus, M. and Truhlar, D.G. (2004). How enzymes work: analysis by modern rate theory and computer simulations. *Science* **303**, 186–195
67. Truhlar, D.G., Gao, J., Alhambra, C., Garcia-Viloca, M., Corchado, J., Sanchez, M.L. and Villa, J. (2002). The incorporation of quantum effects in enzyme kinetics modeling. *Acc. Chem. Res.* **35**, 341–349
68. Gao, J. and Truhlar, D.G. (2002). Quantum mechanical methods for enzyme kinetics. *Annu. Rev. Phys. Chem.* **53**, 467–505
69. Kuznetsov, A.M. and Ulstrup, J. (1999). Proton and hydrogen atom tunnelling in hydrolytic and redox enzyme catalysis. *Can. J. Chem.* **77**, 1085–1096
70. Powell, M.F. and Bruice, T.C. (1983). Effect of isotope scrambling and tunneling on the kinetic and product isotope effects for reduced nicotinamide adenine dinucleotide model hydride transfer reactions. *J. Am. Chem. Soc.* **105**, 7139–7149
71. Doll, K.M., Bender, B.R. and Finke, R.G. (2003). The first experimental test of the hypothesis that enzymes have evolved to enhance hydrogen tunneling. *J. Am. Chem. Soc.* **125**, 10877–10884
72. Doll, K.M. and Finke, R.G. (2003). A compelling experimental test of the hypothesis that enzymes have evolved to enhance quantum mechanical tunneling in hydrogen transfer reactions: the beta-neopentylcobalamin system combined with prior adocobalamin data. *Inorg. Chem.* **42**, 4849–4856
73. Rodgers, J., Femec, D.A. and Schowen, R.L. (1982). Isotopic mapping of transition-state structural features associated with enzymic catalysis of methyl transfer. *J. Am. Chem. Soc.* **104**, 3263–3268
74. Evans, J.P., Ahn, K. and Klinman, J.P. (2003). Evidence that dioxygen and substrate activation are tightly coupled in dopamine β -monooxygenase. *J. Biol. Chem.* **278**, 49691–49698
75. Chen, P. and Solomon, E.I. (2004). Oxygen activation by the noncoupled binuclear copper site in peptidylglycine- α -hydroxylating monooxygenase. Reaction mechanism and role of the noncoupled nature of the active site. *J. Am. Chem. Soc.* **126**, 4991–5000
76. Glad, S.S. and Jensen, F. (1997). Kinetic isotope effects and transition state geometries. A theoretical investigation of E2 model systems. *J. Org. Chem.* **62**, 253–260
77. Albery, W.J. and Knowles, J.R. (1977). The determination of the rate-limiting step in a proton-transfer reaction from the breakdown of the Swain–Schaad relation. *J. Am. Chem. Soc.* **99**, 637–638

One- and two-electron oxidations and reductions of organoselenium and organotellurium compounds

MICHAEL R. DETTY[†] and MARGARET E. LOGAN[‡]

[†]*Department of Chemistry, University at Buffalo, The State University of New York, Buffalo, New York, USA*

[‡]*Department of Chemistry, SUNY College at Brockport, Brockport, New York, USA*

1	Introduction	79
2	Two-electron oxidations and reductions of selenium and tellurium compounds	80
	Diorganochalcogenides and diorganochalcogen(IV) dihalides	80
	Dehalogenation of <i>vicinal</i> -organic dihalides	91
	Halogenation of organic substrates with chalcogen(IV) dihalides	97
	Organochalcogen(II) and organochalcogen(IV) compounds with an odd number of ligands	100
	Oxidation of thiols and related compounds with organoselenium(IV) and organotellurium(IV) compounds	102
	Other oxidations with selenoxides and telluroxides	106
	Thiolperoxidase and haloperoxidase-like activity of organoselenides and organotellurides	108
	Electrochemical reduction of diorganotellurium(IV) species	113
3	One-electron oxidation of selenium and tellurium compounds	117
	Diarylselenides and tellurides	118
	Alkylarylselenides and tellurides	126
	Dialkylselenides and tellurides	131
	Heterocyclic selenides and tellurides: selected examples	137
	Antioxidant activity in functional assays	138
	References	140

1 Introduction

Oxidation and reduction reactions of organotellurium and organoselenium compounds have provided much varied and interesting chemistry with respect to not only physical organic studies, but also to synthetic transformations. One electron oxidation to selenium- and tellurium-centered radical cations has allowed the comparison of substituent effects in various organoselenides and tellurides to the corresponding sulfides and oxygen-containing molecules. These studies have allowed comparison of selenides and tellurides as antioxidants in “functional assays” such as their ability to prevent oxidative chemical processes in azo-initiated

linoleic acid oxidation. Two-electron oxidations of organotellurium(II) and organoselenium(II) compounds to the corresponding chalcogen(IV) compounds have been examined kinetically and, through the process of microscopic reversibility, have provided insight into the two-electron, reductive elimination process from chalcogen(IV) to chalcogen(II). Organochalcogen(II) compounds have been used as synthetic reagents for the dehalogenation of *vicinal*-dihalides and for the reduction of α -halo ketones. Organochalcogen(IV) compounds have been utilized as halogenating agents and as mild oxidants for a variety of transformations.

The oxidations and reductions of organochalcogen compounds all involve the lone-pairs of electrons associated with the chalcogen atoms. These lone-pairs are stereochemically active, which provides well-defined geometries for many of the intermediate species described herein. Oxidized organochalcogen compounds also are stabilized by lone-pair donation from neighboring heteroatoms, which again leads to unusual structures with well-defined geometries as described herein.

2 Two-electron oxidations and reductions of selenium and tellurium compounds

DIORGANOCHALCOGENIDES AND DIORGANOCHALCOGEN(IV) DIHALIDES

One of the oldest general reactions of diorganoselenium(II) and diorganotellurium(II) compounds is the oxidative addition of halogens (F_2 , Cl_2 , Br_2 , and I_2) to these materials to give chalcogen(IV) adducts as shown in equations (1) and (2).¹⁻³ For many years, the resulting diorganoselenium(IV) and tellurium(IV) compounds were drawn as molecular association complexes without defining the covalent or ionic bonding in the systems. McCullough and co-workers determined the crystallographic structures of diorganochalcogen(IV) dihalides **1-5** (Fig. 1), which defined

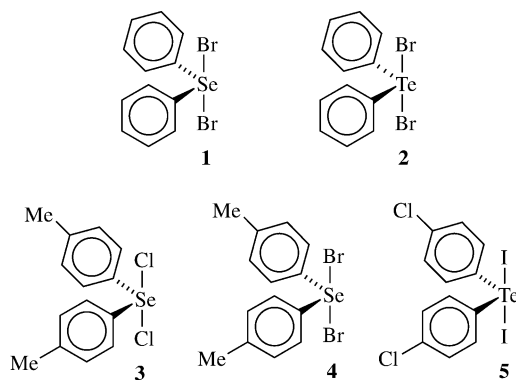
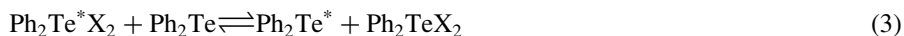


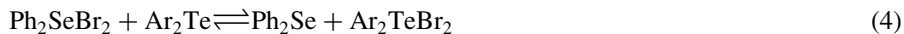
Fig. 1 Representative trigonal bipyramidal diaryltellurium(IV) and selenium(IV) dihalides that have been characterized by X-ray crystallography.

the general structures of molecules of this type:^{4–7} trigonal bipyramids with the selenium or tellurium atom occupying the center, the two organic groups and a lone-pair of electrons occupying the equatorial positions, and the two halogen atoms occupying the axial positions. The halogen–chalcogen–halogen array is nearly linear in these systems and is bent roughly 10–20° away from the equatorial lone-pair of electrons. The chalcogen–halogen bond lengths are long and are typical of “hypervalent” chalcogen–halogen bonds that are half ionic and half covalent.^{8,9} These types of bonds have also been referred to as three-center, four-electron bonds and the bond strengths increase as the difference in electronegativity increases between the central atom and the two electronegative ligands.^{8,9}



The reactions depicted in equations (1) and (2) seem innocently simple: a two-electron oxidation of the chalcogen atom with heterolytic or homolytic cleavage of the halogen–halogen bond. However, mechanistic details for these conversions have been developed only recently. The diorganochalcogen(IV) dihalides often crystallize from the reaction mixture, which drives any equilibria associated with the reaction toward products. In point of fact, however, the oxidative addition of halogen to diorganoselenium(II) and diorganotellurium(II) species has been shown to be reversible and involves rate-determining cleavage of a chalcogen–halogen bond in the reverse direction. Through the principle of microscopic reversibility, mechanistic details learned from oxidative addition or reductive elimination in one direction should be applicable to the opposite process in the other direction. The rates of tellurium–halogen exchange between diphenyltellurium(IV) dihalides and diphenyltelluride (equation (3)) suggest that the bond strengths of the Te–X bonds decrease in the following order: Te–F > Te–Cl > Te–Br > Te–I.^{10,11} One would expect similar orderings in the comparison of Se–X bond strengths, although these bonds should be weaker than the corresponding Te–X bonds, in part, because selenium is more electronegative than tellurium.¹² Experimentally, heating a solution of di-4-methoxyphenyltelluride with diphenylselenium(IV) dibromide (**1**) gives a new solution of diphenylselenide and di-4-methoxyphenyltellurium(IV) dibromide, which is consistent with weaker Se–Br bonds relative to Te–Br bonds (equation (4)). The addition of bromide to a solution of diphenylselenium(IV) dibromide (**1**) gives proton NMR spectra consistent with a mixture of diphenylselenium(IV) dibromide (**1**), diphenylselenide, and tribromide anion (equation (5)).¹² The addition of more bromide drives the equilibrium shown in equation (5) to the right. Heating crystals of diphenylselenium(IV) dibromide (**1**) to 200 °C under a stream of nitrogen gives melting, bromine gas evolution, and isolation of diphenylselenide.¹²





More quantitative energetics for oxidative addition/reductive elimination of halogen from diorganotellurides come from kinetic studies of reductive elimination of chlorine from dyes **6–11** as shown in Fig. 2. Arrhenius and Eyring activation parameters and selected rate constants are compiled in Table 1.^{14,15} As shown in equations (1) and (2), the addition of halogen is a reversible process. However, thermally induced reductive elimination from a diorganochalcogen(IV) dihalide will be limited by the equilibrium constants associated with the process. If the evolved halogen can be scavenged or eliminated efficiently in the reductive elimination direction, then the kinetics of reductive elimination can be monitored more effectively. The trimethine backbone of chalcogenopyrylium dyes related in structure to dyes **6–11** is rapidly halogenated by chlorine or bromine to give halogenated compounds **12** and/or **13**.¹⁶ The rate constants are sufficiently large ($\approx 10^{4-5} \text{ M}^{-1} \text{ s}^{-1}$)¹⁶ that the side chain halogenation can compete with reoxidation of the tellurium atom in these dyes. The initiation of reductive elimination in **6–11** is followed by halogenation of the trimethine backbone and by diffusion of the halogen away from the tellurium(II) center, which allows the reductive elimination to proceed to completion. The data in Table 1 show a range of values of k , the first-order rate constant for reductive elimination, of $5.2 \times 10^{-5} - 1.2 \times 10^{-3} \text{ s}^{-1}$, E_a of 73–100 kJ mol^{-1} and Eyring activation parameters of 70–97 kJ mol^{-1} for ΔH^\ddagger and -4 to 66 $\text{J mol}^{-1} \text{ K}^{-1}$ for ΔS^\ddagger .

In the tellurium(IV) oxidation state, the 5p orbital of the tellurium(IV) atom is involved in the three-center, four-electron bonding to the halides and cannot interact with the carbon π -framework. Long-wavelength absorption maxima for **6–11** are found between 515 and 565 nm in dichloromethane.¹⁴ Reductive elimination generates the tellurium(II) oxidation state in compounds **12** and **13**. The tellurium(II) 5p orbital can now overlap with the carbon π -framework and long-wavelength absorption maxima for **12** and **13** are observed between 765 and 830 nm in dichloromethane. The rate of loss of the 515–565 nm band and the rate of appearance of the 765–830 nm band are identical, which is consistent with reductive elimination as the rate-determining step of this process.

Several trends emerge in these data: (1) The reductive elimination of bromine is 6–13 kJ mol^{-1} more facile than reductive elimination of chlorine in similar structures, which is consistent with weaker chalcogen–bromine bonds relative to chalcogen–chlorine bonds.^{14,15} (2) The reductive elimination of chlorine is accelerated by the presence of a chloride counterion as opposed to a less nucleophilic counterion such as hexafluorophosphate.¹⁴ (3) The rate of reductive elimination is accelerated by the presence of a more polar solvent (acetonitrile) relative to tetrachloroethane,¹⁴ which is consistent with development of charge in the rate-determining step. These observations suggest mechanisms for oxidative

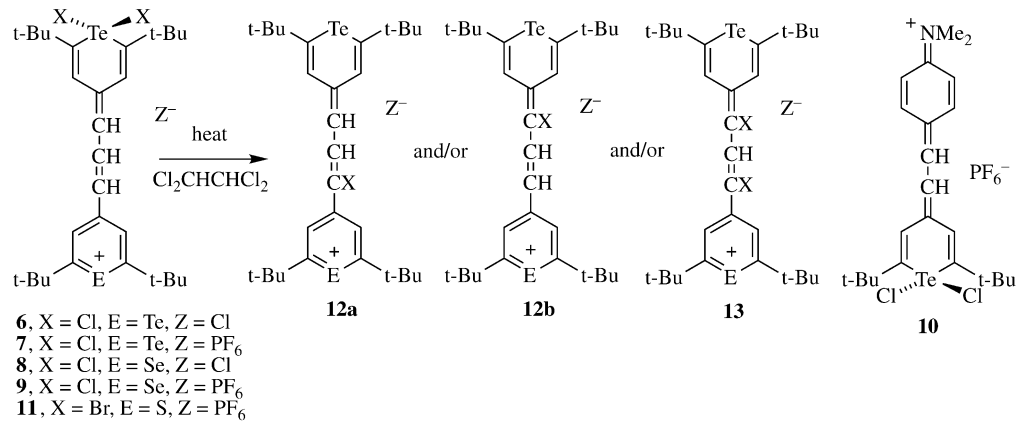
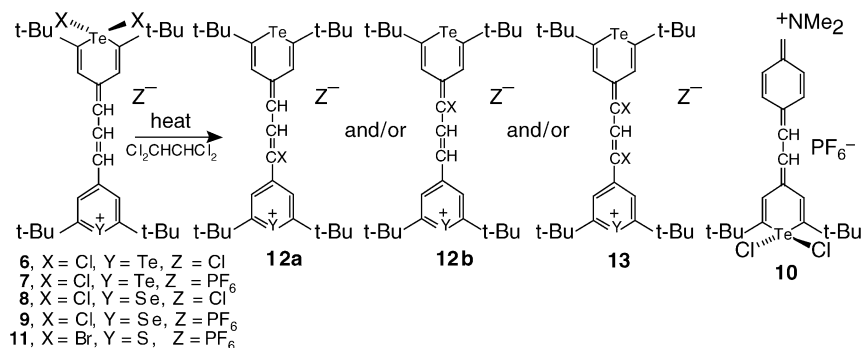


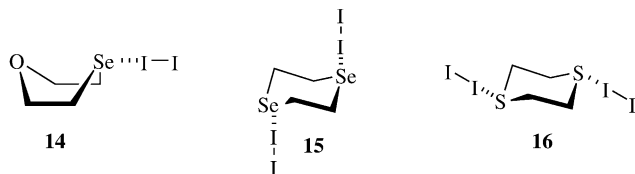
Fig. 2 Reductive elimination of halogens from chalcogenopyrylium dyes **6–11** containing tellurium(IV) dihalide groups.

Table 1 Arrhenius and Eyring activation parameters for the reductive elimination of halogens from chalcogenopyrylium dyes containing tellurium(IV) dihalide groups

Compound	$k \pm 2\sigma$ at 348 K (s ⁻¹)	ΔH^\ddagger (kJ mol ⁻¹)	ΔS^\ddagger (J K ⁻¹ mol ⁻¹)	E_a (kJ mol ⁻¹)	Reference
6	$(4.44 \pm 0.01) \times 10^{-4}$	86 ± 2	33 ± 4	88 ± 2	14
7	$(5.20 \pm 0.01) \times 10^{-5}$	89 ± 1	29 ± 8	93 ± 1	14
8	$(1.20 \pm 0.02) \times 10^{-3}$	94 ± 1	66 ± 24	97 ± 1	14
9	$(7.17 \pm 0.01) \times 10^{-5}$	97 ± 1	54 ± 16	100 ± 1	14
10	$(1.15 \pm 0.02) \times 10^{-3}$	70 ± 2	-4 ± 12	73 ± 2	14
11	$(1.23 \pm 0.02) \times 10^{-3}$	83 ± 2	37 ± 10	87 ± 2	15

addition/reductive elimination of halogens to diorganochalcogenides involving ionic intermediates, halogen–halogen bonding in some intermediate, and rate constants/equilibria driven by chalcogen–halogen bond strengths.

Some mechanistic insights into oxidative addition were gained from studies of iodine–chalcogen complexes that do not form trigonal bipyramidal products with linear iodine–chalcogen–iodine arrays. While diaryltellurium(IV) diiodide **5** (Fig. 1) illustrates the trigonal bipyramidal product formed by oxidative addition of iodine across the tellurium atom of di-4-chlorophenyltelluride,⁷ comparable products are unknown for the addition of iodine to diorganoselenides and sulfides. Linear chalcogen–iodine–iodine arrays have been observed by X-ray crystallographic analysis for the addition of iodine to 1-chalcogen-4-selenanes **14**, 1,4-diselenanes **15**, and 1,4-dithianes **16** as illustrated in Fig. 3.^{17–20} Dissociation

**Fig. 3** Linear chalcogen–iodine–iodine arrays determined by X-ray crystallography.

constants show that selenium–iodine complexes ($K_C \approx 5 \times 10^{-4} \text{ M}$) are stronger than the corresponding sulfur–iodine complexes ($K_C \approx 5 \times 10^{-3} \text{ M}$).²⁰ Even though comparable tellurium–iodine analogues of **14–16** have not been characterized, one might postulate their existence along the path to trigonal bipyramidal derivatives such as **5**.²¹ Cleavage of the iodine–iodine bond would generate $[\text{R}_2\text{Te}-\text{I}]^+ \text{I}^-$ or $[\text{R}_2\text{Se}-\text{I}]^+ \text{I}^-$ species, which might then form a new chalcogen–iodine bond to complete the trigonal bipyramid in the case of organotellurium derivatives.

Physical evidence for the involvement of $[\text{R}_2\text{Te}-\text{X}]^+ \text{X}^-$ or $[\text{R}_2\text{Se}-\text{X}]^+ \text{X}^-$ species comes from X-ray crystallographic studies of iodotelluronium²² and bromotelluronium¹² species. The addition of iodine or bromine to phenyl *N,N*-dimethyl-2-(aminomethyl)phenyltelluride (**17**) gives tellurium(IV) derivative **18** or **19**, respectively (Fig. 4), bearing a formal positive charge. The amino substituent acts as a chelating ligand to the tellurium(IV) center and the nitrogen–tellurium–halogen array is nearly linear.^{12,22} In both examples, the halide counterion is orthogonal to the more covalent tellurium–halogen bond and the distance between the tellurium atom and the halide anion is just under the sum of van der Waals' radii. The intramolecular chelation by the amino substituent blocks the addition of the halide anion to give the halogen–tellurium–halogen linear array found in the examples of Fig. 1.

The structural studies of the various diorganotellurium(IV) and selenium(IV) species provide physical evidence for logical intermediates in the oxidative addition of halogens to diorganochalcogenides. Stopped-flow studies of the kinetics of oxidative addition of bromine¹² and iodine²¹ show several discrete, intermediate reactions leading to the final oxidative addition products. The oxidative additions of bromine to diphenylselenide to give diphenylselenium(IV) dibromide (**1**), to dicyanomethylidene telluropyran **20** to give tellurium(IV) dibromide **21**, and to telluropyranone **22** to give tellurium(IV) dibromide **22a** all display an initial, fast reaction that follows second-order kinetics overall (first-order in chalcogenide and first-order in bromine) followed by a slower, first-order process that is independent of bromine concentration.

As shown in Fig. 5, the initial fast reaction is the association of bromine with the chalcogen atom to form the η_1 -complex of bromine with diphenylselenide, dicyanomethylidene telluropyran **20**, and telluropyranone **22**. These structures are analogous to the 1,4-diselenane iodine complex **15** (Fig. 3), whose structure has been characterized by X-ray crystallography. The second-order rate constants are on the

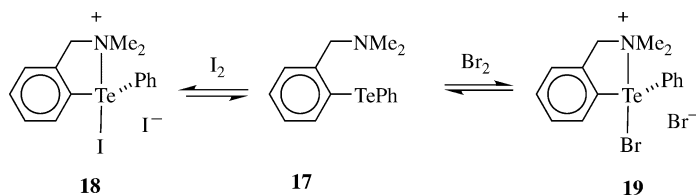


Fig. 4 Halotelluronium species stabilized by intramolecular chelation formed by oxidative addition of halogens to *N,N*-dimethyl-2-(aminomethyl)phenyl phenyltelluride (**17**).

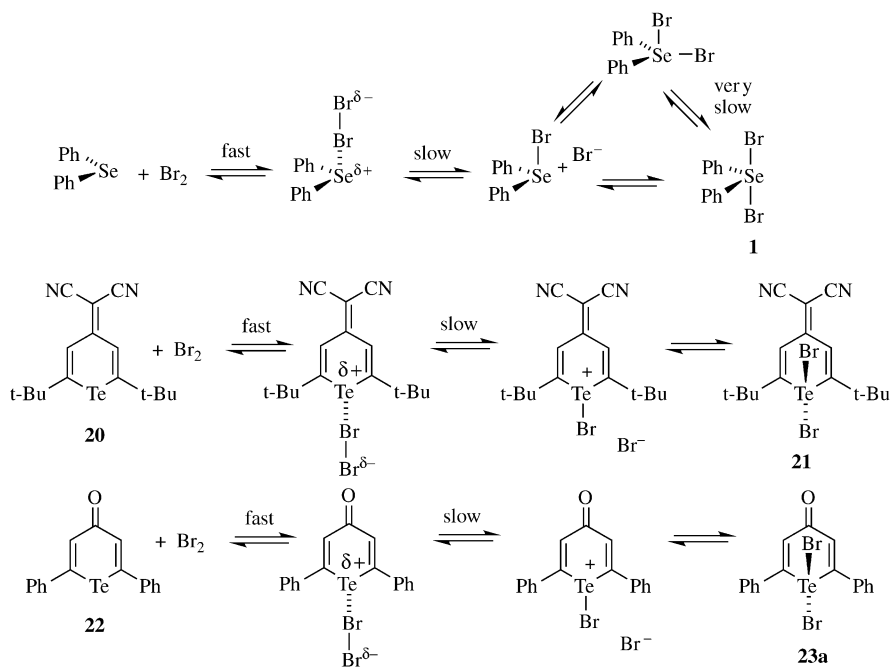


Fig. 5 Plausible mechanistic path for the oxidative addition of bromine to diphenylselenide, dicyanomethylidene telluropyran **20**, and 2,6-diphenyltelluropyran-4-one (**22**) based on stopped-flow kinetics. An initial fast reaction followed second-order kinetics (first order in both bromine and substrate) while a second, slow reaction followed first-order kinetics. For diphenylselenide, a third very-slow reaction was observed.

order of $2 \times 10^3 \text{ M}^{-1} \text{ s}^{-1}$ to $4 \times 10^3 \text{ M}^{-1} \text{ s}^{-1}$. More electron-rich diorganotellurides such as diphenyltelluride (**23**) are much more reactive with second-order rate constants $\geq 10^8 \text{ M}^{-1} \text{ s}^{-1}$ for the association with bromine.¹² These reactions are entropy driven with values of E_a and ΔH^\ddagger near 0 kJ mol^{-1} and values of ΔS^\ddagger between -200 and $-220 \text{ J K}^{-1} \text{ mol}^{-1}$.¹²

The second, slower reaction represents the ionic dissociation of the η_1 -association complex to form bromoselenonium and bromotelluronium intermediates. These intermediates should be similar in structure to iodotelluronium salt **18** and bromotelluronium salt **19** for which X-ray crystallographic structures have been determined.^{12,22} Values of the rate constant, k , are comparable in all three molecules with values of $(4.4 \pm 0.1) \times 10^{-1} \text{ s}^{-1}$ for diphenylselenide, $(2.28 \pm 0.03) \times 10^{-2} \text{ s}^{-1}$ for **20**, and $(3.81 \pm 0.04) \times 10^{-2} \text{ s}^{-1}$ for **22** at 284 K. The slow reaction for the addition of bromine to **22** was discernable over a 20-K temperature range, which allowed activation parameters of $63.0 \pm 0.8 \text{ kJ mol}^{-1}$ for E_a (Table 2), $60.6 \pm 0.8 \text{ kJ mol}^{-1}$ for ΔH^\ddagger (Table 2) and $-54 \pm 12 \text{ J K}^{-1} \text{ mol}^{-1}$ for ΔS^\ddagger to be determined.¹²

Table 2 Arrhenius and Eyring activation parameters for the second, “Slow” reaction observed by stopped-flow spectroscopy in the oxidative addition of halogens to diorgano tellurides **17**, **20**, and **23–25**

Compound	Halogen	Solvent	$k \pm 2\sigma$ at 284 K (s^{-1})	ΔH^\ddagger ($kJ\ mol^{-1}$)	E_a ($kJ\ mol^{-1}$)	Reference
17	I_2	CCl_4	$(1.11 \pm 0.01) \times 10^{-3}$	21.2 ± 0.08	25.2 ± 0.8	21
		EtOAc	$(1.3 \pm 0.3) \times 10^{-1}$	28 ± 2	32 ± 2	21
20	Br_2	CCl_4	$(3.81 \pm 0.04) \times 10^{-2}$	60.6 ± 0.8	63.0 ± 0.8	12
23	I_2	CCl_4	$(1.6 \pm 0.1) \times 10^{-3}$	67 ± 2	71 ± 2	21
		EtOAc	$(4.9 \pm 0.2) \times 10^{-2}$	67 ± 2	48 ± 2	21
24	I_2	CCl_4	$(3.9 \pm 0.3) \times 10^{-3}$	28.5 ± 0.8	31.9 ± 0.8	21
		EtOAc	$(2.2 \pm 0.1) \times 10^{-1}$	48 ± 2	52 ± 2	21
		CH_3CN	1.25 ± 0.02	9 ± 1	13 ± 1	21
25	I_2	CCl_4	$(2.6 \pm 0.9) \times 10^{-3a}$	23.6 ± 0.4	27.4 ± 0.4	21

^aAt 293 K.

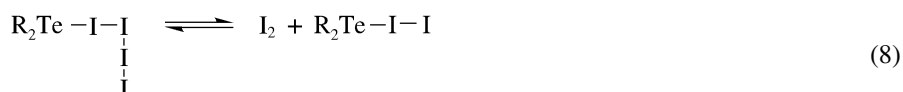
For diphenylselenide and dicyanomethylidene telluropyran **20**, a third, very slow, first-order reaction was discerned. At 284 K, rate constants, k , for this process are $(2.4 \pm 0.1) \times 10^{-3} s^{-1}$ for diphenylselenide and $(2.02 \pm 0.02) \times 10^{-3} s^{-1}$ for **20**. In the collapse of the bromoselenonium bromide or bromotelluronium bromide intermediates to the covalent diorganochalcogen dibromide final products, it might be possible to form a kinetic mixture of initial products in which both linear bromine–chalcogen–bromine and orthogonal bromine–chalcogen–bromine bonds are formed. As noted above in the X-ray crystallographic structures of **18** and **19**, the non-bonding halide ion is less than Van der Waals’ radii away from the tellurium atom and is located orthogonal to the tellurium–halogen bond.^{12,22} The third, very slow reaction may represent conversion from a kinetic mixture of products to a thermodynamic mixture of products via reionization or pseudorotation. This process is illustrated in Fig. 5 for the oxidative addition of bromine to diphenylselenide.

The oxidative addition of iodine to diorganotellurides has also been examined by stopped-flow spectroscopy.²¹ The initial fast reaction of iodine with diphenyltelluride (**23**), di-4-methoxyphenyltelluride (**24**), *N,N*-dimethyl-2-(aminomethyl)phenyltelluride (**17**), and 2,6-di-tert-butyltelluropyran-4-one (**25**) displays inverted Arrhenius behavior (negative values of E_a), which is consistent with a pre-equilibrium involving higher-order iodine species as shown in equation (6). The “ I_4 ” species is the actual oxidant for diorganotellurides as shown in equation (7). Thus, the initial reaction is formation of the η_1 -association complex of I_4 with the

diorganotelluride. Chalcogen–I₄ complexes have been characterized by X-ray crystallography for triphenylphosphine sulfide complex **26** and ethylenethiourea complex **27** (Fig. 6).^{23–25} Covalent complexes of R₂Te–I₄ have been claimed and have been described as having intact I–I bonds by spectroscopic analysis for complexes with telluracyclopentane²⁶ and telluracyclohexane (tellurane).²⁷



In order to give products of oxidative addition, the initial R₂Te–I₄ complex must dissociate to give iodotelluronium ([R₂Te–I]⁺) intermediates. The initial “fast” reaction with iodine is followed by a slow, first-order reaction as was observed with bromination.²¹ Dissociation of the R₂Te–I₄ complex can follow two pathways. In one, as shown in equations (8) and (9), dissociation of the R₂Te–I₄ complex to I₂ and R₂Te–I₂ is followed by ionic dissociation. Alternatively, the R₂Te–I₄ complex may dissociate directly to [R₂Te–I]⁺ and I₃[–] species as shown in equation (10). Based on the effects of added iodide described below, the pathway depicted by equations (8) and (9) is most likely being followed.



The second-order rate constant for the reaction of iodide and iodine is $6.2 \times 10^9 \text{ M}^{-1} \text{ s}^{-1}$ in water at 298 K while the first-order rate constant for the dissociation of triiodide is $8.5 \times 10^6 \text{ s}^{-1}$ at 298 K.²⁸ The dissociation constant, K_C , for this reaction is on the order of 10^{-3} M for the dissociation of triiodide,^{28,29} which is comparable in magnitude to K_C for the R₂Se–I₂ complexes ($5 \times 10^{-3} \text{ M}$).²⁰ Consequently, added iodide should compete for iodine as effectively as the diorganochalcogenides and limit the available concentration of I₄ *in situ*. Thus, equation (9) must be followed to a greater extent in the presence of added iodide.

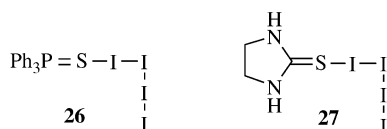


Fig. 6 Chalcogen–I₄ complexes that have been characterized by X-ray crystallography.

The rate constant for the second, “slow” reaction was identical for the addition of iodine to di-4-methoxyphenyltelluride (**24**) in the presence or absence of iodide.²¹

The second, “slow” reaction was followed for **17** and **23–25** in several solvents at several different reaction temperatures.²¹ Arrhenius and Eyring activation parameters for the second, “slow” reaction observed in the addition of iodine to **17** and **23–25** along with those for the addition of bromine to compound **20** are compiled in Table 2. In the examples of Table 2, the rate of reaction increases as the polarity of the solvent increases from CCl₄ to EtOAc to CH₃CN. The “slow” reaction remains first-order in all three solvents. For di-4-methoxyphenyltelluride (**24**), values of E_a and ΔH^\ddagger in CH₃CN are 20–40 kJ mol⁻¹ lower than in CCl₄ or EtOAc. Again, the data from the kinetics studies are consistent with the formation of an ionic intermediate via a dissociative process.

The oxidative addition of halogens to diorganochalcogenides can be summarized as shown in Fig. 7. The initial step is formation of an η_1 -association complex of chalcogen atom with X₂ or a higher-order X₄ halogen species. The rate of initial reaction is dependent on both the concentration of the diorganochalcogenide and the halogen and has very low values for E_a and ΔH^\ddagger and a large, negative value for ΔS^\ddagger . The initial η_1 -association complex then undergoes a first-order, dissociative process to generate a haloselenonium or halotelluronium intermediate. This process has small, positive values of E_a and ΔH^\ddagger and a small, negative value for ΔS^\ddagger . Dissociation of the η_1 -association complex may involve initial loss of X₂ from the X₄ complex prior to dissociation. Collapse of the haloselenonium or halotelluronium intermediate leads to the final diorganoselenium(IV) dihalide or diorganotellurium(IV) dihalide products. The major, thermodynamic product has a trigonal bipyramidal structure with the selenium or tellurium atom occupying the center, the two organic groups and a lone-pair of electrons occupying the equatorial positions, and the two halogen atoms occupying the axial positions. The minor product or, perhaps, a kinetic product, has two orthogonal chalcogen–halogen bonds. If the

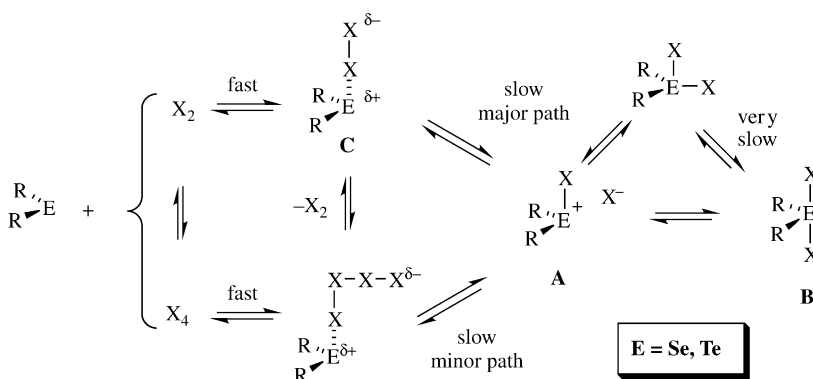


Fig. 7 A summary of oxidative addition of halogens to diorganoselenides and tellurides.

kinetic product mixture is different from the thermodynamic product mixture, the interconversion of the two chalcogen(IV) species can sometimes be observed as a very slow first-order process.

The general mechanism shown in Fig. 7 has implications for all of the redox chemistry associated with diorganochalcogen(II)/diorganochalcogen(IV) complexes as summarized in Fig. 8. The selenium or telluronium intermediate labeled **A** can arise via electrophilic attack of an electrophile on the diorganochalcogen(II) compound or, from microscopic reversibility, via loss of a ligand from the trigonal bipyramidal species **B**. Protonation of a telluroxide or selenoxide leads to hydroxyselenonium and hydroxytelluronium intermediates. Formation of a haloselenonium or halotelluronium intermediate provides a species capable of functioning as a halogenating agent. In the reverse direction, the diorganochalcogen compound can capture the halogen from a halonium ion intermediate and lead to net dehalogenation of *vicinal*-dihalides. Both of these reactions are discussed below.

The reductive elimination reactions of halogen from **6–11** illustrate several examples of ligand loss from trigonal bipyramidal species **B** to generate onium species **A**. Activation parameters in these processes were E_a of 73 to 100 kJ mol⁻¹ and Eyring activation parameters of 70–97 kJ mol⁻¹ for ΔH^\ddagger and -4 to 66 J mol⁻¹ K⁻¹ for ΔS^\ddagger . Thermal reactions of compounds **18** and **19** (Fig. 4) illustrate the cleavage of an unsymmetrical trigonal bipyramidal species **B'** (Fig. 8). Variable temperature ¹H NMR studies show that the tellurium–nitrogen bond is broken to allow the interconversion of **18** and **19** to their mirror images as shown in Fig. 9.²² In these two systems, the lone-pair on tellurium is stereochemically active. The processes were strictly first-order in the sense that reaction rates were identical over a five-fold range of concentrations. Activation parameters of 52 ± 1 kJ mol⁻¹ for E_a , 50 ± 1 kJ mol⁻¹ for ΔH^\ddagger , and -33 ± 17 J K⁻¹ mol⁻¹ for ΔS^\ddagger were measured for **18** and activation parameters of 62 ± 2 kJ mol⁻¹ for E_a ,

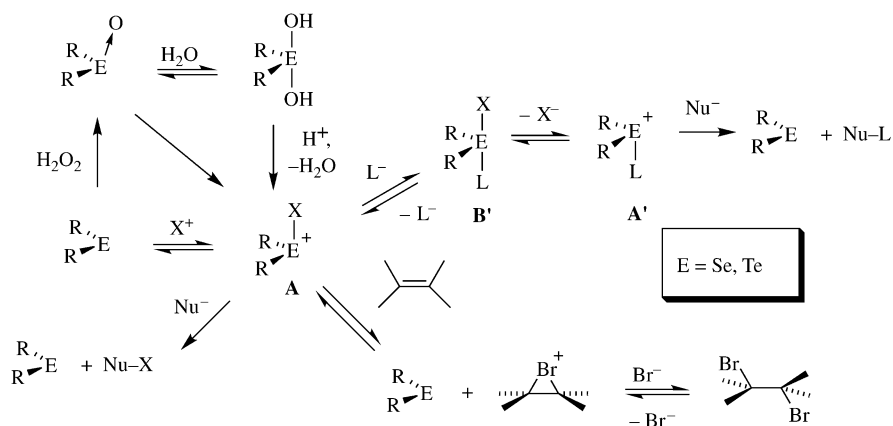


Fig. 8 Redox reactions associated with halotelluronium and hydroxytelluronium intermediates.

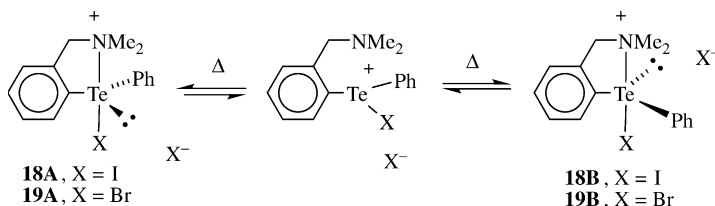


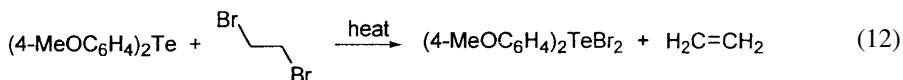
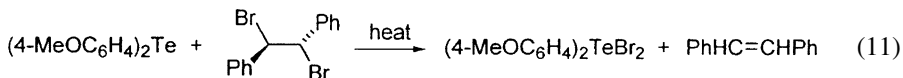
Fig. 9 Interconversion of enantiomers of *N,N*-dimethyl-2-(aminomethyl)phenyl iodo-telluronium iodide (**18**) and *N,N*-dimethyl-2-(aminomethyl)phenyl bromotelluronium bromide (**19**).

$60 \pm 2 \text{ kJ mol}^{-1}$ for ΔH^\ddagger , and $-8 \pm 21 \text{ J K}^{-1} \text{ mol}^{-1}$ for ΔS^\ddagger were measured for **19**. For the cleavage of a tellurium–halogen bond with separation of charge in **6–11**, values of ΔG^\ddagger_{298} fall in the range 71 to 81 kJ mol^{-1} . For **18** and **19**, cleavage of the tellurium–nitrogen bond with no separation of charge give values of ΔG^\ddagger_{298} of 60 kJ mol^{-1} for **18** and 62 kJ mol^{-1} for **19**.²²

Formation of the onium intermediates **A** allows ligand substitution at the chalcogen(IV) atom. Addition of a new ligand, L^- , forms a new trigonal bipyramidal intermediate, **B'**, which can form a new onium intermediate, **A'**, with onium ligand L via loss of X^- . Nucleophilic attack at L^- in **B'** (via intermediate or transition state **C** in Fig. 7) gives formal oxidation of the ligand L^- and reductive elimination at the chalcogen atom. The oxidation of thiols to disulfides with tellurium(IV) species and the oxidation of halide ions to positive halogen species with dihydroxy tellurium(IV) species are examples of this latter transformation. These examples are both discussed below as well.

DEHALOGENATION OF VICINAL-ORGANIC DIHALIDES

In 1960, Campos and Petragrani reported the dehalogenation of *vicinal*-dibromides with diaryltellurides in very high yields.³⁰ Two examples are shown in equations (11) and (12). These reactions represent a formal reduction of the *vicinal*-dibromide with oxidation of tellurium(II) to tellurium(IV). It has also been reported that diaryl ditellurides give the same transformations with the formation of tellurium metal in addition to the alkene and the corresponding diaryltellurium(IV) dibromide.³¹ The high temperatures associated with the diaryl ditelluride reactions most likely give initial detelluration to the corresponding diaryltelluride and tellurium metal. The diaryltelluride then enters into the debromination reactions of *vicinal*-dibromides. Diaryltellurides are also successful reducing agents for the reduction of FeCl_3 , CuCl_2 , and HgCl_2 giving the corresponding diaryltellurium(IV) dichloride.³²



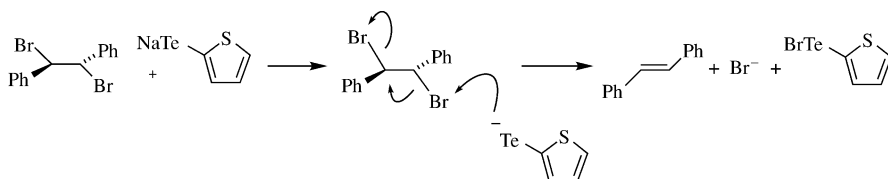


Fig. 10 Plausible mechanism for debromination of *vicinal*-dibromides with 2-thienyltelluride.

A variety of other organotellurium reagents have been used in the debrominations of *vicinal*-dibromides^{33–39} and the dehalogenation of α -haloketones.⁴⁰ Mechanistically, Engman's sodium 2-thienyltelluride³⁹ appears to follow a concerted reaction pathway as shown in Fig. 10 for *vicinal*-dibromides derived from terminal and 1,2-disubstituted alkenes. Nucleophilic attack of the telluride anion at a halogen atom of the *vicinal*-dihalide in an E2-like process (anti-periplanar loss of halogen) gives alkene formation with formal loss of X_2 . More highly substituted *vicinal*-dihalides may follow a different mechanism as described below. Other nucleophilic, dehalogenating agents of *vicinal*-dihalides such as iodide are thought to follow a path similar to the one shown in Fig. 10.^{41,42} Li and Harpp's bis(triphenylstannyl) telluride⁴⁰ follows a similar mechanism as shown in Fig. 11. Nucleophilic attack of the telluride anion at the halogen atom of an α -haloketone generates the dehalogenated enolate anion and a tellurenyl halide. Protonation of the enolate anion generates the reduced ketone.

Debrominations of *vicinal*-dibromides with diorganotellurides appear to follow a different mechanism than that shown in Fig. 10.⁴³ Like debrominations with iodide or telluride anions, debrominations with diorganotellurides follow second-order kinetics and are first-order in both telluride and dibromide. In terms of absolute rates, the anionic iodide and 2-thienyltelluride anions are more nucleophilic than the uncharged diorganotellurides and, consequently, give faster rates of debromination. However, if a similar mechanism were being followed, one would expect the relative rates for debromination of similar substrates to be comparable or, at least, to follow the same trend. Debrominations of *vicinal*-dibromides **27–30** with

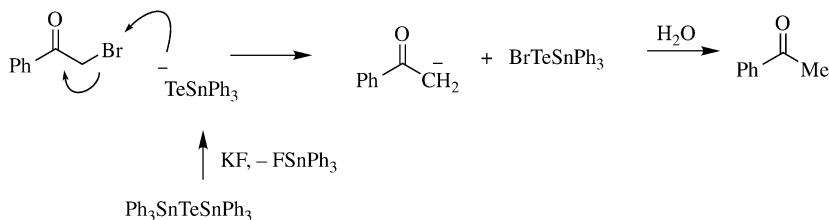
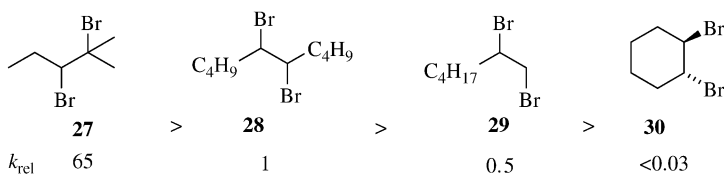


Fig. 11 Plausible mechanism for the debromination of organic substrates with bis(triphenylstannyl) telluride.

di-*n*-hexyltelluride (**26**) followed different relative orderings in comparison to debrominations with tetra-*n*-butylammonium iodide (Fig. 12).⁴⁴ With both debrominating agents, 2,3-dibromo-2-methylpentane was the fastest substrate and was roughly 70-fold more reactive than *erythro*-5,6-dibromodecane (**28**). With di-*n*-hexyltelluride (**26**), the remaining substrates were in the order expected if carbocation/bromonium ion character is developed in the transition state: increased branching in the dibromide leads to faster rates of reaction.^{43,44} With iodide, 1,2-dibromodecane (**29**) is the second most reactive substrate, which one might expect for an E2-like process as depicted in Fig. 10. These results suggested that at least two mechanistic paths were being followed.

trans-1,2-Dibromocyclohexane is essentially unreactive with telluride **26**. Studies have shown that strain impacts bromonium ion stability and that bicyclic bromonium ions such as **31** are less favored relative to bromonium ions derived from acyclic substrates.^{45–47} With the strain of **31** in mind, the order of reactivity of **27–30** with respect to debromination reflects the expected order of bromonium ion stability and suggests the mechanism of Fig. 13 as a viable mechanistic pathway for debrominations with diorganotellurides. The *vicinal*-dibromide would produce its corresponding bromonium ion via an equilibrium process. Increasing concentrations

Debrominations with Te(*n*-C₆H₁₃)₂ (**26**):



Debrominations with Bu₄N⁺ I[−]:

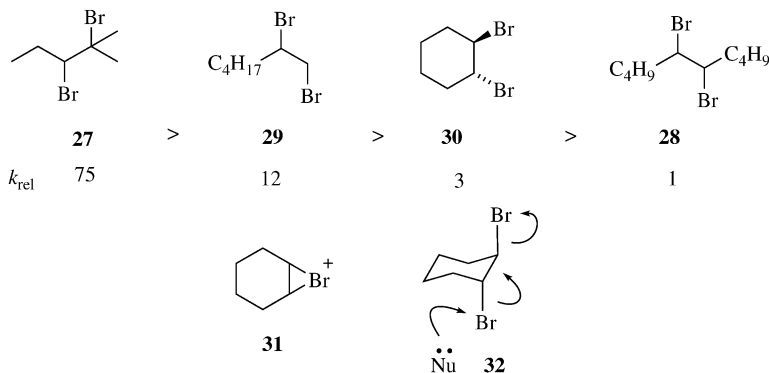


Fig. 12 Relative rates of debromination of *vicinal*-dibromides **27–30** with di-*n*-hexyltelluride (**26**) and tetra-*n*-butylammonium iodide,

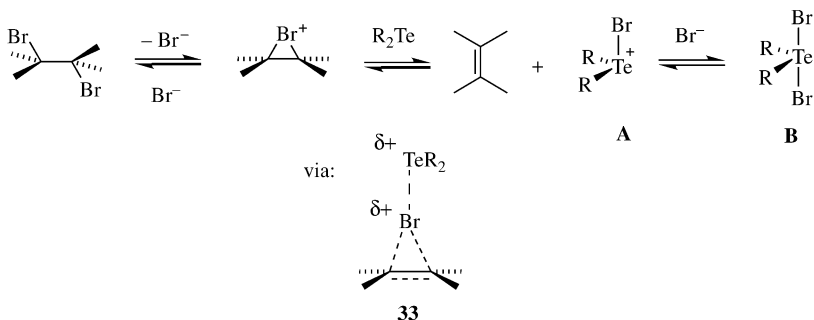


Fig. 13 A plausible mechanism for the debromination of *vicinal*-dibromides with diorganotellurides.

of the *vicinal*-dibromide would give a corresponding increase in the bromonium ion concentration, which explains the first-order dependence on *vicinal*-dibromide concentration. The bromonium ion transfers Br^+ to the tellurium atom of the diorganotelluride to produce the bromotelluronium intermediate **A**, which is the same bromotelluronium intermediate that would be produced during oxidative addition of Br_2 to a diorganotelluride (see Fig. 7). The bimolecular nature of this transfer accounts for the first-order dependence on telluride concentration. Nucleophilic addition of bromide gives the trigonal bipyramidal specie **B**, which is the same trigonal bipyramidal tellurium(IV) species that would be produced during oxidative addition of Br_2 to a diorganotelluride (see Fig. 7).

In contrast to the rate of debromination of **30** with telluride **26**, the debromination of dibromide **30** with iodide is much more rapid. In general, the rate of debromination with the anionic iodide is several orders of magnitude faster than with the uncharged dihexyltelluride **26**. The debromination with iodide most likely proceeds via the E2-like transition state **32** (Fig. 12), which avoids the strain associated with bromonium ion **31**.⁴⁴ Diorganotellurides should also be capable of following a similar mechanism.

The kinetics of debromination of **27** and **29** with di-*n*-hexyltelluride (**26**) and tetra-*n*-butylammonium iodide were followed over a 30 K temperature range, which allowed Eyring and Arrhenius activation parameters to be calculated.⁴⁴ These parameters are summarized in Table 3. For 2,3-dibromo-2-methylpentane (**27**), values of ΔG^\ddagger_{298} are nearly identical for debrominations with either di-*n*-hexyltelluride (**26**) or tetra-*n*-butylammonium iodide (120 ± 21 and 108 ± 21 kJ mol⁻¹, respectively). However, the debromination with di-*n*-hexyltelluride (**26**) is entropy driven with a large negative value of ΔS^\ddagger (-176 J K⁻¹ mol⁻¹) and a small value of ΔH^\ddagger (53 ± 1 kJ mol⁻¹). In contrast, the debromination of **27** with tetra-*n*-butylammonium iodide has a much larger value of ΔH^\ddagger (95 ± 8 kJ mol⁻¹) and a nearly negligible value of ΔS^\ddagger (-21 ± 21 J K⁻¹ mol⁻¹). The highly ordered transition state for debromination with **26** is consistent with the tellurium atom removing “ Br^+ ” from a bromonium ion as shown in Fig. 13 for

Table 3 Arrhenius and Eyring activation parameters for the debrominations of 2,3-dibromo-2-methylpentane (**27**) and 1,2-dibromodecane (**29**) with di-*n*-hexyltelluride (**26**) and tetra-*n*-butylammonium iodide

Substrate	Compound	$k \pm 2\sigma$ at 358 K ($M^{-1} s^{-1}$)	$\Delta G_{298}^{\ddagger}$ (kJ mol $^{-1}$)	$\Delta H_{298}^{\ddagger}$ (kJ mol $^{-1}$)	$\Delta S_{298}^{\ddagger}$ (J K $^{-1}$ mol $^{-1}$)	E_a (kJ mol $^{-1}$)	Reference
27	26	$(7.6 \pm 0.2) \times 10^{-5}$	105 ± 21	53 ± 1	-176 ± 2	56 ± 1	44
27	Bu₄NI	$(3.3 \pm 0.1) \times 10^{-3}$	100 ± 17	95 ± 8	-21 ± 21	100 ± 8	44
29	26	$(1.36 \pm 0.09) \times 10^{-6}$	120 ± 21	91 ± 12	-108 ± 37	91 ± 12	44
29	Bu₄NI	$(2.66 \pm 0.07) \times 10^{-4}$	108 ± 21	83 ± 12	-87 ± 33	83 ± 12	44

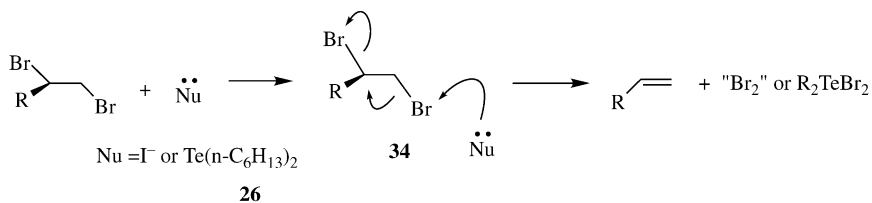


Fig. 14 Plausible E2-like transition state for the debromination of 1,2-dibromoalkanes with either diorganotellurides or iodide.

transition state **33**, while the nucleophilic attack of iodide may cleave the carbon–bromine bond directly to give a carbocation intermediate with a less-ordered transition state.

In contrast to the dichotomy of reaction pathways observed for the debromination of **27**, debromination of 1,2-dibromodecane (**29**) with either di-*n*-hexyltelluride or tetra-*n*-butylammonium iodide gave identical (within experimental error) activation parameters (Table 3).⁴⁴ The large negative values of ΔS^\ddagger (-108 ± 37 and $-87 \pm 12 \text{ J K}^{-1} \text{ mol}^{-1}$, respectively) are consistent with a highly-ordered transition state, but the bromonium ion formed from this dibromide would not be particularly favored. The data suggest that both the telluride and the iodide proceed via the E2-like mechanism of Fig. 14 with anti-periplanar transition state **34**.

With diorganotellurides, the rate of debromination increases as the diorganotelluride becomes more electron rich.^{43,44} Thus, di-*n*-hexyltelluride (**26**) is a much better debrominating agent than diaryltellurides and di-4-dimethylamino telluride is a better debrominating agent than diphenyltelluride. Dramatic increases in the rate of debromination of *vicinal*-dihalides were observed using 1,5-dichalcogenacyclooctanes.⁴⁸ In these molecules, transannular chalcogen–chalcogen interactions drive the debromination processes. Both *vicinal*-dibromides and *vicinal*-dichlorides are dehalogenated with 1,5-ditelluracyclooctane and with 1,5-diselenacyclooctane as shown in Fig. 15. These are the only examples of organoselenide-induced dehalogenation reactions and indicate the importance of the proximity effect of the second chalcogen atom as shown in transition state **35** of Fig. 15.

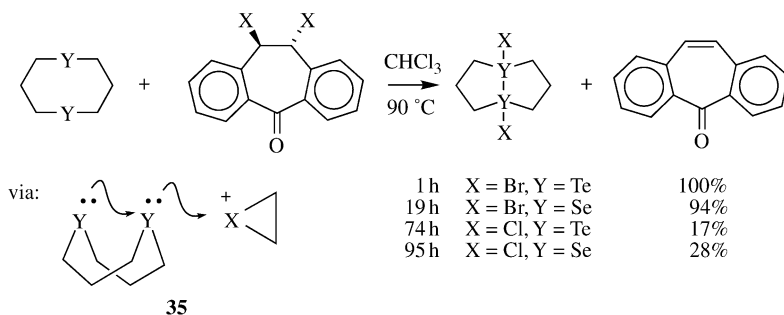


Fig. 15 Dehalogenation of *vicinal*-dibromides and dichlorides with 1,5-ditelluraoctane and 1,5-diselenaoctane.

Catalytic variations of the dehalogenation reactions have been developed that require only a few mole% of the organotelluride compound to be effective. In Engman's 2-thienyltelluride method, the di-2-thienyl ditelluride is formed by reaction of the tellurenyl bromide with telluride anion.³⁹ In the presence of sodium borohydride, a catalytic amount of di-2-thienyl ditelluride can be used to debrominate *vicinal*-dibromides in excellent yield. However, this method can only be used in the presence of functional groups that are stable to sodium borohydride. The ditelluride is reduced to the telluride anion with sodium borohydride. Bisulfite has been used to reduce di-4-methoxyphenyltellurium dibromide to di-4-methoxyphenyltelluride in the debromination of benzylic and heterobenzylic dibromides.⁴⁹ In these reactions, 5 mol% of the telluride was all that was required. Glutathione and sodium ascorbate have also been used to reduce tellurium(IV) dibromides to the corresponding tellurides *in situ* during debrominations of *vicinal*-dibromides.⁵⁰

HALOGENATION OF ORGANIC SUBSTRATES WITH CHALCOGEN(IV) DIHALIDES

As shown in Figs. 6 and 12, halotelluronium and haloselenonium intermediates can be formed via loss of a ligand from the trigonal bipyramidal chalcogen(IV) complex or via oxidative addition of halogen. Through the process of microscopic reversibility, if dehalogenation of *vicinal*-dihalides with diorganochalcogenides occurs, then halogenation of alkenes with diorganochalcogen(IV) dihalides should be possible in the reverse direction. With the exception of 1,5-diselenacyclooctane,⁴⁸ dehalogenation of *vicinal*-dihalides occurs with diorganotellurides and not with diorganoselenides. As noted by Petragnani and Campos,¹³ diaryltellurides will debrominate diarylselenium(IV) dibromides to give the corresponding diaryltellurium(IV) dibromide and diarylselenide. Their results suggest that selenium(IV) dihalides are better oxidants than the corresponding tellurium(IV) dihalide and should function as better halogenating agents for alkenes (a form of oxidation) than the corresponding tellurium(IV) dihalides.

Trigonal bipyramidal selenium(IV) diiodides are unknown, presumably due to the similarity in electronegativities of iodine and selenium.⁵¹ However, diorganotellurium(IV) diiodides form trigonal bipyramidal tellurium(IV) complexes (see Fig. 1) and function as iodinating agents for a variety of organic substrates. Di-4-chlorophenyltellurium(IV) diiodide (**5**) iodinate either 4-pentenoic acid or 4-pentenol in the presence of one equivalent of pyridine as shown in Fig. 16.⁵² These iodinations required 4–5 days in refluxing chloroform to reach completion in contrast to iodinations with iodine and 1 equivalent of pyridine, which were complete within 1 h.

The transfer of iodine to the organic substrate represents a formal reductive elimination at tellurium(IV) to give tellurium(II) as well as oxidation of the alkene. In a series of diaryltellurium(IV) diiodides, iodination of organic substrates is accelerated by electron-withdrawing substituents and is slowed by electron-donating substituents, which is consistent with the substituent effects one would expect for

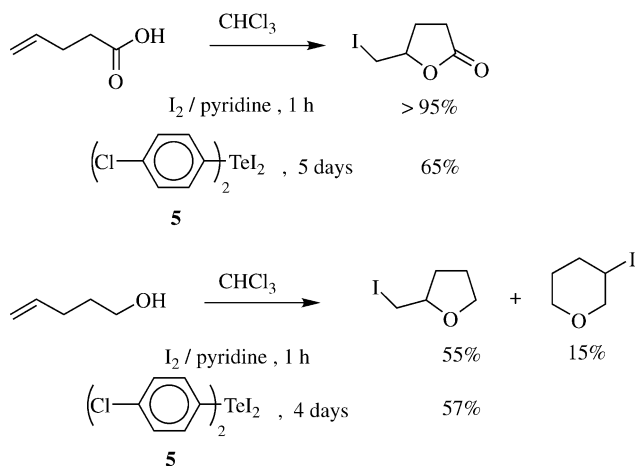


Fig. 16 Iodination of 4-pentenoic acid and 4-penten-1-ol with iodine/pyridine or di-4-chlorophenyltellurium(IV) diiodide (**5**)/pyridine.

stabilizing the tellurium(IV) oxidation state.⁵² While di-4-chlorophenyltellurium(IV) diiodide has a half-life for iodination of 4-pentenoic acid of roughly 20 h, diphenyltellurium(IV) diiodide has a half-life of 3 days, di-4-methylphenyltellurium(IV) diiodide has a half-life of 4 days, and di-4-methoxyphenyltellurium(IV) diiodide is essentially unreactive (a half-life of >14 days). The electron-withdrawing chloro substituent increases the electron demand at the electron-deficient tellurium(IV) center, which facilitates reductive elimination to tellurium(II). The electron-donating methyl substituent increases electron density at the tellurium(IV) center and stabilizes the tellurium(IV) state. The 4-methoxy substituent can back donate a pair of electrons to the tellurium(IV) center to provide even greater stabilization.

Both diorganotellurium(IV) and diorganoselenium(IV) dibromides are known, stable compounds, which permits a direct comparison of the selenium(IV) and tellurium(IV) compounds. Di-4-chlorophenyltellurium(IV) dibromide (**36**) and one equivalent of pyridine were essentially unreactive with respect to bromination of either 4-pentenoic acid or 4-pentenol. With either substrate, **36** gives only 2–3% conversion to brominated products after several days of reaction (Fig. 17).⁵² In contrast, diphenylselenium(IV) dibromide (**1**, Fig. 1) and 2-(dimethylaminomethyl)phenyl phenyl bromoselenonium bromide (**37**) gave essentially complete bromination of either 4-pentenoic acid or 4-pentenol in 1 h in the presence of one equivalent of pyridine as shown in Fig. 17.

Similar trends were observed in the halogenation of 1,3,5-trimethoxybenzene with diorganoselenium(IV) dihalides as shown in Fig. 18.⁵² Di-4-chlorophenyltellurium(IV) dibromide (**36**) gave less than 5% bromination of 1,3,5-trimethoxybenzene after 48 h at reflux in chloroform. Bromination of 1,3,5-trimethoxybenzene with

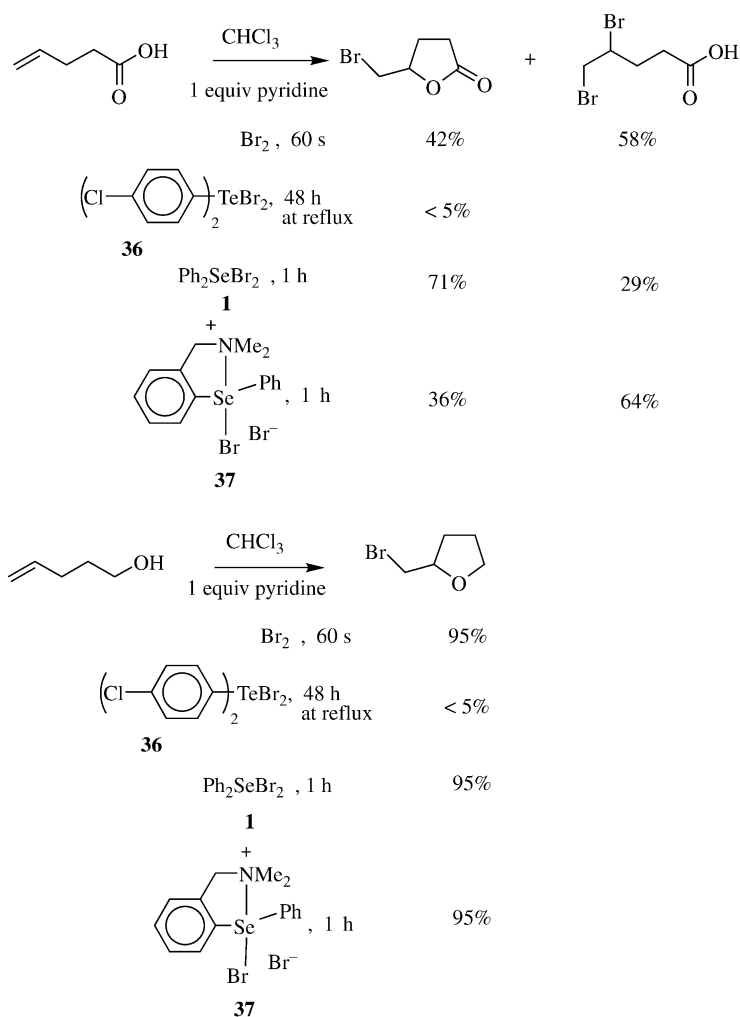


Fig. 17 Bromination of 4-pentenoic acid and 4-penten-1-ol with bromine/pyridine and with di-4-chlorophenyltellurium(IV) dibromide (**36**), diphenylselenium(IV) dibromide (**1**), and *N,N*-dimethyl-2-(aminomethyl)phenyl phenyl bromoselenonium bromide (**37**) and one equivalent of pyridine.

either diphenylselenium(IV) dibromide (**1**) or 2-(dimethylaminomethyl)phenyl phenyl bromoselenonium bromide (**37**) gave 2-bromo-1,3,5-trimethoxybenzene in 80 and 92% isolated yields, respectively, within 5 min of mixing. Chlorination of 1,3,5-trimethoxybenzene with diphenylselenium(IV) dichloride (**38**) gave 2-chloro-1,3,5-trimethoxybenzene in 95% yield within 5 min of mixing.

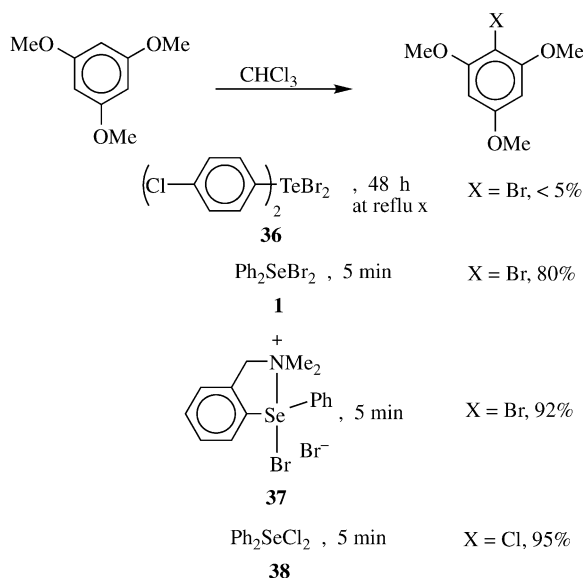


Fig. 18 Halogenation of 1,3,5-trimethoxybenzene di-4-chlorophenyltellurium(IV) dibromide (**36**), diphenylselenium(IV) dibromide (**1**), *N,N*-dimethyl-2-(aminomethyl)phenyl phenyl bromoselenonium bromide (**37**), and diphenylselenium(IV) dichloride (**38**).

ORGANOCHALCOGEN(II) AND ORGANOCHALCOGEN(IV) COMPOUNDS WITH AN ODD NUMBER OF LIGANDS

One method of keeping track of the bonding around the selenium and tellurium atoms of organoselenides and organotellurides, respectively, in various oxidation states is to count the number of electrons around the central selenium or tellurium atom and the number of atoms that are bonded to the central atom.⁵³ Thus, diphenylselenide and diphenyltelluride would be referred to as 8-Se-2 and 8-Te-2 compounds, respectively, to reflect four pairs of electrons around the central atom (two covalently attached atoms and two lone-pairs of electrons). The oxidative addition of halogens produces diphenylselenium(IV) dihalide and diphenyltellurium(IV) dihalide molecules, which are now referred to as 10-Se-4 and 10-Te-4 compounds, respectively, to accommodate 10 electrons around each central atom with four covalently bound atoms and one lone-pair of electrons. The linear halogen-chalcogen-halogen array is a three-center, four-electron bond^{8,9} as discussed above.

Organotellurium(II) compounds can also contain a three-center, four-electron bond as shown for **39** to **42** in Fig. 19. Typically, these molecules contain an odd number ligands around the central atom and an electronegative atom helps to stabilize a tellurenyl halide or selenenyl halide bond through "chelation" to form a four, five, or six membered ring.⁵⁴ Such molecules are described as 10-Te-3 and 10-Se-3

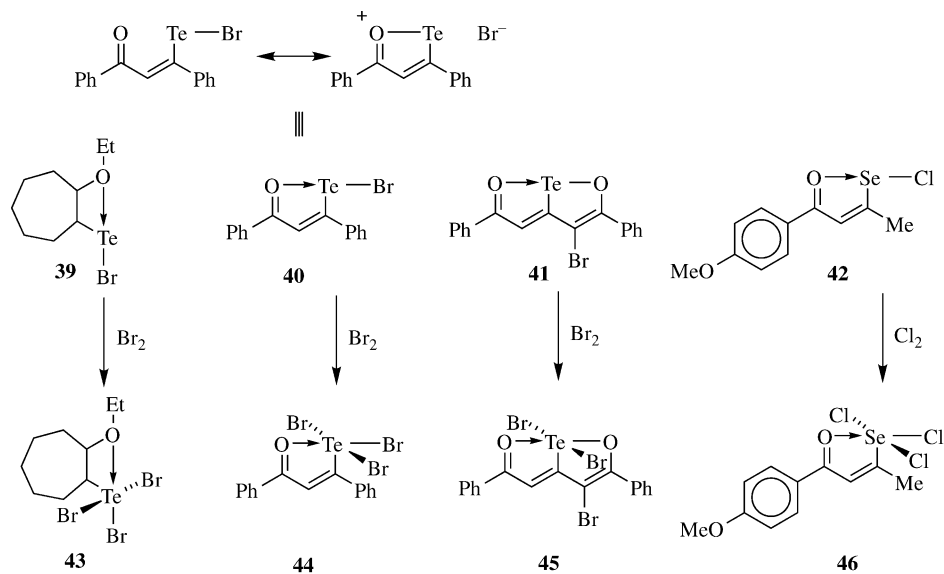
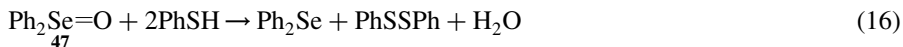
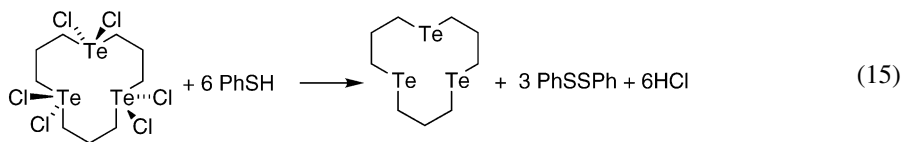
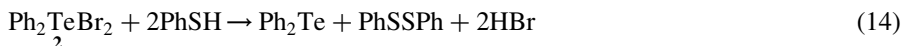
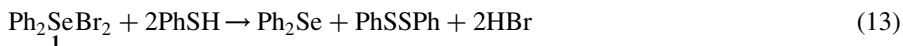


Fig. 19 Representative examples of organoselenenides and tellurides in the +2 and +4 oxidation states with an odd number of ligands to selenium or tellurium.

molecules to account for three “covalently” bound atoms and two lone-pairs of electrons. As illustrated for compound **40**, the three-center, four-electron bond has both ionic and covalent contributions. These molecules can also undergo oxidative addition of halogen to produce tellurium(IV) compounds **43** to **45** and selenium(IV) compound **46**, which are described as 12-Te-5 and 12-Se-5 compounds, respectively.^{54–57} These molecules accommodate one lone-pair of electrons and four “covalently” bonded electronegative atoms. Very few mechanistic details are available for these oxidative addition reactions.

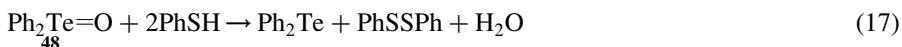
OXIDATION OF THIOLS AND RELATED COMPOUNDS WITH ORGANOSELENIUM(IV) AND ORGANOTELLURIUM(IV) COMPOUNDS

The 10-E-4 chalcogen(IV) species diphenylselenium(IV) dibromide (**1**, Fig. 1) and diphenyltellurium(IV) dibromide (**2**, Fig. 1) oxidize thiophenol to diphenyl disulfide in nearly quantitative yield as shown in equations (13) and (14). Tellurium(IV) dihalides **6–11** also oxidize thiophenol to diphenyl disulfide and benzene selenol to diphenyl diselenide. Similarly, the 12-Te-5 molecule dioxatellurapentalene **45** (Fig. 19) is a mild oxidant for ethylmercaptan, thiophenol, and benzene selenol giving diethyl disulfide, diphenyl disulfide, and diphenyl diselenide in essentially quantitative yield.⁵⁶ As shown in equation (15), 1,1,5,5,9,9-hexachloro-1,5,9-tritelluracyclododecane oxidizes six molecules of thiophenol to diphenyl disulfide and 1,5,9-tritelluracyclododecane in 90% yield.⁵⁷ In contrast, 12-Te-5 pertellurane **44** and 12-Se-5 perselenane **46** do not oxidize thiophenol to diphenyl disulfide. Instead, these molecules undergo a nucleophilic addition of thiophenol followed by cleavage of the tellurium–carbon or selenium–carbon bond.⁵⁸



Selenoxides and telluroxides also function as mild oxidants for the conversion of thiols to disulfides^{59–71} as shown in equations (16) and (17) for the reaction of thiophenol with diphenylselenoxide (**47**) and diphenyltelluroxide (**48**).⁵⁹ Mechanistically, the oxidation of thiols to disulfides with selenoxides and telluroxides is a multi-step process, which takes advantage of the ease with which tellurium(IV) and selenium(IV) species form trigonal bipyramidal

intermediates.



Unlike sulfoxides, which exist primarily as the tetrahedral oxide, both selenoxides and telluroxides add water to give dihydroxy selenanes and telluranes, respectively, which have trigonal bipyramidal structures with two hydroxyl groups as the axial ligands. The hydration step is reversible as shown in Fig. 20.⁷²⁻⁷⁴ Diphenylselenoxide (**47**) and diphenyl dihydroxy selenane (**49**) are both isolable compounds and can be interconverted by stirring in wet solvent to hydrate or by application of heat and vacuum to dehydrate as shown in Fig. 20.⁶⁹ The equilibrium constant for the addition of water to telluroxides in tetrahydrofuran has been measured as between 20 and 30 M⁻¹ for di-4-hydroxyphenyltelluroxide and > 100 M⁻¹ for di-4-aminophenyltelluroxide.⁷³ In water as a solvent, the equilibrium constants lie between 10 and 100 M⁻¹.^{73,74} The enantiomers of *N,N*-dimethyl-2-(aminomethyl)phenyl benzylselenoxide (**50**) and related compounds have been resolved and are configurationally stable. However, traces of water cause the optically active selenoxides to racemize via dihydroxy selenane intermediates such as **51** for the racemization of **50**.⁷⁵ The rate constants for the addition of water to di-4-hydroxyphenyltelluroxide and to di-4-aminophenyltelluroxide in pure water have been measured at 4 × 10³ and 4.5 × 10³ s⁻¹, respectively.⁷³

The chemistry associated with selenoxides and telluroxides in protic solvents is a dynamic process. If other nucleophiles are present in the solution, then these

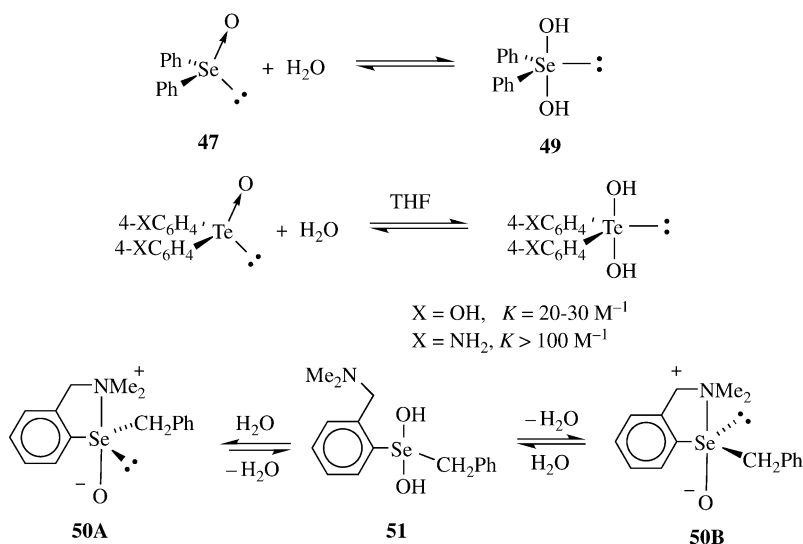


Fig. 20 Reversible hydration/dehydration of diphenylselenoxide (**47**), di-4-hydroxyphenyltelluroxide, di-4-aminophenyltelluroxide, and *N,N*-dimethyl-2-(aminomethyl)phenyl benzylselenoxide (**50**) and the corresponding dihydroxy selenanes/telluranes.

nucleophiles can compete with solvent for addition to the oxide. Thiols are excellent nucleophiles for this process as illustrated in Fig. 21 and can add either to the selenoxide or telluroxide **A** or to the corresponding hydroxyselenonium or hydroxytelluronium intermediates **B**, respectively. The rate constants (k_{FAST}) for the introduction of glutathione to the coordination sphere of diphenylselenoxide (**47**), diphenyltelluroxide (**48**), and chalcogenopyrylium dyes **52** and **53** in phosphate-buffered saline (PBS) have been measured by stopped flow spectroscopy.⁵⁹ The second-order rate constant for the addition of glutathione to selenoxide **47** (k_{FAST}) is $2.26 \times 10^2 \text{ M}^{-1} \text{ s}^{-1}$ (Table 4). The addition of glutathione to tellurium(IV) species **48**, **52**, and **53** is several orders of magnitude faster ranging from 5.2×10^6 to $2.3 \times 10^7 \text{ M}^{-1} \text{ s}^{-1}$ (Table 4). Comparable values of k_{FAST} were measured for the addition of thiophenol to di-4-methoxyphenyltelluroxide (**54**), di-*n*-hexyltelluroxide (**55**), and (*R*)-*N,N*-dimethyl-2-(1-aminoethyl)phenyl phenyltelluroxide (**56**) in methanol with a range of 1.28×10^3 to $1.2 \times 10^6 \text{ M}^{-1} \text{ s}^{-1}$.

Once the thiol is introduced to the coordination sphere of the selenoxide or telluroxide, a second slower reaction occurs. This step is associated with reduction of the chalcogen(IV) oxidation state to the chalcogen(II) oxidation state, which was demonstrated with dihydroxy telluranes **52** and **53**.⁵⁹ In the tellurium(IV) oxidation state of **52** and **53**, the 5p orbital of tellurium is involved in the three-center, four-electron bond and cannot interact with the carbon π -framework. Long-wavelength absorption maxima for **52** and **53** are found at 510 and 500 nm, respectively in water. Reductive elimination generates a tellurium(II) atom, whose 5p orbital can now

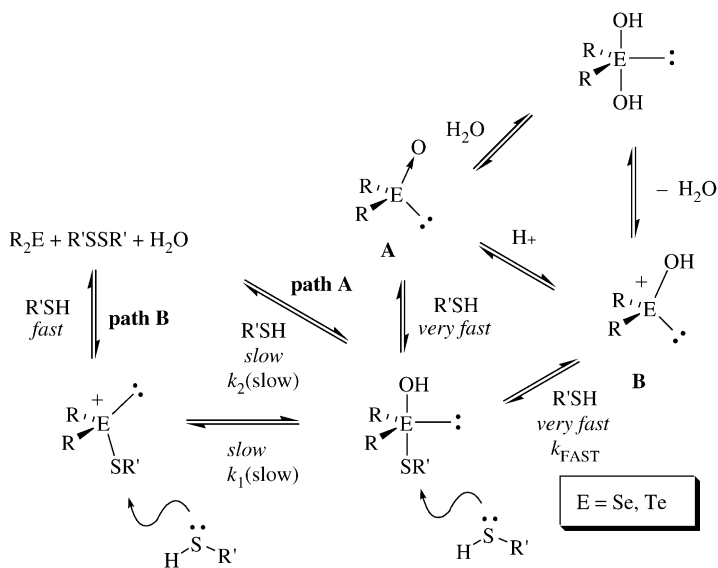
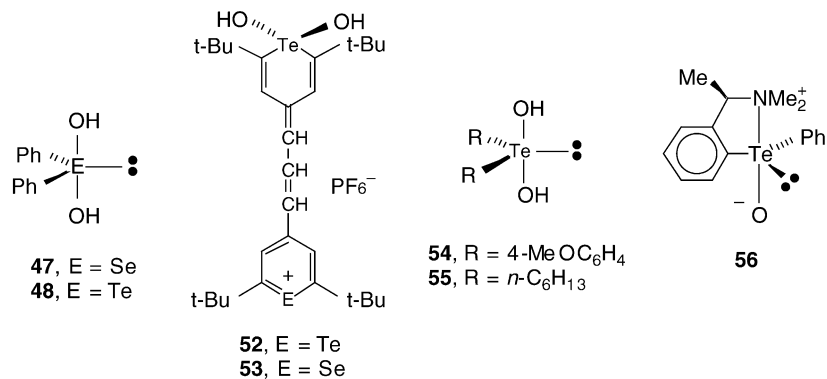


Fig. 21 General mechanism for the oxidation of thiols to disulfides with selenoxides or telluroxides.

Table 4 Rate constants for the fast (k_{FAST}) and slow [$k_2(\text{slow})$ for the second-order path and $k_1(\text{slow})$ for the first-order path] reactions for the addition of glutathione (GSH) to **47**, **48**, **52**, and **53** in PBS at pH 7.4 and for the addition of thiophenol (PhSH) to **54–56** in methanol



Oxide	Thiol	<i>T</i> (K)	k_{FAST} (M ⁻¹ s ⁻¹)	$k_2(\text{slow})$ (M ⁻¹ s ⁻¹)	$k_1(\text{slow})$ (s ⁻¹)	Reference
47	GSG	293.1	$(2.26 \pm 0.04) \times 10^2$	$(6.62 \pm 0.04) \times 10^1$	–	59
48	GSH	285.5	$(5.2 \pm 0.6) \times 10^6$	$(7.6 \pm 0.1) \times 10^3$	–	59
52	GSH	285.4	$(2.30 \pm 0.09) \times 10^7$	$(2.64 \pm 0.03) \times 10^5$	–	59
53	GSH	293.2	$(1.66 \pm 0.04) \times 10^7$	$(3.76 \pm 0.02) \times 10^5$	–	59
54	PhSH	276.8	$(5.5 \pm 0.2) \times 10^5$	$(3.81 \pm 0.06) \times 10^2$	$(2.79 \pm 0.02) \times 10^1$	64
55	PhSH	276.8	$(1.20 \pm 0.01) \times 10^6$	$< 10^1$	2.9 ± 0.1	64
56	PhSH	276.8	$(1.28 \pm 0.08) \times 10^3$	$(1.03 \pm 0.02) \times 10^2$	$(6.2 \pm 0.5) \times 10^{-1}$	64

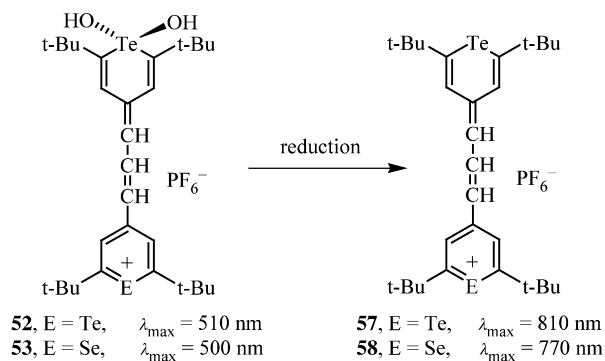


Fig. 22 Changes in the long-wavelength absorption maximum (λ_{\max}) as a function of tellurium oxidation state.

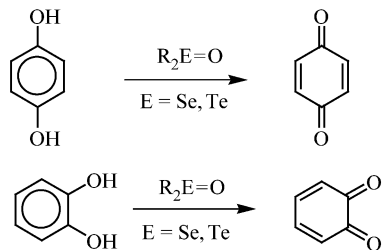
overlap with the carbon π -framework as shown in Fig. 22. The reduced telluropyrylium dyes **57** and **58** have long-wavelength absorption maxima at 810 and 770 nm, respectively, in water. In stopped flow studies of the reaction of **52** and **53** with GSH, loss of the chromophore at 510 or 500 nm was accompanied by the appearance of a new chromophore at 810 or 770 nm, respectively, with identical rates for both processes.

Later stopped-flow studies with **54–56** indicated that the second, slow reductive elimination process can occur by either of two pathways as shown in Fig. 21.⁶⁴ In Path A, a second-order process is observed in which the thiol does a nucleophilic attack at the new sulfide ligand to give the disulfide and the reduced telluride. Only this pathway was observed in the reactions of GSH with **52** and **53**.⁵⁹ In Path B, loss of a hydroxy ligand gives an intermediate thioselenonium or thiotelluronium intermediate via a first-order process, which then undergoes rapid nucleophilic attack by the thiol at the sulfide ligand. This was the predominate pathway observed with **54–56** at low concentrations of PhSH. However, at higher concentrations of PhSH, the second-order process became competitive.⁶⁴ Both the second-order and the first-order process are slow relative to the introduction of the sulfide in the ligand sphere (Table 4).

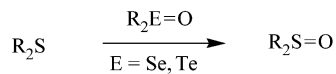
OTHER OXIDATIONS WITH SELENOXIDES AND TELLUROXIDES

Several other oxidation reactions of selenoxides and telluroxides are summarized in Fig. 23. Ley, Barton, and co-workers discovered that di-4-methoxyphenyltelluroxide (**54**) could be used catalytically as an oxidant in the presence of 1,2-dibromotetrachloroethane.^{76,77} After reduction of the telluroxide to the telluride, the di-4-methoxyphenyltelluride (**24**) debrominated the 1,2-dibromotetrachloroethane to give the tellurium(IV) dibromide, which was hydrolyzed *in situ* to give the telluroxide **54**. This process was used to oxidize phosphines to phosphine oxides and

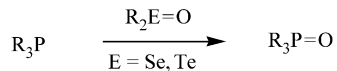
Oxidation of Hydroquinones and Catechols



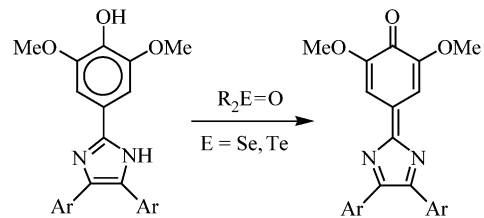
Oxidation of Sulfides to Sulfoxides



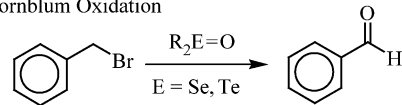
Oxidation of Phosphines to Phosphine Oxides



Oxidation of Leucodyes



Cornblum Oxidation



Thiocarbonyls to Carbonyls

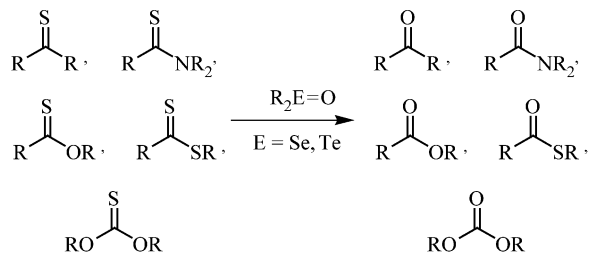


Fig. 23 Other oxidation reactions using delenoxides and telluroxides as mild oxidants.

to convert thiocarbonyl-containing compounds to the corresponding carbonyl-containing compounds. Stoichiometric quantities of telluroxide **54** were also used to convert thioketones, thioamides, thioesters, dithioesters, and thiocarbonates to the corresponding ketones, amides, esters, thioesters, and carbonates, respectively.^{65,66} Polymer-bound selenoxides⁶⁷ and electron-rich, di-4-methoxyphenylselenoxide^{68,69} have been used to oxidize sulfides to sulfoxides, hydroquinones and catechols to quinones, and phosphines to phosphine oxides. Di-4-methoxyphenylselenoxide has also been used as a nucleophilic oxygen source in the Cornblum oxidation of benzylic halides.⁷⁸ Telluroxides have also been used to oxidize imidazole-derived leucodyes to the corresponding dye form.⁶⁰ Selenoxides have been used as a mild oxidant in the osmium-catalyzed oxidation of alkenes to *vicinal*-diols.⁷⁹

Selenoxides are protonated by sulfonic acids and the corresponding hydroxyselenonium sulfonate salts are soluble oxidants for the oxidation of sulfides to sulfoxides.⁸⁰ Chlorooxaselenuranes have also been used for the oxidation of sulfides to sulfoxides.⁸¹

THIOLPEROXIDASE AND HALOPEROXIDASE-LIKE ACTIVITY OF ORGANOSELENIDES AND ORGANOTELLURIDES

Ley and Barton's observation that di-4-methoxyphenyltelluride could be used catalytically was the first entry into the use of *in situ* generated selenoxides or telluroxides as catalysts. As shown in Fig. 8, a variety of different nucleophiles can be introduced via the selenoxide or telluroxide followed by reductive elimination to generate oxidized product and reduced selenide or telluride. If the nucleophile is relatively inert to oxidation by hydrogen peroxide, then the reduced selenide or telluride can be reoxidized by hydrogen peroxide and the overall oxidation of the nucleophile becomes catalytic in the selenide or telluride. In the case of thiols, disulfides are the final product and the selenides or tellurides exhibit thiolperoxidase-like activity.^{60-62,64,82,83} If halide salts (chloride, bromide, iodide) are the nucleophiles, then positive halogen sources are the oxidized products and the selenides and tellurides exhibit haloperoxidase-like activity.⁸⁴⁻⁸⁸ The phenoxypropyltelluride **59** has been used as a catalyst for the iodination and bromination of a variety of organic substrates as shown in Fig. 24.⁸⁷

The catalytic cycle for the thiolperoxidase and haloperoxidase-like activity of diorganoselenides and tellurides is summarized in Fig. 25. Stopped-flow spectroscopy has been used to elicit mechanistic details of the cycle.^{59,64,82,84} Following oxidation to the selenoxide or telluroxide, the catalytic cycle for thiolperoxidase-like activity is shown in Fig. 21. The details of the haloperoxidase-like cycle are not as well defined. Using dihydroxytellurane **52** as a substrate, the addition of 0.5 M sodium iodide in pH 6.8 buffer gave a fast reaction with a second-order rate constant $> 100 \text{ M}^{-1} \text{ s}^{-1}$ followed by a slower, second-order process with a rate constant of $22.5 \pm 0.3 \text{ M}^{-1} \text{ s}^{-1}$.⁸⁴ The two processes could not be resolved by using different wavelengths, which would have allowed a better measurement of the rate constant for the initial process. If we assume that the first, faster process is

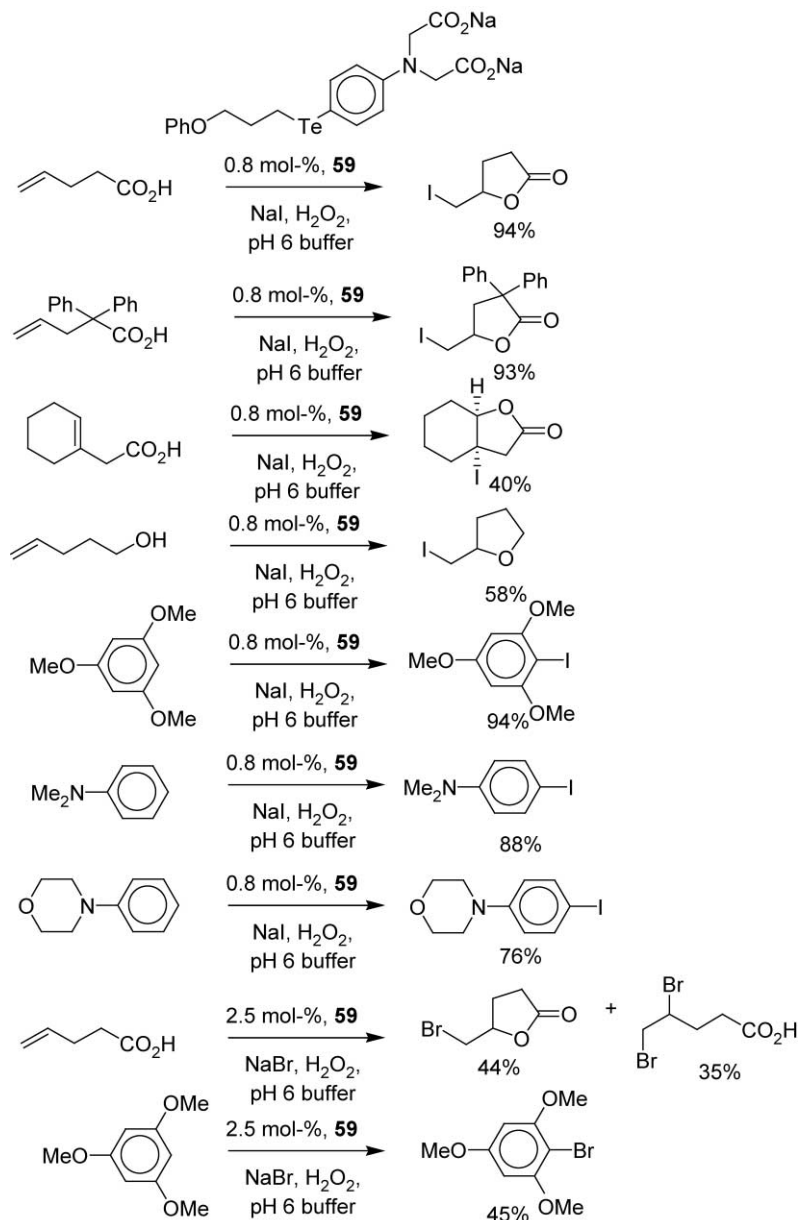


Fig. 24 Iodination and bromination of organic substrates with hydrogen peroxide and sodium iodide or bromide in the presence of phenoxypropyltelluride **59**.

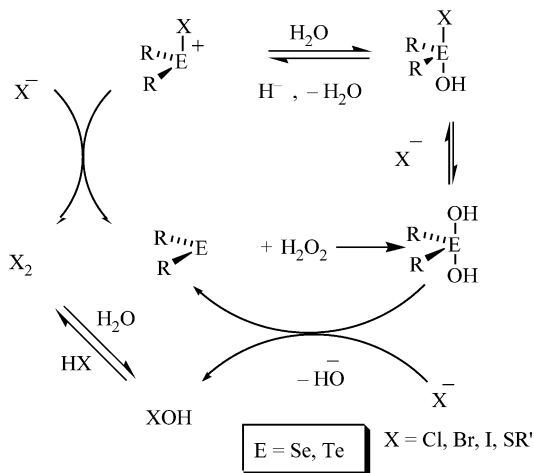


Fig. 25 A summary of haloperoxidase-like and thiolperoxidase-like reactions of diorganoselenenides and tellurides.

introduction of iodide into the coordination sphere of **52**, then the slower, second reaction is the nucleophilic displacement of molecular iodine from the iodotelluronium intermediate of Fig. 25. For this second process, reductive elimination at tellurium was accompanied by an increase in the 810 nm absorption from the reduced dye that was identical in rate to loss of the 510 nm band associated with tellurium(IV). The addition of 0.1 M sodium bromide to **52** gave one resolvable process by stopped-flow spectroscopy with a second-order rate constant of $13.9 \pm 0.5 \text{ M}^{-1} \text{ s}^{-1}$.⁸² A brief induction period was observed (0.2 s) prior to an increase in the 810 nm band corresponding to reductive elimination.

The second-order rate constants above are on the same order of magnitude as those for the second-order reductive elimination of glutathione disulfide from **47** and **48**⁵⁹ and diphenyl disulfide from **54–56**⁶⁴ compiled in Table 4. The introduction of the ligand to be oxidized is a fast process relative to the reductive elimination step. The rate-determining step in the thiolperoxidase- and the haloperoxidase-like activity of diorganoselenenides and tellurides is the rate of oxidation of the chalcogen atom with hydrogen peroxide.^{64,82,84} In general, diorganotellurides are oxidized much more rapidly than the corresponding diorganoselenenides. *N,N*-dimethyl-2-(aminomethyl)phenyl phenyltelluride (**17**) is oxidized by hydrogen peroxide with a second-order rate constant of $17 \text{ M}^{-1} \text{ s}^{-1}$ in pH 6.8 phosphate buffer and dimethyl-2-(1-aminoethyl)phenyl phenyltelluride is oxidized to **56** with a second-order rate constant of $3.6 \text{ M}^{-1} \text{ s}^{-1}$ in methanol.^{64,84} In contrast, the rate of oxidation of *N,N*-dimethyl-2-(aminomethyl)phenyl phenylselenide is $< 0.1 \text{ M}^{-1} \text{ s}^{-1}$. This disparity in rates of oxidation is the reason why *N,N*-dimethyl-2-(aminomethyl)phenyl phenylselenide and related compounds show no thiolperoxidase-like behavior.⁸⁹

Two trends have emerged in structure-activity studies of thiolperoxidase⁶⁴ and haloperoxidase-like⁸⁴ reactions of diorganotellurides. Electron-donating substituents accelerate the rate of oxidation with hydrogen peroxide but retard the rate of reductive elimination of disulfide or positive-halogen products. Electron-withdrawing substituents retard the rate of oxidation with hydrogen peroxide but accelerate the rate of reductive elimination. These same trends have also been observed in the transfer of positive halogen to alkene substrates.⁵²

One approach that has overcome this dichotomy of substituent effects is the use of a combination of statistical effects and cooperativity in dendrimeric catalysts.^{82,85,86} The dendrimer wedges with two, three, and four organotelluride groups and the first-generation Fréchet-type dendrimers based on 3,5-dihydroxybenzyl alcohol and 1,1,1-tris(4-hydroxyphenylethane)^{90,91} shown in Fig. 26 illustrate statistical effects in thiolperoxidase-like reactions. Nearly linear increases in reactivity on a molar basis with increasing numbers of organotelluride groups were observed in the oxidation of

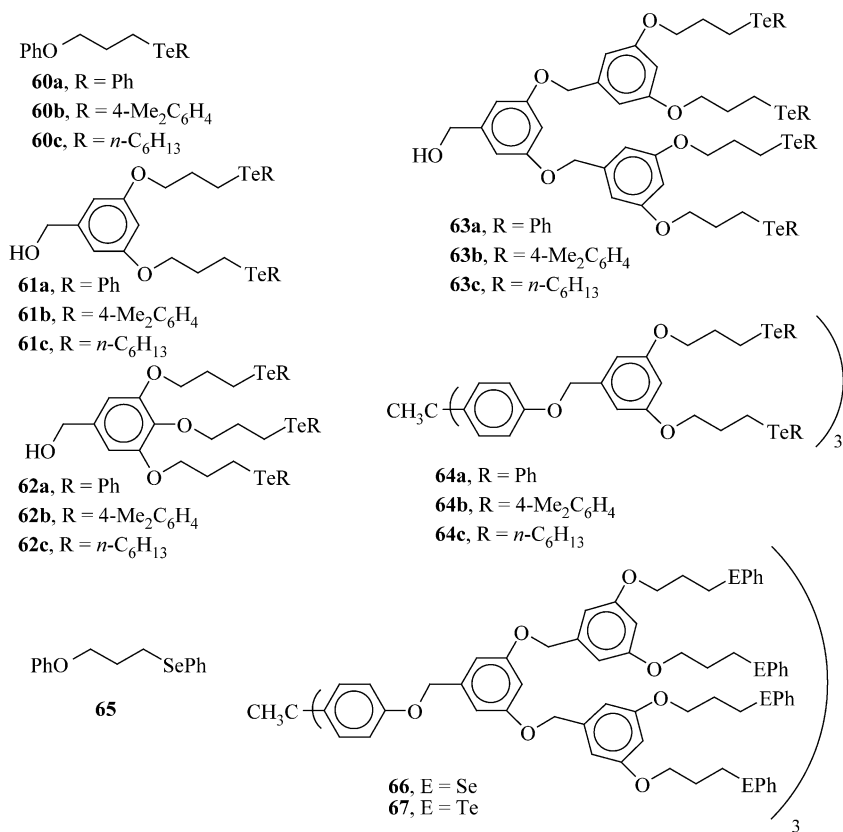


Fig. 26 Dendrimer wedges and first-generation dendrimers that have been used as catalysts with hydrogen peroxide in thiolperoxidase- and haloperoxidase-like reactions.

thiophenol with hydrogen peroxide in methanol as compiled in Table 5.⁸² Thus, the dendrimers **64** with six organotelluride groups were roughly six-times as reactive as the corresponding monotelluride **60**. The thiolperoxidase-like activity increased as the organotelluride groups became more electron rich. The *n*-hexyltelluride-containing molecules (**60c–64c**) were more reactive than the 4-dimethylaminophenyltelluride series (**60b–64b**), which in turn were more reactive than the phenyltelluride series (**60a–64a**). On a molar basis, a 26-fold increase in catalytic activity was realized through a combination of stereoelectronic and statistical effects.

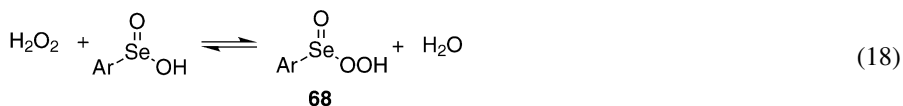
As mentioned above, diorganoselenides have shown little activity in thiolperoxidase- and haloperoxidase-like reactions due to their much slower rates of oxidation with hydrogen peroxide than the corresponding diorganotelluride. As a point of comparison, 1-phenylseleno-3-phenoxypropane (**65**, Fig. 26) has roughly 0.025-times the haloperoxidase-like activity of 1-phenyltelluro-3-phenoxypropane (**60a**) in the bromination of cyclohexene with hydrogen peroxide and sodium bromide.^{85,86} It was unexpected that the second-generation dendrimer **66** with 12 phenylseleno groups has roughly twice the catalytic activity of dendrimer **67** with 12 phenyltelluro groups and that each phenylseleno group in **66** has roughly 80 times the catalytic activity of the one phenylseleno group in **65**.^{85,86} Compound **66** displays cooperativity effects in the increased catalytic activity of the phenylseleno groups. These effects are most likely found in the oxidation of the selenide to the selenoxide and perhaps by the formation of a new catalytic functional group.

Table 5 Thiolperoxidase-like behavior of monotellurides **60**, dendrimer wedges **61–63**, and dendrimers **64** toward the oxidation of thiophenol with hydrogen peroxide in methanol

Catalyst	No. catalyst groups	k_0 ($\Delta A \text{ s}^{-1}$)	v_0 ($\mu\text{M min}^{-1}$)	k_{rel}	k_{rel}/RTe
none	none	$(3.0 \pm 0.2) \times 10^{-6}$	0.72 ± 0.05	0.06	–
60a	1	$(5.3 \pm 0.4) \times 10^{-5}$	12.1 ± 0.9	1.0	1.0
61a	2	$(8.8 \pm 0.5) \times 10^{-5}$	21 ± 1	1.7	0.85
62a	3	$(1.14 \pm 0.02) \times 10^{-4}$	26.9 ± 0.5	2.2	0.73
63a	4	$(1.81 \pm 0.05) \times 10^{-4}$	43 ± 1	3.6	0.9
64a	6	$(4.9 \pm 0.1) \times 10^{-4}$	118 ± 2	9.8	1.6
60b	1	$(1.06 \pm 0.05) \times 10^{-4}$	25 ± 1	2.1	2.1
61b	2	$(1.69 \pm 0.05) \times 10^{-4}$	39 ± 1	3.2	1.6
62b	3	$(3.15 \pm 0.04) \times 10^{-4}$	75.5 ± 0.9	6.2	2.1
63b	4	$(2.77 \pm 0.04) \times 10^{-4}$	66.3 ± 0.9	5.5	1.4
64b	6	$(5.6 \pm 0.1) \times 10^{-4}$	134 ± 2	11	1.8
60c	1	$(1.55 \pm 0.09) \times 10^{-4}$	37 ± 2	3.1	3.1
61c	2	$(2.90 \pm 0.06) \times 10^{-4}$	69 ± 1	5.7	2.9
62c	3	$(3.99 \pm 0.05) \times 10^{-4}$	96 ± 1	7.9	2.6
63c	4	$(5.47 \pm 0.07) \times 10^{-4}$	132 ± 2	10.9	2.7
64c	6	$(1.30 \pm 0.02) \times 10^{-3}$	314 ± 5	26.0	4.3

Data from Ref. 82.

Seleninic acids are another class of selenium(IV) compounds and these molecules have also been efficient catalysts for the activation of hydrogen peroxide. Epoxidation reactions,^{92,93} oxidation of sulfides^{92,93} to sulfoxides and sulfones, Baeyer-Villiger oxidations,^{94–96} oxidation of aldehydes to carboxylic acids,⁹⁶ and oxidation of thiols to disulfides⁹⁷ with H₂O₂ have all been catalyzed with seleninic acids. Selenate esters have also been effective catalysts for the oxidation of thiols to disulfides.⁹⁸ Arylseleninic acids have catalyzed the bromination of organic substrates with hydrogen peroxide and sodium bromide.⁹⁹ Mechanistically, hydrogen peroxide adds to the seleninic acid as shown in equation (18) to give peroxyseleenic acids **68** as the active oxidant. These reactions differ from the reactions of diorganoselenides and tellurides in that the formal oxidation state of the chalcogen atom does not change during the course of the catalytic cycle.



Substituent effects have been examined in epoxidation reactions,⁹³ oxidation of sulfides to sulfoxides,⁹³ Baeyer-Villiger oxidations,^{95,96} and the oxidation of aldehydes to carboxylic acids with hydrogen peroxide in the presence of seleninic acids.⁹⁶ Electron-withdrawing substituents were preferred in these reactions and 3,5-bis(trifluoromethyl)phenylseleninic acid has emerged as the best, general catalyst for activating hydrogen peroxide. In contrast to these results, bromination reactions with hydrogen peroxide and sodium bromide are accelerated by seleninic acids bearing electron-donating substituents such as 4-methyl, 4-methoxy, and 4-dimethylamino.⁹⁹

Diorgano diselenides have been used extensively as precursors to seleninic acids in the presence of hydrogen peroxide.^{100–103} The catalytic activity of preformed seleninic acids and seleninic acids generated *in situ* are identical. Diorgano ditellurides have also been used as catalysts in thiolperoxidase-like reactions for the oxidation of thiols with various peroxides.¹⁰⁴ However, tellurinic acids are not thought to be involved even though RTe(=O)SPh types of structures are proposed as intermediates.

ELECTROCHEMICAL REDUCTION OF DIORGANOTELLURIUM(IV) SPECIES

Hydrogen peroxide is a powerful oxidant releasing roughly 100 kJ mol⁻¹ in its conversion to water and oxygen. However, the kinetics of oxidation with hydrogen peroxide are often slow.¹⁰⁵ Organoselenides and particularly organotellurides are readily oxidized with hydrogen peroxide and, as described above, the resulting chalcogen(IV) compounds are themselves oxidants for a variety of transformations. One measure of the oxidizing power of the tellurium(IV) and selenium(IV) derivatives is the reduction potential to reduce the chalcogen(IV) species to the corresponding chalcogen(II) species. Systematic comparisons have been made on

cationic tellurium(IV) derivatives of chalcogenopyrylium dyes (Fig. 27)⁶⁰ and on neutral tellurium(IV) derivatives (Fig. 28).⁵⁸ Values of the first reduction potential, E_{pc} (V vs. SCE) are compiled in Table 6 for these compounds.

Coulometry studies on cationic dihydroxy tellurium(IV) derivatives **52**, **53**, and **69** indicate that a two-electron reduction occurs ($2 F \text{ mol}^{-1}$) to give chalcogenopyrylium

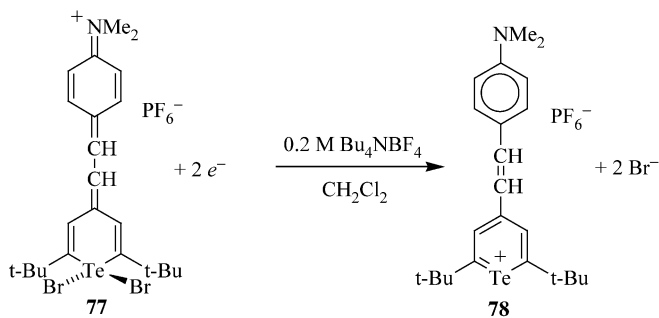
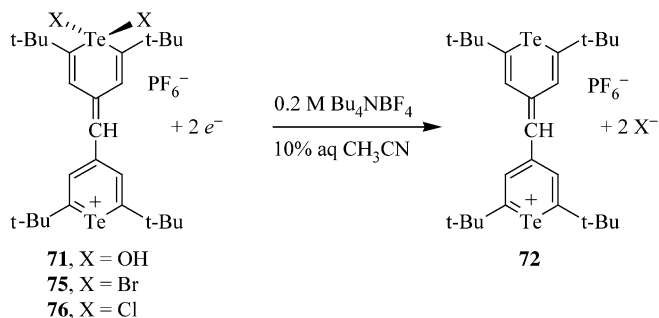
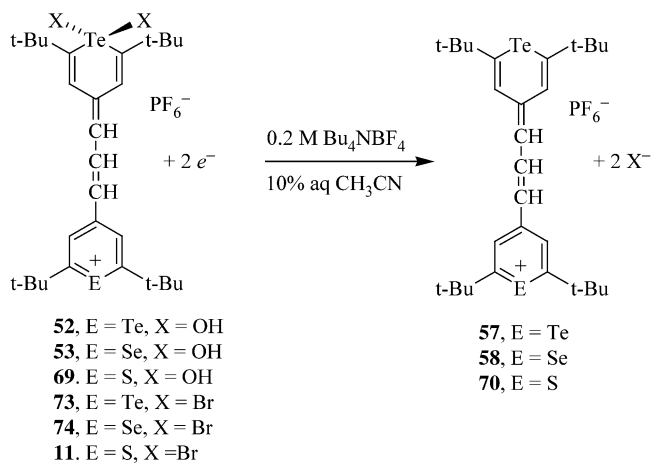


Fig. 27 Two-electron reductions of cationic chalcogenopyrylium dyes with tellurium(IV) atoms in the π -framework.

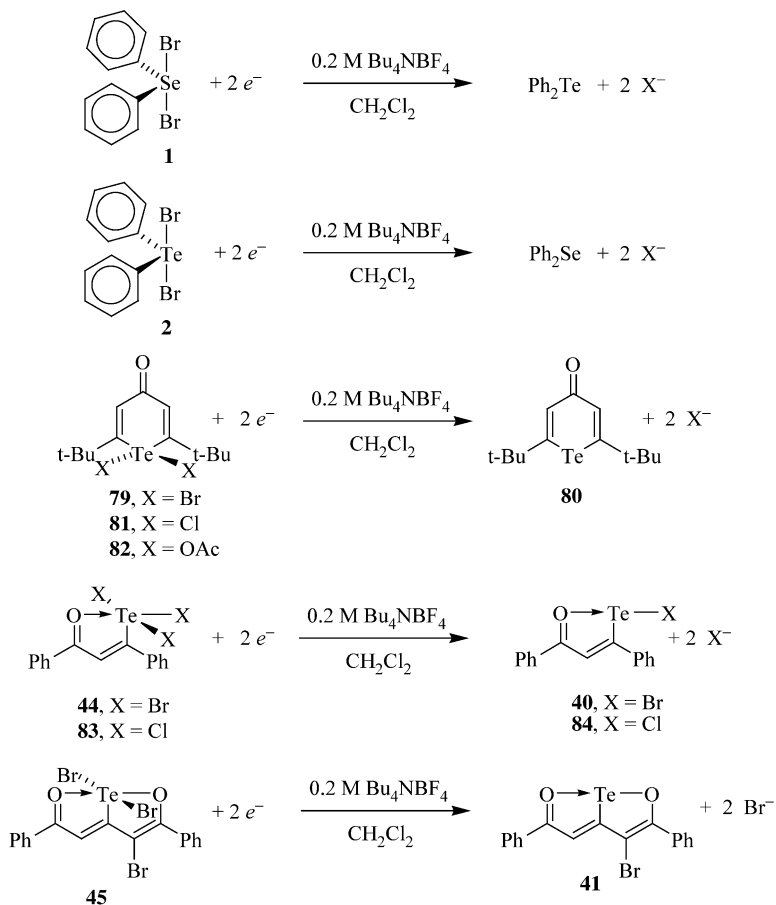


Fig. 28 Two-electron reductions of neutral tellurium(IV) dihalides.

dyes **57**, **58**, and **70**, respectively.⁶⁰ Similarly, dihydroxy monomethine derivative **71** is reduced to telluropyrylium dye **72**. Further reduction of **52**, **53**, and **59** occurs at the same potential as the one-electron reduction¹⁰⁶ of the chalcogenopyrylium dye to the corresponding neutral radical. In the bulk electrolysis, the reduction of **52**, **53**, and **69** is accompanied by the appearance of the near infrared-absorbing band of chalcogenopyrylium dyes **57**, **58**, and **70**, which suggests that two-electron reduction has given the corresponding tellurium(II) compound. There is no evidence for long-lived intermediate tellurium(III) species during the reduction. All four tellurium(IV) compounds are reduced at potentials between -0.10 and -0.22 V (vs. SCE).

The same behavior is observed in the corresponding cationic tellurium(IV) dibromides **11**, **73–75**, and **77** and cationic tellurium(IV) dichloride **76**.⁶⁰ Reduction

Table 6 Electrochemical reduction of organotellurium(IV) compounds and their corresponding organotellurium (II) compounds by cyclic voltammetry and coulometry

Compound	Chalcogen(IV) ligand	E_{Pc}^1 (V) (vs. SCE)	N ($F \text{ mol}^{-1}$)	E_{Pc}^2 (V) (vs. SCE)	Reference
52	OH	-0.10	1.91	-0.42	60
53	OH	-0.22	1.84	-0.45	60
57	-	-0.42	1.01	-	106
58	-	-0.45	0.97	-	106
69	OH	-0.18	2.06	-0.48	60
70	-	-0.48	-	-	106
71	OH	-0.10	-	-0.55	60
72	-	-0.55	-	-	106
73	Br	+0.24	1.95	-0.42	60
74	Br	+0.10	-	-0.44	60
11	Br	-0.05	1.84	-0.48	60
75	Br	+0.18	-	-0.55	60
76	Cl	+0.28	-	-0.55	60
77	Br	+0.48	1.90	-0.45	60
78	-	-0.45	1.01	-	106
79	Br	-0.46	2.10	-1.60	60
80	-	-1.60	-	-	60
81	Cl	-0.68	-	-1.60	60
82	OAc	-1.14	-	-1.60	60
44	Br	+0.11	2.03	-1.36	58
40	-	-1.44	-	-	58
83	Cl	-0.07	-	-0.99	58
84	-	-0.98	-	-	58
45	Br	-0.18	1.97	-1.50	58
41	-	-1.50	-	-	58

Compounds **52**, **53**, **57**, **58**, and **69–72** were measured in 10% aqueous acetonitrile with 0.2 M Bu_4NBF_4 as supporting electrolyte. All other compounds were measured in dichloromethane with 0.2 M Bu_4NBF_4 as supporting electrolyte. A platinum electrode or a platinum gauze basket were the working electrode and all potentials are reported against the saturated calomel electrode (SCE) with a reference potential of 0.0 V. Values of E_{Pc}^1 for **57**, **58**, **70**, **72**, and **78** are actually values of E° , the reversible peak potential. All other values of E_{Pc} are irreversible peak potentials.

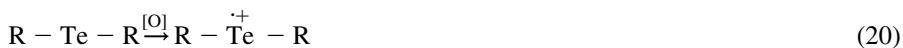
of these species is several hundred millivolts less cathodic in the range of +0.48 V to -0.05 V (vs. SCE). Coulometry again demonstrates that these reductions are two-electron processes ($2 F \text{ mol}^{-1}$) and reduction of the tellurium(IV) species is accompanied by the appearance of the near infrared-absorbing band of the telluropyrylium dye.

In all of the cationic systems described above, reduction of the tellurium(IV) derivative to the tellurium(II) derivative brings the tellurium 5p orbital into conjugation with the carbon π -framework and further delocalizes the positive charge. This drive for conjugation facilitates the reduction. Reduction of neutral tellurium(IV) derivatives such as **44**, **45**, **79**, and **81–83** does not extend conjugation in the same way. As a consequence, reduction of these species is somewhat more cathodic and reduction potentials fall in the range +0.11 to -1.14 V (vs. SCE).⁶⁰

The corresponding selenium(IV) derivatives are less stabilized by the three-center, four-electron bonds in the chalcogen(IV) complex than the tellurium(IV) derivatives. As a consequence, the selenium(IV) derivative is more easily reduced than the tellurium(IV) derivative. Diphenylselenium(IV) dibromide (**1**) undergoes a two-electron reduction with E_{pc}^1 at +0.40 V (vs. SCE) while diphenyltellurium(IV) dibromide (**2**) undergoes a two-electron reduction with E_{pc}^1 at +0.05 V (vs. SCE).¹⁰⁷ Even though selenium(IV) derivatives should be better oxidants than their tellurium(IV) counterparts for thermodynamic reasons, the kinetics associated with ligand exchange at the chalcogen(IV) atom often favor tellurium(IV) as described above.

3 One-electron oxidation of selenium and tellurium compounds

One-electron oxidation of organoselenium and organotellurium compounds results in initial formation of a radical cation (equations (19) and (20)). The eventual fate of the radical cation depends on several variables, but is typically a Se(IV) or Te(IV) compound. The scope of this section will be the one-electron oxidation of selenides and tellurides that are not contained in a heteroaromatic compound, and ones in which the Se and Te are bonded to two carbons, rather than to other heteroatoms. Tellurium- and selenium-containing electron donor molecules have been reviewed.¹⁰⁸



The one-electron oxidations can occur under a range of oxidizing conditions that provide data relative to a reference, so that ease of oxidation can be compared. These methods include cyclic voltammetry (CV) and other electrochemical methods; the use of chemical one-electron oxidants such as the nitronium ion; and pulse and γ -radiolysis, in which extremely reactive oxidizing radicals are generated. Ionization potentials (IPs) have also been determined for some compounds for comparison to the oxidation potentials. Electron spin resonance (ESR) data provide information regarding the spin distribution in the resulting radical cations. Structural information from X-ray crystallographic data is available for starting materials, radical cations, or both in some cases. Molecular orbital calculations have been performed on some radical cations to gain an understanding of the structure of the electron distributions in these species. Finally, the ease of oxidation of selenium and tellurium compounds can be assessed in "functional assays", by measurement of their abilities to prevent oxidative chemical processes such as azo-initiated linoleic acid oxidation. These results are relevant to the use of organoselenium and organotellurium compounds as antioxidants.

In several cases, a series of compounds containing the chalcogens O, S, Se, and Te has been prepared, and the behavior of the compounds under oxidizing conditions evaluated and compared. In other cases, a more limited set of compounds has been evaluated in the same way. In another subset, the impact of substituents has been examined. Finally, the impact of other structural variables, such as the hybridization of the atoms and the structure of the groups to which the chalcogen is attached, have been explored.

CV of many organoselenium and tellurium compounds results in one-electron oxidations that are not reversible, so peak potentials (E_{Pa}) are often given rather than oxidation potentials ($E_{1/2}$). In some cases the peak potential corresponds to two one-electron oxidations due to rapid chemical reaction of the initial radical cation, followed by the loss of a second electron. A further complication is that different solvents, electrodes, and scan speeds can give E_{Pa} or $E_{1/2}$ values that are similar but clearly non-identical. In addition, the time frame of CV with standard electrodes is presumed to be sufficiently long such that equilibrium conditions exist for both the oxidation and reduction processes, and they are microscopically reversible. It is presumed that for a series of structurally related compounds, factors such as solvent reorganization are similar within the series, so that as long as one is examining differences between oxidation behavior, good conclusions can be made regarding trends. Finally, a range of different reference electrodes or redox couples was used in examining one-electron oxidation. The literature data were not changed to reflect this, but it is useful to know the potentials of the reference electrodes relative to the normal hydrogen electrode (NHE).⁵⁴ The relevant numbers are Ag/AgCl (0.223 V), SCE (saturated calomel electrode) (0.241 V), Ag/0.1 M AgNO₃ (0.580 V).

To make clear what type of oxidation potential data are being cited, when thermodynamics-based pulse radiolysis data are cited, such data will be labeled E° , while $E_{1/2}$ will be used for reversible CV data. IPs are obtained under adiabatic conditions, with no gain or loss of heat.

Simply using the electronegativities or IPs of the chalcogens would lead to the prediction that for a series of compounds, the O-containing compound would oxidize least readily and the Te-containing compound would be most easily oxidized (Table 7). In most cases, the oxidation data match this prediction. Only in a small number of cases does it not, and in those cases it can be attributed to the structural environment in which the chalcogen is found.

DIARYLSELENIDES AND TELLURIDES

Diphenylselenides and tellurides

The oxidation potentials of diphenyl selenides^{109–111} and diphenyl tellurides^{110,112} have been measured by electrochemical methods, as well as by pulse radiolysis.⁷⁴ Pulse electrolysis was used to determine E° values for diphenylsulfide (**84**), diphenylselenide (**85**), and diphenyltelluride (**23**).⁷⁴ In each case, equilibrium

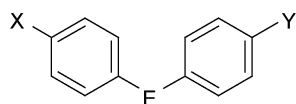
Table 7 Electronegativities and ionization energies of the chalcogens

Chalcogen	Atomic radius (pm)	Electronegativity ^a	Ionization energy (kJ/mol)
O	73	3.5	1314
S	104	2.5	1000
Se	117	2.4	941
Te	137	2.1	869

^aFrom the Pauling scale.

constants from several oxidants were used to generate the E° values (vs. NHE), and led to results that were within 0.04 V of one another (Table 8). The expected trends were observed, with **23** most readily oxidized (1.14 V) and **84** least easily oxidized (1.54 V). These data are consistent with the relevant electrochemical peak potentials E_{Pa} (vs. SCE) obtained for **85** and **23** (Table 8).¹¹⁰

In addition to evaluating the effect of the chalcogen atom on ease of oxidation, series of para-substituted diarylselenides and tellurides have been prepared, and the impacts of the substituents and the heteroatom on the oxidation potentials have been studied.^{110,112} In the most extensive of these studies, the peak potentials of 10 para-substituted diarylselenides **85**, **86a–i** and 14 diaryltellurides **23**, **87a–m** were determined by CV (Table 8).¹¹⁰ For these series, the substituents at the para position had a wide range of Hammett σ_p/σ_p^+ values, ranging from the strongly electron-withdrawing nitro group (0.71/0.79) to the electron-donating dimethylamino group (−0.16/−1.70). The tellurides oxidized at lower potentials than the corresponding selenides, but there was a range of overlap between the two series, with electron-rich selenides **86h–i** oxidizing at a lower potential than all of the tellurides that did not have an electron-donating O- or N-substituent. The di-4-hydroxyphenyltelluride (**87h**) and di-*p*-aminophenyltellurides (**87j**) had E_{Pa} values that correlated reasonably well with the data from pulse radiolysis (Table 8).⁷⁴ Plots of E_{Pa} vs. σ_p^+ for the diarylselenides and diaryltellurides showed strong linear correlations with *R*-values of 0.98 in each case (Fig. 29). The *X*-values were calculated using equation (21), to give $\rho = 0.41$ for the selenides and $\rho = 0.24$ for the tellurides, indicating that the E_{Pa} values in the Se series are more sensitive to substituent effects than in the Te series. This is consistent with the expected poorer overlap between the aryl ring π system and the larger orbitals on Te relative to those on Se. In an effort to better understand the role of the two para substituents, four unsymmetrical diarylselenides (**86j–m**) and two unsymmetrical diaryltellurides (**87n–o**) were prepared and analyzed by CV (Table 8). The results were not clear-cut. When the σ_p^+ values for the two para substituents were dissimilar (**86j–k**), the experimental E_{Pa} was much closer to that of the symmetrical diarylselenides of the more electron-donating substituent, rather than being close to the average of the two symmetrical diarylselenides. That is, it behaves as if predominantly one of the two substituted phenyl rings is interacting with the tellurium orbitals. When both substituents were strongly electron-donating, as

Table 8 Oxidation and peak potentials of diaryl chalcogenides

Compound	E	X, Y	E° (V) (vs. NHE) ^a	E_{Pa} (V) (vs. Ag/AgCl) ^b
84	S	H	1.54	
85	Se	H	1.37	1.38
23	Te	H	1.14	0.95
86a	Se	NO ₂		1.76
86b	Se	CO ₂ H		1.54
86c	Se	Cl		1.44
86d	Se	F		1.38
86e	Se	Me		1.32
86f	Se	NHAc		1.25
86g	Se	OMe		1.22
86h	Se	NH ₂		0.80
86i	Se	NMe ₂		0.68
86j	Se	NO ₂ , NHAc		1.44
86k	Se	NO ₂ , NH ₂		0.98
86l	Se	NH ₂ , NHAc		0.84
86m	Se	NH ₂ , succinimidyl		0.88
87a	Te	NO ₂		1.14
87b	Te	CF ₃		1.12
87c	Te	CO ₂ Me		1.09
87d	Te	Br		0.96
87e	Te	Cl		0.98
87f	Te	F		0.98
87g	Te	Ph		0.89
87h	Te	Me		0.89
87i	Te	OMe		0.80
87j	Te	OH	0.95	0.80
87k	Te	NHPh		0.66
87l	Te	NH ₂	0.80	0.56
87m	Te	NMe ₂		0.50
87n	Te	NMe ₂ , OMe		0.65
87o	Te	OH, H		0.93

^aData from Ref. 74; subtract 0.2 V to obtain the Ag/AgCl values.

^bData from Ref. 110, obtained using a glassy carbon working electrode at 1–3 mM sample and 35 mM Et₄NClO₄ in dry CH₃CN (<0.02% water) at a scan speed of 100 mV s⁻¹.

found in tellurides **87n** and **87o**, the experimental E_{Pa} was closer to the average of the two symmetrical diarylselenides. This leaves ambiguity regarding the role of the two phenyl rings and their role in the oxidation potential.

$$\Delta E_{1/2} = (E_{1/2})_X - (E_{1/2})_H = \rho\sigma \quad (21)$$

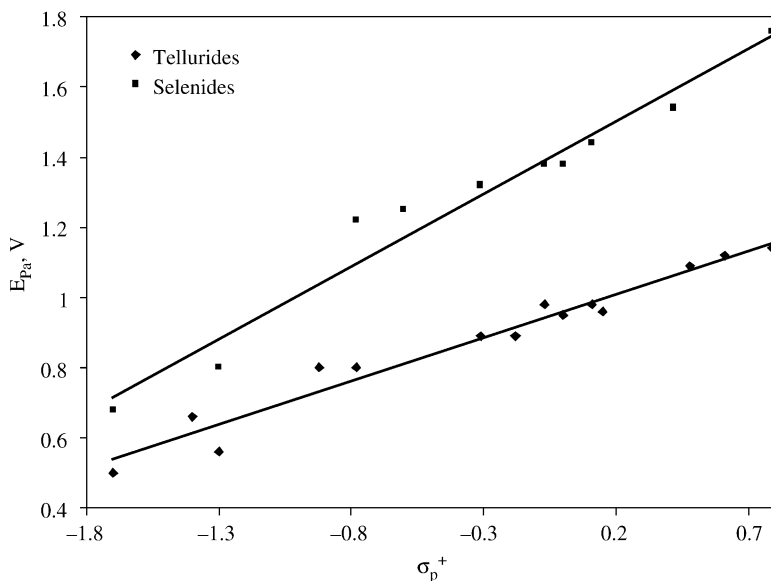


Fig. 29 Correlation of σ_p^+ with E_{Pa} for diaryl tellurides. Data from Ref. 110.

Molecular modeling

Molecular modeling studies were performed on diphenyltelluride (**23**) and nine symmetrical para-substituted diaryltellurides (**87b,d-f,h-j,l-m**), as well as their radical cations.¹¹³ *Ab initio* calculations were performed at the Hartree–Fock level using the 3-21G(d) basis set, providing stabilization energies of the radical cations, Mulliken charges, and orbital energies, among other values. An attempt to use PM-3 calculations resulted in poor geometries for the tellurium compounds. Instead, the 3-21G(d) basis set was used because it had been used previously for generating accurate molecular structures of aryl chalcogenide compounds, and in particular had produced reasonable structures for tellurium-containing compounds, which are typically less well parameterized. Resonance stabilization energies (RSE's) for the 10 tellurides were obtained by calculating the energy difference ΔE between the diaryl telluride radical cation and the diaryl telluride, then subtracting this energy from the ΔE value for diphenyl telluride (**23**) (Table 8). Validation of this approach came from the correlation of these RSEs with the peak potentials of the compounds (Fig. 30). As would be expected, lower E_{Pa} values correlated with more positive RSE values, and vice versa. That is, more easily oxidized tellurides give more stable radical cations. The R -value was 0.93. A similar but slightly less robust correlation was found between the calculated Mulliken charge at the tellurium atom and the peak potentials ($R = 0.87$), with lower peak potentials correlating with less charge on the Te, as would be expected (Fig. 31).

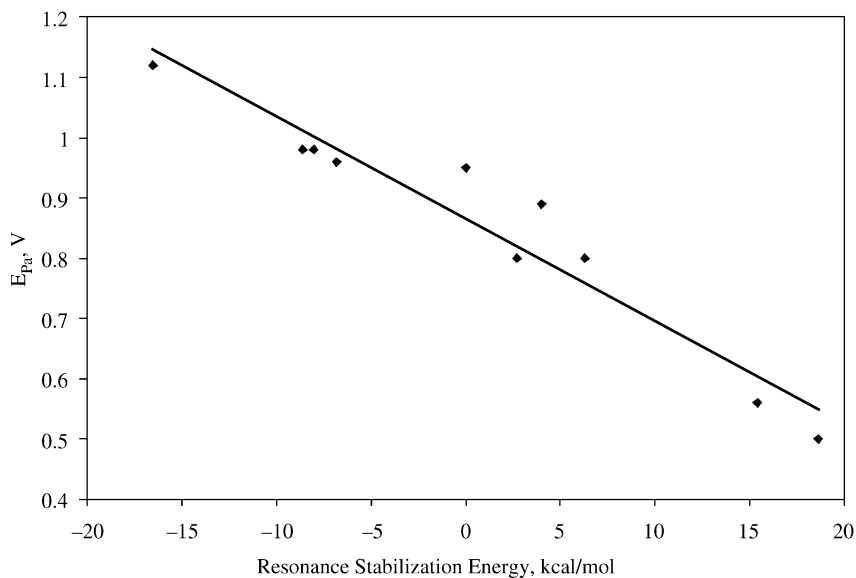


Fig. 30 Correlation of resonance stabilization energy for diaryl telluride radical cations with E_{Pa} . Data from Ref. 113.

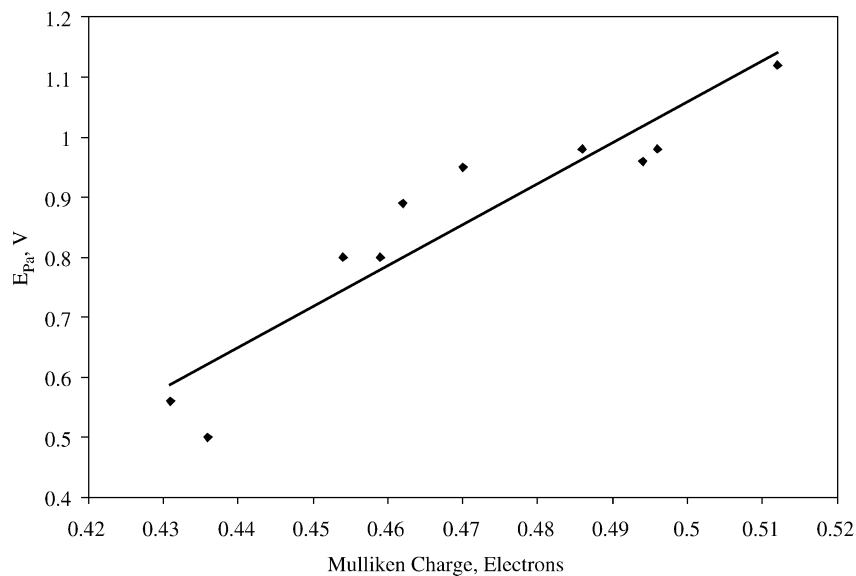


Fig. 31 Correlation of Mulliken charge for diaryl telluride radical cations with E_{Pa} . Data from Ref. 113.

Mechanistic studies

The final products of oxidation of diarylselenides and tellurides (and sulfides as well) in the presence of nucleophiles are the corresponding chalcogen (IV) compounds. In the presence of water, the selenoxide or telluroxide (or the corresponding dihydroxy selenane or tellurane) is the final product. This still leaves several possible pathways, leveraged from early mechanistic studies done using electrochemical techniques on diaryl sulfides¹¹⁴ and outlined by Engman (Fig. 32).¹¹⁰ In these pathways, the initial radical cation can react with a nucleophile present in solution, or the dication resulting from further oxidation or disproportionation can do so.

The details of the first step of the mechanism were studied for diphenylselenide and diphenyltelluride by pulse radiolysis.⁷⁴ The oxidation rates for radical cation formation were large, with rate constants $k = 10^9 - 10^{10} \text{ M}^{-1} \text{ s}^{-1}$. The same radical cations could be made in identical yield by one-electron reduction of the corresponding radicals, $[\text{Ph}_2\text{SeOH}]^\cdot$ and $[\text{Ph}_2\text{TeOH}]^\cdot$. From studies of pH vs. absorbance, the $\text{p}K_a$'s of the selenium and tellurium radical cations could be estimated (equations (22) and (23)). The radical cation from Ph_2Se is significantly less acidic ($\text{p}K_a \geq 13$) than that from Ph_2Te ($\text{p}K_a \geq 10.3$). Concentration studies were undertaken to look for the products of reaction of the radical cations with the starting diaryl chalcogenides to give dimer species having 2-center, 3-electron bonds. Up to the concentration limits studied ($\sim 0.01 \text{ M}$), no spectral changes were observed that could be attributed to dimer radical cation formation. This could reflect the difference in distribution of the odd electron between dialkyl selenides, which are known to form dimer radical cations¹¹⁵ and diaryl selenides. Presumably in the diaryl selenide there is delocalization of the charge and unpaired electron into the aryl ring.

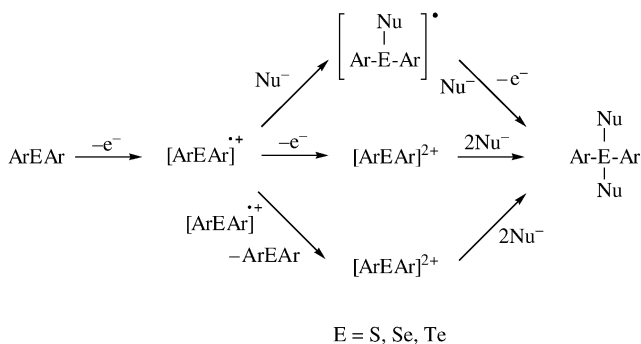
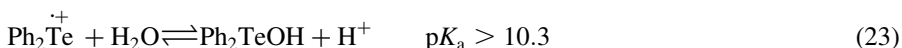
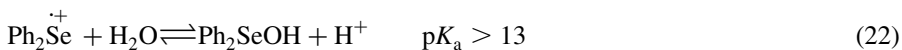


Fig. 32 Pathways for oxidation of diaryl chalcogenides.¹¹⁰

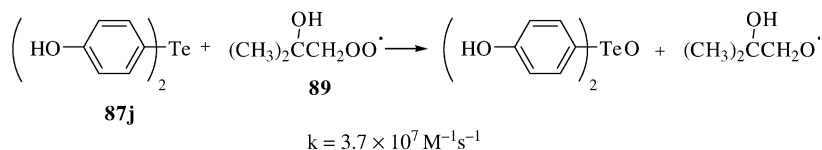
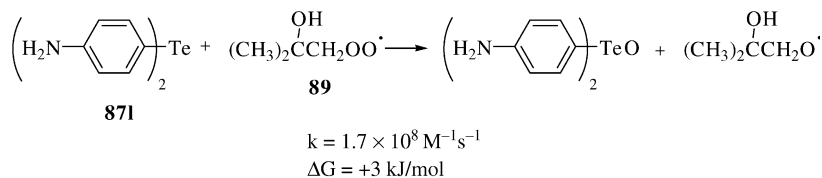
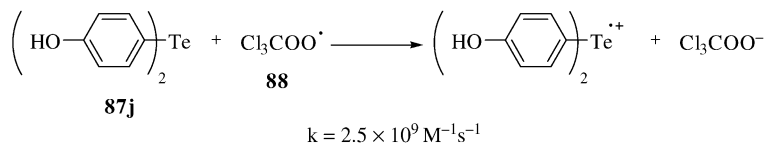
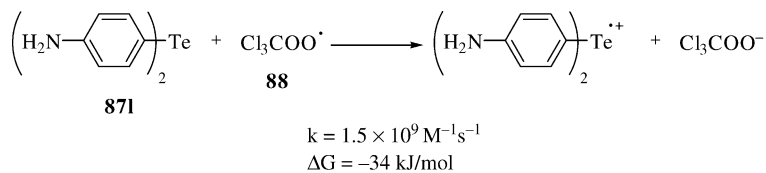
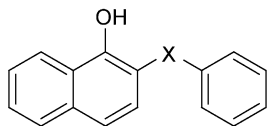


Fig. 34 Reactions of diaryl tellurides with peroxy radicals.⁷³

Table 9 Peak potentials for oxidation of phenyl chalcogenyl-1-naphthols



Compound	X	E_{Pa} (V) (vs. SCE)
90	CH ₂	1.24
91	S	1.27
92	Se	1.25
93	Te	1.00

Data from Ref. 117, obtained using a platinum button working electrode at 1 mM sample and 130 mM Bu₄NClO₄ in dry CH₂Cl₂ at a scan speed of 100 mV s⁻¹.

model system, showing that the oxidation potential is correlated with antioxidant capabilities for this system.

ALKYLARYLSELENIDES AND TELLURIDES

Alkylaryl selenides and tellurides, ArSeR and ArTeR, have much in common with their diaryl counterparts, with trends in oxidation potentials paralleling the electron density at the chalcogen. They differ, though, in the reaction chemistry available to the resulting radical cation. As in the diaryl case, the radical cation is eventually converted to the Se(IV) or Te(IV) compound – which in the presence of water is the selenoxide or telluroxide (likely hydrated). Unlike the diaryl case in which neither carbon–chalcogen bond cleavage nor loss of a proton α to the chalcogen occurs readily, these are possibilities for alkyl aryl selenides and tellurides when water or another good nucleophile is not present (Fig. 35).¹¹⁸ The product distribution is determined by the presence or absence of nucleophiles, the chalcogen, and the structure of the alkyl group.

Aryl methyl selenides and tellurides

The arylmethylselenides ArSeMe and tellurides ArTeMe pose somewhat of a special case in the alkyl aryl compounds, due to the comparatively low reactivity of their radical cations, which do not easily undergo cleavage of the chalcogen–methyl bond, due to the low stability of the resulting methyl radical or cation.

For comparison within the chalcogens, the oxidation potentials of the Ph–E–Me series **94**, **95b**, **96b**, and **97b**, where E = O, S, Se, Te, respectively, were evaluated by pulse radiolysis.^{111,119} Consistent with the analogous diaryl series, the E° values for this series indicate that the compounds are increasingly easy to oxidize, with telluride **97b** most easily oxidized (0.74 V) and ether **94** least easily oxidized (1.62 V), with these values vs. NHE (Table 10). For a broader comparison, series of four or five para-substituted arylmethylsulfides, selenides, and tellurides, **95a–e**, **96a–e**, and **97a–d** were prepared and their E° values determined in the same manner (Table 10).¹¹¹ The same trends were observed, with the thioethers least

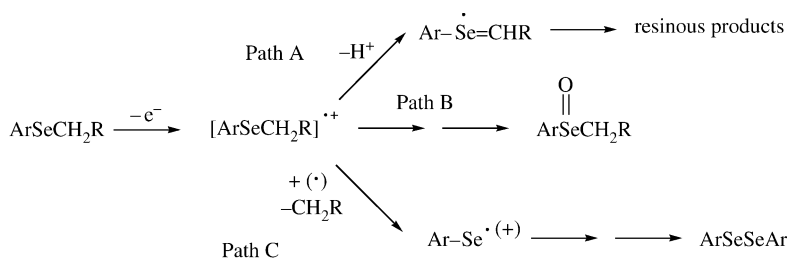
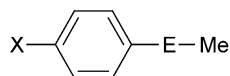


Fig. 35 Reaction pathways for oxidation of alkyl aryl selenides.^{118,128}

Table 10 Oxidation and peak potentials of aryl methyl chalcogenides

Compound	E	X	E° (V) (vs. NHE) ^a	E_{Pa} (V) (vs. Ag/AgCl) ^b	$E_{1/2}$ (V) (vs. Ag/0.1 M AgNO ₃) ^c
94	O	H	1.62		
95a	S	CF ₃	1.45	1.80	
95b	S	H	1.45	1.56	
95c	S	Me	1.42	1.48	
95d	S	OMe	1.43	1.43	
95e	S	NMe ₂	0.65	0.88	
96a	Se	CF ₃	1.20	1.34	
96b	Se	H	1.09	1.22	0.965
96c	Se	Me	1.07	1.20	0.870
96d	Se	OMe	1.09	1.12	0.745
96e	Se	NMe ₂	0.60	0.80	
96f	Se	NH ₂			0.410
96g	Se	NO ₂			1.185
96h	Se	F			0.935
97a	Te	CF ₃	0.75	0.78	
97b	Te	H	0.74	0.77	
97c	Te	Me	0.72	0.71	
97d	Te	OMe	0.73	0.66	
97e	Te	NMe ₂		0.52	

^aData from Ref. 111 except for **94**, from Ref. 119; in water; subtract 0.2 V to obtain the Ag/AgCl values.

^bData from Ref. 110, obtained using a glassy carbon working electrode at 1–3 mM sample and 35 mM Et₄NClO₄ in dry CH₃CN (<0.02% water) at a scan speed of 100 mV s⁻¹.

^cData from Ref. 120, obtained using a platinum rotating disk working electrode at 1 mM sample and 100 mM Et₄NClO₄ in dry CH₃CN at a rotation speed of 24 s⁻¹.

easily oxidized and the tellurides most easily oxidized. However, there was little or no effect of the substituents on E° , with the exception of the strongly electron-donating dimethylamino group, which significantly lowered the oxidation potential. These trends can be compared to those found in electrochemical E_{Pa} values measured in acetonitrile with a glassy carbon electrode (Table 10).¹¹⁰ The E_{Pa} values are consistently higher than the E° values, but the same trends in ease of oxidation are seen across the chalcogens. Relative to the pulse radiolysis conditions, substituents were found to have a much greater impact on the ease of oxidation in these CV measurements. Thus, plots of E_{Pa} vs. σ_p^+ for these three series correlated well, as they did in the diaryl series, with $R = 0.98$ in all cases (Fig. 36). The ρ -values were 0.39 for S, 0.24 for Se, and 0.12 for Te. These ρ -values show that the electron density at sulfur is most sensitive to substituent effects, and tellurium is least sensitive. They also show the E_{Pa} values of the aryl methyl selenides and tellurides to be less sensitive to substituents than are those of their diaryl counterparts, where the corresponding ρ -values were greater. This could mean that

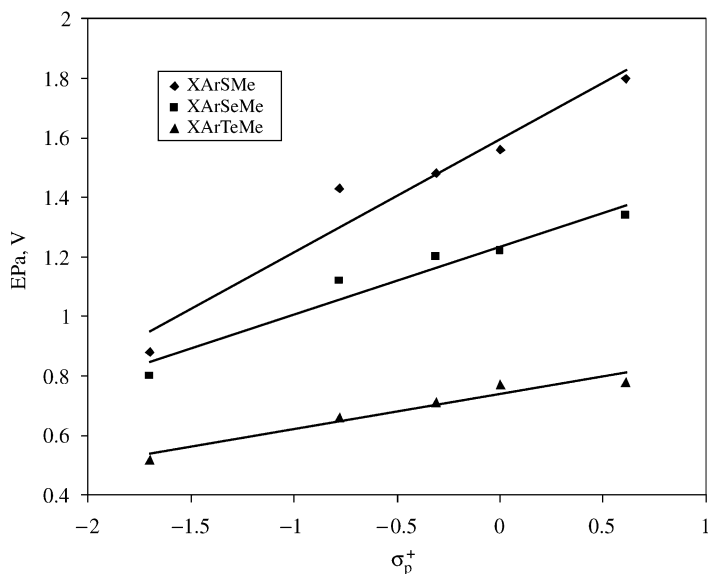


Fig. 36 Correlation of σ_p^+ with E_{Pa} . Data from Ref. 110.

both of the aryl groups are important in interacting with the chalcogen atom, or that for the arylmethylchalcogenides, the electronic effect of the methyl group is dominant. Although the two compounds having the most electron donating substituent, di(4-dimethylaminophenyl)telluride **87m** and methyl(4-dimethylaminophenyl)telluride **97e**, have very similar E_{Pa} values (0.50 V and 0.52 V), the lines showing the correlations of E_{Pa} with σ_p^+ quickly diverge for less electron-donating substituents, with the arylmethylchalcogenides being more easily oxidized. As was true for the diaryltellurides, the calculated RSE values for the arylmethyltelluride radical cations could be correlated with the E_{Pa} values ($R = 0.85$) and the Mulliken charges ($R = 0.93$), but the correlations were weaker.

Electrochemical oxidation potentials ($E_{1/2}$) were also obtained for a series of para-substituted arylmethylselenides (**96b–d,f–h**) using a platinum oxide rotating disk electrode (Table 10).¹²⁰ They showed trends similar to those found in the peak potentials determined by CV: The $E_{1/2}$ values correlated with the electron donating abilities of the substituent, with electron-donating groups giving less positive $E_{1/2}$ values, and with electron-withdrawing groups more positive ones. Very small changes in the potentials were seen when trifluoroacetic acid was added to suppress deprotonation at the methyl group (+0.01 to +0.07 V)¹²¹ and when extrapolations to infinite dilution were made to compensate for adsorption of the selenide to the electrode (−0.01 to −0.05V)¹²², but the trends were unchanged.

The greater impact of substituents on ease of oxidation in acetonitrile than in water (Table 10) is due to the importance of solvation of the radical cation in more

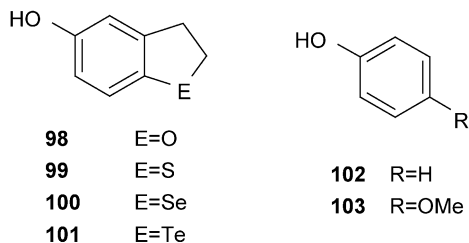
polar solvents, particularly for less stable radical cations.¹²³ In fact, the gas-phase ionization energies for a series of para-substituted arylmethylsulfides showed even more sensitivity to substituent effects than the E_{Pa} values obtained in acetonitrile. A more positive ρ -value was illustrated graphically for this case, although the number was not given.

Alkylarylselenides

Unlike the aryl methyl selenides, the alkyl aryl selenides with alkyl groups of two carbons or more are able to undergo scission of the radical cation at the C_{sp}^3 -Se bond, yielding the ArSe radical (Fig. 35). This can impact product distribution, particularly under conditions in which water is not present to react with the radical cation. Trends in ease of oxidation typically seen in series of chalcogen compounds can still be observed, and are consistent with trends in the diaryl chalcogenides and aryl methyl chalcogenides.

For example, the CV oxidation and peak potentials of the 2,3-dihydrobenzo[b]-furan-5-ol series **98**–**101** in acetonitrile show the expected general trends (Table 11), although the oxidation of **98** is irreversible, that of **99** is quasireversible, and those of **100** and **101** are reversible.¹²⁴ (These data illustrate the difficulty in comparing ease of oxidation even within a series of analogous compounds.) The authors compared the values found for these compounds with those of the arylmethylchalcogenides **94**, **95b**, **96b**, and **97b** (Table 10). They saw good correlation for the selenium and

Table 11 Oxidation potentials of 2,3-dihydrobenzo[b]furan-5-ols



Compound	E_{Pa}^a , $E_{1/2}^b$, or $E^{\circ c}$ (V) (vs. SCE)	Reference
98	1.11 ^a	124
99	1.11 ^b	124
100	0.88 ^b	124
101	0.49 ^b	124
102	1.3 ^c	125
103	~1.1 ^c	125

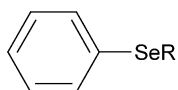
^{a,b}Data from Ref. 124, obtained using a glassy carbon working electrode at 1 mM sample and 100 mM Bu₄NClO₄ in dry CH₃CN at a scan rate of 500 mV s⁻¹.

^cData from Ref. 125, determined by pulse radiolysis in H₂O.

tellurium compounds, but not for the oxygen and sulfur compounds **98** and **99**, which were oxidized much more easily than were **94** and **95b**. They attributed this to the ease of oxidation of the phenol moiety on the aryl ring relative to the O and the S of the ether and thioether, respectively. This view was supported by the literature E° values for both phenol (**102**) and 4-methoxyphenol (**103**) (Table 11).¹²⁵ The values of E° for both **98** and **99** (1.11 V) are essentially identical to that of **102** (~ 1.1 V).

Oxidation potentials of a series of alkylphenylselenides were determined vs. Ag/AgNO₃ using glassy carbon, oxidized platinum, and lead oxide rotating-disc electrodes as the working electrodes, with the data for the oxidized Pt electrode shown (Table 12).¹²⁶ It was found that the $E_{1/2}$ values do not correlate with the Taft inductive parameter σ^* , which is a measure of the electron-donating ability of the alkyl group. Instead they correlate with the steric parameters of the alkyl groups. Thus, *t*-butylphenylselenide **104e** had the highest oxidation potential, 1.13 V. The dominance of steric rather than electronic effects in the correlation obtained reflects the nature of CV, where there is a physical interaction between the surface and the molecules. Presumably this does not reflect relative ease of oxidation under conditions in which electron-transfer would occur with chemical oxidation in solution. The major product of preparative controlled potential electrolysis at 1.0–1.12 V vs. Ag/AgNO₃ of each compound in this series in the absence of nucleophiles except for methylphenylselenide **96b** was the corresponding diaryl diselenide (Fig. 35, Path C).¹²⁷ Because the diselenide is presumably formed via C_{sp}³–Se bond cleavage of the radical cation, it is not surprising that it is not formed from methylphenylselenide radical cation, given the high energy of the methyl cation and radical. Bulk electrolysis in the presence of a nucleophile, excess acetate ion, resulted in α -acetoxylation (equation (24)), probably by two one-electron oxidations and loss of a proton, followed by reaction of the acetate

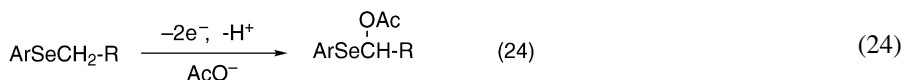
Table 12 Oxidation potentials of alkyl phenyl selenides



Compound	R	$E_{1/2}$ (V) (vs. Ag/0.1 M AgNO ₃)	$-R_s$	σ^*
96b	Me	0.96	1.4	0
104a	Et	0.99	1.82	-0.1
104b	CH ₃ (CH ₂) ₂ -	1.02	2.01	-0.115
104c	(CH ₃) ₂ CH-	1.04	2.24	
104d	(CH ₃) ₂ CHCH ₂ -	1.06	2.36	-0.125
104e	(CH ₃) ₃ C-	1.13	2.79	-0.3
104f	CH ₃ (CH ₂) ₄ -	1.04	2.23	-0.162
104g	(CH ₃) ₂ CH(CH ₂) ₂ -	1.08	2.51	-0.162
104h	CH ₃ (CH ₂) ₅ -	1.05	2.33	

Data from Ref. 126, obtained using an oxidized platinum rotating disk working electrode at 1 mM sample and 10 mM Et₄NClO₄ in dry CH₃CN at a rotation speed of 25 s⁻¹.

ion with the resulting cation.¹²⁷



Aryl trimethylsilylmethyl selenides also yielded the diaryl diselenide as the major product, but possibly through a somewhat different mechanism, due to the increased stability of the initially formed radical cation (Fig. 37).¹²⁸

DIALKYLSELENIDES AND TELLURIDES

Dimethylselenide and telluride

The simplest dialkylchalcogenides R-E-R are the dimethylchalcogenides **105a**–**108a**, with R=Me. The IPs have been calculated from absorption spectra and the expected trend is present, with dimethyltelluride oxidized most readily and dimethyl ether oxidized least readily (Table 12).^{129,130} The electron is removed from a valence p orbital. Radical cations **105b**–**108b** from the ether,¹³¹ sulfide,¹³² selenide,^{115,132} and telluride¹²⁹ have been generated by γ -irradiation in a Freon matrix. In this solid matrix at 77 K, the radical cations can be observed by ESR. The IP values of the radical cations correlate linearly with their proton hyperfine coupling constants $A(^1\text{H})$, which provide a measure of the delocalization of electrons from the C–H σ bonds into the singly occupied chalcogen p orbital (Table 13, Fig. 38).¹²⁹ That is, the larger the IP, the greater the delocalization of the unpaired electron. This relationship is consistent with the best overlap being between the oxygen and carbon valence orbitals that are similar in size, while the increasing size of the chalcogen p orbital in the series S, Se, and Te results in successively poorer overlap.

At higher concentrations or under annealing conditions, radical cations **106b**–**108b** form dimer radical cations **106c**,^{132–134} **107c**,^{132,135} and **108c**,¹²⁹ respectively (Fig. 39). The ESR data for dimethylselenide dimer radical cation **107c** are consistent with two-center three-electron bonding, in which two electrons are in a σ bond between the two chalcogens, while the third electron is in a σ^* orbital.¹¹⁵

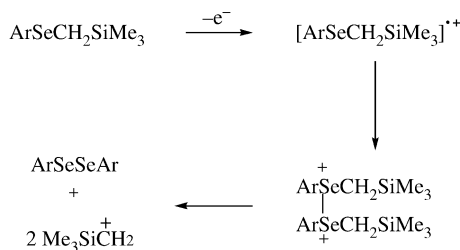
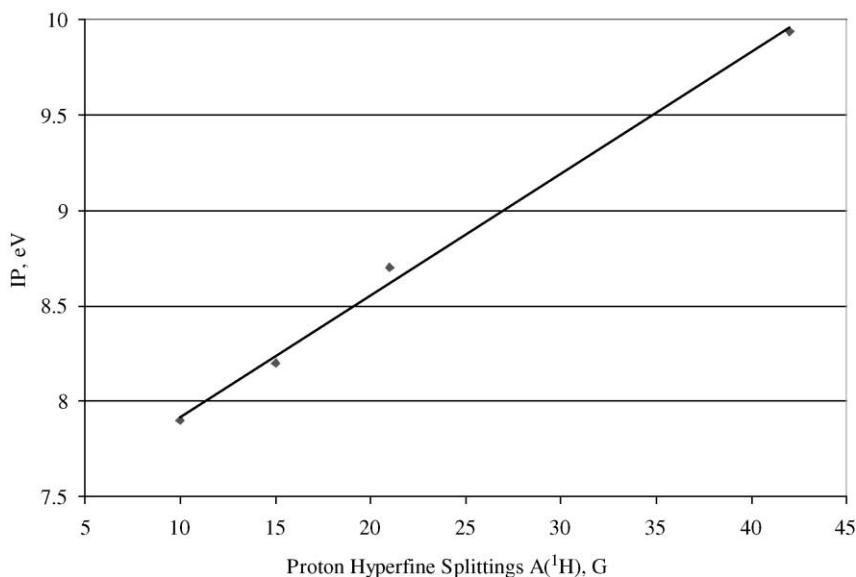


Fig. 37 Reaction pathways for oxidation of aryl trimethylsilylmethyl selenides.¹²⁸

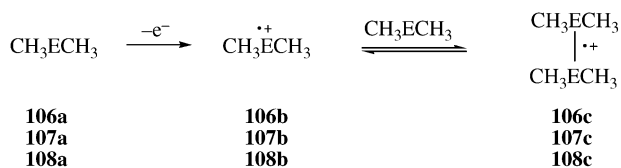
Table 13 Ionization potentials and proton hyperfine splittings for dimethyl chalcogenides, CH_3ECH_3

Compound	E	IP (eV)	$A(^1\text{H}), \text{G}$
105a	O	9.94	42
106a	S	8.7	21
107a	Se	8.2	15
108a	Te	7.9	10

Data from Ref. 129.

**Fig. 38** Correlation of ionization potentials and proton hyperfine splitting constants. Data from Ref. 129.

Molecular orbital calculations using PM3 were performed on the chalcogenides, their radical cations, and the dimer dication. ¹³⁵ The radical cations were calculated to be π radicals, with the unpaired electron in a p orbital perpendicular to the plane containing the two carbons and the chalcogen atom (Fig. 40), as observed experimentally for the S and Se cases. Similar modeling of the corresponding

**Fig. 39** Radical cations and dimer radical cations from dimethyl chalcogenides.

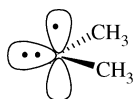


Fig. 40 The structure of the radical cation from dimethyl chalcogenides.

tellurium compounds did not correspond well with experiment, as the calculations showed the radical cation to be a σ radical cation rather than a π radical cation. This probably reflects significantly better parameterization for S and Se than for Te within the PM3 program.¹³⁵

Intramolecular dimer radical cation and dimer dication formation

Just as intermolecular interactions result in dimer radical cation formation from a radical cation and a molecule of starting material, the presence of two chalcogen atoms within a molecule in proximity to one another can result in intramolecular dimer radical cation formation.

The impact of intramolecular interactions on the oxidation potentials of dithioethers compounds has been studied extensively,^{136–138} but there has been much less exploration of the corresponding processes in the selenium and tellurium analogs. However, series of dithioethers (**109a–d**), selenothioethers (**110a–e**), and diselenoethers (**111a–e**) having a range of chain lengths between the two chalcogens of from one to five carbons have been prepared, and their oxidation under electrochemical and free radical oxidation conditions evaluated (Table 14).^{136,137} By CV, the first oxidation peak is a two-electron oxidation, and is not reversible even at high scan speeds. By analogy to the well-documented dithioethers, this presumably represents one-electron oxidation to the intramolecular radical cation, followed by a second one-electron oxidation to a σ^* orbital to give the dication.¹³⁶ The starting dichalcogenodiethers with three methylene groups between the two chalcogens consistently have the lowest E_{Pa} values, possibly indicating that intramolecular interactions of the chalcogen atom are occurring prior to oxidation.¹³⁷ These peak potentials correlate with the λ_{max} values obtained for the radical cations under pulse radiolysis conditions. The radical cations with $n = 3$ have the shortest wavelength transitions.¹³⁷ Because this transition is believed to be a σ/σ^* transition of the two-center three-electron dichalcogen bond, this higher energy transition represents a more stable bonding interaction for the two chalcogens when they are part of a five-membered ring rather than a larger or smaller one.

In related work,¹³⁹ the oxidation of diselenoether **111c** was compared to that of 1,5-diselenacyclooctane (**112**), in which the two selenium atoms are connected by a second $-\text{CH}_2\text{CH}_2\text{CH}_2-$ bridge (Table 15). Just as **111c** was oxidized more easily than dihexylselenide **114** ($E_{Pa} = 0.55$ V vs. $\text{Ag}/0.1$ M AgNO_3 , compared to 0.98 V for **114**), **112** is even more easily oxidized ($E_{Pa} = 0.25$ V), presumably due to the

Table 14 Oxidation peak potentials and λ_{\max} values for the radical cations from dichalcogenoethers, $\text{CH}_3\text{E}^1(\text{CH}_2)_n\text{E}^2\text{CH}_3$

Compound	E^1	E^2	n	E_{pa} (V) (vs. Ag/0.1 M AgNO ₃)	λ_{\max} (nm), for radical cation
106a	S	–	–	1.45	465
107a	Se	–	–	0.970	470
109a	S	S	1	1.130	660
109b	S	S	2	1.095	520
109c	S	S	3	0.742	440
109d	S	S	4	0.900	460
110a	S	Se	1	0.894	620
110b	S	Se	2	0.850	550
110c	S	Se	3	0.600	435
110d	S	Se	4	0.665	455
110e	S	Se	5	0.791	470
111a	Se	Se	1	0.820	680
111b	Se	Se	2	0.600	550
111c	Se	Se	3	0.500	440
111d	Se	Se	4	0.580	460
111e	Se	Se	5	0.660	470

Data from Ref. 137, measured at 2 mM in CH₃CN with 100 mM tetraethylammonium perchlorate, with a platinum or glassy carbon rotating disk electrode and a scan speed of 250 mV s⁻¹.

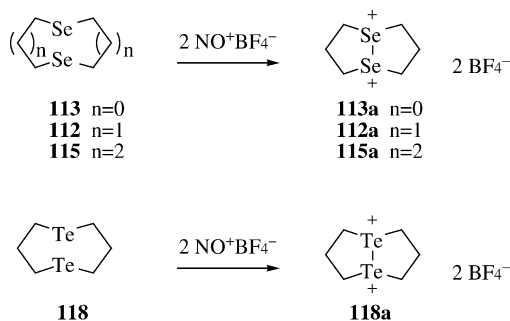
enforced proximity of the two selenium atoms (Table 15). Consistent with ease of oxidation resulting from Se–Se interaction, 1,4-diselenacyclohexane (**113**), in which the two selenium atoms are less able to interact, had a measured peak potential of 0.86 V. The oxidation of **112** was reversible when measured in the range –0.5 to +1.5 V. This is in contrast to the irreversibility found generally for oxidation of diaryl and dialkylselenides, as described above. It was also found that **112**, **113**, and 1,6-diselenacyclodecane (**115**) could be chemically oxidized with two equivalents of the one-electron oxidant NO⁺X⁻, where X is a non-nucleophilic anion, to the stable diselenadication **112a**, **113a**, and **116a**, which were fully characterized (Fig. 41).¹⁴⁰ In contrast to the corresponding dithiadication, **112a** was hydrolytically stable. The X-ray crystal structure of its tetrafluoroborate salt showed the Se–Se bond length (2.38 Å) to be very close to that of a normal Se–Se single bond (2.34 Å).¹⁴⁰

Modification of **112** by fusion of a benzene ring to each “bridge” gave 5H,7H-dibenzo[b,g][1,5]-diselenocin (**116**).¹⁴¹ As for **112**, **116** showed reversible oxidation by CV. However, it occurred at a higher potential: 0.56 V vs Ag/0.1 M AgNO₃ (Table 15). On the other hand, **116** was much more readily oxidized than either diphenylselenide (**85**) or dibenzylselenide (**117**), leading to the conclusion that the proximity of the two selenium atoms to one another has a strong impact on the ease of oxidation. Dication **116a** was also prepared by chemical oxidation of **116** with either two equivalents of the one-electron oxidant NO⁺ or with D₂SO₄, and by treatment of the selenoxide with D₂SO₄ (Fig. 42). The structure was identified by ¹H,

Table 15 Oxidation potentials and peak potentials of selenides and diselenides

	Compound	E_{Pa} (V) (vs. Ag/0.1 M AgNO ₃)
111c		0.55 ^a
112		0.25 ^b
113		0.86 ^a
114	(n-hex) ₂ Se	0.98 ^a
116		0.56 ^c
85	Ph ₂ Se	0.98 ^d
117	(PhCH ₂) ₂ Se	1.05 ^d
118		-0.02 ^e

^aData from Ref. 139, measured at 2 mM in CH₃CN with 100 mM NaClO₄, with a glassy carbon working electrode and a scan speed of 300 mV s⁻¹.

**Fig. 41** Oxidation of 1,5-dichalcogenacyclooctanes to the dication.

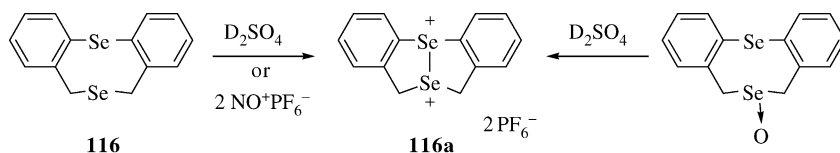


Fig. 42 Oxidation of 5H,7H-dibenzo[b,g][1,5]-diselenocin to the dication.

^{13}C , and ^{77}Se NMR spectroscopy. The compounds having either one or both of the selenium atoms substituted by sulfur showed irreversible oxidation by CV.¹⁴¹

There has been significantly less exploration of the corresponding ditelluroethers. However, by analogy to diselenoether **112**, 1,5-ditelluracyclooctane **118** was prepared, and converted to ditelluradication tetrafluoroborate salt **118a** (Fig. 41) as well as to the hexafluorophosphate salt.¹⁴² As expected, **118** was oxidized reversibly even more readily than **112** ($E_{\text{Pa}} = -0.02 \text{ V}$) (Table 15) and the dication salts were hydrolytically stable.

Other dimer dications have been prepared from dichalcogenoethers by treatment with two equivalents of the one-electron oxidant NO^+ (Fig. 42), but these dimer dications are not sufficiently stable to be isolated and characterized by elemental and spectroscopic analyses, typically undergoing carbon–halogen bond cleavage.^{143,144}

Intramolecular dimer radical cation and dimer dication formation in trichalcogenoethers

By analogy to the dichalcogenoethers, which form dimer dications upon oxidation with two equivalents of a one-electron oxidant, trichalcogenoethers can form a three-center four-electron bonding array.^{143,144} For example, dicationic telluranes **119a** and **120a** can be prepared from 2,6-bis[(phenylthio- or phenylseleno)methyl]-phenyl phenyl telluride with two equivalents of nitronium tetrafluoroborate (Fig. 43).¹⁴⁵ (Alternatively, the bis triflate salt of the phenylthio compound could be prepared from the telluroxide using triflic anhydride.) The bis tetrafluoroborate salts of these compounds were characterized by X-ray crystallographic analysis as well as by elemental and spectroscopic analyses, confirming the nature of the bonding in the dications. The X-ray crystal structures of **119a** and **120a** showed

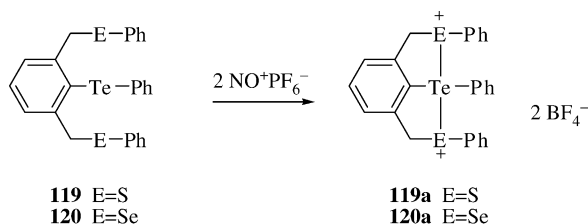


Fig. 43 Oxidative route to dicationic σ -telluranes from tris-chalcogenides.

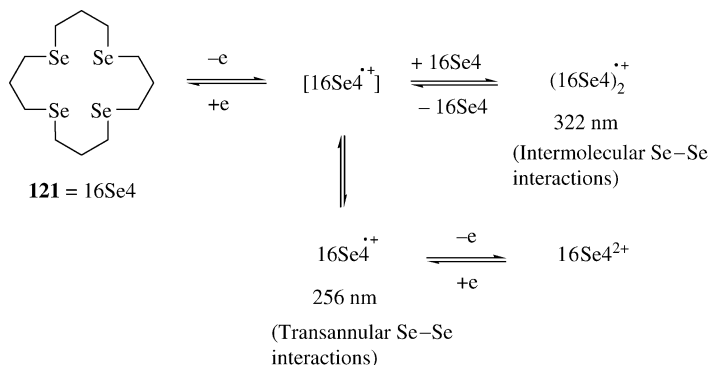


Fig. 44 Redox chemistry of a selenium coronand.

the tellurium to have distorted trigonal bipyramidal bonding geometry, with the two sulfur or selenium atoms at apical positions. The S–Te and Se–Te bond lengths were slightly longer than the normal single bond length, with bond orders of 0.50–0.59, based on Mulliken values. Evidence of interaction between the three chalcogens even prior to oxidation could be seen in the peak potentials, measured vs. Ag/AgCl. While diphenyltelluride (**23**) oxidized irreversibly at 0.90 V, bis-(phenylthio) and bis-(phenylseleno)tellurides **119** and **120** exhibited pseudo-reversible oxidation at 0.67 and 0.62 V, respectively.

The redox chemistry of the selenium coronand, 1,5,9,13-tetraselenacyclohexadecane (Fig. 44, **121**), and of its Cu(II) complex have both been studied through kinetic analysis, electrochemistry, coulometry, and spectroelectrochemistry.¹⁴⁶ Whether formed electrochemically or through a redox reaction involving its Cu(II) complex, the radical cation is formed in a one-electron oxidation, and subsequently undergoes a second one-electron oxidation to the dication. After the first one-electron oxidation ($E_{1/2} = 0.508$ V vs. SCE), the radical cation with transannular interaction between two of the sulfurs can be formed, having an absorbance band at 256 nm. A second UV-absorbing species was formed at higher concentrations of the radical cation, which was identified as the dimer radical cation. Its absorbance band was observed at 322 nm. Loss of the second electron gave the dication, which was characterized by X-ray crystallography, and showed significant transannular interactions between all four selenium atoms.

HETEROCYCLIC SELENIDES AND TELLURIDES: SELECTED EXAMPLES

1,3-Ditelluroles

1,3-Ditellurole (**122**) differs from the compounds described in the previous two sections due to its small ring size, combined with the presence of two sp^2 -hybridized carbons (Fig. 45). As a result, formation of the intramolecular dimer radical cation

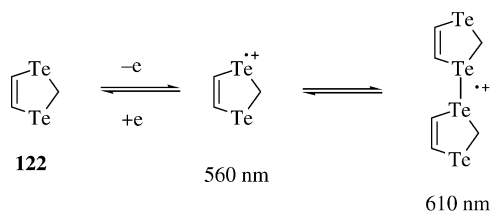


Fig. 45 Redox chemistry of 1,3-ditellurole.

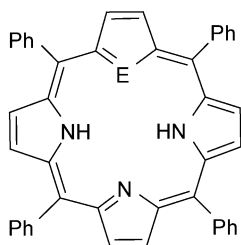
and dimer radical cation is possible, but not as easily accommodated. Oxidation was effected with nitronium tetrafluoroborate, electrochemically, and using X-rays, and the products of one-electron oxidation were studied by absorption, ESR, and ESCA spectroscopy.¹⁴⁷ By CV, **122** is oxidized reversibly at 0.64 V vs. SCE. The data suggest that this one-electron oxidation gives the radical cation, which dimerizes to the dimer dication when conditions permit. The species can be readily distinguished by their absorption spectra (560 and 610 nm, respectively) (Fig. 45). Formation of the radical cation is favored at higher temperature and lower concentration, as would be expected. There is no evidence of either transannular tellurium–tellurium interactions, or of dimer dication formation from two molecules of the radical cation.

Chalcogenaporphyrins and dichalcogenaporphyrins

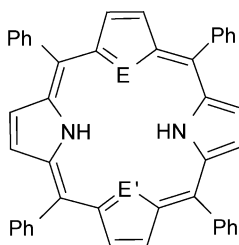
A series of *meso*-tetraphenyl-21-chalcogenaporphyrins **123–125** and *meso*-tetraphenyl-21,23-dichalcogenaporphyrins **126–129** was prepared and the values of E_{Pa} determined using CV (Table 16).¹⁴⁸ The results illustrate the similar ability of sulfur and selenium to give up an electron, while tellurium is more easily oxidized. The two tellurium-containing porphyrin derivatives oxidize at 0.81 V (**125**) and 0.69 V (**129**) vs. SCE, while essentially all the sulfur and selenium-containing analogs have E_{Pa} values between 1.05 and 1.13 V. This is attributed to the close contact between the 21-Te and the 23-N and 23-S in compounds **125** and **129**, respectively, due to the larger van der Waals radius of Te relative to the other chalcogens. The nitrogen or sulfur atom can donate a pair of electrons to the Te, facilitating oxidation and stabilizing the radical cation.

ANTIOXIDANT ACTIVITY IN FUNCTIONAL ASSAYS

The need for antioxidants in both biological and non-biological systems has led to the examination of diorganoselenides and tellurides as glutathione peroxidase mimics (vide supra) and as chain-breaking or hydrogen-donating antioxidants. The role of lipid peroxidation in inflammatory disease has led to the use of model systems for lipid peroxidation to evaluate compounds for potential use against inflammation.^{124,149–152} For example, 2,3-dihydrobenzo[b]furan-5-ol **98** and its S, Se, and Te analogs **99–101** all showed inhibition of lipid peroxidation in both

Table 16 Oxidation and reduction potentials for 21-chalcogenaporphyrins **123–125** and 21,23-dichalcogenaporphyrins **126–129**

123, E = S
124, E = Se
125, E = Te



126, E = E' = S
127, E = Se, E' = S
128, E = E' = Se
129, E = Te, E' = S

Compound	E_{pa} or E_{ox}^0 (V) (vs. SCE)	E_{red}^I (V) (vs. SCE)	E_{red}^{II} (V) (vs. SCE)
123	1.03	-1.15	-1.42
124	1.09	-1.10	-1.42
125	0.81	-1.00	-1.61
126	1.10	-1.07	-1.37
127	1.09	-1.04	-1.33
128	1.10	-1.01	-1.28
129	0.69	-1.00	-1.26

Data from Ref. 148.

a two-phase chlorobenzene and aqueous *N*-acetylcysteine system, as well as in rat liver microsomes stimulated by Fe(II)/ adenosine-5-phosphate (ADP)/ascorbate.¹²⁴ Although none of the compounds approached the antioxidant activity of α -tocopherol, the trends observed for the chalcogenides were consistent with expectation, with telluride **101** showing significantly better activity than the other compounds. This activity was only seen in the presence of *N*-acetylcysteine, which reduces Te(IV) to Te(II), making the reduced telluride available as an antioxidant. In this system, the telluride is acting catalytically, and the *N*-acetylcysteine is stoichiometric.

A series of substituted diaryselenides were examined in three lipid peroxidation model systems: isolated rat liver microsomes treated with Fe(II)/(ADP)/ascorbate; and isolated rat hepatocytes treated with two different initiators of oxidation.¹⁴⁹ In rat hepatocytes, all of the tellurides performed more effectively than the selenides. Particularly for the rat liver microsome system, the substituent effects on lipid peroxidation were consistent with what would be expected: Electron-donating groups give more active compounds, while electron-withdrawing groups give poorer antioxidants. The same trends were seen for substituted diaryltellurides in inhibition of linoleic acid peroxidation in a two-phase model,¹⁵⁰ where the dimethylamino

substituent gave the best antioxidant activity, as well as in linoleic acid peroxidation in methanol.¹⁵² A second method of evaluation of selenides and tellurides is their reaction with the stable radical 2,2-diphenyl-1-picrylhydrazyl, which was examined for diaryl, alkylaryl, and dialkyl selenides and tellurides, including both water-soluble analogs.^{63,152} Although trends are similar to those found for inhibition of linoleic acid peroxidation, with tellurides having more potent antioxidant ability, the exact order of activity is not consistent. This is true whether or not the chalcogenide has an easily donated hydrogen, as can be found when the aryl group is a phenol. However, it is clear that the tellurides are more active than the selenides and sulfides in these assays.

In an effort to better model the evaluation of the protective effect of diarylselenides and tellurides in biological systems, a broad range of these compounds was evaluated for their ability to protect cells by their peroxidase and hydrogen and electron-donating abilities.¹⁵³ For inhibition of tert-butyl hydrogen peroxide-mediated cell toxicity, electron-rich diaryltellurides and one having a carboxylic acid ortho to the tellurium were superior, with activities in the low μM range. On the other hand, the most potent compounds in inhibiting cytotoxicity in Caco-2 cells induced by polymorphonuclear leukocytes were phenol or aniline-type tellurides, probably due to their hydrogen-donating abilities. Finally, the antioxidant properties of diorganotellurides have led to their evaluation in the inhibition of thioredoxin reductase, which is a new anticancer target, and of cancer cell growth in culture.¹⁵⁴ Here, **101** and a broad range of aniline-type tellurides were low μM inhibitors of thioredoxin reductase, but this often did not correlate well with toxicity toward cancer cells.

Polymer stabilization is another area in which the peroxide-decomposing and chain-breaking antioxidant properties of diorganotellurides has found utility.^{155,156} Alone or in combination with phenol and phosphate antioxidants, electron-rich dialkylamino-substituted diaryltellurides and alkylaryltellurides provided greatly enhanced polymer stability for a thermoplastic elastomer and for polypropylene. The effects were unique to the tellurides, with selenides not providing similar protective effects.¹⁵⁶

References

1. Lederer, L. (1916). *Ber. Bynsen-Ges. Phys. Chem.* **49**, 1076–1082
2. Lederer, L. (1916). *Ber. Bynsen-Ges. Phys. Chem.* **49**, 2002–2005
3. Lederer, L. (1912). *Justus Liebigs Ann. Chem.* **391**, 326–347
4. McCullough, J.D. and Hamburger, G. (1941). *J. Am. Chem. Soc.* **63**, 803–807
5. Christofferson, G.D. and McCullough, J.D. (1958). *Acta Crystallogr.* **11**, 249–256
6. McCullough, J.D. and Marsh, R.E. (1950). *Acta Crystallogr.* **3**, 41–45
7. Chao, G.Y. and McCullough, J.D. (1962). *Acta Crystallogr.* **15**, 887–893
8. Drago, R.S. (1973). *J. Chem. Educ.* **50**, 244–245
9. Rundle, R.E. (1962). *Rec. Chem. Prog.* **23**, 195–221

10. Nefedov, V.D., Sinotova, E.N., Sarbash, A.N., Kolobov, E.A. and Kapustin, V.K. (1971). *Radiokhimiya* **13**, 435–439
11. Nefodov, V.D., Sinotova, E.N., Sarbash, A.N. and Timofev, S.A. (1969). *Radiokhimiya* **11**, 154–158
12. Detty, M.R., Friedman, A.E. and McMillan, M. (1994). *Organometallics* **13**, 3338–3345
13. Petragnani, N. and Campos, M. de M. (1961). *Chem. Ber.* **94**, 1759–1762
14. Detty, M.R. and Frade, T.M. (1993). *Organometallics* **12**, 2496–2504
15. Detty, M.R. and Fleming, J.C. (1994). *Adv. Mater.* **6**, 48–51
16. Detty, M.R. and Friedman, A.E. (1994). *Organometallics* **13**, 533–543
17. McCullough, J.D., Chao, G.Y. and Zuccaro, D.E. (1959). *Acta Crystallogr.* **12**, 815–816
18. Maddox, H. and McCullough, J.D. (1966). *Inorg. Chem.* **5**, 522–526
19. McCullough, J.D. (1964). *Inorg. Chem.* **3**, 1425–1428
20. McCullough, J.D. and Brunner, A. (1967). *Inorg. Chem.* **6**, 1251–1252
21. Detty, M.R., Friedman, A.E. and McMillan, M. (1995). *Organometallics* **14**, 1442–1449
22. Detty, M.R., Williams, A.J., Hewitt, J.M. and McMillan, M. (1995). *Organometallics* **14**, 5258–5262
23. Schweikert, W.W. and Meyers, E.A. (1968). *J. Phys. Chem.* **72**, 1561–1565
24. Bransford, J.W. and Meyers, E.A. (1978). *Cryst. Struct. Commun.* **7**, 697
25. Herbstein, F.H. and Schwotzer, W. (1984). *J. Am. Chem. Soc.* **106**, 2367
26. Srivastava, T.N., Srivastava, R.C. and Singh, M. (1979). *Indian J. Chem.* **17A**, 615
27. Morgan, G.T. and Burstall, F.H. (1931). *J. Chem. Soc.* 180
28. Turner, D.H., Flynn, G.W., Sutin, N. and Beitz, J.V. (1972). *J. Am. Chem. Soc.* **94**, 1575–1582
29. Watts, H. (1961). *Aust. J. Chem.* **14**, 15–23
30. Campos, M. de M., Petragnani, N. and Thomé, C. (1960). *Tetrahedron Lett.* **15**, 5–8
31. Petragnani, N. and Campos, M. de M. (1961). *Chem. Ber.* **94**, 1759–1762
32. Campos, M. de M., Suranyi, E.L., de Andrade, H., Jr. and Petragnani, N. (1964). *Tetrahedron* **20**, 2797–2801
33. Ramasamy, K., Kalyanasundarani, S.K. and Shammugan, P. (1978). *Synthesis* 311–312
34. Desilva, K.G.K., Monsef-Mirzai, Z. and McWhinnie, W.R. (1983). *J. Chem. Soc. Dalton Trans.* 2143–2146
35. Suzuki, H. and Inouye, M. (1985). *Chem. Lett.* 225–228
36. Huang, X. and Hou, Yu.Q. (1988). *Synth. Commun.* 2201–2204
37. Barton, D.H.R. and McCombie, S.W. (1975). *J. Chem. Soc. Perkin Trans.* **1**, 1574–1578
38. Barton, D.H.R., Bohe, L. and Lusinchi, X. (1987). *Tetrahedron Lett.* **28**, 6609–6612
39. Engman, L. (1982). *Tetrahedron Lett.* **23**, 3601–3602
40. Li, C.J. and Harpp, D.N. (1991). *Tetrahedron Lett.* **32**, 1545–1548
41. Plattner, P.A., Heusser, H. and Segre, H. (1948). *Helv. Chim. Acta* **31**, 249–255
42. Solo, A.J. and Singh, B.J. (1965). *J. Org. Chem.* **30**, 1658–1659
43. Butcher, T.S., Zhou, F. and Detty, M.R. (1998). *J. Org. Chem.* **63**, 169–176
44. Butcher, T.S. and Detty, M.R. (1999). *J. Org. Chem.* **64**, 5677–5681
45. Olah, G. (1975). *Halonium Ions*, Chapter 7. Wiley, New York
46. Olah, G.A., Bollinger, J.M. and Brinich, J. (1968). *J. Am. Chem. Soc.* **90**, 2587
47. Olah, G.A., Schilling, P., Westerman, P.W. and Lin, H.C. (1974). *J. Am. Chem. Soc.* **96**, 3581–3589
48. Takaguchi, Y., Hosokawa, A., Yamada, S., Motoyoshiya, J. and Aoyama, H. (1998). *J. Chem. Soc. Perkin Trans.* **1**, 3147–3149
49. Suzuki, H., Kondo, A. and Osuka, A. (1985). *Bull. Chem. Soc. Jpn* **58**, 1335–1336
50. Butcher, T.S. and Detty, M.R. (1998). *J. Org. Chem.* **68**, 177–180

51. Pauling, L. (1960). *The Nature of the Chemical Bond* (3rd edn). Cornell University Press, Ithaca, NY
52. Leonard, K.A., Zhou, F. and Detty, M.R. (1996). *Organometallics* **15**, 4285–4292
53. Perkins, S.W., Martin, J.C., Arduengo, A.J., Lau, W., Alegria, A. and Kochi, J.K. (1980). *J. Am. Chem. Soc.* **102**, 7753–7754
54. Detty, M.R. (1994). *The Chemistry of Heterocyclic Compounds. Tellurium-Containing Heterocycles*. vol. 53. Wiley Interscience, New York
55. Cameron, T.S., Amero, R.B., Chan, C. and Cordes, R.E. (1980). *Cryst. Struct. Commun.* **9**, 543–548
56. Detty, M.R. and Luss, H.R. (1983). *J. Org. Chem.* **48**, 5149–5151
57. Takaguchi, Y., Horn, E. and Furukawa, N. (1996). *Organometallics* **15**, 5112–5115
58. Detty, M.R., Luss, H.R., McKelvey, J.M. and Geer, S.M. (1986). *J. Org. Chem.* **51**, 1692–1700
59. Detty, M.R., Friedman, A.E. and Oseroff, A.R. (1994). *J. Org. Chem.* **59**, 8245–8250
60. Detty, M.R. and Gibson, S.L. (1992). *Organometallics* **11**, 2147–2156
61. Andersson, C.M., Hallberg, A., Brattsand, R., Cotgreave, I.A., Engman, L. and Persson, J. (1993). *Bioorg. Med. Chem. Lett.* **3**, 2553–2558
62. Engman, L., Stern, D., Pelcman, M. and Andersson, C.M. (1994). *J. Org. Chem.* **59**, 1973–1979
63. Kanda, T., Engman, L., Cotgreave, I.A. and Powis, G. (1999). *J. Org. Chem.* **64**, 8161–8169
64. You, Y., Ahsan, K. and Detty, M.R. (2003). *J. Am. Chem. Soc.* **125**, 4918–4927
65. Barton, D.H.R., Ley, S.V. and Meerholz, C.A. (1979). *J. Chem. Soc. Chem. Commun.* 755–756
66. Barton, D.H.R., Finet, J.-P., Giannotti, C. and Thomas, M. (1988). *Tetrahedron Lett.* **29**, 2671–2674
67. Ogura, F., Yamaguchi, H., Otsubo, T. and Tanaka, T. (1982). *Bull. Chem. Soc. Jpn* **55**, 641–642
68. Ogura, F., Otsubo, T., Ariyoshi, K. and Yamaguchi, H. (1983). *Chem. Lett.* 1833–1834
69. Hu, N.X., Aso, Y., Otsubo, T. and Ogura, F. (1985). *Chem. Lett.* 603–606
70. Yamaguchi, H., Ogura, F., Otsubo, T., Sakamoto, A. and Fujimoto, M. (1982). *Nippon Kagaku Kaishi* 801–804
71. Ariyoshi, K., Aso, Y., Otsubo, T. and Ogura, F. (1984). *Chem. Lett.* 891–892
72. Detty, M.R. (1980). *J. Org. Chem.* **45**, 274–279
73. Engman, L., Persson, J., Merényi, G. and Lind, J. (1995). *Organometallics* **14**, 3641–3648
74. Engman, L., Lind, J. and Merényi, G. (1994). *J. Phys. Chem.* **98**, 3174–3182
75. Shimizu, T., Enomoto, M., Taka, H. and Kamigata, N. (1999). *J. Org. Chem.* **64**, 8242–8247
76. Ley, S.V., Meerholz, C.A. and Barton, D.H.R. (1981). *Tetrahedron* **37**(Suppl. 1), 213–223
77. Ley, S.V., Meerholz, C.A. and Barton, D.H.R. (1980). *Tetrahedron Lett.* **21**, 1785–1788
78. Ariyoshi, K., Aso, Y., Otsubo, T. and Ogura, F. (1984). *Chem. Lett.* 891–892
79. Abatjoglou, A.G. and Bryant, D.R. (1981). *Tetrahedron Lett.* **22**, 2051–2054
80. Procter, D.J., Thornton-Pett, M. and Rayner, C.M. (1996). *Tetrahedron* **52**, 1841–1854
81. Zhang, J. and Koizumi, T. (2000). *Syn. Commun.* **30**, 979–987
82. Ahsan, K., Drake, M.D., Higgs, D.E., Wojciechowski, A.L., Tse, B.N., Bateman, M.A., You, Y. and Detty, M.R. (2003). *Organometallics* **22**, 2883–2991
83. Ren, X., Xue, Y., Liu, J., Zhang, K., Zheng, J., Luo, G., Guo, C., Mu, Y. and Shen, J. (2002). *ChemBioChem* **3**, 356–363
84. Detty, M.R., Zhou, F. and Friedman, A.E. (1996). *J. Am. Chem. Soc.* **118**, 313–318
85. Francavilla, C., Bright, F.V. and Detty, M.R. (1999). *Org. Lett.* **1**, 1043–1046

86. Francavilla, C., Drake, M.D., Bright, F.V. and Detty, M.R. (2001). *J. Am. Chem. Soc.* **123**, 57–67
87. Higgs, D.E., Nelen, M.I. and Detty, M.R. (2001). *Org. Lett.* **3**, 349–352
88. Abe, M., You, Y. and Detty, M.R. (2002). *Organometallics* **22**, 4546–4551
89. Wilson, S.R., Zucker, P.A., Huang, R.-R.C. and Spector, A. (1989). *J. Am. Chem. Soc.* **111**, 5936–5939
90. Hawker, C. and Fréchet, J.M.J. (1990). *J. Chem. Soc. Chem. Commun.* 1010–1013
91. Hawker, C.J. and Fréchet, J.M.J. (1990). *J. Am. Chem. Soc.* **112**, 7638–7647
92. Reich, H.J., Chow, F. and Peake, S.L. (1978). *Synthesis* 299–301
93. Ten Brink, G.J., Fernandes, B.C.M., Van Vliet, M.C.A., Arends, I.W.C.E. and Sheldon, R.A. (2001). *J. Chem. Soc. Perkin Trans.* **1**, 224
94. Syper, L. and Mlochowski, J. (1987). *Tetrahedron* **43**, 207–213
95. Ten Brink, G.J., Vis, J.-M., Arends, I.W.C.E. and Sheldon, R.A. (2001). *J. Org. Chem.* **66**, 2429–2433
96. Ten Brink, G.J., Vis, M.J., Arends, I.W.C.E. and Sheldon, R.A. (2002). *Tetrahedron* 3977–3983
97. Back, T.G. and Dyck, B.P. (1997). *J. Am. Chem. Soc.* **119**, 2079
98. Back, T.G. and Moussa, Z. (2002). *J. Am. Chem. Soc.* **124**, 12104
99. Drake, M.D., Bateman, M.A. and Detty, M.R. (2003). *Organometallics* ASAP article
100. Reich, H.J. and Jasperse, C.P. (1987). *J. Am. Chem. Soc.* **109**, 5549–5551
101. Iwaoka, M. and Tomoda, S. (1994). *J. Am. Chem. Soc.* **116**, 2557–2561
102. Galet, V., Bernier, J.-L., Hénichart, J.-P., Lesieur, D., Abadie, C., Rochette, L., Lindenbaum, A., Chalas, J., Renaud de la Faverie, J.-F., Pfeiffer, B. and Renard, P. (1994). *J. Med. Chem.* **37**, 2903–2911
103. Mugesh, G., Panda, A., Singh, H.B., Punekar, N.S. and Butcher, R.J. (2001). *J. Am. Chem. Soc.* **123**, 839–850
104. Engman, L., Stern, D., Cotgreave, I.A. and Andersson, C.M. (1992). *J. Am. Chem. Soc.* **114**, 9737–9743
105. Jones, C.W. (1999). Applications of hydrogen peroxide and derivatives. In *RSC Clean Technology Monographs*, Clark, J.H. (ed.). The Royal Society of Chemistry, Cambridge, UK
106. Detty, M.R., McKelvey, J.M. and Luss, H.R. (1988). *Organometallics* **7**, 1131–1141
107. Detty, M.R., unpublished data
108. Detty, M. and O'Regan, M. (1994). *The Chemistry of Heterocyclic Compounds. Tellurium-Containing Heterocycles*. vol. 53, pp. 363–423. Wiley, New York
109. Seeber, R., Cinquantini, A., Zanello, P. and Mazzocchin, G.A. (1978). *Electroanal. Chem.* **88**, 137–145
110. Engman, L., Persson, J., Andersson, C. and Berglund, M. (1992). *J. Chem. Soc. Perkin Trans.* **2**, 1309–1313
111. Jonsson, M., Lind, J., Merényi, G. and Eriksen, T.E. (1995). *J. Chem. Soc. Perkin Trans.* **2**, 67–70
112. Liftman, Y. and Albeck, M. (1983). *Electrochim. Acta* **28**, 1841–1845
113. Frisell, H. and Engman, L. (2000). *J. Mol. Struct.* **526**, 103–114
114. Houghton, D.S. and Humffray, A.A. (1972). *Electrochim. Acta* **17**, 1421–1433
115. Nishikida, K. and Williams, F. (1975). *Chem. Phys. Lett.* **34**, 302–306
116. Jouikov, V.V., Fattakhova, D.S. and Kozhevnikov, A.Y. (2001). *Electrochim. Acta* **46**, 807–812
117. Engman, L., Stern, D., Frisell, H., Vessman, K., Berglund, M., Ek, B. and Andersson, C.-M. (1995). *Bioorg. Med. Chem.* **3**, 1255–1262
118. Latypova, V.Z., Zhuikov, V.V., Kargin, Y.M., Postnikova, M.Y. and Kataev, E.G. (1986). *Zhurnal Obshchei Khimii* **56**, 822–827

119. Jonsson, M., Lind, J., Reitberger, T., Eriksen, T.E. and Merényi, G.J. (1993). *J. Phys. Chem.* **97**, 11278–11282
120. Latypova, V.Z., Kargin, Y.M., Zhuikov, V.V., Chmutova, G.A. and Lisitsyn, Y.A. (1985). *Zhurnal Obshchei Khimii* **55**, 2050–2052
121. Jouikov, V. (2000). *Electrochim. Acta* **45**, 3939–3942
122. Jouikov, V. and Postnikova, M. (1995). *Electrochim. Acta* **40**, 803–807
123. Jonsson, M., Houmam, A., Jocys, G. and Wayner, D.D.M. (1999). *J. Chem. Soc. Perkin Trans. 2*, 425–429
124. Malmström, J., Jonsson, M., Cotgreave, I.A., Hammarström, L., Sjödin, M. and Engman, L. (2001). *J. Am. Chem. Soc.* **123**, 3434–3440
125. Lind, J., Shen, X., Eriksen, T.E. and Merényi, G. (1990). *J. Am. Chem. Soc.* **112**, 479–482
126. Jouikov, V.J. (1995). *Electroanalytical Chem.* **398**, 159–164
127. Jouikov, V., Ivkov, V. and Fattahova, D. (1993). *Tetrahedron Lett.* **34**, 6045–6048
128. Jouikov, V.V. and Fattakhova, D.S. (2000). *J. Organometallic Chem.* **613**, 220–230
129. Almond, M.J., Raqabah, A., Rice, D.A., Symons, M.C.R. and Yates, C.A. (1992). *J. Chem. Soc. Dalton Trans.* 1–4
130. Cradock, S. and Whiteford, R.A. (1972). *J. Chem. Soc. Faraday Trans.* **68**, 281–288
131. Wang, J.R. and Williams, F. (1981). *J. Am. Chem. Soc.* **103**, 6994–6996
132. Wang, J.T. and Williams, F. (1981). *J. Chem. Soc., Chem. Commun.* 1184–1185
133. Petersen, R.L., Nelson, D.J. and Symons, M.C.R. (1978). *J. Chem. Soc. Perkin Trans. 2*, 225–231
134. Gilbert, B.C., Hodgeman, D.K.C. and Norman, R.O.C. (1973). *J. Chem. Soc. Perkin Trans. 2*, 1748–1752
135. Glidewell, C. (1993). *J. Organometal. Chem.* **461**, 15–19
136. Asmus, K.D. (2000). *Nukleonika* **45**, 3–10
137. Tobien, T., Hungerbuehler, H. and Asmus, K.-D. (1994). *Phosphorus, Sulfur Silicon Related Elements* **95–96**, 249–263
138. Asmus, K.-D. (1979). *Accts. Chem. Res.* 436–442
139. Fujihara, H., Akaishi, R. and Furukawa, N. (1990). *Chem. Lett.* 549–550
140. Fujihara, H., Akaishi, R. and Furukawa, N. (1993). *Tetrahedron* **49**, 1605–1618
141. Fujihara, H., Ueno, Y., Chiu, J.-J. and Furukawa, N. (1991). *Chem. Lett.* 1649–1650
142. Fujihara, H., Ninoi, T., Akaishi, R., Erata, R. and Furukawa, N. (1991). *Tetrahedron Lett.* **32**, 4537–4540
143. Furukawa, N., Kobayashi, K. and Sato, S. (2000). *J. Organometal. Chem.* **611**, 116–126
144. For a review, see: Furukawa, N. (1998). *Phosphorus, Sulfur and Silicon and the Related Elements* 43–58, 136–138
145. Bergholdt, A.B., Kobayashi, K., Horn, E., Takahashi, O., Sato, S., Furukawa, N., Yokoyama, M. and Yamaguchi, K. (1998). *J. Am. Chem. Soc.* **120**, 1230–1236
146. Batchelor, R.J., Einstein, F.W.B., Gay, I.D., Gu, J.-H., Pinto, B.M. and Zhou, X.-M. (2000). *Can. J. Chem.* **78**, 598–613
147. DeTTY, M.R., Haley, N.F., Eachus, R.S., Hassett, J.W., Luss, J.R., Mason, M.G., McKelvey, J.M. and Wernberg, A.A. (1985). *J. Am. Chem. Soc.* **107**, 6298–6304
148. Abe, M., Hilmey, D.G., Stilts, C.E., Sukumaran, D.K. and DeTTY, M.R. (2002). *Organometallics* **21**, 2986–2992
149. Andersson, C.-M., Hallberg, A., Linden, M., Brattsand, R., Moldéus, P. and Cotgreave, I. (1994). *Free Rad. Biol. Med.* **16**, 17–28
150. Vessman, K., Ekström, M., Berglund, M., Andersson, C.-M. and Engman, L. (1995). *J. Org. Chem.*, **60**, 4461–4467
151. Andersson, C.-M., Brattsand, R., Hallberg, A., Engman, L., Persson, J., Linden, M., Moldéus, P. and Cotgreave, I. (1994). *Free Rad. Res.* **20**, 401–410

152. Engman, L., Persson, J., Vessman, K., Ekstrom, M., Berglund, M. and Andersson, C.-M. (1995). *Bioorg. Med. Chem.* **19**, 441–452
153. Wieslander, E., Engman, L., Svensjö, E., Erlansson, M., Johansson, U., Linden, M., Andersson, C.-M. and Brattsand, R. (1998). *Biochem. Pharmacol.* **55**, 573–584
154. Engman, L., Al-Maharik, N., McNaughton, M., Birmingham, A. and Powis, G. (2003). *Anticancer Drugs* **14**, 153–161
155. Malmstrom, J., Engman, L., Bellander, M., Jacobsson, K., Stenberg, B. and Lonnberg, V. (1998). *J. Appl. Polym. Sci.* **70**, 449–456
156. Shanks, D., Al-Maharik, N., Malmstrom, J., Engman, L., Ericksson, P., Stenberg, B. and Reitberger, T. (2003). *Polym. Degrad. Stab.* **81**, 261–271

Chiral clusters in the gas phase

MAURIZIO SPERANZA

Dipartimento degli Studi di Chimica e Tecnologia delle Sostanze Biologicamente Attive, Università di Roma "La Sapienza", 00185 Roma, Italy

- 1 Introduction 147
- 2 Ionic and molecular clusters in the gas phase 149
 - Characterization and classification of non-covalent intracomplex interactions 150
 - Noncovalent interactions in supramolecular systems 152
 - Noncovalent interactions in life sciences 152
 - Metal ions in biological systems 153
 - Chiral clusters 154
- 3 Experimental methodologies 155
 - Cluster sources 156
 - Neutral clusters from supersonic beam 157
 - Spectroscopy of neutral clusters 158
 - Sources of ionic clusters 167
 - Mass spectrometry of ionic clusters 170
 - Ion–dipole complexes in dense gases: the radiolytic approach 178
- 4 Chiral recognition in molecular clusters 178
 - Structure of molecular complexes 179
 - Energetics of molecular complexes 192
 - Chiral effects in rydberg electron-bound complexes 194
- 5 Chiral recognition in ionic clusters 196
 - Proton-bound complexes 196
 - Metal-bound complexes 204
 - Enantioselective self-assembling of amino acids 209
 - Host–guest inclusion complexes 213
 - Reactivity of chiral ion–dipole complexes 233
- 6 Concluding remarks 266
 - Acknowledgements 267
 - References 267

His left arm is under my head, and his right arm embraces me. Song of Solomon: 2,6.

1 Introduction

Chemical reactions in solution involve reactants and products in continuous contact with their surroundings. Even a solvent that only weakly perturbs the

E-mail address: maurizio.speranza@uniroma1.it (M. Speranza).

reactants can profoundly influence the course of the reaction by blocking the path of a departing group or by removing excess energy from reactive intermediates. Solvent effects become still more important when the reaction involves charged species, because the forces between an ionic solute and a polar or polarizable solvent can be as strong as the chemical bonding forces between the reactants themselves. The solvent then does not merely interrupt and redirect motion on the potential energy surface (PES) of the isolated solute, it may actually change the topography of the surface. This is not new to chemists, who have long appreciated that a solvent will stabilize the transition state of a reaction differently than it does the reactants or products. Understanding the full impact of solvent–solute interactions on reaction dynamics and mechanisms has nevertheless proved to be a demanding task. The basic models for describing solvent–solute interactions in solution represent just an extension of the gas-phase model, based on non-covalent interactions between reciprocally polarized solute/solvent aggregates. In this perspective, any progress in the comprehension of solvation effects relies on new developments in the description of non-covalent interactions in small gas-phase clusters.

Novel experimental methodologies, capable of characterizing small gas-phase clusters and probing their chemical bond breaking and forming on an extremely short time scale, are now at hand and their results can be now compared with very refined theoretical predictions. Their application fostered important breakthroughs in many scientific fields, which surpass the purely chemical threshold by interlocking the physical and life sciences. The origin of life in the interstellar space or in a drop of water, the nucleation phenomena, the formation of aerosols in the atmosphere and of fine particles in combustion and catalysis share with molecular recognition in biological systems the same queries: what is the nature of non-covalent specific interactions among the components of molecular or ionic aggregates and how do they affect their structure, stability, and reactivity?

Answering these questions is of paramount importance in life sciences. Natural and synthetic enzymes are invariably characterized by asymmetric structures with a cavity of appropriate shape and size holding suitable functionalities in specific positions. Their exceptional enantioselectivity towards chiral molecules is due to shape-specific intermolecular forces acting on their complementary surfaces. However, the precise positioning of reactants functionalities in a chiral molecule–enzyme complex is only one of the factors determining the efficiency of the enzyme catalysis in stabilizing diastereomeric transition states for a particular reaction. Most of the remarkable catalytic proficiency of natural and synthetic enzymes may in fact result from activation of its reactive functionalities by the apolar environment of the active site determined by extensive desolvation of reactants in the host cavity.¹ Thus, solvation/desolvation phenomena may strongly affect chiral recognition and rate acceleration of enzymes and complicate the understanding of the underlying principles.

The state-of-art of the generation, characterization, and evolution of ionic and molecular chiral clusters in the gas phase is illustrated in the present chapter.

An introduction to the non-covalent forces operating in stable ionic and molecular aggregates will be presented in Section 2. A brief description of the experimental methodologies employed in the production, detection, and characterization of clusters will be given in Section 3. The available experimental evidence on the structure of chiral clusters and their intrinsic stability, reactivity, and evolution dynamics will be presented and discussed in Sections 4 (molecular clusters) and 5 (ionic clusters). In the same sections, the experimental data will be interpreted in the light of the available theoretical evidence. Finally, some concluding remarks will be expressed in Section 6.

2 Ionic and molecular clusters in the gas phase

Ionic and molecular clusters have been widely investigated over the last two or three decades,^{2,3} and they are at the forefront of physical and chemical research. The effort to investigate them has become so extensive that many groups refer to ionic and molecular clusters as a new state of matter with neither the properties of their individual constituents nor those of their respective bulk condensed phases. Indeed, the formation of a cluster does affect properties of its components compared to both the isolated molecules and the bulk solution. The stronger are the non-covalent interactions in the cluster, the larger are the changes in the properties of the components. These changes are important for monitoring the formation itself of clusters and for evaluating their stability and reactivity. The importance of research in non-covalent clusters, however, transcends their qualification of a new state of matter. In contrast to bulk systems, both the nature and the number of the interacting molecules can be systematically varied within the clusters and the spectroscopic and kinetic investigation of their behavior may shed light on the structure and the dynamics of bulk solutions and on their effects on chemical reactions.⁴

Tailor-made ionic and molecular clusters have proved to be ideal systems for modeling molecular and chiral recognition processes. In fact, they can be prepared in the isolated state, in the absence of bulk effects that could mask the non-covalent forces governing these processes. In the last few years, it has become possible to study the single interactions acting between the individual components of clusters of biological interest in just that situation, without any interference from the environment and where their structural assignment can provide a benchmark against which the influence of any dynamic environment might be assessed.⁵⁻¹¹

As biological function and morphology are strongly correlated, knowledge of the structure is expected to shed light on the biological function. Structure determination is the primary and probably the most important step in the elucidation of molecular cluster properties. A clear cluster structure permits to face the study of its PES and energy distribution processes and finally to explain chemical reactions occurring in clusters. Structure determination of non-covalent clusters is often a difficult task, due

to both large amplitude motion and cluster flexibility. The latter effect occurs when an aggregate in a given electronic state has more than one energetically accessible potential minimum on its electronic PES. Large amplitude motion for intermolecular cluster modes can involve only one potential minimum, nevertheless it plays a crucial role in the dynamical processes connecting different potential minima on PES. Describing the relative orientation of the components of a flexible cluster is a daunting challenge from both the experimental and theoretical standpoints: a weakly bound cluster should be thought as a dynamic system, rather than one with a well-defined structure.

CHARACTERIZATION AND CLASSIFICATION OF NON-COVALENT INTRACOMPLEX INTERACTIONS

The forces operating in clusters originate from the electrical properties of their components. If involving permanent, induced, or instantaneous time-dependent multipoles among the cluster components, these interactions are defined as non-covalent to distinguish them from the much stronger covalent bonding. The respective energy terms, called electrostatic, induction (charge-transfer), and dispersion are basically attractive (only the electrostatic term, depending on the orientation of the components, can be attractive or repulsive). The repulsive term, due to the overlap of occupied orbitals (exchange-repulsion energy), prevents the cluster components from approaching each other too closely. At variance with covalent bonding, non-covalent forces act at distances of several angstroms or even tens of angstroms. Thus, repulsive interactions, due to the overlap between occupied orbitals (exchange-repulsion energy), are minimized.

The total stabilization energy of a cluster rarely exceeds 25 kcal mol^{-1} , i.e., a small fraction of a strong covalent bond energy (ca. $100 \text{ kcal mol}^{-1}$). Its partitioning into electrostatic, induction, and dispersion terms differs from cluster to cluster. In some cases, one particular energy term is dominant. More typically, many attractive terms contribute to the overall stabilization of non-covalent clusters, as it often happens to hydrogen-bonded complexes. Nevertheless, the electrostatic interaction plays a dominant role, and in the case of polar subsystems, it is possible to identify the total stabilization energy with the electrostatic energy term.¹²

Hydrogen bonding

Hydrogen-bonded complexes are the most important and the most investigated non-covalent complexes.¹³ The hydrogen bonds (H-bonds) are frequent in both molecular and ionic complexes. This strong electrostatic interaction occurs when a hydrogen atom is shared by two atoms ($X-H \cdots Y$). As a rule, X is an electronegative atom ($X = F, O, \text{ or } N$), while Y is either an electronegative atom having one or two lone electron pairs or a group with a region of excess of

electron density (e.g., π -electrons of aromatic systems). The concept of H-bonds has been extended to C–H \cdots Y interactions (acidic CH group; Y = electronegative atom, or π),^{14,15} which however are much weaker than those involving electronegative X and Y atoms. Nevertheless, they could play an important role in biomolecular structures due to their large number. The atom X to which the hydrogen is covalently bound is called the proton donor, whereas the other atom Y is the proton acceptor. Natural bond orbital analysis points to hydrogen bonding as due to charge transfer from the lone pairs or π -molecular orbitals of the electron donor (proton acceptor) to the antibonding orbitals of the X–H bond of the electron acceptor (proton donor).¹⁶ An increase of electron density in these antibonding orbitals causes elongation of the X–H bonds and, therefore, a red-shift of the X–H stretching frequency. This is accompanied by a very small charge transfer. The red-shift is easily observable and provides unambiguous evidence about the formation of H-bonded non-covalent complex. Further stabilization of these complexes arises from electrostatic, charge-transfer, and dispersion energy terms. The electrostatic term, due to ion–dipole or dipole–dipole interactions, is most important and confers to H-bonds their typical (and very important) directionality. Other two types of intermolecular bonds with participation of hydrogen, namely the improper (blue-shifting) H-bond and the dihydrogen bond, less numerous than H-bonds were recently described.^{17–23}

Charge-transfer interactions

The condition for the formation of a charge-transfer interaction in a complex requires that an electron flows from one of its components with a low ionization potential to the other with a high electron affinity. Electron donors and acceptors are classified according to the type of orbital donating or accepting the electrons as follows: donors, n, σ , π (n = nonbonding orbitals); acceptors, v, σ^* , π^* (v = vacant orbitals). The strongest charge-transfer complexes are of n–v type and those of π – π^* type are the weakest.

Electrostatic interactions

The presence of a charged component (electron, anion, cation, proton, or metal ion) in a cluster represents an important source of electrostatic stabilization as well as of strong directionality for the other components. On increasing the size of the charged component, both effects become weaker. This is particularly true for aromatic ions wherein the charge is highly delocalized. Because cations usually possess high electron affinity and anions low ionization potential, the charge-transfer energy term can be an important attractive contribution.

Electrostatic interactions play a dominant role in weak molecular clusters between components, like arenes, exhibiting quadrupole momenta q . The global minimum of the benzene dimer corresponds to structure with monomers located in perpendicular planes (T-shape structure).²⁴ This structure is favored by attractive

$q-q$ interactions between the two benzene molecules. These qualitative estimates are now fully supported by highly accurate *ab initio* calculations.²⁵ The same $q-q$ interactions determine the structure of crystalline phenylalanine.²⁶

The electrostatic motif represents an important recognition feature and also plays a part in determining the structure of biomacromolecules.

Dispersion interactions

While the structure of clusters responds to directionally specific electrostatic interactions, their stabilization energy reflects also the intervention of less specific dispersion interactions. This is, e.g., the case for stacked DNA base pairs. Stability of these pairs stems from dispersion energy while their structure is determined by dipole–dipole electrostatic interactions. Dispersion energy plays an important role in stabilizing clusters of biomacromolecules, where it may be the dominant attractive term.

NONCOVALENT INTERACTIONS IN SUPRAMOLECULAR SYSTEMS

Noncovalent interactions play a special role in synthetic procedures used to assemble various types of supramolecular species. These syntheses rely on the stabilization provided by non-covalent interactions between recognition sites incorporated within precursors. Various types of non-covalent interactions can be used as a recognition motif utilized to guide the synthesis.²⁷ Targeted synthesis of macro- and supramolecular structures of various sizes, shapes, and functionality has now become possible.²⁸ Supramolecular chemistry offers incredible applications in various fields such as medicinal chemistry (drug delivery systems),^{29–32} host–guest chemistry,³³ catalysis,^{34–36} and molecular electronics.³⁷

NONCOVALENT INTERACTIONS IN LIFE SCIENCES

Noncovalent interactions play a key role in biodisciplines. A celebrated example is the secondary structure of proteins.³⁸ The 20 natural amino acids are each characterized by different structures with more or less acidic or basic, hydrophilic or hydrophobic functionalities and thus capable of different intermolecular interactions.³⁹ Due to the formation of hydrogen bonds between nearby C=O and N–H groups, protein polypeptide backbones can be twisted into α -helixes, even in the gas phase in the absence of any solvent.⁴⁰ A protein function is determined more directly by its three-dimensional structure and dynamics than by its sequence of amino acids. Three-dimensional structures are strongly influenced by weak non-covalent interactions between side functionalities, but the central importance of these weak interactions is by no means limited to structural effects. Life relies on biological specificity, which arises from the fact that individual biomolecules “communicate” through non-covalent interactions.^{41,42} Molecular and chiral recognition rely on

these weak bonds which can only be formed if the functionalities of the designated partner are precisely positioned.⁴³

METAL IONS IN BIOLOGICAL SYSTEMS

Metal ions are essential for the structural stability and function of many biological systems.^{44–46} Oxygen is transported around the bodies of mammals by the iron center of hemoglobin. A large fraction of enzymes and proteins contain metal ions at their active sites.^{47–54} In most cases, the selectivity of biomolecules toward metal ions does not depend only on the identity of the metal species, but also on its oxidation state (i.e., Fe^{2+} vs. Fe^{3+}). Metalloenzymes are involved in many biological processes, including methane biogenesis and oxidation,^{55,56} oxygen storage and utilization in evolutionary organisms, and oxidative or reductive degradation of metabolites.^{57,58} Yet, metals (especially heavy metals) can be also deleterious to living organisms which take advantage of efficient metal detoxification resources developed in their evolutionary course. It is only through a detailed understanding of the role of metal ions in metalloenzymes that their biological function can be assessed and the industrial procedures to novel enzyme mimics redesigned.

Metal ions are generally positively charged and, like hydrogen ions, act as electrophiles, seeking the possibility of sharing electron pairs with suitable donors (ligands). However, compared to protons, metal ions have a much larger ionic volume and often a charge greater than one and, therefore, they can accommodate many ligands around them at the same time. The coordination number of a metal ion, i.e., the number of ligand atoms or groups bound to it depends on the size of both the metal ion and the ligands. The binding free energy between them can be subdivided into electrostatic and non-electrostatic terms. The first contribution includes the strong coulombic attraction between the metal center and the ligand. The non-electrostatic contribution includes van der Waals interactions, translational, rotational, vibrational, and configurational entropies, and covalent bonding.⁵⁹ The relative binding free energy of different ions at a particular site will depend on two factors: their ionic radius and the number of ligands surrounding them at the site. These factors are responsible for the ion size dependence of site binding since smaller ions will interact more strongly with the site but have a larger desolvation penalty.⁶⁰

Biologically important ligands may provide one (monodentate), two (bidentate), or more (multidentate) donor atoms to a metal ion. Species that can coordinate to one metal ion with two or more atoms simultaneously are called “chelates”, and the angle described by chelate atom–metal cation–chelate atom is called the “bite angle”. Amino acids are potential bidentate ligands which may coordinate a metal ion through the amino and a carboxylate lone pairs. Those containing an additional donor group in the side chain, i.e., aspartic and glutamic acids, histidine, tryptophan, cysteine, methionine, serine, threonine, tyrosine, asparagine, and glutamine, may act as tridentate ligands. Other multidentate ligands are the macrocycles, exemplified

by the porphyrin ring. In the basic porphyrin structure, the central NH hydrogens are replaced by a metal ion (e.g. iron) located within or slightly out of the macrocycle plane.

Noncovalent interactions in metal complexes of biomolecules may play an important role in the creation of supramolecular structures around the metal center. For instance, extensive three-dimensional hydrogen-bonded structures grow around metal complexes of barbiturates, recognized as the most widely used drugs for the treatment of epilepsy.^{61,62} Electrostatic interactions between a cation and the π ring of an aromatic molecule (cation- π interactions) are common motifs in protein structures.⁶³⁻⁶⁷ Little is known about alkali and alkali-earth cation- π interactions,⁶⁸⁻⁷⁰ although intense Na^+ -benzene binding has been measured (21 kcal mol^{-1}).⁷¹⁻⁷³

Cation- π interactions play a crucial role in molecular recognition.⁶⁴ For example, Na^+/K^+ cation interactions with aromatic rings of some amino acids are implicated in the biological functions of specific enzymes and in the selectivity of Na^+/K^+ channels.⁷⁴⁻⁷⁸ The same factors are responsible of the relative stability of the charge-solvated vs. zwitterionic structure of amino acids.^{70,79-81}

CHIRAL CLUSTERS

The enantiomers of a chiral molecule can have a very different behavior when acting in a chiral environment. A chiral environment can be represented by the circularly polarized light or an asymmetric medium. For instance, when a chiral drug interacts with its chiral receptor, one of the enantiomers of the drug usually displays the desired biological activity while the other is useless or even poisonous. For this reason, the discrimination and separation of enantiomeric pairs are in the focus of intense research and technological developments. Following the notion that the *R* and *S* enantiomers of a chiral molecule have identical properties, except when interacting with a chiral environment, the most commonly employed method for separating enantiomeric pairs is based on their association with a selector of precisely defined configuration, e.g., *R*, to yield the corresponding *R*-*R* and *S*-*R* diastereomeric aggregates. These are no longer mirror images and have different physical and chemical properties and, therefore, can be identified and separated. The most used separation techniques are liquid chromatography (HPLC), gas chromatography (GC), and capillary electrophoresis (CE) using chiral stationary phases acting as selector.⁸²⁻⁸⁴ Pirkle and House⁸⁵ first gave to chiral chromatography a systematic basis with the introduction of the "three-point rule", i.e., there must be at least three simultaneous interactions between a chiral selector and a chiral molecule and one of these must be stereochemically dependent, if chiral resolution is to be effected. After Pirkle and House, researchers devoted a huge effort in defining the principles underlying enantiomeric resolution in chiral chromatography, in particular the specific interactions between the chiral sites of the stationary phase and those of the analyte.⁸⁶⁻⁸⁹

Other techniques such as UV–vis absorbance spectrometry,⁹⁰ circular dichroism,⁹¹ infrared transmission spectrometry,⁹² and NMR spectroscopy⁹³ have also been used for enantiomeric discrimination in liquid phase. In absorbance spectrometry, chiral discrimination of two enantiomers occurs through the measurement of the absorption spectrum of their complexes with a chiral reference (host-guest systems). The two diastereomers show different spectral shift with respect to the absorption spectrum of the bare reference molecule. Also in NMR technique, a chiral reagent is added to obtain different chemical shifts from the proton of two optical isomers. This is possible because the presence of the reagent creates a chiral environment, which makes the protons non-equivalent in the two enantiomers. Fluorescence techniques have often been used to study the interaction between enantiomers and receptors.^{94–97} Receptor systems,^{98–100} such as cyclodextrins and calixarenes, have been observed to selectively bind some enantiomers and produce a complex that can be detected by fluorescence techniques. The centrality of chiral recognition in biology has prompted these investigators to explore the use of biomolecules as receptors for a fluorescence-based determination of enantiomeric purity.

The isolated environment of the supersonic beam and the high resolution of the laser spectroscopy have demonstrated to be very useful tools for enantiodiscriminating van der Waals complexes in the gas phase, where the undesired leveling effects of the solvent are excluded and the intrinsic factors governing enantioselective complexation determinable. Diastereoisomeric R – \mathcal{R} and S – \mathcal{R} complexes, obtained by aggregation of a species with unknown chirality (either R or S) with a chiral selector of defined configuration (\mathcal{R}), can be distinguished through their binding energies, beam populations, fluorescence,¹⁰¹ hole-burning spectra,¹⁰² resonance enhanced multiphoton ionization (REMPI) spectra,¹⁰³ and total dipole moments. The observed chiral discriminations are due to subtle balances between different effects such as steric factors and additive dispersive interactions which are more important in the excited state.

The development of mass spectrometric techniques, such as fast atom bombardment mass spectrometry (FAB-MS),^{90,104} Fourier transform ion cyclotron resonance mass spectrometry (FTICR-MS),¹⁰⁵ and tandem mass spectrometry (MS^n),¹⁰⁶ allowed enantiodiscrimination of chiral ion–dipole complexes the gas phase. These techniques and others will be illustrated in detail in the next Section 3.

3 Experimental methodologies

Atomic and molecular clusters have been studied for more than fifty years, but the last two decades have seen an increasing interest in new experimental methods for cluster production and analysis. The development and improvement of cluster sources lie at the focal point of the technological advances achieved in the study of gas phase clusters. For what concern the molecules of biological interest, the production and analysis of these molecules both isolated or complexed is made

difficult by their thermal properties. In fact, a large fraction of biological molecules have very low vapor pressures, even at temperatures above 200 °C, and easily decompose. As a consequence, it is difficult to bring these molecules into the gas phase as intact molecules, especially as neutral ones. The experimental methodologies for the production, characterization, and detection of both neutral and ionic molecular clusters are illustrated below.

CLUSTER SOURCES

A large number of different sources are available for the production of gas phase clusters, each one having features suitable for particular experimental goals. These include the cluster size range obtainable, versatility in terms of composition, charge and intensity, and the internal temperature of the produced clusters.

Neutral cluster sources are based on either supersonic expansion^{107,108} or inert gas condensation.^{109,110} The latter procedure was first used in 1930 to generate metallic gold smokes for depositing gold “black” on thermal detectors.¹¹¹ Since those early days, other investigators have developed a variety of inert gas condensation cluster sources.^{112–116} Supersonic expansion cluster sources normally operate either in the continuous or the pulsed mode, both providing very effective cooling of the formed clusters. Other important variants and hybrids of nozzle expansion sources are known, including specialized jet cluster sources,¹¹⁷ versatile laser vaporization, pulsed beam cluster source,¹¹⁸ and expansion jet/inert gas condensation combination cluster source.^{119,120}

There are many more types of cluster ion sources than there are neutral cluster sources, in part because of the wide variety of ion-forming techniques available and in part because cluster ion sources are often hybrids of established neutral cluster sources and ion-forming environments. Some non-hybrid ion sources which can generate cluster ions include ion sputter,^{121–125} flow tube,^{126–128} Penning discharge,¹²⁹ and high-pressure mass spectrometry ion sources.^{130–136} The methods of ionization used in these sources include electron beam bombardment,¹³⁷ electrical discharges,¹²⁹ proton beam irradiation,¹³⁸ cesium or xenon ion beam sputtering,¹³⁹ radioactivity,¹⁴⁰ and the photoemission of electrons.¹⁴¹ Among neutral/ion hybrid sources, beams of cluster ions have been produced from supersonic expansion sources with corona discharges,^{142,143} radioactivity,¹⁴⁴ and the photoemission of electrons¹⁴⁵ providing ionization in the high-pressure region behind the nozzle. Cluster ions have also been generated by injecting electrons (either by thermionic emission from a filament or via beams of electrons) directly into the expansion jet just beyond the nozzle orifice on its high-vacuum side^{146–148} and through association reactions with ions emitted from thermionic filaments.¹⁴⁹ Preexisting beams of neutral clusters, well beyond the region of the expansion jet, have also been brought into contact with ion-forming projectiles, such as electrons, photons, fast atoms, and species in excited Rydberg states, to form cluster ions.^{150–154} Other important hybrid sources employing supersonic expansions to generate cluster ions include laser vaporization sources (which makes cluster ions as

well as neutral clusters),¹¹⁸ pulsed arc discharge sources,¹⁵⁵ and the electrospray source.¹⁵⁶

NEUTRAL CLUSTERS FROM SUPERSONIC BEAM

A molecular beam source consists of a high pressure gas reservoir, an orifice to allow the escape of gas, various collimating apertures to shape the downstream flow and an adequate pumping capacity to maintain low pressure. This effusive beam technique has been used for over half a century in many historical beam experiments to establish the basic principles of modern physics. The canonical physics literature on molecular beams^{157,158} stressed that the pressure within the source chamber should be kept low enough and the size orifice should be so small (less than the mean free path λ of the gas) that molecules, as they emerge from it, do not collide with each other. In this effusive flow, the emergent beam provides a true random sample of the gas within the source, undistorted by collisions,¹⁵⁹ with the Maxwell Boltzmann velocity distribution characteristic of the reservoir temperature. Chemists, in desperate need of increasing the density number of the effused species, violated this canonical ideal by using much higher source pressures. Collisions within the orifice than produced hydrodynamic, supersonic flow.^{160,161} Since then, most molecular beam experiments employ supersonic beams.¹⁶²

When a gas at high pressure expands into a low-pressure region through a pinhole nozzle, whose diameter orifice size is larger than the mean free path λ of the gas, the pressure and the temperature both drop abruptly. The nozzle imposes collisional communication that brings the gas molecules to nearly the same direction and velocity. Such a flow regime is termed "hydrodynamic". The gas density decreases along the beam axis, until at some distance the flow changes to a free molecular flow with virtually no molecular collision. It also efficiently relaxes thermal excitation of molecular rotation and (less so) vibration. Thus, not only is the intensity of a supersonic beam far higher than that from an effusive source, but the spreads in velocity and rotational states are markedly narrowed and the effective temperature for relative motion of molecules is typically only a few Kelvin degrees. Temperatures much lower, in the millikelvin range, can readily be attained either by using a pulsed nozzle¹⁶³ to permit operation at higher source pressures or through the interaction of a continuous supersonic flow with ambient gas.¹⁶⁴

The power and beauty of jet techniques is the ability to produce a beam of molecules that are vibrationally and rotationally cold but are still vapors. These advantages of supersonic expansions, however, rely on the possibility of producing sufficient partial vapor pressure of the molecules of interest, typically a few millibars. By regulating the temperature of the beam, it is possible to vary the vapor pressure of the sample to the required values. As an example, liquid molecules, such as aromatic alcohols, have to be heated at about 80 °C to obtain the right vapor concentration in the beam, while other largely volatile molecules, such as aliphatic amines, must be kept in a cold bath around 0 °C to avoid saturation.

Unfortunately, some of the analyzed molecules, as most biologically related molecules (e.g., amino acids), are solids with extremely low vapor pressures at room temperature and rapidly decompose when they are heated. For these molecules, which cannot be thermally vaporized, laser ablation or desorption have been alternatively used to produce neutral species in the gas phase.^{165–172} Both methodologies refer to laser-induced particle removal (laser sputtering) from a surface under the two extremes of massive and negligible rates of surface erosion, respectively.

The low temperatures in a supersonic beam provide a unique environment for the formation of weakly bound molecular complexes. In fact, at the translational temperatures available with supersonic jets, van der Waals clusters are stable because their binding energies can be larger than kT . Their formation proceed through a sequence of association reaction steps with concomitant collisional stabilization.^{173–178} This process can be described by a kinetic model,¹⁷⁹ which considers a diluted binary mixture of weakly interacting molecules expanding in a supersonic beam. The first step, the formation of a dimer, is the critical step in the process. In fact, the formation of a trimer in a three-body collision is too unlikely for dilute systems. The van der Waals condensation energy is dumped into the bond joining the two molecules and an activated complex, containing excess energy, is formed. In general, the complex bond does not couple strongly to the internal vibrations of the molecule, so if the energy is not carried off during the collision, the collision complex will dissociate again. Instead, the complex can be stabilized by a collision with an atom of the monatomic carrier gas or with an incoming third molecule. Further growth of the cluster, which mainly involves cluster–monomer collisions, is easier than dimer formation, since there are more modes into which the “condensation” energy can be temporarily stored.

The rate constants involved in the formation of larger clusters are described in terms of the RRK theory,¹⁸⁰ which states that the substitution reaction rate for the addition of the strongly bound component is much faster than for the addition of the more weakly bound component. This gives rise to the experimental observation that the composition of the clusters does not reflect the composition of the vapor phase from which they are formed. Instead, during the formation stage of the clusters, a non-statistical enrichment toward the more strongly bound species occurs.¹⁸¹

SPECTROSCOPY OF NEUTRAL CLUSTERS

Measuring physical–chemical properties of the clusters, such as ionization potential (IP), binding energy (BE), electron (EA) and proton affinity (PA), fragmentation channels, electronic structure and so on, provides a basis for the comprehension of the intrinsic forces acting in the clusters and governing their dynamics. Theoretical computation of these quantities may provide a feedback to evaluate the quality of the calculations and the accuracy of the experimental determinations.

Recently, a number of reviews on the experimental gas-phase methods applied in the molecular cluster field has been published.^{182–184} Basically, any spectroscopic

method can provide information on the structure and the energetics of clusters in both the neutral and ionized state. Fourier transform (FT) microwave spectroscopy can be used to obtain indirect information on the cluster structure through the measure of rotational constants and moments of inertia.^{185–191} A useful extension of the available frequency range came from the introduction of far-infrared vibration rotation tunneling (FIR-VRT) spectroscopy.^{192,193} Dispersed emission (DE) spectroscopy let to investigate the electronic ground state vibrations of the cluster by dispersing in a monochromator the emission from a particular vibronic level of the cluster. Higher resolution is obtained by stimulated emission pumping spectroscopy (SEP).^{194,195} Also ion-detected stimulated Raman spectroscopy (IDSRS)¹⁹⁶ and the complementary resonance ion-dip IR spectroscopy (RIDIRS)^{197–199} are useful mass selective techniques for the probing of cluster ground state vibrations.

Valuable findings on the electronic ground and excited states of clusters have been derived from laser-induced multi-photon ionization (MPI) investigations,^{200–209} such as laser-induced fluorescence (LIF) and REMPI. This latter technique is particularly promising since it enables mass selection of cluster species and their spectral and thermochemical characterization. The complex is excited from its electronic ground state from a photon and then ionized by a second photon of equal or different frequency, near threshold to avoid cluster fragmentation.^{210–213} Very recently, REMPI spectroscopy has been applied to the study of biomolecules, such as amino acids,^{214–216} peptides,²¹⁷ DNA bases and derivatives,^{218,219} sugars,²²⁰ and others.^{221,222} Hole-burning (HB) and IR fluorescence dip spectroscopy⁵ let to distinguish between isomers of clusters of a given mass. An intense laser beam scans through the wavelength region of interest (the pump) while a counter-propagating laser (the probe), delayed in time, is fixed on a selected resonance whose resulting fluorescence gives a measure of the population of the probed ground-state level. When both lasers excite transitions, which arise from the same ground-state species, the pump beam induced depopulation manifests itself by a decrease in the intensity of the fluorescence excited by the probe (spectral hole). If both lasers excite different ground-state levels, no spectral hole is observed.

Rydberg electron transfer (RET) spectroscopy consists of transferring electrons from highly excited atoms into diffuse orbitals of polar systems and provides a useful method for the discrimination between different geometrical configurations.^{223–226} For cations, two complementary methods provide a wealth of information: zero kinetic energy (ZEKE) photoelectron spectroscopy and mass-analyzed threshold ionization (MATI) spectroscopy. These techniques take advantage of the existence of long-lived molecular Rydberg states ($n > 150$), whose ionization by a delayed pulsed electric field leads to the observation of threshold ions in well-defined energy states.^{227–229} ZEKE is a high-resolution technique²³⁰ that is widely applicable for studies of molecules and clusters.^{231–234} MATI facilitates unambiguous identification of the ionized species, and can be used to follow cluster fragmentation.^{229,235–240} This high-resolution spectroscopy led to partially resolve rotational structure in the molecular cluster cation spectrum.

Three of these experimental laser-based methodologies, LIF, REMPI, and RET, have been successfully applied to the study of the physical–chemical properties of chiral molecular clusters.

Laser-induced multiphoton ionization and hole burning spectroscopy

These techniques are sufficiently sensitive to allow identification of the low-frequency intermolecular vibrations in weakly bonded molecular clusters. Both the LIF and the resonance-enhanced multiphoton ionization (REMPI) techniques are based on the electronic excitation of a supersonically expanded molecule or cluster by absorption of light quanta from a tunable continuous wave (CW) dye laser. In the LIF experiments,²⁰⁴ the resulting fluorescence is usually detected without wavelength dispersion, and the spectrum is then a plot of the total detected fluorescence vs. exciting wavelength. Since the molecule can only fluoresce if it is excited, and it can only be excited if the laser is tuned to an absorption frequency, the fluorescence excitation spectrum is very similar to the absorption spectrum. One important difference arises because some states may decay via radiationless processes. In these cases, the molecule may have a well-developed high-resolution absorption spectrum and no fluorescence spectrum. This difficulty is avoided in the REMPI experiments in that detection is normally carried out using time-of-flight (TOF) mass spectrometers. When different isomers of clusters are present in the jet, the application of hole burning (HB) spectroscopy is of particular advantage.¹⁸³ The population of one isomer can be burned out by employing an additional UV (or IR) laser. The LIF or REMPI spectrum then show the depletion of that isomer and the spectral transitions associated with the isomer can be identified. Recently, additional structural information has come from the deconvolution of the rotational envelopes associated with the electronic transitions.²³¹

Resonant two photon ionization spectroscopy

The simplest version of REMPI uses a two photon ($1 + 1$) process, namely resonant two photon ionization (R2PI). In this, the species M is first promoted from its electronic ground state S_0 to the electronic excited state S_1 via a resonant absorption step. Then, the non-resonant absorption of a second photon takes the species into the ionization continuum. If the frequencies of the excitation and ionization photons are equal, the process is named one color R2PI (1cR2PI), otherwise two colors R2PI (2cR2PI) (Fig. 1).

A large number of R2PI experiments on clusters are reported in literature: these studies allow to explore in detail the nature of the intra- and intermolecular forces acting in molecular clusters. The vast majority of the studies involves simple models consisting in organic species, particularly aromatics, because of the strong electronic spectral transitions (typically the S_0 to S_1 π -electron transitions) available in regions accessible to common tunable dye laser used in 1cR2PI spectroscopy. For what concerns biological molecules, many of them exhibit strong absorption bands in the

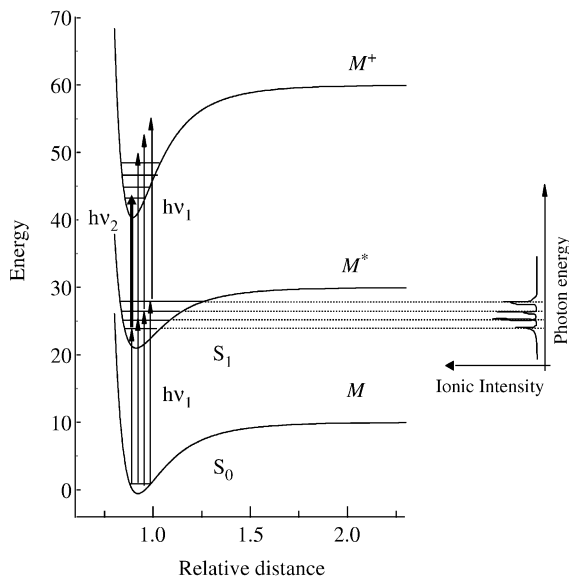


Fig. 1 Schematic representation of the 1cR2PI ($h\nu_1 + h\nu_1$) and 2cR2PI ($h\nu_1 + h\nu_2$) ionization processes for species M.

near-ultraviolet region of the spectrum (200–400 nm). These are generally associated with small conjugated ring systems, both aromatic and heterocyclic, whereas the large conjugated systems absorb in the visible region. Absorption of proteins in the 280 nm region prevalently results from the presence of aromatic amino acidic residues (such as tyrosine, phenylalanine, and tryptophan), which mostly absorb in this range. Similarly, all of the purine and pyrimidines bases absorb strongly in the near ultraviolet. Generally, these absorption bands correspond to transitions of π electrons in the ring to antibonding π orbitals, the so-called $\pi-\pi^*$ transitions. Farther in the ultraviolet, nearly everything absorbs. Transitions in the visible region of the spectrum are relatively low-energy electronic transitions, and only two main kinds of biological structures have energy levels with spacings in this range: some compounds containing metal ions (particularly transition metals), and large aromatic or conjugated double-bond systems. The former include some metalloproteins and the latter such conjugated structures as vitamin A.

One-color resonant two photon ionization (1cR2PI) spectroscopy

1cR2PI measurements consist in tuning the frequency of the excitation and ionization photon ν_1 . Since the ionization cross section is larger for resonant than for non-resonant processes, an increase in the ionization yield of M will be obtained each time the energy $h\nu_1$ excites M from its ground state to a precise vibrational

level of S_1 . Thus, by monitoring the ionic signal M^+ as a function of the laser frequency of the excitation photon, the vibro-electronic spectrum of M is recorded.

The species M is either a simple molecule or its cluster with a chromophore C (henceforth denoted as $[C\cdot M]$). In this latter case, each component of the cluster electronically perturbs the other. This can be seen by comparing the 1cR2PI spectrum of the bare chromophore C with that of the cluster. The spectral shift of the $S_1 \leftarrow S_0$ electronic transition band origin of $[C\cdot M]$ compared to that of the isolated C , provides a measure of the difference in the stabilization energy of the excited and the ground electronic state of the chromophore induced by the solvent. Two opposite situations can be observed: (i) a spectral blue-shift of the $S_1 \leftarrow S_0$ electronic transition in $[C\cdot M]$ with respect of that in the isolated C ("ipsochromic shift"). The complexation of the chromophore results in a larger stabilization of the ground state with respect to the excited state and, thus, an increase in the energy difference between the S_0 and S_1 states; (ii) a spectral red-shift of the $S_1 \leftarrow S_0$ electronic transition in $[C\cdot M]$ with respect to that in the isolated C ("bathochromic shift"). Following the cluster formation, a lower stabilization of the ground state with respect to the excited state takes place and, thus, a reduction of the energy difference between the ground and excited state.

The magnitude and direction of the spectral shift arises from a combination of effects that depends on the nature of the interaction of the molecule with its solvating partners and the effects of excitation on molecular properties including polarizabilities and dipole moments.^{201,241,242} In the case where the interaction is short-range and repulsive effects dominate the potential, blue-shifts can result. This is the situation which typically arises when polar forces such as those from dipole-induced dipole, dipole-dipole, or hydrogen bonding are absent. Instead, a red-shift is most typically observed when dispersive forces give rise to long-range interactions. Polar solvent molecules introduce complications in interpreting spectral shifts. Polar interactions produce red- or blue-shifts, depending on whether the excited state has a larger or smaller permanent dipole moment than the ground state, and whether polar forces are attractive or repulsive in the ground state complex. If an interaction is largely polar and excitation increases the polarity of the chromophore C along the interaction axis, substantial red-shifts are observed.²⁴³ However, if polar forces do not dominate the bonding of the complex in the ground state, then excitation to a more polar state may lead to a blue-shift.²⁴⁴ Zero point energy (ZPE) differences must be considered as well; these can arise from unequal perturbations to ZPE of the two states of the molecule C or unequal contributions to the ZPE by the respective intermolecular (van der Waals) modes in the ground and excited cluster.²⁰¹

Analysis of 1cR2PI spectra has provided evidence for the existence of various conformers²⁴⁵⁻²⁴⁹ in complex molecules, containing multi-ring systems or long side chains. Biological compounds generally belong to this type of complex molecules. The number of aromatic rings also plays an important role in the spectral shifts observed and in the frequencies of the van der Waals modes, which sometimes can be resolved. It is often possible to assign the lower frequency modes observed in the

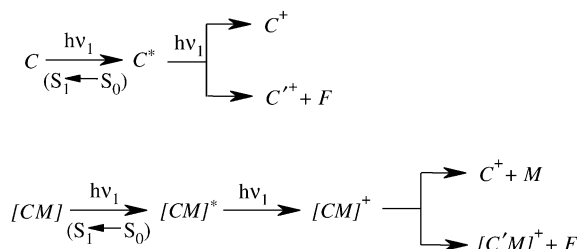
1cR2PI spectra to various stretching and bending modes, but only in the case of small clusters. Thermal broadening of resonant line widths is often observed in large clusters. This is due to the fact that large clusters typically form late in an expansion and retain a considerable amount of their heat of condensation. This leads to a higher internal temperature with a concomitant broader rotational envelope.

The isolated enantiomers S (M_S) and R (M_R) of a chiral molecule M exhibit the same spectral features since their physical properties are identical. However, their aggregation with a chiral chromophore of defined configuration ($C_{R/S}$) leads to the formation of two diastereomeric complexes with different spectral properties, i.e., $[C_{R/S}M_S]$ and $[C_{R/S}M_R]$. The 1cR2PI spectroscopy is able to discriminate between M_R and M_S by measuring the spectral shift of the diastereomeric $[C_{R/S}M_S]$ and $[C_{R/S}M_R]$ complexes with respect to that of the bare chromophore $C_{R/S}$. It is convenient to define the diastereomeric clusters as “homochiral” when the chromophore and the solvent have the same configuration, and “heterochiral” in the opposite case.

The coupling of the 1cR2PI and supersonic beam techniques let to obtain good spectra, not congested by the presence of hot bands, being negligible the population of the high vibrational levels of the ground state. This comes from the cooling of the translational, rotational and vibrational degrees of freedom of the species produced in the supersonic expansion. Obviously, the 1cR2PI methodology presents also some constraints, mostly due to the fact that the method does not permit to choose the frequency of the second ionizing photon. For example, there is the possibility that the ionization of the species comes out from autoionization and, thus, the cross section of this process should be also considered. Autoionization occurs following a resonant absorption of the ionization photon in a vibrational level of the Rydberg states of the neutral. As a consequence it is not possible to prevent exactly the intensities of the ions produced in the 1cR2PI process, nevertheless the energy of the ionizing photon could be controlled, as in the 2cR2PI techniques.^{250,251}

Furthermore, in order to ensure ionization of the species and avoid its fragmentation, the excited states of the species should have high absorption cross sections, lifetimes comparable to the coherence time of the laser, and an energy amount equal or larger than one-half of the appearance potential (AP) of the species. In fact, if the excited state is much higher in energy than one-half of the AP, the ion will be produced with a not negligible excess energy ($2h\nu_1 - \text{AP}$) which is then transferred into vibrational excitation of the ionized species. Sometimes, this excitation causes the formed ion to dissociate: if the species is a molecular ion, fragmentation can occur; if the species is a cluster ion, it can dissociate into its original components or give rise to more complex fragmentation patterns. In general, the fragmentation pattern is that reported in [Scheme 1](#).

When, during the scan of the ν_1 frequency, the photon is resonant with a vibrational level of the electronic excited state, the second photon leads to the ionization of the species. If the overflow energy causes the fragmentation or the dissociation of the ionic species, fragments will compare in the mass spectrum. These fragments keep memory of their parent ions, it is as to say that they have the



Scheme 1

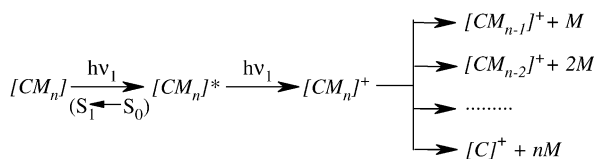
same vibroelectronic spectral patterns. This is an important characteristic of the 1cR2PI method, which in turn allows to study the fragmentation and dissociation processes occurring in molecules and clusters.

A complication in the 1cR2PI spectrum can come from the fragmentation of large clusters, $[C \cdot Mn]$ (Scheme 2). The measured spectral features of a cluster come from the dissociation of a larger cluster ions, which eventually could be not detectable in the spectrum because of a high fragmentation efficiency. In this case, an unambiguous assignment of the vibronic pattern is no longer possible. As been yet mentioned, another complication in the analysis of the 1cR2PI spectrum can come from the presence of various isomers of the studied species, which cannot be always distinguished in the vibroelectronic spectrum.

Two-color resonant two photon ionization (2cR2PI) spectroscopy

All the problems associated with the 1cR2PI laser spectroscopy can be avoided or strongly reduced by means of the 2cR2PI laser spectroscopy, a powerful methodology allowing the measurement of physicochemical properties of the species of interest, such as the ionization and fragmentation potentials and the binding energies. As previously described, in the 2cR2PI a fixed frequency laser (ν_1) pumps a specific vibroelectronic transition, while a second tunable photon ν_2 promotes the species into the ionization continuum.

The ionization and fragmentation thresholds can be obtained by the photoionization efficiency curves through the following sequence: (i) the first exciting laser ($h\nu_1$) is fixed on the $S_1 \leftarrow S_0$ transition of the species of interest; (ii) the laser intensity is lowered to about 1-10% of the initial fluence to minimize the $h\nu_1$



Scheme 2

absorption, and thus avoid one color ionization processes; (iii) a second laser, whose beam intensity is almost five times higher than those of the excitation laser beam, is scanned through the cluster ionization ($h\nu_2$) and dissociation threshold ($h\nu_3$) regions (Fig. 2).

The binding energy of the $[C\cdot M]$ adduct in the ground, excited ($[C\cdot M]^*$), and ionized state ($[C\cdot M]^+$), respectively D_0'' , D_0^* and D_0^+ , are computed from the following relations:

$$D_0'' = h\nu_1 + h\nu_3 - (h\nu_1' + h\nu_2') \quad (1)$$

$$D_0^* = D_0'' - (h\nu_1 - h\nu_1') = D_0'' - \Delta\nu \quad (2)$$

$$D_0^+ = h\nu_3 - h\nu_2 \quad (3)$$

The topic of ionization thresholds and cross sections of clusters has been intensely explored.^{252,253} A general finding is that the ionization energy of molecular clusters ($h\nu_1 + h\nu_2$) tends to decrease with its size, the change being more pronounced for smaller clusters. In the case of homogenous clusters, a linear dependence of the ionization energy on inverse cluster size is often found,^{254,255} justified on the basis of a quantum mechanical independent systems model.^{256,257} In the case of weakly bound systems, the decreases in ionization energies are found to be considerably larger than the spectral shifts of the electronic transitions. Ionization enhances the intermolecular forces by introducing the influence of a charged center.²⁵⁸ This is found, for example, in the case of benzene and its derivatives where their ionization potential decreases upon association with argon by about $100\text{--}200\text{ cm}^{-1}$ compared to spectral shifts for the $S_0 \leftarrow S_1$ transitions around 30 cm^{-1} .^{259,260} This large difference is an indication of the magnitude of the ion-induced dipole effect.

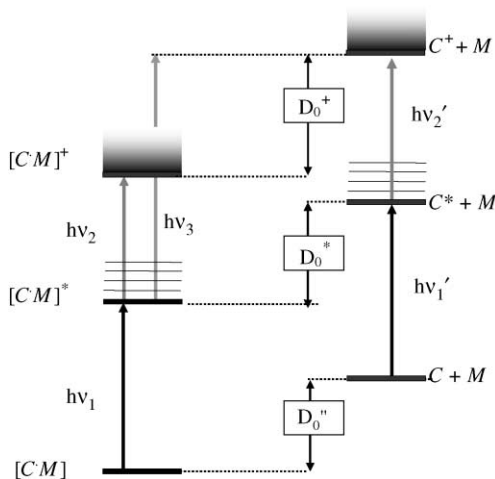


Fig. 2 Schematic representation of the energy levels of the bare C (denoted as $C + M$) and of its complexes with M (denoted as $[C\cdot M]$). D_0'' , D_0^* and D_0^+ as the binding energies of the adducts in the ground, excited, and ionized state, respectively.

Another consequence of the stronger interactions upon ionization is that the equilibrium geometry of the ionized complex may differ significantly from that of the neutral states. Broadened ionization onsets are frequently attributed to the spectral superposition of ionization into several vibrational levels for which Franck-Condon factors are more favorable.²⁶¹ As a result, the adiabatic ionization potential may be considerably lower than the vertical potential, and the observed ionization onsets may occur above the adiabatic potential. Another factor to be considered is the conformation-dependent effect,²¹³ due to the different conformations of the solvent molecules. The most populated form of a complex may involve a less stable form of the solvent. After photoionisation, the lowest-energy dissociation channel in the complex ion leads to the most stable form of isolated solvent, which has to be taken into account for the estimate of the binding energy.

Rydberg electron transfer (RET) spectroscopy

RET spectroscopy is based on the transfer of electrons from highly excited atoms into diffuse orbitals of polar systems and provides a useful method for the discrimination between different geometrical configurations.

When an excess electron is attached to a neutral non-covalent complex of polar molecules with negative valence electron affinities, no stable valence negative ions of this complex can be formed. However, the presence of a large enough total permanent electric dipole moment²⁶² and of a quadrupole moment and polarizability,²⁶³ let the electrostatic field to accommodate a very weakly bound (in the meV range) excess electron in a very diffuse orbital (in the nanometer range), mostly located outside the molecular frame. The formation of a stable anion, called dipole-bound or multipole-bound, only releases very little internal energy into the complex.²⁶⁴ As a consequence, fragmentation processes are very unlikely to occur, even for weakly bound non-covalent complexes, and the structure of the dipole-bound anion is generally very similar to that of its neutral parent. Therefore, information about the original structure can be deduced. This is not always true, and, if a reorganization of the neutral geometry with a low energy expense take places, a higher dipole moment structure, more favorable to dipole-bound anion formation, can be formed.^{226,258}

The dipole-bound anions can be formed by electron transfer collisions between cold molecular complexes and laser-excited Rydberg atoms, in a crossed beam experiment under single collision conditions. The use of Rydberg electrons allows for a very efficient electron transfer and for the stabilization of the created anions, leading to cold negatively charged species. Furthermore RET spectroscopy is selective with respect to the excess electron binding energy in the dipole-bound anion and electron transfer is efficient only if there is an appropriate matching between the initial Rydberg orbital and the final dipole-bound anion orbital. This peculiarity allows to precisely determine the excess electron binding energy in the created dipole-bound anion, EA_{DB} . When rigid complex anions are produced, the Rydberg n -dependencies are sharply peaked, while more peaks appear when a

number of nearly isoenergetic isomers of the neutral complexes are simultaneously present. Each peak corresponds to the production of different anions arising from electron attachment to either large or small resulting dipole configurations. If a neutral complex configuration is floppy, there is no well-defined resulting dipole but rather a broad distribution and the Rydberg n -dependencies for anion production are then sums of different contributions. As an example, the experimental data obtained by Schermann and co-workers for the formation respectively of monomer dipole-bound anions of imidazole and adenine and for their complex are shown in Fig. 3.²⁶⁵ Anion creation rates for the two monomers are clearly peaked around the respective optimum Rydberg quantum numbers $n_{\max} = 12$ and $n_{\max} = 15$, while their complex has mainly one peak centered around $n_{\max} = 8-9$.

From these data, the excess electron binding energy values can be obtained from the $EA_{DB} = 23/n_{\max}^{2.8}$ empirical relationship, which has been verified with a very good precision for many previously studied dipole-bound species.^{223,264} Since excess electron binding energy is strongly related to the electrostatic characteristics (dipole, quadrupole, polarizability, etc.) and thus to the geometry of the complex, it is possible to determine which neutral configuration is likely to have given birth to the observed anions. For a given cluster size, the resulting dipole moment of the different configurations is, in a first approximation, the vector sum of the individual dipoles.

SOURCES OF IONIC CLUSTERS

As for neutral cluster sources, an ever growing array of techniques are being implemented to generate ionic clusters and measure their properties. Mass spectrometry is useful for quantitative determination of atoms or molecules and

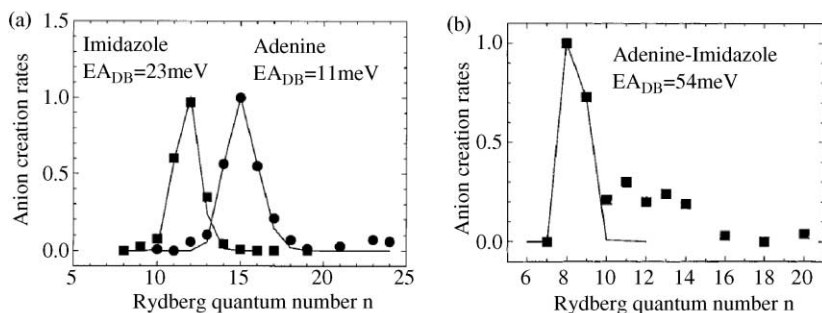


Fig. 3 Relative dipole-bound anion formation rates in RET collisions between Rydberg $Xe(nf)$ atoms with (a) adenine (circles) or imidazole (squares) molecules and (b) adenine–imidazole complex produced in a supersonic beam. Experimental data are fitted to curve-crossing model calculations which lead to the experimental determination of EA_{DB}^{exp} values, equal to 11 meV for adenine, 23 meV for imidazole and 54 meV for adenine–imidazole complex (reproduced by permission of the American Chemical Society).

also for determining chemical and structural information about molecules on the grounds of their distinctive fragmentation pattern.

Electrospray ionization sources

Electrospray ionization (ESI) refers to the overall process by which an intense electric field disperses a sample liquid into a bath gas as a fine spray of highly charged droplets. Evaporation of those charged droplets produces gas-phase ions by mechanisms that remain the subject of much argument and debate. The ESI is a complex of independent component processes, the two most important of which are electrospray dispersion, the electrostatic dispersion of sample liquid into charged droplets, and ionization, the transformation of solute species in those droplets to free ions in the gas phase.

Electrospray dispersion, often shortened to electrospray (ES), is usually accomplished by passing a small flow of the liquid through a narrow-bore injection tube maintained at a substantial electrostatic potential relative to its surroundings which generally include an opposing counter-electrode. Such injection tubes are frequently known as “needles” because they often comprise a short length of the kind of stainless-steel tubing from which hypodermic needles are fashioned. The potential difference between needle and counter-electrode (cathode) creates an intense external electric field in the vicinity of the needle tip that disperses the emerging liquid as a fine spray of charged droplets, usually into an ambient gas at or near atmospheric pressure. In 1991, Blades, Ikonomou and Kebarle²⁶⁶ remarked that the liquid injection “needle” can be regarded as the anode or cathode of a Galvanic cell depending upon the polarity of the applied potential (electrohydrodynamic mass spectrometry (EHMS)).^{267,268} Producing solute ions from charged droplets requires the vaporization of solvent. The energy for this process is provided by the bath gas in which the droplets are dispersed. In ESI systems, that bath gas also served to moderate the translational energy of the charged droplets and the ions they produced.

Electrospray is a very gentle, non-fragmenting ionization technique which can leave unsolvated ions with a memory of their solution phase structure. Weakly bound complexes can be easily studied by electrospray. An uncharged bonus is that ions formed by this method are often multiply charged by the addition of protons. This multiple charging of the ions makes them appear proportionally lighter to the mass spectrometer and so species which would normally be well beyond the mass range of the instrument are brought within its capabilities.

Matrix assisted laser desorption and ionization

Matrix assisted laser desorption and ionization (MALDI) technique has developed in 1987.^{269,270} Since then, it has proven to be one of the most successful ionization methods for the mass spectrometric investigation of large molecules, increasing the

upper mass limit of intact ion molecules to over 100,000 Da and, therefore, enabling the analyses of large biomolecules.²⁷¹

MALDI is a method that allows for vaporization and ionization of non-volatile biological molecules from a solid-state or liquid phase directly into the gas phase. The presence of a solid or liquid matrix (around 1 part in 100–50,000), which strongly absorbs the laser radiation, spares the studied species from degradation, by protecting them from the harsh effects of the laser. It results in the detection of intact molecules.^{272,273}

The desorption and ionization source in MALDI is a laser beam. The ion formation process has two distinct components. First, molecules are ejected from the solid sample with sufficient kinetic energy to escape the surface without introducing large amounts of vibrational or electronic excitation to the molecules themselves. Then, transfer of charge to the molecules occurs during their ejection. This first portion of the mechanism is inherently non-equilibrium. If the translational energy involved in ejecting the molecules from the surface is in equilibrium with the internal degrees of freedom of the molecule, the molecule would disintegrate before it could be extracted from the ion source. The matrix plays a key role in this mechanism by absorbing the laser light energy and causing part of the illuminated substrate to vaporize.

A rapidly expanding matrix plume carries some of the sample molecules into the vacuum. Collisions with the dense expanding gas accelerate the large sample molecules included in the evaporating solid region up to the same speed as the gas. At some point in the expansion process, proton transfer between photoexcited matrix and sample molecules occurs, causing the formation of positively and negatively charged sample ions. The expansion process continues until the density of the matrix cloud becomes low enough that the sample ions can be considered free particles, moving with the velocity imparted by the expansion.

Fast atom bombardment

The fast atom bombardment (FAB) technique^{274–276} involves the bombardment of a solid analyte/matrix mixture by a fast particle beam. The matrix is a small organic species (glycerol or 3-nitrobenzyl alcohol, 3-NBA) which is used to keep a “fresh” homogeneous surface for bombardment, thus extending the spectral lifetime and enhancing sensitivity. The particle beam is generally a neutral inert gas, typically Ar or Xe, at bombardment energies of 4–10 KeV. The particle beam is incident at the analyte surface, where it transfers much of its energy to the surroundings, setting up momentary collisions and disruptions. Some species are ejected off the surface as positive and negative ions by this process, and these “sputtered” or secondary ions are then extracted from the source and analyzed by the mass spectrometer. The polarity of the source extraction can be switched depending on what species are to be analysed. The FAB technique is a comparatively soft ionization method which is therefore suitable for analyzing low-volatility fragile species (M), typically producing large peaks for the pseudo-molecular ion species $[M + H]^+$ or $[M-H]^-$

along with structurally significant fragment ions and some higher mass cluster ions and dimers.

MASS SPECTROMETRY OF IONIC CLUSTERS

The use of mass spectrometry is not restricted to the characterization of chemical species, but it is nowadays increasingly extended to life sciences. Many of the physical and chemical procedures accessible to mass spectrometry, e.g., collision-induced decompositions, ion/molecule reactions, charge exchange processes, etc., are now commonly employed to elucidate biological processes. The variety of ionization methods permits the volatilization of macromolecules in the range of 300,000 Da at sensitivities below 1 picomol, as well as the analysis of small molecules of less than 500 Da at the attomol level. Experimental conditions can be designed to measure the molecular weight of the species of interest or its fragmentation pattern which may provide detailed structural information, e.g., protein sequencing.

A wide variety of mass spectrometry techniques is available, including multiple quadrupole, TOF, and ion cyclotron resonance mass spectrometry.²⁷⁷ Wien filter mass separation, magnetic or electric sector mass separation, and retarding potential analysis share the capability to assign mass-to-charge values to ions, although the principles of operation and the types of experiments that can be done differ greatly. Combinations of several techniques are also possible. Many state-of-the-art commercial mass spectrometers interface electric and magnetic sectors with one or more quadrupoles to achieve high performance mass spectra.¹¹⁰

Mass spectrometers are operated at reduced pressure in order to prevent collisions of ions with residual gas molecules in the analyzer during the flight from the ion source to the detector. The vacuum should be such that the mean free path length of an ion, i.e., the average distance an ion travels before colliding with another gas molecule, is longer than the distance from the source to the detector. For example, at a pressure of 5×10^{-5} torr, the mean free path length of an ion is approximately one meter, i.e., about twice the length of a quadrupole instrument.

Time-of-flight mass spectrometry (TOF-MS)

In a simple TOF mass spectrometer, ions are firstly accelerated in an electric field between two charged grids (electrostatic lenses) and, then, separated in a field-free drift region. At the end of the flight, the ions arrive at the detector. If all ions were instantaneously formed in a single point between the lenses, and with zero initial velocity, they would be accelerated to the same kinetic energy by the extraction field. Under these conditions, ions with large masses fly through the drift region more slowly than ions with little masses.

The mass range of a TOF mass spectrometer is virtually limitless, provided the flight distance does not greatly exceed the mean free collision path with background gases. Typically, the mass resolution of the TOF is a few hundreds, independent of

whether ionization is induced by electron impact or laser techniques. Over the past decades, many methods have been proposed to increase the mass resolution of TOF mass spectrometry.^{278,279} Increased resolution can be achieved using a mass reflectron, a modification of the TOF technique introduced in the early 1970s by Mamyrin.^{280,281} In the reflectron device, a reflection is built into either a V-shaped or linear drift path such that ion packets which have spread due to spatial and energetic difference can be focused back together at the detector. An advantage of the reflectron is that the same mass resolution can be achieved with about 40% of the drift length of a traditional drift tube, and lower voltage are required.²⁸² Resolution of about 10,000–11,000 are reported in literature²⁸³ for this device, although a resolution of about 1000 is more typical. The advantages for cluster beam experiments of TOF mass spectrometry are several-fold. The principal ones are the following: (i) well resolved mass spectra can be rapidly recorded and, thus, it is possible to study the relative intensity of the ion peaks as a function of the experimental condition (for example as a function of the photoionization energy, i.e., wavelength scan); (ii) the entire mass spectrum of a single ion packet can be obtained at one time. This is ideally matched to cluster sources which provide pulsed outputs, e.g., REMPI.

Quadrupole mass spectrometry

The basic principles of the quadrupole mass filter were published in the early 1950s by Paul and Steinwedel.²⁸⁴ It has now become one of the most widely used types of mass spectrometers because of its ease of use, small size, and relatively low cost. Mass separation in a quadrupole mass filter is based on achieving a stable trajectory for ions of specific m/z values in a hyperbolic electrostatic field.

A quadrupole mass spectrometer consists of four parallel metal rods. One pair of diagonally opposite rods have an applied potential consisting of a DC voltage and an rf voltage. To the other pair of rods, a DC voltage of opposite polarity and an rf voltage with a 180° phase shift is applied. The applied voltages affect the trajectory of ions traveling down the flight path centered between the four rods. For a given set of DC voltage and rf voltages and frequency, only ions of a certain mass-to-charge ratio pass through the quadrupole filter and all other ions are thrown out of their original path. A mass spectrum is obtained by monitoring the ions passing through the quadrupole filter as the voltages on the rods are varied.

The resolving power of a quadrupole mass filter depends on the number of cycles experienced by an ion within the rf field, which in turn depends on its velocity. Thus, the resolution will increase with increasing mass, as ions of higher mass have lower velocity. However, the transmission efficiency will decrease, due to the longer time ions of higher masses spend in the quadrupole.

Typical quadrupoles transmit ions with mass-to-charge ratios ranging from 1–300 or greater with a mass-dependent resolution of twice the mass. More sophisticated instruments can achieve m/z of 4000 with comparable resolution. The suitability of a quadrupole mass analyzer depends in large part on the duty cycle

of the cluster experiment and the energy of the incident ions. Continuous ion sources are by far the most suitable for a quadrupole mass spectrometer since m/z is transmitted at one time. Wider m/z ranges can be transmitted only by sacrificing mass resolution. Quadrupoles also require low velocity ions and relatively low ion current densities. Ion beams with high energies or current densities will be passed through a quadrupole sector with little or no mass resolution. Finally, the sensitivity of the quadrupole is mass and energy dependent. In principle, the instrument response function can be obtained using a calibration gas. In practice, however, this is most straightforward using a static pressure of the calibrant and can be difficult to determine from a neutral beam. In addition, the abundance spectrum of gas phase clusters tends to span a large mass range; relative intensities of neighboring cluster sizes are more easily determined than those of clusters of widely different masses. The principal advantages of quadrupole mass filter are its good transmission efficiency, high scan speed, and wide acceptance angle to give high sensitivity.

Fourier-transform ion cyclotron resonance mass spectrometry (FT-ICR)

Although the above mass spectrometric tools have mass ranges and resolving powers adequate for chemical analysis, mass spectral characterization and structural analysis of biopolymers generally demand efficient detection of ions over a wide mass range, accurate mass measurements, and high mass resolution.²⁷⁷ The FT-ICR analyzer is able to combine high resolution and MS^n capabilities.

The basic hardware for FT-ICR consists of an analyzer cell contained within a high-vacuum chambers ($< 10^{-8}$ mbar), which is centered in a strong, homogeneous magnetic field. The ions in the FT-ICR analyzer are constrained to move in circular orbits. Their motion is confined perpendicular to the magnetic field and is restricted parallel to the magnetic field by application of an electrostatic potential to the two plates on the ends of the cell (trapping plates). The trapped ions can be stored in the FT-ICR analyzer for long periods of time (up to several hours), provided that a high vacuum is maintained to reduce the number of destabilizing collisions between ions and residual neutral molecules. The polarity of the voltage applied to the trapping plates determines whether positive or negative ions are retained in the cell.

The ion motion in the cell is complex because of the presence of electrostatic and magnetic trapping fields; it consists of three different modes of oscillation.²⁸⁵ However, the primary mode of interest is the cyclotron motion, whose frequency, ν_c , is directly proportional to the strength of the magnetic field B and inversely proportional to the mass-to-charge ratio m/z of the ion ($\nu_c = kzB/m$).

FT-ICR detection is accomplished by monitoring the image current induced by the orbiting ion packet as it cycles between the two receiver plates of the cell. After formation by an ionization event, all trapped ions of a given m/z have the same cyclotron frequency but have random positions in the FT-ICR cell. The net motion of the ions under these conditions does not generate a signal on the receiver plates of the FT-ICR cell because of the random locations of ions. To detect cyclotron motion, an excitation pulse must be applied to the FT-ICR cell so that the ions bunch

together spatially into a coherently orbiting ion packet. This excitation pulse also increase the radius of the orbiting ion packet so that it closely approaches the receiver plates of the FT-ICR cell.

As a result of this excitation step, the net coherent ion motion produces a time-dependent signal on the receiver plates, termed the “image current”, which represents all ions in the FT-ICR cell. The image current is converted to a voltage, amplified, digitized, and Fourier transformed to yield a frequency spectrum that contains complete information about frequencies and abundances of all ions trapped in the cell. A mass spectrum can then be determined by converting frequency into mass: because frequency can be measured precisely, the mass of an ion can be determined to one part in 10^9 or better.

In a typical FT-ICR experiment, after ion detection, a voltage spike is used to eject all ions from the cell in preparation of a new experiment. However, instead of being ejected from the cell, the ions can be allowed to relax to the center of the cell through collisions with background gases. These ions can then be re-excited and measured several times.²⁸⁶ This remeasurement process may reduce the amount of sample required for FT-ICR analysis, a capability that is very important in biological applications.

Although FT-ICR detection of image current is somewhat less sensitive than ion detection with an electron multiplier, the remeasurement technique significantly lowers the detection limit to the point of detecting a single ion. Because of the inverse relationship between ν_c and m/z , it is more difficult to resolve high-mass (low-frequency) ions than low-mass (high-frequency) ions. Whereas ultrahigh mass resolution can be achieved for small ions ($m/\Delta m > 10^6$ for $m/z = 100$), FT-ICR resolution decreases linearly with increasing mass, implying that a resolution of $m/\Delta m > 10^4$ would be expected for an ion of $m/z = 10000$.

Perhaps, the most attractive features of the FT-ICR are its extensive ion-trapping and manipulation capabilities, useful for measuring the stability and reactivity of ions and for probing their structure. Targeted ions can be selectively trapped in the cell by applying rf pulses to eliminate unwanted ions. After this isolation step, a number of experiments can be carried out. For instance, selected ions can be accelerated into a neutral inert gas (e.g., Ar) to produce fragment ions. This process, called collisionally induced dissociation (CID),^{287,288} can give information upon the structure of a covalently bound ion or upon the relative stability of ionic fragments arising from decomposition of an ion-neutral cluster (see the following section). As an alternative to CID processes, photo-induced or black-body radiation-induced fragmentation can be used with FT-ICR. These techniques are more useful than CID for the differentiation of isomers.²⁸⁹ The reactivity and the stability of the trapped ions can be conveniently probed by measuring the kinetics and the equilibrium constant of their reaction with suitable neutral reactants.

The kinetic method

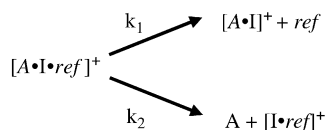
The kinetic method was introduced by Cooks and co-workers about twenty years ago for the determination of proton affinities:^{290,291} since then it has probably

became the most widely used mass spectrometric method for the determination of relative thermochemical properties. It is based on the rates of competitive dissociations of a mass selected cluster ion: under appropriate conditions, the kinetics of the dissociation of a cluster ion can yield relative, but nevertheless quantitative, thermochemical information on the constituent species. Cluster ions bound via protons, electrons, or other atomic or polyatomic anions or cations can be isolated and their dissociations followed in a tandem MS/MS or FT-ICR experiment.

A wide range of thermochemical properties can be measured, including not only proton affinity^{292–295} or gas-phase basicity, but also electron affinity,²⁹⁶ ionization energy,^{297,298} gas-phase acidity^{299–301} and cation affinity.^{45,302,303} Entropy changes upon attachment of an ion to a molecule are also accessible and provide information on both the nature of the bonding and fragmentation mechanisms in cluster ions, especially in biological compounds. Thermochemical determinations by the kinetic method also provide very useful structural information: e.g., two-electron three-center bond has been observed in the gas phase by means of the kinetic method.³⁰⁴ In the last years, the kinetic method has been also applied to characterize chiral ions in the gas phase.

The principal attractions of this method are the ease of use, the large applicability to non-volatile and thermally labile species (including peptides and other biological molecules), and the high sensitivity to small differences in thermochemical values. All these features account for the popularity of the method. Unfortunately, this popularity has also led to incorrect uses of the kinetic method that does not follow the application conditions outlined by Cooks. In fact, a number of assumptions have to be made to correctly apply the kinetic method: (i) the method applies to weakly bound complexes; (ii) comparisons should be made for competitive dissociation of clusters having no other decomposition channels; (iii) there must be no reverse activation barriers to the dissociations process; (iv) the fraction of cluster ions that undergo dissociations can be characterized by an “effective temperature” T_{eff} , defined as the temperature of the canonical ensemble for which fragmentation would yield the same branching ratios as observed experimentally (*vide infra*).

Being valid these assumptions, we can consider the dissociation of the ionic cluster $[A \cdot I \cdot \text{ref}]^+$, where I^+ is a metal ion, a proton, or another cationic species binding the unknown A with a reference molecule ref, whose affinity for I^+ is known. The dissociation channels are shown in Scheme 3, where k_1 and k_2 are the rate constants for the two dissociation processes.



Scheme 3

The difference in the affinity of A and ref for I^+ will be reflected in the experimentally measured branching ratio $[A \cdot I]^+ / [I \cdot \text{ref}]^+$. From the absolute reaction rate theory, the branching ratio can be expressed as:

$$\ln\{[A \cdot I]^+ / [I \cdot \text{ref}]^+\} = \ln(k_1/k_2) = -[(\Delta H_1 - \Delta H_2)/RT_{\text{eff}}] + \ln(Q_1^\ddagger/Q_2^\ddagger) \quad (4)$$

where Q_1^\ddagger , ΔH_1 and Q_2^\ddagger , ΔH_2 are the partition function of the transition state and the dissociation enthalpy for the reactions of the competing processes of Scheme 3. Equation (4) is valid for systems in the thermal equilibrium. If the competing dissociations involve species that are chemically similar, entropic effects are generally ignored, and thus $Q_1^\ddagger = Q_2^\ddagger$. As a consequence, the term $\ln(Q_1^\ddagger/Q_2^\ddagger)$ is neglected in the equation (4), giving:

$$\ln(k_1/k_2) = -(\Delta H_1 - \Delta H_2)/RT_{\text{eff}} \quad (5)$$

The plot of $\ln(k_1/k_2)$ vs. ΔH_2 , named the “kinetic plot”, is a straight line with a slope $m = 1/RT_{\text{eff}}$ and an intercept $q = (-\Delta H_1/RT_{\text{eff}})$. Hence the unknown value of the affinity of A for I^+ can be determined. However the assumption of negligible entropy effects cannot be applied in a large number of cases, and thus, in 1993, Fenselau and co-workers^{305,306} suggested a means to overcome this limitation, which was later refined by Wesdemiotis and co-workers.^{45,307–309} Assuming that $\ln(Q_1^\ddagger/Q_2^\ddagger)$ is constant over the range of effective temperatures sampled experimentally, equation (4) becomes:

$$\ln(k_1/k_2) = -[\Delta H_1 - \Delta H_2]/RT_{\text{eff}} - \Delta(\Delta S)/R \quad (6)$$

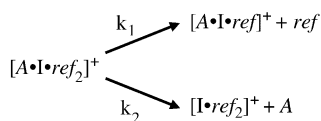
where $\Delta(\Delta S)$ is the difference between the complexation entropies of the molecules A and ref with ion I^+ . The kinetic plot is a straight line with a slope $m_1 = 1/RT_{\text{eff}}$ and an intercept $q_1 = (-\Delta H_1/RT_{\text{eff}}) - \Delta(\Delta S)/R$. The differences in the entropies of dissociation can be estimated by examining the dependence of the competition on the effective temperature of the dissociating cluster ion. The branching ratios are measured at different collision energies, corresponding to different T_{eff} values, in order to independently determine ΔH_1 and $\Delta(\Delta S)$. The plot of the intercepts q_1 obtained from the first kinetic plot (i.e., $\ln(k_1/k_2)$ vs. ΔH_2) vs. the corresponding slopes m_1 will give a straight line, with slope $m_2 = -\Delta H_1$ and intercept $q_2 = -\Delta(\Delta S)/R$.³¹⁰

At this point, it is worthwhile to return on the theoretical basis of the kinetic method, and make some considerations on the assumptions made, in order to better investigate the validity of the information provided by the method. In particular some words have to be spent on the effective temperature T_{eff} . The use of effective parameters is common in chemistry. This usually implies that one wishes to use the form of an established equation under conditions when it is not strictly valid. The effective parameter is always an empirical value, closely related to and defined by the equation one wishes to approximate. Clearly, T_{eff} is not a thermodynamic quantity reflecting a Maxwell–Boltzmann distribution of energies. Rather, T_{eff} represents only a small fraction of the complexes generated that happen to dissociate during the instrumental time window (which can vary from apparatus to apparatus).

Drahos and Vékey³¹¹ have demonstrated that T_{eff} varies from cluster to cluster because it is related to a number of experimental parameters (e.g., the time window for observing dissociation) and unimolecular dissociation kinetics (the lifetimes of the complexes), which depend on the enthalpies of dissociation and the vibrational frequencies and rotational constants of the dissociating complexes. For this reason, the use of a common T_{eff} for different systems is unlikely to be correct. Drahos and Vékey found that the effective temperature shows a very good correlation with the mean internal energy of reacting ions, but not with the mean internal or excess energy of the whole ion population. In fact, the ion population not dissociating in the time window of analysis does not affect the effective temperature: the same T_{eff} can be used to characterize the behavior of the total or the dissociating ion population.

When the system is not in thermal equilibrium, the use of thermodynamic relationships like equations (5) and (6) would not be rigorous. However, it has been shown that these equations can be derived from RRK (Rice–Ramsperger–Kassel) theory¹⁸⁰ without assuming thermal equilibrium for the system.^{312–314} Furthermore, Craig et al.³¹³ have performed RRKM (Rice–Ramsperger–Kassel–Marcus) simulations, which demonstrate the exponential dependence of the branching ratio from the difference in the barrier heights of the two competitive reactions. These observations seem to support the validity of equations (5) and (6), although the authors conclude their works affirming that the use of these equations is not rigorous and can be applied under specific conditions. Recently Laskin and Futrell³¹⁵ have provided a rigorous theoretical basis of the kinetic method by using the finite heat bath theory (FHBT) developed by Klots.^{316–318} According this formalism, Laskin and Futrell describe the reacting population through two different temperatures, T_1^\ddagger and T_2^\ddagger , that characterize the two competitive dissociations. T_{eff} closely resemble the average value of these two temperatures and can effectively characterize the fragmentation process when large clusters are considered. Their results demonstrate that high-quality thermochemical information can be obtained using the extended version of the kinetic method, provided both competing reactions have negligible reverse activation barriers.

At the beginning of this paragraph, it has been mentioned the application of the kinetic method to characterize chiral ions. If A is an unknown chiral molecule and ref is a reference molecule of defined configuration, the stability difference between their homochiral and heterochiral complexes with I^+ , $[A_R \cdot I \cdot \text{ref}]^+$ and $[A_S \cdot I \cdot \text{ref}]^+$, can be determined by the dissociation of the corresponding $[A_R \cdot I \cdot (\text{ref})_2]^+$ and $[A_S \cdot I \cdot (\text{ref})_2]^+$ clusters (Scheme 4).



Scheme 4

According to the kinetic method, dissociation of $[A_R\text{-I}(\text{ref})_2]^+$ is achieved in a MS^2 experiment and occurs by competitive ligand loss to produce dimeric ions: $[A_R\text{-I-ref}]^+$ and $[\text{I}(\text{ref})_2]^+$; by contrast, dissociation of $[A_S\text{-I}(\text{ref})_2]^+$ generates $[A_S\text{-I-ref}]^+$ and $[\text{I}(\text{ref})_2]^+$. Each of the dimeric ions has an associated ion intensity, I , reflecting the free energy diagram of Fig. 4. The small differences in steric interactions in the diastereomeric cluster ions $[A_R\text{-I-ref}]^+$ and $[A_S\text{-I-ref}]^+$ are recognized by easily measured differences in branching ratios for dissociation of the $[A_R\text{-I}(\text{ref})_2]^+$ and $[A_S\text{-I}(\text{ref})_2]^+$ complexes.

The chiral selectivity R_{chiral} is defined as:

$$R_{\text{chiral}} = \frac{R_{\text{homo}}}{R_{\text{hetero}}} = \frac{I_S/I_{\text{ref}(1)}}{I_R/I_{\text{ref}(2)}} \quad (7)$$

if the S enantiomer of ref is employed. In equation (7), the $I_{\text{ref}(1)}$ and $I_{\text{ref}(2)}$ terms refer to the $[\text{I}(\text{ref})_2]^+$ intensities from dissociation of $[A_S\text{-I}(\text{ref})_2]^+$ and $[A_R\text{-I}(\text{ref})_2]^+$, respectively. The R_{chiral} term serves as a numerical indication of the degree of chiral distinction achieved in a particular system and is the ratio of the individual intensity ratios of the fragment ions from the homochiral $[A_S\text{-I}(\text{ref})_2]^+$ and the heterochiral $[A_R\text{-I}(\text{ref})_2]^+$ precursor (if the S enantiomer of ref is employed). The farther R_{chiral} is from unity, the higher the degree of chiral recognition. When $R_{\text{chiral}} < 1$, the heterochiral $[A\text{-I-ref}]^+$ complex is more stable than the homochiral analog. The reverse is true if $R_{\text{chiral}} > 1$. When $R_{\text{chiral}} = 1$, no chiral discrimination occurs, which means that the particular combination of I and ref fails to create stereochemically dependent interactions with the enantiomers under the observation conditions used. The above discussion deals with the recognition of chirally pure compounds by the kinetic method. In cases in which the analyte is a mixture of the R - and S -enantiomers, an $R = (I_R + I_S)/I_{\text{ref}}$ term can be defined which falls between R_{homo} and R_{hetero} , measured with the pure enantiomers. The $\ln R_{\text{chiral}}$ is linearly related to the enantiomeric purity of the analyte, which allows quantitative chiral analysis.

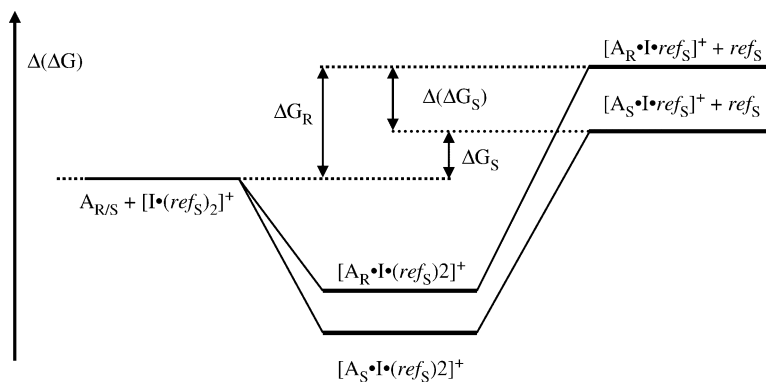


Fig. 4 Free energy schematic representation for the dissociation of trimeric cluster ions $[A_R\text{-I}(\text{ref}_S)_2]^+$ and $[A_S\text{-I}(\text{ref}_S)_2]^+$.

The relative stability, $\Delta(\Delta G)$, of the homo $[A_S\text{-I-ref}]^+$ vs. the hetero $[A_R\text{-I-ref}]^+$ cluster ion is calculated from the following equation, provided that both reaction of [Scheme 4](#) have negligible reverse barriers:

$$\ln R_{\text{chiral}} = \frac{\Delta(\Delta G)}{RT_{\text{eff}}} \quad (8)$$

where \mathcal{R} is the gas constant. The free energy quantity, $\Delta(\Delta G)$, reflects the different attractive electrostatic and repulsive steric interactions operating in the diastereomeric $[A_S\text{-I-ref}]^+$ and $[A_R\text{-I-ref}]^+$ clusters: negative $\Delta(\Delta G)$ values indicate that the heterochiral complexes are more stable than the homochiral analogues, and vice versa.

ION-DIPOLE COMPLEXES IN DENSE GASES: THE RADIOLYTIC APPROACH

Since its first modern application in the late fifties,³¹⁹ radiolysis has been extensively employed for generating transient ion–dipole complexes in the gas phase and to investigate their reactivity in the absence of the perturbing effects of solvation and ion pairing.^{320–328} The growing impact of the radiolytic technique in the gas-phase ion chemistry field is due to its relative simplicity and its unique features that set it apart from most common mass spectrometric methodologies. As in mass spectrometry, ions are generated by the impact on suitable gaseous mixtures of energetic electrons, mainly arising from the interaction of high-energy electromagnetic radiations (x - or γ -rays) with the container of the mixture itself. A steady concentration of ions can be produced at pressures from several torrs to several atmospheres (“stationary radiolysis”). Otherwise, very high transient concentrations of ions can be generated momentarily by a pulse of ionizing radiation (“pulse radiolysis”). The decay kinetics of the transient species formed with this latter technique can be investigated by detecting the transient species of interest by means of conductivity measurements. At the high pressures accessible to stationary radiolysis, the ions undergo efficient complexation with the surrounding neutral and their complete thermal equilibration by collisions with the bulk gas prior to conversion to products. The transient ion–dipole reactivity can be evaluated by standard kinetic procedures and their regio- and stereochemistry assessed by the actual isolation and structural discrimination of the relevant reaction products. These basic features confer upon radiolysis a role in gas-phase ion chemistry complementary to that covered by mass spectrometry, in which thermalization of ionic transients is prevented by the low-pressure operating regime and their structural characterization severely hampered by the inherently limited structural resolution.

4 Chiral recognition in molecular clusters

Molecular complexes represent the simplest model systems for studying the physical and chemical properties of molecules in the transition from the gas phase to the

condensed phase. They are ideal systems for disentangling the intrinsic structural factors affecting molecular reactivity from solvation effects and for gathering information upon the sensitivity of molecular stability to microsolvation. The assessment of the structure of molecular complexes and the microscopic understanding of their intracomplex forces require their spectroscopic investigation in the isolated state. Recent progress in this area was stimulated by the introduction of the experimental methodologies described in previous sections as well as by the growing interest in these systems as models for understanding enantioselectivity in chemistry and biology. Supersonic beams allow the synthesis of otherwise fragile molecular complexes in quantities suitable for their spectroscopic characterization. Laser sources and synchrotron radiation allow precise evaluation of their energetics, dynamics, and structure.

This section will focus on the structure and energetics of chiral molecular complexes studied with Fourier-transform IR (FT-IR), microwave, LIF, hole burning (HB), IR fluorescence dip spectroscopy, resonance-enhanced multiphoton ionization (REMPI; Fig. 5), and RET spectroscopy.

STRUCTURE OF MOLECULAR COMPLEXES

Supersonic expansion of a carrier gas, typically helium or argon, seeded with molecules with many degrees of freedom may result in the production of weakly bound molecular complexes in their electronic ground state S_0 with translational and vibrational temperatures of few Kelvin degrees. Different conformers corresponding to different local minima of the PES can coexist in the cold region of the jet. If separated by significant energy barriers, these forms are relatively stable and can be probed by LIF and REMPI spectroscopies. Owing to the low internal temperature of the probed complexes, their LIF and REMPI spectra are generally very sharp and well resolved. The LIF method combines the formation of a molecular complex containing a fluorescent moiety (F) by supersonic expansion and the measurement of the laser-induced emitted fluorescence. The F molecule is laser excited to the fluorescent S_1 state. The emitted fluorescence is collected at right angles to both the excitation laser pulse and the beam axis and recorded. The fluorescence decay times are measured with a photomultiplier.

Relative to the excitation spectrum of the bare F($h\nu$), complexation with a solvent molecule (M) usually results in the appearance of new spectral features ($h\nu'$) falling at different wavelengths (microscopic solvent shift: $\Delta\nu = h\nu' - h\nu$). The shift may be toward the red (negative $\Delta\nu$ value) or toward the blue (positive $\Delta\nu$ value). A red-shift indicates the decrease of the $S_1 \leftarrow S_0$ energy gap in the [F·M] complex relative to the bare F, while a blue-shift indicates the opposite. In general, diastereomeric pairs from complexation of a chiral M with chiral F are characterized by the non-equivalence of their interaction energy in both the ground and the excited states and, therefore, are expected to exhibit different microscopic solvent shifts $\Delta\nu$. Besides, complexation normally results in a drastic variation of the fluorescence lifetime τ of the chromophore due to change of the radiative lifetime or to a decrease of the

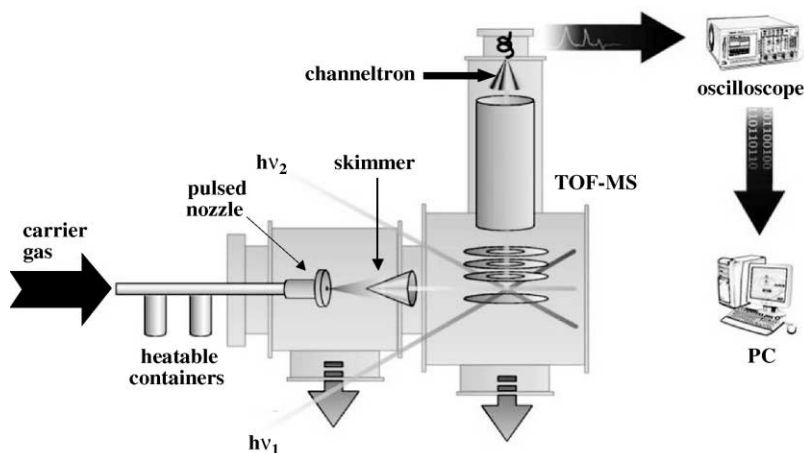


Fig. 5 Schematic representation of REMPI/TOF experimental setup.

intersystem-crossing rate constant. This is the basis of the LIF application to chiral recognition in the isolated state.

The LIF spectral shifts $\Delta\nu$ and the fluorescence lifetimes τ concerning the complexes between $F_R = (R)$ - or $F_S = (S)$ -2-naphthyl-1-ethanol and a variety of primary and secondary aliphatic alcohols and terpenes (M) are listed in [Table 1](#).^{102,329,330}

The origin bands of the $[F \cdot M]$ complexes are red-shifted with respect to that of bare F (negative $\Delta\nu$ in [Table 1](#)). This suggests that the major contribution to the intracomplex forces is due to hydrogen bonding between M and F , with the latter acting as the hydrogen donor. In fact, when the hydrogen donor is M , as in the case of the acidic trifluoroethanol, a blue-shift is observed ($\Delta\nu = +24 \text{ cm}^{-1}$). Similar band shifts are observed for the diastereomeric complexes with chiral $M = 2$ -methyl-1-butanols or 2-chloro-1-propanols. Here, the band origin of the heterochiral complex falls more toward the blue (from 37 to 50 cm^{-1}) relative to that of the homochiral adduct. The trend is fully reversed for the complexes with chiral secondary alcohols. In this case, are the heterochiral complexes which exhibit larger red shifts (11 – 63 cm^{-1}).

In general, the excitation spectra of the selected $[F \cdot M]$ complexes show intense features, accompanied by smaller signals placed at the low energy side. These signals are mainly due to several conformational isomers of the 1:1 complexes, as demonstrated by HB experiments.³³¹

For instance, LIF experiments, carried out on the heterochiral complex between F_S and $M = (R)$ -2-butanol, indicate the presence of three new bands at -136 , -114 , and -73 cm^{-1} from the band origin of the bare F_S . Similar experiments on the homochiral complex between F_S and $M = (S)$ -2-butanol exhibit two new bands at -125 and -69 cm^{-1} from the band origin of the bare F_S . HB experiments show that four different isomers coexist in the jet, two of them corresponding to the

Table 1 Main solvent shifts ($\Delta\nu$) and fluorescence lifetimes (τ) of [F·M] complexes ($F_R = (R)$ -2-naphthyl-1-ethanol; $F_S = (S)$ -2-naphthyl-1-ethanol)

F	M	$\Delta\nu$ (cm^{-1}) (τ (ns) in parentheses)	Reference
	None	0(45), +39(35), +76(20), +278, +339, +434	329
	<i>Primary alcohols</i>		
F_R or F_S	Methanol	-67(33), -55(160), -43(151)	329
F_R or F_S	Ethanol	-61(63), -55, -52(126)	102
F_R or F_S	Trifluoroethanol	+24(84), +51(158)	102
F_R or F_S	1-Propanol	-138(119), -112(54), -60(55), -55(119)	102
F_R or F_S	1-Butanol	-158(112), -144, -125, -71(125)	102
F_R	(<i>S</i>)-2-Chloro-1-propanol	-23(94), +10	329
F_S	(<i>S</i>)-2-Chloro-1-propanol	-60(94), -32	329
F_R	(<i>S</i>)-2-Methyl-1-butanol	-84(135), -51, -34, -19	102
F_S	(<i>S</i>)-2-Methyl-1-butanol	-134(140), -118, -62(123), +54	102
	<i>Secondary alcohols</i>		
F_R	(<i>S</i>)-2-Butanol	-136, -114, -73, -28, +6	102
F_R	(<i>R</i>)-2-Butanol	-125, -87, -69, +29	102
F_R	(<i>S</i>)-2-Pentanol	-147, -133, -119, -52, +50	102

(continued on next page)

Table 1 (*continued*)

F	M	$\Delta\nu$ (cm ⁻¹) (τ (ns) in parentheses)	Reference
F _R	(<i>R</i>)-2-Pentanol	- 85, - 54	102
F _R	(<i>S</i>)-2-Hexanol	- 127(140), - 110(120), + 53	102
F _R	(<i>R</i>)-2-Hexanol	- 106, - 73(55), - 65(75)	102
F _R	(<i>S</i>)-2-Octanol	- 160, - 151, - 142, - 135, - 17	102
F _R	(<i>R</i>)-2-Octanol	- 133, - 122, - 115, - 107, - 91, - 79, - 63, - 38	102
<i>Terpenes</i>			
F _R	(<i>S</i>)- α -Pinene	- 54(44)	330
F _R	(<i>R</i>)- α -Pinene	- 79(34)	330
F _R	(<i>S</i>)-Camphene	- 35(193)	330
F _R	(<i>R</i>)-Camphene	- 35(110)	330
F _R	(<i>S</i>)-Borneol	- 191	330
F _R	(<i>R</i>)-Borneol	- 162	330
F _R	(<i>S</i>)-Camphor	- 89(42)	330
F _R	(<i>R</i>)-Camphor	- 89(25)	330

heterochiral complex (Rs1 (-136 cm^{-1}) and Rs2 (-73 cm^{-1})) and two others to the homochiral one (Ss1 (-125 cm^{-1}) and Ss2 (-69 cm^{-1})) (Fig. 6). The relevant interaction energies have been partitioned into the electrostatic, dispersion, polarization, and repulsion contributions by using the method developed by Claverie.³³² Accordingly, it is assumed that the complex which exhibits the most important dispersion term corresponds to the most red-shifted isomer.

Therefore, the most stable heterochiral *anti-gauche* structure, observed in the HB experiments, is assigned to the more red-shifted Rs1 isomer (Sr(ag) in Fig. 7). In it, the ethyl chain interacts strongly with the aromatic ring of F_S . The H atom of the chiral center of 2-butanol points to the aromatic ring and interacts with it repulsively. The more red-shifted Ss1 diastereomer can also be assigned to the most stable homochiral *anti-gauche* structure Ss(ag) in Fig. 7. In it, the increased repulsive interaction between the methyl group of 2-butanol and the aromatic ring leads to a switch of the ethyl chain on the edge of the ring and, therefore, to a decrease in dispersive interactions (smaller red-shift). The minor red-shift of the Rs2 and Ss2 diastereomers are instead assigned to the corresponding *gauche-anti* structures. This example clearly shows that, in this case, the chiral discrimination is achieved by means of the repulsion–dispersion part of the interaction energy.

The most intense bands observed in the excitation spectra of the complexes often exhibit a decay time τ longer than that of bare F (Table 1). However, some exceptions are observed and τ does not decrease monotonically with the interaction

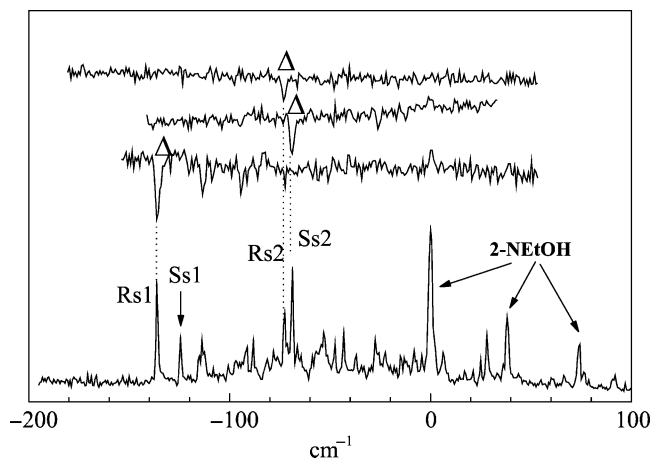


Fig. 6 Bottom-up: (i) fluorescence excitation spectrum of the 1:1 diastereomeric complexes between (*S*)-2-naphthyl-1-ethanol (F_S) and 2-butanol (M_R/M_S); (ii) hole-burning spectrum obtained with the probe tuned on the transition located at -136 cm^{-1} ($[F_S\cdot M_R]$ complex); (iii) (c) hole-burning spectrum obtained with the probe tuned on the transition located at -69 cm^{-1} ($[F_S\cdot M_S]$ complex); (iv) hole-burning spectrum obtained with the probe tuned on the transition located at -73 cm^{-1} ($[F_S\cdot M_R]$ complex). The probed band is denoted by Δ . The bands due to the bare chromophore are denoted by 2-NEtOH (reproduced by permission of the American Chemical Society).

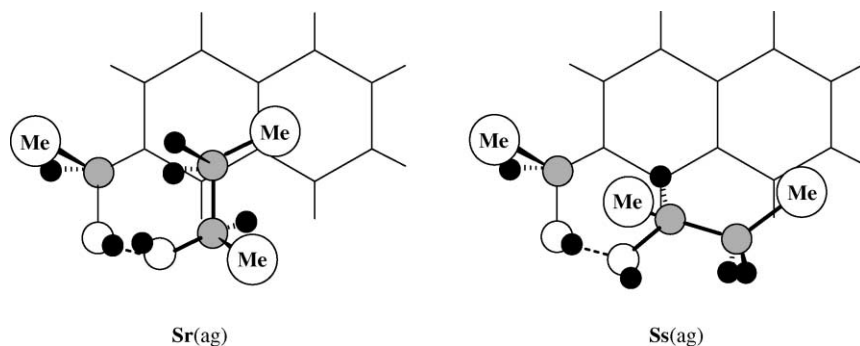


Fig. 7 Calculated geometry of the 1:1 diastereomeric complexes of (*S*)-2-naphthyl-1-ethanol with either (*R*)-2-butanol (Sr(ag)) and (*S*)-2-butanol (Ss(ag)).

energy as could be expected. The τ variations can be rather associated with the effect of complexation on the photophysics of the chromophore F. Thus, no clear-cut relationship can be established between τ and the structure and configuration of M. Nonetheless, because of the peculiar sensitivity of the excited state dynamics to the subtle perturbation induced by complexation, the decay time τ can be seen as a phenomenological tool for enantiodifferentiating chiral molecules in the isolated state. For instance, the diastereomeric complexes between F_R and camphor exhibit the same LIF spectra, characterized by an intense single band red-shifted by 89 cm^{-1} from the origin of bare F_R .^{330,333} Thus, no discrimination can be achieved between the two diastereoisomeric complexes on the exclusive basis of the excitation energy. However, in contrast to the LIF spectra, the lifetimes of the diastereoisomeric complexes differ markedly ($25 \pm 3\text{ ns}$ (homochiral complex); $42 \pm 3\text{ ns}$ (heterochiral complex)). Besides, both are shorter than that of bare F_R ($45 \pm 3\text{ ns}$). This observation is attributed to a strong chirality effect on the electronic overlap between the excited states of the components of the complexes which reduces the fluorescence decay time.

The structure of weakly bound diastereomeric complexes between F_S and the enantiomers of 2-amino-1-propanol (alaninol) has been interrogated by means of LIF and IR fluorescence dip spectroscopy.^{5,334} The homochiral complex exhibits two new bands red-shifted by 94 and 28 cm^{-1} from the origin of bare F_S , while the heterochiral one only one new signal red-shifted by 59 cm^{-1} from the origin of bare F_S . The structures associated with these signals are determined by fluorescence dip spectroscopy, coupled with *ab initio* calculations of the most stable structures of the complexes and of their associated harmonic frequencies. Accordingly, the fluorescence dip spectrum recorded with the probe set on the transition located at -59 cm^{-1} from the origin of bare F_S is consistent with a chainlike structure of the heterochiral complex involving the oxygen center of the chromophore (henceforth denoted as **O**) and the two *n*-type centers of alaninol, i.e., $\text{OH} \cdots \text{OH} \cdots \text{N}$. A similar chainlike structure is associated with the homochiral complex with the transition

located at -28 cm^{-1} from the origin of bare F_S . A completely different IR spectrum is associated with the homochiral complex with the transition located at -94 cm^{-1} from the origin of bare F_S , which is more consistent with a bridged structure characterized by an intense $\text{OH}\cdots\text{NH}_2$ intermolecular bond coupled with a weaker $\text{OH}\cdots\pi$ interaction between the OH group of M and the aromatic ring of F_S .

Further insights into the structural features of supersonically expanded molecular complexes is obtained using the REMPI spectroscopy.^{335–338} The supersonically expanded species under investigation is ionized through absorption of several laser photons of adequate energy and mass selected by a TOF mass spectrometer (Fig. 5).

The mass resolved 1cR2PI spectrum of the bare chiral chromophore $C_R = (R)\text{-}(+)\text{-1-phenyl-1-propanol}$, shows three intense signals at 37577 (A), 37618 (B), and 37624 cm^{-1} (C) in the electronic $S_1 \leftarrow S_0$ band origin region. A similar triplet falls at 38106, 38148, and 38155 cm^{-1} . This pattern is common to substituted arenes and is interpreted as due to three stable conformers. Quantum chemical calculations at the RHF/3-21G and B3LYP/6-31G levels of theory confirm this hypothesis.

In qualitative agreement with the previous LIF results, the 1cR2PI absorption spectra of the complexes between $C_R = (R)\text{-}(+)\text{-1-phenyl-1-propanol}$ and a variety of primary and secondary alcohols and amines exhibit major characteristic peaks (for instance, α and β signals in Fig. 8) which somewhat reproduce the pattern of the bare chromophore but shifted toward the red or the blue by an extent denoted as $\Delta\nu_\alpha$ and $\Delta\nu_\beta$, respectively (Table 2).

Table 2 REMPI band shifts relative to jet-cooled 1:1 complexes between $C_R = (R)\text{-}(+)\text{-1-phenyl-1-propanol}$ and primary and secondary alcohols and amines (M)

M	$\Delta\nu_\alpha\text{ (cm}^{-1}\text{)}^a$	$\Delta\nu_\beta\text{ (cm}^{-1}\text{)}^b$	PA (kcal mol ⁻¹) ^c
Methanol	-2	-6	180.3
Ethanol	-78	-63	185.6
1-Propanol	-90	-	188.0
1-Butanol	-96	-101	188.6
1-Pentanol	-118	-136	189.2
2-Propanol	-87	-71	189.5
3-Pentanol	-108	-	195.6
(R)-2-Butanol	-79	-102	195.0
(S)-2-Butanol	-92	-119	195.0
(R)-2-Pentanol	-64	-92	195.6
(S)-2-Pentanol	ca. + 25	-	195.6
(R)-2-Butylamine	-109	-	222.2
(S)-2-Butylamine	-127	-	222.2

^aBand shifts of the α peaks, relative to the band origin A of bare C_R .

^bBand shifts of the β peaks, relative to the band origin B of bare C_R .

^cLias, S.G., Bartmess, J.E., Liebman, J.F., Holmes, J.L., Levin, R.D. and Mallard, W.G. (1988). *J. Phys. Chem. Ref. Data* **17**, Suppl. 1. Values in italic estimated from the PA limits of primary and secondary alcohols (Long, J. and Munson, B. (1977). *J. Am. Chem. Soc.* **99**, 6822), using the group additivity method (Benson, S.W. (1968). *Thermochemical Kinetics*. Wiley, New York).

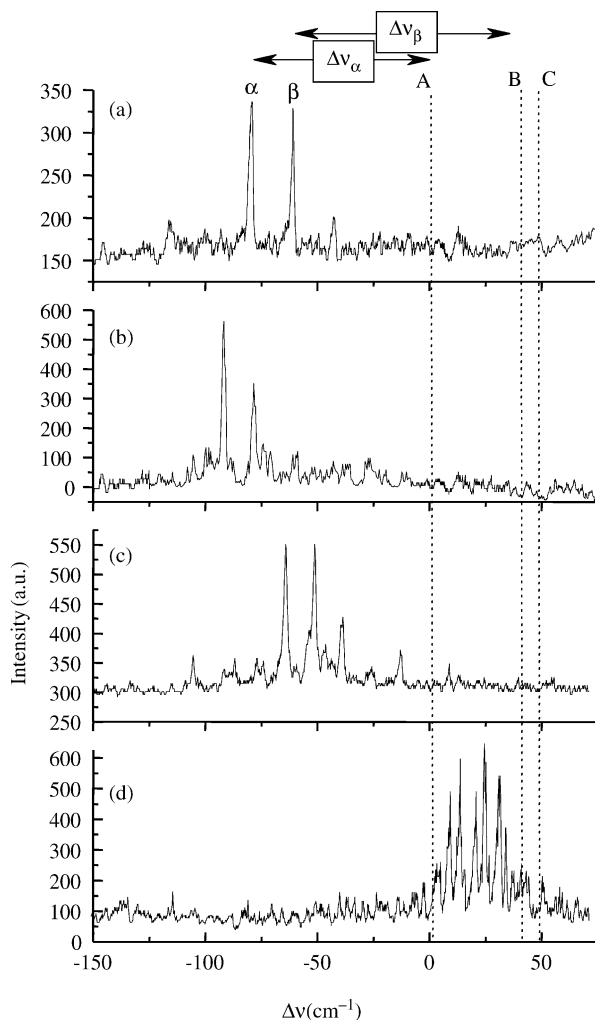


Fig. 8 2cR2PI excitation spectra of the 1:1 diastereomeric complexes between (*R*)-(+)-1-phenyl-1-propanol (C_R) and (*R*)-2-butanol (a), (*S*)-2-butanol (b), (*R*)-2-pentanol (c), and (*S*)-2-pentanol (d), measured at their m/z values and at a total stagnation pressure of 4×10^5 Pa.

The $\Delta\nu_\alpha$ and $\Delta\nu_\beta$ shifts from the complexes with primary alcohols are linearly correlated to the proton affinity (PA) of primary M ($\text{PA}(\text{M})$ (kcal mol^{-1}) = $(180 \pm 0.6) - (0.076 \pm 0.006)\Delta\nu(\text{cm}^{-1})$; $r^2 = 0.951$), which in turn determines the strength of the $\text{OH}\cdots\text{O}$ hydrogen bond between the C_R donor and the M acceptor (Fig. 9).

These features allow to assign the α and β spectral signatures of Fig. 8 to two different sets of $[C_R\cdots M]$ complexes, where C_R is in a given conformation and acts as the hydrogen-bond donor to M and where the alkyl group of M maintains a specific

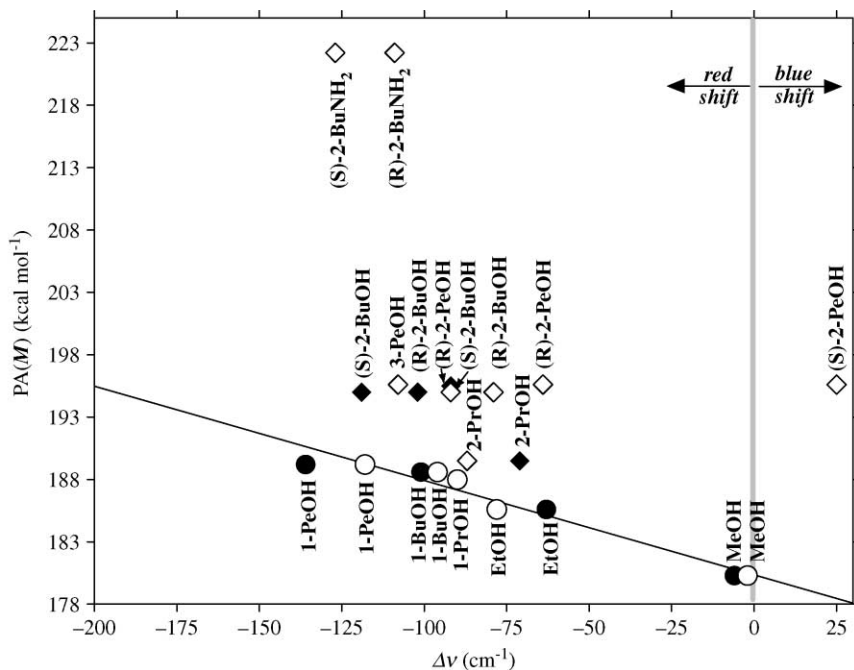


Fig. 9 Diagram of the band origin shifts $\Delta\nu$ of the molecular complexes between (*R*)-(+)-1-phenyl-1-propanol (C_R) and primary and secondary alcohols and amines. The circles refer to primary alcohols (open circles = $\Delta\nu_\alpha$; full circles = $\Delta\nu_\beta$); the diamonds refer to secondary alcohols and amines (open diamonds = $\Delta\nu_\alpha$; full diamonds = $\Delta\nu_\beta$).

spatial orientation toward the aromatic ring of C_R . In this case, both the electrostatic and the dispersive (polarization, charge exchange, etc.) interactions cooperate in stabilizing the adducts in the ground and excited states.

According to Fig. 9, the signals of the complexes with secondary alcohols and amines display $\Delta\nu$ values which are less negative than expected on the grounds of the linear correlation obtained for the primary alcohols. These deviations suggest that the relative contributions of electrostatic and dispersive forces in these systems are substantially different from those operating in the corresponding complexes with primary alcohols.

Comparison of the $\Delta\nu$ values of diastereomeric complexes with 2-butanols, 2-pentanol, and 2-butylamines indicates that relative extent of electrostatic and dispersive forces depends upon the nature, the bulkyness, and the configuration of M . The $\Delta(\Delta\nu_\alpha) = ((\Delta\nu_\alpha)_{\text{homo}} - (\Delta\nu_\alpha)_{\text{hetero}}) = +13 \text{ cm}^{-1}$ difference between the red shifts of the homochiral and the heterochiral complexes with 2-butanols finds a close analogy with LIF red-shift difference of the corresponding adducts with $F_R = (R)\text{-}(+)\text{-}2\text{-naphthyl-1-ethanol}$ ($\Delta(\Delta\nu) = ((\Delta\nu)_{\text{homo}} - (\Delta\nu)_{\text{hetero}}) = +11 \text{ cm}^{-1}$; Table 1). However, while LIF results from the diastereomeric $[F_R\text{-}M]$ ($M = 2\text{-pentanol}$) complexes are qualitatively similar to those with the other secondary

alcohols, the homochiral and the heterochiral $[C_R \cdot M]$ ($M = 2$ -pentanol) complexes display a negative spectral shift difference ($\Delta(\Delta\nu\alpha) = ca. -89 \text{ cm}^{-1}$) which strikingly contrasts with the positive one observed for the $[C_R \cdot M]$ ($M = 2$ -butanol) pair. This marked spectral diversity can be attributed to the shorter side chain and the wider “ π -electron bed” of F_R , relative to C_R , which allows establishment of a synergy between attractive electrostatic and dispersive forces in $[F_R \cdot M]$ ($M = 2$ -pentanol) in both the S_0 and S_1 states. In the $[C_R \cdot M]$ ($M = 2$ -pentanol) complexes, a similar cooperation is hindered by the greater steric congestion due to the relatively bulky side chain and relatively small π -system of the chromophore. This is particularly evident in the heterochiral complex with $M = (S)$ -2-pentanol, whose blue shift is rationalized in terms of a predominant $\text{OH} \cdots \pi$ electrostatic interaction (or even a changeover in the hydrogen-bond donor/acceptor pair) determined by its high steric congestion. Indeed, a similar blue shift is observed in the 1cR2PI absorption spectrum of the 1:1 cluster between C_R and water, where the solvent can establish with the aromatic ring of the chromophore only electrostatic $\text{OH} \cdots \pi$ interactions.³³⁹

Insight into the forces intervening in the supersonically expanded isomeric complexes of $(2R,3R)$ -(M_{RR}), $(2S,3S)$ -(M_{SS}), and $(2R,3S)$ -butanediols (M_{RS}) with C_R is achieved by 1cR2PI-TOF experiments.³⁴⁰ Fig. 10 illustrates the corresponding excitation spectra together with that of bare C_R .

Their spectral patterns are characterized by the presence of several bands red-shifted relative to the 0_0^0 electronic $S_1 \leftarrow S_0$ origin of the bare chromophore C_R at 37618 cm^{-1} (peak B). The most intense one is separated from the peak B of the chromophore by the $\Delta\nu$ values reported in the figure. Since a red-shifted $S_1 \leftarrow S_0$ origin denotes an increase of attractive interactions in the complex by the electronic transition, the $\Delta\nu$ values of Fig. 10b, c, and d, indicate that bond strengthening follows the order: $[C_R \cdot M_{RR}] > [C_R \cdot M_{RS}] > [C_R \cdot M_{SS}]$.

These results point to a significant effect of the configuration of the diol moiety on the intracomplex forces involved in the isomeric $[C_R \cdot M_{RR}]$, $[C_R \cdot M_{RS}]$, and $[C_R \cdot M_{SS}]$ adducts. The $\text{OH} \cdots \text{O}$ hydrogen bonding in these complexes is responsible for the bathochromic shifts observed in the corresponding spectra.³⁴¹ Different spectral shifts for diastereomeric complexes are often due to the superimposing effects of attractive dispersive (polarization) and repulsive (steric) interactions.³³⁷

As pointed out before, the IR/UV double resonance spectra of the complexes between F_S and the enantiomers of 2-amino-1-propanol (alaninol) exhibit spectral features due to structures involving not only the expected intermolecular hydrogen bonding (either $\text{OH} \cdots \text{O}$ or $\text{OH} \cdots \text{N}$), but also extensive intramolecular $\text{OH} \cdots \text{N}$ and $\text{OH} \cdots \pi$ hydrogen bonding.³³¹ Similar intramolecular interactions are present in the isomeric $[C_R \cdot M_{RR}]$, $[C_R \cdot M_{RS}]$, and $[C_R \cdot M_{SS}]$ adducts as well.

Fig. 11 reports the optimized $[C_R \cdot M_{RR}]$, $[C_R \cdot M_{RS}]$, and $[C_R \cdot M_{SS}]$ structures, calculated at the MM3 force-field level of theory. For $[C_R \cdot M_{RR}]$ and $[C_R \cdot M_{SS}]$, two different stable structures, involving intramolecular $\text{OH} \cdots \text{O}$ hydrogen bonding, were found, characterized by the diol moiety in a *gauche* ($[C_R \cdot M_{RR}]_g$ and $[C_R \cdot M_{SS}]_g$ in Fig. 11) or the *anti* conformation ($[C_R \cdot M_{RR}]_a$ and $[C_R \cdot M_{SS}]_a$ in Fig. 11).

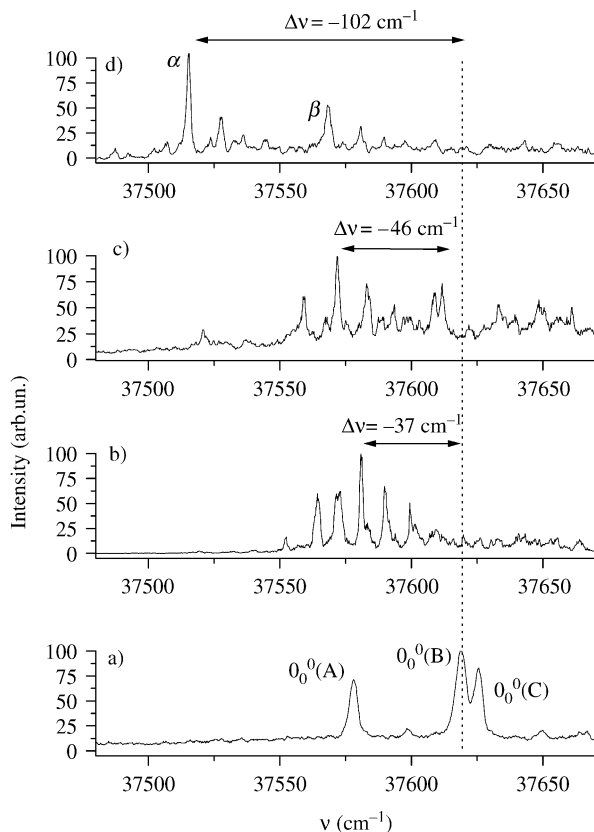


Fig. 10 Mass resolved 1cR2PI excitation spectrum of: (a) the bare (*R*)-(+)-1-phenyl-1-propanol (C_R); (b) the $[C_R \cdot M_{SS}]$ cluster; (c) the $[C_R \cdot M_{RS}]$ cluster; (d) the $[C_R \cdot M_{RR}]$ cluster (total stagnation pressure = 2×10^5 Pa).

Two different structures have been identified for the $[C_R \cdot M_{RS}]$ isomer as well, one with the $\text{OH} \cdots \text{O}(\text{H})\text{-}C_{(R)}$ intermolecular arrangement ($[C_R \cdot M_{RS}]_R$ in Fig. 11) and the other with the $\text{OH} \cdots \text{O}(\text{H})\text{-}C_{(S)}$ one ($[C_R \cdot M_{SR}]_S$ in Fig. 11).

According to the $\text{OH} \cdots \text{OH} \cdots \text{OH}$ interaction distances of the structures of Fig. 11, the α band of $[C_R \cdot M_{RR}]$, which displays the largest red-shift, is assigned to the tightest *gauche* structure $[C_R \cdot M_{RR}]_g$. No significant structural and energetic differences can be appreciated in the *gauche* and *anti* conformers of $[C_R \cdot M_{SS}]$ and $[C_R \cdot M_{RS}]$. In particular, irrespective of the specific conformation and orientation of the diol moiety, the $\text{OH} \cdots \text{O}$ distance in these structures ranges around 2.01–2.03 Å and are much closer to that of $[C_R \cdot M_{RR}]_a$ (2.04 Å) than of $[C_R \cdot M_{RR}]_g$ (1.96 Å). This analogy may explain the minor red-shifts observed in $[C_R \cdot M_{RS}]$ and $[C_R \cdot M_{SS}]$, relative to $[C_R \cdot M_{RR}]$.

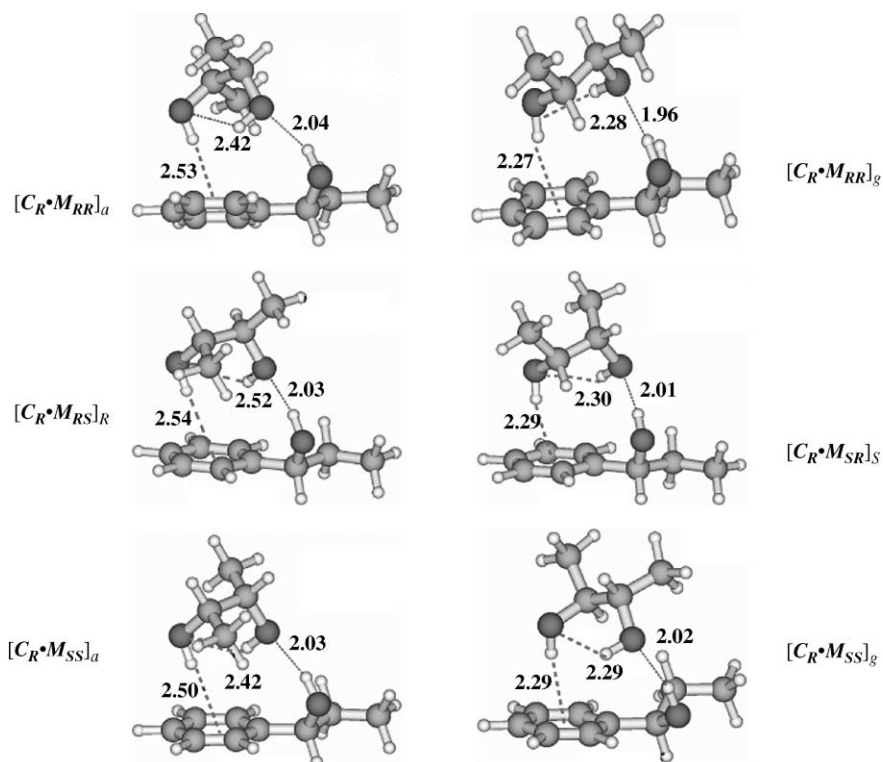


Fig. 11 H-bond distances (in Å) in the isomeric $[C_R \cdot M_{SS}]$, $[C_R \cdot M_{RS}]$ and $[C_R \cdot M_{RR}]$ structures.

The effect of changing the nature of the chromophore has been investigated by comparing the R2PI spectra of diastereomeric $[C_R \cdot M]$ ($M = 2$ -butanol or 2-hexanol) complexes with the corresponding spectra with (R)-(+)-1-phenylethanol (E_R) and (R)-(–)-indanol (I_R), as chromophores. As for $[C_R \cdot M]$, the diastereomeric $[E_R \cdot M]$ ($M = 2$ -butanol) and $[I_R \cdot M]$ ($M = 2$ -hexanol) complexes exhibit spectral signatures characterized by a significant red-shift $\Delta\nu$ of the $0_0^0 S_1 \leftarrow S_0$ transition relative to that of the bare chromophore. These spectral shifts reflect the combined effect of the electrostatic and dispersive interactions between M and the HOMO and LUMO of the chromophore. As expected, the homochiral clusters exhibits a red-shift ($\Delta\nu_{\text{homo}}$) less negative than that displayed by the heterochiral analogue. Their differences, $\Delta(\Delta\nu) = \Delta\nu_{\text{homo}} - \Delta\nu_{\text{hetero}} = +12 \text{ cm}^{-1}$ (E_R ; $M = 2$ -butanol)³⁴² and $+30 \text{ cm}^{-1}$ (I_R ; $M = 2$ -hexanol),³⁴³ are consistent with a $S_1 \leftarrow S_0$ energy gap of the heterochiral complex which is smaller than that of the corresponding homochiral adduct.

A strict correspondence is also observed between the 1cR2PI spectral shifts $\Delta\nu$ of the selected diastereomeric clusters and the relevant 1cR2PI mass fragmentation patterns. In the 1cR2PI ionization experiments, some excess energy is imparted to the adduct to an extent which somewhat reflects its HOMO–LUMO energy gap

(and, therefore, $\Delta\nu$). Since $|\Delta\nu_{\text{homo}}| < |\Delta\nu_{\text{hetero}}|$, one should expect that homochiral clusters display 1cR2PI/TOF fragmentation patterns which are qualitatively similar, though less abundant than those exhibited by the corresponding heterochiral adducts. The experimental 1cR2PI/TOF mass spectra are fully consistent with this expectation (Table 3).³³⁵

Microwave spectroscopy is a well-established technique for detecting the rotational spectrum of a molecule or a complex. From the rotational spectrum, the moments of inertia can be extracted which can be used to determine in detail the structure of the species of interest. The high resolution attached to this approach makes it particularly suitable for singling out the small structural differences of diastereomeric complexes between chiral molecules. This methodology has been recently applied to the study of the supersonically expanded hydrogen-bonded dimer of 2-butanol.³⁴⁴ The microwave spectrum is consistent with a heterochiral structure for the 2-butanol dimer. Indeed, a completely different spectrum is obtained by analyzing the spectra of the dimer obtained from enantiomerically pure 2-butanol. By comparing the experimental values of the rotational constant of the dimer with those predicted on the grounds of MP2/6-311G* calculations, it was possible to assign to the dimer the energetically most stable structure **R2S** of Fig. 12.

A FT-IR methodology has been employed to investigate chiral self-recognition phenomena in supersonically expanded glycidol. Glycidol dimers exhibit dominant OH-stretching absorption peaks at 3492 (homochiral dimers) and 3488 cm^{-1} (heterochiral dimer) within a rich line FT-IR spectrum with sizeable variations between enantiomerically pure and racemic dimers.³⁴⁵ A systematic quantum mechanical study of the conformational degrees of freedom reveals important types of hydrogen bond topology in glycidol dimers and up to 10 conformations in the adiabatic expansion. These dimer conformations derive from two out of eight monomer conformations which are preformed and stabilized by intramolecular hydrogen bond contacts. All important conformations have two intermolecular OH...O interactions. In the most stable conformations, the homochiral pair interacts more strongly than the heterochiral one. Secondary CH...O interactions may contribute to chiral discrimination.³⁴⁶

Table 3 Relative ion abundance from the R2PI-TOF mass spectra of supersonically expanded 1:1 [C:M] complexes

C	M	$\Delta\nu$ (cm^{-1})	[C:M] ⁺	[C-M-C ₂ H ₅] ⁺	[C] ⁺	[C-C ₂ H ₅] ⁺
C _R	(R)-2-Butanol	-79	41	100	28	42
C _R	(S)-2-Butanol	-92	11	100	15	35
E _R	(R)-2-Butanol	-113	33	-	100	-
E _R	(S)-2-Butanol	-127	11	-	100	-
I _R	(R)-2-Hexanol	-134	98	-	100	-
I _R	(S)-2-Hexanol	-164	83	-	100	-

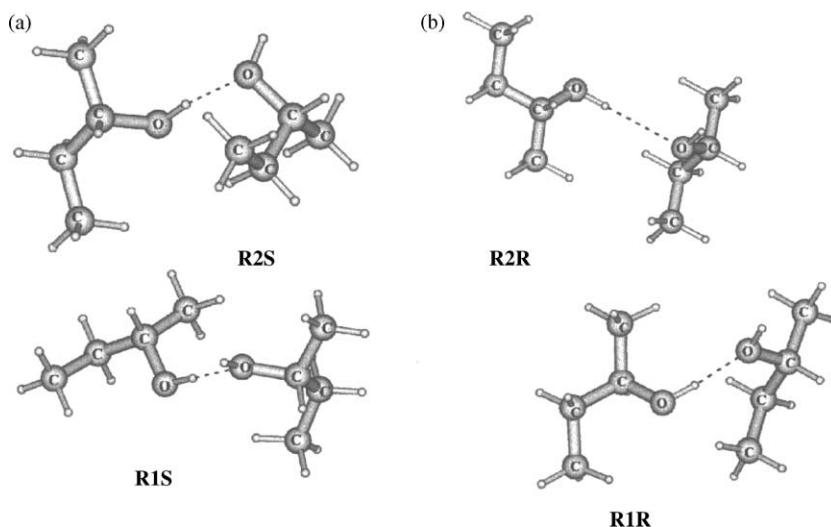


Fig. 12 (a) The structure of the two heterochiral dimers of 2-butanol; (b) The structure of the two homochiral dimers of 2-butanol.

ENERGETICS OF MOLECULAR COMPLEXES

Further insights into the forces operating in the molecular complexes between $C_R = (R)\text{-}(+)\text{-}1\text{-phenyl-}1\text{-propanol}$ (and $E_R = (R)\text{-}(+)\text{-}1\text{-phenylethanol}$) and chiral secondary alcohols is obtained from the measurement of their binding energies.^{212,337,340,347} The used procedure is summarized in Fig. 2. Accordingly, the binding energy D_0'' of a molecular complexes is derived from the difference between its dissociative ionization threshold ($h\nu_1 + h\nu_3$) and the ionization threshold of bare $C_R(h\nu_1' + h\nu_2')$ (equation (1)). The binding energy D_0'' of the molecular complexes in the S_1 excited state is taken as equal to $D_0'' - \Delta\nu$, using the appropriate $\Delta\nu$ terms of Table 2 (equation (2)). The dissociation energy D_0^+ of ionic cluster is estimated from the difference between its dissociative ionization threshold ($h\nu_1 + h\nu_3$) and its ionization threshold ($h\nu_1 + h\nu_2$) (equation 3). The relevant results are listed in Table 4.

The D_0'' value of the complex between C_R and 1-butanol ($2.6 \pm 0.2 \text{ kcal mol}^{-1}$) well conforms to the approximate value of $2\text{--}3 \text{ kcal mol}^{-1}$ indirectly estimated for the dissociation energy of the complex between $F_R = (R)\text{-}(+)\text{-}2\text{-naphthyl-}1\text{-ethanol}$ and methanol.¹⁰² Concerning the diastereomeric complexes, the homochiral adducts are invariably more stable than the heterochiral ones. This trend extends to the corresponding S_1 excited complexes as well. This observation, coupled with the appreciable deviation from linearity of the corresponding $\Delta\nu$ values (Fig. 9), corroborates the view that the interaction forces in these complexes are affected by steric congestion to a different extent. Their sensitivity to steric factors is demonstrated by the diverging observations that (Table 4): (i) in the diastereomeric

Table 4 Spectral shifts ($\Delta\nu$) and binding energies (D_0'' , D_0' and D_0^+ (see text)) of the molecular complexes between C_R and some alcohols (M) ($1 \text{ kcal mol}^{-1} = 349.77 \text{ cm}^{-1}$)

C	M	$\Delta\nu (\text{cm}^{-1})$	$D_0'' (\text{kcal mol}^{-1})$	$D_0^* (\text{kcal mol}^{-1})$	$D_0^+ (\text{kcal mol}^{-1})$
C_R	Water	+88	4.8 ± 0.2	4.6 ± 0.2	5.4 ± 0.2
C_R	2-Propanol	-87	3.7 ± 0.2	3.9 ± 0.2	-
C_R	1-Butanol	-96	2.6 ± 0.2	2.9 ± 0.2	6.5 ± 0.2
C_R	(<i>S</i>)-2-Butanol	-92	4.8 ± 0.2	5.1 ± 0.2	6.8 ± 0.2
C_R	(<i>R</i>)-2-Butanol	-79	5.9 ± 0.2	6.1 ± 0.2	8.4 ± 0.2
C_R	(<i>S</i>)-2-Pentanol	+25	3.1 ± 0.2	3.1 ± 0.2	4.6 ± 0.2
C_R	(<i>R</i>)-2-Pentanol	-64	4.7 ± 0.2	4.9 ± 0.2	8.5 ± 0.2
E_R	Water	+54	4.5 ± 0.2	4.3 ± 0.2	-
E_R	(<i>S</i>)-2-Butanol	-131	0.9 ± 0.5	1.3 ± 0.5	-
E_R	(<i>R</i>)-2-Butanol	-119	1.9 ± 0.5	2.3 ± 0.2	-

pairs with 2-butanols, the larger red-shift is associated with the less stable heterochiral complex. This trend is confirmed by replacing C_R with E_R (Table 4)³⁴⁸ or with F ($\Delta\nu_{\text{hom}} = -125 \text{ cm}^{-1}$; $\Delta\nu_{\text{hetero}} = -136 \text{ cm}^{-1}$);³⁴² (ii) in the diastereomeric pair with 2-pentanol, the less stable heterochiral complex exhibits a blue-shift and the most stable homochiral complex a red-shift. This trend is confirmed by replacing C_R with E_R ($\Delta\nu_{\text{hom}} = -101 \text{ cm}^{-1}$; $\Delta\nu_{\text{hetero}} = +5 \text{ cm}^{-1}$).³⁴⁸ This implies that the relatively high steric congestion, making the heterochiral complexes with (*S*)-2-butanol less stable than the homochiral analogs, is insufficient to alter significantly the nature of the attractive intracomplex forces. This is no longer true in going from the homochiral complexes with (*R*)-2-butanol to the homochiral complexes with (*R*)-2-pentanol. In fact, steric congestion in the latter complexes is so high to modify to some extent the nature of the attractive intracomplex forces and, therefore, the magnitude of its binding energy in both the ground and the excited states, relative to those operating in the homologous complexes with (*R*)-2-butanol. This trend goes to extremes in the least stable heterochiral adducts with (*S*)-2-pentanol. The low binding energy of these complexes and the blue shift accompanying their $S_1 \leftarrow S_0$ transition point to an exceedingly high steric congestion, which dramatically perturbs the spatial arrangement of the two moieties so as to favor attractive O-H $\cdots\pi$ -ring electrostatic forces more than dispersive interactions.

Inspection of the data in Table 4 reveals that the D_0^+ values always exceed the corresponding D_0'' interaction energies. The slow rise of the ion current observed in the 2cR2PI spectra suggests significant geometry change of the complex in its excited and the ionic state and, therefore, the phenomenological D_0^+ terms of Table 4 are probably not representative of the actual binding energies of the ionized molecular complexes, but rather must be considered as lower limits.³⁴² Nevertheless, they provide an additional phenomenological tool for chiral recognition in the isolated state.

CHIRAL EFFECTS IN RYDBERG ELECTRON-BOUND COMPLEXES

A large number of molecules of biological interest are strongly polar, and thus they can efficiently capture low energy electrons, giving rise to Rydberg electron-bound complexes. As seen above, a Rydberg electron is localized in a very diffuse orbital mainly outside the neutral molecular frame and its binding energy is generally very low (0.5–100 meV). For this reason the formation of the Rydberg electron-bound anion does not perturb the neutral parent structure. On the contrary, if valence anions are formed, the excess electron enters a valence orbital which participates into the chemical bonding and the geometrical structure of the neutral parent system is modified. Analogous considerations can be made if we consider the electron transfer process on a molecular complex.

For each molecule and molecular complex, it is possible to measure the dependence of the anion creation rate as a function of the Rydberg atom principal quantum number n . This n -dependence allows the experimental measure of the excess electron binding energy EA_{DB}^{calc} , with the help of a curve-crossing model, according to the equations reported above. From the computed electrostatic parameters (μ , Q , α), a semi-empirical electrostatic model provides the corresponding dipole-bound electron affinity EA_{DB}^{calc} . RET spectroscopy has proven to be a very useful tool to investigate the weak non-covalent interactions between polar biological molecules,^{184,263,267,349} but only recently it has been applied to investigate chiral clusters.³⁵⁰ In particular, the diastereomeric complexes of (*R*)-1-phenyl-1-ethanol (E_R) with (*R*)-(-)-(P_R) and (*S*)-(+)-2-pyrrolidinmethanol (P_S) (prolinol) have been investigated.

Fig. 13 shows the B3LYP/6-31++G**^{*}-calculated optimized structures of neutral diastereomeric $[E_R \cdot P_R]$ and $[E_R \cdot P_S]$ complexes. Two structures have been predicted for both the homochiral (I_{HOMO} and II_{HOMO}) and heterochiral (I_{HETERO} and II_{HETERO}) complexes. Their electrostatic parameters, binding energies and computed dipole-bound electron affinities EA_{DB}^{calc} are reported in Table 5.

Table 5 Calculated energy value and electrostatic parameters for the optimized $[E_R \cdot P_R]$ isomers, I_{HOMO} and II_{HOMO} , and $[E_R \cdot P_S]$ isomers, I_{HETERO} and II_{HETERO}

Calculated parameters ^a	$[E_R \cdot P_R]$		$[E_R \cdot P_S]$	
	I_{HOMO}	II_{HOMO}	I_{HETERO}	II_{HETERO}
D_e'' (meV)	355	486	365	511
$\Delta D_e''$ (meV)	0	131	0	146
μ (D)	3.59	3.46	3.91	3.34
Q_μ (DA)	-8	+9	-16	+9
EA_{DB}^{calc} (meV)	13	19	16	17

^a D_e'' is the cluster binding energy, $\Delta D_e''$ is the relative energy between the most stable and less stable structures of both $[E_R \cdot P_R]$ and $[E_R \cdot P_S]$ clusters; μ is the dipole moment of the complex; Q_μ is the quadrupole moment of the complex; EA_{DB}^{calc} is the calculated dipole-bound electron affinity.

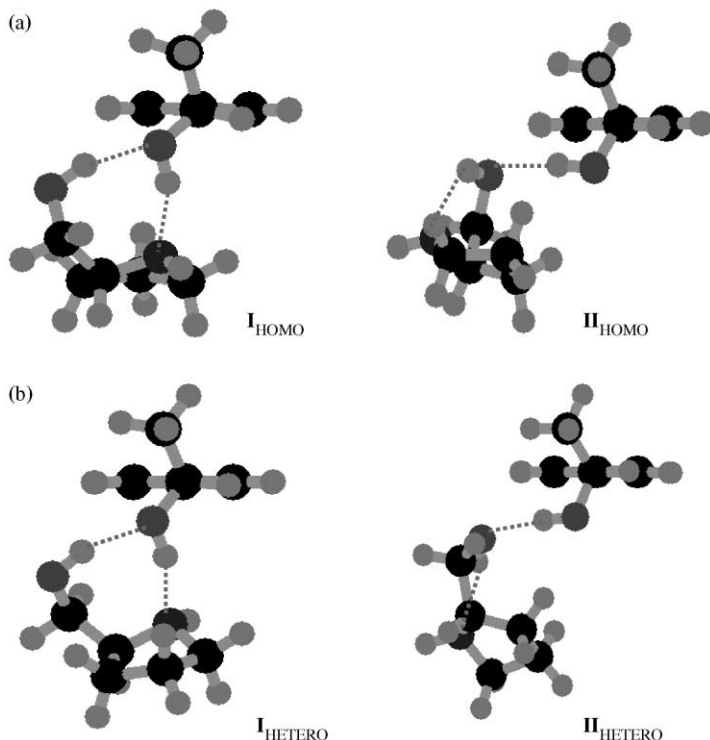


Fig. 13 Calculated structures of the neutral homochiral (a) and heterochiral (b) complexes between (*R*)-1-phenylethanol (E_R) and 2-pyrrolidinmethanols (P_R and P_S).

The two more stable structures I_{HOMO} and I_{HETERO} are characterized by a double hydrogen bond between E_R and P_R or P_S . The E_R molecule acts as proton donor towards the nitrogen of prolinol, and as acceptor towards the alcoholic proton of $P_{R/S}$. In the two less stable structure II_{HOMO} and II_{HETERO} , the prolinol maintains an intramolecular H-bond between the alcoholic oxygen and nitrogen and, thus, only one hydrogen bond with the E_R molecule is possible, in which the oxygen of $P_{R/S}$ accepts a proton.

These calculations can be compared with the experimental RET spectroscopy data obtained on separate mixtures of E_R with P_R , and E_R with P_S . Fig. 14 reports the n -dependency of the relative formation rate for the two diastereomeric complexes. As can be seen, a small discrimination between the two sets of data is possible: the plot of $[E_R \cdot P_R]$ data is peaked at Rydberg quantum number $n = 12$, while the one of $[E_R \cdot P_S]$ at $n = 13$. From these values the experimental dipole-bound electron affinities result to be: $EA_{\text{DB}}^{\text{exp}}([E_R \cdot P_R]) = 19 \text{ meV}$ and $EA_{\text{DB}}^{\text{exp}}([E_R \cdot P_S]) = 16 \text{ meV}$. The $EA_{\text{DB}}^{\text{exp}}([E_R \cdot P_R])$ value appears in better agreement with the calculated $EA_{\text{DB}}^{\text{calc}}$

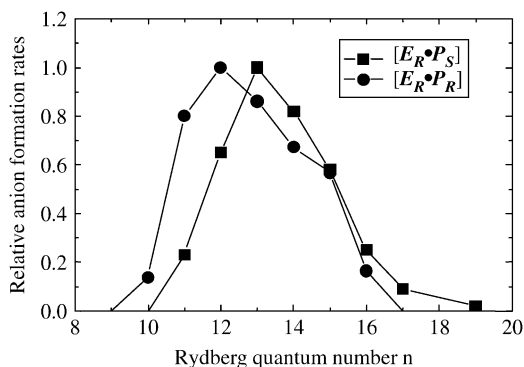


Fig. 14 Relative dipole bound anion formation rates in RET collisions between Rydberg Xe(nf) atoms and a supersonic beam of (*R*)-1-phenylethanol (E_R) with 2-pyrrolidinmethanols (P_R and P_S).

one corresponding to the predicted less stable structure $\mathbf{II}_{\text{HOMO}}$ (Table 5). This may indicate that conformational effects favor formation of structures \mathbf{II} in the supersonic beam expansion.

5 Chiral recognition in ionic clusters

In principle, mass spectrometry is not suitable to differentiate enantiomers. However, mass spectrometry is able to distinguish between diastereomers and has been applied to stereochemical problems in different areas of chemistry. In the field of chiral cluster chemistry, mass spectrometry, sometimes in combination with chiral chromatography, has been extensively applied to studies of proton- and metal-bound clusters, self-recognition processes, cyclodextrin and crown ethers inclusion complexes, carbohydrate complexes, and others. Several excellent reviews on this topic are nowadays available.^{351–356} A survey of the most relevant examples will be given in this section. Most of the studies was based on ion abundance analysis, often coupled with MIKE and CID ion fragmentation on MS^n and FT-ICR mass spectrometric instruments, using CI, MALDI, FAB, and ESI, and atmospheric pressure ionization (API) methods.

PROTON-BOUND COMPLEXES

Proton-bound dimers and trimers of tartrates

The detection of chiral recognition with a mass spectrometer was reported first in 1977 by Fales and Wright.³⁵⁷ Their study showed that the chirality of dialkyltartrates (**T**) strongly influences the stability of their diastereomeric proton-bound dimers, generated by isobutane chemical ionization (CIMS) of their racemic mixtures.^{358,359} In order to differentiate the protonated species of the homochiral self-dimers

($[T_D \cdot T_D \cdot H]^+$ and $[T_L \cdot T_L \cdot H]^+$) from the heterochiral one ($[T_D \cdot T_L \cdot H]^+$), the CIMS experiments were carried out on an equimolar mixture of one enantiomer, deuterium-labeled at the estereal function (T_D^*), with the other unlabeled enantiomer (T_L). The abundances of the three protonated diastereomeric dimers ($[T_D^* \cdot T_D^* \cdot H]^+$, $[T_D^* \cdot T_L \cdot H]^+$, and $[T_L \cdot T_L \cdot H]^+$) indicated a chiral recognition pattern. The chirality effect or the chiroselective ratio of the virtual equilibrium constants $K_{\text{homo}}/K_{\text{hetero}}$ (internal chirality effect), regarded as a measure of the relative stability of the homochiral vs. the heterochiral dimers, is defined as $K_{\text{homo}}/K_{\text{hetero}} = 2\{[T_D^* \cdot T_D^* \cdot H]^+ \times [T_L \cdot T_L \cdot H]^+\}^{1/2}/[T_D^* \cdot T_L \cdot H]^+$. If a third chiral component is added as the reference substrate (ref) to the above racemate, the CIMS of the mixture typically gives five ions in the dimer region, i.e., $[\text{ref} \cdot T_D^* \cdot H]^+$, $[\text{ref} \cdot T_L \cdot H]^+$, $[T_D^* \cdot T_D^* \cdot H]^+$, $[T_D^* \cdot T_L \cdot H]^+$, and $[T_L \cdot T_L \cdot H]^+$, and a new chirality effect (external chirality effect) can be defined as $K_{\text{homo}}^{\text{ref}}/K_{\text{hetero}}^{\text{ref}} = \{[\text{ref} \cdot T_D^* \cdot H]^+ / [\text{ref} \cdot T_L \cdot H]^+\} / \{[T_D^* \cdot T_D^* \cdot H]^+ / [T_L \cdot T_L \cdot H]^+\}^{1/2}$ (if ref has the *D* configuration).³⁵⁸

Since the monochiral experiment reported on the last row of Table 6 excludes any significant deuterium isotope effect in the formation of the proton-bound dimers, the other figures demonstrate that the homochiral dimer is relatively more stable than the heterochiral one. The lower stability of the heterochiral dimer is ascribed to steric repulsion between the estereal functions of the two monomers in the hydrogen bonded basket-type structure of the complex. Similar chirality effects have been measured for the same systems using FAB as the ionization mode.³⁶⁰ A linear correlation is observed between the optical purity of a ref = diethyltartrate specimen and the $K_{\text{homo}}^{\text{ref}}/K_{\text{hetero}}^{\text{ref}}$ value. These findings suggest the possibility of using the FAB-MS method for chirally titrating ref.

The $K_{\text{homo}}/K_{\text{hetero}}$ was also estimated by B/E linked scanning of FAB-MS.^{359,360} It can be expressed as $K_{\text{homo}}/K_{\text{hetero}} = \{[T_D^* \cdot H]^+ / [T_D^* \cdot T_D^* \cdot H]^+\} / \{([T_D^* \cdot H]^+ + [T_L \cdot H]^+) / [T_D^* \cdot T_L \cdot H]^+\}$, where $[T_D^* \cdot H]^+$ and $[T_L \cdot H]^+$ correspond to the peak intensities of monomer ions produced by unimolecular decomposition of the relevant protonated dimer species. The experimental results ($K_{\text{homo}}/K_{\text{hetero}} = 0.67$ (diPrⁱ-D-tartrate + diPrⁱ-D-tartrate-d₁₄); 0.77 (diEt-D-tartrate + diEt-D-tartrate-d₁₀)) confirm the higher stability of the homochiral dimer relative to the heterochiral one by indicating that the latter has a higher tendency toward unimolecular decomposition.

More comprehensive CIMS investigations on tartrate systems indicate that the dimer chirality effects disappear when the ester functions of tartrates is replaced by H or an alkyl function, e.g., methyl or cyclohexyl.³⁵⁹ A similar effect is observed when the proton in the proton-bound dimers is replaced by lithium or ammonium ion.^{358–360} These observations are attributed to a dramatic change in the basket-type structure of tartrate dimer ions.

The same CIMS approach has been used for investigating the self-recognition processes in proton-bound tartrate trimers.^{359–363} The trimer chirality effect is consistent with the heterochiral trimers as more stable than the homochiral ones. The reverse is true when the proton in the proton-bound trimers is replaced by hydronium, ammonium ion, or primary aminium ions.^{364,365} This changeover is

Table 6 Chirality effects in the dimerization of homologous tartrate esters

T	T ^{tr}	ref	$K_{\text{homo}}/K_{\text{hetero}}$	$K_{\text{homo}}^{\text{ref}}/K_{\text{hetero}}^{\text{ref}}$	ext/int
diPr ⁱ -D-Tartrate	diPr ⁱ -L-Tartrate-d ₁₄	diMe-D-Tartrate	1.57 ± 0.16	1.54 ± 0.17	0.99 ± 0.12
diPr ⁱ -D-Tartrate	diPr ⁱ -L-Tartrate-d ₁₄	diMe-L-Tartrate	1.51 ± 0.16	1.35 ± 0.14	0.88 ± 0.11
diPr ⁱ -D-Tartrate	diPr ⁱ -L-Tartrate-d ₁₄	diEt-D-Tartrate	1.47 ± 0.04	1.55 ± 0.10	1.05 ± 0.08
diPr ⁱ -D-Tartrate	diPr ⁱ -L-Tartrate-d ₁₄	diEt-L-Tartrate	1.49 ± 0.05	1.46 ± 0.10	0.98 ± 0.08
diPr ⁱ -D-Tartrate	diPr ⁱ -L-Tartrate-d ₁₄	diPy-D-Tartrate ^a	1.43 ± 0.05	1.23 ± 0.14	0.86 ± 0.10
diPr ⁱ -D-Tartrate	diPr ⁱ -L-Tartrate-d ₁₄	–	1.71 ± 0.04		
diPr ⁱ -L-Tartrate	diPr ⁱ -L-Tartrate-d ₁₄	–	1.01 ± 0.05		

^aPy = pyrrolidyl.

ascribed to the formation of an especially stable supramolecular propeller structure accessible only to the homochiral aggregation.

The relative stability of the homochiral and the heterochiral dimers arising from self-CI of an equimolar mixture of the L and the D enantiomers of dimethyl- and di-isopropyltartrate has been evaluated by Nikolaev et al. using the FT-ICR technique.^{366–369} The dimer chirality effect, $K_{\text{homo}}/K_{\text{hetero}} = 0.33$ corresponds to a $\Delta\Delta G_{298}^0 = -RT \ln(K_{\text{homo}}/K_{\text{hetero}}) = 0.65 \text{ kcal mol}^{-1}$ value at 20 °C, a value which is slightly larger than those measured in the CIMS experiments (0.25–0.50 kcal mol⁻¹).^{358,359} The lack of chirality effects, observed when the used tartrates are replaced by the L and the D enantiomers of methyl lactate, alaninamide, and *N*-acetyl- α -methyl-benzylamine, is attributed to their extensive racemization after protonation.

Proton-bound carboxylic acid/amino acid complexes

Proton-induced association of a number of chiral compounds, including carboxylic acids, amino acids, and amines has been investigated using CIMS and FABMS techniques. The first controversial³⁶⁰ evidence of chiral discrimination in these systems was based upon the relative peak intensities of proton-bound complexes generated by CIMS of mixtures containing a chiral selector S_R (i.e., (*R*)-2-methyl-1-butanol) and the enantiomers of a target molecule $M_{R/S}$ (i.e., mandelic acid or phenylalanine).³⁷⁰ The resulting chiral discrimination term, defined as $[S_S \cdot M_R \cdot H]^+ / [S_S \cdot M_S \cdot H]^+$, ranged from >9 (mandelic acid) to 2.3 (phenylalanine). The same approach has been applied to a number of systems,^{371–376} whose results are summarized in Table 7.

Analysis of Table 7 reveals that the stability of the homochiral complexes is higher than that of the heterochiral ones, except in the cases with chiral succinic anhydrides. Similar results have been obtained by using (*R*)- and (*S*)-1-naphthylethylamine as optically resolving reagents.³⁷⁷

An approach, similar to that employed in the analysis of tartrate mixtures, has been used for the chiral discrimination of amino acid ($M_{R/S}$) mixtures, using an amino acid of defined configuration as reference (*S*). The proton-bound trimers $[S_2 \cdot M \cdot H]^+$ form $[S \cdot M \cdot H]^+$ and $[S_2H]^+$ fragments upon CID or MIKE decay (equations (9)–(12)). With two independent measurements of the fragmentation ratio $[S \cdot M \cdot H]^+ / [S_2H]^+$ from either $[S_2 \cdot M_R \cdot H]^+$ and $[S_2 \cdot M_S \cdot H]^+$, the differences in binding energies can be determined.³⁷⁸ The relative gas phase basicities (GB) of the molecular pairs $[S \cdot M]$ and $[S_2]$ can be derived from equations (13) and (14).

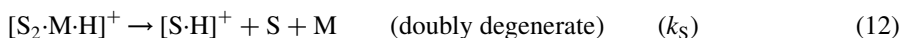
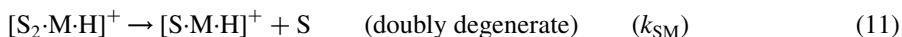
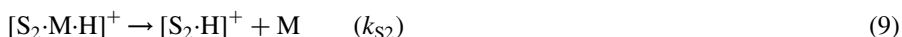


Table 7 Relative abundances of diastereomeric proton-bound complexes from CI, FAB, and API mass spectrometry

MS techniques	<i>S</i> ^a	<i>M</i> ^b	[<i>S</i> · <i>M</i> · <i>H</i>] ⁺ / <i>[S</i> · <i>H</i>] ⁺	Reference
CI	(<i>S</i>)-Alanine	(<i>S</i>)-Mandelic acid	0.05 ^c	371
CI	(<i>S</i>)-Alanine	(<i>R</i>)-Mandelic acid	0.01 ^c	371
CI	(<i>R</i>)-Alanine	(<i>S</i>)-Mandelic acid	0.08 ^c	371
CI	(<i>R</i>)-Alanine	(<i>R</i>)-Mandelic acid	0.17 ^c	371
CI	(<i>S</i>)-Phenylalanine	(<i>S</i>)-2-Methylbutanoic acid	0.09	371
CI	(<i>S</i>)-Phenylalanine	(<i>R</i>)-2-Methylbutanoic acid	0.04	371
CI	(<i>R</i>)-Phenylalanine	(<i>S</i>)-2-Methylbutanoic acid	0.07	371
CI	(<i>R</i>)-Phenylalanine	(<i>R</i>)-2-Methylbutanoic acid	0.11	371
CI	(<i>S</i>)-Proline	(<i>S</i>)-Mandelic acid	1.39	372
CI	(<i>S</i>)-Proline	(<i>R</i>)-Mandelic acid	0.09	372
CI	(<i>R</i>)-Proline	(<i>S</i>)-Mandelic acid	0.04	372
CI	(<i>R</i>)-Proline	(<i>R</i>)-Mandelic acid	0.82	372
CI	(1 <i>S</i> ,3 <i>S</i> ,5 <i>S</i>)-ABOCA	(1 <i>S</i>)-Camphanic acid	5.00	372
CI	(1 <i>S</i> ,3 <i>S</i> ,5 <i>S</i>)-ABOCA	(1 <i>R</i>)-Camphanic acid	1.27	372
CI	(1 <i>R</i> ,3 <i>R</i> ,5 <i>R</i>)-ABOCA	(1 <i>S</i>)-Camphanic acid	1.52	372
CI	(1 <i>R</i> ,3 <i>R</i> ,5 <i>R</i>)-ABOCA	(1 <i>R</i>)-Camphanic acid	5.56	372
FAB	(<i>S</i>)-Cinchonine	(<i>S</i> , <i>S</i>)-DBOSA	0.02	373
FAB	(<i>S</i>)-Cinchonine	(<i>R</i> , <i>R</i>)-DBOSA	0.16	373
FAB	(<i>R</i>)-Cinchonidine	(<i>S</i> , <i>S</i>)-DBOSA	0.30	373
FAB	(<i>R</i>)-Cinchonidine	(<i>R</i> , <i>R</i>)-DBOSA	0.05	373
LC/API	(<i>S</i>)-Mandelic acid methyl ester	(<i>S</i>)-1-Phenylethylamine	7.11	374
LC/API	(<i>S</i>)-Mandelic acid methyl ester	(<i>R</i>)-1-Phenylethylamine	5.31	374
LC/API	(<i>R</i>)-Mandelic acid methyl ester	(<i>S</i>)-1-Phenylethylamine	3.70	374
LC/API	(<i>R</i>)-Mandelic acid methyl ester	(<i>R</i>)-1-Phenylethylamine	8.50	374
GC/CI	(+)-Isoborneol	(<i>R</i>)-2-Amino-1-propanol	0.12	375
GC/CI	(+)-Isoborneol	(<i>S</i>)-2-Amino-1-propanol	0.01	375
GC/CI	(-)-Isoborneol	(<i>R</i>)-2-Amino-1-propanol	0.02	375
GC/CI	(-)-Isoborneol	(<i>S</i>)-2-Amino-1-propanol	0.09	375

Table 7 (continued)

MS techniques	S ^a	M ^b	[S·M·H] ⁺ /[S·H] ⁺	Reference
HPLC/API	(<i>S</i>)-Phenylalanine	(<i>S</i>)-Mandelic acid	0.84	376
HPLC/API	(<i>S</i>)-Phenylalanine	(<i>R</i>)-Mandelic acid	0.46	376
HPLC/API	(<i>R</i>)-Phenylalanine	(<i>S</i>)-Mandelic acid	0.53	376
HPLC/API	(<i>R</i>)-Phenylalanine	(<i>R</i>)-Mandelic acid	0.75	376
HPLC/API	(<i>S</i>)-Phenylalanine	(<i>S</i>)-Mandelic acid methyl ester	0.85	376
HPLC/API	(<i>R</i>)-Phenylalanine	(<i>S</i>)-Mandelic acid methyl ester	0.53	376

^aABOCA, 2-azabicyclo[3,3,0]octane-3-carboxylic acid.

^bDBOSA, dibenzoyloxysuccinic acid anhydride.

^c[S·M·H-H₂O]⁺/[S·H]⁺ value.

$$\ln([S_2 \cdot H]^+ / [M \cdot H]^+) = \ln(k_{S_2} / k_M) = \{GB(S_2) - GB(M)\} / RT_{\text{eff}} \quad (13)$$

$$\ln(\{[S \cdot M \cdot H]^+ / 2\} / [S_2 \cdot H]^+) = \ln(\{k_{SM} / 2\} / k_{S_2}) = \{GB(SM) - GB(S_2)\} / RT_{\text{eff}} \quad (14)$$

The chiral discrimination factor, ΔR^{chiral} , is defined by equation (15). The $[S \cdot M \cdot H]^+ / [S_2 \cdot H]^+$ ratios from CID of various mixtures of chiral amino acids are reported in Table 8.

$$\begin{aligned} \Delta R^{\text{chiral}} &= \frac{[SMH]_{\text{hetero}}^+ / [S_2H]^+}{[SMH]_{\text{homo}}^+ / [S_2H]^+} \\ &= \frac{\{[SMH]^+ / [S_2H]^+\}_{DL} + \{[SMH]^+ / [S_2H]^+\}_{LD}}{\{[SMH]^+ / [S_2H]^+\}_{DD} + \{[SMH]^+ / [S_2H]^+\}_{LL}} \end{aligned} \quad (15)$$

Using equations (13) and (14), the relative GB ($\Delta GB^{\text{chiral}}$) of the hetero- vs. homochiral proton-bound complexes can be expressed as in equation (16).

$$\Delta GB^{\text{chiral}} = GB([S \cdot M]_{\text{hetero}}) - GB([S \cdot M]_{\text{homo}}) = RT_{\text{eff}} \ln\{\Delta R^{\text{chiral}}\} \quad (16)$$

The relevant $\Delta GB^{\text{chiral}}$ values, calculated by using $T_{\text{eff}} = 970 \text{ K}$,³⁷⁹ are listed in Table 8. According to the reported values, the heterochiral Trp/Pro and Phe/Ala complexes are more stable than the homochiral ones. The reverse is true for the Phe/Pro and Phe/Val complexes. By the same token, the chiral discrimination factor, ΔR^{chiral} , measured by ESI-MS² for 19 amino acids was found to vary between 0.3 and 3.³⁸⁰ The stereochemistry associated to the CID of diastereomeric peptides has been investigated using a similar approach. The results suggest that the secondary structure of protonated peptides may play an important role in their gas-phase behavior.³⁸¹

The kinetic method, described by equations (9)–(12), has been successfully employed for enantiodiscriminating important chiral residues from post-translationally modified proteins, such as O-phospho- α -amino acids and α -aminophosphonic acids. The CID decomposition of their mixed proton and Na^+ -bound trimers, carried out in a ESI-MS² instrument as a function of the collision energy (4–14 eV), points to a greater stability of the heterochiral proton- and Na^+ -bound dimers between O-phospho-serine and (1-aminoethyl) phosphonic acid (or O-phospho-threonine) relative to the homochiral ones.³⁸² The stability trend of the proton-bound dimers of α -aminophosphonic acids, $\text{H}_2\text{O}_3\text{P-CH}(\text{NH}_2)\text{-R}$ ($\text{R} = \text{CH}_3$, $i\text{-C}_3\text{H}_7$, and $n\text{-C}_5\text{H}_{11}$) is less evident and is found to depend critically on their structural features.³⁸³ Thus, when the components of the dimers have the largest alkyl groups $\text{R} = i\text{-C}_3\text{H}_7$ and $n\text{-C}_5\text{H}_{11}$, no stability difference is observed. Instead, the heterochiral complex is more stable than the homochiral one when the R alkyl substituents have a different bulkiness, e.g., $\text{R} = \text{CH}_3$ and $i\text{-C}_3\text{H}_7$. The reverse is true with $\text{R} = \text{CH}_3$ and $n\text{-C}_5\text{H}_{11}$.

Table 8 Fragment-ion abundance ratios from CID of proton-bound $[S_2 \cdot M \cdot H]^+$ clusters

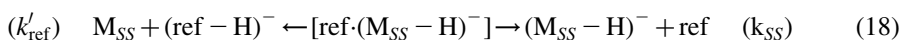
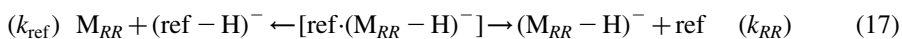
Amino acid, M	Selector, S	$[S \cdot M \cdot H^+]/[S_2 \cdot H^+]$	ΔR^{chiral}	SD^a of ΔR^{chiral}	$\Delta GB^{\text{chiral}}$ (kcal mol ⁻¹) ^b
Trp	Pro	1.528(<i>DD</i>); 1.529(<i>LL</i>); 1.656(<i>DL</i>); 1.643(<i>LD</i>)	1.079	0.004	0.2
Pro	Trp	2.936(<i>DD</i>); 3.049(<i>LL</i>); 3.429(<i>DL</i>); 3.461(<i>LD</i>)	1.151	0.008	0.3
Phe	Ala	0.291(<i>DD</i>); 0.291(<i>LL</i>); 0.315(<i>DL</i>); 0.313(<i>LD</i>)	1.079	0.008	0.2
Phe	Pro	15.221(<i>DD</i>); 15.098(<i>LL</i>); 9.346(<i>DL</i>); 9.901(<i>LD</i>)	0.645	0.015	-0.8
Phe	Val	0.786(<i>DD</i>); 0.776(<i>LL</i>); 0.744(<i>DL</i>); 0.749(<i>LD</i>)	0.956	0.004	-0.1

^aSD, standard deviation.^bPositive values indicate higher basicity for the heterochiral complex.

Proton-bound diol complexes

The relative stability of diastereomeric complexes between some chiral selectors $\text{ref} = (S)\text{-}(+)\text{-}3\text{-hydroxy-tetrahydrofuran}$ or methyl- $(R)\text{-}(+)\text{-}2\text{-chloro-propionate}$, and the conjugate bases $(\text{M}_{RR}\text{-H})^-$ and $(\text{M}_{SS}\text{-H})^-$, respectively) and acids $(\text{M}_{RR} + \text{H})^+$ and $(\text{M}_{SS} + \text{H})^+$, respectively) of $(2R,3R)\text{-}(\text{M}_{RR})$ and $(2S,3S)\text{-}2,3\text{-butanediol}$ (M_{SS}), was evaluated by using the kinetic method.^{384,385}

This method is based on the CID of the diastereomeric complexes, e.g., $[\text{ref}\cdot(\text{M}_{RR}\text{-H})^-]$ and $[\text{ref}\cdot(\text{M}_{SS}\text{-H})^-]$ ($\text{ref} = (S)\text{-}(+)\text{-}3\text{-hydroxy-tetrahydrofuran}$), and the measurement of relative abundances of the corresponding fragment ions, i.e., $(\text{M}_{RR}\text{-H})^-$ (or $(\text{M}_{SS}\text{-H})^-$) and $(\text{ref-H})^-$, which reflect the corresponding fragmentation rate constants k_{RR} (or k_{SS}) and k_{ref} (or k'_{ref}) (equations (17) and (18))



$$\ln([\text{M}_{RR}\text{-H})^-]/[(\text{ref-H})^-]) = \ln(k_{RR}/k_{\text{ref}}) = \ln K_{\text{eq}}^{RR} = -\Delta(\Delta G)^{RR}/RT_{\text{eff}} \quad (19)$$

$$\ln([\text{M}_{SS}\text{-H})^-]/[(\text{ref-H})^-]) = \ln(k_{SS}/k'_{\text{ref}}) = \ln K_{\text{eq}}^{SS} = -\Delta(\Delta G)^{SS}/RT_{\text{eff}} \quad (20)$$

Theoretical treatments lead to the approximate expression in equations (19) and (20),³⁸⁴ where T_{eff} is the effective temperature of the complexes, and the $\Delta(\Delta G)$ s are the differences in their dissociation free energies. If the entropy effects of the two competing fragmentation processes cancel, then the $\Delta(\Delta G)$ s can be substituted by the $\Delta(\Delta H)$ s.

The average effective temperature T_{eff} , which is a measure of excess internal energy content per degree of freedom of the ion/molecule complexes, was determined as 333 K from the slopes of the $1/RT$ dependence of the logarithm of the branching ratios similar to those of equations (19) and (20) involving ions $(\text{M}_{RR}\text{-H})^-$, $(\text{M}_{SS}\text{-H})^-$, $(\text{M}_{RR} + \text{H})^+$, and $(\text{M}_{SS} + \text{H})^+$ and a number of reference molecules. With $T_{\text{eff}} = 333$ K, the CID fragmentation ratios correspond to the $\Delta(\Delta G)$ values reported in Table 9, where I_{diol} represents the abundance of the $(\text{M}_{RR}\text{-H})^-$, $(\text{M}_{SS}\text{-H})^-$, $(\text{M}_{RR} + \text{H})^+$, and $(\text{M}_{SS} + \text{H})^+$ ions from paths k_{RR} and k_{SS} and I_{ref} refers to the abundance of the fragments from paths k_{ref} and k'_{ref} , involving the appropriate chiral selector $\text{ref} = (S)\text{-}(+)\text{-}3\text{-hydroxy-tetrahydrofuran}$ or methyl- $(R)\text{-}(+)\text{-}2\text{-chloro-propionate}$.

The differences between the $\Delta(\Delta G)$ values of diastereomeric complexes ($\Delta\Delta(\Delta G) = \Delta(\Delta G)^{RR} - \Delta(\Delta G)^{SS}$ in Table 9) demonstrate that the kinetic method can be used to enantiodifferentiate chiral ions and molecules in the gas phase.

METAL-BOUND COMPLEXES

Li^+ -Bound diol complexes

Chiral diols and tartrates have been studied as metal complexes as well. The enantiomers of 1,1'-bi-2-naphthol (Y) and diisopropyltartrate (T) have been

Table 9 Fragment-ion abundance ratios from CID of diastereomeric complexes

Diastereomeric complex	Chiral selector, ref	$I_{\text{diol}}/I_{\text{ref}}$	$\Delta(\Delta G)$ (kcal mol ⁻¹)	$\Delta\Delta(\Delta G)$ (kcal mol ⁻¹)
[ref-(M _{RR} -H) ⁻]	(S)-(+)-3-Hydroxy-tetrahydrofuran	(M _{RR} -H) ⁻ /(ref-H) ⁻ = 12.4	- 1.67	0.47
[ref-(M _{SS} -H) ⁻]	(S)-(+)-3-Hydroxy-tetrahydrofuran	(M _{SS} -H) ⁻ /(ref-H) ⁻ = 25.6	- 2.14	
[ref-(M _{RR} + H) ⁺]	Methyl-(R)-(+)-2-Chloro-propionate	(M _{RR} + H) ⁺ /(ref + H) ⁺ = 19.0	- 1.94	0.23
[ref-(M _{SS} + H) ⁺]	Methyl-(R)-(+)-2-Chloro-propionate	(M _{SS} + H) ⁺ /(ref + H) ⁺ = 26.7	- 2.17	

discriminated by generating their Li^+ complexes (using (*R,R*)-threohydrobenzoyl (S_{RR}) as the chiral selector) in the FAB source of a tandem mass spectrometer.¹⁰⁶ Unimolecular dissociation (MIKE) of the diastereomeric $[\text{S}_{RR}\text{Li}\cdot\text{Y}]^+$ (or $[\text{S}_{RR}\text{Li}\cdot\text{T}]^+$) complexes yields the corresponding fragments $[\text{S}_{RR}\text{Li}]^+$ and $[\text{Y}\cdot\text{Li}]^+$ (or $[\text{T}\cdot\text{Li}]^+$), whose relative abundance is taken as a measure of the relative stability of their precursor. According to kinetic energy release (KER) associated to the unimolecular fragmentation, this stability difference is attributed to the different structure of the diastereomeric $[\text{S}_{RR}\text{Li}\cdot\text{Y}]^+$ (or $[\text{S}_{RR}\text{Li}\cdot\text{T}]^+$) complexes, rather than to their internal energy.

Co³⁺-Bound complexes

Statistically significant differences have been observed in the KER measurements of the fragments arising from MIKE dissociation of the transition-metal complex $[\text{Co}(\text{acac})_2\cdot\text{T}]^+$, generated in FAB source of a tandem mass spectrometer from the diisopropyltartrate (T) enantiomers and cobalt trisacetonylacetate ($\text{Co}(\text{acac})_3$) in the presence of the chiral selector of defined configuration, either (*R,R*)- or (*S,S*)-1,1'-bi-2-naphthol (Y).³⁸⁶ Indeed, different KER values were measured for the $[\text{Co}(\text{acacH})\cdot\text{T}]^+$ fragments, which have been considered to reflect different precursor $[\text{Co}(\text{acac})_2\cdot\text{T}]^+$ ion structures. In these experiments, the chiral 1,1'-bi-2-naphthol selector Y is thought to serve as a chemical kinetic resolving agent.

Metal ion-bound amino acid complexes

Accurate quantification of the optical isomers in mixtures of tartaric acid and other α -hydroxy acids was performed by Cooks and coworkers by using the mass spectrometric kinetic method.^{387,388} In a series of elegant studies, they used the same approach for enantiodiscriminating amino acids, peptides, pharmaceuticals, and drugs. Chiral recognition and quantitation of these molecules, recognized as building blocks in life sciences, are based on the competing fragmentation of the diastereomeric complexes $[\text{A}_R\text{Me}^{\text{II}}\cdot(\text{ref})_2\text{-H}]^+$ and $[\text{A}_S\text{Me}^{\text{II}}\cdot(\text{ref})_2\text{-H}]^+$ in which Me^{II} is generally a divalent transition-metal ion, such as Cu(II), Zn(II), Ni(II), or Co(II), A is the chiral analyte, and ref is a reference molecule of defined configuration (Scheme 4, with $\text{I} = \text{Me}^{\text{II}}$).³⁸⁹

Using this procedure, D- and L- α -amino acids have been enantiodifferentiated in the gas phase.^{390,391} ESI of hydroalcoholic solutions of the amino acid and CuCl_2 into the source of an ion trap mass spectrometer reveals the presence of singly charged, covalently bound dimeric and trimeric ions. Table 10 reports the CID results of the diastereomeric complexes $[\text{A}_R\text{Cu}^{\text{II}}\cdot(\text{ref})_2\text{-H}]^+$ and $[\text{A}_S\text{Cu}^{\text{II}}\cdot(\text{ref})_2\text{-H}]^+$.

The degree of chiral discrimination is defined from the relative copper(II) affinity $\Delta\text{Cu}(\text{II})' = RT_{\text{eff}}\ln R_{\text{chiral}}$, with R_{chiral} as expressed in equation (7). The $\Delta\text{Cu}(\text{II})'$ terms in Table 10 indicate that irrespective of the ref used, the heterochiral complexes of most amino acids are more stable than the homochiral analogues

Table 10 Fragment ion abundance ratios in the MS² spectra of Cu(II)-bound trimer complexes

Entry	A	ref	I_L/I_{ref}^a	I_D/I_{ref}^a	R_{chiral}^a	$\Delta Cu(II)^c$ (kcal mol ⁻¹) ^b
i	Leu	L-Val	2.5	2.4	1.05	0.0
ii	Leu	L-Pro	0.11	0.099	1.11	+0.1
iii	Leu	L-Ser	10	9.5	1.05	0.0
iv	Leu	L-Phe	0.41	0.96	0.43	-0.6
v	Met	L-Pro	33	60	0.50	-0.4
vi	Met	4-OH-L-Pro	33	59	0.56	-0.4
vii	Met	L-Glu	18	27	0.67	-0.3
viii	Met	L-Trp	0.23	1.8	0.13	-1.4
ix	Tyr	L-Met	0.90	2.8	0.32	-0.8
x	Tyr	L-Glu	8.0	16	0.50	-0.5
xi	Tyr	L-Pro	4.7	43	0.11	-1.5
xii	Tyr	L-Trp	0.02	0.21	0.09	-1.6
xiii	Phe	L-Pro	2.1	16	0.13	-1.4
xiv	Thr	L-Pro	0.88	0.89	1.00	0.0
xv	Asp	L-Pro	3.2	4.5	0.71	-0.2
xvi	Ala	L-Phe	0.024	0.049	0.49	-0.5
xvii	Val	L-Phe	0.17	0.75	0.23	-1.0
xviii	Ile	L-Phe	0.36	1.7	0.21	-1.1
xix	Pro	L-Phe	2.2	12	0.18	-1.2
xx	Asp	L-Phe	1.1	3.0	0.37	-0.7
xxi	Glu	L-Phe	3.7	11	0.34	-0.8
xxii	Ser	L-Phe	0.18	0.28	0.64	-0.3
xxiii	Thr	L-Phe	0.76	1.4	0.54	-0.4
xxiv	Phe	L-Trp	0.013	0.11	0.12	-1.5
xxv	Asn	L-Trp	3.3	6.1	0.54	-0.4
xxvi	Gln	L-Trp	7.3	50	0.15	-1.3
xxvii	Trp	L-Asn	3.3	6.1	0.54	-0.4
xxviii	His	L-Arg	0.046	0.022	2.09	+0.5
xxix	Lys	L-His	1.6	0.91	1.76	+0.4

^aChiral resolution factor, R_{chiral} , as the ratio between the homochiral and the heterochiral ion abundance ratios.

^bSee text, $T_{eff} = 350$ K.

($R_{chiral} < 1$). Analysis of entries i–xii of Table 10 provides some insights into the effects of the ref on leucine, methionine, and tyrosine enantiodiscrimination. The L-valine (entry i) and L-serine (entry iii) references, like L-proline (entry ii), give low enantioselectivity for leucine as analyte ($R_{chiral} \approx 1$). Instead, with an aromatic amino acid as ref, i.e., L-phenylalanine (entry iv), high chiral selectivity is achieved. A similar behavior is observed for the methionine enantiodiscrimination (cf. entries v–vii with entry viii of Table 10). An excellent enantioselectivity is achieved for tyrosine with ref = L-proline (entry xi of Table 10). However, even greater chiral selectivity is observed with ref = L-tryptophan (entry xii of Table 10). The selectivity decreases dramatically when non-aromatic references are used (entries ix and x of Table 10). The great selectivity of aromatic ref, such as L-phenylalanine or

tryptophan, if compared to that of a rigid, non-aromatic ref, like L-proline, is confirmed by extending the comparison to the corresponding Ala, Thr, and Asp systems.

Structural studies of the dimeric clusters $[A_R\text{-Me}^{\text{II}}\text{-ref-H}]^+$ and $[A_S\text{-Me}^{\text{II}}\text{-ref-H}]^+$, arising from CID of the corresponding $[A_R\text{-Me}^{\text{II}}\text{-(ref)}_2\text{-H}]^+$ and $[A_S\text{-Me}^{\text{II}}\text{-(ref)}_2\text{-H}]^+$ precursors, reveal that two ligands are covalently bound to the metal ion through multiple binding sites, which provide the basis for efficient chiral distinction.^{391,392} In the case of amino acids, two of the interactions between the two ligands are Me(II)-mediated, resulting from the coordination of the amino and carboxylate groups to the central metal ion, whereas the third interaction involves the substituents at or near the asymmetric α -carbon of each of the two ligands (Fig. 15).

Although relatively weak, it is this last interaction that is essential for determining chiral discrimination. The superior chiral recognition achieved when ref has an aromatic side chain (Table 10) suggests that π -cation interactions play an important role in the stereoselectivity. Evidence for such a π -cation interaction is observed in the CID spectra of the dimeric $[A_R\text{-Me}^{\text{II}}\text{-ref-H}]^+$ and $[A_S\text{-Me}^{\text{II}}\text{-ref-H}]^+$ diastereomers, in which one ligand is an aromatic amino acid, and is supported by *ab initio* calculations. When an L-aromatic amino acid, such as L-phenylalanine, is used as ref, these interactions are disrupted by the side group on the α -asymmetric carbon of the L-analyte, whereas the side-chain group in the D-analyte has little steric effect on

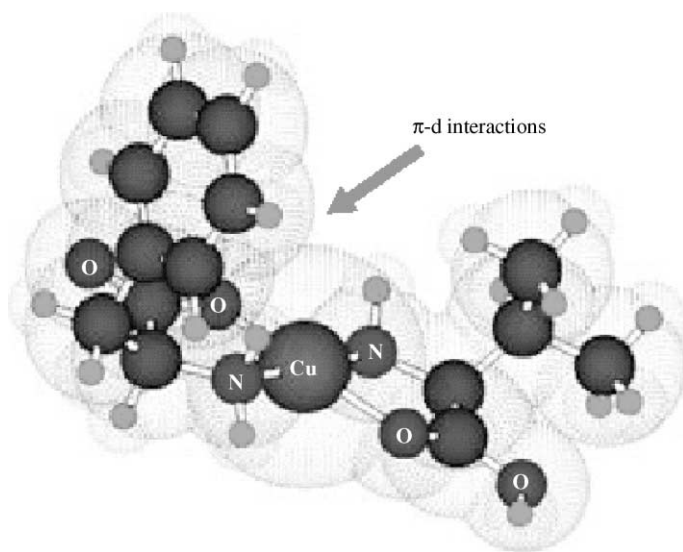


Fig. 15 π -Cation interactions responsible for chiral distinction observed in the recognition of *D,L*-valine using Cu(II) with *L*-phenylalanine as the reference. Calculations show overlap between the π orbitals of the phenyl group in *L*-phenylalanine and the d orbitals of Cu(II) in $[\text{Cu}^{\text{II}}(\text{L-Phe})(\text{L-Val})\text{-H}]^+$ (reproduced by permission of the American Chemical Society).

the interaction because it is located at the opposite side of the square planar structure (Fig. 15). This interpretation is consistent with the observation that the heterochiral dimeric fragment ions are more stable than the homochiral analogues in cases where an aromatic amino acid is used as either analyte or ref. As the size of the side-chain group on the analyte increases in the series: Ala < Leu < Val < Ile, the interactions between ref = L-Phe and the side group on the α -asymmetric carbon of the L-analyte are more and more inhibited. A increasingly large preference for the heterochiral complexes over the homochiral ones should result as well as a decrease of the corresponding R_{chiral} values (Table 10).

In this connection, the nature of the metal ion is expected to play an important role and the experimental data indeed show intriguing effects.³⁹³ In the case of amino acids, for example, Cu(II) offers much larger chiral selectivity than does Zn(II) or Ni(II), which is due to the formation of a square planar structure.³⁹⁴

The enantioselectivity factors in Table 10 indicate that amino acid samples with different enantiomeric excess (ee) should show differences in the $R = (I_R + I_S)/I_{\text{ref}}$ term. Indeed, $\ln R_{\text{chiral}}$ is linearly related to optical purity of the specimen and the relevant calibration curve can be established. Accordingly, it is possible to rapidly determine ee of an amino acid sample by a single measurement of R_{chiral} in a tandem mass spectrometer.^{390,391}

This behavior is typified by Clevudine (L-FMAU; 2'-fluoro-5-methyl- β ,L-arabinofuranosyluracil), a potent antiviral nucleoside against hepatitis B.³⁹³ To optimize its chiral discrimination, several metal ions have been checked together with a variety of amino acids as ref. Differently from amino acid analytes which clearly prefer Cu(II) as metal ion center, FMAU prefers transition metals as Co(II) and Zn(II) since these ions have a high affinity for its heteroaromatic ring which is distant from the stereocenters. Using *N*-acetyl-L-proline, as ref, and Co^{2+} as the metal ion, the data for various enantiomeric mixtures of FMAU display a linear relationship between $\ln R_{\text{chiral}}$ and ee with a correlation coefficient, r^2 , of 0.9995. This calibration curve is then used to measure the percent ee of various unknown samples. An average accuracy of 0.6% ee is obtained for this particular case from four unknown samples. Calibration curves can be constructed also by using slightly modified methods which require only one sample of the analyte with known optical purity.³⁹⁵ They can be used for days, and the method can be applied to samples that contain only few percent of one enantiomer. Calibration curves can be established for the simultaneous chiral analysis of different amino acids in mixtures.³⁹⁶ Quantitative enantiomeric determination of this sort can be made using protocols based not only on the kinetic method, but also on host-guest exchange reactions (*vide infra*). The same procedure has been applied to the chiral analysis of peptides,³⁹⁷⁻⁴⁰⁰ neurotransmitters,⁴⁰¹ thalidomide,⁴⁰² and antibiotics.⁴⁰³

ENANTIOSELECTIVE SELF-ASSEMBLING OF AMINO ACIDS

Is homochirality a consequence of life or did it precede life? In the latter case, the question is: what is the mechanism for homochirogenesis, i.e., the spontaneous

generation of homochirality? Homochirogenesis may be achieved by at least three fundamental mechanisms: (i) selective synthesis of only one enantiomer of a chiral molecule (symmetry breaking); (ii) preferential destruction of one enantiomer of a heterochiral mixture (chiral enrichment); and, (iii) separation of a racemic mixture into distinct homochiral parts (chiral transmission). Enantioselective self-assembling of chiral molecules may have important implications in the latter mechanism of homochirogenesis.

The term “self-assembling” describes a process in which a larger, complex structure is formed from smaller building blocks in a specific manner. Usually, self-assembling processes are driven by thermodynamics. The different species that could be formed are separated by rather low barriers so that finally the global minimum structure is realized. Which final structure of the resulting multi-component architecture is formed can be determined by programming the necessary structural information into the starting subunits. Binding sites must be present in just the right arrangement for the systems to assemble. With chiral building blocks, an enantioselective self-assembling process may take place in which the complex structure is constituted exclusively by a single enantiomeric form of a racemate.

The discovery and explanation of abiogenic sources of homochirality is an important step towards the explanation of the origin of life. Chirogenesis usually leads to racemates, but spontaneous symmetry breaking has been achieved through only a handful of methods. The spontaneous resolution of racemates during crystallization is an example of this kind of symmetry breaking. The formation of homochiral crystals from racemates suggests that chiral non-covalent interactions can greatly influence molecular aggregation. ESI-MS is an excellent method for generating molecular clusters from biologically important molecules, including amino acids and peptides, and for investigating their properties in the gas phase in the absence of medium effects.

The structure, the function, and the activity of biological molecules are greatly affected by hydrophobic, hydrogen-bonding, and electrostatic interactions between constituent amino acids, whose form in turn depends upon environmental conditions. In contrast with solution, the zwitterionic form of amino acids is destabilized in the gas phase due to the absence of solvation. For example, the N-terminus of glycine is not basic enough to deprotonate the carboxylic acid on its C-terminus,^{404,405} a result predicted by *ab initio* calculations.^{406–408} By contrast, the high basicity of the guanidino side-chain functional group of arginine makes it a better candidate for a gas-phase stable zwitterion.⁴⁰⁹ However, first experimental⁴¹⁰ and theoretical^{411,412} evidence seem to exclude a stable zwitterionic form for an isolated arginine monomer in the gas phase. On the other hand, recent experiments, supported by theory,⁴¹³ suggest that arginine in the presence of a net charge may exist in the zwitterionic state.^{414,415}

Theoretical calculations predict that, compared to other amino acids, arginine may dimerize and trimerize in the zwitterionic state.⁴¹⁶ Soft-sampling ESI of the racemate of arginine, with one of the enantiomer isotopically labeled, reveals the formation of stable trimers with NO_3^- present as counterion. No preference for

the chirality of the individual aminoacidic components is observed.⁴¹⁷ In the positive ion mode, ESI of arginine solutions leads to abundant singly- and multiprotonated clusters.⁴¹⁸ The singly-protonated cluster $[(\text{Arg})_n\text{H}]^+$ ($n = 4$) displays enhanced stability so as it is preferentially formed also by CID of larger clusters ($n > 4$). In the doubly-charged ion series, the dications $[(\text{Arg})_n\text{2H}]^{+2}$ ($n = 12-15$) have enhanced stability relative to those of immediately smaller size.

As for arginine, ESI-MS analysis of serine solutions reveals an unusually abundant protonated serine octamers $[(\text{Ser})_8\text{H}]^{+n}$ ($n = 1-3$), which demonstrate a strong preference for homochirality.^{419,420} In addition to them, the positive ion spectrum displays a series of Na^+ -bound serine octamers $[(\text{Ser})_8\text{nNa}]^{+n}$ ($n = 1-3$).⁴²¹ CID of protonated and sodiated serine octamers provides some information on their structure. Thus, $[(\text{Ser})_8\text{nH}]^{+n}$ ($n = 1-3$) show preferential fragmentation to the singly charged $[(\text{Ser})_n\text{H}]^+$ ($n = 6$), with small contribution of $[(\text{Ser})_n\text{H}]^+$ ($n = 4, 5$). By comparison, $[(\text{Ser})_8\text{nNa}]^{+n}$ ($n = 1-3$) show *inter alia* the formation of a variety of multicharged fragments with $[(\text{Ser})_n\text{Na}]^+$ ($n = 6$) as only a minor one. These results suggest that $[(\text{Ser})_8\text{H}]^+$ is composed of four hydrogen-bonded dimers, stabilized by further extensive proton bonding. The final drum-shaped structure has incomplete hydrogen bonding, i.e., lone pairs on oxygen and amino hydrogens atoms available for further interactions (Fig. 16). They can be regarded as “sticky ends” present on the top and bottom faces of the drum-shaped structure and are responsible of the formation of multicharged structures. The situation is rather different for $[(\text{Ser})_8\text{Na}]^+$ which, instead, exhibits the Na^+ ion inside the octamer in a crown-ether-like structure (Fig. 17a). The formation of multicharged sodiated structures is due in this case to simple hydrogen bonding between two $[(\text{Ser})_8\text{Na}]^+$ units (Fig. 17b). Density functional calculations and ion mobility experiments⁴²² support these models and show that the protonated homochiral octamer is energetically stabilized relative to its possible fragments (e.g., dimer plus protonated hexamer). The calculations also show that heterochiral octamers are less stable than homochiral octamers. For instance, $[(\text{L-Ser})_7\text{D-Ser-H}]^+$ is 2.1 kcal mol⁻¹ less stable than $[(\text{L-Ser})_8\text{H}]^+$.

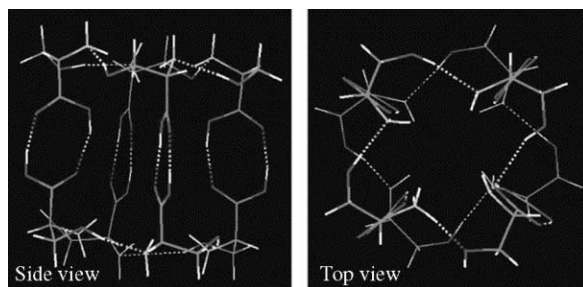


Fig. 16 Calculated HF/6-31G structure (two views) of the protonated serine octamer: left, side view; right, top-down view (reproduced by permission of the American Chemical Society).

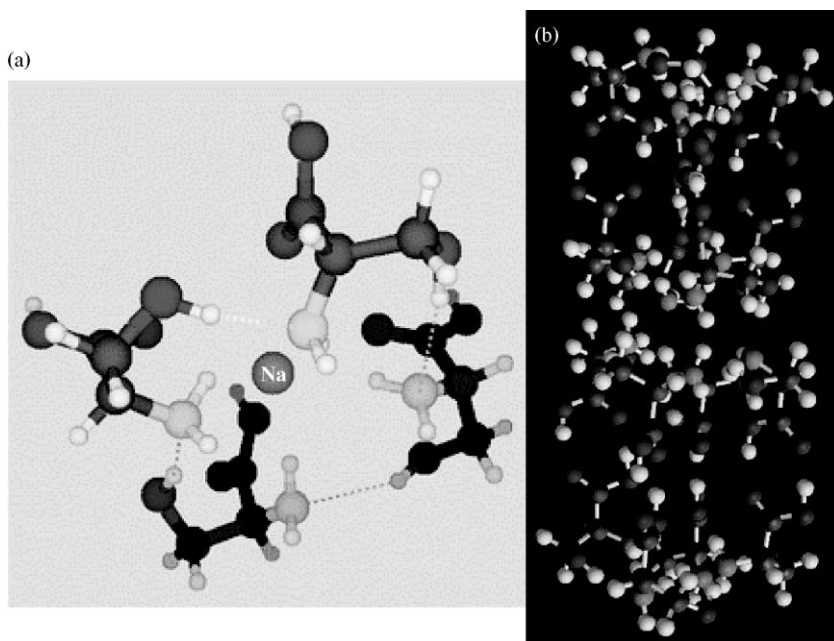


Fig. 17 (a) Calculated position of Na^+ near one face of the serine octamer; (b) calculated structure of $[(\text{Ser})_{16} + 2\text{Na}]^{2+}$ (reproduced by permission of The Royal Society of Chemistry).

Differently from serine, ESI-MS analysis of homoserine (HSer) solutions reveals an unusually abundant diprotonated homoserine octamers $[(\text{HSer})_8\text{2H}]^{+2}$, but not the expected monoprotinated $[(\text{HSer})_8\text{H}]^+$ one.⁴²² A 3/1 mixture of L-serine and L-homoserine yields abundant mixed serine octamers with the incorporation of one or two homoserine molecules into the cluster. CID of the isolated $[(\text{Ser})_6(\text{HSer})_2\text{H}]^+$ cluster leads to the preferentially loss of two neutral serine molecules. Homoserine is always retained. The ESI-MS spectral patterns of threonine and allothreonine solutions is similar to that of homoserine. A 1/1 mixture of D-serine and D-threonine yields abundant mixed singly- and doubly-charged octamers incorporating from 2 to 6 threonine molecules. Their relative abundance indicates that threonine may incorporate freely into serine clusters because the additional methyl group does not interfere with the bonding of the cluster.

ESI-MS of cysteine solutions yields only the singly protonated hexamer $[(\text{Cys})_6\text{H}]^+$. No preference for the chirality of the individual aminoacidic components is observed.⁴²³ Addition of cysteine to a serine solution yields abundant homochiral mixed octamer $[(\text{L-Ser})_{8-m}(\text{L-Cys})_m\text{H}]^+$ ($m = 0-2$). No $[(\text{L-Ser})_{8-m}(\text{D-Cys})_m\text{H}]^+$ ($m = 1, 2$) octamers, but only $[(\text{L-Ser})_8\text{H}]^+$ are observed by using the wrong D-cysteine enantiomer. A similar picture is observed by replacing cysteine with other aminoacid, such as aspartic acid, asparagine, leucine, and methionine.

The enantioselective incorporation of these amino acids into the serine octamers represents an example of chiral transmission to elementary biomolecules and a possible way of chirality amplification on primitive earth.

HOST–GUEST INCLUSION COMPLEXES

Chiral crown ether hosts

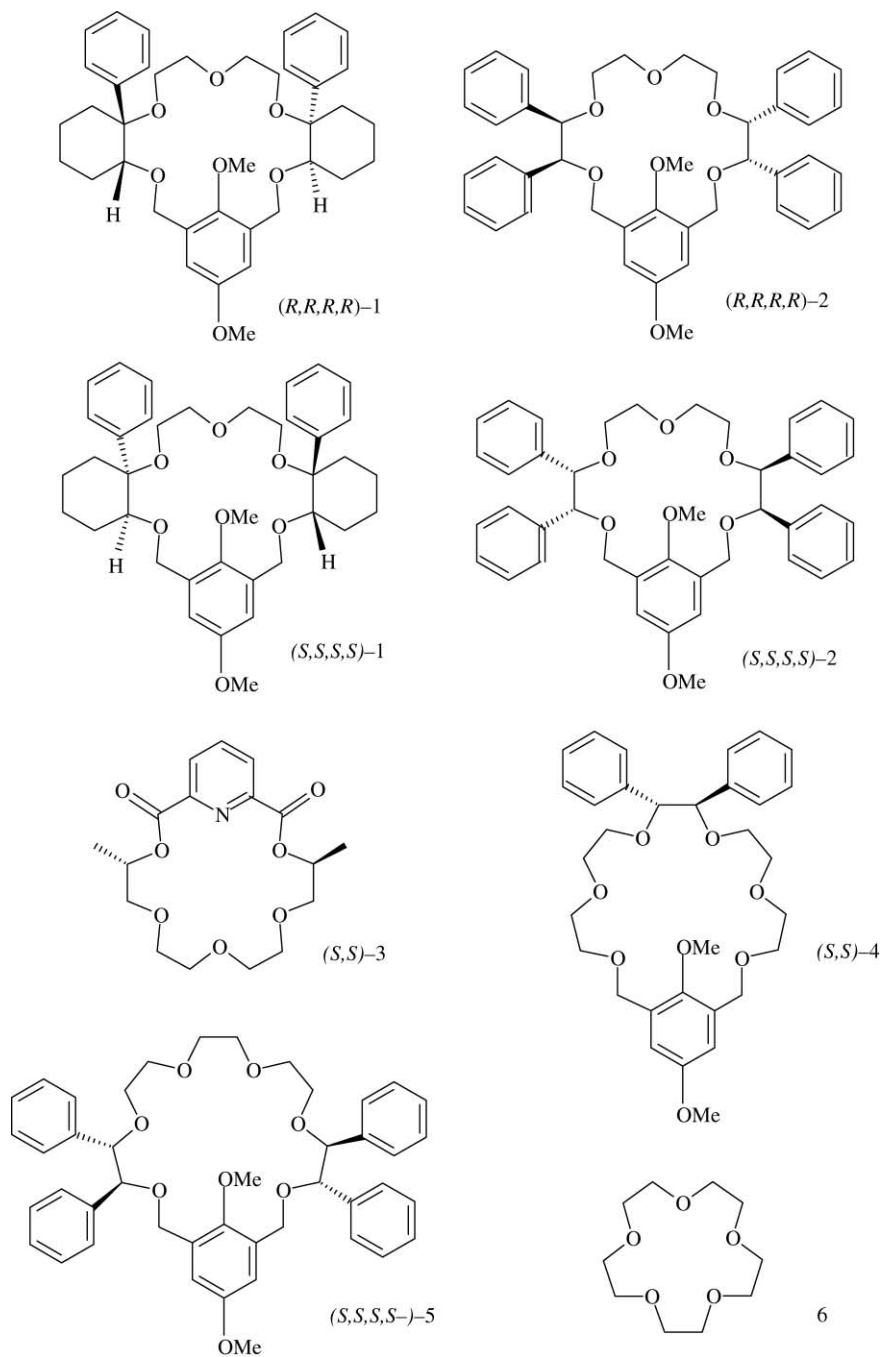
Multiple hydrogen bonding is responsible for the exceedingly high affinity of ammonium ions towards crown ethers. Thus, when employed as chiral selectors, crown ethers reveals particularly suitable for chiral recognition of a variety of ammonium ion derivatives.^{351,352,354,356,359} Research in this area has been first directed towards the enantiodifferentiation of chiral ions, normally generated by FAB or ESI. Later on, the relative stability of diastereomeric crown ether–ammonium ion complexes was investigated by FT-ICR equilibrium measurements of the exchange of chiral and achiral hosts in chiral guests. More recently, the performance of the ESI sources of generating ions from non-volatile compounds enabled ESI-FT-ICR studies of the exchange of the chiral and achiral guests in a chiral host.

There are several methods to enantiodifferentiate chiral ammonium ions by FAB-MS. One is the so-called enantiomer-labeled (EL) guest method.⁴²⁴ The method is based on the preparation of a mixture containing the enantiopure host (denoted as U) and the racemate of the guest. One of the guest enantiomers is isotopically labeled (e.g., $[M_S^d]^+$) and the other is not (e.g., $[M_R]^+$). Consequently, the signals for the two diastereomeric host–guest pairs (i.e., $[U\cdot M_R]^+$ and $[U\cdot M_S^d]^+$ of equations (21) and (22)) appear at different m/z ratios.



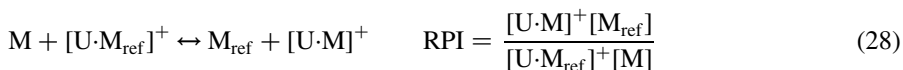
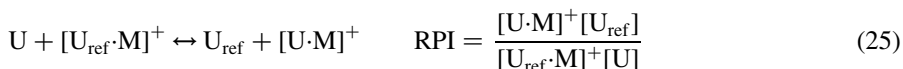
If no thermodynamic isotope effect is operative, the relative stability of the diastereomeric $[U\cdot M_R]^+$ and $[U\cdot M_S^d]^+$ complexes can be represented approximately by their relative peak intensity, i.e., the IRIS value ($IRIS = [U\cdot M_R]^+ / [U\cdot M_S^d]^+$). Usually, isotope effects on non-covalent binding are small. However, both stereochemical and isotope effects can easily be separated by performing a control experiments using the other enantiomer of the host under the same conditions.

This experimental procedure has been applied to the crown ethers **1** and **2** of Scheme 5, first with FAB as the ionization method,^{425,426} later with ESI-MS.^{427,428} A number of amino acid methyl esters have been used as guests, including those of methionine (Met–O–Me), phenylalanine (Phe–O–Me), and phenylglycine (Pgly–O–Me). For instance, the FAB spectra of Met–O–Me/(*R,R,R,R*)-**1** reveal that the host recognizes (*R*)-Met–O–Me much better than (*S*)-Met–O–Me (over five-fold excess). Chiral recognition of Met–O–Me by (*R,R,R,R*)-**2** is much less pronounced. Quite surprisingly, the large 5.3:1 excess of (*R*)-Met–O–Me /(*R,R,R,R*)-**1** over



Scheme 5

(*S*)-Met-O-Me/(*R,R,R,R*)-**1** in the FAB spectra reduces to ca. 1.5:1, if ESI is used to generate the ionic complexes. This observation appears to be general for all host-guest pairs studied and it was attributed to the electrospray process, although no real explanation was advanced as to the observed ESI effect on stereochemistry.^{427,428} Enantiomer labeling can also be applied to the host.^{428–430} An enantiopure guest is combined with a 1:1 mixture of the enantiomers of the host, one of them isotopically labeled. This enantiomer-labeled host method have been applied using (*R,R,R,R*)-**2** and [d₆]-(*S,S,S,S*)-**2** labeled at the two methyl groups. After calibration, the method can also be used to determine the enantiomeric excess of an unknown mixture of the guest enantiomers. Extension of these methods to spiroacetal polyethers have been reported.⁴³¹



Another method for enantiodifferentiating chiral ammonium ions by FAB-MS is called the relative peak intensity (RPI) method. It does not require labeling procedures, but rather it is based on two independent measurements of each host enantiomer (i.e., U_R and U_S) with a given guest (M) relative to an achiral reference host (U_{ref}) or guest (M_{ref}) (equations (23)–(25) and (26)–(28), respectively). According to equation (25), the RPI value, derived from the combination of equations (23) and (24), can be regarded as a measure of the degree of cation transfer equilibria (25). Two RPI values (RPI_R and RPI_S) can be measured, depending upon the configuration of the guest (i.e., M_R and M_S). Because U_{ref} is achiral, the relationship $\text{RPI}_R/\text{RPI}_S = [U \cdot M_R]^+/[U \cdot M_S]^+$ holds, provided that $[U]/[U_{\text{ref}}]$ remains constant in the two sets of experiments. In a similar way, the RPI value, derived from the combination of equations (26) and (27), can be regarded as a measure of the degree of cation transfer equilibria 28. Again, two RPI values (RPI_R and RPI_S) can be measured, depending upon the configuration of the chiral guest (i.e., M_R and M_S). Because M_{ref} is achiral, the relationship $\text{RPI}_R/\text{RPI}_S = [U \cdot M_R]^+/[U \cdot M_S]^+$ holds, provided that $[M_R]/[M_{\text{ref}}] = [M_S]/[M_{\text{ref}}]$ in the two sets of experiments. These methods have been used to study chiral recognition properties of crown ether (*S,S*)-**3** with a several ammonium ions (M_R and M_S), including N-protonated α -methylbenzylamine and 1-(1-naphthyl)ethylamine. The method has been extended to a variety of other crown ethers (Scheme 5).^{432–436} A 1.17-fold preference of the host for N-protonated (*R*)-(+)-1-(1-naphthyl) ethylamine over the

(*S*)-(–)-enantiomer was observed with (*S,S*)-**3**, which further increases to 1.70:1 ratio upon replacement of the two methyl groups of (*S,S*)-**3** with phenyl substituents.⁴³²

Chiral selectivity factors, $RPI_R/RPI_S = [U \cdot M_R]^+ / [U \cdot M_S]^+$ as defined in equation (25), for a variety of host-guest inclusion complexes are reported in Table 11.^{434,435} Thus, chiral crown ethers (*S,S*)-**4** and (*R,R,R,R*)-**2** bind the (*R*)-enantiomers of the selected guests more strongly than the (*S*)-enantiomers. In contrast to (*R,R,R,R*)-**2**, crown (*S,S,S,S*)-**5** shows no chiral differentiation. This result is rationalized in terms of structural complementarity of the relevant host–guest complex ions. The larger size of the crown ring and the accompanying shift of the attached phenyl groups (chiral barriers) result in looser intermolecular complementarity with the guest ammonium ion, even if a sterically bulky naphthyl unit exists.

The studies discussed in this section use MS in order to compare chiral recognition as it occurs in a medium (a solvent in ESI-MS, a matrix in FAB-MS). Although one might argue that the only difference is the stereochemistry and, thus, the solvent and the ionization conditions should not have a distinct influence, the differences between FAB and ESI-determined chiral selectivity should be a clear warning. Consequently, clear-cut determinations of intrinsic chiral recognition in the gas phase must rely on true gas-phase equilibrium and kinetic studies. Such investigations with host **3** and, among others, the α -methylbenzylamine and 1-(1-naphthyl)ethylamine guests have been performed.^{437,438} Both procedures in equations (23)–(28) were used in these studies. The protonated host ions were generated in the ESI source of a FT-ICR mass spectrometer and were allowed to react with the chiral amine and an achiral reference until equilibrium was reached. A second experiment with the other enantiomer of the chiral guest provides the chiral selectivity factor, $RPI_R/RPI_S = [U \cdot M_R]^+ / [U \cdot M_S]^+$ as defined in equations (25) and (28), wherefrom the difference in the free energies of binding for the two guests can be derived.

The procedure has been applied to the gas-phase exchange equilibria of the N-protonated (*R*)-(+) and (*S*)-(–) α -methylbenzylamine ligands between chiral (*S,S*)-**3** and the achiral 18-crown-6, as reference (U_{ref}).⁴³⁷ The achiral crown ether U_{ref}

Table 11 Chiral selectivity factors, $RPI_R/RPI_S = [U \cdot M_R]^+ / [U \cdot M_S]^+$ (equation (25)) for chiral crown ethers complexed with enantiomeric alkylammonium ions ($U_{ref} = 6$ in Scheme 5)

U	M	$RPI_R/RPI_S = [U \cdot M_R]^+ / [U \cdot M_S]^+$
(<i>S,S</i>)- 4	N-Protonated 1-amino-2-propanol	1.0
(<i>S,S</i>)- 4	N-Protonated 1-(1-naphthyl)ethylamine	1.2
(<i>S,S</i>)- 4	N-Protonated α -methylbenzylamine	1.1
(<i>S,S</i>)- 4	N-Protonated phenylalanine methyl ester	0.9
(<i>R,R,R,R</i>)- 2	N-Protonated 1-(1-naphthyl)ethylamine	1.2
(<i>R,R,R,R</i>)- 2	N-Protonated phenylalanine methyl ester	1.5
(<i>S,S,S,S</i>)- 5	N-Protonated 1-(1-naphthyl)ethylamine	1.0
(<i>S,S,S,S</i>)- 5	N-Protonated phenylalanine methyl ester	1.1

displays an affinity for the N-protonated (*R*)-(+)- and (*S*)-(–)- α -methylbenzylamine ligands which is higher than that of the chiral crown ether (*S,S*)-**3**. The equilibrium constants for reactions 25 with the N-protonated (*R*)-(+)- and (*S*)-(–)- α -methylbenzylamine ligands amount to 130 ± 15 and 567 ± 68 , respectively, which correspond to a difference of 1.0 ± 0.1 kcal mol⁻¹ between the stability of the heterochiral [(*S,S*)-3-H-(*R*)-(+)- α -methylbenzylamine]⁺ complex and the homochiral [(*S,S*)-3-H-(*S*)-(–)- α -methylbenzylamine]⁺ one. This stability difference is greater than that measured in methanol solution (0.5 kcal mol⁻¹), but similar to that seen in CD₂Cl₂ (1.1 kcal mol⁻¹).⁴³⁹ This provides experimental support to the concept that solvation moderates those short-range intracomplex forces that play a major role in chiral discrimination, such as the π - π stacking interactions between the N-protonated (*R*)-(+)- and (*S*)-(–)- α -methylbenzylamine guests and the host (*S,S*)-**3**.

With the same methodology, it was possible to quantify the gas-phase exchange equilibria of the (*R*)-enantiomer of the chiral amines (*M_R*), sec-butylamine, 1-cyclohexylethylamine, α -methylbenzylamine, and 1-(1-naphthyl)ethylamine with protonated (*S,S*)-**3** ([U_{SS}]⁺) or protonated (*R,R*)-**3** ([U_{RR}]⁺).⁴³⁸ One among the selected amines was introduced together with a reference achiral amine (*M_{ref}*), i.e., isopropylamine or cyclohexylamine, into the FT-ICR cell, where they react with [U_{SS}]⁺ or [U_{RR}]⁺ to form the corresponding [U_{SS}-*M_R*]⁺ and [U_{RR}-*M_R*]⁺ adducts. The equilibrium constant for the exchange of the chiral and the achiral amine guests (equation (28)) was determined from the relevant RPI = [U·*M_R*]⁺/[U·*M_{ref}*]⁺ ratios and the enantioselectivity of the process was inferred from their RPI_R/RPI_S = [U_{RR}-*M_R*]⁺/[U_{SS}-*M_R*]⁺ ratio. As observed before, binding of the guest with the absolute configuration opposite to that of the stereocenters of [U]⁺ is invariably preferred. The enantiomeric preference of [U_{SS}]⁺ vs. [U_{RR}]⁺ towards *M_R* is expressed by the relevant $\Delta\Delta G^0 = \Delta G^0([U_{RR}\text{-}M_R]^+) - \Delta G^0([U_{SS}\text{-}M_R]^+)$ terms which amount to 0.07 ± 0.10 kcal mol⁻¹ (sec-butylamine), 0.21 ± 0.05 kcal mol⁻¹ (1-cyclohexylethylamine), 0.57 ± 0.12 kcal mol⁻¹ (α -methylbenzylamine), and 0.84 ± 0.14 kcal mol⁻¹ (1-(1-naphthyl)ethylamine). This trend corroborates the hypothesis that the π - π stacking interactions between the guest and the host as well as the steric hindrance to complexation represent main intrinsic factors for chiral recognition. Another important factor, which is entropic in nature, may be related to the conformational space available for the most favorable complexation geometry. Molecular modeling points to a facile attainment of the best complexation geometry for the systems of Scheme 5, but this may occur at the expenses of entropically unfavorable partial locking of methyl rotors and it is probable that the degree to which this occurs differs for the two enantiomers. Indeed, space-filling models of the complexes suggest that partial locking of the methyl rotors is more important for the homochiral complex.

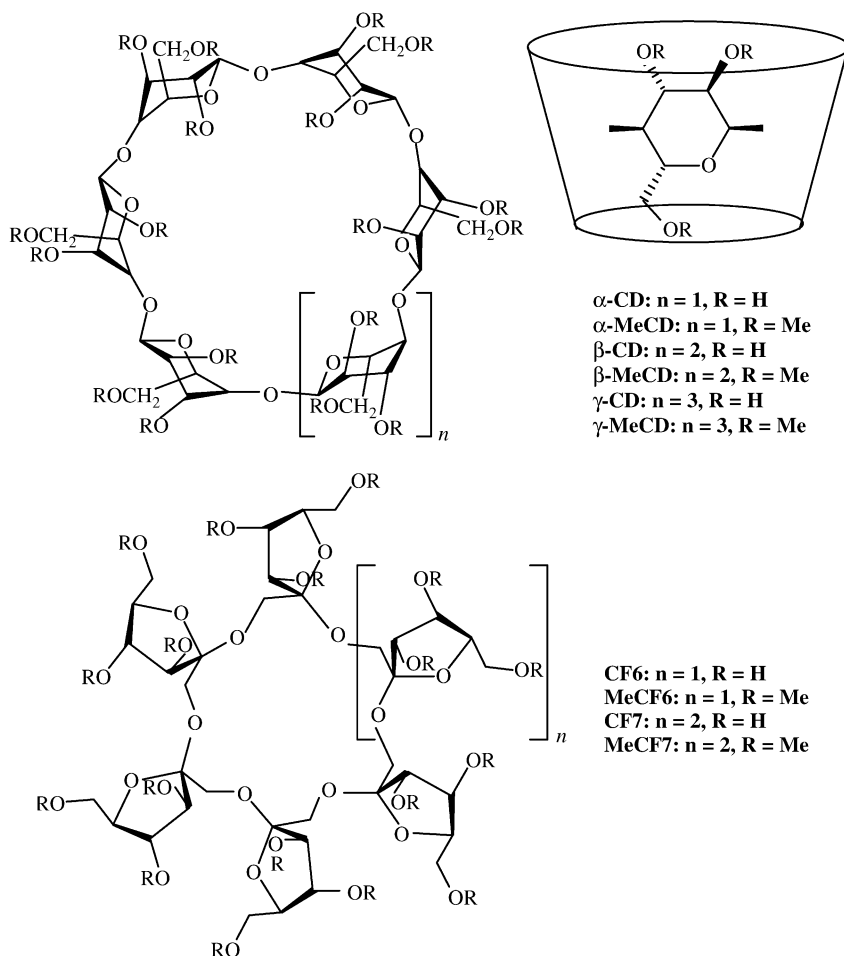
Using cyclohexylamine, as *M_{ref}*, the data for various enantiomeric mixtures of 1-(1-naphthyl)ethylamine (*M*) display a linear relationship between RPI_R/RPI_S and ee. Enantiomeric impurities as small as about 2% can currently be detected with this method.⁴⁴⁰ Variable-temperature FT-ICR-MS measurements of the ligand

exchange equilibria on the diastereomeric complexes between α -methylbenzylamine (and 1-(1-naphthyl)ethylamine) and protonated (*S,S*)-**3** ($[U_{SS}]^+$) and (*R,R*)-**3** ($[U_{RR}]^+$) allowed to establish the enthalpy and entropy contribution to their thermodynamic stability.⁴⁴¹ Thus, the heterochiral $[U_{SS}M_R]^+$ complexes have more favorable enthalpy in both cases than the homochiral $[U_{RR}M_R]^+$ complexes; the differences are: -1.6 ± 0.2 kcal mol⁻¹ for α -methylbenzylamine and -2.4 ± 0.3 kcal mol⁻¹ for 1-(1-naphthyl)ethylamine. Entropy disfavors the heterochiral complexes by -3.5 ± 0.5 cal mol⁻¹ K⁻¹ for α -methylbenzylamine and by -4.8 ± 0.9 cal mol⁻¹ K⁻¹ for 1-(1-naphthyl)ethylamine. Enthalpy–entropy compensation is evident. The results suggest that enantiodiscrimination in these complexes is enthalpic and that locking of methyl rotors in the thermodynamically disfavored complexes is probably not important. Although theoretical calculations correctly conform to the observed heterochiral > homochiral stability trend, nevertheless they failed to reproduce the experimental finding that enantiodiscrimination of 1-(1-naphthyl) ethylamine is greater than that of α -methylbenzylamine.

Cyclic oligosaccharide hosts

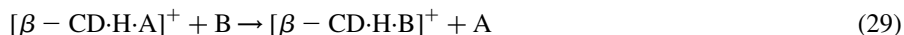
Cyclodextrins (CDs) are a group of cyclic oligosaccharides composed of α (1,4)-linked glucopyranose units. The most common have six, seven, and eight units with the common names α -, β -, and γ -CD, respectively. The utility of CDs stems from their truncated-cone molecular shape with a sizable inner cavity (Scheme 6). In water, cyclodextrins (CDs) are believed to form inclusion complexes that are mostly stabilized by hydrophobic interactions between the unpolar surface inside the CD cavity and the surface of the guest. In the gas phase, the energetics that benefit from this arrangement do not exist any more, because there is no water that surrounds the complex. Consequently, there are no benefits from hydrophobic interactions in the gas phase. Rather, van der Waals' forces and, if possible, hydrogen bonding remain. However, the gas-phase complexes are ions, usually positive ions generated by MALDI, FAB, or ESI. For example, the higher basicity of an amino group will lead to the generation of CD complexes with the ammonium form of an amino acid. Strong interactions can be expected for a host with so many hydroxy dipoles that may arrange in a favorable fashion around the cationic guest. For a maximization of the number of such interactions, it is likely that the guest is located inside the cavity to provide a geometrically reasonable fit between guest and cavity. The conclusion from these considerations is that the complexes exist in solution as well as in the gas phase, but for different reasons.

Because of their asymmetry, CDs exhibit chiral effects towards chiral molecules under FAB⁴⁴² and MALDI⁴⁴³ conditions. The main ambiguity of these studies remains regarding the environment in which chiral recognition occurs, whether in the bulk matrix, in the seldge vaporization region, or in the gas phase. Besides, neither MALDI nor FAB ensure attainment of purely kinetic or equilibrium conditions so as that quantitative interpretation of the MS patterns in terms of relative stability of diastereomeric host/guest intermediates or transition structures



Scheme 6

is precluded. For this reason, the problem of gas-phase CDs enantioselectivity was tackled by Lebrilla et al. from the kinetic side by using an FT-ICR methodology.^{355,444} Protonated β -cyclodextrin/amino acid complexes ($[\beta\text{-CD}\cdot\text{H}\cdot\text{A}]^+$), isolated in the reaction cell of an FT-ICR instrument, react with gaseous alkyl amine (B) to undergo the gas-phase guest-exchange reaction 29.



The rate of reaction 29 is found to be sensitive to the configuration of the guest A, making β -CD a gas-phase chiral selector. Its enantioselectivity, defined by the measured k_D/k_L ratio, is as large as far k_D/k_L is from unit. Table 12 indicates that the β -CD increases from alanine ($k_D/k_L = 0.62$) to valine ($k_D/k_L = 0.32$), leucine

Table 12 Reaction selectivity (k_D/k_L) of various protonated β -CD/amino acid complexes with 1-propylamine

Amino acid	$k_L (\times 10^{11} \text{ cm}^3 \text{ molecule}^{-1} \text{ s}^{-1})$	k_D/k_L
Ala	2.4	0.62
Cys	3.4	0.45
Glu	0.011	0.53
Ile	1.0	0.26
Alle ^a	1.9	0.24
Leu	0.50	0.28
Met	0.014	2.70
Phe	1.4	1.22
Pro	1.2	0.67
HPro ^b	0.031	0.71
Ser	0.64	0.83
HSer	0.35	0.45
Thr	0.12	1.59
AThr ^c	0.18	0.045
Val	3.1	0.32

^aAlle, allo-isoleucine.

^bHPro, *cis* - 4-hydroxyproline.

^cAThr, *allo*-threonine.

($k_D/k_L = 0.28$), isoleucine ($k_D/k_L = 0.26$), and *allo*-isoleucine ($k_D/k_L = 0.24$) when B = 1-propylamine.^{444–446} Even when the side chain is hydroxylated, which would make the interaction with the CD cavity favorable, the enantioselectivity increases with the size of the side chain (cf. HSer, Thr, and AThr with Ser in Table 12). Proline and *cis* - 4-hydroxyproline (HPro) have low selectivities because these molecules are rigid and compact. However, phenylalanine ($k_D/k_L = 1.22$) and tyrosine ($k_D/k_L = 1.49$) with relatively bulky substituent groups exhibit significantly smaller enantioselectivities. Similar trends are obtained when more basic alkylamines B are used, including 2-butylamine and 1-amino-2-propanol.⁴⁴⁷ These results indicate that increasing the size of the side chain of A increases enantioselectivity to a point (Fig. 18).

According to molecular modeling,^{445,446} the different enantioselectivities of Table 12 can be accounted for by the structure of the relevant $[\beta\text{-CD}\cdot\text{H}\cdot\text{A}]^+$ complexes. Leucine, isoleucine, and *allo*-isoleucine with four carbons in the side chain have the optimal size to fit into the permethylated β -CD cavity, while phenylalanine and tyrosine with seven carbons are too large to fit into the same cavity. Noticeable differences in the interactions of the two enantiomers of A with the permethylated β -CD host are observed. Chiral differentiation occurs when the access to the protonated amino group of A is limited either by its alkyl side chain or by the methoxy groups of the host that are drawn in by hydrogen-bonding interactions. These differences in binding translate to differences in reaction rates.

Phenylalanine behaves differently from valine in permethylated β -CD. Both L- and D-phenylalanine interact in the same way. In fact, the predominant interaction of

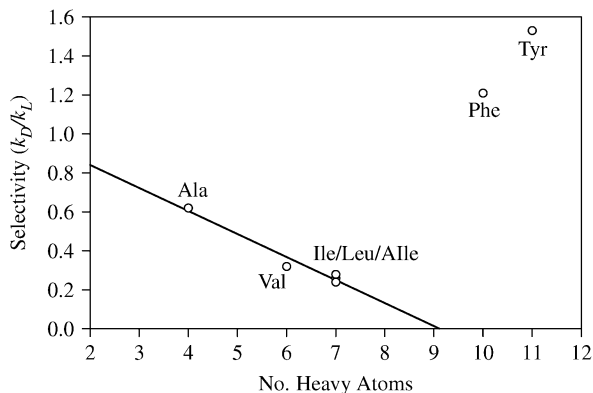
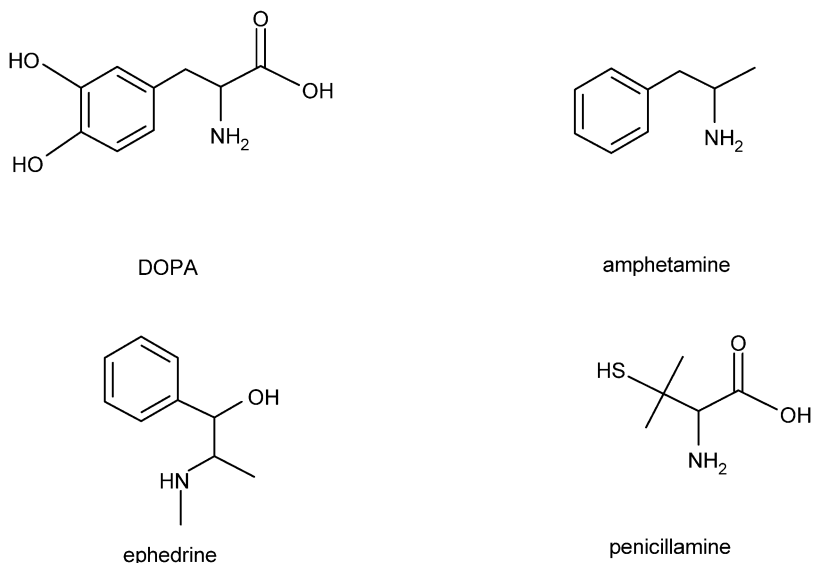


Fig. 18 Chiral selectivity (k_D/k_L) as a function of the number of non-hydrogen atoms on the amino acid. Hosts: permethylated β -CD; reagent base: 1-propylamine. Chiral selectivity tends to increase with the size of the amino acids. Phe and Tyr, however, do not follow this trend.

both the ammonium and the carboxylic acid group of phenylalanine forces its phenyl group to remain inside the cavity. The similarity in the binding of the two enantiomers is responsible of the observed small enantioselectivity ($k_D/k_L = 1.22$). In contrast, both the ammonium and the carboxylic acid group of L-valine interacts preferentially with the narrow rim of permethylated β -CD, whereas only the ammonium of D-valine interacts in the same way and its carboxylic acid group interacts preferentially with the wider rim of the host. Such a difference in the binding of the two enantiomers accounts for the observed high (and reverse) enantioselectivity ($k_D/k_L = 0.32$).

Additional experiments were performed to examine the role of the molecular size of the host enantioselectivity. Since the methyl groups in methylated β -CD orient themselves toward the center of the cavity, it is expected that decreasing the extent of methyl derivatization in β -CD from 21 (the permethylated β -CD) to 14 methyl groups increases the effective size of the cavity.⁴⁴⁵ As a matter of fact, the enantioselectivity of valine ($k_D/k_L = 0.32$ with 21-methyl β -CD) increases to $k_D/k_L = 0.18$ with 14-methyl β -CD. No significant effect of the cavity size is observed with the smaller alanine.

Another way to increase the host cavity is by using exchange reactions in γ -CD (diameter of the cavity from 7.5 to 8.3 Å) instead of β -CD (diameter of the cavity from 6.0 to 6.5 Å).⁴⁴⁵ The larger cavity size of γ -CD decreases (and inverts) the enantioselectivity of valine from $k_D/k_L = 0.32$ to $k_D/k_L = 1.41$ and that of isoleucine from $k_D/k_L = 0.26$ to $k_D/k_L = 2.28$. This observation indicates that the three amino acids have optimal enantioselectivity with β -CD. Conversely, phenylalanine increases in selectivity from $k_D/k_L = 1.2$ (with β -CD) to $k_D/k_L = 1.8$ (with γ -CD). This observation suggests that the larger cavity of γ -CD allows each enantiomer of the larger amino acid to find more distinct interactions with the larger host.



Scheme 7

The gas-phase guest-exchange reaction 29 has been employed to probe the enantioselectivity of permethylated β -CD for pharmacologically important compounds, such as DOPA, amphetamine, ephedrine, and penicillamine (Scheme 7).⁴⁴⁸

A variety of alkyl amines B, including 1-propylamine, ethylene diamine, 1,3-diaminopropane, and (*R*)-1-amino-2-propanol have been used as reactants. The guest exchange kinetic results are reported in Table 13. The presence of more than one reacting $[\beta\text{-CD}\cdot\text{H}\cdot\text{A}]^+$ structure is observed with A = DOPA and penicillamine. The results have been rationalized in terms of specific interactions in the relevant inclusion complexes which determine their structure and relative stability.

Closely related analogues of cyclodextrins are the cyclofructans (CFs), depicted in Scheme 6. Permethylated six- (MeCF₆) and seven-membered CFs (MeCF₇) exhibit an appreciable enantioselectivity towards a number of amino acid isopropyl esters using the FAB-MS-EL (amino ester) guest method.^{449–451} The relevant IRIS values are reported in Table 14 and compared with those obtained by using CDs and crown ethers, as chiral selectors. Relative to these, MeCF₆ shows a higher enantioselectivity for the esters of tryptophan and tert-leucine, while MeCF₇ for the esters of phenylglycine, serine, and proline.

Linear oligosaccharide hosts

The maltose-based oligomers are exact linear analogues of CDs. For example, maltoheptaose is composed of seven α (1-4)-linked glucose units such as β -CD. Its linear chain is sufficiently flexible to wrap around guest molecules and form “quasi-inclusion” complexes in the gas phase.⁴⁴⁷

Table 13 Selectivities for the CD hosts ($k \times 10^{11} \text{ cm}^3 \text{ molecule}^{-1} \text{ s}^{-1}$)

Guest	1-Propylamine	(<i>R</i>)-1-amino-2-propanol	Ethylene diamine	1,3-Diaminopropane
DOPA				
k_D	$< 10^{-15}$	$< 10^{-15}$	0.0024	Fast: 0.131; slow: 0.014
k_L	$< 10^{-15}$	0.0047	0.0121	Fast: 0.122; slow: 0.0131
k_D/k_L	–	–	0.20	Fast: 1.07; slow: 0.46
Amphetamine				
k_D	0.27	1.34	–	–
k_L	0.40	1.78	–	–
k_D/k_L	0.68	0.75	–	–
Ephedrine				
$k_{(+)}$	0.031	0.53	–	–
$k_{(-)}$	–	0.64	–	–
$k_{(+)}/k_{(-)}$	–	0.83	–	–
Penicillamide				
k_D	Fast: 1.80; slow: 0.55	–	–	–
k_L	3.4	–	–	–
k_D/k_L	Fast: 0.53; slow: 0.16	–	–	–

Table 14 I_R/I_{S-Dn} values of permethylated cyclic oligosaccharide hosts with amino acid ester hydrochloride guests

Guest (counterion, Cl ⁻)	MeCF6	MeCF7	α -MeCD	β -MeCD	γ -MeCD	18-C-6
[Trp-O-Pr ⁱ] ⁺	1.38	1.29	1.29	1.23	1.17	0.98
[Pgly-O-Pr ⁱ] ⁺	0.99	0.76	0.94	0.91	0.89	0.99
[Phe-O-Pr ⁱ] ⁺	1.00	1.01	1.02	1.01	1.00	1.02
[Tle-O-Pr ⁱ] ⁺	1.18	1.00	0.95	0.94	0.93	0.97
[Met-O-Pr ⁱ] ⁺	1.04	0.95	0.91	0.91	0.92	0.96
[Ser-O-Pr ⁱ] ⁺	1.01	1.18	0.95	1.15	0.99	0.96
[Pro-O-Pr ⁱ] ⁺	1.08	1.16	1.07	1.07	1.14	0.96
[Gly-O-Pr ⁱ] ⁺	1.01	0.99	0.97	0.98	–	0.99

Phenomenological chiral discrimination of various permethylated linear oligosaccharides toward organic amines has been examined by using the FAB-MS-EL guest method.^{451–454} As shown in Table 15, permethylated fructo-oligosaccharides, especially the permethylated 1^F-fructonystose (MeFruNys in Scheme 8), display a remarkable chiral discrimination ability.⁴⁵² If compared to MeCF₆,^{450,455,456} linear permethylated fructo-oligosaccharides exhibit a much greater enantioselectivity due to their low molecular symmetry and high flexibility. The dynamic conformation changes of linear fructo-oligosaccharides emphasize the difference in the host/guest complex stability.

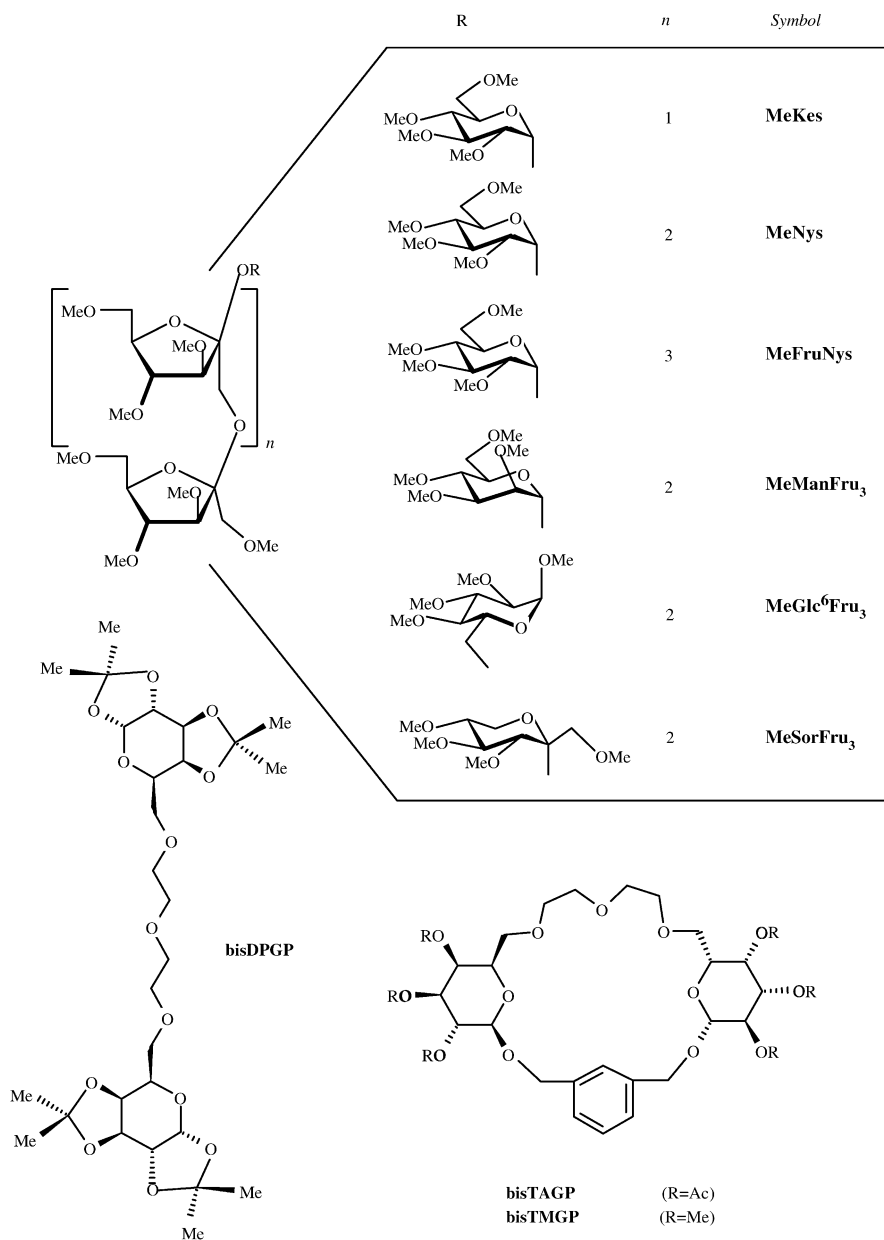
Along this line, several new linear hosts and flexible cyclic hosts having a C₂-symmetry axis (bisDPGP, bisTAGP, and bisTMGP; Scheme 8) have been designed and synthesized based on the structural feature of the highly selective MeFruNys.⁴⁵⁷ However, these tailor-made flexible hosts prove less effective than MeFruNys as chiral selector (Table 15).

Exchange experiments of aminoacids “wrapped” in permethylated linear oligosaccharides were carried out in a ESI-FT-ICR instrument.⁴⁴⁷ Table 16 lists the k_D/k_L values for the exchange reactions of a selected group of amino acids complexed to permethylated maltoheptaose and reacted with 1-propylamine. The enantioselectivities of the exchange reactions are slightly less than those with CDs for most amino acids. However, the same trend is observed as a function of the side-chain size of the guests. Remarkably, the reaction on the maltoheptaose complexes with tyrosine and phenylalanine exhibits a significantly greater enantioselectivity relative to β -CD. For example, the k_D/k_L value for phenylalanine decreases from 1.21 with β -CD to 0.25 with maltoheptaose. A plot with maltoheptaose and the aminoacids with alkyl side chains shows that phenylalanine and tyrosine are now in linear agreement with the other aminoacids (Fig. 19).

Molecular modeling calculations give important insight into the origin of such a large enantioselectivity. Unlike the rigid β -CD, the linear maltoheptaose allows each enantiomer of phenylalanine to find the most favorable conformation. The phenyl group of L-phenylalanine is oriented towards the C6 center of the hosts, while that of D-phenylalanine is oriented towards the C2 and C3 centers of the hosts.

Table 15 Chiral discrimination ability (I_R/I_{S-Dn} values) of permethylated cyclic and acyclic oligosaccharide hosts toward amino acid 2-propyl ester salts by FAB-MS

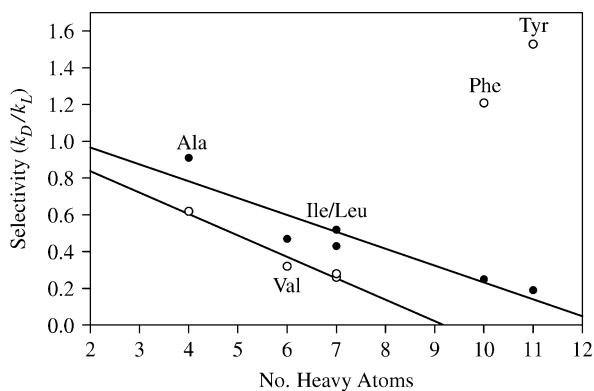
Guest	MeKes	MeNys	MeFruNys	MeManFru ₃	MeGlc ⁶ Fru ₃	MeSorFru ₃	18C6	MeCF6	bisDPGP	bisTAGP	bisTMGP
[Ala-O-Pr ⁱ] ⁺	1.11	1.16	0.45	1.09	0.60	0.80	0.99		1.43	1.46	1.40
[Val-O-Pr ⁱ] ⁺	1.19	0.87	0.14	0.84	0.49	0.51	1.00		0.85	1.39	1.18
[Met-O-Pr ⁱ] ⁺	1.18	1.54	0.28	1.28	0.79	0.83	1.01	1.04	1.33	1.50	1.27
[Phe-O-Pr ⁱ] ⁺	1.15	1.08	0.18	0.98	0.64	0.67	1.00	1.00	1.78	1.88	0.85
[Trp-O-Pr ⁱ] ⁺	1.18	1.28	0.56	1.25	0.84	0.77	1.00	1.38	2.64	2.09	1.91
[Pro-O-Pr ⁱ] ⁺	1.16	1.19	1.23	1.06	1.16	1.16	1.02	1.08	1.98	1.77	1.09
[Pgly-O-Pr ⁱ] ⁺	0.93	1.56	0.26	1.20	0.79	0.72	1.00	0.99	0.76	0.96	0.55
[Tle-O-Pr ⁱ] ⁺	1.23	0.85	0.33	0.98	0.40	0.40	1.04	1.18	1.03	1.57	1.63



Scheme 8

Table 16 Rate constants ($k \times 10^{11} \text{ cm}^3 \text{ molecule}^{-1} \text{ s}^{-1}$) and selectivities (k_D/k_L) of selected amino acids with CD and linear oligosaccharides. All hosts are permethylated

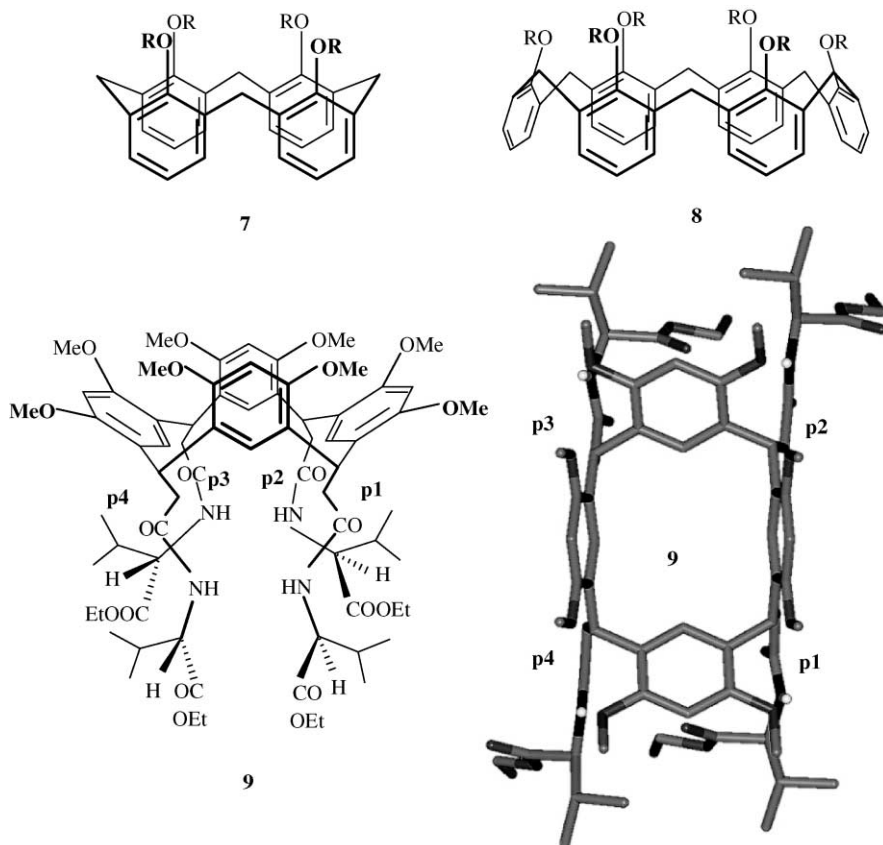
Amino acids	Met- β -CD	Met-Heptaose	Met-Hexaose	Met-Pentaose
Ala				
k_D	1.5	3.1	–	3.9
k_L	2.4	3.4	–	4.2
k_D/k_L	0.62	0.91	–	0.93
Val				
k_D	1.1	1.6	–	3.1
k_L	3.4	3.4	–	3.2
k_D/k_L	0.32	0.47	–	0.97
Ile				
k_D	0.26	1.3	–	1.1
k_L	1.0	3.0	–	1.6
k_D/k_L	0.26	0.43	–	0.69
Leu				
k_D	0.14	1.3	2.1	0.85
k_L	0.50	2.5	2.9	1.5
k_D/k_L	0.28	0.52	0.72	0.57
Phe				
k_D	1.7	0.14	0.89	0.69
k_L	1.4	0.63	1.1	0.86
k_D/k_L	1.21	0.25	0.81	0.77
Tyr				
k_D	0.029	0.005	–	–
k_L	0.019	0.026	–	–
k_D/k_L	1.53	0.19	–	–

**Fig. 19** Plot of the enantioselectivity (k_D/k_L) as a function of the number of non-hydrogen atoms on the amino acid. Hosts: permethylated β -CD (open circles); permethylated maltoheptaose (full circles); reagent base: 1-propylamine.

Smaller linear hosts, such as maltohexaose and maltopentaose, show lower enantioselectivities (Table 16). Molecular modeling calculations predict that these hosts are too small to fully envelop the guest and create an environment for high enantioselectivity.

Chiral calixarene hosts

Calixarene and their resorcinarene relatives are similar to CDs with respect to their ability to form a concave cavity in which guests can bind. Calixarenes are conformationally more flexible than the resorcinarenes, and depending on the substituents attached to their wider upper rim or to the narrower lower rim they may exist in a highly-symmetric bowl-shaped, so-called cone conformation or in several other conformations that do not exhibit an as perfect cavity as does the cone conformation (Scheme 9). Cationic guests, such as alkali metal or ammonium ions,



Scheme 9

bind quite strongly inside the cavity mostly by electrostatic interactions with the n - or π -centers of the host.

Chiral recognition by calixarenes in the gas phase is virtually unknown.^{458–460} To date, only few very recent gas-phase studies on this subject can be retrieved from the literature, i.e., (i) a gas-phase study on the displacement of several amino acids from the chiral amido⁴resorcinarene **9** (Scheme 9) carried out by Speranza and coworkers using an electrospray-ionization Fourier-transform ion cyclotron resonance (ESI-FT-ICR) mass spectrometer,^{461,462} and (ii): Lebrilla and coworkers' study on the ability of the achiral calix[4]arene **7** and calix[6]arene **8** to form inclusion complexes with natural amino acids under matrix-assisted laser desorption ionization (MALDI) conditions.⁴⁵⁹



The molecular asymmetry of **9** is due to the four axial pendants containing the chiral L-valine group. The efficiency of the gas-phase exchange reaction 30 where A are representative amino acids and B is either (S)-(+)- or (R)-(–)-2-butylamine is appreciably affected by the configuration of both A and B. The guest exchange kinetic results are reported in Table 17. The presence of more than one reacting $[\mathbf{9}\cdot\text{H}\cdot\text{A}]^+$ structure is observed with A = DOPA. A similar behavior was observed with permethylated β -CD as the host.⁴⁴⁸

The results of Table 17 indicates that the efficiency of the gas-phase exchange reaction 30 is affected by the nature and the configuration of the amino acid guest $S_A = (k_D/k_L)$ and the configuration of the amine B $S_B = (k_R/k_S)$. The emerging selectivity picture, discussed in the light of molecular mechanics and molecular dynamics calculations, points to chiral recognition by **9** as determined by the effects of the host asymmetric frame upon the structure, stability, and rearrangement dynamics of the diastereomeric $[\mathbf{9}\cdot\text{H}\cdot\text{A}]^+$ complexes and the orientation of the amine reactant B in the encounters with $[\mathbf{9}\cdot\text{H}\cdot\text{A}]^+$. Indeed, docking (MM) and molecular dynamics (MD) calculations on several $[\mathbf{9}\cdot\text{H}\cdot\text{A}]^+$ (A = alanine, serine, and DOPA) complexes points to three regions of the host as most suited for hosting the amino acid A, i.e., (i) inside the achiral upper rim cavity (UP); (ii) among the four chiral pendants in correspondence of its chiral lower rim cavity (DOWN); and, (iii) in the external position in proximity of two adjacent pendants (EXT).

MD simulations on low-energy $[\mathbf{9}\cdot\text{H}\cdot\text{A}]^+$ (A = alanine) docking geometries point to EXT as the thermodynamically most favored structures at room temperature. The relevant diastereomeric structures are almost equally stable. Therefore, the observed enantioselectivity has to be attributed to specific stabilization of the exchange transition structures. In this view, the small effects of the configuration of B $S_B = (k_R/k_S)$ in Table 17 indicates that the B amine displaces alanine from the relevant EXT structure without getting completely into the chiral cavity of the host.

Docking (MM) and molecular dynamics (MD) calculations on $[\mathbf{9}\cdot\text{H}\cdot\text{A}]^+$ (A = serine) complexes point to DOWN as the most favored hosting region for both L- and D-serine, although the complex with L-serine is ca. 6 kcal mol⁻¹ less stable than with D-serine. In addition, while DOWN with D-serine persists

Table 17 Rate constants of the displacement reactions 30^a

Amino acid (A)	PA (A) (kcal mol ⁻¹)	(R)-(-)-C ₄ H ₉ NH ₂		(S)-(+)-C ₄ H ₉ NH ₂		S _B	Reaction efficiency	
		k _R ^a	S _A ^R	k _S ^a	S _A ^S		k _R /k _{coll}	k _S /k _{coll}
D-Ala	215.5 ^b	7.69 ± 0.12	1.52 ± ^{0.05} _{0.06}	7.06 ± 0.11	1.20 ± ^{0.04} _{0.04}	1.09 ± ^{0.03} _{0.03}	0.69	0.63
L-Ala		5.05 ± 0.10		5.89 ± 0.09		0.86 ± ^{0.03} _{0.03}	0.45	0.53
D-Ser	218.6 ^c	4.59 ± 0.06	0.67 ± ^{0.02} _{0.01}	3.70 ± 0.06	0.49 ± ^{0.01} _{0.01}	1.24 ± ^{0.06} _{0.04}	0.41	0.34
L-Ser		6.87 ± 0.05		7.56 ± 0.06		0.91 ± ^{0.01} _{0.02}	0.62	0.68
D-Leu	218.6 ^b	3.76 ± 0.02	1.33 ± ^{0.02} _{0.01}	4.68 ± 0.05	1.29 ± ^{0.05} _{0.05}	0.80 ± ^{0.02} _{0.01}	0.34	0.42
L-Leu		2.82 ± 0.02		3.64 ± 0.10		0.77 ± ^{0.03} _{0.02}	0.25	0.32
D-DOPA	221.0 ^d	2.28 ± 0.06	0.76 ± ^{0.04} _{0.04}	1.26 ± 0.05	0.69 ± ^{0.09} _{0.12}	1.81 ± ^{0.12} _{0.12}	0.20	0.11
L-DOPA		3.00 ± 0.09		1.82 ± 0.20		1.65 ± ^{0.26} _{0.21}	0.27	0.16
D-DOPA		0.07 ₃ ± 0.00 ₈	0.73 ± ^{0.13} _{0.15}	0.06 ₄ ± 0.00 ₈	0.81 ± ^{0.17} _{0.21}	1.14 ± ^{0.31} _{0.24}	0.00 ₆	0.00 ₆
L-DOPA		0.10 ₀ ± 0.00 ₈		0.07 ₉ ± 0.00 ₉		1.27 ± ^{0.27} _{0.23}	0.00 ₉	0.00 ₇
D-Pro	224.9 ^e	1.51 ± 0.01	0.92 ± ^{0.01} _{0.01}	1.38 ± 0.02	0.92 ± ^{0.03} _{0.03}	1.09 ± ^{0.03} _{0.02}	0.13	0.12
L-Pro		1.64 ± 0.01		1.50 ± 0.03		1.09 ± ^{0.03} _{0.03}	0.15	0.14
D-Pip	225.6 ^e	0.14 ₇ ± 0.00 ₂	0.91 ± ^{0.03} _{0.01}	0.11 ₇ ± 0.00 ₂	0.74 ± ^{0.02} _{0.03}	1.26 ± ^{0.04} _{0.04}	0.01 ₃	0.01 ₀
L-Pip		0.16 ₁ ± 0.00 ₃		0.15 ₇ ± 0.00 ₃		1.02 ± ^{0.04} _{0.03}	0.01 ₄	0.01 ₄

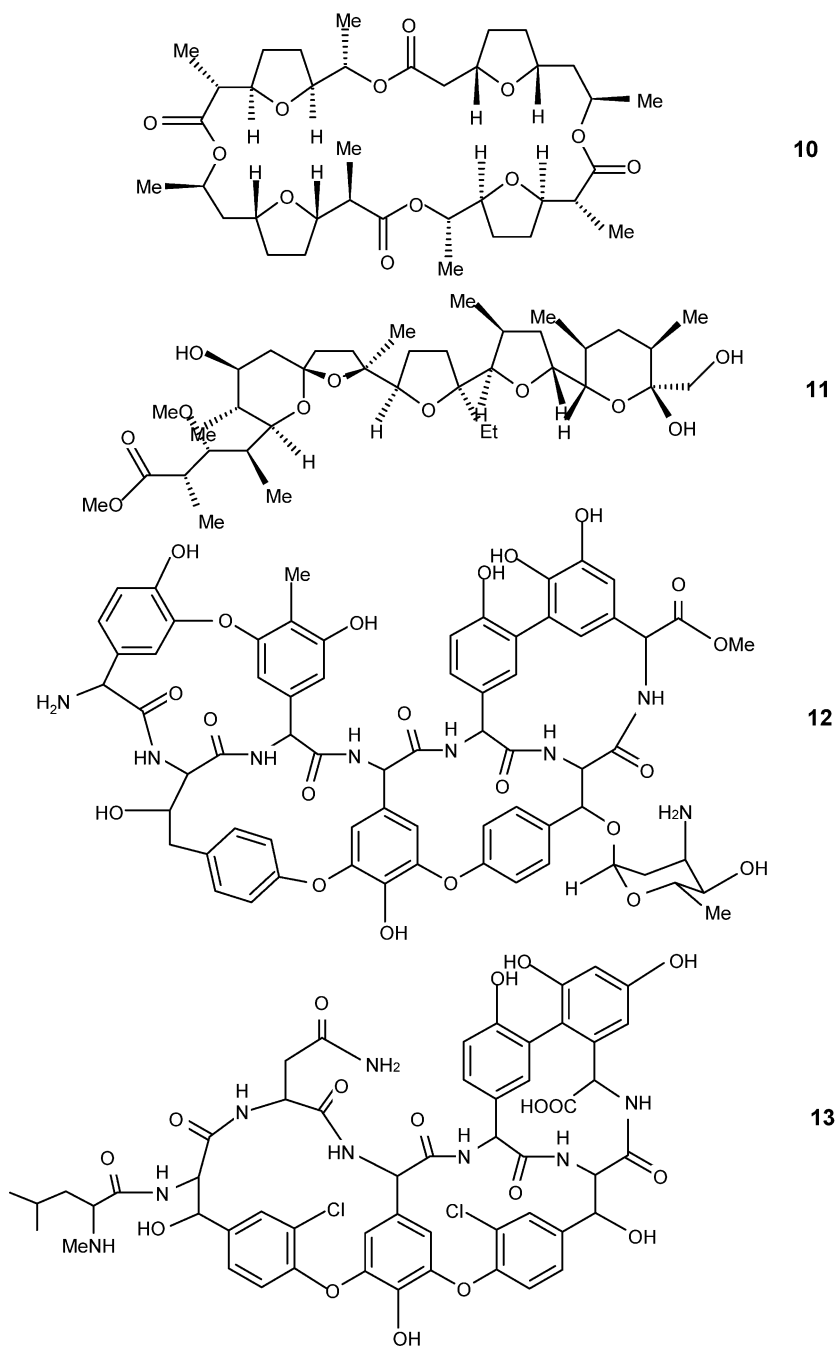
^ak × 10⁻¹⁰ cm³ molecule⁻¹ s⁻¹.^bArmentrout, P.B. (2000). *J. Am. Soc. Mass Spectrom.* **11**, 371.^c<http://webbook.nist.gov/chemistry/name-ser.html>.^dTaken as equal to the PA of tyrosine.^eKuntz, A.F., Boynton, A.W., David, G.A., Colyer, K.E. and Poutsma, J.C. (2002). *J. Am. Soc. Mass Spectrom.* **13**, 72.

unchanged up to 20 ns, that with L-serine moves to the quasi-degenerate EXT within the same lapse of time. Accordingly, the pronounced effect of the serine configuration on the exchange reaction 30 ($S_A = k_D/k_L$ in Table 17) is accounted for by the greater stability of $[\mathbf{9}\cdot\text{H}\cdot\text{A}]_{\text{DOWN}}^+$ (A = D-serine) relative to $[\mathbf{9}\cdot\text{H}\cdot\text{A}]_{\text{EXT}}^+$ (A = L-serine). This latter complex exhibits a limited effect of the B configuration ($S_B = k_R/k_S$ in Table 17), much like that measured with the $[\mathbf{9}\cdot\text{H}\cdot\text{A}]_{\text{EXT}}^+$ (A = alanine) complexes. This coincidence reflects a common exchange mechanism in which amine B pushes away the guest A from EXT without getting completely into the chiral cavity of the host. In contrast, the comparatively large effect of the B configuration on the slower reaction between B and $[\mathbf{9}\cdot\text{H}\cdot\text{A}]_{\text{DOWN}}^+$ (A = L-serine) (Table 17) reflects the involvement of a more congested, higher-energy transition structures with B partially inside the host chiral cavity while pushing D-serine away from it.

MC/MD simulations on $[\mathbf{9}\cdot\text{H}\cdot\text{A}]^+$ (A = DOPA) complexes indicate that DOPA, irrespective of its configuration, can be permanently trapped not only into the chiral DOWN region of the host, but also onto its achiral UP region. The relevant diastereomeric structures are almost equally stable, with the DOWN structures ca. 5 kcal mol⁻¹ more stable than the UP ones. This computational result is consistent with the formation of more than one reacting $[\mathbf{9}\cdot\text{H}\cdot\text{A}]^+$ (A = DOPA) structures, the most reactive corresponding to UP and the less reactive to DOWN. The UP structure displays the highest effect of the B configuration ($S_B = k_R/k_S$ in Table 17). This implies that the B amine must get completely inside the empty chiral cavity of $[\mathbf{9}\cdot\text{H}\cdot\text{A}]_{\text{UP}}^+$ (A = DOPA) to displace the guest. In contrast, the slower exchange reaction with $[\mathbf{9}\cdot\text{H}\cdot\text{A}]_{\text{DOWN}}^+$ (A = DOPA) exhibits a much smaller effect of the B configuration which is similar to that accompanying the reaction with $[\mathbf{9}\cdot\text{H}\cdot\text{A}]_{\text{DOWN}}^+$ (A = D-serine). This observation indicates the involvement of a congested, high-energy transition structures with B not fully inserted into the host chiral cavity which, therefore, may exert only in part the effects of its asymmetry toward it. The above results represent the first attempt to a dynamic model of chiral recognition of biomolecules by enzyme mimics in the unsolvated state.

Antibiotic hosts

Chiral recognition of phenylglycine methyl ester by antibiotic host nonactine **10** and monensin methyl ester **11** (Scheme 10) was detected and evaluated using the FAB-MS-EL (amino ester) guest method.⁴²⁶ The relevant IRIS = 0.54 value was essentially on the same line as the results derived independently from the ion-selective electrode method in water.⁴⁶³ No distinct selectivity of the aglycones of ristocetin A **12** and vancomycin **13** has been observed toward the cell wall analog peptide *N*-acetyl-D-ala-D-ala and *N*-acetyl-L-ala-L-ala.⁴⁶⁴ The same study has been repeated by using the ESI-MS²-EL (amino ester) guest method.⁴⁶⁵ CID experiments have been carried out to probe the gas phase stability of isomeric 1:1 non-covalent complexes formed between vancomycin and tripeptide stereoisomers. In the negative ion mode, the CID results show that a complex between vancomycin and a -L-Ala-L-Ala ligand fragments more readily than a complex formed between



Scheme 10

vancomycin and a -D-Ala-D-Ala ligand. The difference in gas phase stability is in agreement with what would be expected if the non-covalent complexes had retained their structural specific interactions from living cells to the gas phase. In positive ion mode, no significant difference in the gas phase stabilities of the isomeric complexes is observed. This is attributed to a protonation of the C-terminus of the peptide ligand which destroys the specific interaction between antibiotic and peptide ligand.

Proteic hosts

The proton transfer from multiply charged [cytochrome *c*]^{+*n*} (*n* = 7–9) to (*R*)- and (*S*)-2-butylamine show a significant enantioselectivity.^{466,467} Ions [cytochrome *c*]^{+*n*} (*n* = 7–9) were produced by ESI and introduced into the analyzer cell of a FT-ICR containing an alkylamine, i.e., (*R*)- and (*S*)-2-butylamine, 1-propylamine, or tert-butylamine. Rate constants for the proton transfer are listed in Table 18.

Proton transfer to (*R*)-2-butylamine is invariably faster than that to (*S*)-2-butylamine, irrespective of the charge state of cytochrome *c*. In any instances, the reaction is very inefficient (0.1–0.001%) due to the endoergonicity of the process and the large steric interactions in the corresponding transition structures. The decay of the [cytochrome *c*]⁺⁹ ions with reaction time is best represented by a single rate constant, while that of the [cytochrome *c*]^{+*n*} (*n* = 7, 8) ions is best represented by two rate constants (fast and slow in Table 18). This is indicative of a single conformer for [cytochrome *c*]⁺⁹ and of two conformers for [cytochrome *c*]^{+*n*} (*n* = 7, 8).⁴⁶⁸ The relative amount of these conformers (percent in Table 18) are the same for the *R*- and *S*-enantiomer. (*S*)-2-butylamine exhibits decreasing reactivity with decreasing *n*, as expected from purely Coulombic considerations. In this regard, either 1-propylamine and tert-butylamine behave in the same manner. With (*R*)-2-butylamine, the rate constant with *n* = 9 and the highest rates with *n* = 7, 8 are approximately equal, suggesting a possible reactive site for the three charged states. Comparison of the rate constants of Table 18 indicates that 1-propylamine is approximately as reactive as (*S*)-2-butylamine, despite the 1.6 kcal mol⁻¹ lower basicity. Toward [cytochrome *c*]^{+*n*} (*n* = 8, 9), tert-butylamine is one order of magnitude less reactive of 1-propylamine, despite the 2.9 kcal mol⁻¹ higher basicity. These findings are interpreted in terms of the strong influential role of steric effects in the highly specific arrangement of the alkylamine toward the multiply charged protein.

REACTIVITY OF CHIRAL ION–DIPOLE COMPLEXES

As illustrated in the previous sections, an array of MS methodologies are nowadays available to enantiodiscriminate chiral molecules by complexation with chiral selectors and to investigate the intrinsic factors affecting their stability in the gas phase. The advantages connected with studying enantioselectivity in simple ionic and neutral complexes in the gas phase instead of in complicated associations in solution come from the possibility to make precise statements upon the nature of

Table 18 Rate constants for the proton transfer from [cytochrome *c*]⁺ⁿ (n = 7–9) to alkylamines^a

[Cytochrome <i>c</i>] ⁺ⁿ		<i>(R)</i> -(-)-2-aminobutane (GB, 211.7)		<i>(S)</i> -(+)-2-aminobutane (GB, 211.7)		1-Propylamine (GB, 210.1) <i>k</i> ^b	tert-Butylamine (GB, 213.0) <i>k</i> ^b
<i>n</i>	Type	<i>k</i> _R ^b	Percent	<i>k</i> _S ^b	Percent		
9		1.5 ± 0.3(-11)		2.5 ± 0.2(-12)		2.2(-12)	6.1(-13)
8 ^c		2.3 ± 0.5(-12)		4.6 ± 1.1(-13)		2.9(-13)	3.8(-14)
8	Fast	1.0 ± 0.3(-11)	45	1.9 ± 0.4(-12)	46	3.1(-13)	3.7(-13)
8	Slow	1.4 ± 0.1(-12)	55	3.7 ± 1.0(-13)	54		
7 ^c		2.3 ± 0.1(-13)		8.4 ± 3.6(-14)		7.2(-14)	
7	Fast	1.1 ± 0.1(-11)	21	1.4 ± 0.3(-12)	30	1.4(-13)	5.1(-14)
7	Slow	1.3 ± 1.1(-13)	79	1.4 ± 1.9(-13)	70		

^a*k* in cm³ molecule⁻¹ s⁻¹.^bThe figures in parentheses refer to the power of ten. GB, gas-phase basicity (kcal mol⁻¹).^cFurther reaction of the lower charged state arising from proton transfer.

the non-covalent forces holding them together. The relevant results demonstrate that chiral discrimination in ionic and molecular aggregates is mainly determined by short-range attractive and repulsive (steric) forces and that these forces may be dramatically affected by solvation. The next step is to verify how these forces (and their sensitivity to environmental conditions) determine the reactivity of diastereomeric encounter complexes, namely how they affect the diastereomeric transition structures involved in their evolution to chiral products (kinetic enantioselectivity).

Low-pressure reactions in chiral ion–dipole complexes

MS proves not only as a powerful tool for chiral discrimination, but it is increasingly becoming recognized as a means for studying the mechanistic details of fundamental chemical reactions involving chiral species. In this connection, MS as well as molecular and ion beams occupy prominent positions since operating under collision-free conditions ensuring against radiationless dispersal of the internal energy acquired by ion–molecule or molecule–molecule complexation. It is this energy which is used to overcome the activation barrier for the evolution of the complex.

Proton-transfer reactions in chiral ion–dipole complexes. Low-energy FT-ICR–CID experiments on complexes composed of permethylated β -cyclodextrin (Met- β -CD) or permethylated maltoheptaose (Met-Heptaose) and protonated amino acids (A) induces an endothermic proton-transfer reaction.⁴⁶⁹ Experiments were performed with the amino acids reported in Table 19 as the guests.⁴⁷⁰ The resulting product ions are fragments of the host, corresponding to the losses of methanol and one or two glycosidic residues. The net reaction in each case is a proton transfer from AH^+ to the host with charge being retained on the less basic host fragments. This implies that energetically favored back-protonation is slow relative to fragmentation.

Table 19 reports multicollisional dissociation thresholds of the selected complexes. A direct correlation exists between them and the proton affinity (PA) of the guest. However, although chiral specificity has been observed in similar systems using ligand-exchange reactions (see previous sections), the results of Table 19 show no such specificity. The differences in binding of the Ala and Phe enantiomers are evidently too small to be measured with this method.

Hydrogen–deuterium exchange in chiral ion–dipole complexes. The rates of gas phase H/D exchange reactions are most conveniently measured in a FT-ICR cell in which the ions can be trapped for extended periods of time in the presence of a fixed concentration of the exchange reagent.⁴⁶⁹ Generally, multiple exchanges are possible, and one observes the decay of the parent peak at m/z and the growth of peaks at $(m + n)/z$ corresponding to the products containing n deuteriums.

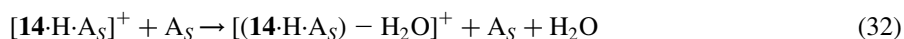
Table 19 Multicollisional dissociation threshold of [Met- β -CD-H.A]⁺ complexes

Amino acid A	Proton affinity (kcal mol ⁻¹)	Threshold E_{com} (eV)
D-Phe	216.5	1.8 ± 0.2
L-Phe	216.5	1.6 ± 0.2
D-Ala	215.7	1.7 ± 0.2
L-Ala	215.7	1.7 ± 0.5
L-Lys	238.3	2.6 ± 0.2
L-Hys	236.4	2.6 ± 0.6

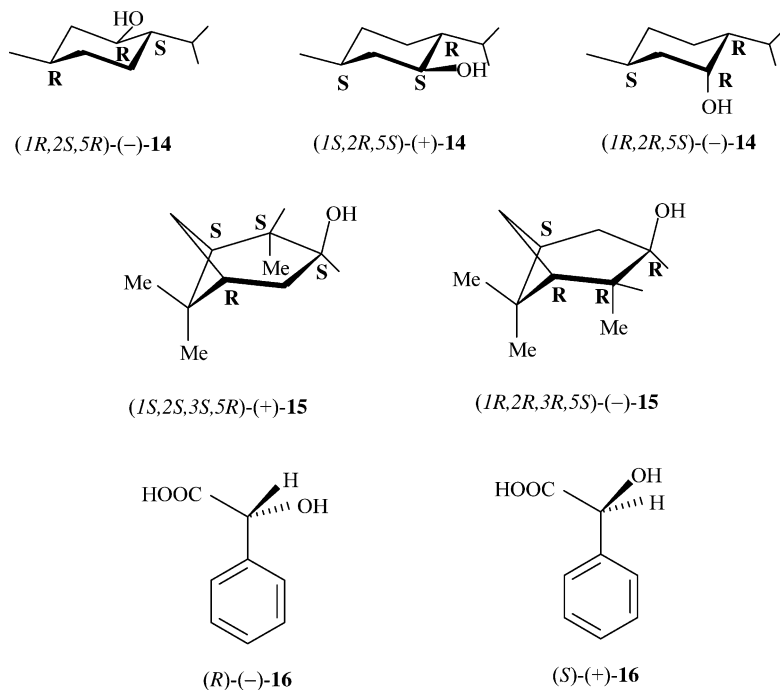
This approach has been applied to the H/D exchange reaction in complexes composed of tetradeuterated dipeptides (GlyAla, GlyVal, AlaGly, AlaAla, AlaVal, ValGly, and ValVal) and (*R*)-(-)- or (*S*)-(+)-2-butanol.⁴⁷¹ While extensive exchange is observed, no difference in the exchange rate is appreciated by changing the configuration of the alcohol. This lack of stereoselectivity is attributed to the small difference in proton affinity between 2-butanol and the selected dipeptides ($\Delta\text{PA} = 19\text{--}26$ kcal mol⁻¹). As a result, H/D exchange takes place in loosely bound, almost equally stable diastereomeric complexes.

Stereospecific nucleophilic substitution in chiral ion-dipole complexes. Chiral molecules can be discriminated in the CI source of a CIMS instrument by specific ion-molecule reactions induced by chiral reagent gas. This method has been applied with success to distinguish between enantiomeric and diastereomeric forms of menthols ((*1R,2S,5R*)-(-)-**14**, (*1S,2R,5S*)-(+)-**14**, and (*1R,2R,5S*)-(-)-**14** in Scheme 11) through the nucleophilic displacement of their hydroxyl group by (*S*)-2-amino-1-butanol (A_S).⁴⁷² Self-protonation of A_S under CIMS conditions (0.5 torr, 100 °C) leads to the predominant formation of the corresponding ammonium ion $A_S\text{H}^+$ which is able to react with menthols **14** yielding the corresponding adducts [**14**·H· A_S]⁺ and substituted ionic products [(**14**·H· A_S)-H₂O]⁺.

As shown in Fig. 20, the MIKE/CID of the substituted products [(**14**·H· A_S)-H₂O]⁺ m/z 228 exhibit an appreciable dependence on the configuration of **14**. The origin of substituted products [(**14**·H· A_S)-H₂O]⁺ has been investigated and attributed to a stereospecific bimolecular S_N2 process 32:



The exclusive loss of H₂O from MIKE/CID of [(**14**·H· A_S)-H₂O]⁺ indicates that its formation process 32 is also regioselective in the sense that it is the amino group of the A_S nucleophile that exclusively attacks the activated [**14**·H· A_S]⁺ precursor. Steric interactions in the isomeric [(**14**·H· A_S)-H₂O]⁺ ions are responsible for the differences observed in the relevant MIKE/CID spectra of Fig. 20.



Scheme 11

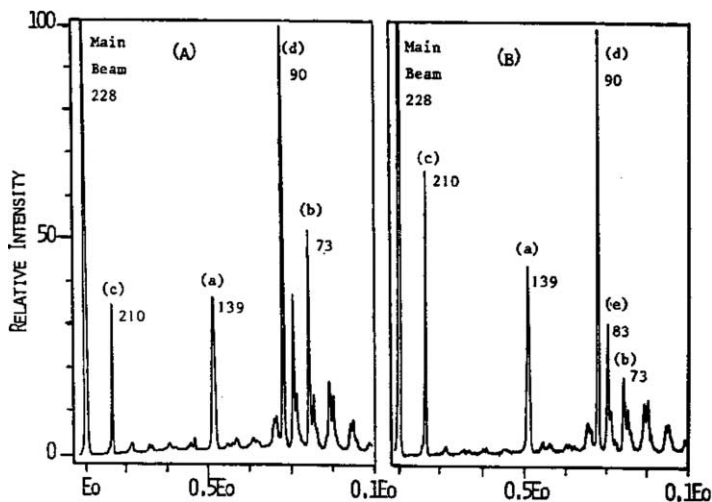


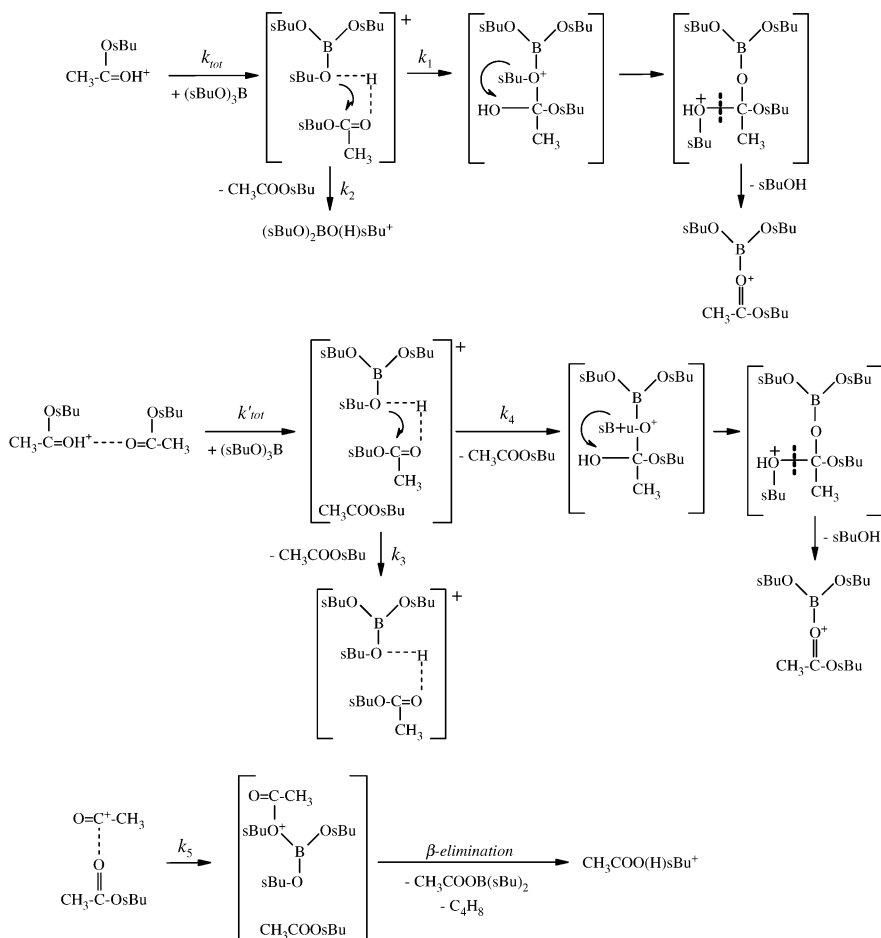
Fig. 20 MIKE/CID spectra of the substituted $m/z228$ ions from the enantiomers of menthol ($(1R,2S,5R)\text{-}(-)\text{-14}$ (A) and $(1S,2R,5S)\text{-}(+)\text{-14}$ (B)) formed under CI/ (S) -2-amino-1-butanol (A_S) conditions (the $m/z210$ and $m/z90$ daughter ions are also produced during unimolecular decomposition of the $m/z228$ ions) (reprinted from ref. 472, with permission from Elsevier).

The same approach has been employed for enantiodiscriminating isopinocampheols (*1S,2S,3S,5R*)-(+)-**15** and (*1R,2R,3R,5S*)-(–)-**15**⁴⁷³ and mandelic acids (*R*)-(–)-**16** and (*S*)-(+)-**16**⁴⁷⁴ (Scheme 11). Several chiral reagent gases were used, including (*R*)-2-amino-1-propanol, (*S*)-2-amino-1-butanol, (*S*)-2-pyrrolidinemethanol, and (*S*)- and (*R*)-1-phenylethylamine.

The reactivity of the encounter complexes between protonated and acetylated (*R*)- and (*S*)-2-butyl acetate, $(\text{CH}_3\text{COOsBu})_n\text{M}^+$ (sBu = (*R*)-, (*S*)-, or (\pm)-2-butyl; M = H ($n = 1, 2$); CH_3CO ($n = 1$)), and (*S,S,S*)-tri-sec-butylborate has been measured by FT-ICR–MS. The relevant ion patterns are shown in Scheme 12.⁴⁷⁵ The kinetic data of Table 20 reveal some differences in both the overall reactivity of chiral $(\text{CH}_3\text{COOsBu})_n\text{M}^+$ ions toward (*S,S,S*)-tri-sec-butylborate (k_{tot} , k'_{tot} , and k_5) and the relative extent of the competing addition/elimination (k_1 and k_4), proton transfer (k_2), and ligand exchange (k_3) channels. They clearly indicate that (*S,S,S*)-tri-sec-butylborate reacts more efficiently with the homochiral (*S*)-2-butyl acetate ions, than with the heterochiral (*R*)-2-butyl acetate ones. As expected, the reaction efficiency of the racemate (\pm)-2-butyl acetate ions falls in between.

Nucleophilic substitution is a cornerstone reaction of organic chemistry studied for more than 100 years.⁴⁷⁶ Immense progress has been made in the 20th century in unveiling how this reaction occurs. A major contribution is due to gas-phase studies, which provided the deepest insight into the mechanistic details of a reaction normally conducted in solution. In addition, these studies revealed the critical effects of the solvent not only on the reaction coordinate but also on the actual topography of the PES.⁴⁷⁷ The most serious limitation of these studies is the almost complete lack of information on the stereochemistry of the process and the identity of their neutral products. For these reasons, most of the gas-phase investigations on the mechanism of nucleophilic substitutions has been carried out using the experimental techniques (mostly stationary radiolysis and electron bombardment flow (EBF) radiolysis, but also ICR-MS) which allow for the isolation of the reaction products and their structural identification. The first contribution on this area was provided by a sophisticated trapped-ion ICR experiment by Lieder and Brauman,⁴⁷⁸ who elucidated the stereochemistry of a single negative-ion substitution reaction between Cl^- and *cis*- and *trans*-4-bromocyclohexanols. Identification and structural discrimination of the substituted neutral products, i.e., *cis*- and *trans*-4-chlorocyclohexanols, were based on their positive ion pattern after switching the apparatus from negative to positive ion mode. The results indicate that nucleophilic Cl-to-Br displacement on *cis*-4-bromocyclohexanol involves $91 \pm 14\%$ inversion of configuration, whereas the same reaction on *trans*-4-bromocyclohexanol involves $86 \pm 19\%$ inversion of configuration.

Independent evidence for backside attack in gas-phase acid-induced nucleophilic substitutions was provided by a number of studies, carried out using stationary radiolysis.^{479–488} Further confirmation was provided by Morton and coworkers,⁴⁸⁹ who investigated the stereochemistry of the proton-induced nucleophilic substitution on (*S*)-(+)- and (*R*)-(–)-2-butanol in the gas-phase at 10^{-3} torr in their 70-eV EBF radiolysis reactor. In the presence of a strong base, i.e., tri-*n*-propylamine



Scheme 12

(PA = 226 kcal mol⁻¹), the predominant formation (6.4 to 1) of the (*R,S*)-di-2-butyl ether over the (*R,R*)- and (*S,S*)-forms is attributed to a simple backside displacement in the proton-bound adduct of the starting 2-butanol enantiomer with inversion of configuration of the reaction site and loss of a molecule of water. When tri-*n*-propylamine is replaced by the less basic NH₃ (PA = 196 kcal mol⁻¹), fast neutralization of the proton-bound dimers of the starting 2-butanol is prevented and, therefore, they can grow, producing aggregates that resemble solution microenvironments in which S_N1 pathways may be accessible as well. In them or in their primary substituted derivatives, consecutive nucleophilic displacements may take place. As a consequence, the stereospecificity of the process is lost and the [(*R,S*)-di-2-butyl ether]/[(*R,R*)- and (*S,S*)-di-2-butyl ethers] ratio falls down to 1.2. In this case,

Table 20 Phenomenological rate constants ($\times 10^{10} \text{ cm}^3 \text{ molecule}^{-1} \text{ s}^{-1}$) and efficiencies ($\text{eff} = k_{\text{obs}}/k_{\text{coll}}$) (in parentheses) of the reaction of chiral 2-butylacetate ions with (*S,S,S*)-tri-*sec*-butylborate (Scheme 12)

sBu	M	<i>n</i>	k_{tot}	k_1	k_2	k_{coll}
(<i>R</i>)-2-Butyl	H	1	4.89 (0.36)	3.47 (0.29)	1.42 (0.12)	11.89
(<i>S</i>)-2-Butyl	H	1	6.26 (0.52)	3.95 (0.33)	2.31 (0.19)	11.89
(±)-2-Butyl	H	1	5.12 (0.43)	3.81 (0.32)	1.31 (0.11)	11.89
			k'_{tot}	k_3	k_4	k_{coll}
(<i>R</i>)-2-Butyl	H	2	0.07 (0.007)	0.03 (0.003)	0.04 (0.004)	9.73
(<i>S</i>)-2-Butyl	H	2	0.08 (0.008)	0.03 (0.003)	0.05 (0.005)	9.73
(±)-2-Butyl	H	2	0.08 (0.008)	0.03 (0.003)	0.05 (0.005)	9.73
			k_5			k_{coll}
(<i>R</i>)-2-Butyl	CH ₃ CO	1	4.44 (0.41)			10.80
(<i>S</i>)-2-Butyl	CH ₃ CO	1	5.37 (0.50)			10.80
(±)-2-Butyl	CH ₃ CO	1	5.35 (0.49)			10.80

consecutive S_N2 displacements in large ionic aggregates lead to predominant racemization, although this observation is commonly associated with S_N1 mechanisms in solution. It is concluded that the classical S_N1/S_N2 paradigm with its relationship between stereochemistry and reaction order is at best very complicated and often misleading.

High-pressure reactions in chiral ion–dipole complexes

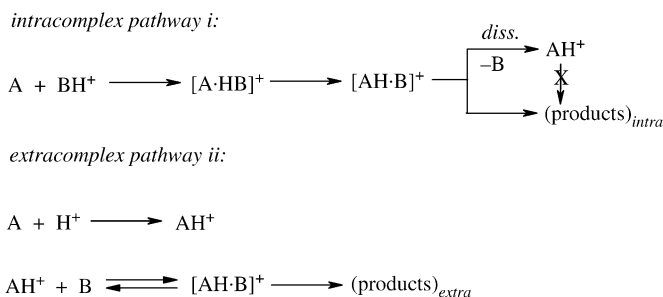
Physical organic chemists are interested in experimental approaches for reproducing in the gas phase reactions that formerly could be carried out only in solution with the aim of determining the effects of solvation and ion-pairing upon the intrinsic properties of the reactants involved. In this case, it is necessary that the gas-phase study is carried out under conditions ensuring thermal equilibration for all the species involved. To achieve this important condition, the reaction must be performed in the gas phase at sufficiently high pressures where the internal energy acquired by ion–molecule complexation is efficiently removed by unreactive collisions with the bulk gas prior to reaction. The ion–molecule encounter complexes are thermally coupled with the gaseous environment much like with the solvent in solution.

At high pressures, a non-covalent ionic complex can be regarded as a “microsolvated” ion. It represents the simplest model for ions generated in a dynamic environment, such as in a solvent cage in solution. The main difference is that the behavior of a “microsolvated” ion is not perturbed by those environmental factors (solvation, ion pairing, etc.) which normally affect the fate of intimate ion–dipole pairs in solution. Hence, a detailed study of the dynamics and the reactivity of microsolvated ions may provide valuable information on the intrinsic factors governing the reaction and how these factors may be influenced by the solvent cage in solution.

The evolution of an ion-neutral complex may be accompanied by the rearrangement of its components or simply by their mutual re-orientation before reaction or dissociation. Thus, the knowledge of the structure, the configuration, and the initial orientation of the components of the microsolvated systems is crucial for understanding its reaction stereochemistry. This section deals with the stereochemistry of representative addition and substitution reactions taking place within gaseous complexes $[\text{AH}\cdot\text{B}]^+$, wherein AH^+ is the formally charged moiety generated by stationary γ -radiolysis and B is a nucleophilic molecule. The microsolvated systems investigated contain: i- protonated (*R*)-(-)-2-chlorobutane and an arene,⁴⁹⁴ ii- deuterated 2-butyl/toluene pair from protonated (*S*)-(+)-1-D₁-3-(para-tolyl) butane;⁴⁹⁵ (iii) chiral oxonium ions and methanol;^{496,497} (iv) chiral phenonium ions and ROH (R = H, CH₃);^{498,499} (v) prochiral allyl cation and ROH (R = H, CH₃);⁵⁰⁰⁻⁵⁰² (vi) prochiral α -methyl benzyl cation and methanol;^{503,504} and, (vii) an O-protonated (*R*)-(+)-1-arylethanol and ¹⁸O-methanol.⁵⁰⁵

Complexes $[\text{AH}\cdot\text{B}]^+$ are generated in an inert gaseous medium at pressures high enough (700–750 torr) to allow their complete thermal equilibration. A tailor-made procedure has been used which ensures that the reaction products arise exclusively from the intracomplex reorganization of $[\text{AH}\cdot\text{B}]^+$. Thus, adducts $[\text{AH}\cdot\text{B}]^+$ are generated by intracomplex proton transfer in the $[\text{A}\cdot\text{HB}]^+$ adduct obtained by coordination of molecule A around ion BH^+ (pathway i of Scheme 13). The BH^+ precursor is prepared by a route excluding the presence of its conjugate base B. For instance, the $[\text{AH}\cdot\text{B}]^+$ complex with $\text{AH}^+ = \text{O-protonated } (R)\text{-}(+)\text{-1,2-propene oxide}$ and $\text{B} = \text{CH}_3^{18}\text{OH}$ is generated by intracomplex proton transfer within the adduct between (*R*)-(+)-1,2-propene oxide (A) with $\text{CH}_3^{18}\text{OH}_2^+(\text{BH}^+)$. Ions $\text{CH}_3^{18}\text{OH}_2^+$ are in turn formed in the gas phase by methylation of H_2^{18}O with the $(\text{CH}_3)_2\text{F}^+$ ions obtained in known yields by γ -radiolysis of CH_3F . In this way, ions $\text{CH}_3^{18}\text{OH}_2^+$ are generated in complete absence of their conjugate $\text{CH}_3^{18}\text{OH}$ base and, hence, their reaction products, i.e., the ¹⁸O-labeled 1-methoxy-2-propanols, are bound to arise exclusively from the intracomplex substitution on the incipient O-protonated (*R*)-(+)-1,2-propene oxide by the putative $\text{CH}_3^{18}\text{OH}$ molecule.

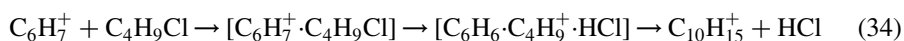
In some instances, the outcome of the intracomplex process *i* of Scheme 13 is confronted with that of the direct reaction between unsolvated AH^+ ion (or its



Scheme 13

rearranged form) and an external B molecule (the “extracomplex” pathway ii of Scheme 13). Taking again the above example, $\text{AH}^+ = \text{O-protonated (R)-(+)-1,2-propene oxide}$ is simply obtained by protonation of (R)-(+)-1,2-propene oxide with C_nH_5^+ ($n = 1, 2$) ions, formed by γ -radiolysis of gaseous CH_4 . The “extracomplex” pathway ii of Scheme 13 takes place by coordination of the so-formed O-protonated (R)-(+)-1,2-propene oxide with external $\text{CH}_3^{18}\text{OH}$ molecules, present as a massive additive in the irradiated mixture.

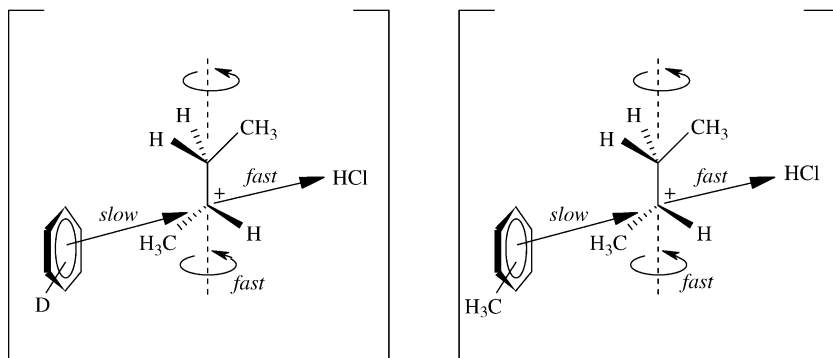
The arenium ion/(R)-(-)-2-chlorobutane adducts. A crucial question concerns the chemical identity and the relative spatial arrangement of the components of a microsolvated system, two features of paramount importance to assess the kinetic and the mechanistic role of the corresponding ion–dipole pairs in solution. In the example reported in this section, Cacace and coworkers consider the ion–molecule complexes involved in the classical Friedel–Crafts alkylation of arenes.⁴⁹⁴ At 300 K and under FT-ICR conditions, the benzenium ion C_6H_7^+ reacts with 2-chlorobutane $\text{C}_4\text{H}_9\text{Cl}$ to give the $\text{C}_{10}\text{H}_{15}^+$ ion with a rate constant of $5 \times 10^{-11} \text{ cm}^3 \text{ molecule}^{-1} \text{ s}^{-1}$, corresponding to a collision efficiency of 2.5% (equations (33) or (34)).⁹



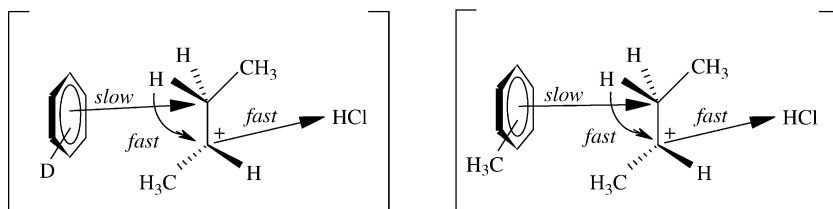
No information is available from this experiment as to the detailed path of formation of $\text{C}_{10}\text{H}_{15}^+$, whether via equation (33) or (34). Besides, no information is available as to the spatial relationship and the dynamics of the species present in the second complexes of equations (33) and (34). To answer these questions, the $^{12}\text{C}_6\text{H}_6\text{D}^+$ arenium ion was prepared in the gas phase by deuteration of $^{12}\text{C}_6\text{H}_6$ with radiolytic C_nD_5^+ ($n = 1, 2$) ions. Similarly, the $^{12}\text{C}_6\text{H}_6\text{CH}_3^+$ arenium ion was generated in the gas phase by methylation of $^{12}\text{C}_6\text{H}_6$ with radiolytic $(\text{CH}_3)_2\text{F}^+$. Both arenium ions were allowed to react at 700–750 torr with (R)-(-)-2-chlorobutane. The corresponding 2-arylbutanes, recovered among the radiolytic products, display complete racemization which points to their formation as proceeding exclusively via equation (34). This implies that alkylation follows a $\text{S}_{\text{N}}1$ mechanism, i.e., a process wherein covalent bond breaking precedes covalent bond formation as in the three body adduct of equation (34), whose individual components are not constrained in a fixed geometry, but are free to re-orientate or to rearrange before addition (Scheme 14).

Noncovalent isomeric 2-butyl ion/toluene complexes. As pointed out in the previous section, key features of ion–neutral complexes, such as the mutual orientation of their components and their evolution dynamics, usually escape precise determination because of intrinsic limitations of the available experimental methodologies. This lack of information is particularly unsatisfactory since, in principle, the nature and the dynamics of an ion–neutral complex may determine its evolution to products and, thus, the reaction selectivity. Filippi and coworkers⁴⁹⁵ recently

Re-orientation process



H-scrambling in the butyl ion



Scheme 14

provided novel indications of the factors governing the positional selectivity in a representative gas-phase electrophilic aromatic substitution, i.e., the *sec*-butylation of toluene, based on a careful investigation of the nature and the dynamics of the ion–neutral complexes involved. Ring-protonated (*S*)-(+)-1-D₁ – 3-(*para*-tolyl)-butane was generated by attack of radiolytic C_nH₅⁺ (*n* = 1, 2) ions on (*S*)-(+)-1-D₁ – 3-(*para*-tolyl)butane and its isomerization kinetics and stereochemistry investigated in the gas phase at 70 torr and *T* = 100–160 °C. The process leads to the exclusive formation of the relevant *meta* isomer with complete racemization and partial 1,2-H shift in the migrating 2-butyl group. These results, together with the relevant activation parameters ($\Delta H^* = 10.3 \pm 1.2 \text{ kcal mol}^{-1}$; $\Delta S^* = -5.3 \pm 3.6 \text{ cal mol}^{-1} \text{ K}^{-1}$), point to the occurrence of tightly bound, isomeric 2-butyl ion/toluene complexes of defined structure and stability placed ca. 10 kcal mol⁻¹ below the classical electrostatically bound π -complexes on the relevant PES. The existence and the η^1 -type structure of these low-energy intermediates are confirmed by *ab initio* calculations (Fig. 21).

Formation of the tightly-bound η^1 -type complexes in the isomerization of ring-protonated (*S*)-(+)-1-D₁ – 3-(*para*-tolyl)butane rises some questions about the role

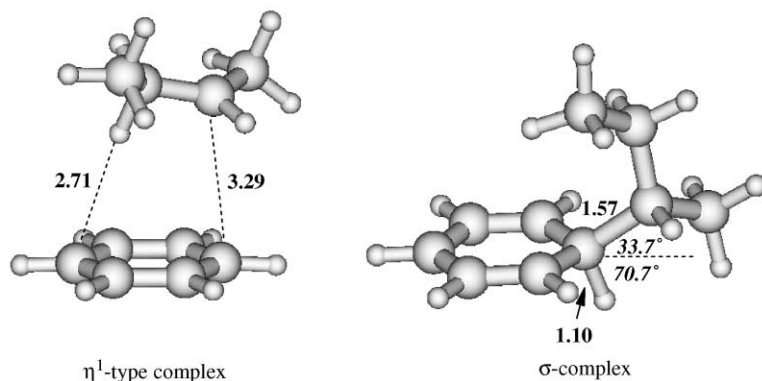


Fig. 21 HF/6-31 + G** -optimized structures and main geometrical parameters of the stable σ - and η^1 -type complexes located on the potential energy surface (PES) of protonated sec-butyl benzene (bond lengths in Ångströms; angles in degrees (in italic)).

of these intermediates in determining the substrate and positional selectivity of the gas-phase ionic alkylation of arenes. Indeed, the classical mechanistic model of gas-phase aromatic alkylations involves the preliminary formation of an electrostatically bound π -complex acting as a microscopic reaction “vessel” wherein the reactants are confined by electrostatic forces. The substrate selectivity of the alkylation reaction essentially reflects the competition between the collisional stabilization of the individual π -complexes and their back-dissociation. The positional selectivity reflects instead the different activation free energies for the conversion of the π -complex to isomeric σ -bonded arenium ions.

Filippi and coworkers’ discovery of tightly-bound, isomeric η^1 -type complexes on the 2-butyl ion/toluene PES put into question this widely accepted model.⁴⁹⁵ Indeed, their occurrence provide a rationale for the significant pressure effect on the isomeric product pattern observed in the gas-phase sec-butylation of toluene ($T = 24\text{ }^\circ\text{C}$).⁵⁰⁶ This pressure effect can be explained only by acknowledging the intermediacy of isomeric η^1 -type complexes with lifetimes comparable with their collision time with the bulk gas at 70–710 torr ($5 \times 10^{-10} \div 5 \times 10^{-11}$ s).

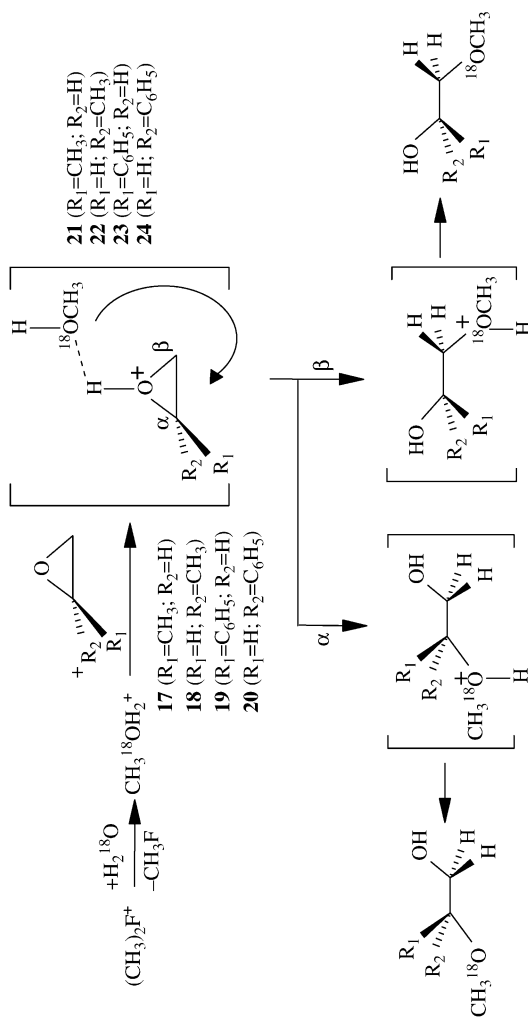
In this frame, the positional selectivity of the gas-phase sec-butylation of toluene, a model reaction for electrophilic aromatic substitutions, is determined by the relative population of isomeric η^1 -type complexes and the activation free energies for their conversion to the relevant σ -bonded arenium ions. When collisional cooling of the η^1 -type complexes is efficient (high pressure), the reaction is essentially controlled by enthalpy factors favoring the formation of their *ortho* and *para* isomers and their conversion to the corresponding σ -arenium intermediates. When instead collisional cooling of the η^1 -type complexes is not so efficient (low pressure), their relative population and conversion to the corresponding σ -arenium ion can be significantly altered by the contribution of the entropic factors.

Acid-induced ring opening of chiral alkene oxides. The detailed knowledge of ring opening in 1,2-epoxides represents the basis for understanding the mutagenic and carcinogenic activity of aromatic hydrocarbons and their metabolites in biological tissues. The mechanism and the stereochemistry of this class of reactions are heavily affected in solution by environmental factors. For instance, depending upon the pH of the reaction medium, alcoholysis of epoxides may follow either a unimolecular or a bimolecular pathway with a stereochemistry ranging from complete retention to complete inversion of configuration. Discrimination between intrinsic structural and environmental factors on ring opening of epoxides arises from a detailed investigation of the reaction in the gas phase, where the nature of the active intermediates is well defined and their evolution to products is unaffected by solvation and ion-pairing phenomena.

Gas-phase acid-induced ring opening of enantiomerically pure 1,2-propene (**17** and **18**) and styrene oxides (**19** and **20**) has been investigated at room temperature using $\text{CH}_3^{18}\text{OH}$, CD_3OH , and H_2^{18}O , as nucleophiles, and C_nH_5^+ ($n = 1, 2$) and $(\text{CH}_3)_2\text{F}^+$, as gaseous acids, generated by γ -radiolysis of CH_4 and CH_3F (720 torr), respectively (Scheme 15).^{496,497} No racemization of the starting chiral epoxide is observed under all experimental conditions. Therefore, the ring opening takes place on the O-protonated (or O-methylated) **17-20** retaining the original configuration of their precursors. Ring opening proceeds via two different reaction pathways. In the $\text{CH}_3\text{F}/\text{H}_2^{18}\text{O}$ systems, the reaction follows the intracomplex mechanism depicted in Scheme 13. It involves protonation of the oxygen of the epoxide by the $\text{CH}_3^{18}\text{OH}_2^+$ ion, generated in the gaseous mixture by $(\text{CH}_3)_2\text{F}^+$ -methylation of H_2^{18}O . The neutral $\text{CH}_3^{18}\text{OH}$ molecule, arising from the proton transfer, moves around the oxonium ions ($k < 10^8 \text{ s}^{-1}$) before attacking their ring carbons. The attack exclusively occurs at the α carbon of **23** and **24** with slightly predominant inversion of the configuration (55–67%). With **21** and **22**, instead, the attack takes place at both ring carbons ($\alpha/\beta = 0.72 \pm 0.05$) with exclusive inversion of their configuration.

In the $\text{CH}_4/\text{CH}_3^{18}\text{OH}$ systems, the intracomplex pathway is preceded by the extracomplex attack of an external $\text{CH}_3^{18}\text{OH}$ molecule. Both the intracomplex and the extracomplex pathways display the same regio- and stereoselectivity. The different regio- and stereoselectivity observed for **21/22** and **23/24** is explained in terms of a different extent of $\text{C}_\alpha\text{-O}$ bond rupture in the relevant TS. Ring-opening of **23/24** involves a loose TS characterized by extensive $\text{C}_\alpha\text{-O}$ bond cleavage promoted by conjugative delocalization of the C_α positive charge over the phenyl ring. The same stabilization mechanism is not operative in the ring opening of **21/22** whose TS is therefore characterized by a much less advanced $\text{C}_\alpha\text{-O}$ cleavage.

Acid-induced wagner-meerwein rearrangements in chiral alcohols. In view of the considerable interest on ion-molecule complexes involved in gas-phase analogues of solvolytic reactions,^{490,493} a sustained research effort has been directed to the study of Wagner-Meerwein rearrangements in cationized β -arylalkyl systems, under conditions excluding nucleophilic assistance by the solvent which in these systems normally interferes with anchimeric assistance of groups adjacent to the



Scheme 15

reaction center. In particular, a great deal of the efforts has been directed to the assessment of the kinetics and the stereochemistry of the unimolecular H₂O loss from the chiral oxonium ions **26** and **28** (A = H or CH₃; Scheme 16).^{498,499}

Ions **26** and **28** arise from the corresponding chiral alcohols **25** and **27** by reaction with gaseous acids (GA⁺), either C_nH₅⁺ (n = 1, 2) (A = H) or (CH₃)₂F⁺ (A = CH₃), formed respectively by γ -radiolysis of CH₄ and CH₃F (750 torr). The reaction sequences of Scheme 16 have been investigated in the temperature range 25–140 °C, in the presence of CH₃¹⁸OH or H₂¹⁸O, as nucleophiles (NuOH). The experimental results conform to the unimolecular loss of H₂O from **26** and **28** (A = H), anchimerically assisted by all the groups adjacent to the leaving moiety (Scheme 17). Anchimeric assistance to the CH₃OH loss from **26** and **28** (A = CH₃) appears much less effective.

The linear Arrhenius plots of the $k_{\text{Ph}}^{\text{back}}/k_{\text{Ph}}^{\text{front}}$, $k_{\text{Ph}}^{\text{back}}/k_{\text{H}}$, and $k_{\text{Ph}}^{\text{front}}/k_{\text{H}}$, ratios and of the $k_{\text{Ph}}/k_{\text{Me}}$, $k_{\text{Ph}}/k_{\text{H}}$, and $k_{\text{Me}}/k_{\text{H}}$ ratios (Scheme 17), taken in the 25–140 °C interval, obey to the differential activation parameters listed in Table 21. From the reported values, the absolute activation energy for the backside phenyl, frontside phenyl, methyl, and hydrogen participation to the H₂O loss in **26** and **28** (A = H) can be estimated as ranging around 9, 8, 4, and 2 kcal mol⁻¹, respectively.

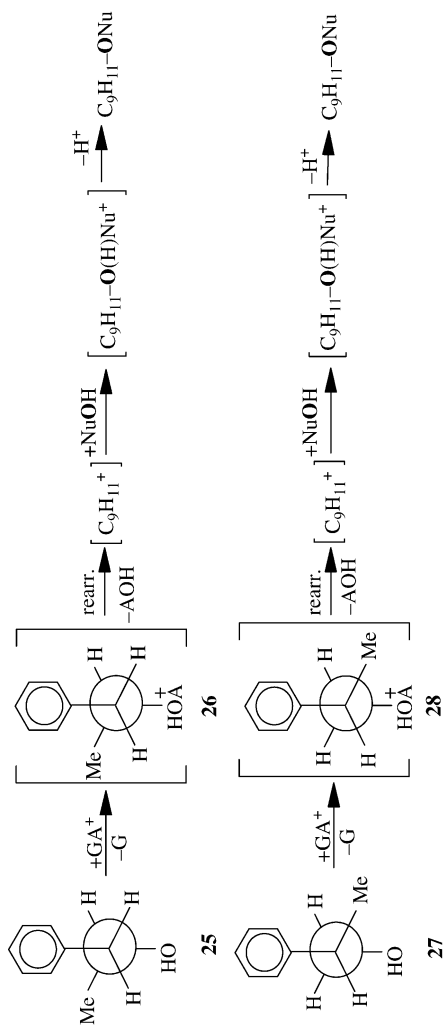
Analysis of Table 21 indicates that, in the 25–140 °C temperature interval, the neighboring-group assistance in **26** and **28** (A = H) is mainly controlled by entropic, rather than enthalpic factors. Furthermore, the counterintuitive observation that the frontside phenyl-group participation involves an activation barrier lower than that of the competing backside participation finds a rationale in the *gauche-anti* conformation of the oxonium ion **26** (A = H), most favored in the gas phase, and on the stabilizing electrostatic interactions between the leaving H₂O moiety and the ring of the phenonium ion in the transition structure **34** (Scheme 18).

Unequivocal characterization of the transition structures involved in the anchimeric assistance to H₂O loss from **26** and **28** (A = H) is obtained by the measurement of the relevant deuterium primary and secondary kinetic effects.

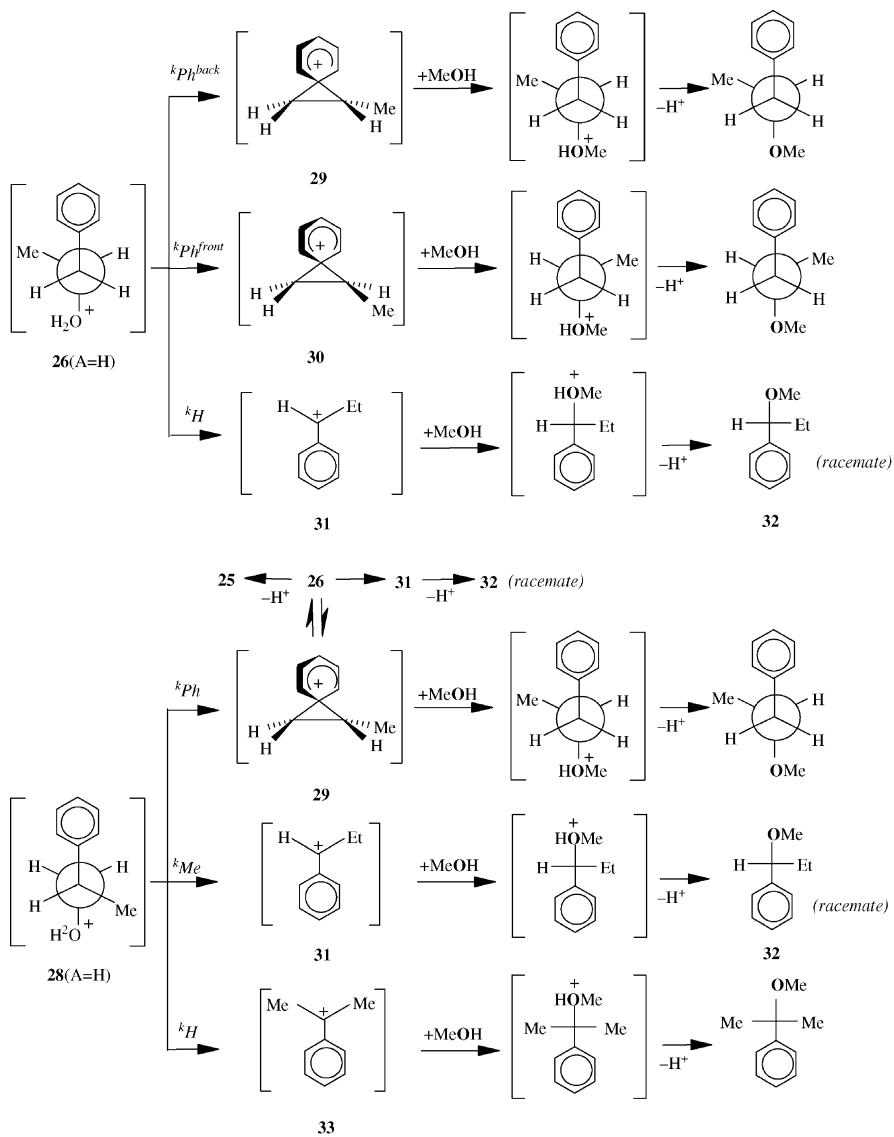
Acid-induced racemization and isomerization of chiral allylic alcohols. Bimolecular nucleophilic displacements in allylic compounds are known to proceed via the four possible pathways shown in Scheme 19.

The existence itself of the S_N2' mechanism, the question of its concertedness, and the origin of its stereochemistry, have been matter of lively debate for the last half-century. The controversy was continuously sustained by the paucity of firm proofs of the S_N2' mechanism in solution and by the coincidence of the S_N2' products with those arising from alternative competing mechanisms, i.e., S_N1, unimolecular rearrangement of the starting alcohol before substitution and of its derivatives after S_N2 substitution, etc.

This ambiguity was removed by the results of a comprehensive investigation on the gas-phase acid-induced nucleophilic substitution on several allylic alcohols showing that the concerted S_N2' reaction competes with the classical S_N2 pathway in the absence of solvation and ion-pairing factors.^{507–509} Assessment of the



Scheme 16



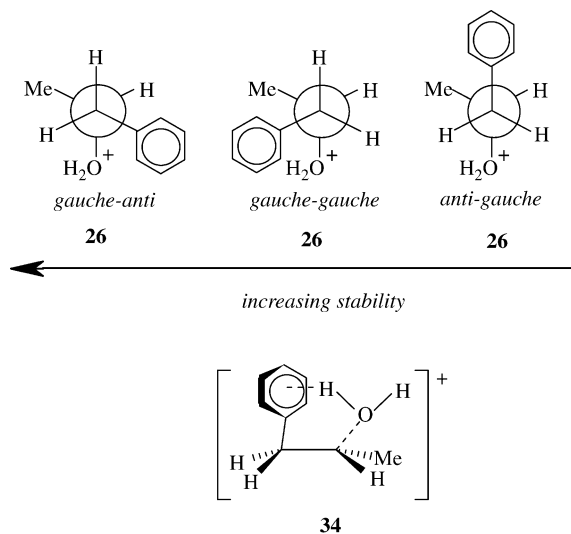
Scheme 17

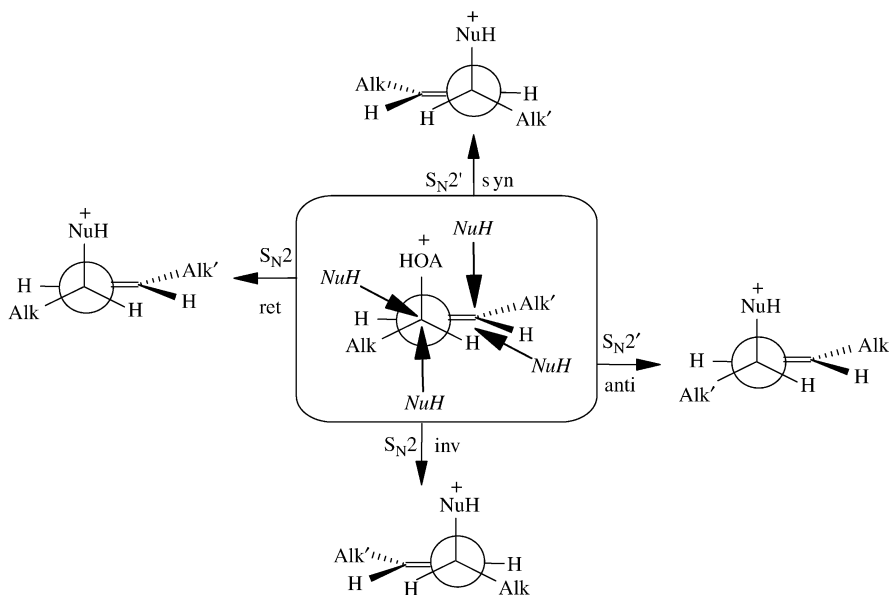
Table 21 Differential Arrhenius parameters for the competing neighboring-group participation to the unimolecular H_2O loss in the chiral oxonium ions **26** and **28** ($A = \text{H}$)

Reaction	Arrhenius equation ($x = 1000/2.303RT$)	Corr. coeff. (r)
29 \leftarrow 26 \rightarrow 31	$\log(k_{\text{Ph}}^{\text{back}}/k_{\text{H}}) = (5.0 \pm 0.3) - (7.0 \pm 0.3)x$	0.960
30 \leftarrow 26 \rightarrow 31	$\log(k_{\text{Ph}}^{\text{front}}/k_{\text{H}}) = (3.2 \pm 0.3) - (5.6 \pm 0.3)x$	0.964
29 \leftarrow 26 \rightarrow 30	$\log(k_{\text{Ph}}^{\text{back}}/k_{\text{Ph}}^{\text{front}}) = (1.7 \pm 0.5) - (1.3 \pm 0.5)x$	0.927
29 \leftarrow 28 \rightarrow 31	$\log(k_{\text{Ph}}/k_{\text{Me}}) = (4.7 \pm 0.2) - (5.7 \pm 0.2)x$	0.997
29 \leftarrow 28 \rightarrow 33	$\log(k_{\text{Ph}}/k_{\text{H}}) = (6.0 \pm 0.2) - (7.1 \pm 0.2)x$	0.997
31 \leftarrow 28 \rightarrow 33	$\log(k_{\text{Me}}/k_{\text{H}}) = (1.3 \pm 0.5) - (1.4 \pm 0.5)x$	0.906

stereochemistry of the gas-phase $\text{S}_{\text{N}}2'$ reactions in these systems requires a detailed knowledge of the extent of conceivable rearrangements in the starting intermediate **35** prior to nucleophilic attack (Scheme 20).

To this purpose, the oxonium ion **35** ($A = \text{H}$; Alk = ethyl; Alk' = methyl) has been generated in the gas phase (720 torr) by protonating the corresponding allylic alcohol with C_nH_5^+ ($n = 1, 2$) and sC_3H_7^+ , obtained respectively by γ -radiolysis of CH_4 and C_3H_8 . Ion **35** was found to undergo appreciable inversion to **36** ($A = \text{H}$; Alk = ethyl; Alk' = methyl) and isomerization to racemate **37** ($A = \text{H}$; Alk = ethyl; Alk' = methyl) in yields (Y_{racem} and Y_{isom} , respectively) which depend on the temperature of the gaseous mixture (40–120 °C) and on the reaction time t . This is defined by the concentration of the powerful $(\text{CH}_3)_3\text{PO}_4$ base (proton affinity (PA) = 212 kcal mol $^{-1}$)⁵⁰⁰ deliberately added to the system. The experimental results, combined with *ab initio* calculations on the model $[\text{C}_3\text{H}_5^+/\text{H}_2\text{O}]$ system, point

**Scheme 18**



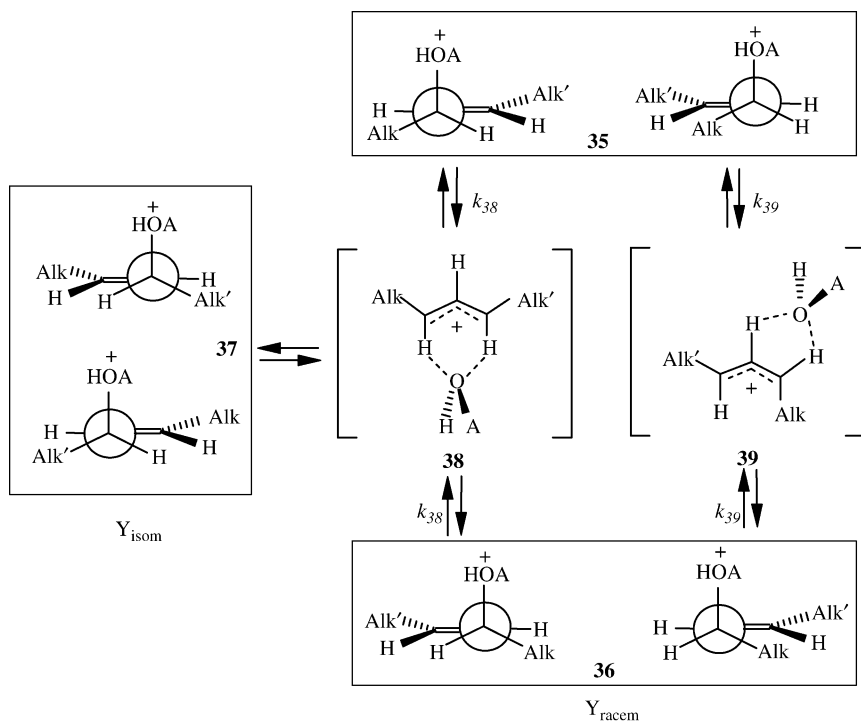
Scheme 19

to the rearrangement of **35** as proceeding through structurally distinct intermediates **38** and **39** characterized by site-specific hydrogen bonding (Scheme 20). If the probabilities of conversion of complex **38** to the **35/36** enantiomeric pair and to isomer **37** are equal, the rate constant for the formation of **38** from **35** can be expressed by $k_{38} = t^{-1} \ln(1 - 2Y_{\text{isom}})^{-1}$ and that for the formation of **39** by $k_{39} = t^{-1} \ln[1 - 2(Y_{\text{racem}} - 0.5Y_{\text{isom}})]^{-1}$. The relevant values are respectively plotted in Fig. 22 as a function of the reaction temperature.

The observation that essentially the same rate constants are measured in methane and propane at 40 and 100 °C demonstrates that the starting oxonium ion **35** is in thermal equilibrium with the bulk gas and that its unimolecular rearrangement depends exclusively on the reaction temperature.

Similar plots have been obtained for the gas-phase rearrangement of **35** ($A = \text{CH}_3$; $\text{Alk} = \text{ethyl}$; $\text{Alk}' = \text{methyl}$) and **36** ($A = \text{CH}_3$; $\text{Alk} = \text{methyl}$; $\text{Alk}' = \text{ethyl}$) in 720 torr methyl chloride in the temperature range from 40 to 120 °C.⁵⁰¹ Regression analysis of the relevant Arrhenius curves leads to the activation parameters listed in Table 22.

The activation parameters of Table 22 suggest that the energy, the charge distribution, and the location of the relevant transition structures (TS) along the reaction coordinate depend significantly on the nature of the moving AOH moiety. When $A = \text{H}$, the racemization and isomerization TS are located early on the reaction coordinate, whereas they are late with $A = \text{CH}_3$ and are characterized by comparatively stronger H-bond interactions.



Scheme 20

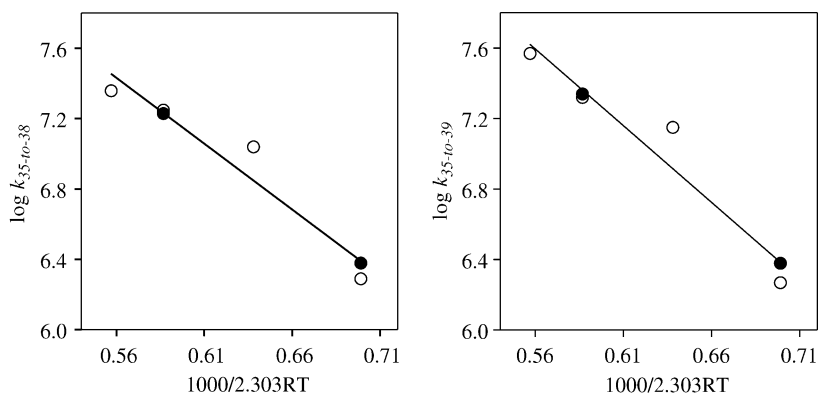


Fig. 22 Left: Arrhenius plots for the formation of intermediate **38** in 720 torr of methane (circles) and propane (diamonds); right: Arrhenius plots for the formation of intermediate **39** in 720 torr of methane (circles) and propane (diamonds).

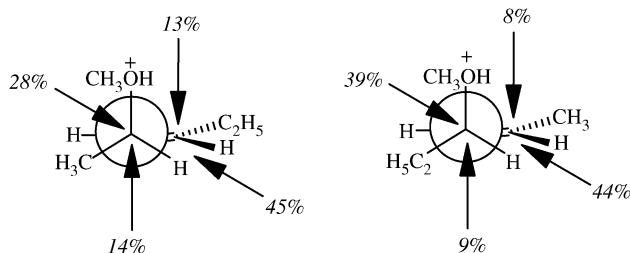
Table 22 Arrhenius parameters for the gas-phase racemization and isomerization of chiral ions **35** and **36**

Reaction	Arrhenius equation ($x = 1000/2.303RT$)	Corr. coeff. (r)	ΔH^* (kcal mol ⁻¹)	ΔS^* (cal mol ⁻¹ K ⁻¹)
35 (A = H; alk = C ₂ H ₅ ; alk' = CH ₃) → 38	$\log k_{38} = (11.6 \pm 0.4) - (7.4 \pm 0.5)x$	0.960	6.7 ± 0.5	-7.9 ± 2.4
35 (A = H; alk = C ₂ H ₅ ; alk' = CH ₃) → 39	$\log k_{39} = (12.5 \pm 0.4) - (8.7 \pm 0.6)x$	0.963	8.0 ± 0.6	-3.7 ± 2.8
35 (A = CH ₃ ; alk = C ₂ H ₅ ; alk' = CH ₃) → 38	$\log k_{38} = (10.6 \pm 0.4) - (5.4 \pm 0.5)x$	0.978	4.7 ± 0.5	-12.4 ± 2.1
35 (A = CH ₃ ; alk = C ₂ H ₅ ; alk' = CH ₃) → 39	$\log k_{39} = (10.1 \pm 0.4) - (6.3 \pm 0.5)x$	0.960	5.6 ± 0.5	-14.6 ± 2.1
36 (A = CH ₃ ; alk = CH ₃ ; alk' = C ₂ H ₅) → 38	$\log k_{38} = (10.9 \pm 0.4) - (5.8 \pm 0.5)x$	0.987	5.1 ± 0.5	-11.2 ± 1.9
36 (A = CH ₃ ; alk = CH ₃ ; alk' = C ₂ H ₅) → 39	$\log k_{39} = (10.3 \pm 0.4) - (6.5 \pm 0.6)x$	0.988	5.8 ± 0.6	-13.6 ± 2.1

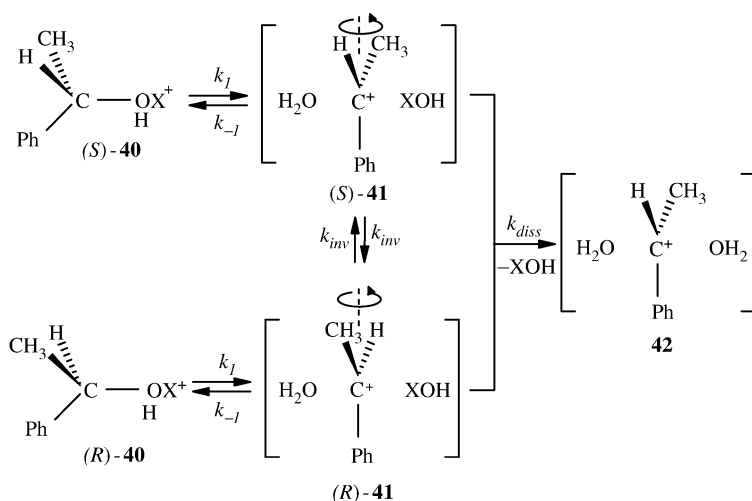
The limited extent of intramolecular rearrangements undergone by the chiral oxonium ions **35** and **36** at 720 torr and at 40 °C (Table 22) allows their use for probing the regio- and stereochemistry of the displacement reactions of Scheme 19. In this case, the allylic alcohol, precursor of the chiral oxonium ions **35** and **36**, acts as the nucleophile NuH.⁵⁰² The relevant results are condensed in Scheme 21.

They are fully consistent with modern concepts^{510–512} pointing to concerted acid-catalyzed S_N2' reactions which are feasible in the gas phase and which efficiently compete with the classical S_N2 processes. According to these concepts, a preferred *anti* relationship between the NuH and the leaving group is observed in gas-phase S_N2'. The relevant TS is only marginally influenced by stereoelectronic factors, while it is strongly favored by the lack of the non-bonding and repulsive Coulombic interactions between NuH and leaving group, which usually play a critical role in the gas phase.

Racemization of chiral α -methyl benzyl cation/methanol adducts. The rate of ¹⁸O exchange between water and the chiral labeled alcohols as a function of racemization has been extensively used as a criterion for discriminating the S_N2 from the S_N1 solvolytic mechanisms in solution. The expected ratio of exchange vs. racemization rate is 0.5 for the S_N2 mechanism and 1.0 for a pure S_N1 process.⁵¹³ With chiral ¹⁸O-enriched 1-phenylethanol in aqueous acids, this ratio is found to be equal to 0.84 ± 0.05. This value has been interpreted in terms of the kinetic pattern of Scheme 22 involving the reversible dissociation of the oxonium ion (*S*)-**40** (XOH = H₂¹⁸O) to the chiral intimate ion–dipole pair (*S*)-**41** ($k_{-1} > k_{inv}$). In (*S*)-**41**, the leaving H₂¹⁸O molecule does not equilibrate immediately with the solvent (i.e., H₂¹⁶O), but remains closely associated with the ion. This means that k_{inv} is of the same order of magnitude of k_{diss} .^{514,515} In contrast, the rate constant ratio of exchange vs. racemization of chiral 1-phenyl-1-methoxyethane in acidic acetonitrile-water solutions is as large as 0.99. The closeness of this value to that of a pure S_N1 mechanism indicates that, in Scheme 22 (XOH = CH₃OH), either k_{inv} is many orders of magnitude lower than k_{diss} or, if not, that internal return is negligible ($k_{-1} \ll k_{inv}$).⁵¹⁶ This kinetic ambiguity prevents identification of the actual factors hindering inversion in (*S*)-**41** (XOH = CH₃OH).

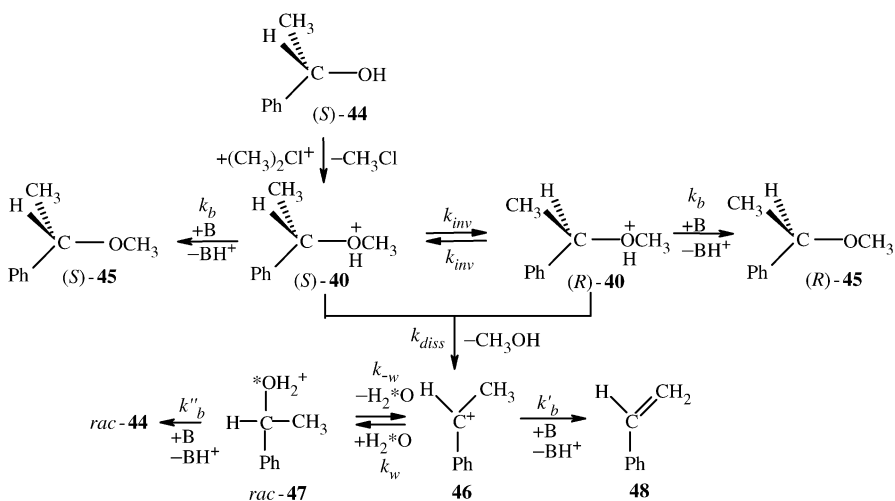


Scheme 21



Scheme 22

Removal of this ambiguity was due to Speranza et al.⁵⁰³ who prepared the chiral oxonium ion (S)-40 (XOH = CH₃OH) in the gas phase by methylation of S(-)-1-phenylethanol ((S)-44) with (CH₃)₂Cl⁺ ions (Scheme 23). The latter ions are generated by γ -radiolysis of CH₃Cl, present as bulk component (720 torr; 25–160 °C) of gaseous mixtures containing traces of the alcoholic substrate (S)-44, of H₂¹⁸O, of a radical scavenger (i.e., O₂), and of a powerful base (i.e., (C₂H₅)₃N).



Scheme 23

Detailed information on the reorganization dynamics of the intimate ion–dipole pair (*S*)-**41**, arising from (*S*)-**40** by C–O bond dissociation, is inferred from the kinetic study of the intracomplex inversion of configuration of (*S*)-**40** vs. its dissociation to α -methylbenzyl cation (**46**) and CH₃OH. The results point to k_{inv} values that are anything but negligible relative to k_{diss} rate constants within the entire temperature range investigated (25–160 °C). Indeed, k_{inv} are just 2–4 time lower than k_{diss} . This implies that, in acidic media, the hindered inversion of (*S*)-**40** (XOH = CH₃OH) has to be ascribed to the lack of appreciable (*S*)-**41** \rightarrow (*S*)-**40** (and (*R*)-**41** \rightarrow (*R*)-**40**) internal return ($k_{-1} \ll k_{\text{inv}}$; Scheme 22), rather than to k_{inv} negligible relative to k_{diss} .⁵¹⁶ Accordingly, the difference in the behavior of (*S*)-**41** (and (*R*)-**41**) in acidic solution essentially reduces to $k_{-1} > k_{\text{diss}}$, when XOH = H₂¹⁸O, and $k_{-1} \ll k_{\text{diss}}$, when XOH = CH₃OH.

Quantum-chemical calculations at the B3LYP/6-31G* level of theory have been employed to gather some insights into the reasons for this dual behavior. The calculations qualitatively indicate that the (*S*)-**40** \rightarrow (*R*)-**40** (XOH = CH₃OH) transition structures are placed late along the reaction coordinate. The CH₃OH moiety is enough removed from the benzyl ion moiety to start interacting with the solvent cage. These interactions favor (*S*)-**41** \rightarrow **42** dissociation and prevent efficient (*S*)-**41** \rightarrow (*S*)-**40** internal return ($k_{-1} < k_{\text{diss}}$ in Scheme 22).⁵¹² The (*S*)-**40** \rightarrow (*R*)-**40** (XOH = H₂¹⁸O) transition structures are instead placed much earlier along the reaction coordinate so as to resemble the starting (*S*)-**40** ion. In them, the moving H₂¹⁸O, less basic than CH₃OH, sits nearby the departure face of the still flexible benzylic residue and does not appreciably interact with its acidic hydrogens. A surplus of energy is needed to remove the H₂¹⁸O moiety far enough to establish appreciable interactions with the solvent cage and to promote (*S*)-**41** \rightarrow **42** dissociation. As a consequence, (*S*)-**41** \rightarrow (*S*)-**40** internal return can efficiently compete with H₂¹⁸O diffusion to the aqueous cage ($k_{-1} > k_{\text{diss}}$). Besides, the shielding effect of the H₂¹⁸O leaving group accounts for the observed prevalence of the inversion of configuration in the H₂O-to-H₂¹⁸O exchange in solution.^{514,515}

Using the same experimental approach, a family of enantiomerically pure oxonium ions, i.e., O-protonated 1-aryl-1-methoxyethanes (aryl = 4-methylphenyl ((*S*)-**49**); 4-chlorophenyl ((*S*)-**50**); 3-(α,α,α -trifluoromethyl)phenyl ((*S*)-**51**); 4-(α,α,α -trifluoromethyl)phenyl ((*S*)-**52**); 1,2,3,4,5-pentafluorophenyl ((*R*)-**53**)) and 1-phenyl-1-methoxy-2,2,2-trifluoroethane ((*R*)-**54**), has been generated in the gas phase by (CH₃)₂Cl⁺-methylation of the corresponding 1-arylethanol.⁵⁰⁴ Some information on their reaction dynamics was obtained from a detailed kinetic study of their inversion of configuration and dissociation. Figs. 23 and 24 report respectively the Arrhenius plots of k_{inv} and k_{diss} for all the selected alcohols, together with (*R*)-**40** of Scheme 23. The relevant linear curves obey the equations reported in Tables 23 and 24, respectively. The corresponding activation parameters were calculated from the transition-state theory.

The activation parameters of the inversion reaction are found to obey two different isokinetic relationships (IKR) depending upon the nature and the position of the substituents in the oxonium ions. In contrast, the activation parameters of the

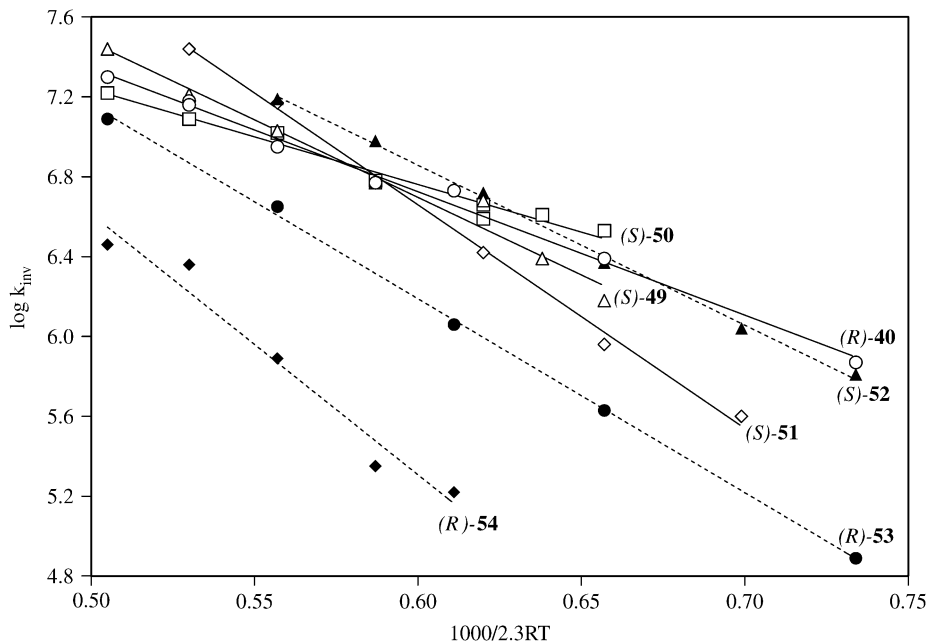


Fig. 23 Arrhenius plots for the inversion of configuration of O-protonated 1-aryl-1-methoxyethanes (aryl = 4-methylphenyl ((S)-49); 4-chlorophenyl ((S)-50); 3-(α,α,α -trifluoromethyl) phenyl ((S)-51); 4-(α,α,α -trifluoromethyl)phenyl ((S)-52); 1,2,3,4,5- pentafluorophenyl ((R)-53); phenyl ((R)-40)) and 1-phenyl-1-methoxy-2,2,2-trifluoroethane ((R) – 54).

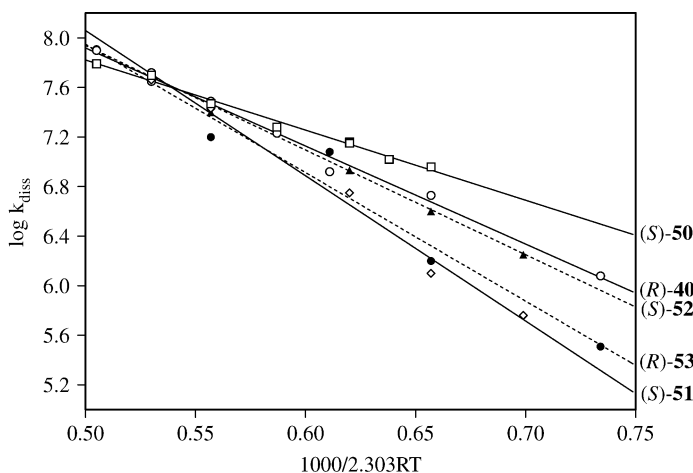


Fig. 24 Arrhenius plots for the dissociation of O-protonated 1-aryl-1-methoxyethanes (aryl = 4-chlorophenyl ((*S*)-**50**); 3-(α,α,α -trifluoromethyl)phenyl ((*S*)-**51**); 4-(α,α,α -trifluoromethyl)phenyl ((*S*)-**52**); 1,2,3,4,5-pentafluorophenyl ((*R*)-**53**); phenyl ((*R*)-**40**)).

dissociation reaction obey a single isokinetic relationship. The curves of Fig. 25 show the existence of two different enthalpy–entropy compensation effects on the gas-phase inversion of **40** and **49–54** ions related to the nature and the position of the substituent(s) in their structure, i.e., the F family (**49**, **50**, **51**, and **40**) and the G family (**52**, **53**, and **54**). In contrast, the curve of Fig. 26 points to the existence of a single enthalpy–entropy compensation in the gas-phase dissociation of the same ions, i.e., the E family (**50**, **51**, **52**, **53**, and **40**).

The definition of IKR implies that, at the isokinetic temperature (T_{iso}), $\Delta G_{\text{iso}}^* = \Delta H^* - T_{\text{iso}} \Delta S^* = \text{const}$. Therefore, the slopes of the linear curves of Figs. 25 and 26 provide the relevant T_{iso} values, while the Y-intercepts give an estimate of the corresponding ΔG_{iso}^* terms. Accordingly, the isokinetic parameters for the F inversion reactions are $T_{\text{iso}} = 376 \pm 2$ K, $\Delta G_{\text{iso}}^* = 10.37 \pm 0.02$ kcal mol $^{-1}$, and $\log k_{\text{iso}} = 6.84$, whereas those for the G inversion reactions are $T_{\text{iso}} = 767 \pm 10$ K, $\Delta G_{\text{iso}}^* = 13.00 \pm 0.05$ kcal mol $^{-1}$, and $\log k_{\text{iso}} = 9.35$. Similarly, the isokinetic parameters for the E dissociations are $T_{\text{iso}} = 409 \pm 5$ K, $\Delta G_{\text{iso}}^* = 9.89 \pm 0.04$ kcal mol $^{-1}$, and $\log k_{\text{iso}} = 7.61$.

The origin of IKR can be interpreted in terms of Linert’s model.⁵¹⁷ The rate constant of a given reaction taking place in a constant-temperature “heat bath” (HB) depends on the collision number between the reacting system (M) and HB molecules, the energy barrier height of the given process, the temperature of the “heat bath”, and the quantum-mechanical transition probability between any reactant level and the transition structure. When the “heat bath” contains energy stored in the form of vibrational degrees, the transition probabilities for vibrational–vibrational energy transfer is expressed by $P_{l,m} = l \exp(\omega/\nu)$ (where m is the HB vibrational level

Table 23 Arrhenius parameters for the gas-phase intracomplex inversion of O-protonated 1-aryl-1-methoxyethanes

Process	Arrhenius equation ($y = 1000/2.303RT$)	Corr. coeff. (r^2)	ΔH_{inv}^* (kcal mol $^{-1}$)	ΔS_{inv}^* (cal mol $^{-1}$ K $^{-1}$)
(<i>S</i>) – 49 → (<i>R</i>) – 49	$\log k_{\text{inv}} = (11.3 \pm 0.3) - (7.8 \pm 0.5)y$	0.978	7.0 ± 0.5	-9.0 ± 0.9
(<i>S</i>) – 50 → (<i>R</i>) – 50	$\log k_{\text{inv}} = (9.6 \pm 0.2) - (4.8 \pm 0.3)y$	0.973	4.0 ± 0.4	-16.9 ± 0.9
(<i>S</i>) – 51 → (<i>R</i>) – 51	$\log k_{\text{inv}} = (13.3 \pm 0.2) - (11.1 \pm 0.3)y$	0.997	10.4 ± 0.3	$+0.1 \pm 1.1$
(<i>R</i>) – 40 → (<i>S</i>) – 40	$\log k_{\text{inv}} = (10.4 \pm 0.1) - (6.2 \pm 0.2)y$	0.994	5.4 ± 0.3	-13.3 ± 1.0
(<i>S</i>) – 52 → (<i>R</i>) – 52	$\log k_{\text{inv}} = (11.7 \pm 0.1) - (8.0 \pm 0.2)y$	0.998	7.3 ± 0.3	-7.4 ± 0.8
(<i>R</i>) – 53 → (<i>S</i>) – 53	$\log k_{\text{inv}} = (12.0 \pm 0.1) - (9.7 \pm 0.2)y$	0.999	8.9 ± 0.2	-5.4 ± 0.5
(<i>R</i>) – 54 → (<i>S</i>) – 54	$\log k_{\text{inv}} = (13.1 \pm 0.8) - (13.0 \pm 1.5)y$	0.964	12.3 ± 1.5	-0.9 ± 1.0

Table 24 Arrhenius parameters for the gas-phase dissociation of O-protonated 1-aryl-1-methoxyethanes

Process	Arrhenius equation ($y = 1000/2.303RT$)	Corr. coeff. (r^2)	ΔH_{diss}^* (kcal mol ⁻¹)	ΔS_{diss}^* (cal mol ⁻¹ K ⁻¹)
(<i>S</i>) - 50 → pClC ₆ H ₄ CHCH ₃ ⁺ + MeOH	$\log k_{\text{diss}} = (10.6 \pm 0.1) - (5.7 \pm 0.2)y$	0.989	4.9 ± 0.3	-12.2 ± 0.7
(<i>S</i>) - 51 → mCF ₃ C ₆ H ₄ CHCH ₃ ⁺ + MeOH	$\log k_{\text{diss}} = (13.9 \pm 0.4) - (11.7 \pm 0.7)y$	0.990	10.9 ± 0.6	+2.6 ± 2.0
(<i>R</i>) - 40 → C ₆ H ₅ CHCH ₃ ⁺ + MeOH	$\log k_{\text{diss}} = (11.9 \pm 0.3) - (7.9 \pm 0.2)y$	0.992	7.1 ± 0.3	-6.7 ± 1.2
(<i>S</i>) - 52 → pCF ₃ C ₆ H ₄ CHCH ₃ ⁺ + MeOH	$\log k_{\text{diss}} = (12.1 \pm 0.3) - (8.4 \pm 0.5)y$	0.990	7.7 ± 0.5	-5.4 ± 1.4
(<i>R</i>) - 53 → C ₆ F ₅ CHCH ₃ ⁺ + MeOH	$\log k_{\text{diss}} = (13.1 \pm 0.7) - (10.3 \pm 1.1)y$	0.965	9.6 ± 1.1	-0.9 ± 1.9

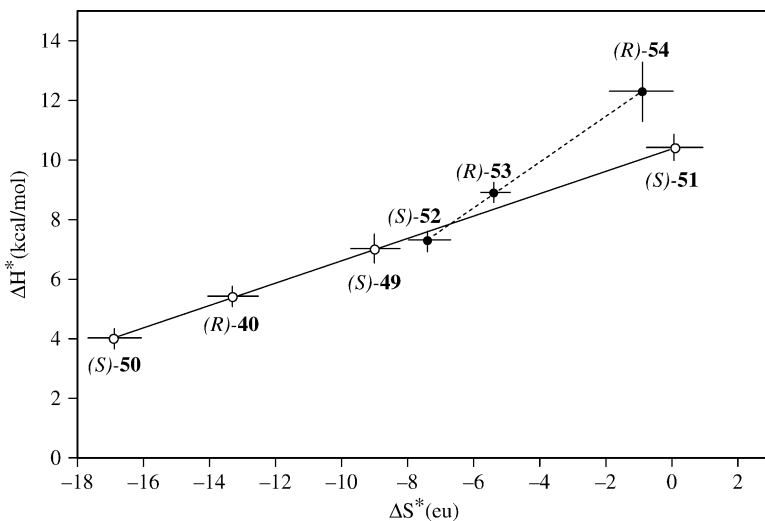


Fig. 25 Enthalpy–entropy compensation plots for the inversion of (S)-49; (S)-50; (S)-51; (R)-40 (the F family) and (S)-52; (R)-53; (R)-54 (the G family).

associated with ν and l is that associated with M) and reach the maximum value for a resonant vibrational–vibrational coupling, i.e., when $\nu m = \omega l$. In the condensed phase, cooperative supramolecular effects normally make available HB vibrational frequencies (ν) which are much smaller than those of M (ω). In this case, the only

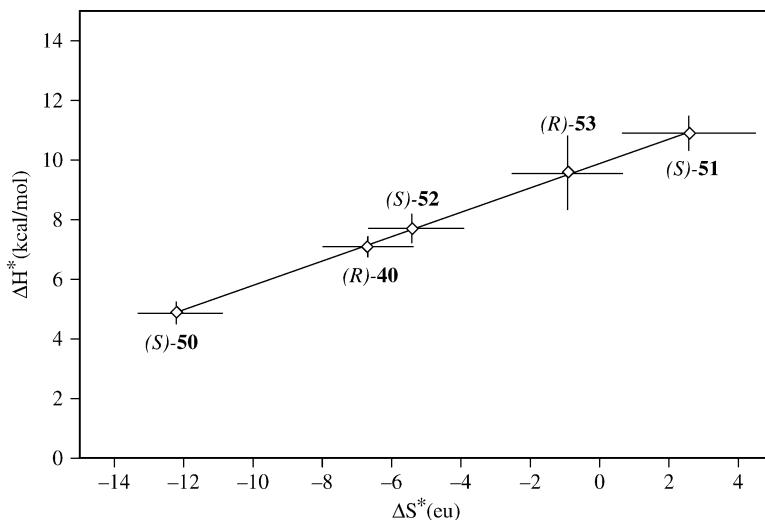


Fig. 26 Enthalpy–entropy compensation plots for the dissociation of (S)-50; (S)-51; (S)-52; (R)-53; (R)-40 (the E family).

variable parameter for a family of reactions is ω and, therefore, the IKR can be expressed mathematically as $\text{dlnk}(\omega)/\text{d}\omega = 0$ at T_{iso} . Accordingly, for a homogeneous family of reactions, such as those involving O-protonated 1-aryl-1-methoxyethanes, a single T_{iso} should be expected whose value (in Kelvin degrees) is related to the characteristic vibrational frequency ν (in cm^{-1}) predominantly exchanging energy in HB by the $T_{\text{iso}} = h\nu/2k_{\text{B}}$ equation, where k_{B} is the Boltzmann constant and h , Planck constant.

While this is the case for the gas-phase E dissociation (Figs. 24 and 26), the observation in the same gaseous HB (CH_3Cl at 720 torr) of two isokinetic temperatures for **40** and **49–54** inversion (Figs. 23 and 25) underlines the existence of a point of discontinuity in the ν/ω coupling which may be peculiar for gaseous media where cooperative supramolecular effects are negligible and, thus, the variable parameters for a family of reactions are both ν and ω .⁵¹⁷

In this frame, the two IKR of Fig. 23 can be rationalized in terms of Larsson's selective energy transfer (SET) model,⁵¹⁸ which introduces in Linert's model the notion of possible switchovers in the resonant ν/ω coupling. Thus, in the assumption of full ν/ω resonance ($T_{\text{iso}} = h\nu/2k_{\text{B}}$), $T_{\text{iso}} = 376 \pm 2$ K for the inversion of configuration of the F family corresponds to a vibrational frequency ν_{F} predominantly exchanging energy of 523 ± 3 cm^{-1} , while $T_{\text{iso}} = 767 \pm 10$ K for the inversion of the G family to a predominant vibrational frequency $\nu_{\text{G}} = 1067 \pm 14$ cm^{-1} . According to theory, these frequencies should correspond to intense absorption bands of the vibrational spectrum of gaseous CH_3Cl . As a matter of fact, the IR spectrum of gaseous CH_3Cl shows characteristic vibrational bands around 1015 cm^{-1} , assigned to its $\nu_6(\text{e})$ CH_3 -rocking mode. On the contrary, none of the characteristic absorption bands of the CH_3Cl spectrum can account for $T_{\text{iso}} = 376 \pm 2$ K obtained for the F series. Rather, this T_{iso} value reflects the activation of the F ions by a more intimate mechanism involving their transient complexation with a CH_3Cl molecule. Indeed, HF/6-31G* calculations of a model complex between O-protonated benzyl methyl ether and CH_3Cl indicate the presence of nine vibrational frequencies over those characteristic of the two isolated components. Among these, that related to the out-of-plane C–Cl \cdots H–O bending mode falls at 572 cm^{-1} , a value which is close to the experimental $\omega_{\text{F}} = 523 \pm 3$ cm^{-1} one. The same 572 cm^{-1} vibrational mode coincides with the critical $\omega_{\text{diss}} = 569$ cm^{-1} value for the dissociation of the E family ($T_{\text{iso}} = 409 \pm 5$ K).

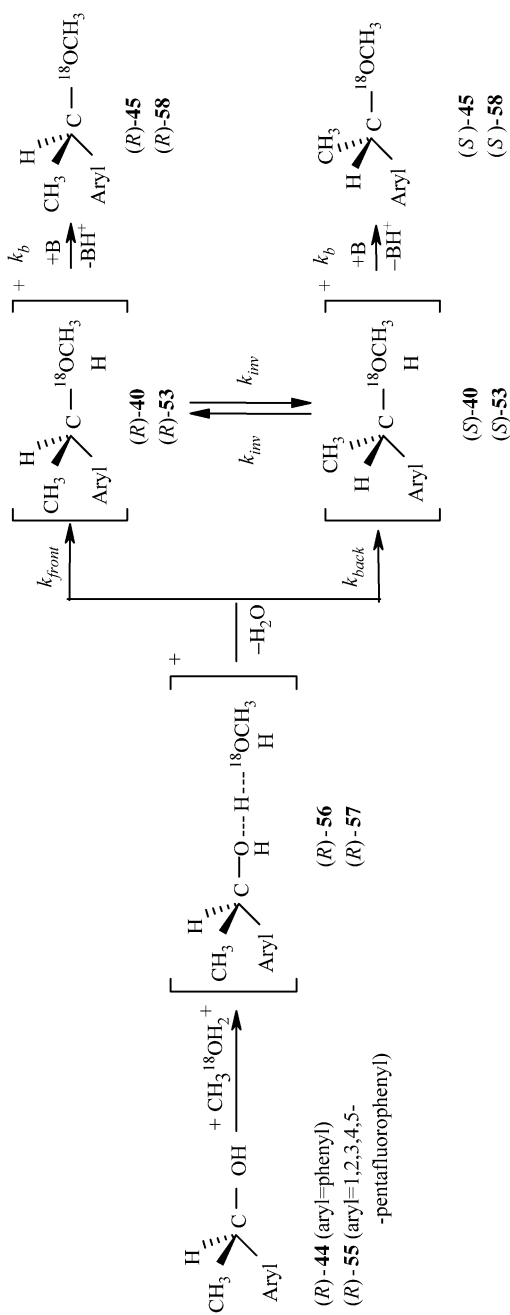
It is concluded that the inversion of configuration of the selected family of O-protonated 1-aryl-1-methoxyethanes obey two different reaction dynamics driven by the activation dynamics from the bulk gas (CH_3Cl). Thus, if activation predominantly proceeds through a resonant energy exchange with $\nu_6(\text{e}) = 1015$ cm^{-1} CH_3 -rocking mode of the unperturbed molecule of the bath gas (CH_3Cl), the inversion reaction proceeds through the dynamically most accessible TS involving unassisted C α –O bond rupture (the G family). If, instead, activation involves the out-of-plane C–Cl \cdots H–O bending vibration developed in the intimate encounter complex between CH_3Cl and the oxonium ions, the inversion

reaction proceeds through the energetically most accessible TS where the CH_3OH motion is assisted by coordination with the acidic hydrogens of the benzylic residue (the F family). The same vibrational mode is active in promoting the dissociation of most of members of the oxonium ions **40/49-54** family, irrespective of their belonging to the F or G sets.

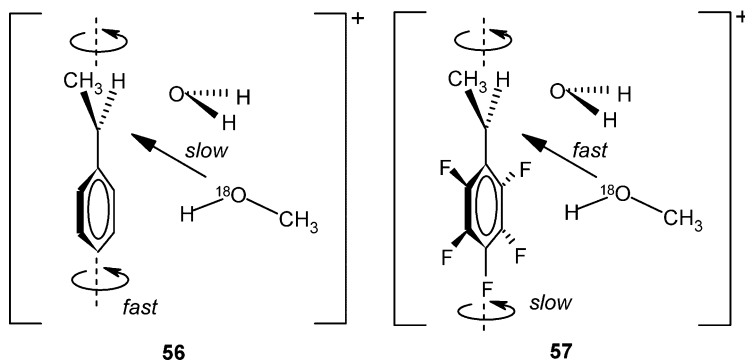
Gas-phase intracomplex substitution in (R)-(+)-1-arylethanol/ $\text{CH}_3^{18}\text{OH}_2^+$ adducts. It is well established that bimolecular $\text{S}_{\text{N}}2$ reactions generally involve predominant inversion of configuration of the reaction center. Unimolecular $\text{S}_{\text{N}}1$ displacements instead proceed through the intermediacy of free carbocations and, therefore, usually lead to racemates. However, many alleged $\text{S}_{\text{N}}1$ solvolyses do not give fully racemized products. The enantiomer in excess often, but not always, corresponds to inversion. Furthermore, the stereochemical distribution of products may be highly sensitive to the solvolytic conditions.⁵¹⁹ These observations have led to the concept of competing^{520–522} or mixed^{522–524} $\text{S}_{\text{N}}1$ - $\text{S}_{\text{N}}2$ mechanisms. More recently, the existence itself of $\text{S}_{\text{N}}1$ reactions has been put into question.⁵²⁵

Some obscure facets of this intricate picture have been unveiled by Filippi and Speranza who investigated the stereochemistry and the intimate mechanism of a model “solvolytic” reaction taking place in an ion-dipole pair in the gaseous phase.⁵⁰⁵ Adducts (R)-**56** and (R)-**57** are obtained in the gas phase by association of the relevant chiral alcohols, i.e., (R)-(+)-1-phenyl-ethanol ((R)-**44**) and (R)-(+)-1-(pentafluorophenyl)ethanol ((R)-**55**), with the $\text{CH}_3^{18}\text{OH}_2^+$ ion, generated by γ -radiolysis of $\text{CH}_3\text{F}/\text{H}_2^{18}\text{O}$ mixtures (Scheme 24). As mentioned above, the absence of neutral nucleophile molecules, i.e., $\text{CH}_3^{18}\text{OH}$, in the reaction medium ensures that the ^{18}O -labeled ethers **45** and **58** of Scheme 24 arise exclusively from the intracomplex “solvolysis” of (R)-**56** and (R)-**57**, respectively.

The experimental results point to intracomplex “solvolysis” in (R)-**56** and (R)-**57** as proceeding through the intermediacy of the relevant benzyl cation (a pure $\text{S}_{\text{N}}1$ mechanism). “Solvolysis” of (R)-**56** leads to complete racemization at $T > 50^\circ\text{C}$, whereas at $T < 50^\circ\text{C}$ the reaction displays a preferential retention of configuration. Predominant retention of configuration is also observed in the intracomplex “solvolysis” of (R)-**57**. The exothermic intracomplex displacement in (R)-**56** proceeds through TS's characterized by non-covalent interactions between the stable benzyl cation and the nucleophile/leaving group pair (an $\text{S}_{\text{N}}1$ process). The formation of the (R/S)-**40** racemate from (R)-**56** at $T > 50^\circ\text{C}$ is entirely consistent with this view. In this frame, the slight predominance of retained (R)-**40** over the inverted (S)-**40**, observed at $T < 50^\circ\text{C}$, is accounted for by a free rotation of the benzylic moiety of complex **56** (Scheme 25) slower than its bonding to $\text{CH}_3^{18}\text{OH}$. In fact, the procedure adopted to generate (R)-**56** in the gas phase requires that the $\text{CH}_3^{18}\text{OH}$ moiety resides initially in the same region of space containing the leaving group. In the absence of any intracomplex rotation of the benzylic moiety of **56**, $\text{CH}_3^{18}\text{OH}$ is spatially situated to attack from the frontside (a “troposelective” reaction).⁵⁰⁵ At higher temperatures, this positional advantage is annulled and the (R/S)-**40** racemate is formed.



Scheme 24



Scheme 25

The intracomplex “solvolysis” of (*R*)-**57** can be considered highly troposelective since it involves predominant retention of configuration (88% at 25 °C). Inductive and resonance effects of the ring fluorine substituents reduce appreciably the stabilization energy of α -methyl pentafluorobenzyl cation relative to the unsubstituted homologue. This implies that the interactions between the nucleophile/leaving group and benzylic moiety in complex **57** (Scheme 25) is stronger than those operating in adduct **56**. As a consequence, free rotation of benzylic moiety in **57** is slow relative to covalent bonding with $\text{CH}_3^{18}\text{OH}$.

The above gas-phase picture may represent a guideline for understanding the mechanism and the stereochemistry of substitution reactions in the solvent cage. The results of gas-phase (*R*)-**44** “solvolysis” demonstrate the existence of a pure $\text{S}_{\text{N}}1$ mechanism. Fast rotation of the benzylic moiety in the complex **56** of Scheme 25 ($T > 50^\circ$) explains the formation of the product racemate. If rotation is hampered by significant ion-nucleophile interactions (as in (*R*)-**55** and (*R*)-**44** at $T < 50^\circ$), predominant retention of configuration is observed. This may explain why some solvolytic reactions lead to a slight excess of the retained product in the liquid phase. However, the presence of the solvent cage may alter this picture and favor inversion of configuration even if a pure $\text{S}_{\text{N}}1$ solvolysis is taking place. This may happen when reorientation of the ion in the cage is slow and if the presence of the leaving group somewhat hampers the approach of the nucleophile from the frontside. However, inversion of configuration predominates even when the relative motionlessness of the ion in the solvent cage is due to a partial covalency of its interactions with the leaving group and the nucleophilic solvent (a $\text{S}_{\text{N}}2$ process). It is concluded that the solvolytic reactions are mostly governed by the lifetime and the dynamics of the species involved and, if occurring in solution, by the nature of the solvent cage. Their rigid subdivision into the $\text{S}_{\text{N}}1$ and $\text{S}_{\text{N}}2$ mechanistic categories appears inadequate and the use of their stereochemistry as a mechanistic probe can be highly misleading.

6 Concluding remarks

In the present excursion through the world of non-covalent clusters in the gas phase, the reader can readily realize the exceptional experimental and conceptual know-how needed for generating weakly-bonded aggregates in the gas phase and for examining their structural and stability features at the microscopic level. The huge effort unfolded along this direction by most advanced spectroscopic and mass spectrometric methodologies is fully rewarded by precious information about the nature of the intrinsic non-covalent interactions in gaseous clusters and their impact on the physics, the chemistry, and the biochemistry of species involved.

The energy of non-covalent interactions under ambient conditions is comparable to the average thermal energy of the kinetic motion of molecules. This has an important consequence: even strong non-covalent bonds can be easily broken under ambient conditions, while most covalent bonds cannot. Thus, non-covalent aggregates are often dynamic systems of limited stability and high structural flexibility. Sometimes, however, the combination of several non-covalent bonds confers a pronounced stability even to very flexible aggregates. This combination represents the keystone of living matter: biomacromolecules “communicate” through multiple non-covalent interactions which must be sufficiently strong to ensure preferential bonding among them, but not so strong to allow thermodynamic sinks which would be incompatible with the existence of living matter itself. Thus, understanding the way biomacromolecules “communicate” in living systems or the forces holding molecules together in supramolecular assemblies require a deep knowledge of non-covalent interactions in simplified models. Of particular interest for understanding chiral recognition and rate acceleration of biomacromolecules are those involving chiral species. A key step along this direction requires the study the single interactions acting between the individual chiral components of tailor-made ionic and molecular clusters in the gas phase, without any interference from the environment.

A compendium of the most relevant studies on the structure, stability, reactivity, and dynamics of chiral molecular and ionic clusters in the gas phase has been reported in the present chapter, together with a presentation of the experimental and theoretical methodologies adopted. REMPI, LIF, HB, and RET spectroscopies, coupled with supersonic beam expansion, have allowed to establish the structure and the energetics of diastereomeric molecular clusters at very low temperatures. The introduction of ESI, MALDI, and FAB sources in mass spectrometry has allowed the generation of chiral clusters of biological interest and their characterization beyond the mere mass determination. Thus, precious information on the interaction of biomolecules around metal centers, the energetics of chiral host/guest inclusion pairs, and the enantioselectivity of chiral molecules in enzyme mimics are nowadays available. Comprehensive mechanistic and dynamic studies on the most classical stereoselective reactions involving chiral encounter complexes has been made possible by a careful application of the radiolytic method.

These gas-phase studies were driven by the continuing interest in chiral species, whether involved in enantioselective reactions, or in the origin of life, or in biochemical cycles. The body of information arising from these huge experimental and theoretical efforts represents the basis for unravelling the details of complicated chemical and biochemical processes occurring in condensed phases. It is only a matter of time before relatively simple reactions of biological significance, such as an enantioselective reaction in a receptor cavity, can be studied in the gas phase.

Acknowledgements

The author acknowledges the contribution of his coworkers, as cited in the references. In particular, thanks are due to Antonello Filippi and Anna Giardini and her group for their contribution to the continuing work in the field of gaseous chiral clusters. Special acknowledgements are addressed to his recently deceased advisor, Fulvio Cacace, for his tireless support and encouragement.

References

1. Hollfelder, F., Kirby, A.J. and Tawfik, D.S. (1996). *Nature* **383**, 60
2. Van der Waals Molecules I (1988). *Chem. Rev.* **88** (6)
3. Van der Waals Molecules II (1994). *Chem. Rev.* **94** (7)
4. Castleman, A.W., Jr. and Bowen, K., Jr. (1996). *J. Phys. Chem.* **100**, 12911
5. Robertson, E.G. and Simons, J.P. (2001). *Phys. Chem. Chem. Phys.* **3**, 1
6. Rizzo, T.R., Park, Y.D., Peteanu, L.A. and Levy, D.H. (1985). *J. Chem. Phys.* **85**, 4819
7. Rizzo, T.R., Park, Y.D., Peteanu, L.A. and Levy, D.H. (1986). *J. Chem. Phys.* **86**, 2534
8. Rizzo, T.R., Park, Y.D. and Levy, D.H. (1986). *J. Chem. Phys.* **86**, 6945
9. Philips, L.A. and Levy, D.H. (1986). *J. Chem. Phys.* **90**, 4921
10. Plützer, C., Nir, E., de Vries, M.S. and Kleinermanns, K. (2001). *Phys. Chem. Chem. Phys.* **3**, 5466
11. Nir, E., Janzen, Ch., Imhof, P., Kleinermanns, K. and de Vries, M.S. (2001). *J. Chem. Phys.* **115**, 4604
12. Buckingham, A.D., Fowler, P.W. and Hutson, J.M. (1988). *Chem. Rev.* **88**, 963
13. Scheiner, S. (1997). *Hydrogen Bonding. A Theoretical Perspective*. Oxford University Press, New York
14. Steiner, T. and Desiraju, G.R. (1998). *Chem. Commun.* 891
15. Djafari, S., Barth, H.D., Buchhold, K. and Brutschy, B. (1997). *J. Chem. Phys.* **107**, 10573
16. Reed, A., Curtiss, L.A. and Weinhold, F. (1988). *Chem. Rev.* **88**, 899
17. Hobza, P., Spirko, V., Selzle, H.L. and Schlag, E.W. (1998). *J. Phys. Chem. A* **102**, 2501
18. Hobza, P., Spirko, V., Havlas, Z., Buchhold, K., Reinmann, B., Barth, H.D. and Brutschy, B. (1999). *Chem. Phys. Lett.* **299**, 180
19. Hobza, P. and Havlas, Z. (1999). *Chem. Phys. Lett.* **303**, 447
20. Lee, J.C., Peris, E., Rheingold, A.L. and Crabtree, R.H. (1994). *J. Am. Chem. Soc.* **116**, 11014
21. Richardson, T.B., De Gala, S. and Crabtree, R.H. (1995). *J. Am. Chem. Soc.* **117**, 12875
22. Klooster, W.T., Koetzle, T.F., Siegbahn, P.E.M., Richardson, T.B. and Crabtree, R.H. (1999). *J. Am. Chem. Soc.* **121**, 6337

23. Liu, Q. and Hoffmann, R. (1995). *J. Am. Chem. Soc.* **117**, 10108
24. Hobza, P., Selzle, H.L. and Schlag, E.W. (1994). *Chem. Rev.* **94**, 1767
25. Hobza, P., Selzle, H.L. and Schlag, E.W. (1996). *J. Phys. Chem.* **100**, 18790
26. Hunter, C.A., Singh, J. and Thornton, J.M. (1991). *J. Mol. Biol.* **218**, 837
27. Lehn, J.M., Atwood, J.L., Davies, J.E.D., MacNicol, D.D. and Vögtle, F. (eds) (1996). In *Comprehensive Supramolecular Chemistry*. Pergamon, Oxford
28. Nanostructures (1999). *Chem. Rev.* **99** (7)
29. Duncan, R. and Kopecek, J. (1984). *Adv. Polym. Sci.* **57**, 51
30. Peppas, N.A., Nagai, T. and Miyajima, M. (1994). *Pharm. Technol. Jpn* **10**, 611
31. Bieniarz, C. (1999). *Technology Encyclopedia of Pharmaceutical*, p. 55. Marcel Dekker, New York
32. Akiyoshi, K. (1994). *Kagaku (Kyoto)* **49**, 442
33. Tzalis, D. and Tor, Y. (1996). *Tetrahedron Lett.* **37**, 8293
34. Huck, W.T.S., Prins, L.J., Fokkens, R.H., Nibbering, N.M.M., van Veggel, F.C.J.M. and Reinhoudt, D.N. (1998). *J. Am. Chem. Soc.* **120**, 6240
35. Knapen, J.W.J., van der Made, A.W., de Wilde, J.C., van Leeuwen, P.W.W.N.M., Wijkens, P., Grove, D.M. and van Koten, G. (1994). *Nature* **372**, 659
36. Kokufuta, E. (1993). *Adv. Polym. Sci.* **110**, 157
37. Warshel, A., Papazyan, A. and Kollman, P.A. (1995). *Science* **269**, 102
38. Saenger, W. (1984). *Principles of Nucleic Acid Structure*. Springer, New York
39. Massova, I. and Kollman, P.A. (1999). *J. Am. Chem. Soc.* **121**, 8133
40. Hudgins, R.R. and Jarrold, M.F. (1999). *J. Am. Chem. Soc.* **121**, 3494
41. Kauzman, W. (1959). *Rev. Mod. Phys.* **31**, 549
42. Schnier, P.D., Klassen, J.S., Strittmatter, E.F. and Williams, E.R. (1998). *J. Am. Chem. Soc.* **120**, 9605
43. Pichierri, F., Aida, M., Gromiha, M.M. and Sarai, A. (1999). *J. Am. Chem. Soc.* **121**, 6152
44. Lippard, S. and Berg, J.M. (1994). *Principles of Bioinorganic Chemistry*. University Science Books, Mill Valley, CA
45. Cerda, B.A. and Wesdemiotis, C. (1996). *J. Am. Chem. Soc.* **118**, 11884
46. Misra, V.K. and Draper, D.E. (1998). *Biopolymers* **48**, 113
47. Curtain, C.C., Ali, F., Volitakis, I., Cherny, R.A., Norton, R.S., Beyreuther, K., Barrow, C.J., Masters, C.L., Bush, A.I. and Barnham, K.J. (2001). *J. Biol. Chem.* **276**, 20466
48. Curtain, C.C., Ali, F., Volitakis, I., Cherny, R.A., Norton, R.S., Beyreuther, K., Barrow, C.J., Masters, C.L., Bush, A.I. and Barnham, K.J. (2001). *J. Neurochem.* **76**, 1509
49. Sakoda, S., Ogawa, Y., Nagano, S., Fukada, K., Konaka, K., Nakanishi, T., Shimizu, A., Tohyama, C. and Satoh, M. (2002). *Biomed. Res. Trace Elements* **13**, 11
50. Rodriguez, J.A., Valentine, J.S., Eggers, D.K., Roe, J.A., Tiwari, A., Brown, R.H., Jr. and Hayward, L.J. (2002). *J. Biol. Chem.* **277**, 15932
51. Reglinski, J., Armstrong, D.R., Sealey, K. and Spicer, M.D. (1999). *Inorg. Chem.* **38**, 733
52. Roehm, P.C. and Berg, J.M. (1997). *Biochemistry* **36**, 10240
53. Zheng, L., Pan, H., Li, S., Flesken Nikitin, A., Chen, P.L., Boyer, T.G. and Lee, W.H. (2000). *Mol. Cell.* **6**, 757
54. Bodrossy, L. and Kovacs, K.L. (1994). *Indian J. Exp. Biol.* **32**, 443
55. Jablonski, P.E., Lu, W.P., Ragsdale, S.W. and Ferry, J.G. (1993). *J. Biol. Chem.* **268**, 325
56. Rosenzweig, A.C., Nordlund, P., Takahara, P.M., Frederick, C.A. and Lippard, S.J. (1995). *Chem. Biol.* **2**, 409
57. Vallee, B.L. and Auld, D.S. (1992). *Matrix Suppl.* **1**, 5
58. Crack, P.J., Wu, T.J., Cummins, P.M., Ferro, E.S., Tullai, J.W., Glucksman, M.J. and Roberts, J.L. (1999). *Brain Res.* **835**, 113
59. Ajay, M.A.M. (1995). *J. Med. Chem.* **38**, 4953
60. Eisenman, G. (1962). *Biophys. J.* **2**, 259
61. Wang, B.C. and Craven, B.M. (1971). *Chem. Commun.* 290

62. Bernhardt, P.V. (1999). *Inorg. Chem.* **38**, 3481
63. Dougherty, D.A. (1996). *Science* **271**, 163
64. Ma, J.C. and Dougherty, D.A. (1997). *Chem. Rev.* **97**, 1303
65. Caldwell, J.W. and Kollman, P.A. (1995). *J. Am. Chem. Soc.* **117**, 4177
66. Minoux, H. and Chipot, C. (1999). *J. Am. Chem. Soc.* **121**, 10366
67. Gallivan, J.P. and Dougherty, D.A. (1999). *Proc. Natl Acad. Sci. USA* **96**, 9459
68. Hu, P., Sorensen, C. and Gross, M.L. (1995). *J. Am. Soc. Mass Spectrom.* **6**, 1079
69. Cerda, B.A., Cornett, L. and Wesdemiotis, C. (1999). *Int. J. Mass Spectrom.* **193**, 205
70. Ryzhov, V., Dunbar, R.C., Cerda, B.A. and Wesdemiotis, C. (2000). *J. Am. Soc. Mass Spectrom.* **11**, 1037
71. Armentrout, P.B. and Rodgers, M.T. (2000). *J. Phys. Chem. A* **104**, 2238
72. Castleman, A.W., Jr., Peterson, K.I., Upschulte, B.I. and Schelling, F.J. (1983). *Int. J. Mass Spectrom. Ion Process.* **47**, 203
73. Hoyau, S., Norman, K., McMahon, T.B. and Ohanessian, G. (1999). *J. Am. Chem. Soc.* **121**, 8864
74. Nayal, M. and Di Cera, E. (1996). *J. Mol. Biol.* **256**, 228
75. Wouters, J. (1998). *Protein Sci.* **7**, 2472
76. De Wall, S.L., Meadows, E.S., Barbour, L.J. and Gokel, G.W. (2000). *Proc. Natl Acad. Sci. USA* **97**, 6271
77. Silvermann, S.K., Lester, H.A. and Dougherty, D.A. (1998). *Biophys. J.* **75**, 1330
78. Nakamura, R.L., Anderson, J.A. and Gaber, R.F. (1997). *J. Biol. Chem.* **272**, 1011
79. Jockusch, R.A., Price, W.D. and Williams, E.R. (1999). *J. Phys. Chem. A* **103**, 9266
80. Dunbar, R.C. (2000). *J. Phys. Chem. A* **104**, 8067
81. Siu, F.M., Ma, N.L. and Tsang, C.W. (2001). *J. Am. Chem. Soc.* **123**, 3397
82. Schreier, P., Bernreuther, A. and Huffer, M. (1995). *Analysis of Chiral Organic Molecules. Methodology and Applications*, Chapter 3. Walter de Gruyter, Berlin
83. Koppenhoefer, B., Epperlein, U. and Schwierskott, M. (1997). *Fresenius' J. Anal. Chem.* **359**, 107
84. Desiderio, C. and Fanali, S. (1998). *J. Chromatogr. A* **807**, 37
85. Pirkle, W.H. and House, D.W. (1979). *J. Org. Chem.* **44**, 1957
86. Taylor, D.R. and Maher, K. (1992). *J. Chromatogr. Sci.* **30**, 67
87. Gubitz, G. (1990). *Chromatographia* **30**, 555
88. Agnew-Heard, K.A., Pena, M.S., Shamsi, S.A. and Warner, I.M. (1997). *Anal. Chem.* **69**, 958
89. Dzygiel, P., Rudzinska, E., Wieczorek, P. and Kafarski, P. (2000). *J. Chromatogr. A* **895**, 301
90. Kubo, Y., Maeda, S., Tokita, S. and Kubo, M. (1996). *Nature (London)* **382**, 522
91. Fleischhauer, J., Harmata, M., Kahraman, M., Koslowski, A. and Welch, C.J. (1997). *Tetrahedron Lett.* **38**, 8655
92. Chappell, J.S. (1997). *Analyst (Cambridge UK)* **122**, 755
93. Kram, T.C. and Lurie, I.S. (1992). *Forensic Sci. Int.* **55**, 131
94. James, T.D., Sandanayake, K. and Shinkai, S. (1995). *Nature (London)* **374**, 345
95. Takeuchi, M., Yoda, S., Imada, T. and Shinkai, S. (1997). *Tetrahedron* **53**, 8335
96. Parker, K.S., Townshend, A. and Bale, S.J. (1995). *Anal. Proc.* **32**, 329
97. Parker, K.S., Townshend, A. and Bale, S.J. (1996). *Anal. Commun.* **33**, 265
98. Grady, T., Harris, S.J., Smyth, M.R. and Diamond, D. (1996). *Anal. Chem.* **68**, 3775
99. Schuette, J.M., Will, A.Y., Agbaria, R.A. and Warner, I.M. (1994). *Appl. Spectrosc.* **48**, 581
100. Yang, H. and Bohne, C. (1995). *J. Photochem. Photobiol. A* **86**, 209
101. Lahmani, F., Barbu, K.L. and Zenacker-Rentien, A. (1999). *J. Phys. Chem. A* **103**, 1991
102. Al-Rabaa, A.A., Barbu, K.L., Lahmani, F. and Zenacker-Rentien, A. (1997). *J. Phys. Chem. A* **101**, 3273

103. Latini, A., Toja, D., Giardini Guidoni, A., Palleschi, A., Piccirillo, S. and Speranza, M. (1999). *Chirality* **11**, 376
104. Sawada, M., Okumura, Y., Shizuma, M., Yamada, H., Kaneda, T. and Hanafusa, T. (1993). *J. Am. Chem. Soc.* **115**, 7381
105. Camara, E., Green, M.K., Penn, S.G. and Lebrilla, C.B. (1996). *J. Am. Chem. Soc.* **118**, 8751
106. Hofmeister, G. and Leary, J.A. (1991). *Org. Mass Spectrom.* **26**, 811
107. Hagen, O.F. and Obert, W. (1972). *J. Chem. Phys.* **56**, 1793
108. Ryali, S.B. and Fenn, J.B. (1984). *Ber. Bunsen-Ges. Phys. Chem.* **88**, 245
109. Mann, D.M. and Broida, H.P. (1973). *J. Appl. Phys.* **44**, 4950
110. Mandich, M.L., Reents, W.D., Jr. and Bondybey, V.E. (1990). *Atomic and Molecular Clusters*. Bernstein, E.R. (ed.). Elsevier, Amsterdam
111. Pfund, A.H. (1930). *Rev. Sci. Instr.* **1**, 397
112. Yokozeki, A. and Stein, G.D. (1978). *J. Appl. Phys.* **49**, 2224
113. Mühlbach, J., Pfau, P., Sattler, K. and Recknagel, E. (1982). *Z. Phys. B* **47**, 233
114. Frank, F., Schulze, W., Tesche, B., Urban, J. and Winter, B. (1985). *Surf. Sci.* **156**, 90
115. Martin, T.P. (1984). *J. Chem. Phys.* **81**, 4426
116. Riley, S.J., Parks, E.K., Mao, C.R., Pobo, L.G. and Wexler, S. (1982). *J. Phys. Chem.* **86**, 3911
117. Campargue, R. (1964). *Rev. Sci. Instrum.* **35**, 111
118. Powers, D.E., Hansen, S.G., Geusic, M.E., Pulu, A.C., Hopkins, J.B., Dirtz, T.G., Duncan, M.A., Langridge-Smith, P.R.R. and Smalley, R.E. (1982). *J. Phys. Chem.* **86**, 2556
119. Bowles, R.S., Kolstad, J.J., Calo, J.M. and Andres, R.P. (1981). *Surf. Sci.* **106**, 117
120. Patil, A.N., Paithankar, D.Y., Otsuka, N. and Andres, R.P. (1993). *Z. Phys. D* **26**, 135
121. Hortig, G. and Muller, M. (1969). *Z. Phys.* **221**, 119
122. Krohn, V.E., Jr. (1962). *J. Appl. Phys.* **33**, 3523
123. Middleton, R. (1977). *Nucl. Instrum. Methods* **144**, 373
124. Leleyter, M. and Joyes, P. (1974). *J. Phys (Paris)* **35**, L8
125. Orth, R.G., Jonkman, H.J. and Michl, J. (1981). *J. Am. Chem. Soc.* **103**, 1564
126. Fehsenfeld, F.C. and Ferguson, E.E. (1974). *J. Chem. Phys.* **61**, 3181
127. Paulson, J.F. and Dale, F. (1982). *J. Chem. Phys.* **77**, 4006
128. Leopold, D.G., Ho, J. and Lineberger, W.C. (1987). *J. Chem. Phys.* **86**, 1715
129. Kaiser, H.J., Heinicke, E., Baumann, H. and Bethge, K. (1971). *Z. Phys.* **243**, 46
130. Arshadi, M., Yamdagni, R. and Kebarle, P. (1970). *J. Phys. Chem.* **74**, 1475
131. Castleman, A.W., Jr. and Tang, I.N. (1971). *Nature* **234**, 129
132. Castleman, A.W., Jr. and Tang, I.N. (1971). *Nature* **234**, 324
133. Tang, I.N., Munkelwitz, H.R. and Castleman, A.W., Jr. (1971). *Nature Phys. Sci.* **230**, 175
134. Tang, I.N., Munkelwitz, H.R. and Castleman, A.W., Jr. (1971). *Nature Phys. Sci.* **230**, 431
135. Castleman, A.W., Jr., Tang, I.N. and Munkelwitz, H.R. (1971). *Science* **173**, 1025
136. Castleman, A.W., Jr., Holland, P.M., Lindsay, D.M. and Peterson, K.I. (1978). *J. Am. Chem. Soc.* **100**, 6039
137. Moseley, J.T., Cosby, P.C., Bennett, R.A. and Peterson, J.R. (1975). *J. Chem. Phys.* **62**, 4826
138. Collins, J.C. and Kebarle, P. (1967). *J. Chem. Phys.* **46**, 1082
139. Colton, R.J., Campana, J.E., Bariak, T.M., De Corpo, J.J. and Wright, J.R. (1980). *Rev. Sci. Instrum.* **51**, 1685
140. Kebarle, P., Searles, S.K., Zolla, A., Scarborough, J. and Arshadi, M. (1967). *J. Am. Chem. Soc.* **89**, 6393
141. Moruzzi, J.L. and Phelps, A.V. (1966). *J. Chem. Phys.* **45**, 509

142. Beuhler, R.J. and Friedman, L. (1982). *J. Chem. Phys.* **77**, 2549
143. Friedman, L. and Beuhler, R.J. (1983). *J. Chem. Phys.* **78**, 4669
144. Siegel, M.W. and Fite, W.L. (1976). *J. Phys. Chem.* **80**, 2871
145. Haberland, H., Langosch, H., Schindler, H.G. and Worsnop, D.R. (1983). *Proc. 9th Int. Symp. Mol. Beams* 123
146. Haberland, H., Schindler, H.G. and Worsnop, D.R. (1984). *Ber. Bunsen-Ges Phys. Chem.* **88**, 270
147. Coe, J.V., Snodgrass, J.T., Friedhoff, C.B., McHugh, K.M. and Bowen, K.H. (1987). *J. Chem. Phys.* **87**, 4302
148. Miller, T.M., Leopold, D.G., Murray, K.K. and Lineberger, W.C. (1985). *Bull. Am. Phys. Soc.* **30**, 880
149. Tang, I.N. and Castleman, A.W., Jr. (1972). *J. Chem. Phys.* **57**, 3638
150. Gspann, J. and Korting, J. (1973). *J. Chem. Phys.* **59**, 4726
151. Compton, R.N. (1977). *J. Chem. Phys.* **67**, 1779
152. Bowen, K.H., Liesegang, G.W., Sanders, R.A. and Herschbach, D.H. (1983). *J. Phys. Chem.* **87**, 557
153. Kondow, T. (1987). *J. Phys. Chem.* **91**, 1307
154. Desfrancois, C., Abdoul-Carine, H., Adjoure, C. and Khelifa Schermann, J.P. (1994). *Europhys. Lett.* **26**, 25
155. Sickman, H.R., Luder, Ch., Faehrmann, J., Lutz, H.O. and Meiwes-Broer, K.H. (1991). *Z. Phys. D* **20**, 417
156. Meng, C.K. and Fenn, J.B. (1991). *Org. Mass Spectrom.* **26**, 542
157. Stern, O. (1926). *Zeits. F. Phys.* **39**, 751 U.z.M.1
158. Stern, O. (1927). *Zeits. F. Phys.* **41**, 563 U.z.M.5
159. Ramsey, N.F. (1956). *Molecular Beam*. Oxford University Press, Oxford
160. Kantrovitz, A. and Grey, J. (1951). *Rev. Sci. Instrum.* **22**, 328
161. Pauly, H. and Tonnie, J.P. (1968). *Methods Exp. Phys.* **7A**, 237
162. Fenn, J.B. (1996). *Ann. Rev. Phys. Chem.* **47**, 1
163. Gentry, W.R. and Giese, C.F. (1978). *Rev. Sci. Instrum.* **49**, 595
164. Campargue, R. (1984). *J. Phys. Chem.* **88**, 4466
165. Ready, J.F. (1971). *Effects of High Power Laser Radiation*. Academic Press, New York
166. Hughes, T.P. (1975). *Plasmas and Laser Light*. Wiley, New York
167. Bekefi, G. (1976). *Principles of Laser Plasmas*. Wiley, New York
168. Radziemski, L.J. and Cremers, D.A. (eds) (1989). *Laser-Induced Plasma and Applications*. Marcel Dekker, New York
169. Lubman, D.M. (ed.) (1990). *Lasers and Mass Spectrometry*. Oxford University Press, Oxford
170. Miller, J.C. (1994). Laser ablation principles and applications. In *Springer Series in Material Science*, vol. 28. Springer, Berlin
171. Bauerle, D. (1996). *Laser Processing and Chemistry* (2nd edn.). Springer, Berlin
172. Miller, J.C. and Haglund, R.F. (eds) (1998). In *Laser Ablation and Desorption, Experimental Methods in the Physical Sciences*. vol. 30. Academic Press, London
173. Anderson, J.B. (1974). In *Molecular Beams and Low Density Gas Dynamics*, Wegener, P.P. (ed.). Dekker, New York
174. Hagen, O.F. (1974). In *Molecular Beams and Low Density Gas Dynamics*, Wegener, P.P. (ed.). Dekker, New York
175. Milne, T.A. and Greene, F.T. (1968). *Adv. Chem. Ser.* **72**, 68
176. Bauchert, J. and Hagen, O.F. (1965). *Z. Naturforsch.* **20**, 1135
177. Hagen, O.F. and Henkes, W. (1965). *Z. Naturforsch.* **20**, 1344
178. Breen, J.J., Kilgore, K., Stephan, K., Hofmann-Sievert, R., Kay, B.D., Keese, R., Märk, T.D., Van Doren, J.M. and Castleman, A.W., Jr. (1984). *Chem. Phys.* **91**, 305
179. Veenstra, B.R., Jonkman, H.T. and Kommandeur, J. (1994). *J. Phys. Chem.* **98**, 3538

180. Robinson, P.J., Holbrook, K.A. (1972) *Unimolecular Reactions*. Wiley, New York
181. Jonkman, H.T., Even, U. and Kommandeur, J. (1985). *J. Phys. Chem.* **89**, 4240
182. Castleman, A.W., Jr. and Bowen, K.H. (1996). *J. Phys. Chem.* **100**, 12911
183. Müller-Dethlefs, K. and Hobza, P. (2000). *Chem. Rev.* **100**, 143
184. Desfrancois, C., Carles, S. and Schermann, J.P. (2000). *Chem. Rev.* **100**, 3943
185. Breen, P.J., Warren, J.A., Bernstein, E.R. and Seeman, J.I. (1987). *J. Chem. Phys.* **87**, 1917
186. Breen, P.J., Warren, J.A., Bernstein, E.R. and Seeman, J.I. (1987). *J. Chem. Phys.* **87**, 1927
187. Breen, P.J., Warren, J.A., Bernstein, E.R. and Seeman, J.I. (1987). *J. Am. Chem. Soc.* **109**, 3453
188. Gutowsky, H.S., Emilsson, T. and Arunan, E.J. (1993). *J. Chem. Phys.* **99**, 4883
189. Canagaratna, M., Phillips, J.A., Ott, M.E. and Leopold, K.R. (1998). *J. Phys. Chem. A* **102**, 1489
190. Leopold, K.R., Canagaratna, M. and Phillips, J.A. (1997). *Acc. Chem. Res.* **30**, 57
191. Leopold, K.R., Fraser, G.T., Novick, S.E. and Klemperer, W. (1994). *Chem. Rev.* **94**, 1807
192. Blake, G.A., Laughlin, K.B., Cohen, R.C., Busarow, K.L., Gwo, D.H., Schmuttenmaer, C.A., Steyert, D.W. and Saykally, R.J. (1991). *Rev. Sci. Instrum.* **62**, 1701
193. Liu, K., Fellers, R.P., Viant, M.R., McLaughlin, R.P., Brown, M.G. and Saykally, R.J. (1996). *Rev. Sci. Instrum.* **67**, 410
194. Ebata, T., Furukawa, M., Suzuki, T. and Ito, M. (1990). *J. Opt. Soc. Am.* **7**, 1890
195. Hamilton, C.E., Kinsey, J.L. and Field, R.W. (1986). *Annu. Rev. Phys. Chem.* **37**, 493
196. Felker, P.M., Maxtone, P.M. and Schaeffer, M.W. (1994). *Chem. Rev.* **94**, 1787
197. Pribble, R.N. and Zwier, T.S. (1994). *Science* **265**, 75
198. Cooper, D.E., Kilmcak, C.M. and Wessel, J.E. (1981). *Phys. Rev. Lett.* **46**, 324
199. Suzuki, T., Mikami, N. and Ito, M. (1986). *J. Phys. Chem.* **90**, 6431
200. Smalley, R.E., Wharton, L. and Levy, D.H. (1977). *Acc. Chem. Res.* **10**, 139
201. Amirav, A., Even, U. and Jortner, J. (1981). *J. Chem. Phys.* **75**, 2489
202. Babbitt, R.J., Ho, C.J. and Topp, M.R. (1988). *J. Phys. Chem.* **92**, 2422
203. Wittmeyer, S.A. and Topp, M.R. (1989). *Chem. Phys. Lett.* **163**, 261
204. Smalley, R.E., Levy, D.H. and Wharton, L. (1976). *J. Chem. Phys.* **64**, 3266
205. Kenny, J.E., Johnson, K.E., Sharfin, W. and Levy, D.H. (1980). *J. Chem. Phys.* **72**, 1109
206. Weber, Th., Riedel, E., Neusser, H.J. and Schlag, E.W. (1991). *Chem. Phys. Lett.* **183**, 77
207. Scherzer, W., Selzle, H.L. and Schlag, E.W. (1992). *Chem. Phys. Lett.* **195**, 11
208. Leutwyler, S. and Bosiger, J. (1990). *Chem. Rev.* **90**, 489
209. Dao, P.D., Morgan, S., Breen, J.J., Kilgore, K., Wei, S., Tzeng, W.B., Keesee, R.G. and Castleman, A.W., Jr. (1989). *J. Chem. Phys.* **90**, 11
210. Helm, R.M., Clara, M., Grebner, T.L. and Neusser, H.J. (1998). *J. Phys. Chem.* **102**, 3268
211. Courty, A., Mons, M., Calvé, J.L., PiuZZi, F. and Dimicoli, I. (1997). *J. Phys. Chem.* **101**, 1445
212. Latini, A., Toja, D., Giardini Guidoni, A., Palleschi, A., Piccirillo, S. and Speranza, M. (1999). *Angew. Chem. Int. Ed. Engl.* **38**, 815
213. Mons, M., PiuZZi, F., Dimicoli, I., Zehnacker, A. and Lahmani, F. (2000). *Phys. Chem. Chem. Phys.* **2**, 5065
214. Lubman, D.M. and Li, L. (1990). In *Laser and Mass Spectrometry*, Lubman, D.M. (ed.), Chapter XVI. Oxford University Press, Oxford
215. Snoek, L.C., Robertson, E.G., Kroemer, R.T. and Simons, J.P. (2000). *Chem. Phys. Lett.* **321**, 49
216. Snoek, L.C., Kroemer, R.T. and Simons, J.P. (2002). *Phys. Chem. Chem. Phys.* **4**, 2130

217. Cohen, R., Brauer, B., Nir, E., Grace, L. and de Vries, M.S. (2000). *J. Phys. Chem. A* **104**, 6351
218. Nir, E., Imhof, P., Kleinermanns, K. and de Vries, M.S. (2000). *J. Am. Chem. Soc.* **122**, 8091
219. Nir, E., Janzen, C., Imhof, P., Kleinermanns, K. and de Vries, M.S. (2002). *Phys. Chem. Chem. Phys.* **4**, 732
220. Talbot, F.O. and Simons, J.P. (2002). *Phys. Chem. Chem. Phys.* **4**, 3562
221. Weinkauff, R., Schanen, P., Yang, D., Soukara, S. and Schlag, E.W. (1995). *J. Phys. Chem.* **99**, 11255
222. Nir, E., Grace, L., Brauer, B. and de Vries, M.S. (1999). *J. Am. Chem. Soc.* **121**, 4896
223. Desfrancois, C. (1995). *Phys. Rev. A* **51**, 3667
224. Carles, S., Desfrancois, C., Schermann, J.P., Bergès, J. and Houée-Levin, C. (2001). *Int. J. Mass Spectrom.* **205**, 227
225. Zheng, Y.J. and Ornstein, R.L. (1996). *J. Am. Chem. Soc.* **118**, 4175
226. Carles, S., Desfrancois, C., Schermann, J.P., Smith, D.M.A. and Adamowicz, L. (2000). *J. Chem. Phys.* **112**, 3726
227. Dopfer, O. and Müller-Dethlefs, K. (1994). *J. Chem. Phys.* **101**, 8508
228. Lembach, G. and Brutschy, B. (1997). *J. Chem. Phys.* **107**, 6156
229. Braun, J.E., Grebner, T.L. and Neusser, H.J. (1998). *J. Phys. Chem. A* **102**, 3273
230. Reiser, G., Habenicht, W., Müller-Dethlefs, K. and Schlag, E.W. (1988). *Chem. Phys. Lett.* **152**, 119
231. Müller-Dethlefs, K. (1995). *High-Resolution Laser Photoionisation and Photoelectron Studies*. Wiley, Chichester, England
232. Merkt, F. and Softley, T.P. (1993). *Int. Rev. Phys. Chem.* **12**
233. Müller-Dethlefs, K., Dopfer, O. and Wright, T.G. (1994). *Chem. Rev.* **94**, 1845
234. Müller-Dethlefs, K. and Schlag, E.W. (1998). *Angew. Chem. Int. Ed. Engl.* **37**, 1346
235. Zhu, L. and Johnson, P. (1991). *J. Chem. Phys.* **94**, 5769
236. Krause, H. and Neusser, H.J. (1993). *J. Chem. Phys.* **99**, 6278
237. Lembach, G. and Brutschy, B. (1997). *Chem. Phys. Lett.* **273**, 421
238. Lembach, G. and Brutschy, B. (1998). *J. Phys. Chem. A* **102**, 6068
239. Pitts, J.D. and Knee, J.L. (1999). *J. Chem. Phys.* **110**, 3389
240. Pitts, J.D. and Knee, J.L. (1998). *J. Chem. Phys.* **109**, 7113
241. Keese, R.G. and Castleman, A.W., Jr. (1990). In *Atomic and Molecular Clusters*, Bernstein, E.R. (ed.). Elsevier, Amsterdam
242. Amirav, A., Even, U., Leutwyler, S., Ondrechen, M.J., Berkovitch-Yellon, Z. and Jortner, J. (1982). *Faraday Discuss. Chem. Soc.* **73**, 153
243. Bombach, R., Honnegger, E. and Leutwyler, S. (1985). *Chem. Phys. Lett.* **118**, 449
244. Even, U. and Jortner, J. (1983). *J. Chem. Phys.* **78**, 3445
245. Dao, P.D., Morgan, S. and Castleman, A.W., Jr. (1984). *Chem. Phys. Lett.* **111**, 38
246. Schauer, M. and Bernstein, E.R. (1985). *J. Chem. Phys.* **82**, 726
247. Bahatt, D., Even, U., Shalev, E., Ben-Horin, N. and Jortner, J. (1991). *Chem. Phys.* **156**, 223
248. Leutwyler, S. and Jortner, J. (1987). *J. Phys. Chem.* **91**, 5558
249. Amirav, A., Even, U. and Jortner, J. (1982). *J. Phys. Chem.* **86**, 3345
250. Hager, J.W., Smith, M.A. and Wallace, S.C. (1986). *J. Chem. Phys.* **83**, 4820
251. Hager, J.W., Smith, M.A. and Wallace, S.C. (1986). *J. Chem. Phys.* **84**, 6771
252. Mark, T.D. and Castleman, A.W., Jr. (1984). *Adv. At. Mol. Phys.* **20**, 65
253. Jortner, J. (1984). *Ber. Bunsenges. Phys. Chem.* **88**, 188
254. Ng, C.Y. (1983). *Adv. Chem. Phys.* **52**, 263
255. Walters, E.A. and Blais, N.C. (1981). *J. Chem. Phys.* **75**, 4208
256. Trott, W.M., Blais, N.C. and Walters, E.A. (1978). *J. Chem. Phys.* **69**, 3150

257. Simpson, W.T. (1962). *Theories of Electrons in Molecules*. Prentice-Hall, Englewood Cliffs, NJ
258. Dao, P.D., Morgan, S. and Castleman, A.W., Jr. (1985). *Chem. Phys. Lett.* **113**, 219
259. Gonohe, N., Abe, H., Mikami, N. and Ito, M. (1985). *J. Phys. Chem.* **89**, 3642
260. Fung, K.H., Henke, W.E., Hays, T.R., Selzle, H.L. and Schlag, E.W. (1981). *J. Phys. Chem.* **85**, 3560
261. Fuke, K., Yoshiuchi, H., Kaya, K., Achiba, Y., Sato, K. and Kimura, K. (1984). *Chem. Phys. Lett.* **108**, 179
262. Desfrancois, C., Abdoul-Carime, H., Adjoure, C., Khelifa, N. and Schermann, J.P. (1994). *Phys. Rev. Lett.* **73**, 2436
263. Abdoul-Carime, H. and Desfrancois, C. (1998). *Eur. Phys. J. D* **2**, 149
264. Desfrancois, C., Abdoul-Carime, H. and Schermann, J.P. (1996). *Int. J. Modern Phys.* **10**, 1339
265. Carles, S., Lecomte, F., Schermann, J.P. and Desfrancois, C. (2000). *J. Phys. Chem. A* **104**, 10662
266. Blades, A.T., Ikononou, M.G. and Kebarle, P. (1991). *Anal. Chem.* **63**, 2109
267. Van Berkel, G.J. (1997). In *Electrospray Ionization Mass Spectrometry*, Cole, R.B. (ed.). Wiley, New York
268. Simons, D.S., Colby, B.N. and Evans, C.A., Jr. (1974). *Int. J. Mass Spectrom. Ion Phys.* **15**, 291
269. Karas, M., Bachmann, D., Bahr, U. and Hillenkamp, F. (1987). *Int. J. Mass Spectrom. Ion Process.* **78**, 53
270. Carroll, J.A. and Beavis, R.C. (1998). In *Laser Ablation and Desorption*, Miller, J.C. and Haglund, R.F. (eds), Chapter IX. Academic Press, London
271. Karas, M., Bahr, U. and Hillenkamp, F. (1989). *Int. J. Mass Spectrom. Ion Processes* **92**, 231
272. Karas, M. and Hillenkamp, F. (1988). *Anal. Chem.* **60**, 2299
273. Beavis, R.C., Chaudhary, T. and Chait, B.T. (1989). *Rapid Commun. Mass Spectrom.* **3**, 432
274. Barber, M., Bordoli, R.S., Sedgewick, R.D. and Tyler, A.N. (1981). *Chem. Commun.* 325
275. Barber, M., Bordoli, R.S., Sedgewick, R.D. and Tyler, A.N. (1981). *Nature* **293**, 270
276. Barber, M., Bordoli, R.S., Elliott, G.J., Sedgewick, R.D. and Tyler, A.N. (1982). *Anal. Chem.* **54**, 645A
277. Comisarow, M. (1978). In *Advances in Mass Spectrometry*, Daly, N.R. (ed.), vol. 7B, 1042. Heyden, London
278. Marable, N.L. and Sanzone, G. (1974). *Int. J. Mass Spectrom. Ion Phys.* **13**, 185
279. Browder, J.A., Miller, R.L., Thomas, W.A. and Sanzone, G. (1981). *Int. J. Mass Spectrom. Ion Phys.* **37**, 99
280. Mamyrin, B.A., Karataev, V.I., Shmikk, D.V. and Zagulin, B.A. (1973). *Sov. Phys. – JETP* **37**, 45
281. Mamyrin, B.A. and Shmikk, D.V. (1979). *Sov. Phys. – JETP* **49**, 762
282. Walter, K., Boesl, U. and Schlag, E.W. (1986). *Int. J. Mass Spectrom. Ion Proc.* **71**, 309
283. Grotemeyer, J., Boesl, U., Walter, K. and Schlag, E.W. (1986). *Org. Mass Spectrom.* **21**, 645
284. Paul, W. and Steinwedel, H. (1953). *Z. Naturforsch.* **8a**, 448
285. Marshall, A.G. and Grosshans, P.B. (1991). *Anal. Chem.* **63**, 215A
286. Williams, E.R., Henry, K.D. and McLafferty, F.W. (1990). *J. Am. Chem. Soc.* **112**, 6157
287. McLafferty, F.W. (ed.) (1983). In *Tandem Mass Spectrometry*. Wiley, New York
288. Busch, K.L., Glish, G.L. and McLuckey, S.A. (1988). *Mass Spectrometry/Mass Spectrometry*. VCH Publishers, Deerfield, FL
289. Williams, E.R. and McLafferty, F.W. (1990). *J. Am. Soc. Mass Spectrom.* **1**, 361

290. Cooks, R.G. and Kruger, T.L. (1977). *J. Am. Chem. Soc.* **99**, 1279
291. McLuckey, S.A., Cameron, D. and Cooks, R.G. (1981). *J. Am. Chem. Soc.* **103**, 1313
292. McLuckey, S.A., Cooks, R.G. and Fulford, J.E. (1983). *Int. J. Mass Spectrom. Ion Phys.* **52**, 165
293. Bojesen, G. (1987). *J. Am. Chem. Soc.* **109**, 5557
294. Li, X. and Harrison, A.G. (1993). *Org. Mass Spectrom.* **28**, 366
295. Kuntz, A.F., Boynton, A.W., David, G.A., Colyer, K.E. and Poutsma, J.C. (2002). *J. Am. Chem. Soc.* **13**, 72
296. Burinsky, D.J., Fukuda, E.K. and Campana, J.E. (1984). *J. Am. Chem. Soc.* **106**, 2770
297. Chen, G. and Cooks, R.G. (1997). *J. Mass Spectrom.* **31**, 333
298. Wong, P.S.H., Ma, S.G. and Cooks, R.G. (1996). *Anal. Chem.* **68**, 4254
299. Wright, L.G., McLuckey, S.A. and Cooks, R.G. (1982). *Int. J. Mass Spectrom. Ion Phys.* **42**, 115
300. Graul, S.T., Schnute, M.E. and Squires, R.R. (1990). *Int. J. Mass Spectrom. Ion Process.* **96**, 181
301. Ma, S.G., Wang, F. and Cooks, R.G. (1998). *J. Mass Spectrom.* **33**(10), 943
302. McLuckey, S.A., Shoen, A.E. and Cooks, R.G. (1982). *J. Am. Chem. Soc.* **104**, 848
303. Andersen, U.N. and Bojesen, G. (1997). *J. Chem. Soc., Perkin Trans.* **2**, 323
304. Sheng, S.Y., Wong, P., Shuguang, M. and Cooks, R.G. (1996). *J. Am. Soc. Mass Spectrom.* **7**, 198
305. Cheng, X.H., Wu, Z.C. and Fenselau, C. (1993). *J. Am. Chem. Soc.* **115**, 4844
306. Wu, Z.C. and Fenselau, C. (1994). *Rapid Commun. Mass Spectrom.* **8**, 777
307. Cerda, B.A., Nold, M.J. and Wesdemiotis, C. (1997). In *Selected Topics in Mass Spectrometry in the Biomolecular Sciences*, Caprioli, R.M., Malorni, A. and Sindona, G. (eds). Kluwer Academic, Dordrecht
308. Cerda, B.A., Hoyau, S., Ohanessian, G. and Wedemiotis, C. (1998). *J. Am. Chem. Soc.* **120**, 2437
309. Nold, M.J., Cerda, B.A. and Wesdemiotis, C.J. (1999). *J. Am. Soc. Mass Spectrom.* **10**, 1
310. Armentrout, P.B. (2000). *J. Am. Soc. Mass Spectrom.* **11**, 371
311. Drahos, L. and Vékely, K. (1999). *J. Mass Spectrom.* **34**, 79
312. Bojesen, G. and Breindahl, T. (1994). *J. Chem. Soc., Perkin Trans.* **2**, 1029
313. Craig, S.L., Zhong, M., Choo, B. and Brauman, J.L. (1997). *J. Phys. Chem. A* **101**, 19
314. Ervin, K.M. (2000). *Int. J. Mass Spectrom.* **195/196**, 271
315. Laskin, J. and Futrell, J.H. (2000). *J. Phys. Chem. A* **104**, 5484
316. Klots, C.E. (1989). *J. Chem. Phys.* **90**, 4470
317. Klots, C.E. (1993). *J. Chem. Phys.* **98**, 206
318. Klots, C.E. (1994). In *Unimolecular and Bimolecular Reaction Dynamics*, Ng, C.Y., Baer, T. and Powis, I. (eds). Wiley, New York
319. Meisels, G.G., Hamill, W.H. and Williams, R.R., Jr. (1957). *J. Phys. Chem.* **61**, 1456
320. Lias, S.G. (1975). In *Interactions Between Ions and Molecules*, Ausloos, P. (ed.). Plenum, New York
321. Cacace, F. (1979). In *Kinetics of Ion-Molecule Reactions*, Ausloos, P. (ed.), p 199. Plenum, New York
322. Cacace, F. (1982). In *Radiat. Phys. Chem.*, Ausloos, P. (ed.), **20**, p. 99
323. Speranza, M. (1983). *Gazz. Chim. Ital.* **113**, 37
324. Speranza, M. (1987). *Spectrosc. Int. J.* **5**, 1
325. Cacace, F. (1988). *Acc. Chem. Res.* **21**, 215
326. Speranza, M. (1992). *Mass Spectrom. Rev.* **11**, 73
327. Speranza, M. (1999). In *Fundamentals and Applications of Gas Phase Ion Chemistry*, Jennings, K.R. (ed.). Kluwer, Dordrecht
328. Fornarini, F. and Crestoni, M.E. (1998). *Acc. Chem Res.* **31**, 827

329. Al-Rabaa, A.R., Br  h  ret, E., Lahmani, F. and Zehnacker, A. (1995). *Chem. Phys. Lett.* **237**, 480
330. Lahmani, F., Le Barbu, K. and Zehnacker-Rentien, A. (1999). *J. Phys. Chem. A* **103**, 1991
331. Le Barbu, K., Brenner, V., Milli  , Ph., Lahmani, F. and Zehnacker-Rentien, A. (1998). *J. Phys. Chem. A* **102**, 128
332. Claverie, O. (1978). In *Intermolecular Interactions from Diatomics to Biopolymers*, Pullman, B. (ed.). Wiley, New York
333. Al-Rabaa, A.R., Le Barbu, K., Lahmani, F. and Zehnacker, A. (1997). *J. Photochem. Photobiol. A: Chem.* **105**, 277
334. Le Barbu, K., Lahmani, F. and Zehnacker-Rentien, A. (2002). *J. Phys. Chem. A* **106**, 6271
335. Piccirillo, S., Bosman, C., Toja, D., Giardini Guidoni, A., Pierini, M., Troiani, A. and Speranza, M. (1997). *Angew. Chem. Int. Ed. Engl.* **36**, 1729
336. Giardini Guidoni, A. and Piccirillo, S. (1997). *Isr. J. Chem.* **37**, 439
337. Latini, A., Satta, M., Giardini Guidoni, A., Piccirillo, S. and Speranza, M. (2000). *Chem. Eur. J.* **6**, 1042
338. Latini, A., Toja, D., Giardini Guidoni, A., Palleschi, A., Piccirillo, S. and Speranza, M. (1999). *Chirality* **11**, 376
339. Satta, M., Latini, A., Piccirillo, S., Di Palma, T.M., Scuderi, D., Speranza, M. and Giardini Guidoni, A. (2000). *Chem. Phys. Lett.* **316**, 94
340. Giardini Guidoni, A., Piccirillo, S., Scuderi, D., Satta, M., Di Palma, T.M. and Speranza, M. (2000). *Phys. Chem. Chem. Phys.* **2**, 4139
341. Scuderi, D., Paladini, A., Piccirillo, S., Satta, M., Catone, D., Giardini, A., Filippi, A. and Speranza, M. (2002). *Chem. Commun.* 2438
342. Le Barbu, K., Zehnacker, A., Lahmani, F., Mons, M., Piu  zi, F. and Dimicoli, I. (2001). *Chirality* **13**, 715
343. Scuderi, D., Paladini, A., Satta, M., Catone, D., Piccirillo, S., Speranza, M. and Giardini Guidoni, A. (2002). *Phys. Chem. Chem. Phys.* **4**, 4999
344. King, A.K. and Howard, B.J. (2001). *Chem. Phys. Lett.* **348**, 343
345. Bohro, N., Haeber, T. and Suhm, M.A. (2001). *Phys. Chem. Chem. Phys.* **3**, 1945
346. Bohro, N. and Suhm, M.A. (2002). *Phys. Chem. Chem. Phys.* **4**, 2721
347. Giardini Guidoni, A., Piccirillo, S., Scuderi, D., Satta, M., Di Palma, T.M., Speranza, M., Filippi, A. and Paladini, A. (2001). *Chirality* **13**, 727
348. Giardini Guidoni, A., Piccirillo, S., Scuderi, D., Satta, M., Di Palma, T.M., Speranza, M., Filippi, A. and Paladini, A. (2001). *Int. J. Photoenergy* **3**, 1
349. Carles, S., Lecomte, F., Schermann, J.P., Desfrancois, C., Xu, S., Nilles, J.M., Bowen, K.H., Berges, J. and Houee-Levin, C. (2001). *J. Phys. Chem. A* **105**, 5622
350. Lecomte, F., Lucas, B., Gregoire, G., Schermann, J.P. and Desfrancois, C. (2004). *Eur. Phys. J.* in press
351. Sawada, M. (1994). In *Biological Mass Spectrometry: Present and Future*, Matsuo, T., Caprioli, R.M., Gross, M.L. and Seyama, T. (eds) Wiley, New York
352. Sawada, M. (1997). *Mass Spectrom. Rev.* **16**, 733
353. Schalley, C.A. (2000). *Int. J. Mass Spectrom.* **194**, 11
354. Filippi, A., Giardini, A., Piccirillo, S. and Speranza, M. (2000). *Int. J. Mass Spectrom.* **198**, 137
355. Lebrilla, C.B. (2001). *Acc. Chem. Res.* **34**, 653
356. Dearden, D., Liang, Y., Nicoll, J.B. and Kellersberger, K.A. (2001). *J. Mass Spectrom.* **36**, 989
357. Fales, H.M. and Wright, G.J. (1977). *J. Am. Chem. Soc.* **99**, 2339
358. Winkler, F.J., Stahl, D. and Maquin, F. (1986). *Tetrahedron Lett.* **27**, 335

359. Winkler, F.J. and Splitter, J.S. (1994). In *Applications of Mass Spectrometry to Organic Stereochemistry*, Splitter, J.S. and Tureek, F. (eds). VCH Publishers, New York
360. Baldwin, M.A., Howell, S.A., Welham, K.J. and Winkler, F.J. (1988). *Biomed. Environ. Mass Spectrom.* **16**, 357
361. Winkler, F.J., Medina, R., Winkler, J. and Krause, H. (1994). *J. Chromatog. A.* **666**, 549
362. Sussmuth, R., Jung, G., Winkler, F.J. and Medina, R. (1999). *Eur. Mass Spectrom.* **5**, 298
363. Nikolaev, E.N., Denisov, E.V., Nikolaeva, M.I., Futrell, J.H., Rakov, V.S. and Winkler, F.J. (1998). *Adv. Mass Spectrom.* **14**, 279, Chapter 12
364. Winkler, F.J., Medina, R., Winkler, J. and Krause, H.J. (1997). *Mass Spectrom.* **32**, 1072
365. Denisov, E.V., Shustriakov, V., Nikolaev, E.N., Winkler, F.J. and Medina, R. (1997). *Int. J. Mass Spectrom. Ion Proc.* **167/168**, 259
366. Nikolaev, E.N., Goginashvili, G.T., Tal'rose, V.L. and Kostyanovsky, R.G. (1988). *Int. J. Mass Spectrom. Ion Proc.* **86**, 249
367. Nikolaev, E.N., McMahon, T.B. (1995). Proceedings of the 43rd Annual Conference on Mass Spectrometry and Allied Topics, Atlanta, Georgia, 973
368. Nikolaev, E.N., Denisov, E.V. (1996). Proceedings of the 44th Annual Conference on Mass Spectrometry and Allied Topics, Portland, Oregon, 415
369. Nikolaev, E.N., Denisov, E.V., Rakov, V.S. and Futrell, J.H. (1999). *Int. J. Mass Spectrom.* **182/183**, 357
370. Hua, S., Chen, Y., Jiang, L. and Xue, S. (1986). *Org. Mass Spectrom.* **21**, 7
371. Chen, Y.Z., Li, H., Yang, H.J., Hua, S.M., Li, H.Q., Zhao, F.Z. and Chen, N.Y. (1988). *Org. Mass Spectrom.* **23**, 821
372. Martens, J., Lübben, S. and Schwarting, W. (1991). *Z. Naturforsch.* **46b**, 320
373. Yang, H.J. and Chen, Y.Z. (1992). *Org. Mass Spectrom.* **27**, 736
374. Hashimoto, K., Sumida, Y., Terada, S. and Okamura, K. (1993). *J. Mass Spectrom. Soc. Jpn.* **41**, 87
375. Hashimoto, K., Sumida, Y., Terada, S. and Okamura, K. (1993). *J. Mass Spectrom. Soc. Jpn.* **41**, 95
376. Okamura, K., Sumida, Y., Fujiwara, Y., Terada, S., Kim, H. and Hashimoto, K. (1995). *J. Mass Spectrom. Soc. Jpn.* **43**, 97
377. Hashimoto, K., Okamura, K., Fujiwara, Y., Sumida, Y. and Terada, S. (1998). *Adv. Mass Spectrom.* **14**, 1
378. Vékey, K. and Czira, G. (1997). *Anal. Chem.* **69**, 1700
379. Vékey, K. and Czira, G. (1995). *Rapid Commun. Mass Spectrom.* **9**, 783
380. Yao, Z.P., Wan, T.S.M., Kwong, K.P. and Che, C.T. (1999). *Chem. Commun.* 2119
381. Vaisar, T., Urban, J. and Nakanishi, H. (1996). *J. Mass Spectrom.* **31**, 937
382. Fago, G., Filippi, A., Giardini, A., Laganà, A., Paladini, A. and Speranza, M. (2001). *Angew. Chem., Int. Ed. Engl.* **40**, 4051
383. Paladini, A., Scuderi, D., Laganà, A., Giardini, A., Filippi, A. and Speranza, M. (2003). *Int. J. Mass Spectrom.* **228**, 349
384. Cooks, R.G., Patrick, J.S., Kotiaho, T. and McLuckey, S.A. (1994). *Mass Spectrom. Rev.* **13**, 287
385. Shen, W., Wong, P.S.H. and Cooks, R.G. (1997). *Rapid Commun. Mass Spectrom.* **11**, 71
386. Dang, T.T., Pedersen, S.F. and Leary, J.A. (1994). *J. Am. Soc. Mass Spectrom.* **5**, 452
387. Tao, W.A., Wu, L. and Cooks, R.G. (2000). *Chem. Commun.* 2023
388. Tao, W.A., Clark, R.L. and Cooks, R.G. (2003). *Chem. Commun.* 136
389. Tao, W.A. and Cooks, R.G. (2003). *Anal. Chem.* **75**, 25A
390. Tao, W.A., Zhang, D., Wang, F., Thomas, P.D. and Cooks, R.G. (1999). *Anal. Chem.* **71**, 4427
391. Tao, W.A., Zhang, D., Nikolaev, E.N. and Cooks, R.G. (2000). *J. Am. Chem. Soc.* **122**, 10598

392. Tao, W.A. and Cooks, R.G. (2002). *Eur. J. Mass Spectrom.* **8**, 107
393. Tao, W.A., Wu, L., Cooks, R.G., Wang, F., Begley, J.A. and Lampert, B. (2001). *J. Med. Chem.* **44**, 3541
394. Zhang, D., Tao, W.A. and Cooks, R.G. (2001). *Int. J. Mass Spectrom.* **204**, 159
395. Tao, W.A., Clark, R.L. and Cooks, R.G. (2002). *Anal. Chem.* **74**, 3783
396. Wu, L., Tao, W.A. and Cooks, R.G. (2003). *J. Mass Spectrom.* **38**, 386
397. Tao, W.A., Wu, L. and Cooks, R.G. (2001). *J. Am. Soc. Mass Spectrom.* **12**, 490
398. Tao, W.A. and Cooks, R.G. (2001). *Angew. Chem. Int. Ed. Engl.* **40**, 757
399. Chen, J., Zhu, C.J., Chen, Y. and Zhao, Y.F. (2002). *Rapid Commun. Mass Spectrom.* **16**, 1251
400. Wu, L., Lemr, K., Aggerholm, T. and Cooks, R.G. (2003). *J. Am. Soc. Mass Spectrom.* **14**, 152
401. Tao, W.A., Gozzo, F.G. and Cooks, R.G. (2001). *Anal. Chem.* **73**, 1692
402. Augusti, D.V., Augusti, R., Carazza, F. and Cooks, R.G. (2002). *Chem. Commun.* 2242
403. Wu, L. and Cooks, R.G. (2003). *Anal. Chem.* **75**, 678
404. Locke, M.J., Hunter, R.L. and McIver, R.T. (1979). *J. Am. Chem. Soc.* **101**, 272
405. Locke, M.J. and McIver, R.T. (1983). *J. Am. Chem. Soc.* **105**, 4226
406. Hu, C.H., Shen, M.Z. and Schaefer, H.F. (1993). *J. Am. Chem. Soc.* **115**, 2923
407. Gordon, M.S. and Jensen, J.H. (1996). *Acc. Chem. Res.* **29**, 536
408. Bertran, J., Rodriguez-Santiago, L. and Sodupe, M. (1999). *J. Phys. Chem. B* **103**, 2310
409. Jockusch, R.A., William, P.D. and Williams, E.R. (1997). *J. Am. Chem. Soc.* **119**, 11988
410. Chapo, C.J., Paul, J.B., Provencal, R.A., Roth, K. and Saykally, R.J. (1998). *J. Am. Chem. Soc.* **120**, 12956
411. Maksic, Z.B. and Kovacevic, B. (1999). *J. Chem. Soc., Perkin Trans. 2*, 2623
412. Skurski, P., Gutowski, M., Barrios, R. and Simons, J. (2001). *Chem. Phys. Lett.* **337**, 143
413. Gutowski, M., Skurski, P. and Simons, J. (2000). *J. Am. Chem. Soc.* **122**, 10159
414. Skurski, P., Rak, J., Simons, J. and Gutowski, M. (2001). *J. Am. Chem. Soc.* **123**, 11073
415. Rak, J., Skurski, P., Simons, J. and Gutowski, M. (2001). *J. Am. Chem. Soc.* **123**, 11695
416. Julian, R.R., Beauchamp, J.L. and Goddard, W.A., III (2002). *J. Phys. Chem. A* **106**, 32
417. Hodyss, R., Julian, R.R. and Beauchamp, J.L. (2001). *Chirality* **13**, 703
418. Zhang, D., Wu, L., Koch, K.J. and Cooks, R.G. (1999). *Eur. Mass Spectrom.* **5**, 353
419. Cooks, R.G., Zhang, D., Koch, K.J., Gozzo, F.C. and Eberlin, M.N. (2001). *Anal. Chem.* **73**, 3646
420. Takats, Z., Nanita, S.C., Cooks, R.G., Schlosser, G. and Vekey, K. (2003). *Anal. Chem.* **75**, 1514
421. Koch, K.J., Gozzo, F.C., Zhang, D., Eberlin, M.N. and Cooks, R.G. (2001). *Chem. Commun.* 1854
422. Julian, R.R., Hodyss, R., Kinnear, B., Jarrold, M.F. and Beauchamp, J.L. (2002). *J. Phys. Chem. B* **106**, 1219
423. Koch, K.J., Gozzo, F.C., Nanita, S.C., Takats, Z., Eberlin, M.N. and Cooks, R.G. (2002). *Angew. Chem. Int. Ed. Engl.* **41**, 1721
424. Guo, J., Wu, J., Siuzdak, G. and Finn, M.G. (1999). *Angew. Chem., Int. Ed. Engl.* **38**, 1755
425. Sawada, M., Takai, Y., Yamada, H., Kaneda, T., Kamada, K., Mizooku, T., Hirose, K., Tobe, Y. and Naemura, K. (1994). *Chem. Commun.* 2497
426. Sawada, M., Takai, Y., Yamada, H., Hirayama, S., Kaneda, T., Tanaka, T., Kamada, K., Mizooku, T., Takeuchi, S., Ueno, K., Hirose, K., Tobe, Y. and Naemura, K. (1995). *J. Am. Chem. Soc.* **117**, 7726
427. Sawada, M., Takai, Y., Kaneda, T., Arakawa, R., Okamoto, M., Doe, H., Matsuo Naemura, K., Hirose, K. and Tobe, Y. (1996). *Chem. Commun.* 1735
428. Sawada, M., Takai, Y., Yamada, H., Nishida, J., Kaneda, T., Arakawa, R., Okamoto, M., Hirose, K., Tanaka, T. and Naemura, K. (1995). *J. Chem. Soc., Perkin Trans. 2*, 701

429. Sawada, M., Yamaoka, H., Takai, Y., Kawai, Y., Yamada, H., Azuma, T., Fujioka, T. and Tanaka, T. (1998). *Chem. Commun.* 1569
430. Sawada, M., Yamaoka, H., Takai, Y., Kawai, Y., Yamada, H., Azuma, T., Fujioka, T. and Tanaka, T. (1999). *Int. J. Mass Spectrom.* **193**, 123
431. Garcia, C., Guyot, J., Jeminet, G., Leize-Wagner, E., Nierengarten, H. and Van Dorselaer, A. (1999). *Tetrahedron Lett.* **40**, 4997
432. Pócsfalvi, G., Lipták, M., Huszthy, P., Bradshaw, J.S., Izatt, R.M. and Vékey, K. (1996). *Anal. Chem.* **68**, 792
433. Dobó, A., Lipták, M., Huszthy, P. and Vékey, K. (1997). *Rapid Commun. Mass Spectrom.* **11**, 889
434. Sawada, M., Shizuma, M., Takai, Y., Yamada, H., Kaneda, T. and Hanafusa, T. (1992). *J. Am. Chem. Soc.* **114**, 4405
435. Sawada, M., Okamura, Y., Shizuma, M., Takai, Y., Hidaka, Y., Yamada, H., Tanaka, T., Kaneda, T., Hirose, K., Misumi, S. and Takahashi, S. (1993). *J. Am. Chem. Soc.* **115**, 7381
436. Sawada, M., Okamura, Y., Yamada, H., Takai, Y., Takahashi, S., Kaneda, T., Hirose, K. and Misumi, S. (1993). *Org. Mass Spectrom.* **28**, 1525
437. Chu, I.H., Dearden, D.V., Bradshaw, J.S., Huszthy, P. and Izatt, R.M. (1993). *J. Am. Chem. Soc.* **115**, 4318
438. Dearden, D.V., Dejsupa, C., Liang, Y., Bradshaw, J.S. and Izatt, R.M. (1997). *J. Am. Chem. Soc.* **119**, 353
439. Davidson, R.B., Bradshaw, J.S., Jones, B.A., Dalley, N.K., Christensen, J.J., Izatt, R.M., Morin, F.G. and Grant, D.M. (1984). *J. Org. Chem.* **49**, 353
440. Liang, Y., Bradshaw, J.S., Izatt, R.M., Pope, R.M. and Dearden, D.V. (1999). *Int. J. Mass Spectrom.* **185/186/187**, 977
441. Liang, Y., Bradshaw, J.S. and Dearden, D.V. (2002). *J. Phys. Chem. A.* **106**, 9665
442. Haskins, N.J., Saunders, M.R. and Camilleri, P. (1994). *Rapid Commun. Mass Spectrom.* **8**, 423
443. So, M.P., Wan, T.S.M. and Chan, T.W.D. (2000). *Rapid Commun. Mass Spectrom.* **14**, 692
444. Ramirez, J., He, F. and Lebrilla, C.B. (1998). *J. Am. Chem. Soc.* **120**, 7387
445. Ramirez, J., Ahn, S., Grigorean, G. and Lebrilla, C.B. (2000). *J. Am. Chem. Soc.* **122**, 6884
446. Gal, J.F., Stone, M. and Lebrilla, C.B. (2003). *Int. J. Mass Spectrom.* **222**, 259
447. Ahn, S., Ramirez, J., Grigorean, G. and Lebrilla, C.B. (2001). *J. Am. Soc. Mass Spectrom.* **12**, 278
448. Grigorean, G. and Lebrilla, C.B. (2001). *Anal. Chem.* **73**, 1684
449. Sawada, M. (1997). *J. Mass Spectrom. Soc. Jpn* **45**, 439
450. Takai, Y., Okamura, Y., Tanaka, T., Sawada, M., Takahashi, S., Shiro, M., Kawamura, M. and Uchiyama, T. (1994). *J. Org. Chem.* **59**, 2967
451. Sawada, M., Shizuma, M., Takai, Y., Adachi, H., Takeda, T. and Uchiyama, T. (1998). *Chem. Commun.* 1453
452. Shizuma, M., Adachi, H., Kawamura, M., Takai, Y., Takeda, T. and Sawada, M. (2001). *J. Chem. Soc. Perkin Trans. 2*, 592
453. Shizuma, M., Adachi, H., Amemura, A., Takai, Y., Takeda, T. and Sawada, M. (2001). *Tetrahedron* **57**, 4567
454. Shizuma, M., Adachi, H., Takai, Y., Hayashi, M., Tanaka, J., Takeda, T. and Sawada, M. (2001). *Carbohydr. Res.* **335**, 275
455. Takai, Y., Okamura, Y., Takahashi, S., Sawada, M., Kawamura, M. and Uchiyama, T. (1993). *Chem. Commun.* 53
456. Shizuma, M., Takai, Y., Kawamura, M., Takeda, T. and Sawada, M. (2001). *J. Chem. Soc. Perkin Trans. 2*, 1306

457. Shizuma, M., Kadoya, Y., Takai, Y., Imamura, H., Yamada, H., Takeda, T., Arakawa, R., Takahashi, S. and Sawada, M. (2002). *J. Org. Chem.* **67**, 4795 and references therein
458. Vincenti, M. and Irico, A. (2002). *Int. J. Mass Spectrom.* **214**, 23
459. Stone, M.M., Franz, A.H. and Lebrilla, C.B. (2002). *J. Am. Soc. Mass Spectrom.* **13**, 964
460. Liang, T.M., Laali, K.K., Cordero, M. and Wesdemiotis, C. (1991). *J. Chem. Res (S)* 354
461. Botta, B., Botta, M., Filippi, A., Tafi, A., Delle Monache, G. and Speranza, M. (2002). *J. Am. Chem. Soc.* **124**, 7658
462. Tafi, A., Botta, B., Botta, M., Delle Monache, G., Filippi, A. and Speranza, M. (2004). *Chem. Eur. J.* **10**, 1
463. Tsukube, H. and Sohmiya, H. (1991). *J. Org. Chem.* **56**, 875
464. Williams, D.H., Bradley, C., Bojesen, G., Shantikarn, S. and Taylor, L.C.E. (1981). *J. Am. Chem. Soc.* **103**, 5700
465. Jørgensen, T.J.D., Delforge, D., Remacle, J., Bojesen, G. and Roepstorff, P. (1999). *Int. J. Mass Spectrom.* **188**, 63
466. Camara, E., Green, M.K., Penn, S.G. and Lebrilla, C.B. (1996). *J. Am. Chem. Soc.* **118**, 8751
467. Gong, S., Camara, E., Fei, H., Green, M.K. and Lebrilla, C.B. (1999). *Int. J. Mass Spectrom.* **185/186/187**, 401
468. Clemmer, D.E., Hudgins, R.R. and Jarrold, M.F. (1995). *J. Am. Chem. Soc.* **117**, 10141
469. Green, M.K. and Lebrilla, C.B. (1997). *Mass Spectrom. Rev.* **16**, 53
470. He, F., Ramirez, J. and Lebrilla, C.B. (1999). *J. Am. Chem. Soc.* **121**, 4726
471. Gur, E.H., De Koning, L.J. and Nibbering, N.M.M. (1996). *J. Mass Spectrom.* **31**, 325
472. Tabet, J.C. (1987). *Tetrahedron* **43**, 3413
473. Sellier, N.M., Bouillet, C.T., Douay, D.L. and Tabet, J.C.E. (1994). *Rapid Commun. Mass Spectrom.* **8**, 891
474. Tabet, J.C. (1987). *Spectrosc. Int. J.* **5**, 83
475. Filippi, A. and Speranza, M. (2000). *Int. J. Mass Spectrom.* **199**, 211
476. Walden, P. (1893). *Ber.* **26**, 210
477. Laerdahl, J.K. and Uggerud, E. (2002). *Int. J. Mass Spectrom.* **214**, 277
478. Lieder, C.A. and Brauman, J.I. (1974). *J. Am. Chem. Soc.* **96**, 4028
479. Angelini, G. and Speranza, M. (1978). *Chem. Commun.* 213
480. Speranza, M. and Angelini, G. (1980). *J. Am. Chem. Soc.* **102**, 3115
481. Angelini, G. and Speranza, M. (1981). *J. Am. Chem. Soc.* **103**, 3792
482. Angelini, G. and Speranza, M. (1981). *J. Am. Chem. Soc.* **103**, 3800
483. Crotti, P., Macchia, M., Pizzabiocca, A., Renzi, G. and Speranza, M. (1987). *Tetrahedron Lett.* **28**, 3383
484. Crotti, P., Macchia, M., Pizzabiocca, A., Renzi, G. and Speranza, M. (1987). *Gazz. Chim. Ital.* **117**, 739
485. Fornarini, S., Sparapani, C. and Speranza, M. (1988). *J. Am. Chem. Soc.* **110**, 34
486. Fornarini, S., Sparapani, C. and Speranza, M. (1988). *J. Am. Chem. Soc.* **110**, 42
487. Cecchi, P., Pizzabiocca, A., Renzi, G., Chini, M., Crotti, P., Macchia, F. and Speranza, M. (1989). *Tetrahedron* **45**, 4227
488. Cecchi, P., Chini, M., Crotti, P., Pizzabiocca, A., Renzi, G. and Speranza, M. (1991). *Tetrahedron* **47**, 4683
489. Hall, D.G., Gupta, C. and Morton, T.H. (1981). *J. Am. Chem. Soc.* **103**, 2416
490. Morton, T.H. (1982). *Tetrahedron* **38**, 3195
491. Bowen, R.D. (1991). *Acc. Chem. Res.* **24**, 364
492. Morton, T.H. (1992). *Org. Mass Spectrom.* **27**, 353
493. McAdoo, D.J. and Morton, T.H. (1993). *Acc. Chem. Res.* **26**, 295
494. Aschi, M., Cacace, F. and Troiani, A. (1997). *Angew. Chem. Int. Ed. Engl.* **36**, 83
495. Filippi, A., Roselli, G., Renzi, G., Grandinetti, F. and Speranza, M. (2003). *Chem. Eur. J.* **9**, 2072

496. Troiani, A., Filippi, A. and Speranza, M. (1997). *Chem. Eur. J.* **3**, 2063
497. Filippi, A. and Speranza, M. (1999). *Int. J. Mass Spectrom.* **185/186/187**, 425
498. Speranza, M. and Filippi, A. (1999). *Chem. Eur. J.* **5**, 834
499. Speranza, M. and Filippi, A. (1999). *Chem. Eur. J.* **5**, 845
500. Troiani, A., Gasparri, F., Grandinetti, F. and Speranza, M. (1997). *J. Am. Chem. Soc.* **119**, 4525
501. Troiani, A. and Speranza, M. (1998). *J. Org. Chem.* **63**, 1012
502. Speranza, M. and Troiani, A. (1998). *J. Org. Chem.* **63**, 1020
503. Filippi, A., Gasparri, F. and Speranza, M. (2001). *J. Am. Chem. Soc.* **123**, 2251
504. Filippi, A. and Speranza, M. (2003). *Chem. Eur. J.* **9**, 5274
505. Filippi, A. and Speranza, M. (2001). *J. Am. Chem. Soc.* **123**, 6077
506. Cacace, F., Ciranni, G. and Giacomello, P. (1981). *J. Am. Chem. Soc.* **103**, 1513
507. Dezi, E., Lombardozi, A., Pizzabiocca, A., Renzi, G. and Speranza, M. (1995). *Chem. Commun.* 547
508. Renzi, G., Lombardozi, A., Dezi, E., Pizzabiocca, A. and Speranza, M. (1996). *Chem. Eur. J.* **2**, 316
509. Dezi, E., Lombardozi, A., Renzi, G., Pizzabiocca, A. and Speranza, M. (1996). *Chem. Eur. J.* **2**, 323
510. Carrion, F. and Dewar, M.J.S. (1984). *J. Am. Chem. Soc.* **106**, 3531
511. Bach, R.D. and Wolber, G.J. (1985). *J. Am. Chem. Soc.* **107**, 1352
512. Park, Y.S., Kim, C.K., Lee, B.S. and Lee, I. (1995). *J. Phys. Chem.* **99**, 13103
513. For a review, see: Samuel, D., Silver, B (1965). *Adv. Phys. Org. Chem.* **3**, 128
514. Merritt, M.V., Bell, S.J., Cheon, H.J., Darlington, J.A., Dugger, T.L., Elliott, N.B., Fairbrother, G.L., Melendez, C.S., Smith, E.V. and Schwartz, P.L. (1990). *J. Am. Chem. Soc.* **112**, 3560 and references therein
515. Merritt, M.V., Anderson, D.B., Basu, K.A., Chang, I.W., Cheon, H.J., Mukundan, N.E., Flannery, C.A., Kim, A.Y., Vaishampayan, A. and Yens, D.A. (1994). *J. Am. Chem. Soc.* **116**, 5551 and references therein
516. Thibblin, A. (1993). *J. Phys. Org. Chem.* **6**, 287 and references therein
517. Linert, W. and Jameson, R.F. (1989). *Chem. Soc. Rev.* **18**, 477 and references therein
518. Larsson, R. (1988). *Catal. Today* **3**, 387
519. March, J. (1985). *Advanced Organic Chemistry*, 357. Wiley, New York
520. Dostrovsky, I., Hughes, E.D. and Ingold, C.K. (1946). *J. Chem. Soc.* 173
521. Bentley, T.W., Bowen, C.T., Parker, W. and Watt, C.I.F. (1979). *J. Am. Chem. Soc.* **101**, 2486
522. Jencks, W.P. (1982). *Chem. Soc. Rev.* **10**, 345
523. Bentley, T.W., Bowen, C.T., Morten, D.H. and Schleyer, P.v.R. (1981). *J. Am. Chem. Soc.* **103**, 5466
524. Bentley, T.W. and Bowen, C.T. (1978). *J. Chem. Soc. Perkin Trans. II* 557
525. Dale, J. (1998). *J. Chem. Educ.* **75**, 1482

Dynamics for the reactions of ion pair intermediates of solvolysis

JOHN P. RICHARD,^{†,*} TINA L. AMYES,[†] MARIA M. TOTEVA[†] and YUTAKA TSUJI[‡]

[†]*Department of Chemistry, University at Buffalo, SUNY, Buffalo, NY 14260-3000, USA*

[‡]*Department of Biochemistry and Applied Chemistry, Kurume National College of Technology, Komorinomachi, Kurume 830-8555, Japan*

1	Introduction	1
2	A “Global” scheme for solvolysis	2
3	Clocks for reactions of ion pairs	3
4	Addition of solvent to carbocation–anion pairs	6
5	Protonation of a carbocation–anion pair	11
6	Isomerization of ion pair reaction intermediates	12
	Reorganization of ion pairs in water	13
	Internal return of isotopically labeled ion pairs	18
7	Racemization of ion pairs	22
8	Concluding remarks	24
	Acknowledgements	24
	References	24

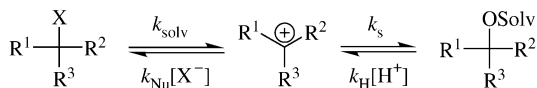
1 Introduction

Carbon atoms in organic molecules are most often neutral. Positively charged carbocations have attracted the interest of synthetic organic chemists, because of their use as intermediates in reactions leading to formation of carbon–carbon bonds. Our work on carbocations has focused on defining the stability of these species as intermediates of solvolysis reactions,^{1–4} through the determination of rate and equilibrium constants for these stepwise reactions (Scheme 1).^{5–14} This has led to the development of experimental methods to characterize these parameters for carbocations that are sufficiently stable to form in aqueous solution.

Heterolytic cleavage of bonds between carbon and an electron deficient leaving group produces, initially, a carbocation–anion or an ion–dipole pair depending upon whether the leaving group, at the reactant, is neutral or positively charged. It was fashionable in 1979, when I became interested in solvolysis reaction mechanisms, to write a “general” mechanism which included contact ion-pairs, solvent-separated ion-pairs, and free ions (Scheme 2).¹⁵ At this time the study of ion

* Corresponding author. Tel.: (716) 645-6800 ext 2194; Fax: (716) 645-6963.

E-mail address: jrichard@acsu.buffalo.edu (J.P. Richard).



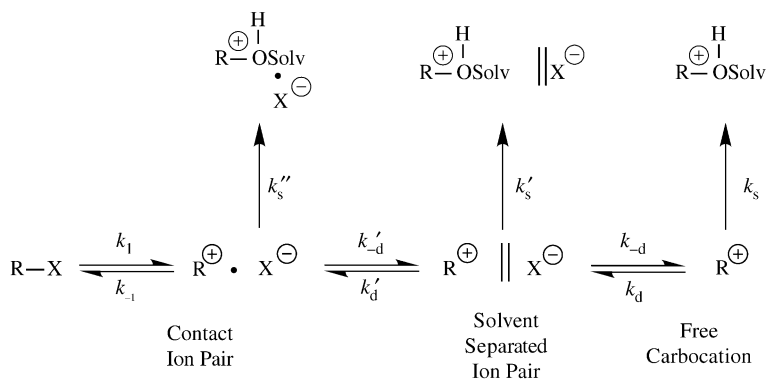
Scheme 1

pair intermediates of $\text{D}_{\text{N}} + \text{A}_{\text{N}}$ ¹⁶ reactions was central to investigations of solvolysis reaction mechanisms. However, the complexities inherent in a multistep reaction with several intermediates of similar structure and energy had resulted in contentious disputes. The reasons for the declining interest in polar reaction mechanisms are seldom discussed, however, it is likely that these fractious debates may have encouraged young scientists to consider other research problems. My preference is to avoid controversy by working on soluble problems, and I was fortunate to have the guidance of Bill Jencks who assured me that there were significant problems on solvolysis reaction mechanisms that could be addressed through experiments in aqueous solution, where the dominant reaction of ion pairs is their separation to free ions. This judgment has since been confirmed.^{1,14,17-21}

In retrospect, it should have been clear to me – as I am sure it was to Bill Jencks – that the rate and equilibrium constants for addition of solvent to 1-phenylethyl carbocation intermediates of solvolysis of 1-phenylethyl derivatives would serve as the first step in the characterization of the dynamics of the reactions of their ion pair intermediates.^{14,18} Therefore, this earlier work has served as a point of departure for our experiments to determine relative and absolute barriers to the reactions of ion pair intermediates of solvolysis.

2 A “Global” scheme for solvolysis

It is convenient to separate heterolytic bond cleavage and bond formation (k_1 and k_{-1}) from the transport steps (k'_{-d} , k_{-d} , k'_d and k_d) for Scheme 2. The values of



Scheme 2

the rate constants for bond cleavage and formation depend strongly on substrate structure and are generally similar, respectively, to the experimental rate constants for solvolysis of R–X and capture of the carbocation reaction intermediate R⁺ by X[−], respectively. By comparison, the rate constants for reversible separation of ion pairs to free ions show a much smaller dependence on the structure of the ions and a significant dependence on the solvent.

Contact- and solvent-separated ion pairs form whenever solvolysis proceeds to the free carbocation. However, these intermediates are generally only thought of as “significant” when their formation can be detected by experiment. We have focused on several different reactions of ion pairs that leave detectable *signatures*.

- (1) The addition of solvent to a carbocation paired with its leaving group anion (k_s'' and k_s' , Scheme 2). The effect of direct addition of solvent to an ion-pair reaction intermediate is to cause the rate of solvolysis to become faster than for a reaction where products form exclusively by addition of solvent to the unpaired carbocation (k_s), and it is possible to detect this as a deviation from a rate law for the latter reaction.
- (2) Protonation of the leaving group anion, which prevents internal return of the ion pair to reactant, and has the effect of making substrate ionization irreversible.
- (3) Isomerization of the ion-pair followed by internal return that leads to formation of a neutral isomerized reaction product.

In water, ion pairs undergo fast separation to free ions, because of the strong attenuation in this solvent of stabilizing electrostatic interactions between ions. Consequently, the ion-pair intermediates of solvolysis in water are most often too short-lived to undergo these *signature* reactions, because they experience faster separation to free ions. Since ion pair reactions in water are rare they can often be neglected entirely, which greatly simplifies the interpretation of experimental data.^{22,23} On the other hand, the determination of absolute rate constants for the various reactions of ion pairs in water remains a challenging problem of significant intellectual interest.

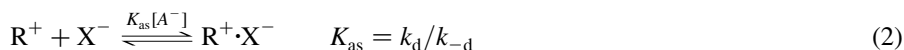
3 Clocks for reactions of ion pairs

We have focused on determining partition rate constant ratios for a variety of reactions of ion pairs, and of absolute rate constants from these ratios. This has been accomplished by use of one of the rate constants from this product ratio as a “clock” for the second reaction.

Values of $k_{\text{az}} = 5 \times 10^9 \text{ M}^{-1} \text{ s}^{-1}$ have been determined for diffusion-controlled addition of azide ion to a variety of ring-substituted benzhydryl²⁴ and α -substituted 4-methoxybenzyl²⁵ carbocations. This rate constant have seen extensive use as a “clock” to determine absolute rate constants for addition of a variety of nucleophiles to benzylic carbocations.⁵ Relative rate constants for addition of azide ion

($k_{\text{az}}, \text{M}^{-1} \text{s}^{-1}$) and solvent ($k_{\text{s}}, \text{s}^{-1}$) to a carbocation intermediate of solvolysis are first determined from the ratio of the yields the azide ion and solvent adducts (equation (1)). The value for k_{s} may then be calculated from this product rate constant ratio ($k_{\text{az}}/k_{\text{s}}, \text{M}^{-1}$), and $k_{\text{az}} = 5 \times 10^9 \text{M}^{-1} \text{s}^{-1}$ for the diffusion limited reaction of azide ion (Scheme 3).

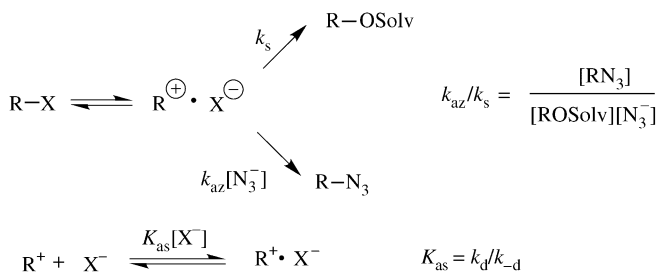
$$k_{\text{az}}/k_{\text{s}} = \frac{[\text{RN}_3]}{[\text{ROSolv}][\text{N}_3^-]} \quad (1)$$



Separation of an ion-pair to free ions, with rate constant $k_{-\text{d}}$, has been used as a “clock” for other reactions of the ion pair. Estimates of $k_{-\text{d}}$ can be obtained from the simple relationship between the association constant for ion-pair formation (K_{as} , equation (2)) and the rate constant for diffusion-controlled encounter ($k_{\text{d}} = 5 \times 10^9 \text{M}^{-1} \text{s}^{-1}$) of anions and carbocations.

Ionic complexes in water are generally are weak. For example, the association constant for formation of complexes between stable monocations and monanions ions in water are typically $K_{\text{as}} \approx 0.1 \text{M}^{-1}$.²⁶ Values of K_{as} (M^{-1}) for association of nucleophilic anions and neutral electrophilic substrates for solvolysis have been estimated from the limiting rate constant ratios determined for stepwise nucleophilic substitution reactions through highly unstable carbocation reaction intermediates.^{2,20,27} Justification for these estimates of K_{as} is provided by the representative plot shown in Fig. 1 of nucleophile selectivity $k_{\text{az}}/k_{\text{s}}$ (M^{-1}) against carbocation reactivity for stepwise aliphatic nucleophilic substitution.^{14,17,28}

The descending nucleophile selectivity ($(k_{\text{az}}/k_{\text{s}})_{\text{obsd}}$ (M^{-1}) on the left-hand limb of Fig. 1 for stepwise solvolysis of R-X is due to the increase in k_{s} (s^{-1}), with decreasing stability of the carbocation intermediate, relative to the constant value of k_{az} ($\text{M}^{-1} \text{s}^{-1}$) for the diffusion-limited addition of azide anion. The lifetime for the carbocation intermediate R^+ eventually becomes so short that essentially no azide ion adduct forms by diffusion-controlled trapping, because addition of solvent to R^+ occurs faster than escape of the carbocation from the solvent cage followed by addition of azide ion ($k'_{\text{s}} \gg k_{-\text{d}}$). Now, the nucleophile adduct must form through a preassociation mechanism, where the azide anion comes together in an association



Scheme 3

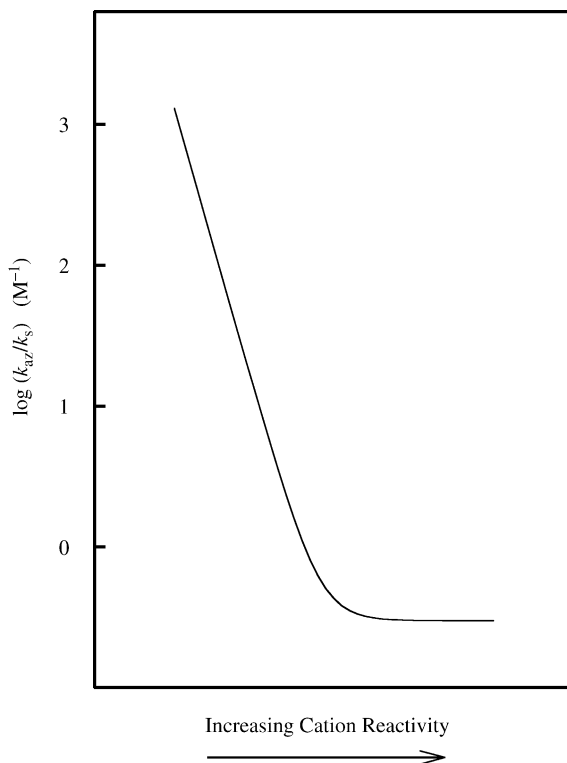
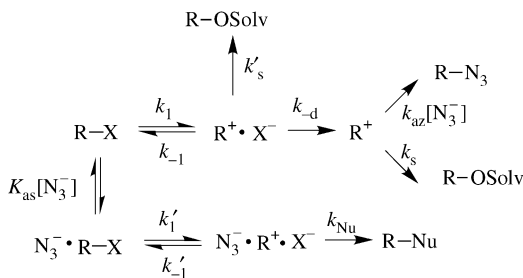


Fig. 1 A hypothetical plot of azide ion selectivity $k_{\text{az}}/k_{\text{s}}$ (M^{-1}) against the reactivity of the carbocation intermediate of solvolysis of R-X in aqueous solution (Scheme 4). The descending limb on the left hand side of this plot is for reactions where the value of k_{s} (s^{-1}) is increasing relative to the constant value of k_{az} ($\text{M}^{-1} \text{s}^{-1}$) for diffusion-limited addition of azide ion to the carbocation. The constant nucleophile selectivity is for reaction of R-X by a preassociation mechanism.

complex with substrate (K_{as} , Scheme 4), which then ionizes (k_1') to form a triple ion complex. This complex will react to form mainly R-Nu , because of the greater reactivity azide ion compared with solvent. The nucleophile selectivity for reaction by a preassociation mechanism is equal to the value of the association constant for formation of $\text{Nu}^- \cdot \text{R-X}$ ($k_{\text{Nu}}/k_{\text{s}} = K_{\text{as}}$ (M^{-1})), in the case of a stepwise reaction mechanism in which there is no nucleophilic assistance to ionization of neutral substrate ($k_1 \approx k_1'$). This association constant should not show a strong dependence on substrate structure, so that a nearly constant value of $k_{\text{Nu}}/k_{\text{s}} = K_{\text{as}}$ is expected to be observed by experiment (Fig. 1).

The azide ion product selectivity $(k_{\text{az}}/k_{\text{s}})_{\text{obsd}} = 0.7 \text{ M}^{-1}$ observed for reactions of ring-substituted cumyl derivatives $[\text{XC}_6\text{H}_4\text{C}(\text{Me}_2)\text{Y}]$ when X is strongly electron-withdrawing is consistent with $K_{\text{as}} \approx 0.7 \text{ M}^{-1}$ for formation of an association



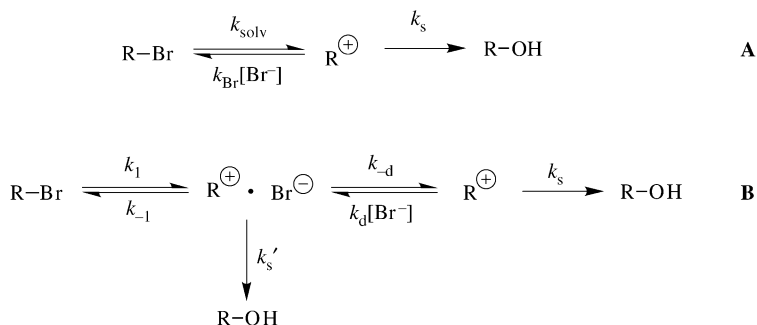
Scheme 4

complex between the substrate and azide ion, provided there is no nucleophilic assistance by azide ion.² There is no detectable bimolecular substitution of azide ion at any ring-substituted cumyl derivative² and this is consistent with little or no nucleophilic assistance by azide ion. However, it is possible that a small rate increase from bimolecular substitution is masked by a compensating decrease in k_{obsd} from a specific azide ion salt effect. Values of $K_{\text{as}} = 0.2 \text{ M}^{-1}$ (Ref. 27) and $K_{\text{as}} = 0.3 \text{ M}^{-1}$ (Ref. 20), respectively, have been determined from the small nucleophile selectivities observed for addition of azide ion to 3,5-(bis)trifluoromethylbenzyl diazonium ion and for addition of propanethiol to 1-(4-fluorophenyl)ethyl chloride in 50:50 (v:v) trifluoroethanol water.

We have assumed that the values of K_{as} for formation weak encounter complexes between nucleophile and substrate, and between nucleophile and carbocation are similar. This is supported by the observation of similar values of K_{as} [see above] for formation of encounter complexes between neutral substrate and anionic nucleophile (0.7 M^{-1}),² between cationic substrate and anionic nucleophile (0.2 M^{-1}),²⁷ and between neutral substrate and neutral nucleophile (0.3 M^{-1}).²⁰ We use the value of $k_{-d} = 1.6 \times 10^{10} \text{ s}^{-1}$ that can be calculated from $K_{\text{as}} = 0.3 \text{ M}^{-1}$ formation of encounter complexes with 1-phenylethyl derivatives and $k_d = 5 \times 10^9 \text{ M}^{-1} \text{ s}^{-1}$ (equation (2)).²⁰ The uncertainty in this value for k_{-d} is approximately equal to the range of experimental values for K_{as} ($0.2\text{--}0.7 \text{ M}^{-1}$).^{2,20,27}

4 Addition of solvent to carbocation–anion pairs

The addition of water to a free carbocation intermediate of solvolysis can be distinguished from addition to an ion-pair intermediate by an examination of common ion inhibition of solvolysis.^{29–31} Common leaving group inhibition of solvolysis is observed when the leaving group ion (X^-) acts, by mass action, to convert the free carbocation (R^+ , Scheme 5A) to substrate (R-X). This results in a decrease in the steady-state concentration of R^+ that leads directly to a decrease in the velocity of solvolysis. Some fraction of the solvolysis reaction products form by direct addition of solvent to the carbocation–anion pair intermediate. The external



Scheme 5

leaving group ion will have little effect on the rate of reaction of solvent with R^+ that is already paired to this ion at the intermediate. Therefore, large concentrations of X^- that reduce the concentration of “free” R^+ to close to zero are predicted to cause the velocity for solvolysis to level off at a constant value at the point when all of the solvent reaction is from capture of the ion pair intermediate (Scheme 5B).

1-(4-Methoxyphenyl)-2,2,2-trifluoroethyl bromide (**1-Br**) undergoes solvolysis by a $\text{D}_\text{N} + \text{A}_\text{N}$ reaction mechanism in water at 25 °C and $I = 6.00$ (NaClO_4) through the 1-(4-methoxyphenyl)-2,2,2-trifluoroethyl carbocation intermediate (1^+) which partitions between addition of azide ion ($k_{\text{az}} = 5 \times 10^9 \text{ M}^{-1} \text{ s}^{-1}$, Scheme 4) and solvent ($k_s = 2.3 \times 10^7 \text{ s}^{-1}$).³² Fig. 2 shows the effect of increasing concentrations of bromide ion on the observed rate constant for solvolysis of **1-Br** under the same reaction conditions. The data for reactions at low $[\text{Br}^-]$ show a good fit to equation (3A) derived for Scheme 5A (inset to Fig. 2) using $k_{\text{Br}^-}/k_s = 77 \text{ M}^{-1}$.

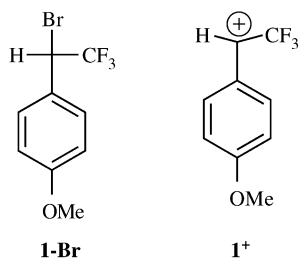


Fig. 2 shows that there is a 300-fold decrease in k_{obsd} for solvolysis of **1-Br** as $[\text{Br}^-]$ is increased from 0 to 5.00 M. This 300-fold decrease shows that at least 99.7% of the solvolysis reaction product forms by the addition of solvent to the liberated intermediate 1^+ , because the concentration of this species has been reduced 99.7% by mass action of bromide ion. Fig. 3 shows the fit to equation (3B) of the data for reaction of **1-Br** at low $[\text{NaBr}]$ of 0.0–0.03 M using $k_{\text{solv}} = 0.049 \text{ s}^{-1}$ and $k_{\text{Br}^-}/k_s = 77 \text{ M}^{-1}$ (Scheme 5A). A comparison of the calculated and observed rate constants for solvolysis of **1-Br** (Fig. 3) shows that k_{obsd} for the reaction of **1-Br**

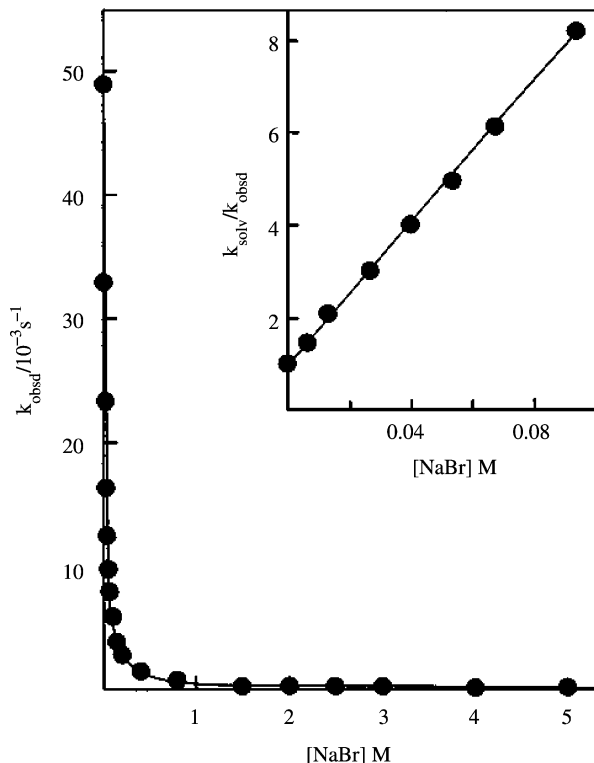


Fig. 2 Effect of added NaBr on the pseudo-first-order rate constants, k_{obsd} , for solvolysis of **1-Br** in water at 25 °C and $I = 6.00$ (NaClO_4). The inset shows the linear replot of the data according to equation (3A) of the text. [Reprinted with permission of the American Chemical Society from Ref. 32].

at $[\text{NaBr}] = 2.00\text{--}5.00$ M is larger than k_{calc} by an amount that is significantly greater than the experimental uncertainty of $\pm 5\%$.

The difference between k_{obsd} and k_{calc} might be due to a specific salt effect on the rate constant for solvolysis. However, this is unlikely because perchlorate ion acts to stabilize carbocations relative to neutral substrates.³³ At high concentrations of sodium bromide, the rate-limiting step for solvolysis of **1-Br** is the capture of $\mathbf{1}^+$ by solvent (k_s Scheme 5A). Substitution of Br^- for ClO_4^- should destabilize the carbocation-like transition state for this step relative to the starting neutral substrate, and this would lead to a *negative*, rather than positive deviation of k_{obsd} for equations (3A) and (3B).

$$k_{\text{solv}}/k_{\text{obsd}} = 1 + (k_{\text{Br}}/k_s)[\text{Br}^-] \quad (3A)$$

$$k_{\text{calc}} = \frac{k_{\text{solv}}k_s}{k_s + k_{\text{Br}}[\text{Br}^-]} \quad (3B)$$

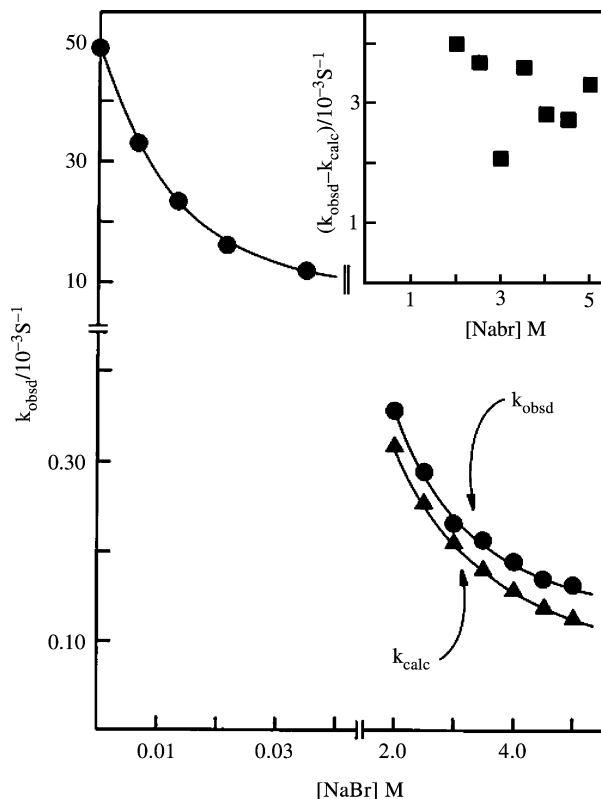


Fig. 3 Expansion of the plot in Fig. 1, which shows a comparison of the values for k_{obsd} , the observed rate constant for the reaction of **1-Br** and k_{calc} , the value calculated from equation (3B) as described in the text. The inset shows a plot of $(k_{\text{obsd}} - k_{\text{calc}})/10^{-3}\text{s}^{-1}$ against the concentration of bromide ion. [Reprinted with permission of the American Chemical Society from Ref. 32].

The rate law for Scheme 5B is given in equation (4). The first and second terms in the numerator of equation (4) describe, respectively, the relative contribution to k_{obsd} of the pathways which proceed through the free carbocation (k_s) and the ion-pair intermediate (k'_s). At low $[\text{Br}^-]$ the reaction of **1-Br** proceeds largely through the free carbocation intermediate $\mathbf{1}^+$ and the second term in the numerator of equation (3) is not significant. The values of k_{calc} determined by extrapolation of rate constants determined for reactions in the presence of low $[\text{Br}^-]$, where the reaction proceeds by capture of free $\mathbf{1}^+$, provide an estimate for the contribution of this reaction pathway to k_{obsd} for reactions in the presence of high $[\text{Br}^-]$. The difference between k_{obsd} and k_{calc} for the reaction of **1-Br** through free $\mathbf{1}^+$ (inset Fig. 3) is equal to the observed rate constant for that small fraction of the reaction that proceeds with addition of solvent to the ion-pair reaction intermediate (equation (5)). The average value of $(k_{\text{obsd}} - k_{\text{calc}})$ over $[\text{NaBr}] = 2.00\text{--}5.00\text{ M}$ is $(3 \pm 1) \times 10^{-5}\text{ s}^{-1}$. This provides an estimate for the limiting velocity at infinite

$[\text{Br}^-]$ where the solvolysis reaction would proceed solely by the capture of the ion-pair intermediate $\mathbf{1}^+\cdot\text{Br}^-$. Equation (5) simplifies to equation (6) for reactions at $[\text{Br}^-] \geq 2.0 \text{ M}$ because $k'_s \approx k_s = 2.3 \times 10^7 \text{ s}^{-1}$ are negligible in comparison with k_{-d} , k_{-1} and $k_d[\text{Br}^-]$.³²

$$k_{\text{obsd}} = \frac{k_1 k_{-d} k_s + k_1 k'_s (k_s + k_d [\text{Br}^-])}{k_s (k_{-1} + k'_s + k_{-d}) + k_d [\text{Br}^-] (k_{-1} + k'_s)} \quad (4)$$

$$k_{\text{obsd}} - k_{\text{calc}} = \frac{k_1 k'_s k_d [\text{Br}^-]}{k_s (k_{-1} + k'_s + k_{-d}) + k_d [\text{Br}^-] (k_{-1} + k'_s)} \quad (5)$$

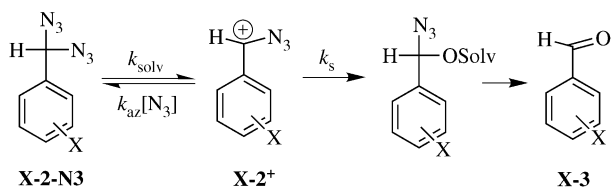
$$k_{\text{obsd}} - k_{\text{calc}} = k_1 k'_s / k_{-1} \quad (6)$$

This limiting velocity $(k_{\text{obsd}} - k_{\text{calc}}) = (3 \pm 1) \times 10^{-5} \text{ s}^{-1}$ is only 0.06% of the value of $k_{\text{solv}} = 0.049 \text{ s}^{-1}$. This provides evidence that the ion pair reaction intermediate $\mathbf{1}^+\cdot\text{Br}^-$ is trapped by solvent less than once for every 1000 times the the substrate undergoes ionization to form the ion pair intermediate. Since this trapping reaction is rare and only results in formation of a significant fraction of total products for reactions in the presence of high concentrations of bromide ion ($>2.0 \text{ M}$), we suggest that it should generally be omitted when writing the mechanism for stepwise aliphatic nucleophilic substitution reactions in water.

The value of $(k_{\text{obsd}} - k_{\text{calc}})$ at a given concentration of bromide anion depends on the association constant for formation of the ion pair from free ions ($K_{\text{as}} = k_d/k_{-d}$), and on the relative reactivity of the ion-pair and free carbocation toward addition of solvent (k'_s/k_s). For example, if K_{as} is small, then the concentration of the ion-pair intermediate will be low and its reaction will make a small contribution to k_{obsd} ; or, if (k'_s/k_s) is small then the ion pair intermediate will be unreactive compared with the free cation.³² Equation (7) shows the relationship between the experimental parameters, K_{as} and (k'_s/k_s) where: $k_{\text{obsd}} - k_{\text{calc}} = (3 \pm 1) \times 10^{-5} \text{ s}^{-1}$ (equation (6)); $k_{\text{solv}} = 0.049 \text{ s}^{-1}$ [$(k_{\text{solv}} = k_1 k_{-d} / (k_{-1} + k_{-d})$]; $k_{\text{Br}}/k_s = 77 \text{ M}^{-1}$ ($k_{\text{Br}}/k_s = k_d k_{-1} / [k_s (k_{-1} + k_{-d})]$, see equation (4)); and $K_{\text{as}} = k_d/k_{-d}$ for formation of an encounter complex between $\mathbf{1}^+$ and Br^- .

The value of 0.05 M from equation (7) is consistent with values of $K_{\text{as}} < 1$ and $(k'_s/k_s) < 1$ for reactions in water. For example, $K_{\text{as}} = 0.3 \text{ M}^{20}$ gives $(k'_s/k_s) = 0.17$ for the relative rate constants for addition of solvent to the carbocation-anion pair and free carbocation. By comparison, the three-fold smaller rate constant for addition of water to an intramolecular trityl carbocation-sulfonate ion pair compared with addition to the analogous substituted trityl carbocation *o*-sulfonyl methyl ester has been used to estimate a value of $(k_s/k'_s) = 0.33$.³⁴

$$\left(\frac{k_{\text{obsd}} - k_{\text{calc}}}{k_{\text{solv}}} \right) \left(\frac{k_{\text{Br}}}{k_s} \right) = \frac{K_{\text{as}} k'_s}{k_s} = \frac{(3 \times 10^{-5} \text{ s}^{-1})(77 \text{ M}^{-1})}{(4.9 \times 10^{-2} \text{ s}^{-1})} = 0.05 \text{ M} \quad (7)$$



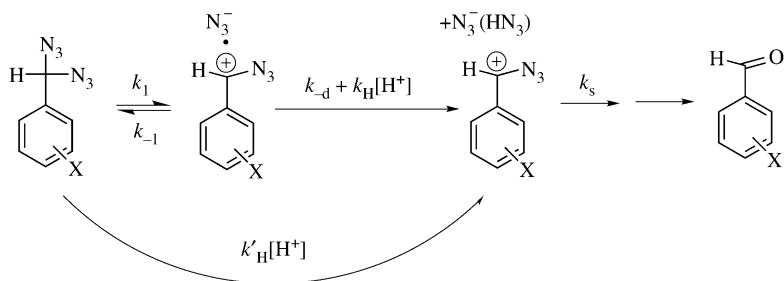
Scheme 6

5 Protonation of a carbocation–anion pair

Azide ion is a modest leaving group in $A_N + D_N$ nucleophilic substitution reactions, and at the same time a potent nucleophile for addition to the carbocation reaction intermediate. Consequently, ring-substituted benzaldehyde *gem*-diazides (**X-2-N₃**) undergo solvolysis in water in reactions that are subject to strong common-ion inhibition by added azide ion from reversible trapping of an α -azido carbocation intermediate (**X-2⁺**) by diffusion controlled addition of azide anion (Scheme 6).^{9,35,36}

The observed first-order rate constants for solvolysis (k_{obsd} , s^{-1}) of **4-MeO-2-N₃** in water at 25 °C and constant ionic strength of 2.0 maintained with NaClO_4 show a sharp dependence on the concentration of perchloric acid up until $[\text{HClO}_4] \approx 0.1 \text{ M}$, at which point there is a downward break to a much weaker linear dependence on the acid concentration up to 1.0 M HClO_4 . Plots of k_{obsd} against $[\text{H}^+]$ (not shown here) have been determined for a broad range of **X-2-N₃**. It was found that as the ring-substituent $-X$ is made progressively more electron-withdrawing, the dependence of k_{obsd} on acid concentration changes gradually from biphasic for reaction of **4-MeO-2-N₃** to linear, with a very steep dependence on $[\text{H}^+]$ for the reaction of **4-NO₂-2-N₃**.³⁷

These data have been fit to a rate law derived for Scheme 7.³⁷ Ionization of **4-MeO-2-N₃** in neutral solution is fast and reversible, and the rate determining step for solvolysis is separation of the ion pair to free ions ($k_{-1} \gg k_{-d}$). Specific acid-catalysis is observed in cases where ionization gives a moderately stabilized



Scheme 7

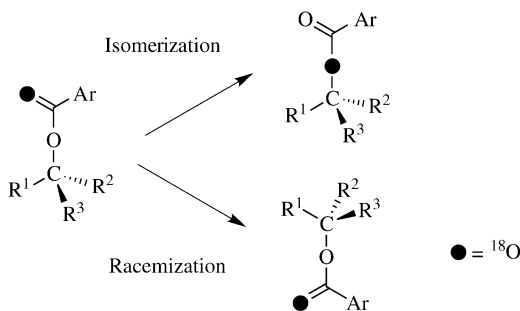
carbocation that undergoes fast internal return to regenerate reactant, because thermodynamically favorable protonation of azide anion to form the much more weakly nucleophilic HN_3 ($k_{\text{H}}[\text{H}^+]$, Scheme 7) eliminates return and makes ionization of **4-MeO-2-N₃** nearly irreversible. This causes an increase in the observed rate constant for solvolysis, by increasing the fraction of times that ionization of the substrate with rate constant k_1 leads to formation of solvolysis product. At high $[\text{HClO}_4]$, essentially every ionization results in formation of solvolysis product [$(k_{-d} + k_{\text{H}}[\text{H}^+]) \gg k_{-1}$], ionization (k_1) becomes rate determining for solvolysis, and a downward break in the plot of k_{obsd} against $[\text{H}^+]$ is observed. The reaction does not change to zero-order in $[\text{H}^+]$, because of competing acid-catalyzed cleavage by a concerted mechanism that converts **4-MeO-2-N₃** directly to **4-MeO-2⁺**. The Hammett reaction constant ρ for this concerted acid-catalyzed cleavage of **X-2-N₃** (k_{H}') is over one unit more positive than for the stepwise ionization (k_1). Therefore, the concerted acid-catalyzed reaction becomes more significant with increasing values of σ_{X} for **X-2-N₃**, and is essentially the only pathway observed for the reaction of **4-NO₂ - 2-N₃**.

The details of our analysis of the dependence of k_{obsd} (s^{-1}) on the concentration of hydronium ion over the region where the rate determining step for solvolysis changes from substrate ionization to formation of the free carbocation awaits the full publication of our experimental data. This analysis will provide two rate constant ratios for partitioning of the ion-pair reaction intermediate (Scheme 7): (1) A value of k_{-1}/k_{-d} for partitioning of the intermediate between internal return and diffusional separation to free ions can be estimated from the ratio of k_{obsd} determined in the absence of acid, and of k_{obsd} determined at very high acid concentrations for which substrate ionization is rate determining. (2) A value of k_{H}/k_{-1} for partitioning of the ion-pair intermediate between thermodynamically favorable bimolecular protonation by hydronium ion and internal return to neutral reactant can be estimated from the concentration of acid at which k_{obsd} is 50% of the maximum value observed at high concentrations of acid when there is a full change in rate determining step. Absolute values of k_{-1} and k_{H} can then be obtained from these rate constant ratios and a value of $k_{-d} = 1.6 \times 10^{10} \text{ s}^{-1}$.

6 Isomerization of ion pair reaction intermediates

The observation of “hidden” reactions during solvolysis, through the use of chiral or isotopically labeled substrates has created considerable excitement in communities interested in the mechanisms of nonenzymatic¹⁵ and enzyme catalyzed reactions.^{38,39} These hidden reactions reveal something interesting about reaction mechanisms. However, chemists and biochemists are still working on the problem of extracting simple and definitive conclusions from analysis of data for these isomerization reactions.

The racemization of chiral substrate or the exchange of bridging and nonbridging oxygens during solvolysis (Scheme 8) may occur through an ion-pair reaction

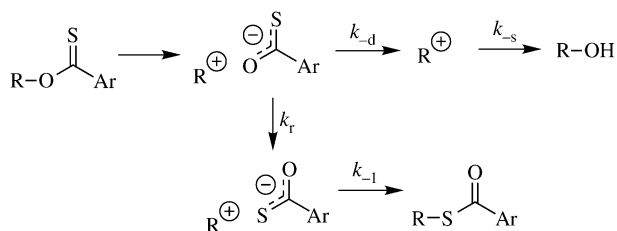


Scheme 8

intermediate that is sufficiently long-lived to undergo reorganization in a solvent cage,¹⁵ or it may proceed by an effectively “concerted” mechanism over an energy maximum that closely resembles the carbocation–anion pair intermediate, but which is flat and avoids formation of a potential energy well for the reaction intermediate.^{40,41} This ambiguity in reaction mechanism can sometimes be resolved by interpreting the experimental results within the broad context of what is known about the lifetime of the putative carbocation reaction intermediate from other experiments.

REORGANIZATION OF ION PAIRS IN WATER

Much is known about the lifetimes of carbocation intermediates of solvolysis, and these data have proven critical in the design of experiments to estimate absolute rate constants for reorganization of ion pairs. Consider reorganization of an ion-pair reaction intermediate that exchanges the positions of the nucleophilic atoms of the leaving group (k_r , Scheme 9) and that occurs in competition with diffusional separation to free ions (k_{-d}) which is much faster than addition of solvent to the ion pair. Ion-pair separation is irreversible and will result in formation of solvolysis reaction products (k_s, s^{-1}). Reorganization of the ion pair will result in formation of isomerization reaction product and the yield of this reaction product will provide a measure of the relative rate constant



Scheme 9

for ion-pair reorganization when internal return is significantly faster than separation of the ion-pair to free ions ($k_{-1} \gg k_{-d}$, [Scheme 9](#)).⁴²

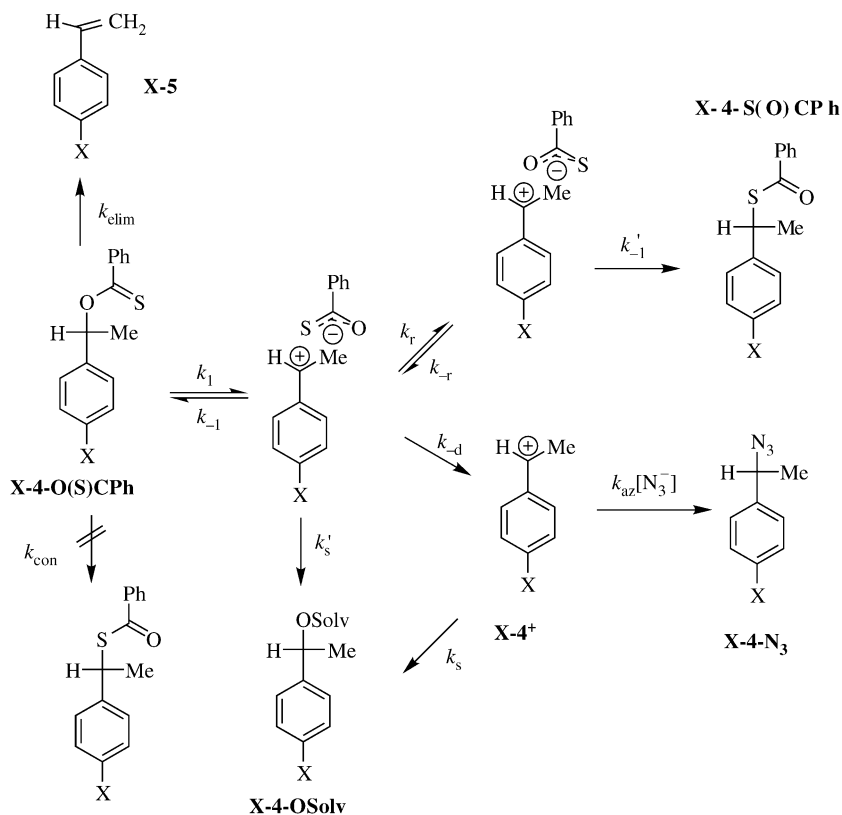
Equation (8) will hold for [Scheme 9](#) in the rare cases where the leaving group is sufficiently weakly basic to allow for heterolysis to form the carbocation reaction intermediate, and the leaving anion is sufficiently nucleophilic to ensure that no escape to free ions can occur after isomerization of the ion pair.⁴² This is true for thionobenzoates, whose reactivity towards C–O bond cleavage is comparable to that of the corresponding ring-substituted pentafluorobenzoate, and whose leaving group anion, thiobenzoate, is highly nucleophilic and undergoes diffusion-limited addition to ring-substituted 1-phenylethyl carbocations even when the ring-substituent is the electron-donating 4-SMe group.⁴²

$$\frac{k_r}{k_{-d}} = \frac{[\text{R-SC(O)Ar}]}{[\text{R-OH}]} \quad (8)$$

The yield of products from the reaction of ring-substituted 1-phenylethyl thionobenzoates provide a unique experimental measure of the relative rate constants for reorganization of an ion pair that exchanges the position of oxygen and sulfur at the thiocarboxylate group (k_r), and diffusional separation of the ion pair to free ions (k_{-d}). The 86% yield of the isomerization reaction product **MeS-4-S(O)CPh** and 14% yield of total solvent adducts **MeS-4-OSolv** ([Table 1](#)) from the reaction of **X-4-O(S)CPh** in 50:50 trifluoroethanol at 25 °C and $I = 0.50$ (NaClO_4) can be used to calculate a value of $k_r/k_{-d} = 6/1$ for partitioning of an ion pair reaction intermediate ([Scheme 10](#)), provided: (1) The reaction proceeds through an intermediate, and (2) Reorganization of the ion-pair is irreversible and results in quantitative formation of **MeS-4-S(O)CPh** ($k_r \gg k_{-d}$, [Scheme 10](#)).

The solvolysis of **MeS-4-O(S)CPh** in aqueous/trifluoroethanol at 25 °C is zero-order in $[\text{N}_3^-]$.⁴² [Fig. 4A](#) shows that formation of **MeS-4-N₃** occurs at the expense of **MeS-4-OSolv** but not **MeS-4-S(O)CPh**. The reaction of **MeS-4-(3,5-dinitrobenzoate)** under the same conditions proceeds through the liberated carbocation intermediate **MeS-4⁺** which partitions between addition of solvent to form **MeS-4-OSolv** and azide anion to form **MeS-4-N₃**.¹⁴ [Fig. 4B](#) shows that the yields of **MeS-4-N₃**, calculated as a fraction of the sum of the yields of **MeS-4-N₃** and **MeS-4-OSolv**, from the reactions of **MeS-4-O(S)CPh** and **MeS-4-(3,5-dinitrobenzoate)** are identical. These data show that essentially 100% of the ion-pair intermediate of reaction of **MeS-4-(3,5-dinitrobenzoate)** undergoes separation to the free carbocation which is trapped by azide ion, while 14% of the reaction of **MeS-4-O(S)CPh** proceeds by this pathway and 86% proceeds by the competing isomerization reaction.⁴²

Solvolysis and isomerization may either proceed through a common ion-pair reaction intermediate, or the isomerization reaction may proceed by a separate concerted reaction pathway that avoids formation of this intermediate (k_{con} , [Scheme 10](#)). Hammett reaction constants of $\rho_{\text{solv}}^+ = -4.9$ and $\rho_{\text{isom}}^+ = -5.5$ for reactions of **X-4-O(S)CPh** were calculated from the data in [Table 1](#).⁴² The larger negative value



for ρ_{isom}^+ than for ρ_{solv}^+ is inconsistent with a concerted isomerization reaction, which would be expected to proceed through a transition state in which cleavage of the C–O bond is accompanied by formation of a C–S bond. This would increase the extent of bonding to the benzylic carbon in the transition state for isomerization compared with solvolysis, so that $\rho_{\text{isom}}^+ > \rho_{\text{solv}}^+$ would have been observed.

The ratio of the yields of the products of isomerization and solvolysis of **X-4-O(S)CPh**, 84/16, gives a value of $k_r/k_{-d} = 6$ for partitioning of the ion-pair intermediate between diffusional separation and reorganization (equation (8)). Combining this ratio²⁰ with $k_{-d} = 1.6 \times 10^{10}$ gives $k_r = 1 \times 10^{11} \text{ s}^{-1}$ for reorganization of the ion pair that exchanges the position of oxygen and sulfur at the thiocarboxylate. These results are consistent with an earlier proposal⁴³ that the rate constant for reorganization of ion pair intermediates of heterolytic reactions in water is similar to the rotational correlation time for water, $k_r \approx 10^{11} \text{ s}^{-1}$.^{44–46}

The rate constants for addition of solvent to **X-4⁺** approach the value of $k_r \approx 10^{11} \text{ s}^{-1}$, so that the ion pair reaction intermediate will undergo addition of

Table 1 Rate constants and product yields for the reactions of ring-substituted 1-phenylethyl thionobenzoates **X-4-OC(S)CPh** (Scheme 10) in 50:50 (v:v) trifluoroethanol/water at 25 °C and $I = 0.50$ (NaClO_4)^a

X	Product yield % ^b			k_{obsd} (s^{-1}) ^c	$k_{\text{s}} \approx k_{\text{s}}'$ (s^{-1}) ^{d,e}	$k_{-\text{d}}$ (s^{-1}) ^{d,f}	k_{r} (s^{-1}) ^{d,g}
	X-4-OSolv	X-4-SC(O)CPh	X-5				
4-MeS	14 (14)	86 (86)	none detected	5.5×10^{-4}	6×10^7 ^h	1.6×10^{10}	1×10^{11}
4-Me	21 (16)	73 (78)	6	2.0×10^{-5}	6×10^9 ⁱ	1.6×10^{10}	1×10^{11}
4-F	25 (24)	64 (65)	12	4.1×10^{-7}	2×10^{10} ⁱ	1.6×10^{10}	1×10^{11}

^aThe details of the calculation of the rate constants for reaction of the carbocation–anion pair are given in Ref. 42.

^bProduct yields determined by HPLC analysis. The values in parenthesis are theoretical product yields calculated as described in Ref. 42.

^cThe observed first order rate constant for the disappearance of **X-4-OC(S)CPh**.

^dRate constants for partitioning of the ion-pair intermediate (Scheme 10).

^eThe rate constant for addition of solvent to the free carbocation, which is assumed to be equal to k_{s}' for addition of solvent to the ion pair [Ref. 32].

^fEstimated rate constant for diffusional separation of the ion pair [Ref. 20].

^gRate constant for reorganization of the ion-pair intermediate, which is assumed to be equal to the dielectric relaxation of water.

^hData from Ref. 42.

ⁱData from Ref. 20.

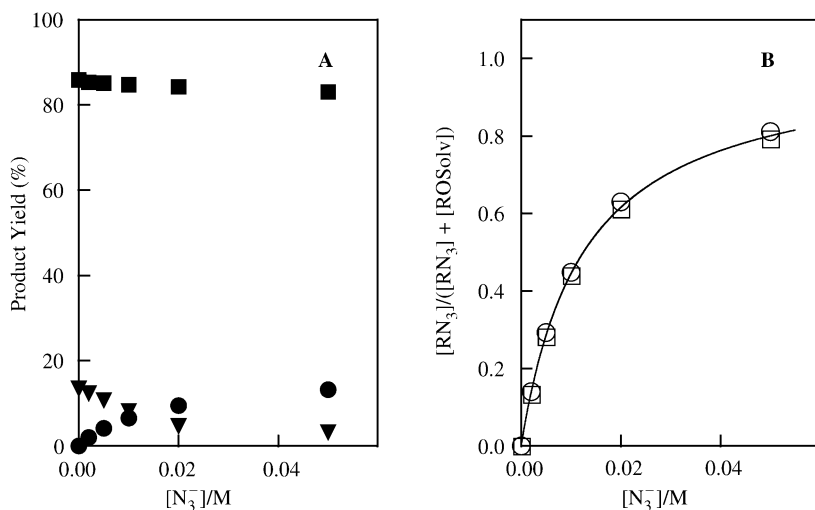


Fig. 4 (A) Dependence of the yields of the products from the reaction of **MeS-1-O(S)CPh** on the concentration of added azide anion in 50:50 (v/v) TFE/H₂O at 25 °C and $I = 0.50$ (NaClO₄): (■), **MeS-1-S(O)CPh**; (▼), **MeS-1-OSolv**; (●), **MeS-1-N₃**. (B) Dependence of the yield of **MeS-1-N₃**, calculated as a fraction of the sum of the yields of **MeS-1-N₃** and **MeS-1-OSolv**, on the concentration of added azide ion in 50:50 (v/v) TFE/H₂O at 25 °C and $I = 0.50$ (NaClO₄): (○), data for reaction of **MeS-1-O(S)CPh**; (□), data for reaction of **MeS-1-(3,5-dinitrobenzoate)**. The solid line was calculated using $k_{az}/k_s = 80 M^{-1}$ for partitioning of **MeS-1⁺** between addition of azide ion and solvent (Scheme 10). [Reprinted with permission of the American Chemical Society from Ref. 42].

solvent at a rate competitive with reorganization.¹⁴ This provides a simple explanation for the increase in the yield of solvolysis products from reactions of **X-4-O(S)CPh** observed as $-X$ is changed from electron-donating to electron withdrawing. Equations (9) and (10) were derived for Scheme 10 where the products of isomerization and solvolysis of **X-4-O(S)CPh** form by partitioning of a common reaction intermediate (see above) and the alkene product of the elimination reaction of **X-4-O(S)CPh** forms by a competing concerted elimination reaction.⁴² The parenthetical values reported in Table 1 are theoretical product yields calculated from the estimated rate constants k_r , k_{-d} and k'_s reported in Table 1 using equations (9) and (10). The good agreement between the calculated and observed product yields provides strong evidence that there are no large errors in the *relative* values of the rate constants used to calculate the product yields.⁴²

$$f_{\text{isom}} = (1 - f_{\text{alk}}) \left(\frac{k_r}{k_r + k_{-d} + k'_s} \right) \quad (9)$$

$$f_{\text{solv}} = (1 - f_{\text{alk}}) \left(\frac{k_{-d} + k'_s}{k_r + k_{-d} + k'_s} \right) \quad (10)$$

INTERNAL RETURN OF ISOTOPICALLY LABELED ION PAIRS

Compounds labeled with multiple isotopes of the same atom provide the opportunity to observe “virtual” isomerization reactions that go undetected in conventional studies.¹⁵ There have been relatively few modern studies of these virtual isomerization reactions,^{47–49} because the reactions themselves are not common and because of difficulties in drawing general conclusions from the observation of the scrambling of isotopic label during solvolysis (Scheme 8).

The exchange of isotopically labeled oxygen between bridging and nonbridging positions is not common, because of the generally incompatible requirements that the solvolysis reaction should occur at a reasonable rate and that internal return of the reactant to substrate be competitive with irreversible separation of the ion pair to free ions. The former requirement is favored when the leaving group is weakly basic, while the later is favored when the leaving group anion is strongly nucleophilic. Substituted benzoate ions (Scheme 8) are not good leaving groups in solvolysis,⁵⁰ and are relatively weakly reactive as nucleophiles towards addition to carbocations.²⁰ Consequently, heterolysis of benzoates substrates (Scheme 8) is only easily observed at ambient temperature when the reaction proceeds through a moderately stable carbocation intermediates, but this favors separation of the carbocation–anion pair to free ions, so that internal return will often not be observed.

Sulfonate anions are better leaving groups than carboxylate ions, but solvolysis of sulfonates in water can only be easily monitored when the putative carbocation intermediate is highly unstable. For example *s*-butyl bromobenzosulfonate undergoes competing solvolysis and scrambling of oxygens between bridging and nonbridging positions in trifluoroethanol,⁵¹ but the putative *s*-butyl carbocation intermediate of this reaction is far too unstable to exist in water for the time of a bond vibration.⁵¹ The formation of this intermediate may also be avoided in the more weakly nucleophilic solvent trifluoroethanol, in which case the mechanisms for the competing ¹⁸O scrambling and solvolysis reactions of *s*-butyl bromobenzosulfonate are best described as concerted.⁴¹

We have examined the competing isomerization and solvolysis reactions of 1-(4-(methylphenyl)ethyl) pentafluorobenzoate with two goals in mind:⁵² (1) We wanted to use the increased sensitivity of modern analytical methods to extend oxygen-18 scrambling studies to mostly aqueous solutions, where we have obtained extensive data for nucleophilic substitution reactions of 1-phenylethyl derivatives. (2) We were interested in comparing the first-order rate constant for internal return of a carbocation–carboxylate anion pair with the corresponding second-order rate constant for the bimolecular combination of the same carbocation with a carboxylate anion, in order to examine the effect of aqueous solvation of free carboxylate anions on their reactivity toward addition to carbocations.

1-(4-(Methylphenyl)ethyl) pentafluorobenzoate (**Me-4-OC(O)C₆F₅**) was prepared labeled with carbon-13 at the benzylic carbon (99% enriched) and oxygen-18 at the bridging benzoate oxygen (45% enriched). The solvolysis reaction and the

isomerization reaction to form $\text{Me-4-OC}^{(18\text{O})}\text{C}_6\text{F}_5$ with oxygen-18 at the nonbridging oxygen were monitored by ^{13}C -NMR in a solvent of 50:50 (v/v) water/trifluoroethanol. The ^{13}C NMR spectrum of the ester substrate showed peaks at 75.520 ppm and 75.481 ppm for the benzylic carbons of $\text{Me-4-OC}(\text{O})\text{C}_6\text{F}_5$ and $\text{Me-4-}^{18}\text{OC}(\text{O})\text{C}_6\text{F}_5$, respectively, because of an oxygen-18 perturbation of carbon-13 chemical shift. Solvolysis resulted in the disappearance of ^{13}C NMR peaks for the benzylic carbon of substrate, and isomerization in the appearance of a new peak at (75.514 ppm) for the isomerization product $\text{Me-4-OC}^{(18\text{O})}\text{C}_6\text{F}_5$.

$$(A_{\text{nor}})_{\text{nonbridging}} = 0.5(e^{-k_{\text{solv}}t} - e^{-(2k_{\text{iso}}+k_{\text{solv}})t}) \quad (11)$$

Fig. 5 (■) shows the fractional conversion with time of $\text{Me-4-}^{18}\text{OC}(\text{O})\text{C}_6\text{F}_5$ (oxygen-18 bridging) to isomerization product $\text{Me-4-OC}^{(18\text{O})}\text{C}_6\text{F}_5$

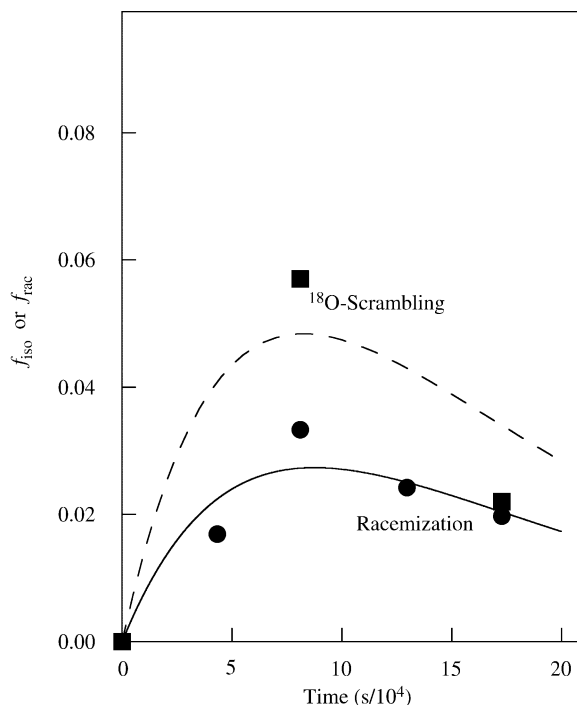
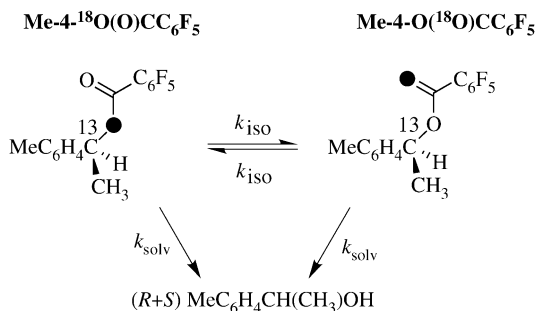


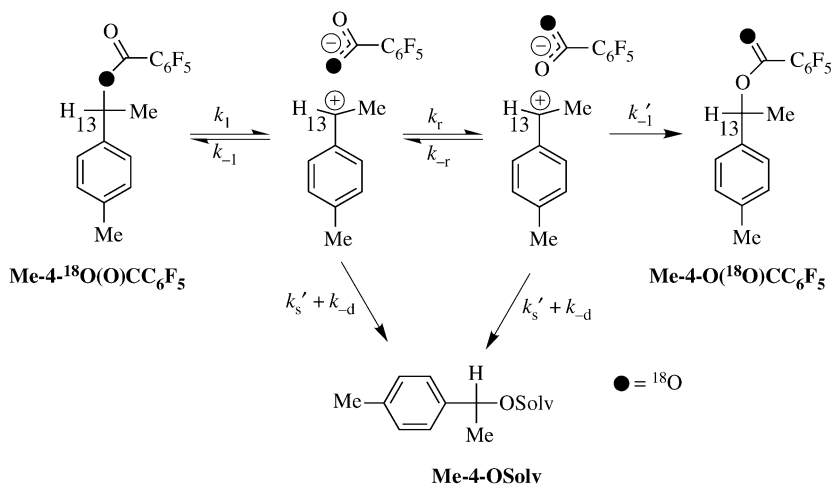
Fig. 5 Time course for isomerization of $\text{Me-4-}^{18}\text{OC}(\text{O})\text{C}_6\text{F}_5$ and the racemization of $(S)\text{-1-OC}(\text{O})\text{C}_6\text{F}_5$ during the solvolysis of these esters in 50/50 (v/v) trifluoroethanol/water at 25 °C. (■): Fractional conversion with time of $\text{Me-4-}^{18}\text{OC}(\text{O})\text{C}_6\text{F}_5$ (oxygen-18 bridging) to isomerization product $\text{Me-4-OC}^{(18\text{O})}\text{C}_6\text{F}_5$. The dashed line shows the fit of the data to equation (11) derived for Scheme 11 using $k_{\text{solv}} = 1.06 \times 10^{-5} \text{ s}^{-1}$ and $k_{\text{iso}} = 1.6 \times 10^{-6} \text{ s}^{-1}$. (●): Fractional conversion with time of $(S)\text{-Me-4-OC}(\text{O})\text{C}_6\text{F}_5$ to $(R)\text{-Me-4-OC}(\text{O})\text{C}_6\text{F}_5$. The solid line shows the fit of the data to equation (15) derived for Scheme 14 using $k_{\text{solv}} = 1.06 \times 10^{-5} \text{ s}^{-1}$ and $k_{\text{rac}} = 8.5 \times 10^{-7} \text{ s}^{-1}$.



Scheme 11

(oxygen-18 nonbridging) during the solvolysis of **Me-4-¹⁸O(O)C₆F₅** in 50/50 trifluoroethanol/water, that has been calculated from published data.⁵² The dashed line shows the fit of the experimental data to equation (11), derived for **Scheme 11** using values of $k_{\text{solv}} = 1.06 \times 10^{-5} \text{ s}^{-1}$ determined for the overall solvolysis reaction of substrate and $k_{\text{iso}} = 0.16 \times 10^{-5} \text{ s}^{-1}$ for the isomerization reaction.⁵² A direct comparison of these rate constants shows that this substrate undergoes internal return that leads to isomerization about once for every six substrate ionizations.

Scheme 12 shows a minimal mechanism for solvolysis and isomerization of **Me-4-¹⁸O(O)C₆F₅**. Values of $k'_s = 6 \times 10^9 \text{ s}^{-1}$ for the direct nucleophilic addition of solvent to the ion-pair intermediate, and $k_{-d} = 1.6 \times 10^{10} \text{ s}^{-1}$ for the irreversible diffusional separation of the intermediate to free ions have been reported in earlier work.²⁰ Both of these reactions result, eventually, in formation of the solvent



Scheme 12

adducts **Me-4-OSolv**. The reorganization of the ion pair intermediate of the reaction of **Me-4-OC(S)C₆F₅**, $k_r = k_{-r} = 10^{11} \text{ s}^{-1}$,⁴² is significantly faster than the total rate addition of solvent to the carbocation–anion pair, and diffusional separation of this ion pair, $k_r > (k'_s + k_{-d}) = 2.2 \times 10^{10} \text{ s}^{-1}$ (see above). Therefore, the observation that isomerization is slower than the solvolysis of **Me-4-¹⁸OC(O)C₆F₅** requires that reaction of the ion pair to form **Me-4-OSolv** be faster than unimolecular collapse of the ion pair, $(k'_s + k_{-d}) > k'_{-1}$ (Scheme 12). This allows the conclusion that isomerization of **Me-4-¹⁸OC(O)C₆F₅** to give **Me-4-OC(¹⁸O)C₆F₅** takes place by rapid reorganization of the first-formed ion pair intermediate (k_r) followed by rate-limiting ion pair collapse (k'_{-1}).⁵²

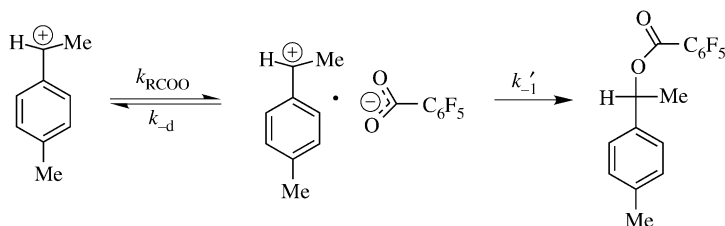
Equations (12)–(14) were derived for Scheme 12 by making the assumption that $k_{-1} = k'_{-1}$ and that the degenerate reorganization of the ion pair that exchanges the two equivalent benzoate oxygens ($k_r = k_{-r}$) is much faster than the other reactions of the ion pair, so that $k_r \gg (k'_s + k_{-d}), k'_{-1}$. A value of $k'_{-1} = 7 \times 10^9 \text{ s}^{-1}$ for unimolecular ion pair collapse was calculated from the ratio of experimental rate constants $k_{\text{iso}}/k_{\text{solv}} = 0.15$ using equation (13), with $k'_s = 6 \times 10^9 \text{ s}^{-1}$ and $k_{-d} = 1.6 \times 10^{10} \text{ s}^{-1}$.⁵²

$$k_{\text{solv}} = \frac{k_1(k'_s + k_{-d})}{k'_s + k_{-d} + k_{-1}} \quad (12)$$

$$k_{\text{iso}} = \frac{k_1 k'_{-1}}{2(k'_s + k_{-d} + k_{-1})} \quad (13)$$

$$\frac{k_{\text{iso}}}{k_{\text{solv}}} = \frac{k'_{-1}}{2(k'_s + k_{-d})} \quad (14)$$

The value of $k'_{-1} = 7 \times 10^9 \text{ s}^{-1}$ for the first-order rate constant for collapse of an ion pair between **Me-4⁺** and pentafluorobenzoate ion is larger than the second-order rate constant $k_{\text{RCOO}} = 5 \times 10^8 \text{ M}^{-1} \text{ s}^{-1}$ reported for the bimolecular addition of alkane carboxylates to **Me-4⁺**.²⁰ This second-order rate constant is limited by the rate constant for formation of an ion pair between **Me-4⁺** and a carboxylate ion. The larger barrier to encounter-limited reactions of carboxylate ions compared with the diffusion-limited reactions of anions such as azide ion, $k_{\text{az}} = 5 \times 10^9 \text{ M}^{-1} \text{ s}^{-1}$ represents the barrier to desolvation of nucleophile that must precede formation of an ion pair between **Me-4⁺** and a carboxylate ion (Scheme 13).⁵²



Scheme 13

7 Racemization of ion pairs

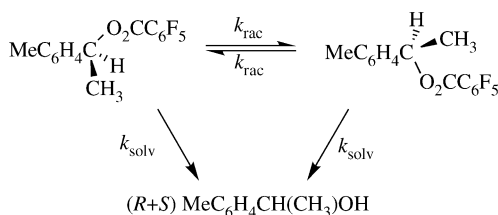
Another historically important reaction is the reorganization of “chiral” ion pair intermediates of solvolysis of a chiral substrate that leads to racemization of substrate during solvolysis. This reorganization competes with other reactions of the ion pair intermediate of solvolysis of a chiral substrate, so that the relative rate constant for ion-pair “racemization” can be obtained by determining the relative rates of formation of products from partitioning of the ion pair reaction intermediate, including the enantiomer of substrate (Scheme 14).

$$(A_{\text{nor}})_{\text{R}} = 0.5(e^{-k_{\text{solv}}t} - e^{-(2k_{\text{rac}}+k_{\text{solv}})t}) \quad (15)$$

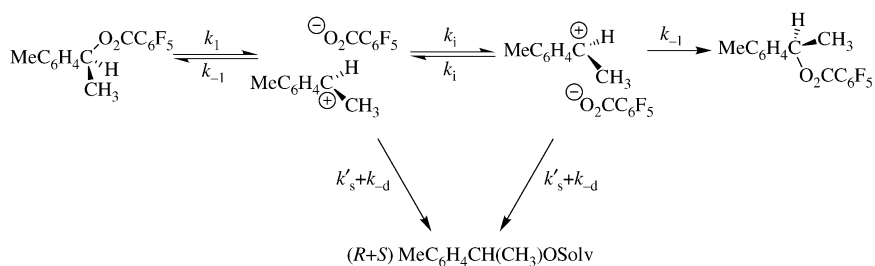
We prepared the chiral ester (*S*)-1-(4-methylphenyl)ethyl pentafluorobenzoate, (**S**)-**Me-4-OC(O)C₆F₅** and monitored the formation of (*R*)-**Me-4-OC(O)C₆F₅** during solvolysis in 50:50 (v/v) water/trifluoroethanol by using a chiral shift reagent to resolve the signals for the benzylic protons of the (*R*) and (*S*) isomers of reactant.⁵³ Fig. 5 (●) shows the fractional conversion with time of (*R*)-**Me-4-OC(O)C₆F₅** to (*S*)-**Me-4-OC(O)C₆F₅** during solvolysis of the (*R*)-enantiomer in 50:50 (v/v) trifluoroethanol/water. The data from Fig. 5 have been fit to equation (15) derived for Scheme 14 using $k_{\text{solv}} = 1.06 \times 10^{-5} \text{ s}^{-1}$ for the solvolysis of **Me-4-OC(O)C₆F₅** to give a value of $k_{\text{rac}} = 8.5 \times 10^{-7} \text{ s}^{-1}$ for racemization of (*R*)-**Me-4-OC(O)C₆F₅**.⁵² This value of k_{rac} is 12-fold smaller than $k_{\text{solv}} = 1.06 \times 10^{-5} \text{ s}^{-1}$ for solvolysis of **Me-4-OC(O)C₆F₅**, and 2-fold smaller than $k_{\text{iso}} = 1.6 \times 10^{-6} \text{ s}^{-1}$ for degenerate isomerization which exchanges the position of the ester bridging and nonbridging oxygens of **Me-4-OC(O)C₆F₅** (see above).⁵² This shows that inversion of the ion-pair intermediate is a relatively rare event during solvolysis in a largely aqueous solvent.

$$\frac{k_{\text{rac}}}{k_{\text{iso}}} = \frac{2k_{\text{i}}}{2k_{\text{i}} + k_{-1} + k_{-d} + k'_{\text{s}}} \quad (16)$$

Equation (16) gives the relationship between the rate constant ratio $k_{\text{rac}}/k_{\text{iso}} = 0.53$ and the rate constants from Scheme 15 for partitioning of the ion pair reaction intermediate.⁵³ Racemization and isomerization will proceed at similar rates, if inversion of the ion pair is much faster than the other reactions



Scheme 14



Scheme 15

from Scheme 15 ($2k_i \gg k'_s + k_{-d} + k_{-1}$, equation (16)). The observed ratio of $k_{\text{rac}}/k_{\text{iso}} = 0.53$ requires that $2k_i \approx k'_s + k_{-d} + k_{-1}$. Substitution of $k_{-d} = 1.6 \times 10^{10} \text{ s}^{-1}$, $k'_s = 6 \times 10^9 \text{ s}^{-1}$, and $k_{-1} = 7 \times 10^9 \text{ s}^{-1}$ into equation (16) gives $k_i = 1.5 \times 10^{10} \text{ s}^{-1}$ for inversion of the ion pair in 50/50 (v/v) water/trifluoroethanol. This is similar to the value of $k_{-d} \approx 1.6 \times 10^{10} \text{ s}^{-1}$ for separation of the ion pair to free ions. We have concluded that the barrier to separation of this ion pair to free ions, which involves complete loss of intermolecular ionic interactions, is similar to the barrier to “inversion”, which involves substantial reorganization but maintains the intermolecular interactions between these ions.⁵³

Racemization of neutral substrates by solvolysis through an ion-pair or ion-dipole reaction intermediate will rarely be observed for reactions in water, because few substrates will meet the following strict requirements for the observation of racemization:

- (1) The reactant must undergo ionization to form a carbocation intermediate in water with a rate constant of between 10^{-1} and 10^{-8} s^{-1} , in order to be able to conveniently monitor this reaction.
- (2) The ion-pair intermediate must undergo internal return to reactant at a rate competitive with diffusional separation to free ions ($k_{-1} \geq k_{-d} \approx 1.6 \times 10^{10} \text{ s}^{-1}$).
- (3) The carbocation intermediate must exist in water long enough to allow for racemization of the carbocation–anion or ion dipole pair to occur, so that $k'_s < 1 \times 10^{11} \text{ s}^{-1}$ for addition of solvent (Scheme 15). In the case of solvolysis of (*R*)-1-phenylethanol in H_2^{18}O , which proceeds by a stepwise mechanism through a 1-phenylethyl carbocation intermediate that is captured by water with an estimated rate constant of $k'_s \approx 1 \times 10^{11} \text{ s}^{-1}$,¹⁴ only a barely detectable 1–3% of (*S*)-1-phenylethanol forms by migration of the ¹⁶O-water leaving group from the *re* to the *si* face of the carbocation.⁵⁴ Similarly, internal return to reactant that accompanies the stepwise solvolysis of 1-phenylethyl 4-nitrobenzoate in 70% aqueous acetone does not result in detectable racemization of the remaining ester, because of the fast competing direct addition of solvent to the ion pair intermediate.⁵⁵

The situation is different for solvolysis reactions in most other solvents, where the intermolecular interactions between ions at an ion pair are stronger than the compensating interactions with solvent that develop when the ion pair separates to free ions. This favors the observation of racemization during solvolysis. There are numerous reports from studies on solvolysis in solvents with relatively low dielectric constant such as acetic acid, of polarimetric rate constants (k_{α} , s^{-1}) for racemization of chiral substrates that greatly exceed the titrimetric rate constant (k_t , s^{-1}) for formation of acid from the solvolysis reaction.¹⁵

8 Concluding remarks

The rise of physical organic chemistry in the United States can be traced through the papers leading to Winstein's "global" mechanism for stepwise solvolysis through intimate and solvent separated ion pair intermediates. The neglect of this model in recent years is a result of the declining fashionability of physical organic chemistry in the US the onset of which, perhaps, was marked by Winstein's untimely death. This neglect is easily understood. The perils of ignoring fashion in science are more severe than ignoring fashion in everyday dress, and no one who suffers the consequences of ignoring fashion can expect sympathy from those who set it. The result is a more than 20-year gap in the chemical literature on many problems similar to those discussed here, whose solution will require the more enthusiastic support by the organic community of curious investigators.

Acknowledgements

This work was supported by grant GM 39754 from the National Institutes of Health.

References

1. Richard, J.P. and Jencks, W.P. (1982). *J. Am. Chem. Soc.* **104**, 4691–4692
2. Richard, J.P., Amyes, T.L. and Vontor, T. (1991). *J. Am. Chem. Soc.* **113**, 5871–5873
3. Amyes, T.L. and Richard, J.P. (1990). *J. Am. Chem. Soc.* **112**, 9507–9512
4. Amyes, T.L. and Richard, J.P. (1991). *J. Am. Chem. Soc.* **113**, 8960–8961
5. Richard, J.P., Amyes, T.L. and Toteva, M.M. (2001). *Acc. Chem. Res.* **4**, 981–988
6. Richard, J.P., Amyes, T.L. and Williams, K.B. (1998). *Pure Appl. Chem.* **70**, 2007–2014
7. Richard, J.P., Lin, S.-S. and Williams, K.B. (1996). *J. Org. Chem.* **61**, 9033–9034
8. Richard, J.P. (1995). *Tetrahedron* **51**, 1535–1573
9. Richard, J.P., Amyes, T.L., Jagannadham, V., Lee, Y.-G. and Rice, D.J. (1995). *J. Am. Chem. Soc.* **117**, 5198–5205
10. Amyes, T.L., Stevens, I.W. and Richard, J.P. (1993). *J. Org. Chem.* **58**, 6057–6066
11. Amyes, T.L., Richard, J.P. and Novak, M. (1992). *J. Am. Chem. Soc.* **114**, 8032–8041
12. Richard, J.P., Amyes, T.L. and Rice, D.J. (1993). *J. Am. Chem. Soc.* **115**, 2523–2524
13. Richard, J.P. (1989). *J. Am. Chem. Soc.* **111**, 1455–1465

14. Richard, J.P., Rothenberg, M.E. and Jencks, W.P. (1984). *J. Am. Chem. Soc.* **106**, 1361–1372
15. Harris, J.M. (1974). *Prog. Phys. Org. Chem.* **11**, 89–173
16. Guthrie, R.D. and Jencks, W.P. (1989). *Acc. Chem. Res.* **22**, 343–349
17. Richard, J.P. and Jencks, W.P. (1982). *J. Am. Chem. Soc.* **104**, 4689–4691
18. Richard, J.P. and Jencks, W.P. (1984). *J. Am. Chem. Soc.* **106**, 1396–1401
19. Richard, J.P. and Jencks, W.P. (1984). *J. Am. Chem. Soc.* **106**, 1383–1396
20. Richard, J.P. and Jencks, W.P. (1984). *J. Am. Chem. Soc.* **106**, 1373–1383
21. Rothenberg, M.E., Richard, J.P. and Jencks, W.P. (1985). *J. Am. Chem. Soc.* **107**, 1340–1346
22. Raber, D.J., Harris, J.M. and Schleyer, P.V.R. (1974). In *Ions and Ion Pairs in Organic Reactions*, Szwarc M. (ed.), vol. 2. Wiley, New York
23. Richard, J.P. and Jencks, W.P. (1984). *J. Am. Chem. Soc.* **106**, 1383–1396
24. McClelland, R.A., Kanagasabapathy, V.M., Banait, N.S. and Steenken, S. (1991). *J. Am. Chem. Soc.* **113**, 1009–1014
25. McClelland, R.A., Cozens, F.L., Steenken, S., Amyes, T.L. and Richard, J.P. (1993). *J. Chem. Soc., Perkin Trans. 2*, 1717–1722
26. Davies, C.W. (1962). *Ion Association*. pp. 77–87. Butterworths, Washington
27. Finnemann, J.I. and Fishbein, J.C. (1995). *J. Am. Chem. Soc.* **117**, 4228–4239
28. Ta-Shma, R. and Rappoport, Z. (1983). *J. Am. Chem. Soc.* **105**, 6082–6095
29. Rappoport, Z., Apeloig, Y. and Greenblatt, J. (1980). *J. Am. Chem. Soc.* **102**, 3837–3848
30. Winstein, S., Clippinger, E., Fainberg, A.H., Heck, R. and Robinson, G.C. (1956). *J. Am. Chem. Soc.* **78**, 328–335
31. Winstein, S., Klinedinst, P.E. and Robinson, G.C. (1961). *J. Am. Chem. Soc.* **83**, 885–895
32. Richard, J.P. (1992). *J. Org. Chem.* **57**, 625–629
33. Bunton, C.A. and Huang, S.K. (1972). *J. Am. Chem. Soc.* **94**, 3536–3544
34. Ritchie, C.D. and Hofelich, T.C. (1980). *J. Am. Chem. Soc.* **102**, 7039–7044
35. Amyes, T.L. and Richard, J.P. (1991). *J. Am. Chem. Soc.* **113**, 1867–1869
36. Jagannadham, V., Amyes, T.L. and Richard, J.P. (1993). *J. Am. Chem. Soc.* **115**, 8465–8466
37. Amyes, T.L. and Richard, J.P. Unpublished results.
38. Midelfort, C.F. and Rose, I.A. (1976). *J. Biol. Chem.* **251**, 5881–5887
39. Kokesh, F.C. and Kakuda, Y. (1977). *Biochemistry* 2467–2473
40. Richard, J.P. (1989). *Adv. Carbocation Chem.* **1**, 122–169
41. Jencks, W.P. (1981). *Chem. Soc. Rev.* **10**, 345–375
42. Richard, J.P. and Tsuji, Y. (2000). *J. Am. Chem. Soc.* **122**, 3963–3964
43. Paradisi, C. and Bunnett, J.F. (1985). *J. Am. Chem. Soc.* **107**, 8223–8233
44. Kaatze, U., Pottel, R. and Schumacher, A. (1992). *J. Phys. Chem.* **96**, 6017–6020
45. Giese, K., Kaatze, U. and Pottel, R. (1970). *J. Phys. Chem.* **74**, 3718–3725
46. Kaatze, U. (1989). *J. Chem. Engng Data* **34**, 371–374
47. Tsuji, Y., Yatsugi, K., Fujio, M. and Tsuno, Y. (1995). *Tetrahedron Lett.* **36**, 1461–1464
48. Tsuji, Y., Kim, S.H., Saeki, Y., Yatsugi, K.-i., Fujio, M. and Tsuno, Y. (1995). *Tetrahedron Lett.* **36**, 1465–1468
49. Allen, A.D., Fujio, M., Tee, O.S., Tidwell, T.T., Tsuji, Y., Tsuno, Y. and Yatsugi, K.-I. (1995). *J. Am. Chem. Soc.* **117**, 8974–8981
50. Noyce, D.S. and Virgilio, J.A. (1972). *J. Org. Chem.* **37**, 2643–2647
51. Dietze, P.E. (1987). *J. Am. Chem. Soc.* **109**, 2057–2062
52. Tsuji, Y., Mori, T., Richard, J.P., Amyes, T.L., Fujio, M. and Tsuno, Y. (2001). *Organic Lett.* **3**, 1237–1240

53. Tsuji, Y., Mori, T., Toteva, M.M. and Richard, J.P. (2003). *J. Phys. Org. Chem.* **16**, 484–490
54. Merritt, M.V., Anderson, D.B., Basu, K.A., Chan, I.-W., Cheon, H.-J., Mukundan, N.E., Flannary, C.A., Kim, A.Y., Vaishampayan, A. and Yens, D.A. (1994). *J. Am. Chem. Soc.* **116**, 5551–5559
55. Goering, H.L., Briody, R.G. and Sandrock, G. (1970). *J. Am. Chem. Soc.* **92**, 7401–7407

Subject Index

- 1-(4-Methoxyphenyl)-2,2,2-trifluoroethyl bromide, 7
- 1-(4-(Methylphenyl)ethyl pentafluorobenzoate, 18
- 1,3-Ditelluroles, 137–138
- 1,5-Dichalcogenacyclooctanes, 135*f*
- 1cR2PI spectroscopy, 185, 189*f*
- 2-amino-1-propanol (alaninol), 184
- 2-Butanol clusters, 187–188, 191, 193*f*
- 2-Butyl acetate ions, 240*t*
- 2'-Fluoro-5-methyl- β -L-arabinofuranosyluracil, 209
- 2-Pyrrolidinmethanols, 196*f*
- 2,3-Dihydrobenzo[b]furan-5-ols, 129*t*
- 2,4,6-Collidine, 31
- 2cR2PI spectroscopy, 186
- Alcohol dehydrogenases, 57–62
- from *Bacillus stearothermophilus*, 53*t*, 60–61
 - from horse liver, 51*t*, 57–59
 - reaction diagram, 54*f*
- Alkali-earth cation- π interactions, 154
- Alkene oxides, 245
- Alkyl phenyl selenides, oxidation potentials, 130*t*
- Alkylarylselenides, 129–131
- arylmethylselenides, 126–129
 - reaction pathways for oxidation, 126*f*
- Alkylaryltellurides, 126–129
- α -Methyl benzyl cation/methanol adducts, 254–263
- α -Secondary isotope effects, 35, 40
- for dihydrofolate reductases, 54
 - exaltation, 40–42
- Amino acid complexes, 199–203
- Amino acids
- charge-solvated vs. zwitterionic structure, 154
 - enantioselectivity and non-hydrogen atoms, 227*f*
 - as ligands, 153
 - metal-bound complexes, 206–209
 - self-assembling, 209–213
 - size and chiral selectivity, 221*f*
 - wrapped in permethylated linear oligosaccharides, 224–225
- Ammonium ion enantiodifferentiation
- by enantiomer-labeled guest method, 213–215
 - by relative peak intensity method, 215–216
- Antibiotic hosts, 231–233
- Arrhenius activation parameters
- for debromination reactions, 94, 95*t*
 - for gas-phase intracomplex inversion of O-protonated 1-aryl-1-methoxyethanes, 259*f*
 - for gas-phase isomerization/racemization of chiral ions **35** and **36**, 253*t*
 - H₂O loss in chiral oxonium ions, 250*t*
 - for oxidative addition of halogens to diorganotellurides, 87*t*
 - for reductive elimination of halogens from chalcogenopyrylium dyes, 84*t*
- Arrhenius plot
- dissociation of O-protonated 1-aryl-1-methoxyethanes, 258*f*
 - inversion of configuration of O-protonated 1-aryl-1-methoxyethanes, 256
 - as quantum tunneling indicator, 70–71
- Aryl trimethylsilylmethyl selenides, 131*f*
- Arylmethyl chalcogenides
- oxidation and peak potentials, 127*t*
- Arylmethylselenides, 126–129
- Arylmethyltellurides, 126–129
- Arylseleninic acids, 113
- Azide ion, 4
- as clock for solvolysis reaction, 4–6
 - as leaving group in nucleophilic substitution reactions, 11
- Bell quantum tunneling model, 33, 34–35, 72
- β -Cyclodextrin/amino acid complexes, 220*t*
- Bidentate ligands, 153
- Biomacromolecules
- dispersion energy, 152
 - structure, 152
- Bite angle, 153
- Bromination
- with diorganoselenium(IV) dihalides, 98, 99*f*
 - with hydrogen peroxide using seleninic acids, 113

- phenoxypropyltelluride 59 as catalyst, 108, 109*f*
- Bromine. *see also* Debromination reactions
addition/reduction from diorganotellurides, 82
oxidative addition to diorganoselenium, 85–87
- Calixarenes, 155
host-guest inclusion, 228–231
- Capillary electrophoresis (CE), 154
- Carbocation-ion pair
addition of solvent, 6–10
protonation, 11–12
- Carbocations
description, 1
as intermediates of solvolysis reactions, 1
lifetime and solvolysis reaction mechanisms, 13
- Carboxylate ions, as leaving group in solvolysis, 18
- Carboxylic acid complexes, 199–203
- Catalysis. *see also* Organoselenium compounds;
Organotellurium compounds; Quantum tunneling experimental studies
and conformational flexibility of thermophilic enzymes, 61–62
enzyme commitment, 55
enzyme structure and tunneling, 59
and quantum tunneling, 28
- Chalcogen dihalides, halogenation of organic substrates, 97–99
- Chalcogen- I_4 complexes, 88
- Chalcogen-iodine-iodine arrays, 84
- Chalcogen (IV) adducts, 80
- Chalcogenaphyrins, 138
- Chalcogenopyrylium dyes, 82
activation parameters for reductive elimination of halogens, 84*t*
halogen elimination, 83*f*
two-electron reduction, 114*f*, 115*f*
- Chalcogens
chalcogenaporphyrins, 138
dichalcogenoethers, 134
electronegativities, 119*t*
intramolecular dimer radical cation formation, 133–134
ionization energies, 119*t*
trichalcogenoethers, 136–137
- Chelates, 153
- Chemical ionization mass spectrometry, 196–197
- Chiral alcohols
acid-induced racemization and isomerization, 247–254
acid-induced Wagner-Meerwein rearrangements, 245–247
- Chiral cluster spectroscopy
hole burning spectroscopy, 160
laser-induced multiphoton excitation, 160
one-color resonant two photon ionization (1cR2P1), 161–164
resonant two photon ionization spectroscopy, 160–161
Rydberg electron transfer (RET) spectroscopy, 166–167
two-color resonant two photon ionization (2cR2P1), 164–166
- Chiral clusters. *see also* Ionic clusters
enantiomer behavior, 154–155
radiolysis, 178
and solvation/desolvation, 148
sources, 156–157
spectroscopy, 158–160
three point rule, 154
- Chiral ion-dipole complexes
acid-induced racemization and isomerization of chiral allylic alcohols, 247–254
acid-induced ring opening of chiral alkene oxides, 245, 246*f*
acid-induced Wagner-Meerwein rearrangements, 245–247
arenium ion/(R)-(-)-2-chlorobutane adducts, 242
gas-phase intracomplex substitution, 263–266
high-pressure reactions, 240–242
hydrogen-deuterium exchange, 235–236
low pressure reactions, 235
noncovalent isomeric 2-butyl ion/toluene complexes, 242–245
proton-transfer reactions, 234*t*, 235
racemization of chiral α -methyl benzyl cation/methanol adducts, 254–263
stereospecific nucleophilic substitution, 236–240
- Chiral recognition. *see also* Host-guest inclusion complexes
2-butanol, 2-pentanol, 2-butylamines
diastereomeric complexes, 187–188
Co³⁺-bound complexes, 206
decay time, 183–184
electrostatic and dispersive interactions, 187
fluorescence dip spectroscopy, 184–185
FTIR, 191–192
kinetic method, 202
Li⁺-bound diol complexes, 204–206
LIF method, 179–180

- metal-bound amino acid complexes, 206–209
- microwave spectroscopy, 191
- proton-bound amino acid complexes, 199–203
- proton-bound carboxylic acid complexes, 199–203
- proton-bound complexes, 196–204
- proton-bound diol complexes, 204
- REMPI spectroscopy, 185
- repulsion-dispersion energy, 183
- Chlorination, with diorganoselenium(IV) dihalides, 99
- Chlorine, addition/reduction from diorganotellurides, 82
- CID spectrometry
 - fragment-ion abundance ratios, 205*t*
 - proton-bound amino acid complexes, 203*t*
- Clevudine, 209
- Co³⁺-bound complexes, 206
- Coupled motion, 40
 - experimental results, 38–39*t*
 - test in 1983, 40–42
- Crown ether hosts, 213–218
- Cu(II)-bound trimer complexes, 207*t*
- Cyclodextrins, 155
 - and host-guest inclusion complexes, 218–222
 - host selectivities, 223*t*
 - as linear oligosaccharide hosts, 222–228
- Cyclofructans, 219*f*, 222
- Debromination reactions
 - of 1,2-dibromoalkanes, 96*f*
 - with diorganotellurides, 92–93, 94*f*
 - with iodide, 92
 - reaction rate, 96
 - with telluride, 92
- Decay time, and enantiomeric differentiation, 184
- Dehalogenation reactions, 96*f*
- Dendrimer wedges, 111
- Di-4-aminophenyltelluroxide
 - hydration/dehydration, 103*f*
- Di-4-chlorophenyltellurium(IV) diiodide, 98
- Di-4-hydroxyphenyltelluroxide
 - hydration/dehydration, 103*f*
- Di-4-methoxyphenyltelluride, 81
- Di-4-methoxyphenyltellurium(IV) diiodide, 98
- Di-4-methylphenyltellurium(IV) diiodide, 98
- Di-*n*-hexyltelluride, 93
- Dialkylselenides
 - dimethylselenide, 131–133
 - intramolecular dimer radical cation formation, 133–134
- Dialkyltellurides, 131–133
- Dialkyltartrates, 196
- Diaryl chalcogenides
 - oxidation and peak potentials, 120*t*
 - oxidation pathways, 123*f*
 - phenylchalcogenyl-1-naphthols, 124
- Diaryl Ditelluride reactions, 91
- Diarylselenides
 - diphenylselenides, 119–121
 - mechanistic studies, 123–124
- Diaryltellurides
 - diphenyltellurides, 119–121
 - mechanistic studies, 123–124
 - molecular modeling, 121
 - reactions with peroxy radicals, 125*f*
- Dichalcogenaporphyrins, 138
- Dichalcogenoethers, 134*t*
- Dihydrofolate reductases, 49*t*
 - reaction diagram, 54*f*
- Dihydrofolate reductases (DHFR), 48, 54, 56
- Dimethyl chalcogenides, 131–133
- Dimethylselenide, 131–133
- Dimethyltellurides, 131–133
- Diorgano diselenides, 113
- Diorgano ditellurides, 113
- Diorganochalcogen(IV) dihalides
 - crystallographic structure, 80*f*
 - redox reactions, 90
- Diorganoselenides
 - antioxidant activity, 138–140
 - and dehalogenation of *vicinal*-dihalides, 97
 - haloperoxidase-like activity, 110*f*
 - oxidative addition of halogens, 89*f*
 - oxidative addition of iodine, 84–85
 - structural studies, 85–87
 - thiolperoxidase-like reactions, 110*f*
- Diorganoselenium(IV) bromides, 98
- Diorganotellurides
 - antioxidant activity, 138–140
 - debromination reactions, 92–93, 94*f*, 96
 - and dehalogenation of *vicinal*-dihalides, 97
 - halogen elimination, 82
 - haloperoxidase-like activity, 110*f*
 - oxidation rate, 110
 - oxidative addition of halogens, 89*f*
 - structural studies, 85–87
 - thiolperoxidase-like reactions, 110*f*
- Diorganotellurium(IV) bromides, 98
- Diorganotellurium(IV) diiodides, 97
- Diphenylselenides, 119–121
- Diphenylselenium(IV) dibromide, 81
- Diphenylselenoxide, hydration/dehydration, 103*f*

- Diphenyltellurides, 119–121
 molecular modeling, 121
- Diselenides, oxidation potentials, 135*t*
- Effusive beam technique, 157–158
- Electron bombardment flow radiolysis, 238
- Electrospray ionization and ionic clusters, 168
- Enantiomers, separation techniques, 154–155
- Enantioselectivity of enzymes, 148
- Enthalpy-entropy compensation plots, 261
- Enthalpy of activation, and quantum tunneling, 67, 70–71
- Enzyme-catalyzed reactions
 breakthroughs in quantum tunneling, 42–48
 conformational flexibility of thermophilic enzyme, 61–62
 early indications of quantum tunneling, 35, 40–42
 enzyme commitment, 55
 enzyme structure and tunneling, 59
 failure to satisfy Swain-Schaad relationship, 43–48
 quantum tunneling during, 28
- Enzymes
 alcohol dehydrogenases, 51*t*, 53*t*, 54*f*, 57–59
 dihydrofolate reductases, 54*f*
 dihydrofolate reductase, 49*t*
 glucose oxidase, 50*t*, 54*f*
 horse liver alcohol dehydrogenase, 51*t*
 human 15-lipoxygenase, 52*t*
 lipoxygenases, 54*f*
 malic enzyme, 54*f*
 methylamine dehydrogenase, 54*f*
 morphinone reductase, 50*t*, 54*f*
 NAD-malic enzyme, 52*t*
 pentaerythritol tetranitrate (PETN) reductase, 50*t*
 peptidyl- α -hydroxylating monooxygenase, 54*f*
 peptidylglycine α -hydroxylating monooxygenase, 49*t*
 sarcosine oxidase, 54*f*
 soybean LO-1, 52*t*
 thymidylate synthase, 49*t*, 54*f*
- Enzymes, enantioselectivity, 148
- Equilibrium chemical isotope effects, 28
 for NCMH model, 40–41
- ESI-MS analysis
 antibiotic hosts, 231
 cysteine solutions, 212–213
 serine solutions, 211–212
- Eyring activation parameters
 for debromination reactions, 94, 95*t*
 for oxidative addition of halogens to diorganotellurides, 87*t*
 for reductive elimination of halogens from chalcogenopyrylium dyes, 84*t*
- Eyring plot, as quantum tunneling indicator, 70–71
- FAB mass spectrometry, 199–203
 enantiodifferentiation of chiral ammonium ions, 213–216
- Fast atom bombardment mass spectrometry (FAB-MS), 155
 as ionic cluster source, 169–170
- Finite heat bath theory (FHBT), 176
- Fluorescence techniques
 for enantiomer discrimination, 155
 excitation spectra for 1:1 diastereomeric complexes, 183*f*
 fluorescence dip spectroscopy, 184–185
- FMAU, 209
- Fourier transform ion cyclotron resonance mass spectrometry (FTIC-MS), 155
 of ionic clusters, 172–173
- FTIR spectroscopy, 191–192
- Gas chromatography (GC), 154
- Glucose oxidase, 50*t*, 66–67
 reaction diagram, 54*f*
- Glutathione, 104, 105*t*
- Glycidol dimers, 191–192
- Halogenation, with chalcogen(IV) dihalides, 97–99
- Halogens
 addition/reduction from diorganotellurides, 82
 bond strength with tellurium, 81
 dehalogenation of *vicinal*-organic dihalides, 91–99
 oxidative addition to diorganoselenium compounds, 80–91
 reductive elimination from chalcogenopyrylium dyes, 83*f*
- Haloperoxidase-like activity, 108–113
- Halotelluronium species, 85
- Hammett reaction constants, 14, 16*t*
- Heisenberg Uncertainty Principle, 28
- Hole burning spectroscopy, 160
 excitation spectra for 1:1 diastereomeric complexes, 183*f*
- Homochirogenesis, 209–210
- Horse liver alcohol dehydrogenase, 51*t*

- Host-guest inclusion complexes, 262–263
antibiotic hosts, 231–233
calixarene hosts, 228–231
chiral crown ether hosts, 213–218
cyclic oligosaccharide hosts, 218–222
cyclodextrin host selectivities, 223*t*
host molecular size, 221
linear oligosaccharide hosts, 222–228
 π - π stacking interactions, 217
proteic hosts, 231
- Human 15-lipoxygenase, 52*t*
- Huskey's rules, 63–64
- Hydride-transfer reactions
dihydrofolate reductases, 48
involving nicotinamide cofactors, 48, 54, 56
- Hydrogen isotope effects, 36
- Hydrogen peroxide oxidation, 113
- Hydrogen tunneling, 28–29
Bell model, 34*f*, 35
early studies, 29–30
and indications of quantum tunneling, 46–48
- Imaginary frequency, 33, 41
- Iodination
4-pentenoic acid, 98*f*
phenoxypropyltelluride 59 as catalyst, 108, 109*f*
- Iodine
oxidative addition to diorganoselenium, 84–85
oxidative addition to diorganotellurides, 87–89
- Iodotellurium, 85
- Ion clusters, sources, 156–157
- Ion-dipole complex, 178
- Ion pairs
and capture and solvolysis velocity, 7
isomerization and solvolysis reaction, 12–21
racemization, 22–24
reaction rate as clock for solvolysis, 3–6
reorganization in water, 13–14
signatures in solvolysis reactions, 3
- Ionic clusters
in gas phase, 149–155
kinetic method, 173–178
quadrupole mass spectrometry, 171–172
radiolysis, 178
sources, 167–170
time-of-flight mass spectrometry, 170–171
trimeric, dissociation, 177*f*
- Isokinetic relationships (IKR), 256, 258
and Larsson's selective energy transfer model, 262–263
- Isomerization reactions
of chiral allylic alcohols, 247–254
virtual, 18–19
- Isotope effect. *see* Kinetic isotope effect
- Isotopes, and virtual isomerization reactions, 18–19
- Kinetic complexity
definition, 43
Klinman's approach, 46
- Kinetic isotope effects, 28
for 2,4,6-collidine, 31
 α -secondary, 35
and coupled motion, 35, 40
in enzyme-catalyzed reactions, 35
as indicators of quantum tunneling, 70
in multistep enzymatic reactions, 44–45
normal temperature dependence, 37
Northrop notation, 45
Northrop's method of calculation, 55
rule of geometric mean, 36
secondary effects and transition state, 37
semiclassical treatment for hydrogen transfer, 31*f*
and Swain-Schaad relationship, 36–37
temperature dependence, 29, 30*f*, 32, 48, 60
temperature-independence and quantum tunneling, 71
temperature independent cases, 65
and violations of Swain-Schaad relationship, 42–48
- Kinetic method, 173–178
and chiral recognition, 202
- Klinman's approach to kinetic complexity, 46
- Larsson's selective energy transfer model, 262–263
- Laser-induced multiphoton excitation, 160
- Laser sputtering, 158
- Li⁺-bound diol complexes, 204
- LIF spectroscopy
[F-M] complexes, 181–182*t*
and chiral recognition, 179–180, 183
- Ligands, 153
- Lipoxygenases, 68–69
reaction diagram, 54*f*
- Liquid chromatography (HPLC), 154
- Malic enzyme, 54*f*
- Mass spectrometry
carboxylic acid/amino acid complexes, 199–203

- chemical ionization, 196–197
fast atom bombardment mass spectrometry, 169–170
Fourier transform ion cyclotron resonance mass spectrometry (FTIC-MS), 172–173
of ionic clusters, 170–178
kinetic method, 173–178
quadrupole mass spectrometry, 171–172
time-of-flight mass spectrometry, 170–171
Matrix assisted laser desorption and ionization (MALDI), 168–169
mechanism for solvolysis, 20–21
solvolysis and racemization of ion pairs, 22–24
Metal-bound amino acid complexes, 206–209
Metal ions, in biological systems, 153–154
Methylamine dehydrogenase, 69–70
reaction diagram, 54*f*
Microsolvated ion, 240
spatial arrangement and chemical identities, 242
Microwave spectroscopy, 191
Molecular clusters
charge-transfer interactions, 151
in gas phase, 149–155
hydrogen bonding, 150–151
neutral clusters from supersonic beam, 157–158
non-covalent interactions, 150–158
sources, 156–157
spectroscopy, 158–160
stabilization energy, 150
structure and function, 149–150
in supramolecular systems, 152
Molecular complexes
energetics, 192–196
Monotellurides, 112*t*
Morphinone reductase, 50*t*, 57, 64–66
reaction diagram, 54*f*
Multidentate ligands, 153
NAD-malic enzyme, 52*t*, 62–63
N,N-dimethyl-2-(aminomethyl)phenyl benzylselenoxide, 103
N,N-dimethyl-2-(aminomethyl)phenyl bromotelluronium iodide, 91
N,N-dimethyl-2-(aminomethyl)phenyl iodotelluronium iodide, 91
N,N-dimethyl-2-(aminomethyl)phenyl phenyltelluride, 110
Non-covalent molecular structures
attractive interactions, 150
charge-transfer interactions, 151
dispersion interactions, 152
electrostatic interactions, 151–152
hydrogen bonding, 150–151
interactions in metal complexes, 153–154
in life sciences, 152–153
repulsive interactions, 150
structure, 149–150
in supramolecular systems, 152
Non-unit kinetic isotope effects, 28
Nucleophilic substitution
acid-induced of allylic alcohols, 247–254
in chiral ion-dipole complexes, 236–240
O-protonated 1-aryl-1-methoxyethanes
Arrhenius parameters for gas-phase dissociation, 260*t*
Arrhenius parameters for gas-phase intracomplex inversion, 259*t*
Arrhenius plot for configuration inversion, 257*f*
Arrhenius plot for dissociation, 258*f*
Oligosaccharide hosts
cyclic, 218–222
linear, 222–228
One-color resonant two photon ionization (1cR2P1), 161–164
Organochalcogen(II) compounds, 100–102
Organochalcogen(IV) compounds, 100–102
Organoselenium compounds
dehalogenation reactions, 96
electrochemical reduction, 113–117
haloperoxidase-like activity, 108–113
with odd number of ligands, 100–102
one-electron oxidation, 117–118
oxidation of thiols, 102–106
redox reactions, 79–80
thioperoxidase-like activity, 108–113
Organotellurium compounds
electrochemical reduction, 113–117, 113–117, 116*t*
haloperoxidase-like activity, 108–113
with odd number of ligands, 100–102
one-electron oxidation, 117–118
oxidation of thiols, 102–106
redox reactions, 79–80
thioperoxidase-like activity, 108–113
Pentaerythritol tetranitrate (PETN) reductase, 50*t*
Pentaerythritoltetranitrate reductase, 57
Pentafluorobenzoate, 14

- Peptidyl- α -hydroxylating monooxygenase, 67–68
Peptidylglycine α -hydroxylating monooxygenase, 49*t*
 reaction diagram, 54*f*
Phenoxypropyltelluride, 108, 109*f*
Phenyl *N,N*-dimethyl-2-(aminomethyl)phenyltelluride, 85
Phenylalanine, 152
Phenylchalcogenyl-1-naphthols, 124
 peak potentials for oxidation, 125*f*
Phenylglycine methyl ester, 231
Porphyrin, 154
Potential energy surface (PES), 148
Primary isotope effects
 temperature dependence, 48
 temperature independence, 56
Proteic hosts, 231
Protein vibrations, 28, 72–73
Proteins, secondary structure, 152–153
Proton-bound dimers of tartrates, 196–199
- Quadrupole mass spectrometry, 171–172
Quantum tunneling
 assisted by protein dynamics, 72–73
 Bell model, 33, 72
 breakthroughs in enzyme-catalyzed reactions, 42–48
 in chemical reactions, 28–29
 and conformational flexibility of thermophilic enzymes, 61–62
 and coupled motion, 38–39*t*
 diagnostic criteria, 42–48
 early indications in enzyme-catalyzed reactions, 35, 40–42
 and enthalpy of activation, 67
 environmentally modulated, 56
 Huskey's rules, 63–64
 indicators, 70–72
 and motion of C-H/D bonds, 29–30
 reactant ground-state tunneling hypothesis, 68–69
 in solution reactions, 29–35
 steric hindrance, 31–34
 unmasking by active site mutation, 58–60
 vibrational assisted, 56, 69
Quantum tunneling experimental studies, 56
 alcohol dehydrogenases, 57–62
 dihydrofolate reductases (DHFR), 48, 54–57
 glucose oxidase, 66–67
 hydrogen-atom transfer reactions, 67–69
 lipoxygenases, 68–69
 methylamine dehydrogenase, 69–70
 morphinone reductase, 57, 64–66
 NAD-malic enzyme, 62–63
 pentaerythritol tetranitrate reductase, 57
 peptidyl- α -hydroxylating monooxygenase, 67–68
 proton-transfer reactions, 69–70
 summaries, 49–53*t*
 thymidylate synthase, 57
- (*R*)-1-phenylethanol, 196*f*
R2PI spectroscopy, 160–161
R2PI-TOF spectroscopy, 191*t*
Racemization
 of chiral allylic alcohols, 247–254
 chiral α -methyl benzyl cation/methanol adducts, 254–263
 of chiral substrate during solvolysis, 12–13
 of ion pairs during solvolysis, 22–24
Radiolysis, 178
 ion-dipole complexes, 178
 and nucleophilic substitution, 238
Rate constant ratio
 and non-unit kinetic isotope effects, 28
 and Swain-Schaad relationship, 36–37
Rate constants
 amino acids with cyclodextrin and linear oligosaccharides, 227*t*
 as clock for solvolysis reaction, 3–6
 displacement reactions 30, 230*t*
 for formation of large molecular clusters, 158
 for halogen addition/reduction from diorganotellurides, 82
 in multistep enzymatic reactions, 43
 proton transfer from [cytochrome *c*] to alkylamines, 234*t*
 for reorganization of ion pairs in water, 13
 for solvolysis reactions, 2–3
 for thiolperoxidase-like activity of organoselenides, 110
Rate-limiting step
 and enthalpy of activation, 67
 and enzyme commitment, 55
Redox reactions
 for diorganochalcogen(II)/diorganochalcogen(IV) complexes, 90*f*
 halogen elimination/addition to diorganotellurides, 82
 reduction of organotellurium compounds, 113–117
REMPI spectra, 155
REMPI/TOF setup, 180*f*

- Resonance-enhanced multiphoton ionization (REMPI)
description, 160
- Resonant two photon ionization spectroscopy, 160–161
- Rice-Ramsperger-Kassel-Marcus (RRKM) simulations, 176
- Rule of geometric mean, 36
Huskey's rules for violations, 63–64
- Rydberg electron transfer (RET) spectroscopy, 166–167
- (S)-2-naphthyl-1-ethanol, 184
- Salt effect, and solvolysis reaction rate, 8
- Sarcosine oxidase, 69
reaction diagram, 54f
- Secondary isotope effect, 37
and substituent effects, 40
and Swain-Schaad relationship, 47
- Selenides
heterocyclic, 137–138
oxidation potentials, 135t
- Seleninic acids, 113
- Selenium-halogen bond strength, 81
- Selenium(IV) dihalides
crystallographic structure, 80f
- Selenoxides, 102
oxidation reactions, 106–108
in protic solvents, 103–104
in situ generated, 108
thiol oxidation mechanism, 104f
- Selenate esters, 113
- Serine
HF/6-31G structure, 211f
Na⁺ position, 212f
- Solvent effects, 148
- Solvolysis
addition of solvent to carbocation-ion pairs, 6–10
6–10
carbocations as intermediates, 1
general mechanisms of reaction, 2–3
intracomplex in (R)-(+)-1-arylethanol/CH₃¹⁸OH₂⁺, 263–266
ion pair isomerization, 12–21
leaving group inhibition, 6–7
mechanism, 254
and racemization of ion pairs, 22–24
reaction rate and bromide ion concentration, 7–9
salt effect and reaction rate, 8
study by virtual isomerization reactions, 18–19
of X-4-O(S)CPh, 14–15, 16t, 17
Soybean lipoxigenases, 52t, 68–69
- Spectroscopy. *see also* Chiral cluster spectroscopy
enantiomer discrimination, 155
of molecular clusters, 158–160
- Stationary radiolysis, 178
and nucleophilic substitution, 238
- Steric hindrance, 31–34
- Sulfonate anions, as leaving group in solvolysis, 18
- Supersonic expansion of carrier gas, 179
2-butanol, 191
- Swain-Schaad relationship, 36–37
Huskey's rules for violations, 63–64
for primary vs. secondary isotope effects, 47–48
- Tandem mass spectrometry (MS), 155
- Tartrate systems, CIMS investigation, 196–197, 198t
- Tellurides, heterocyclic, 137–138
- Tellurium-halogen bond strength, 81
- Tellurium(IV) species
addition of glutathione, 104
- Telluroxides, 102
oxidation reactions, 106–108
in protic solvents, 103–104
in situ generated, 108
thiol oxidation mechanism, 104f
- Tetra-*n*-butylammonium iodide, 93
- Thiol oxidation, 102–106
and addition of glutathione, 105t
mechanism for solvolysis, 104f
thioperoxidase-like activity of
organoselenides/tellurides, 108
- Thiolperoxidase-like activity, 108–113
- Thionobenzoates, 14
- Three point rule, 154
- Thymidylate synthase, 49t
reaction diagram, 54f
- trans*-1,2-Dibromocyclohexane, 93
- Trichalogenoethers, 136–137
- Tridentate ligands, 153
- Trifluoroethanol, 180
- Trigonal bipyramidal diaryltellurium(IV), 80f
- Trigonal bipyramidal selenium(IV) diiodides, 97
- Trimeric ion cluster dissociation, 177f
- Two-color resonant two photon ionization (2cR2P1), 164–166
- Two-electron redox reactions
diorganochalcogen (IV) dihalides, 80–91
diorganochalcogenides, 80–91

Vibration of enzymes, 72–73

Vicinal-dihalides

dehalogenation, 97–99

Vicinal-organic dihalides

dehalogenation, 91–99

Virtual isomerization reactions, 18–19

Wagner-Meerwein rearrangements, 245–247

Water

and ion complex strength, 4

as solvent in solvolysis reactions, 23–24

X-ray crystallography

Chalcogen-iodine-iodine arrays, 84

chalcogen-L₄ complexes, 88

iodotelluronium, 85

Author Index

- Abadie, C., 143
Abatjoglou, A.G., 142
Abdoul-Carime, H., 274
Abdoul-Carime, H., 271, 274
Abe, H., 274
Abe, M., 143, 144
Achiba, Y., 274
Adachi, H., 279
Adamowicz, L., 273
Adjoure, C., 271, 274
Agbaria, R.A., 269
Aggerholm, T., 278
Agnew-Heard, K.A., 269
Agrawal, N., 57, 74
Ahlberg, P., 77
Ahn, K., 77
Ahn, S., 279
Ahsan, K., 142
Aida, M., 268
Ajay, M.A.M., 268
Akaishi, R., 144
Akiyoshi, K., 268
Al-Maharik, N., 145
Al-Rabaa, A.A., 269
Al-Rabaa, A.R., 276
Albeck, M., 143
Albery, W.J., 77
Alegria, A., 142
Alhambra, C., 77
Ali, F., 268
Allemann, R.K., 56, 75
Allen, A.D., 25
Allinger, N.L., 74
Almond, M.J., 144
Amemura, A., 279
Amero, R.B., 142
Amirav, A., 272, 273
Amyes, T.L., 1, 24, 25
Andersen, U.N., 275
Anderson, D.B., 26, 281
Anderson, J.A., 269
Anderson, J.B., 271
Andersson, C., 143
Andersson, C.-M., 143, 144, 145
Andersson, C.M., 142, 143
Andres, R.P., 270
Angelini, G., 280
Antoniou, D., 75
Aoyama, H., 140
Apeloig, Y., 25
Arakawa, R., 278, 280
Arduengo, A.J., 142
Arends, I.W.C.E., 143
Ariyoshi, K., 142
Armentrout, P.B., 269, 275
Armstrong, D.R., 268
Arshadi, M., 270
Arunan, E.J., 272
Aschi, M., 280
Asmus, K.-D., 144
Asmus, K.D., 144
Aso, Y., 142
Augusti, D.V., 278
Augusti, R., 278
Auld, D.S., 268
Azuma, T., 279
Babbitt, R.J., 272
Bach, R.D., 281
Bachmann, D., 274
Back, T.G., 143
Bahatt, D., 273
Bahnsen, B.J., 58, 59, 75, 76
Bahr, U., 274
Baldwin, M.A., 277
Bale, S.J., 269
Banait, N.S., 25
Barber, M., 274
Barbour, L.J., 269
Barbu, K.L., 269
Bariak, T.M., 270
Barnham, K.J., 268
Barrios, R., 278
Barrow, C.J., 268
Barth, H.D., 267
Bartolucci, S., 60, 75
Barton, D.H.R., 140, 142
Basran, J., 57, 64, 70, 75, 76
Basu, K.A., 26, 281
Batchelor, R.J., 144
Bateman, M.A., 142, 143
Bauchert, J., 271
Bauerle, D., 271
Baumann, H., 270
Beauchamp, J.L., 278
Beavis, R.C., 274
Begley, J.A., 278
Beitz, J.V., 140
Bekefi, G., 271
Bell, R.P., 34, 74

- Bell, S.J., 281
 Bellander, M., 145
 Ben-Horin, N., 273
 Bender, B.R., 77
 Benkovic, S.J., 48, 74, 75
 Bennett, R.A., 270
 Bentley, T.W., 281
 Berg, J.M., 268
 Bergès, J., 273
 Berges, J., 276
 Bergholdt, A.B., 144
 Berglund, M., 143, 144, 145
 Berkovitch-Yellon, Z., 273
 Bernhardt, P.V., 269
 Bernier, J.-L., 143
 Bernreuther, A., 269
 Bernstein, E.R., 272, 273
 Berry, J.A., 77
 Bertran, J., 278
 Bethge, K., 270
 Beuhler, R.J., 271
 Beyreuther, K., 268
 Bibbs, J.A., 76
 Bieniarz, C., 268
 Birmingham, A., 145
 Blackburn, N.J., 67, 68, 75
 Blades, A.T., 168, 274
 Blais, N.C., 273
 Blake, G.A., 272
 Blanchard, J.S., 35, 74
 Bodrossy, L., 268
 Boesl, U., 274
 Bohe, L., 140
 Bohne, C., 269
 Bohro, N., 276
 Bojesen, G., 275, 280
 Bollinger, J.M., 140
 Bombach, R., 273
 Bondybey, V.E., 270
 Bordoli, R.S., 274
 Bosiger, J., 272
 Bosman, C., 276
 Botta, B., 280
 Botta, M., 280
 Bouillet, C.T., 280
 Bowen, C.T., 281
 Bowen, K., Jr., 267
 Bowen, K.H., 271, 272, 276
 Bowen, R.D., 280
 Bowles, R.S., 270
 Boyer, T.G., 268
 Boynton, A.W., 275
 Bradley, C., 280
 Bradshaw, J.S., 279
 Bransford, J.W., 140
 Brattsand, R., 142, 144, 145
 Brauer, B., 273
 Brauman, J.I., 238, 280
 Brauman, J.L., 275
 Braun, J.E., 273
 Breen, J.J., 271, 272
 Breen, P.J., 272
 Bréhéret, E., 276
 Breindahl, T., 275
 Brenner, V., 276
 Bright, F.V., 142, 143
 Brinich, J., 140
 Briody, R.G., 26
 Broida, H.P., 270
 Browder, J.A., 274
 Brown, M.G., 272
 Brown, R.H., Jr., 268
 Bruice, T.C., 77
 Brunner, A., 140
 Brutschy, B., 267, 273
 Bryant, D.R., 142
 Buchhold, K., 267
 Buchold, K., 267
 Buckingham, A.D., 267
 Bunnett, J.F., 25
 Bunton, C.A., 25
 Burinsky, D.J., 275
 Burkert, U., 74
 Burstall, F.H., 140
 Busarow, K.L., 272
 Busch, K.L., 274
 Bush, A.I., 268
 Butcher, R.J., 143
 Butcher, T.S., 140
 Cacace, F., 275, 280, 281
 Caldin, E.F., 29, 31, 74
 Caldwell, J.W., 269
 Calo, J.M., 270
 Calvé, J.L., 272
 Camara, E., 270, 280
 Cameron, D., 275
 Cameron, T.S., 142
 Camilleri, P., 279
 Campana, J.E., 270, 275
 Campargue, R., 270, 271
 Campos, M. de M., 140
 Canagaratna, M., 272
 Cannio, R., 60, 75
 Caratzoulas, S., 75
 Carazza, F., 278
 Carles, S., 272, 273, 274, 276
 Carrion, F., 281
 Carroll, J.A., 274
 Castleman, A.W., Jr, 270
 Castleman, A.W., Jr., 267, 269, 270, 271, 272, 273, 274
 Catone, D., 276
 Cecchi, P., 280
 Cerda, B.A., 268, 269, 275
 Cha, Y., 43, 42, 74, 75

- Chait, B.T., 274
 Chalas, J., 143
 Chan, C., 142
 Chan, I.-W., 26
 Chan, T.W.D., 279
 Chang, I.W., 281
 Chao, G.Y., 140
 Chapo, C.J., 278
 Chappell, J.S., 269
 Chaudhary, T., 274
 Che, C.T., 277
 Chen, G., 275
 Chen, J., 278
 Chen, N.Y., 277
 Chen, P., 77
 Chen, P.L., 268
 Chen, Y., 277, 278
 Chen, Y.Z., 277
 Cheng, X.H., 275
 Cheon, H.-J., 26
 Cheon, H.J., 281
 Cherny, R.A., 268
 Chin, J.K., 58, 59, 75, 76
 Chini, M., 280
 Chipot, C., 269
 Chiu, J.-J., 144
 Chmutova, G.A., 144
 Choo, B., 275
 Chow, F., 143
 Christensen, J.J., 279
 Christofferson, G.D., 140
 Christofferson, R.E., 74
 Chu, I.H., 279
 Cinquantini, A., 143
 Ciranni, G., 281
 Clara, M., 272
 Clark, R.L., 277, 278
 Claverie, O., 183, 276
 Cleland, W.W., 35, 74
 Clemmer, D.E., 280
 Clippinger, E., 25
 Coe, J.V., 271
 Cohen, R., 273
 Cohen, R.C., 272
 Colby, B.N., 274
 Colby, T.D., 58, 59, 76
 Collins, J.C., 270
 Colton, R.J., 270
 Colyer, K.E., 275
 Comisarow, M., 274
 Compton, R.N., 271
 Cook, P.F., 35, 62, 74, 75, 76
 Cooks, R.G., 275, 277, 278
 Cooper, D.E., 272
 Corchado, J., 77
 Cordero, M., 280
 Cordes, R.E., 142
 Cornett, L., 269
 Cosby, P.C., 270
 Cotgreave, I., 144
 Cotgreave, I.A., 142, 143, 144
 Courty, A., 272
 Cozens, F.L., 25
 Crabtree, R.H., 267
 Crack, P.J., 268
 Cradock, S., 144
 Craig, 176
 Craig, S.L., 275
 Craven, B.M., 268
 Creighton, D.J., 40, 74
 Crestoni, M.E., 275
 Crotti, P., 280
 Cummins, P.M., 268
 Curtain, C.C., 268
 Curtiss, L.A., 267
 Czira, G., 277
 Dale, F., 270
 Dale, J., 281
 Dalley, N.K., 279
 Dang, T.T., 277
 Dao, P.D., 272, 273, 274
 Darlington, J.A., 281
 David, G.A., 275
 Davidson, R.B., 279
 Davies, C.W., 25
 de Andrade, H., Jr., 140
 De Corpo, J.J., 270
 De Gala, S., 267
 De Koning, L.J., 280
 de Vries, M.S., 267, 273
 De Wall, S.L., 269
 de Wilde, J.C., 268
 Dearden, D., 276
 Dearden, D.V., 279
 Dejsupa, C., 279
 Delforge, D., 280
 Delle Monache, G., 280
 Demuth, H.U., 76
 Denisov, E.V., 277
 Desfrancois, C., 271, 272, 273, 274, 276
 Desfrancois, C., 276
 Desiderio, C., 269
 Desilva, K.G.K., 140
 Desiraju, G.R., 267
 Detty, M., 143
 Detty, M.R., 79, 140, 142, 143, 144
 Dewar, M.J.S., 281
 Dezi, E., 281
 Di Cera, E., 269
 Di Palma, T.M., 276
 Diamond, D., 269
 Dietze, P.E., 25
 Dimicoli, I., 272, 276
 Dirtz, T.G., 270
 Djafari, S., 267

- Dobó, A., 279
 Doe, H., 278
 Doll, K.M., 77
 Dopfer, O., 273
 Dostrovsky, I., 281
 Douay, D.L., 280
 Dougherty, D.A., 269
 Drago, R.S., 140
 Drahos, L., 176, 275
 Drake, M.D., 142, 143
 Draper, D.E., 268
 Dugger, T.L., 281
 Dunbar, R.C., 269
 Duncan, M.A., 270
 Duncan, R., 268
 Dyck, B.P., 143
 Dzygiel, P., 269
- Eachus, R.S., 144
 Ebata, T., 272
 Eberlin, M.N., 278
 Eggers, D.K., 268
 Einstein, F.W.B., 144
 Eisenman, G., 268
 Ek, B., 143
 Ekström, M., 144
 Ekstrom, M., 145
 Elliott, G.J., 274
 Elliott, N.B., 281
 Emilsson, T., 272
 Engman, L., 140, 142, 143, 144, 145
 Enomoto, M., 142
 Epperlein, U., 269
 Erata, R., 144
 Ericksson, P., 145
 Eriksen, T.E., 143, 144
 Erlansson, M., 145
 Ervin, K.M., 275
 Evans, C.A., Jr., 274
 Evans, J.P., 77
 Even, U., 272, 273
- Faehrmann, J., 271
 Fago, G., 277
 Fainberg, A.H., 25
 Fairbrother, G.L., 281
 Fales, H.M., 196, 276
 Fanali, S., 269
 Fattahova, D., 144
 Fattakhova, D.S., 143, 144
 Fehsenfeld, F.C., 270
 Fei, H., 280
 Felker, P.M., 272
 Fellers, R.P., 272
 Femec, D.A., 77
 Fenn, J.B., 270, 271
 Fenselau, C., 275
- Ferguson, E.E., 270
 Fernandes, B.C.M., 143
 Ferro, E.S., 268
 Ferry, J.G., 268
 Field, R.W., 272
 Filippi, A., 242, 276, 277, 280, 281
 Finet, J.-P., 142
 Finke, R.G., 77
 Finn, M.G., 278
 Finnemann, J.I., 25
 Fishbein, J.C., 25
 Fite, W.L., 271
 Flannary, C.A., 26
 Flannery, C.A., 281
 Fleischhauer, J., 269
 Fleming, J.C., 140
 Flesken Nikitin, A., 268
 Flynn, G.W., 140
 Fokkens, R.H., 268
 Fornarini, F., 275
 Fornarini, S., 280
 Fowler, P.W., 267
 Frade, T.M., 140
 Francavilla, C., 142, 143
 Francisco, W.A., 67, 68, 75
 Frank, F., 270
 Franz, A.H., 280
 Fraser, G.T., 272
 Fréchet, J.M.J., 143
 Fredenburg, M.E., 74
 Frederick, C.A., 268
 Frieden, C., 35, 40, 74
 Friedhoff, C.B., 271
 Friedman, A.E., 140, 142
 Friedman, L., 271
 Frisell, H., 143
 Fujihara, H., 144
 Fujimoto, M., 142
 Fujio, M., 25
 Fujioka, T., 279
 Fujiwara, Y., 277
 Fukada, K., 268
 Fuke, K., 274
 Fukuda, E.K., 275
 Fulford, J.E., 275
 Funderburk, L., 29, 30, 74
 Fung, K.H., 274
 Furukawa, M., 272
 Furukawa, N., 142, 144
 Futrell, J.H., 176, 275, 277
- Gaber, R.F., 269
 Gal, J.F., 279
 Galet, V., 143
 Gallivan, J.P., 269
 Gao, J., 77
 Garcia, C., 279
 Garcia-Viloca, M., 77

- Gasparrini, F., 281
Gavva, S.R., 76
Gay, I.D., 144
Geer, S.M., 142
Gentry, W.R., 271
Geusic, M.E., 270
Giacomello, P., 281
Giannotti, C., 142
Giardini Guidoni, A., 270, 272, 276
Giardini, A., 276, 277
Gibson, S.L., 142
Giese, C.F., 271
Giese, K., 25
Gilbert, B.C., 144
Glad, S.S., 77
Glidewell, C., 144
Glish, G.L., 274
Glucksman, M.J., 268
Goddard, W.A., III, 278
Goering, H.L., 26
Goginashvili, G.T., 277
Gokel, G.W., 269
Goldstein, B.M., 58, 59, 76
Gong, S., 280
Gonohe, N., 274
Gordon, M.S., 278
Gozzo, F.C., 278
Gozzo, F.G., 278
Grace, L., 273
Grady, T., 269
Grandinetti, F., 242, 280, 281
Grant, D.M., 279
Graul, S.T., 275
Grebner, T.L., 272, 273
Green, M.K., 270, 280
Greenblatt, J., 25
Greene, F.T., 271
Gregoire, G., 276
Grey, J., 271
Grigorean, G., 279
Gromiha, M.M., 268
Gross, M.L., 269
Grosshans, P.B., 274
Grottemeyer, J., 274
Grove, D.M., 268
Gspann, J., 271
Gu, J.-H., 144
Gubitz, G., 269
Guo, C., 142
Guo, J., 278
Gupta, C., 238, 280
Gur, E.H., 280
Guthrie, R.D., 25
Gutowski, M., 278
Gutowsky, H.S., 272
Guyot, J., 279
Gwo, D.H., 272
Habenicht, W., 273
Haberland, H., 271
Haeber, T., 276
Hagen, O.F., 270, 271
Hager, J.W., 273
Haley, N.F., 144
Hall, D.G., 238, 280
Hallberg, A., 142, 144
Hamburger, G., 140
Hamill, W.H., 275
Hamilton, C.E., 272
Hammarström, L., 144
Hammes-Schiffer, S., 75
Hanafusa, T., 270, 279
Hansen, S.G., 270
Harmata, M., 269
Harpp, D.N., 140
Harris, J.M., 25
Harris, R.J., 57, 64, 69, 75
Harris, S.J., 269
Harrison, A.G., 275
Hashimoto, K., 277
Haskins, N.J., 279
Hassett, J.W., 144
Havlas, Z., 267
Hawker, C., 143
Hawker, C.J., 143
Hayashi, M., 279
Hays, T.R., 274
Hayward, L.J., 268
He, F., 279, 280
Heck, R., 25
Heisenberg, 28
Helm, R.M., 272
Hénichart, J.-P., 143
Henke, W.E., 274
Henkes, W., 271
Henry, K.D., 274
Herbstein, F.H., 140
Herschbach, D.H., 271
Heusser, H., 140
Hewitt, J.M., 140
Hidaka, Y., 279
Higgs, D.E., 142, 143
Hillenkamp, F., 274
Hilmey, D.G., 144
Hirayama, S., 278
Hirose, K., 278, 279
Ho, C.J., 272
Ho, J., 270
Hobza, P., 267, 268, 272
Hodgeman, D.K.C., 144
Hodyss, R., 278
Hofelich, T.C., 25
Hoffmann, R., 268
Hofmann-Sievert, R., 271
Hofmeister, G., 270
Holland, P.M., 270

- Hollfelder, F., 267
 Holman, T.R., 69, 75
 Hong, B., 57, 74
 Honnegger, E., 273
 Hopkins, J.B., 270
 Horn, E., 142, 144
 Hortig, G., 270
 Hosokawa, A., 140
 Hou, Yu.Q., 140
 Houée-Levin, C., 273
 Houee-Levin, C., 276
 Houghton, D.S., 143
 Houmam, A., 144
 House, D.W., 269
 Howard, B.J., 276
 Howell, S.A., 277
 Hoyau, S., 269, 275
 Hu, C.H., 278
 Hu, N.X., 142
 Hu, P., 269
 Hua, S., 277
 Hua, S.M., 277
 Huang, R.-R.C., 143
 Huang, S.K., 25
 Huang, X., 140
 Huck, W.T.S., 268
 Hudgins, R.R., 268, 280
 Huffer, M., 269
 Hughes, E.D., 281
 Hughes, T.P., 271
 Humffray, A.A., 143
 Hungerbuehler, H., 144
 Hunter, C.A., 268
 Hunter, R.L., 278
 Huskey, W.P., 40, 42, 63 74, 76
 Huszthy, P., 279
 Hutson, J.M., 267
 Hvidt, A., 76
 Hwang, C.C., 62, 75

 Ikonomidou, M.G., 168, 274
 Imada, T., 269
 Imamura, H., 280
 Imhof, P., 267, 273
 Ingold, C.K., 281
 Inouye, M., 140
 Irico, A., 280
 Ito, M., 272, 274
 Ivkov, V., 144
 Iwaoka, M., 143
 Izatt, R.M., 279

 Jablonski, P.E., 268
 Jacobsson, K., 145
 Jagannadham, V., 24, 25
 James, T.D., 269
 Jameson, R.F., 281
 Janzen, C., 273
 Janzen, Ch., 267
 Jarrold, M.F., 268, 278, 280
 Jasperse, C.P., 143
 Jeminet, G., 279
 Jencks, W.P., 24, 25, 281
 Jensen, F., 77
 Jensen, J.H., 278
 Jiang, L., 277
 Jockusch, R.A., 269, 278
 Jocys, G., 144
 Johansen, E., 69, 75
 Johansson, U., 145
 Johnson, K.E., 272
 Johnson, P., 273
 Johnston's, H.S., 28
 Johnston, H.S., 74
 Jones, B.A., 279
 Jones, C.W., 143
 Jonkman, H.J., 270
 Jonkman, H.T., 271, 272
 Jonsson, M., 143, 144
 Jonsson, T., 66, 77
 Jørgensen, T.J.D., 280
 Jortner, J., 272, 273
 Jouikov, V., 144
 Jouikov, V.J., 144
 Jouikov, V.V., 143, 144
 Joyes, P., 270
 Julian, R.R., 278
 Jung, G., 277

 Kaatz, U., 25
 Kadoya, Y., 280
 Kafarski, P., 269
 Kahraman, M., 269
 Kaiser, H.J., 270
 Kakuda, Y., 25
 Kaldor, S.B., 74
 Kalyanaraman, C., 75
 Kalyanasundaram, S.K., 140
 Kamada, K., 278
 Kamigata, N., 142
 Kanagasabapathy, V.M., 25
 Kanda, T., 142
 Kaneda, T., 270, 278, 279
 Kantrovitz, A., 271
 Kapustin, V.K., 140
 Karas, M., 274
 Karataev, V.I., 274
 Kardos, J., 76
 Kargin, Y.M., 143, 144
 Karplus, M., 77
 Karsten et al., 63
 Karsten, W.E., 62, 75, 76
 Kataev, E.G., 143
 Kauzman, W., 268
 Kauzmann, W., 74
 Kawai, Y., 279

- Kawamura, M., 279
 Kay, B.D., 271
 Kaya, K., 274
 Kebarle, P., 168, 270, 274
 Keese, R.G., 273
 Keesee, R., 271
 Keesee, R.G., 272
 Kellersberger, K.A., 276
 Kenny, J.E., 272
 Khelifa Schermann, J.P., 271
 Khelifa, N., 274
 Kilgore, K., 271, 272
 Kilmcak, C.M., 272
 Kim, A.Y., 26, 281
 Kim, C.K., 281
 Kim, H., 277
 Kim, K., 58, 76
 Kim, S.H., 25
 Kimura, K., 274
 King, A.K., 276
 Kinnear, B., 278
 Kinsey, J.L., 272
 Kirby, A.J., 267
 Klassen, J.S., 268
 Kleinermanns, K., 267, 273
 Klemperer, W., 272
 Klinedinst, P.E., 25
 Klinman, J.P., 40, 42, 43, 58, 59, 60, 61, 66, 67, 68, 71, 74, 75, 76, 77
 Klooster, W.T., 267
 Klots, C.E., 176, 275
 Knapen, J.W.J., 268
 Knapp, M.J., 67, 75, 76, 77
 Knee, J.L., 273
 Knowles, J.R., 77
 Kobayashi, K., 144
 Koch, K.J., 278
 Kochi, J.K., 142
 Koetzle, T.F., 267
 Kohen, A., 48, 57, 60, 61, 66, 74, 75, 76, 77
 Koizumi, T., 142
 Kokesh, F.C., 25
 Kokufuta, E., 268
 Kollman, P.A., 268, 269
 Kolobov, E.A., 140
 Kolstad, J.J., 270
 Kommandeur, J., 271, 272
 Konaka, K., 268
 Kondo, A., 140
 Kondow, T., 271
 Kopecek, J., 268
 Koppenhoefer, B., 269
 Korting, J., 271
 Koslowski, A., 269
 Kostyanovsky, R.G., 277
 Kotiaho, T., 277
 Kovacevic, B., 278
 Kovacs, K.L., 268
 Kozhevnikov, A.Y., 143
 Kram, T.C., 269
 Krause, H., 273, 277
 Krause, H.J., 277
 Krishtalik, L.I., 65, 76
 Kroemer, R.T., 272
 Krohn, V.E., Jr., 270
 Kruger, T.L., 275
 Kubo, M., 269
 Kubo, Y., 269
 Kuntz, A.F., 275
 Kurz, L.C., 35, 40, 74
 Kuznetsov, A.M., 73, 77
 Kwong, K.P., 277
 Laali, K.K., 280
 Laerdahl, J.K., 280
 Laganà, A., 277
 Lahmani, F., 269, 272, 276
 Lampert, B., 278
 Langosch, H., 271
 Langridge-Smith, P.R.R., 270
 Larsson, R., 281
 Laskin, J., 176, 275
 Latini, A., 270, 272, 276
 Latypova, V.Z., 143, 144
 Lau, W., 142
 Laughlin, K.B., 272
 Le Barbu, K., 276
 Leary, J.A., 270, 277
 Lebrilla, C.B., 270, 276, 279, 280
 Lecomte, F., 274, 276
 Lederer, L., 140
 Lee, B.S., 281
 Lee, I., 281
 Lee, J.C., 267
 Lee, W.H., 268
 Lee, Y.-G., 24
 Leize-Wagner, E., 279
 Leleyter, M., 270
 Lembach, G., 273
 Lemr, K., 278
 Leonard, K.A., 142
 Leopold, D.G., 270, 271
 Leopold, K.R., 272
 Lesieur, D., 143
 Lester, H.A., 269
 Leutwyler, S., 272, 273
 Levy, D.H., 267, 272
 Lewis, E.R., 69, 75
 Lewis, E.S., 30, 74
 Ley, S.V., 142
 Li, C.J., 140
 Li, H., 277
 Li, H.Q., 277
 Li, L., 272
 Li, S., 268
 Li, X., 275

- Liang, T.M., 280
 Liang, Y., 276, 279
 Lias, S.G., 275
 Lieder, C.A., 238, 280
 Liesegang, G.W., 271
 Liftman, Y., 143
 Lin, H.C., 140
 Lin, S.-S., 24
 Lind, J., 142, 143, 144
 Linden, M., 144, 145
 Lindenbaum, A., 143
 Lindsay, D.M., 270
 Lineberger, W.C., 270, 271
 Linert, W., 281
 Lippard, S., 268
 Lippard, S.J., 268
 Lipták, M., 279
 Lisitsyn, Y.A., 144
 Liu, J., 142
 Liu, K., 272
 Liu, Q., 268
 Locke, M.J., 278
 Logan, M.E., 79
 Lombardozi, A., 281
 Lonngberg, V., 145
 Lu, W.P., 268
 Lübben, S., 277
 Lubman, D.M., 272
 Lucas, B., 276
 Luder, Ch., 271
 Luo, G., 142
 Lurie, I.S., 269
 Lusinchi, X., 140
 Luss, H.R., 142, 143
 Luss, J.R., 144
 Lutz, H.O., 271
- Ma, J.C., 269
 Ma, N.L., 269
 Ma, S.G., 275
 Macchia, F., 280
 Macchia, M., 280
 Maddox, H., 140
 Maeda, S., 269
 Maglia, G., 56, 75
 Maher, K., 269
 Maksic, Z.B., 278
 Malmström, J., 144
 Malmstrom, J., 145
 Mamyryn, B.A., 171, 274
 Mandich, M.L., 270
 Mann, D.M., 270
 Mao, C.R., 270
 Maquin, F., 276
 Marable, N.L., 274
 March, J., 281
 Märk, T.D., 271
 Mark, T.D., 273
- Markham, K.A., 74
 Marsh, R.E., 140
 Marshall, A.G., 274
 Martens, J., 277
 Martin, J.C., 142
 Martin, T.P., 270
 Mason, M.G., 144
 Massova, I., 268
 Masters, C.L., 268
 Matsuo Naemura, K., 278
 Maxtone, P.M., 272
 Mazzocchin, G.A., 143
 McAdoo, D.J., 280
 McClelland, R.A., 25
 McCombie, S.W., 140
 McCullough, J.D., 140
 McHugh, K.M., 271
 McIver, R.T., 278
 McKelvey, J.M., 142, 143, 144
 McLafferty, F.W., 274
 McLaughlin, R.P., 272
 McLuckey, S.A., 274, 275, 277
 McMahan, T.B., 269
 McMillan, M., 140
 McNaughton, M., 145
 McWhinnie, W.R., 140
 Meadows, E.S., 269
 Medina, R., 277
 Meerholz, C.A., 142
 Meisels, G.G., 275
 Meiwes-Broer, K.H., 271
 Melander, L., 34, 74
 Melendez, C.S., 281
 Meng, C.K., 271
 Merényi, G., 142, 143, 144
 Merényi, G.J., 144
 Merkt, F., 273
 Merritt, M.V., 26, 281
 Meskys, R., 69, 75
 Meyers, E.A., 140
 Michl, J., 270
 Middleton, R., 270
 Midelfort, C.F., 25
 Mihai, C., 57, 74
 Mikami, N., 272, 274
 Miller, J.C., 271
 Miller, R.L., 274
 Miller, S.M., 76, 77
 Miller, T.M., 271
 Millié, Ph., 276
 Milne, T.A., 271
 Mincer, J.S., 75
 Minoux, H., 269
 Misra, V.K., 268
 Misumi, S., 279
 Miyajima, M., 268
 Mizooku, T., 278
 Mlochowski, J., 143

- Moldéus, P., 144
Mons, M., 272, 276
Monsef-Mirzai, Z., 140
Mordy, C.W., 76
Morgan, G.T., 140
Morgan, S., 272, 273, 274
Mori, T., 25, 26
Morin, F.G., 279
Morten, D.H., 281
Morton, T.H., 238, 280
Moruzzi, J.L., 270
Moseley, J.T., 270
Motoyoshiya, J., 140
Moussa, Z., 143
Mu, Y., 142
Mugesh, G., 143
Mühlbach, J., 270
Mukundan, N.E., 26, 281
Muller, M., 270
Müller-Dethlefs, K., 272, 273
Munkelwitz, H.R., 270
Murray, C.J., 42, 43, 74, 75
Murray, K.K., 271
- Naemura, K., 278
Nagai, T., 268
Nagano, S., 268
Nakamura, R.L., 269
Nakanishi, H., 277
Nakanishi, T., 268
Nanita, S.C., 278
Nayal, M., 269
Nefedov, V.D., 140
Nefodov, V.D., 140
Nelen, M.I., 143
Nelson, D.J., 144
Neusser, H.J., 272, 273
Ng, C.Y., 273
Nibbering, N.M.M., 268, 280
Nicoll, J.B., 276
Nierengarten, H., 279
Nikolaev, E.N., 277
Nikolaeva, M.I., 277
Nilles, J.M., 276
Ninoi, T., 144
Nir, E., 267, 273
Nishida, J., 278
Nishikida, K., 143
Nold, M.J., 275
Nordlund, P., 268
Norman, K., 269
Norman, R.O.C., 144
Northrop, D.B., 76
Norton, R.S., 268
Novak, M., 24
Novick, S.E., 272
Noyce, D.S., 25
- O'Regan, M., 143
Obert, W., 270
Ogawa, Y., 268
Ogura, F., 142
Ohanessian, G., 269, 275
Okamoto, M., 278
Okamura, K., 277
Okamura, Y., 279
Okumura, Y., 270
Olah, G., 140
Olah, G.A., 140
Ondrechen, M.J., 273
Oppenheimer, N.J., 74
Ornstein, R.L., 273
Orth, R.G., 270
Oseroff, A.R., 142
Osuka, A., 140
Otsubo, T., 142
Otsuka, N., 270
Ott, M.E., 272
- Paithankar, D.Y., 270
Paladini, A., 276, 277
Palleschi, A., 270, 272, 276
Pan, H., 268
Panda, A., 143
Papazyan, A., 268
Paradisi, C., 25
Park, D.H., 58, 76
Park, S.H., 76
Park, Y.D., 267
Park, Y.S., 281
Parker, K.S., 269
Parker, W., 281
Parks, E.K., 270
Patil, A.N., 270
Patrick, J.S., 277
Paul, J.B., 278
Paul, W., 171, 274
Pauling, L., 142
Paulson, J.F., 270
Pauly, H., 271
Peake, S.L., 143
Pedersen, S.F., 277
Pelcman, M., 142
Pena, M.S., 269
Penn, S.G., 270, 280
Peppas, N.A., 268
Peris, E., 267
Perkins, S.W., 142
Persson, J., 142, 143, 144, 145
Peteanu, L.A., 267
Petersen, R.L., 144
Peterson, J.R., 270
Peterson, K.I., 269, 270
Petraghani, N., 97, 140
Petsko, G.A., 76
Pfau, P., 270

- Pfeiffer, B., 143
 Pfund, A.H., 270
 Phelps, A.V., 270
 Philips, L.A., 267
 Phillips, J.A., 272
 Piccirillo, S., 270, 272, 276
 Pichierri, F., 268
 Pierini, M., 276
 Pinto, B.M., 144
 Pirkle, W.H., 269
 Pitts, J.D., 273
 Piuze, F., 272, 276
 Pizzabocca, A., 280, 281
 Plapp, B.V., 58, 76
 Plattner, P.A., 140
 Plützer, C., 267
 Pobo, L.G., 270
 Pócsfalvi, G., 279
 Pope, R.M., 279
 Postnikova, M., 144
 Postnikova, M.Y., 143
 Pottel, R., 25
 Poutsma, J.C., 275
 Powell, M.F., 77
 Powers, D.E., 270
 Powis, G., 142, 145
 Pribble, R.N., 272
 Price, W.D., 269
 Prins, L.J., 268
 Procter, D.J., 142
 Provencal, R.A., 278
 Pulu, A.C., 270
 Punekar, N.S., 143

 Raber, D.J., 25
 Ragsdale, S.W., 268
 Rak, J., 278
 Rakov, V.S., 277
 Ramasamy, K., 140
 Ramirez, J., 279, 280
 Ramsey, N.F., 271
 Rappoport, Z., 25
 Raqabah, A., 144
 Ravi Rajagopalan, P.T., 74
 Rayner, C.M., 142
 Ready, J.F., 271
 Recknagel, E., 270
 Reed, A., 267
 Reents, W.D., Jr., 270
 Reglinski, J., 268
 Reich, H.J., 143
 Reinhoudt, D.N., 268
 Reinmann, B., 267
 Reiser, G., 273
 Reitberger, T., 144, 145
 Remacle, J., 280
 Ren, X., 142
 Renard, P., 143

 Renaud de la Faverie, J.-F., 143
 Renzi, G., 280, 281
 Rheingold, A.L., 267
 Rice, D.A., 144
 Rice, D.J., 24
 Richard, J.P., 1, 24, 25, 26
 Richardson, T.B., 267
 Rickert, K., 77
 Rickert, K.W., 68, 75
 Riedel, E., 272
 Riley, S.J., 270
 Ritchie, C.D., 25
 Rizzo, T.R., 267
 Roberts, J.L., 268
 Robertson, E.G., 267, 272
 Robinson, G.C., 25
 Rochette, L., 143
 Rodgers, J., 77
 Rodgers, M.T., 269
 Rodriguez, J.A., 268
 Rodriguez-Santiago, L., 278
 Roe, J.A., 268
 Roehm, P.C., 268
 Roepstorff, P., 280
 Romesberg, F.E., 27
 Rose, I.A., 25
 Roselli, G., 242, 280
 Rosenzweig, A.C., 268
 Roth, K., 278
 Rothenberg, M.E., 25
 Rudzinska, E., 269
 Rundle, R.E., 140
 Ryali, S.B., 270
 Ryzhov, V., 269

 Saeki, Y., 25
 Saenger, W., 268
 Sakamoto, A., 142
 Sakoda, S., 268
 Sanchez, M.L., 77
 Sandanayake, K., 269
 Sanders, R.A., 271
 Sandrock, G., 26
 Sanzone, G., 274
 Sarai, A., 268
 Sarbash, A.N., 140
 Sato, K., 274
 Sato, S., 144
 Satoh, M., 268
 Satta, M., 276
 Sattler, K., 270
 Saunders, M.R., 279
 Saunders, W. H., 34
 Saunders, W.H., 47, 74
 Sawada, M., 270, 276, 278, 279, 280
 Saykally, R.J., 272, 278
 Scarborough, J., 270
 Schaefer, H.F., 278

- Schaeffer, M.W., 272
 Schalley, C.A., 276
 Schanen, P., 273
 Schauer, M., 273
 Scheiner, S., 267
 Schelling, F.J., 269
 Schermann, J.P., 272, 273, 274, 276
 Scherzer, W., 272
 Schilling, P., 140
 Schindler, H.G., 271
 Schlag, E.W., 267, 268, 272, 273, 274
 Schleyer, P.V.R., 25
 Schleyer, P.v.R., 281
 Schlosser, G., 278
 Schmuttenmaer, C.A., 272
 Schnier, P.D., 268
 Schnute, M.E., 275
 Schowen, R.L., 27, 40, 42, 74, 76, 77
 Schreier, P., 269
 Schuette, J.M., 269
 Schulze, W., 270
 Schumacher, A., 25
 Schwarting, W., 277
 Schwartz, P.L., 281
 Schwartz, S.D., 75
 Schweikert, W.W., 140
 Schwiarskott, M., 269
 Schwotzer, W., 140
 Scrutton, N.S., 57, 64, 69, 70, 75, 76
 Scuderi, D., 276, 277
 Sealey, K., 268
 Searles, S.K., 270
 Sedgewick, R.D., 274
 Seeber, R., 143
 Seeman, J.I., 272
 Segre, H., 140
 Sellier, N.M., 280
 Selzle, H.L., 267, 268, 272, 274
 Seymour, S.L., 66, 71, 75
 Shalev, E., 273
 Shammugan, P., 140
 Shamsi, S.A., 269
 Shanks, D., 145
 Shantikarn, S., 280
 Sharfin, W., 272
 Sheldon, R.A., 143
 Shen, J., 142
 Shen, M.Z., 278
 Shen, W., 277
 Shen, X., 144
 Sheng, S.Y., 275
 Shimizu, A., 268
 Shimizu, T., 142
 Shinkai, S., 269
 Shiro, M., 279
 Shizuma, M., 270, 279, 280
 Shmikk, D.V., 274
 Shoen, A.E., 275
 Shuguang, M., 275
 Shustryakov, V., 277
 Sickman, H.R., 271
 Siegbahn, P.E.M., 267
 Siegel, M.W., 271
 Sikorski, R.S., 74
 Silvermann, S.K., 269
 Simons, D.S., 274
 Simons, J., 278
 Simons, J.P., 267, 272, 273
 Simpson, W.T., 274
 Singh, B.J., 140
 Singh, H.B., 143
 Singh, J., 268
 Singh, M., 140
 Sinotova, E.N., 140
 Siu, F.M., 269
 Siuzdak, G., 278
 Sjödin, M., 144
 Skurski, P., 278
 Smalley, R.E., 270, 272
 Smith, D.M.A., 273
 Smith, E.V., 281
 Smith, M.A., 273
 Smyth, M.R., 269
 Snodgrass, J.T., 271
 Snoek, L.C., 272
 So, M.P., 279
 Sodupe, M., 278
 Softley, T.P., 273
 Sohmiya, H., 280
 Solo, A.J., 140
 Solomon, E.I., 77
 Sorensen, C., 269
 Soukara, S., 273
 Sparapani, C., 280
 Spector, A., 143
 Speranza, 255
 Speranza, M., 242, 270, 272, 275, 276, 277, 280, 281
 Spicer, M.D., 268
 Spirko, V., 267
 Splitter, J.S., 277
 Squires, R.R., 275
 Srivastava, R.C., 140
 Srivastava, T.N., 140
 Stahl, D., 276
 Steenken, S., 25
 Stein, G.D., 270
 Steiner, T., 267
 Steinwedel, H., 171, 274
 Stenberg, B., 145
 Stephan, K., 271
 Stern, D., 142, 143
 Stern, O., 271
 Stevens, I.W., 24
 Steyert, D.W., 272
 Stülts, C.E., 144

- Stone, M., 279
 Stone, M.M., 280
 Strittmatter, E.F., 268
 Suhm, M.A., 276
 Sukumaran, D.K., 144
 Sumida, Y., 277
 Suranyi, E.L., 140
 Sussmuth, R., 277
 Sutcliffe, M.J., 57, 64, 69, 70, 75, 76
 Sutin, N., 140
 Suzuki, H., 140
 Suzuki, T., 272
 Svensjö, E., 145
 Svingor, A., 76
 Symons, M.C.R., 144
 Syper, L., 143
- Ta-Shma, R., 25
 Tabet, J.C., 280
 Tabet, J.C.E., 280
 Tafi, A., 280
 Taka, H., 142
 Takaguchi, Y., 140, 142
 Takahara, P.M., 268
 Takahashi, O., 144
 Takahashi, S., 279, 280
 Takai, Y., 278, 279, 280
 Takats, Z., 278
 Takeda, T., 279, 280
 Takeuchi, M., 269
 Takeuchi, S., 278
 Tal'rose, V.L., 277
 Talbot, F.O., 273
 Tanaka, J., 279
 Tanaka, T., 142, 278, 279
 Tang, I.N., 270, 271
 Tao, W.A., 277, 278
 Tawfik, D.S., 267
 Taylor, D.R., 269
 Taylor, L.C.E., 280
 Tee, O.S., 25
 Ten Brink, G.J., 143
 Terada, S., 277
 Tesche, B., 270
 Thibblin, A., 281, 77
 Thomas, M., 142
 Thomas, P.D., 277
 Thomas, W.A., 274
 Thomé, C., 140
 Thornton, J.M., 268
 Thornton-Pett, M., 142
 Tian, G., 77
 Tidwell, T.T., 25
 Timofev, S.A., 140
 Tiwari, A., 268
 Tobe, Y., 278
 Tobien, T., 144
 Tohyama, C., 268
- Toja, D., 270, 272, 276
 Tokita, S., 269
 Tomoda, S., 143
 Tonnies, J.P., 271
 Topp, M.R., 272
 Tor, Y., 268
 Toteva, M.M., 1, 24, 26
 Townshend, A., 269
 Troiani, A., 276, 280, 281
 Trott, W.M., 273
 Truhlar, D.G., 77
 Tsai, S., 60, 75
 Tsang, C.W., 269
 Tse, B.N., 142
 Tsuji, Y., 1, 25, 26
 Tsukube, H., 280
 Tsuno, Y., 25
 Tullai, J.W., 268
 Turner, D.H., 140
 Tyler, A.N., 274
 Tzalis, D., 268
 Tzeng, W.B., 272
- Uchiyama, T., 279
 Ueno, K., 278
 Ueno, Y., 144
 Uggerud, E., 280
 Ulstrup, J., 73, 77
 Upschulte, B.I., 269
 Urban, J., 270, 277
- Vaisar, T., 277
 Vaishampayan, A., 26, 281
 Valentine, J.S., 268
 Vallee, B.L., 268
 Van Berkel, G.J., 274
 van der Made, A.W., 268
 Van Doren, J.M., 271
 Van Dorsseleer, A., 279
 van Koten, G., 268
 van Leeuwen, P.W.W.N.M., 268
 van Veggel, F.C.J.M., 268
 Van Vliet, M.C.A., 143
 Ve'key, K., 176
 Veenstra, B.R., 271
 Vékey, K., 275, 277, 279
 Vekey, K., 278
 Vessman, K., 143, 144, 145
 Viant, M.R., 272
 Villa, J., 77
 Vincenti, M., 280
 Virgilio, J.A., 25
 Vis, J.-M., 143
 Vis, M.J., 143
 Volitakis, I., 268
 Vontor, T., 24

- Walden, P., 280
Wallace, S.C., 273
Wallevik, K., 76
Walter, K., 274
Walters, E.A., 273
Wan, T.S.M., 277, 279
Wang, B.C., 268
Wang, F., 275, 277, 278
Wang, J.R., 144
Wang, J.T., 144
Wang, L., 74
Warner, I.M., 269
Warren, J.A., 272
Warshel, A., 268
Watt, C.I.F., 281
Watts, H., 140
Wayner, D.D.M., 144
Weber, Th., 272
Wedemiotis, C., 275
Wei, S., 272
Weinhold, F., 267
Weinkauff, R., 273
Welch, C.J., 269
Welham, K.J., 277
Welsh, K.M., 40, 74
Wernberg, A.A., 144
Wesdemiotis, C., 268, 269, 275, 280
Wesdemiotis, C.J., 275
Wessel, J.E., 272
Westerman, P.W., 140
Wexler, S., 270
Wharton, L., 272
Whiteford, R.A., 144
Wieczorek, P., 269
Wieslander, E., 145
Wijkens, P., 268
Will, A.Y., 269
William, P.D., 278
Williams, A.J., 140
Williams, D.H., 280
Williams, E.R., 268, 269, 274, 278
Williams, F., 143, 144
Williams, K.B., 24
Williams, R.R., Jr., 275
Wilson, S.R., 143
Winkler, F.J., 276, 277
Winkler, J., 277
Winstein, S., 25
Winter, B., 270
Wittmeyer, S.A., 272
Wojciechowski, A.L., 142
Wolber, G.J., 281
Wong, P., 275
Wong, P.S.H., 275, 277
Worsnop, D.R., 271
Wouters, J., 269
Wright, G.J., 196, 276
Wright, J.R., 270
Wright, L.G., 275
Wright, T.G., 273
Wu, J., 278
Wu, L., 277, 278
Wu, T.J., 268
Wu, Z.C., 275
Xu, S., 276
Xue, S., 277
Xue, Y., 142
Yamada, H., 270, 278, 279, 280
Yamaguchi, H., 142
Yamaguchi, K., 144
Yamaoka, H., 279
Yamda, S., 140
Yamdagni, R., 270
Yang, D., 273
Yang, H., 269
Yang, H.J., 277
Yao, Z.P., 277
Yates, C.A., 144
Yatsugi, K., 25
Yatsugi, K.-I., 25
Yens, D.A., 26, 281
Yoda, S., 269
Yokoyama, M., 144
Yokozeki, A., 270
Yoshiuchi, H., 274
You, Y., 142, 143
Zagulin, B.A., 274
Zanello, P., 143
Zavodszky, P., 76
Zehnacker, A., 272, 276
Zehnacker-Rentien, A., 276
Zenacker-Rentien, A., 269
Zenacker-Retien, A., 269
Zhang, D., 277, 278
Zhang, J., 142
Zhang, K., 142
Zhao, F.Z., 277
Zhao, Y.F., 278
Zheng, J., 142
Zheng, L., 268
Zheng, Y.J., 273
Zhong, M., 275
Zhou, F., 140, 142
Zhou, X.-M., 144
Zhu, C.J., 278
Zhu, L., 273
Zhuikov, V.V., 143, 144
Zolla, A., 270
Zuccaro, D.E., 140
Zucker, P.A., 143
Zwier, T.S., 272

Cumulative Index of Authors

- Abboud, J.-L.M., **37**, 57
 Ahlberg, P., **19**, 223
 Albery, W.J., **16**, 87; **28**, 139
 Alden, J.A., **32**, 1
 Alkorta, I., **37**, 57
 Allinger, N.I., **13**, 1
 Amyes, T.L., **35**, 67; **39**, 1
 Anbar, M., 7, 115
 Arnett, E.M., **13**, 83; **28**, 45
 Ballester, M., **25**, 267
 Bard, A.J., **13**, 155
 Baumgarten, M., **28**, 1
 Beer, P.D., **31**, 1
 Bell, R.P., **4**, 1
 Bennett, J.E., **8**, 1
 Bentley, T.W., **8**, 151; **14**, 1
 Berg, U., **25**, 1
 Berger, S., **16**, 239
 Bernasconi, C.F., **27**, 119;
37, 137
 Berti, P.J., **37**, 239
 Bethell, D., 7, 153; **10**, 53
 Blackburn, G.M., **31**, 249
 Blandamer, M.J., **14**, 203
 Bond, A.M., **32**, 1
 Bowden, K., **28**, 171
 Brand, J.C.D., 1, 365
 Brändström, A., **15**, 267
 Brinkman, M.R., **10**, 53
 Brown, H.C., 1, 35
 Buncel, E., **14**, 133
 Bunton, C.A., **21**, 213
 Cabell-Whiting, P.W., **10**, 129
 Cacace, F., **8**, 79
 Capon, B., **21**, 37
 Carter, R.E., **10**, 1
 Chen, Z., **31**, 1
 Collins, C.J., **2**, 1
 Compton, R.G., **32**, 1
 Cornelisse, J., **11**, 225
 Cox, R.A., **35**, 1
 Crampton, M.R., 7, 211
 Datta, A., **31**, 249
 Dávalos, J.Z., **37**, 57
 Davidson, R.S., **19**, 1; **20**, 191
 de Gunst, G.P., **11**, 225
 de Jong, F., **17**, 279
 Denham, H., **31**, 249
 Desvergne, J.P., **15**, 63
 Detty, M.R., **39**, 79
 Dosunmu, M.I., **21**, 37
 Drechsler, U., **37**, 315
 Ebersson, K., **12**, 1; **18**, 79;
31, 91
 Ebersson, L., **36**, 59
 Ekland, J.C., **32**, 1
 Emsley, J., **26**, 255
 Engdahl, C., **19**, 223
 Farnum, D.G., **11**, 123
 Fendler, E.J., **8**, 271
 Fendler, J.H., **8**, 271; **13**, 279
 Ferguson, G., 1, 203
 Fields, E.K., **6**, 1
 Fife, T.H., **11**, 1
 Fleischmann, M., **10**, 155
 Frey, H.M., **4**, 147
 Fujio, M., **32**, 267
 Gale, P.A., **31**, 1
 Gao, J., **38**, 161
 Garcia-Viloca, M., **38**, 161
 Gilbert, B.C., **5**, 53
 Gillespie, R.J., **9**, 1
 Gold, V., 7, 259
 Goodin, J.W., **20**, 191
 Gould, I.R., **20**, 1
 Greenwood, H.H., **4**, 73
 Gritsan, N.P., **36**, 255
 Hammerich, O., **20**, 55
 Harvey, N.G., **28**, 45
 Hasegawa, M., **30**, 117
 Havinga, E., **11**, 225
 Henderson, R.A., **23**, 1
 Henderson, S., **23**, 1
 Hibbert, F., **22**, 113; **26**, 255
 Hine, J., **15**, 1
 Hogen-Esch, T.E., **15**, 153
 Hogeveen, H., **10**, 29, 129
 Huber, W., **28**, 1
 Ireland, J.F., **12**, 131
 Iwamura, H., **26**, 179
 Johnson, S.L., 5, 237
 Johnstone, R.A.W., **8**, 151
 Jonsäll, G., **19**, 223
 José, S.M., **21**, 197
 Kemp, G., **20**, 191
 Kice, J.L., **17**, 65
 Kirby, A.J., **17**, 183; **29**, 87
 Kitagawa, T., **30**, 173
 Kluger, R.H., **25**, 99
 Kochi, J.K., **29**, 185; **35**, 193
 Kohnstam, G., **5**, 121
 Korolev, V.A., **30**, 1
 Korth, H.-G., **26**, 131
 Kramer, G.M., **11**, 177
 Kreevoy, M.M., **6**, 63;
16, 87
 Kunitake, T., **17**, 435
 Kurtz, H.A., **29**, 273
 Le Fèvre, R.J.W., **3**, 1
 Ledwith, A., **13**, 155
 Lee, I., **27**, 57
 Lee, J.K., **38**, 183
 Liler, M., **11**, 267
 Lin, S.-S., **35**, 67
 Lodder, G., **37**, 1
 Logan, M.E., **39**, 79
 Long, F.A., 1, 1
 Lüning, U., **30**, 63
 Maccoll, A., **3**, 91
 McWeeny, R., **4**, 73
 Mandolini, L., **22**, 1
 Maran, F., **36**, 85
 Matsson, O., **31**, 143
 Melander, L., **10**, 1
 Mile, B., **8**, 1
 Miller, S.I., **6**, 185
 Mo, Y., **38**, 161
 Modena, G., **9**, 185
 More O'Ferrall, R.A., **5**, 331
 Morsi, S.E., **15**, 63
 Müllen, K., **28**, 1
 Müller, P., **37**, 57
 Nefedov, O.M., **30**, 1
 Neta, P., **12**, 223
 Nibbering, N.M.M., **24**, 1
 Norman, R.O.C., **5**, 33
 Novak, M., **36**, 167
 Huber, W., **28**, 1
 Nyberg, K., **12**, 1
 O'Donoghue, A.M.C., **35**, 67
 Okamoto, K., **30**, 173
 Okuyama, T., **37**, 1
 Olah, G.A., **4**, 305
 Oxgaard, J., **38**, 87
 Paddon-Row, M.N., **38**, 1
 Page, M.I., **23**, 165
 Parker, A.J., **5**, 173
 Parker, V.D., **19**, 131;
20, 55
 Peel, T.E., **9**, 1
 Perkampus, H.H., **4**, 195

- Perkins, M.J., **17**, 1
Pittman, C.U, Jr., **4**, 305
Platz, M.S., **36**, 255
Pletcher, D., **10**, 155
Poulsen, T.D., **38**, 161
Pross, A., **14**, 69; **21**, 99
Quintanilla, E., **37**, 57
Rajagopal, S., **36**, 167
Ramirez, F., **9**, 25
Rappoport, Z., **7**, 1; **27**, 239
Rathore, R., **35**, 193
Reeves, L.W., **3**, 187
Reinhoudt, D.N., **17**, 279
Richard, J.P., **35**, 67; **39**, 1
Ridd, J.H., **16**, 1
Riveros, J.M., **21**, 197
Robertson, J.M., **1**, 203
Romesberg, F.E., **39**, 27
Rose, P.L., **28**, 45
Rosenthal, S.N., **13**, 279
Rotello, V.M., **37**, 315
Ruisse, M.-F., **28**, 207
Russell, G.A., **23**, 271
Saettel, N.J., **38**, 87
Samuel, D., **3**, 123
Sanchez, M. de N. de M.,
21, 37
Sandström, J., **25**, 1
Savéant, J.-M., **26**, 1;
35, 117
Savelli, G., **22**, 213
Schaleger, L.L., **1**, 1
Scheraga, H.A., **6**, 103
Schleyer, P. von R., **14**, 1
Schmidt, S.P., **18**, 187
Schowen, R.L., **39**, 27
Schuster, G.B., **18**, 187;
22, 311
Scorrano, G., **13**, 83
Shatenshtein, A.I., **1**, 156
Shine, H.J., **13**, 155
Shinkai, S., **17**, 435
Siehl, H.-U., **23**, 63
Silver, B.L., **3**, 123
Simonyi, M., **9**, 127
Sinnott, M.L., **24**, 113
Speranza, M., **39**, 147
Stock, L.M., **1**, 35
Strassner, T., **38**, 131
Sugawara, T., **32**, 219
Sustmann, R., **26**, 131
Symons, M.C.R., **1**, 284
Takashima, K., **21**, 197
Takasu, I., **32**, 219
Takeuchi, K., **30**, 173
Tanaka, K.S.E., **37**, 239
Tantillo, D.J., **38**, 183
Ta-Shma, R., **27**, 239
Tedder, J.M., **16**, 51
Tee, O.S., **29**, 1
Thatcher, G.R.J., **25**, 99
Thomas, A., **8**, 1
Thomas, J.M., **15**, 63
Tidwell, T.T., **36**, 1
Tonellato, U., **9**, 185
Toteva, M.M., **35**, 67; **39**, 1
Toullec, J., **18**, 1
Tsuji, Y., **35**, 67; **39**, 1
Tsuno, Y., **32**, 267
Tüdös, F., **9**, 127
Turner, D.W., **4**, 31
Turro, N.J., **20**, 1
Ugi, I., **9**, 25
Walton, J.C., **16**, 51
Ward, B., **8**, 1
Watt, C.I.F., **24**, 57
Wayner, D.D.M., **36**, 85
Wentworth, P., **31**, 249
Westaway, K.C., **31**, 143
Westheimer, F.H., **21**, 1
Whalley, E., **2**, 93
Wiest, O., **38**, 87
Williams, A., **27**, 1
Williams, D.L.H., **19**, 381
Williams, J.M., Jr., **6**, 63
Williams, J.O., **16**, 159
Williams, K.B., **35**, 67
Williams, R.V., **29**, 273
Williamson, D.G., **1**, 365
Wilson, H., **14**, 133
Wolf, A.P., **2**, 201
Wolff, J.J., **32**, 121
Workentin, M.S., **36**, 85
Wortmann, R., **32**, 121
Wyatt, P.A.H., **12**, 131
Zimmt, M.B., **20**, 1
Zipse, H., **38**, 111
Zollinger, H., **2**, 163
Zuman, P., **5**, 1

Cumulative Index of Titles

- Abstraction, hydrogen atom, from O—H bonds, **9**, 127
Acid–base behaviour macrocycles and other concave structures, **30**, 63
Acid–base properties of electronically excited states of organic molecules, **12**, 131
Acid solutions, strong, spectroscopic observation of alkylcarbonium ions in, **4**, 305
Acids, reactions of aliphatic diazo compounds with, **5**, 331
Acids, strong aqueous, protonation and solvation in, **13**, 83
Acids and bases, oxygen and nitrogen in aqueous solution, mechanisms of proton transfer between, **22**, 113
Activation, entropies of, and mechanisms of reactions in solution, **1**, 1
Activation, heat capacities of, and their uses in mechanistic studies, **5**, 121
Activation, volumes of, use for determining reaction mechanisms, **2**, 93
Addition reactions, gas-phase radical directive effects in, **16**, 51
Aliphatic diazo compounds, reactions with acids, **5**, 331
Alkene oxidation reactions by metal-oxo compounds, **38**, 131
Alkyl and analogous groups, static and dynamic stereochemistry of, **25**, 1
Alkylcarbonium ions, spectroscopic observation in strong acid solutions, **4**, 305
Ambident conjugated systems, alternative protonation sites in, **11**, 267
Ammonia liquid, isotope exchange reactions of organic compounds in, **1**, 156
Anions, organic, gas-phase reactions of, **24**, 1
Antibiotics, β -lactam, the mechanisms of reactions of, **23**, 165
Aqueous mixtures, kinetics of organic reactions in water and, **14**, 203
Aromatic photosubstitution, nucleophilic, **11**, 225
Aromatic substitution, a quantitative treatment of directive effects in, **1**, 35
Aromatic substitution reactions, hydrogen isotope effects in, **2**, 163
Aromatic systems, planar and non-planar, **1**, 203
N-Arylnitrenium ions, **36**, 167
Aryl halides and related compounds, photochemistry of, **20**, 191
Arynes, mechanisms of formation and reactions at high temperatures, **6**, 1
A-S_E2 reactions, developments in the study of, **6**, 63
- Base catalysis, general, of ester hydrolysis and related reactions, **5**, 237
Basicity of unsaturated compounds, **4**, 195
Bimolecular substitution reactions in protic and dipolar aprotic solvents, **5**, 173
Bond breaking, **35**, 117
Bond formation, **35**, 117
Bromination, electrophilic, of carbon–carbon double bonds: structure, solvent and mechanisms, **28**, 207
- ¹³C NMR spectroscopy in macromolecular systems of biochemical interest, **13**, 279
Captodative effect, the, **26**, 131
Carbanion reactions, ion-pairing effects in, **15**, 153
Carbene chemistry, structure and mechanism in, **7**, 163
Carbenes having aryl substituents, structure and reactivity of, **22**, 311
Carbocation rearrangements, degenerate, **19**, 223
Carbocationic systems, the Yukawa–Tsuno relationship in, **32**, 267
Carbocations, partitioning between addition of nucleophiles and deprotonation, **35**, 67
Carbocations, thermodynamic stabilities of, **37**, 57
Carbon atoms, energetic, reactions with organic compounds, **3**, 201
Carbon monoxide, reactivity of carbonium ions towards, **10**, 29
Carbonium ions, gaseous, from the decay of tritiated molecules, **8**, 79

- Carbonium ions, photochemistry of, **10**, 129
Carbonium ions, reactivity towards carbon monoxide, **10**, 29
Carbonium ions (alkyl), spectroscopic observation in strong acid solutions, **4**, 305
Carbonyl compounds, reversible hydration of, **4**, 1
Carbonyl compounds, simple, enolisation and related reactions of, **18**, 1
Carboxylic acids, tetrahedral intermediates derived from, spectroscopic detection and investigation of their properties, **21**, 37
Catalysis, by micelles, membranes and other aqueous aggregates as models of enzyme action, **17**, 435
Catalysis, enzymatic, physical organic model systems and the problem of, **11**, 1
Catalysis, general base and nucleophilic, of ester hydrolysis and related reactions, **5**, 237
Catalysis, micellar, in organic reactions; kinetic and mechanistic implications, **8**, 271
Catalysis, phase-transfer by quaternary ammonium salts, **15**, 267
Catalytic antibodies, **31**, 249
Cation radicals, in solution, formation, properties and reactions of, **13**, 155
Cation radicals, organic, in solution, and mechanisms of reactions of, **20**, 55
Cations, vinyl, **9**, 135
Chain molecules, intramolecular reactions of, **22**, 1
Chain processes, free radical, in aliphatic systems involving an electron transfer reaction, **23**, 271
Charge density-NMR chemical shift correlation in organic ions, **11**, 125
Charge distribution and charge separation in radical rearrangement reactions, **38**, 111
Chemically induced dynamic nuclear spin polarization and its applications, **10**, 53
Chemiluminescence of organic compounds, **18**, 187
Chiral clusters in the gas phase, **39**, 147
Chirality and molecular recognition in monolayers at the air–water interface, **28**, 45
CIDNP and its applications, **10**, 53
Computational studies of alkene oxidation reactions by metal-oxo compounds, **38**, 131
Computational studies on the mechanism of orotidine monophosphate decarboxylase, **38**, 183
Conduction, electrical, in organic solids, **16**, 159
Configuration mixing model: a general approach to organic reactivity, **21**, 99
Conformations of polypeptides, calculations of, **6**, 103
Conjugated molecules, reactivity indices, in, **4**, 73
Cross-interaction constants and transition-state structure in solution, **27**, 57
Crown-ether complexes, stability and reactivity of, **17**, 279
Crystallographic approaches to transition state structures, **29**, 87
Cyclodextrins and other catalysts, the stabilization of transition states by, **29**, 1
- D₂O—H₂O mixtures, protolytic processes in, **7**, 259
Degenerate carbocation rearrangements, **19**, 223
Deuterium kinetic isotope effects, secondary, and transition state structure, **31**, 143
Diazo compounds, aliphatic, reactions with acids, **5**, 331
Diffusion control and pre-association in nitrosation, nitration, and halogenation, **16**, 1
Dimethyl sulphoxide, physical organic chemistry of reactions, in, **14**, 133
Diolefin crystals, photodimerization and photopolymerization of, **30**, 117
Dipolar aprotic and protic solvents, rates of bimolecular substitution reactions in, **5**, 173
Directive effects, in aromatic substitution, a quantitative treatment of, **1**, 35
Directive effects, in gas-phase radical addition reactions, **16**, 51
Discovery of mechanisms of enzyme action 1947–1963, **21**, 1
Displacement reactions, gas-phase nucleophilic, **21**, 197
Donor/acceptor organizations, **35**, 193
Double bonds, carbon–carbon, electrophilic bromination of: structure, solvent and mechanism, **28**, 171
Dynamics for the reactions of ion pair intermediates of solvolysis, **39**, 1
- Effective charge and transition-state structure in solution, **27**, 1
Effective molarities of intramolecular reactions, **17**, 183
Electrical conduction in organic solids, **16**, 159
Electrochemical methods, study of reactive intermediates by, **19**, 131

- Electrochemical recognition of charged and neutral guest species by redox-active receptor molecules, **31**, 1
- Electrochemistry, organic, structure and mechanism in, **12**, 1
- Electrode processes, physical parameters for the control of, **10**, 155
- Electron donor–acceptor complexes, electron transfer in the thermal and photochemical activation of, in organic and organometallic reactions, **29**, 185
- Electron spin resonance, identification of organic free radicals, **1**, 284
- Electron spin resonance, studies of short-lived organic radicals, **5**, 23
- Electron storage and transfer in organic redox systems with multiple electrophores, **28**, 1
- Electron transfer, **35**, 117
- Electron transfer, in thermal and photochemical activation of electron donor-acceptor complexes in organic and organometallic reactions, **29**, 185
- Electron transfer, long range and orbital interactions, **38**, 1
- Electron-transfer, single, and nucleophilic substitution, **26**, 1
- Electron-transfer, spin trapping and, **31**, 91
- Electron-transfer paradigm for organic reactivity, **35**, 193
- Electron-transfer reaction, free radical chain processes in aliphatic systems involving an, **23**, 271
- Electron-transfer reactions, in organic chemistry, **18**, 79
- Electronically excited molecules, structure of, **1**, 365
- Electronically excited states of organic molecules, acid-base properties of, **12**, 131
- Energetic tritium and carbon atoms, reactions of, with organic compounds, **2**, 201
- Enolisation of simple carbonyl compounds and related reactions, **18**, 1
- Entropies of activation and mechanisms of reactions in solution, **1**, 1
- Enzymatic catalysis, physical organic model systems and the problem of, **11**, 1
- Enzyme action, catalysis of micelles, membranes and other aqueous aggregates as models of, **17**, 435
- Enzyme action, discovery of the mechanisms of, 1947–1963, **21**, 1
- Equilibrating systems, isotope effects in NMR spectra of, **23**, 63
- Equilibrium constants, NMR measurements of, as a function of temperature, **3**, 187
- Ester hydrolysis, general base and nucleophilic catalysis, **5**, 237
- Ester hydrolysis, neighbouring group participation by carbonyl groups in, **28**, 171
- Excess acidities, **35**, 1
- Exchange reactions, hydrogen isotope, of organic compounds in liquid ammonia, **1**, 156
- Exchange reactions, oxygen isotope, of organic compounds, **2**, 123
- Excited complexes, chemistry of, **19**, 1
- Excited molecular, structure of electronically, **3**, 365
- Fischer carbene complexes, **37**, 137
- Force-field methods, calculation of molecular structure and energy by, **13**, 1
- Free radical chain processes in aliphatic systems involving an electron-transfer reaction, **23**, 271
- Free Radicals 1900–2000, The Gomberg Century, **36**, 1
- Free radicals, and their reactions at low temperature using a rotating cryostat, study of, **8**, 1
- Free radicals, identification by electron spin resonance, **1**, 284
- Gas-phase heterolysis, **3**, 91
- Gas-phase nucleophilic displacement reactions, **21**, 197
- Gas-phase pyrolysis of small-ring hydrocarbons, **4**, 147
- Gas-phase reactions of organic anions, **24**, 1
- Gaseous carbonium ions from the decay of tritiated molecules, **8**, 79
- General base and nucleophilic catalysis of ester hydrolysis and related reactions, **5**, 237
- The Gomberg Century: Free Radicals 1900–2000, **36**, 1
- Gomberg and the Nobel Prize, **36**, 59
- H₂O–D₂O mixtures, protolytic processes in, **7**, 259
- Halides, aryl, and related compounds, photochemistry of, **20**, 191
- Halogenation, nitrosation, and nitration, diffusion control and pre-association in, **16**, 1
- Heat capacities of activation and their uses in mechanistic studies, **5**, 121
- Heterolysis, gas-phase, **3**, 91

- High-spin organic molecules and spin alignment in organic molecular assemblies, **26**, 179
Homoaromaticity, **29**, 273
How does structure determine organic reactivity, **35**, 67
Hydrated electrons, reactions of, with organic compounds, **7**, 115
Hydration, reversible, of carbonyl compounds, **4**, 1
Hydride shifts and transfers, **24**, 57
Hydrocarbon radical cations, structure and reactivity of, **38**, 87
Hydrocarbons, small-ring, gas-phase pyrolysis of, **4**, 147
Hydrogen atom abstraction from O—H bonds, **9**, 127
Hydrogen bonding and chemical reactivity, **26**, 255
Hydrogen isotope effects in aromatic substitution reactions, **2**, 163
Hydrogen isotope exchange reactions of organic compounds in liquid ammonia, **1**, 156
Hydrolysis, ester, and related reactions, general base and nucleophilic catalysis of, **5**, 237
- Interface, the air-water, chirality and molecular recognition in monolayers at, **28**, 45
Intermediates, reactive, study of, by electrochemical methods, **19**, 131
Intermediates, tetrahedral, derived from carboxylic acids, spectroscopic detection and investigation of their properties, **21**, 37
Intramolecular reactions, effective molarities for, **17**, 183
Intramolecular reactions, of chain molecules, **22**, 1
Ionic dissociation of carbon-carbon α -bonds in hydrocarbons and the formation of authentic hydrocarbon salts, **30**, 173
Ionization potentials, **4**, 31
Ion-pairing effects in carbanion reactions, **15**, 153
Ions, organic, charge density-NMR chemical shift correlations, **11**, 125
Isomerization, permutational, of pentavalent phosphorus compounds, **9**, 25
Isotope effects and quantum tunneling in enzyme-catalyzed hydrogen transfer.
Part I. The experimental basis, **39**, 27
Isotope effects, hydrogen, in aromatic substitution reactions, **2**, 163
Isotope effects, magnetic, magnetic field effects and, on the products of organic reactions, **20**, 1
Isotope effects, on NMR spectra of equilibrating systems, **23**, 63
Isotope effects, steric, experiments on the nature of, **10**, 1
Isotope exchange reactions, hydrogen, of organic compounds in liquid ammonia, **1**, 150
Isotope exchange reactions, oxygen, of organic compounds, **3**, 123
Isotopes and organic reaction mechanisms, **2**, 1
- Kinetics, and mechanisms of reactions of organic cation radicals in solution, **20**, 55
Kinetics and mechanism of the dissociative reduction of C—X and X—X bonds (X=O, S), **36**, 85
Kinetics and spectroscopy of substituted phenylnitrenes, **36**, 255
Kinetics, of organic reactions in water and aqueous mixtures, **14**, 203
Kinetics, reaction, polarography and, **5**, 1
- β* -Lactam antibiotics, mechanisms of reactions, **23**, 165
Least nuclear motion, principle of, **15**, 1
- Macrocycles and other concave structures, acid-base behaviour in, **30**, 63
Macromolecular systems of biochemical interest, ^{13}C NMR spectroscopy in, **13**, 279
Magnetic field and magnetic isotope effects on the products of organic reactions, **20**, 1
Mass spectrometry, mechanisms and structure in: a comparison with other chemical processes, **8**, 152
Matrix infrared spectroscopy of intermediates with low coordinated carbon silicon and germanium atoms, **30**, 1
Mechanism and reactivity in reactions of organic oxyacids of sulphur and their anhydrides, **17**, 65
Mechanism and structure, in carbene chemistry, **7**, 153
Mechanism and structure, in mass spectrometry: a comparison with other chemical processes, **8**, 152
Mechanism and structure, in organic electrochemistry, **12**, 1
Mechanism of the dissociative reduction of C—X and X—X bonds (X=O, S), kinetics and, **36**, 85

- Mechanisms, nitrosation, **19**, 381
- Mechanisms, of proton transfer between oxygen and nitrogen acids and bases in aqueous solutions, **22**, 113
- Mechanisms, organic reaction, isotopes and, **2**, 1
- Mechanisms of reaction, in solution, entropies of activation and, **1**, 1
- Mechanisms of reaction, of β -lactam antibiotics, **23**, 165
- Mechanisms of solvolytic reactions, medium effects on the rates and, **14**, 10
- Mechanistic analysis, perspectives in modern voltammeter: basic concepts and, **32**, 1
- Mechanistic applications of the reactivity–selectivity principle, **14**, 69
- Mechanistic studies, heat capacities of activation and their use, **5**, 121
- Medium effects on the rates and mechanisms of solvolytic reactions, **14**, 1
- Meisenheimer complexes, **7**, 211
- Metal complexes, the nucleophilicity of towards organic molecules, **23**, 1
- Methyl transfer reactions, **16**, 87
- Micellar catalysis in organic reactions: kinetic and mechanistic implications, **8**, 271
- Micelles, aqueous, and similar assemblies, organic reactivity in, **22**, 213
- Micelles, membranes and other aqueous aggregates, catalysis by, as models of enzyme action, **17**, 435
- Molecular recognition, chirality and, in monolayers at the air-water interface, **28**, 45
- Molecular structure and energy, calculation of, by force-field methods, **13**, 1
- N*-Arylnitrenium ions, **36**, 167
- Neighbouring group participation by carbonyl groups in ester hydrolysis, **28**, 171
- Nitration, nitrosation, and halogenation, diffusion control and pre-association in, **16**, 1
- Nitrosation, mechanisms, **19**, 381
- Nitrosation, nitration, and halogenation, diffusion control and pre-association in, **16**, 1
- NMR chemical shift-charge density correlations, **11**, 125
- NMR measurements of reaction velocities and equilibrium constants as a function of temperature, **3**, 187
- NMR spectra of equilibrating systems, isotope effects on, **23**, 63
- NMR spectroscopy, ^{13}C , in macromolecular systems of biochemical interest, **13**, 279
- Nobel Prize, Gomberg and the, **36**, 59
- Non-linear optics, organic materials for second-order, **32**, 121
- Non-planar and planar aromatic systems, **1**, 203
- Norbornyl cation: reappraisal of structure, **11**, 179
- Nuclear magnetic relaxation, recent problems and progress, **16**, 239
- Nuclear magnetic resonance *see* NMR
- Nuclear motion, principle of least, **15**, 1
- Nuclear motion, the principle of least, and the theory of stereoelectronic control, **24**, 113
- Nucleophiles, partitioning of carbocations between addition and deprotonation, **35**, 67
- Nucleophilic aromatic photosubstitution, **11**, 225
- Nucleophilic catalysis of ester hydrolysis and related reactions, **5**, 237
- Nucleophilic displacement reactions, gas-phase, **21**, 197
- Nucleophilic substitution, in phosphate esters, mechanism and catalysis of, **25**, 99
- Nucleophilic substitution, single electron transfer and, **26**, 1
- Nucleophilic substitution reactions in aqueous solution, **38**, 161
- Nucleophilic vinylic substitution, **7**, 1
- Nucleophilic vinylic substitution and vinyl cation intermediates in the reactions of vinyl iodonium salts, **37**, 1
- Nucleophilicity of metal complexes towards organic molecules, **23**, 1
- O–H bonds, hydrogen atom abstraction from, **9**, 127
- One- and two-electron oxidations and reductions of organoselenium and organotellurium compounds, **39**, 79
- Orbital interactions and long-range electron transfer, **38**, 1
- Organic materials for second-order non-linear optics, **32**, 121
- Organic reactivity, electron-transfer paradigm for, **35**, 193
- Organic reactivity, structure determination of, **35**, 67
- Orotidine monophosphate decarboxylase, the mechanism of, **38**, 183

- Oxyacids of sulphur and their anhydrides, mechanisms and reactivity in reactions of organic, **17**, 65
Oxygen isotope exchange reactions of organic compounds, **3**, 123
- Partitioning of carbocations between addition of nucleophiles and deprotonation, **35**, 67
Perchloro-organic chemistry: structure, spectroscopy and reaction pathways, **25**, 267
Permutational isomerization of pentavalent phosphorus compounds, **9**, 25
Phase-transfer catalysis by quaternary ammonium salts, **15**, 267
Phenylnitrenes, Kinetics and spectroscopy of substituted, **36**, 255
Phosphate esters, mechanism and catalysis of nucleophilic substitution in, **25**, 99
Phosphorus compounds, pentavalent, turnstile rearrangement and pseudorotation in permutational isomerization, **9**, 25
Photochemistry, of aryl halides and related compounds, **20**, 191
Photochemistry, of carbonium ions, **9**, 129
Photodimerization and photopolymerization of diolefin crystals, **30**, 117
Photosubstitution, nucleophilic aromatic, **11**, 225
Planar and non-planar aromatic systems, **1**, 203
Polarizability, molecular refractivity and, **3**, 1
Polarography and reaction kinetics, **5**, 1
Polypeptides, calculations of conformations of, **6**, 103
Pre-association, diffusion control and, in nitrosation, nitration, and halogenation, **16**, 1
Principle of non-perfect synchronization, **27**, 119
Products of organic reactions, magnetic field and magnetic isotope effects on, **30**, 1
Protic and dipolar aprotic solvents, rates of bimolecular substitution reactions in, **5**, 173
Protolytic processes in H₂O–D₂O mixtures, **7**, 259
Proton transfer between oxygen and nitrogen acids and bases in aqueous solution, mechanisms of, **22**, 113
Protonation and solvation in strong aqueous acids, **13**, 83
Protonation sites in ambident conjugated systems, **11**, 267
Pseudorotation in isomerization of pentavalent phosphorus compounds, **9**, 25
Pyrolysis, gas-phase, of small-ring hydrocarbons, **4**, 147
- Radiation techniques, application to the study of organic radicals, **12**, 223
Radical addition reactions, gas-phase, directive effects in, **16**, 51
Radical rearrangement reactions, charge distribution and charge separation in, **38**, 111
Radicals, cation in solution, formation, properties and reactions of, **13**, 155
Radicals, organic application of radiation techniques, **12**, 223
Radicals, organic cation, in solution kinetics and mechanisms of reaction of, **20**, 55
Radicals, organic free, identification by electron spin resonance, **1**, 284
Radicals, short-lived organic, electron spin resonance studies of, **5**, 53
Rates and mechanisms of solvolytic reactions, medium effects on, **14**, 1
Reaction kinetics, polarography and, **5**, 1
Reaction mechanisms, in solution, entropies of activation and, **1**, 1
Reaction mechanisms, use of volumes of activation for determining, **2**, 93
Reaction velocities and equilibrium constants, NMR measurements of, as a function of temperature, **3**, 187
Reactions, in dimethyl sulphoxide, physical organic chemistry of, **14**, 133
Reactions, of hydrated electrons with organic compounds, **7**, 115
Reactive intermediates, study of, by electrochemical methods, **19**, 131
Reactivity, organic, a general approach to: the configuration mixing model, **21**, 99
Reactivity indices in conjugated molecules, **4**, 73
Reactivity-selectivity principle and its mechanistic applications, **14**, 69
Rearrangements, degenerate carbocation, **19**, 223
Receptor molecules, redox-active, electrochemical recognition of charged and neutral guest species by, **31**, 1
Redox and recognition processes, interplay between, **37**, 315
Redox systems, organic, with multiple electrophores, electron storage and transfer in, **28**, 1
Reduction of C–X and X–X bonds (X=O, S), kinetics and mechanism of the dissociative, **36**, 85

- Refractivity, molecular, and polarizability, **3**, 1
- Relaxation, nuclear magnetic, recent problems and progress, **16**, 239
- Selectivity of solvolyses and aqueous alcohols and related mixtures, solvent-induced changes in, **27**, 239
- Short-lived organic radicals, electron spin resonance studies of, **5**, 53
- Small-ring hydrocarbons, gas-phase pyrolysis of, **4**, 147
- Solid state, tautomerism in the, **32**, 129
- Solid-state chemistry, topochemical phenomena in, **15**, 63
- Solids, organic, electrical conduction in, **16**, 159
- Solutions, reactions in, entropies of activation and mechanisms, **1**, 1
- Solvation and protonation in strong aqueous acids, **13**, 83
- Solvent effects, reaction coordinates, and reorganization energies on nucleophilic substitution reactions in aqueous solution, **38**, 161
- Solvent, protic and dipolar aprotic, rates of bimolecular substitution-reactions in, **5**, 173
- Solvent-induced changes in the selectivity of solvolyses in aqueous alcohols and related mixtures, **27**, 239
- Solvolytic reactions, medium effects on the rates and mechanisms of, **14**, 1
- Spectroscopic detection of tetrahedral intermediates derived from carboxylic acids and the investigation of their properties, **21**, 37
- Spectroscopic observations of alkylcarbonium ions in strong acid solutions, **4**, 305
- Spectroscopy, ¹³C NMR, in macromolecular systems of biochemical interest, **13**, 279
- Spectroscopy of substituted phenylnitrenes, kinetics and, **36**, 255
- Spin alignment, in organic molecular assemblies, high-spin organic molecules and, **26**, 179
- Spin trapping, **17**, 1
- Spin trapping, and electron transfer, **31**, 91
- Stability and reactivity of crown-ether complexes, **17**, 279
- Stereochemistry, static and dynamic, of alkyl and analogous groups, **25**, 1
- Stereoelectronic control, the principle of least nuclear motion and the theory of, **24**, 113
- Stereoselection in elementary steps of organic reactions, **6**, 185
- Steric isotope effects, experiments on the nature of, **10**, 1
- Structure, determination of organic reactivity, **35**, 67
- Structure and mechanism, in carbene chemistry, **7**, 153
- Structure and mechanism, in organic electrochemistry, **12**, 1
- Structure and reactivity of carbenes having aryl substituents, **22**, 311
- Structure and reactivity of hydrocarbon radical cations **38**, 87
- Structure of electronically excited molecules, **1**, 365
- Substitution, aromatic, a quantitative treatment of directive effects in, **1**, 35
- Substitution, nucleophilic vinylic, **7**, 1
- Substitution reactions, aromatic, hydrogen isotope effects in, **2**, 163
- Substitution reactions, bimolecular, in protic and dipolar aprotic solvents, **5**, 173
- Sulphur, organic oxyacids of, and their anhydrides, mechanisms and reactivity in reactions of, **17**, 65
- Superacid systems, **9**, 1
- Tautomerism in the solid state, **32**, 219
- Temperature, NMR measurements of reaction velocities and equilibrium constants as a function of, **3**, 187
- Tetrahedral intermediates, derived from carboxylic acids, spectroscopic detection and the investigation of their properties, **21**, 37
- Thermodynamic stabilities of carbocations, **37**, 57
- Topochemical phenomena in solid-state chemistry, **15**, 63
- Transition state analysis using multiple kinetic isotope effects, **37**, 239
- Transition state structure, crystallographic approaches to, **29**, 87
- Transition state structure, in solution, effective charge and, **27**, 1
- Transition state structure, secondary deuterium isotope effects and, **31**, 143
- Transition states, structure in solution, cross-interaction constants and, **27**, 57
- Transition states, the stabilization of by cyclodextrins and other catalysts, **29**, 1

- Transition states, theory revisited, **28**, 139
Tritiated molecules, gaseous carbonium ions from the decay of, **8**, 79
Tritium atoms, energetic reactions with organic compounds, **2**, 201
Turnstile rearrangements in isomerization of pentavalent phosphorus compounds, **9**, 25
- Unsaturated compounds, basicity of, **4**, 195
- Vinyl cation intermediates, **37**, 1
Vinyl cations, **9**, 185
Vinyl iodonium salts, **37**, 1
Vinylic substitution, nucleophilic, **7**, 1; **37**, 1
Voltammetry, perspectives in modern: basic concepts and mechanistic analysis, **32**, 1
Volumes of activation, use of, for determining reaction mechanisms, **2**, 93
- Water and aqueous mixtures, kinetics of organic reactions in, **14**, 203
- Yukawa–Tsuno relationship in carboration systems, the, **32**, 267